GEM TN-91-00009

GEM Calorimetry Questions and Answers

September 5, 1991

Abstract:

Proponents of candidate calorimetry technologies respond to questions and concerns.

Liquid Scintillator Technology for GEM Hadron Calorimeter

Answers to questions of concern

of GEM collaborators

September 4, 1991, Dallas

GENERAL REMARK

We consider two options for liquid scintillator (LS) technique for calorimetery in GEM detector :

Option # 1 BaF_2 (or Liq. Xe) EM calorimeter followed by LS HC

Option # 2 EM and hadron calorimeter as two separate LS sections

Answers to questions addressed by

Howard Gordon

Question 1. Describe the uniformity needed for the hadron calorimeter and show either data or a schedule for achieving this uniformity.

Answer :

We assume the hadronic energy resolution Delta(E)/E = (50)%/sqrt(E) + 2% for Pb/LS hadron calorimeter with sampling fraction 4:1 = 20mmPb : 5mmLS behind BaF2 electromagnetic calorimeter [1,2]. Non-uniformity of the response can affect the resolution, particulary the constant term. We can assume that BaF2 uniformity is perfect for hadron calorimetry purposes.

Uniformity issue can be addressed for three possible kinds of non-uniformities :

1. non-uniformity of the response from point to point in one cell (non-correctable);
2. cell to cell response non-uniformity (in principle, correctable by calibration, but not correctable within group of cells ganged together for common readout channel);
3. non-uniformity introduced by structural elements or readout paths (correctable with cluster centroid measurement)

One can look at these cases separatly :

1. Hadronic shower energy loss in HC of 1 GeV will produce in the scintillation detector the signal equivalent of 15-20 mips [3]. We can assume that this signal consists from 15-20 hits in different parts of the detection cells. This number increases linearly with deposited energy. Difference in response for different hits will be averaged according to :

   Sigma(non-unif.)/SQRT(15*0.4*EGeV)

   Here a 40% total jet energy deposition in the HC was assumed together with a 15% nonuniformity. This corresponds to a 6%/sqrt(E) term which has to be added to (50)%/sqrt(E)+2% in quadrature.

   Measured result of liquid scintillator cell nonuniformity obtained with prototype cell of the size 6 x 6 x 0.5 cm3 is shown in Figure 1. Observed non-uniformity is approx. 12%

2. Nonuniformity due to cell to cell sensitivity variation. Suppose that we have no calibration as well as cell grouping. Then the non-uniformity will be improved with number of cells occupied by the event. This number depends on energy and can be estimated [3,4] as

   10 * {1+Log(E_GeV)}

   According to existing mechanical design of liquid scintillator calorimeter only cells of equal size will be combined into one readout group. The difference in sensitivity between these cells depends on the stability and tolerances of mass production and can be conservatively assumed to be approx. 3%. The contribution to resolution is then

   3%/SQRT{10*(1+Log(0.4*E_GeV))}

   i.e. 0.6% at 100 GeV, which should be added quadratically to the base resolution of 50%/sqrt(E)+2%.

We are building prototype of the LS detector plane which will be tested in ITEP test beam starting from December 1991. The plane will consist from 36 cells of the same size made with uniform technology. We plan to perform the uniformity scan of this plane as well as to determine cell to cell gain variation. Each cell will be equipped with an individual U-235 calibration source.

Beam tests at CERN with prototype of LS HC module is scheduled for the end 1992-beginning 1993. Energy resolution will be measured at high energies, and calibration with radioactive sources and effects of cell to cell response nonuniformity will be studied.

3. In the existing LS hadron calorimeter design all structural elements and readout paths are non-projective (Figures 2-4). Since the design is similar to that of the existing L3 detector, where structural elements in phi view are projective and in theta view are non-projective, we can examine the L3 [4] data in order to understand the effects of structural elements. Figure 5 shows the layout of L3 hadron calorimeter with the BGO (barrel part) in front. In Figure 6 the reconstructed energy of two jets (from Z0 -> 2 jets) is shown vs azimuthal angle and versus the cosine of the polar angle. In phi-view projective structural elements (behind the BGO) do not show any effect on resolution; in theta-view the resolution worsens in both directions from 90 degree polar angle. This is mainly because sampling becomes coarser at smaller angles. Apart from this the complicated structure of supports and flanges doesn't seem to affect the resolution.

   Experimental study of structural elements effects is possible with a set of several hadron calorimeter modules. In our test beam plans for the end 1992-beginning 1993 only one module is envisaged. But it is conceivable to extend the scope of these measurements provided that corresponding financial support will be available.

Referencies :

[1] L* EoI to SSCL, May 1990
[2] L* LoI to SSCL, November 1990
[3] H.Bruckmann et al., Hadron sampling calorimetry, DESY 86-155 and ref. therein
[4] O.Adriani et al, NIM A302(1991)53-62

Measured LS cell non-uniformity – 12% (Ru^{106})

77	88	99	97	78	78
95	109	103	105	101	87
100	113	93	91	104	90
105	116	103	110	100	90
95	116	122	117	103	99
81	94	105	119	115	94

Fig. 1

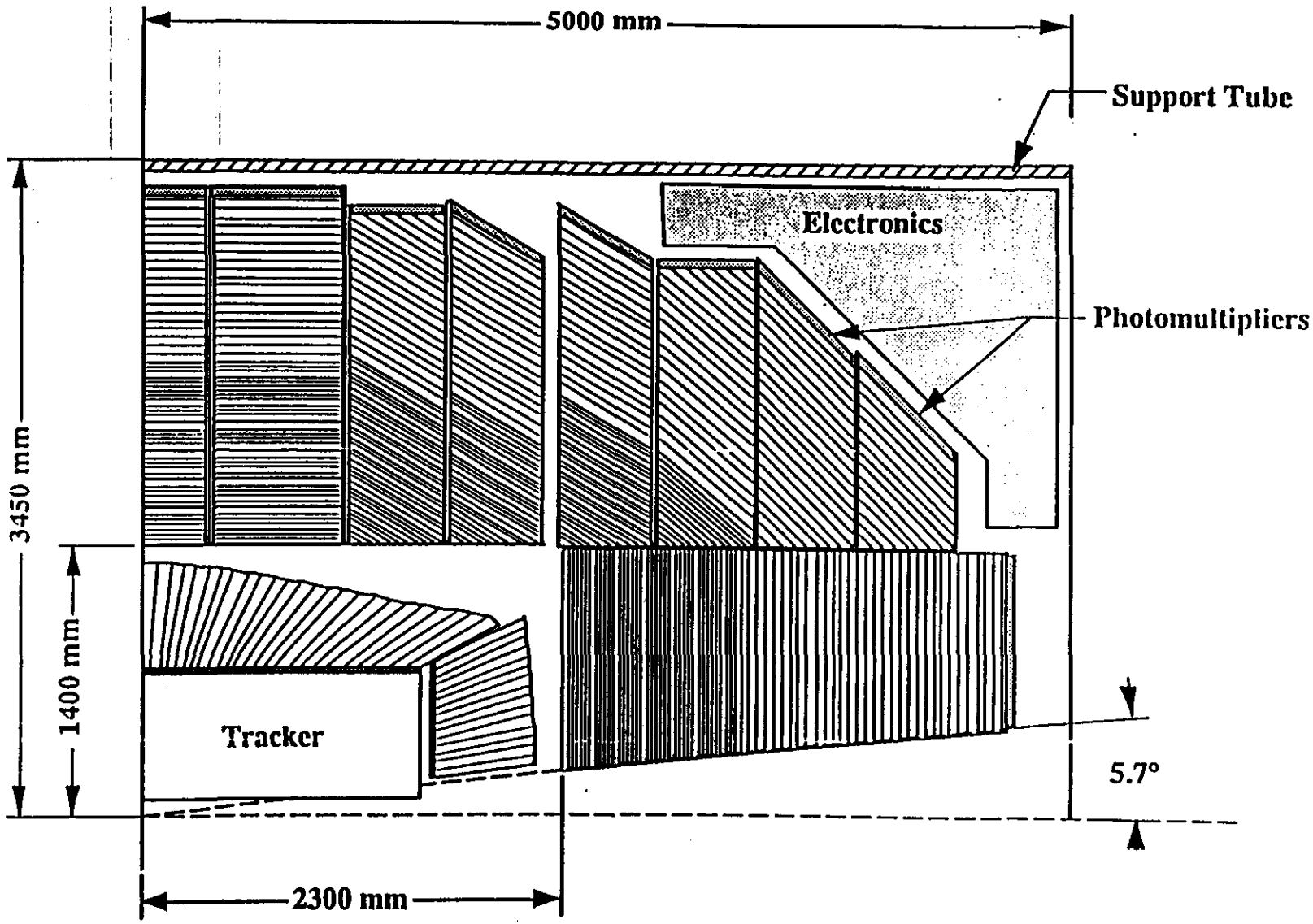

Liquid Scintillator Hadron Calorimeter
Barium Fluoride EM Calorimeter

Fig 2

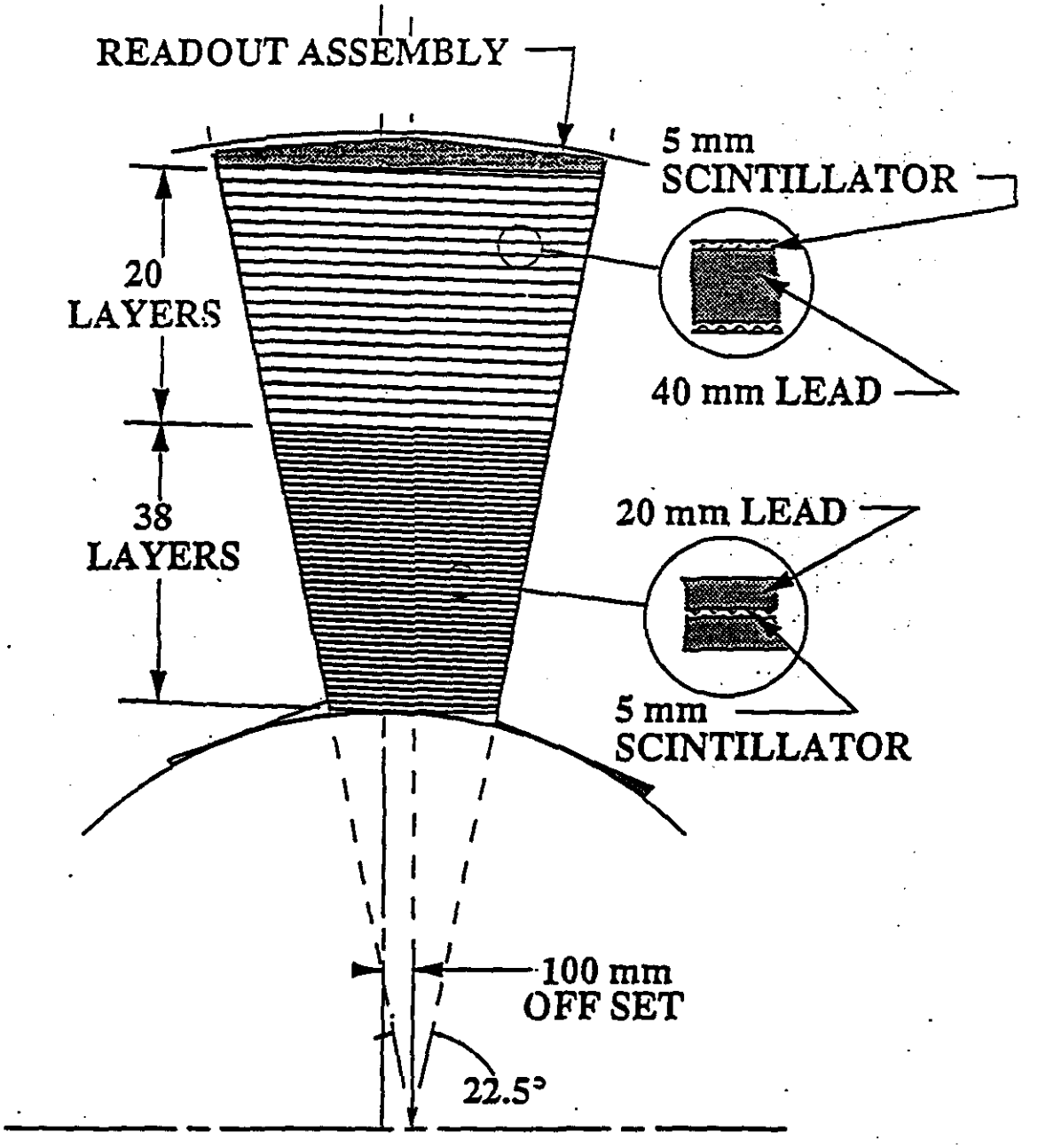

HADRON CALORIMETER
TOWER ASSEMBLY

Fig. 3

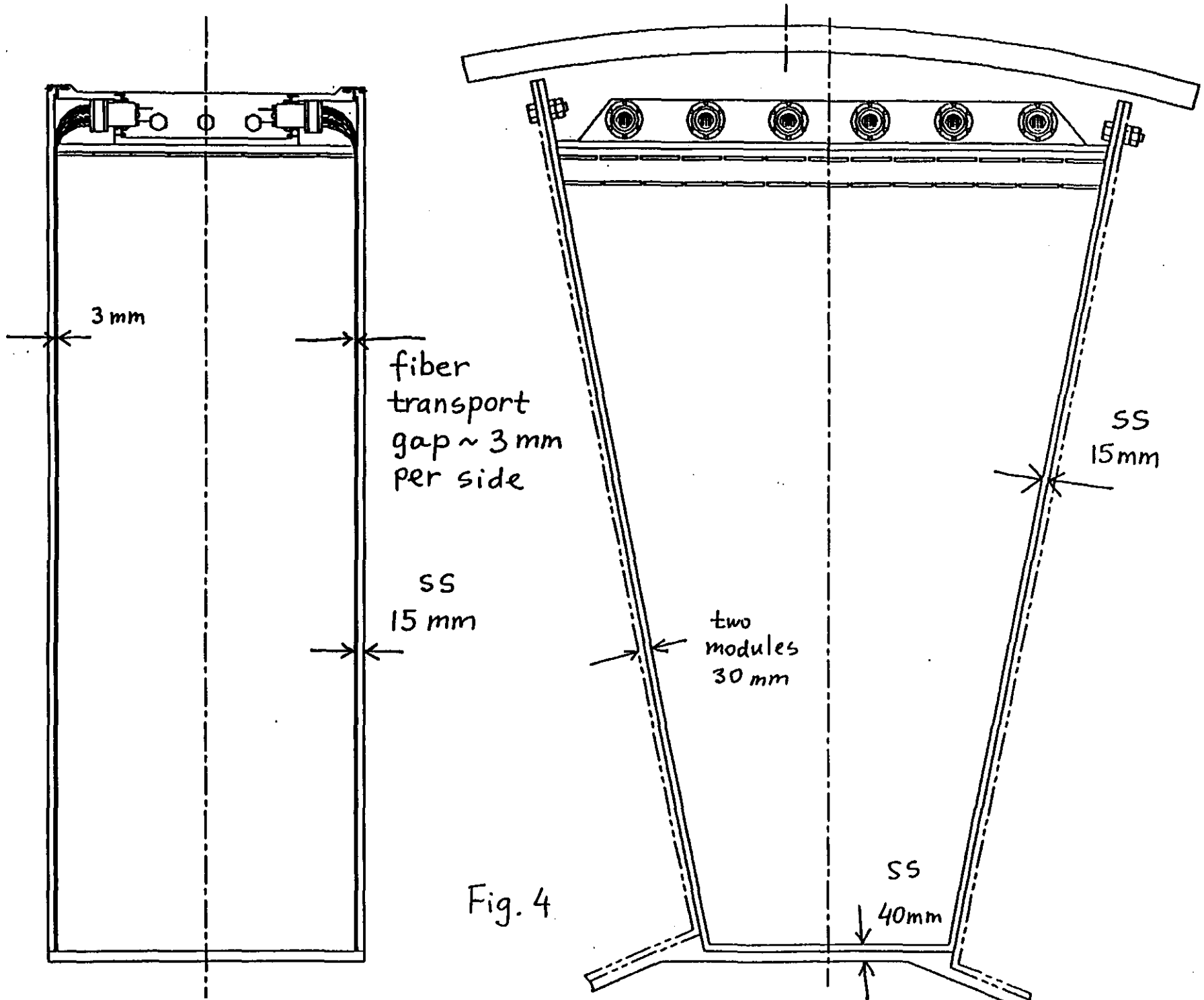
3 mm
fiber
transport
gap ~ 3 mm
per side
SS
15 mm
two
modules
30 mm
SS
15mm
SS
40mm

Fig. 4

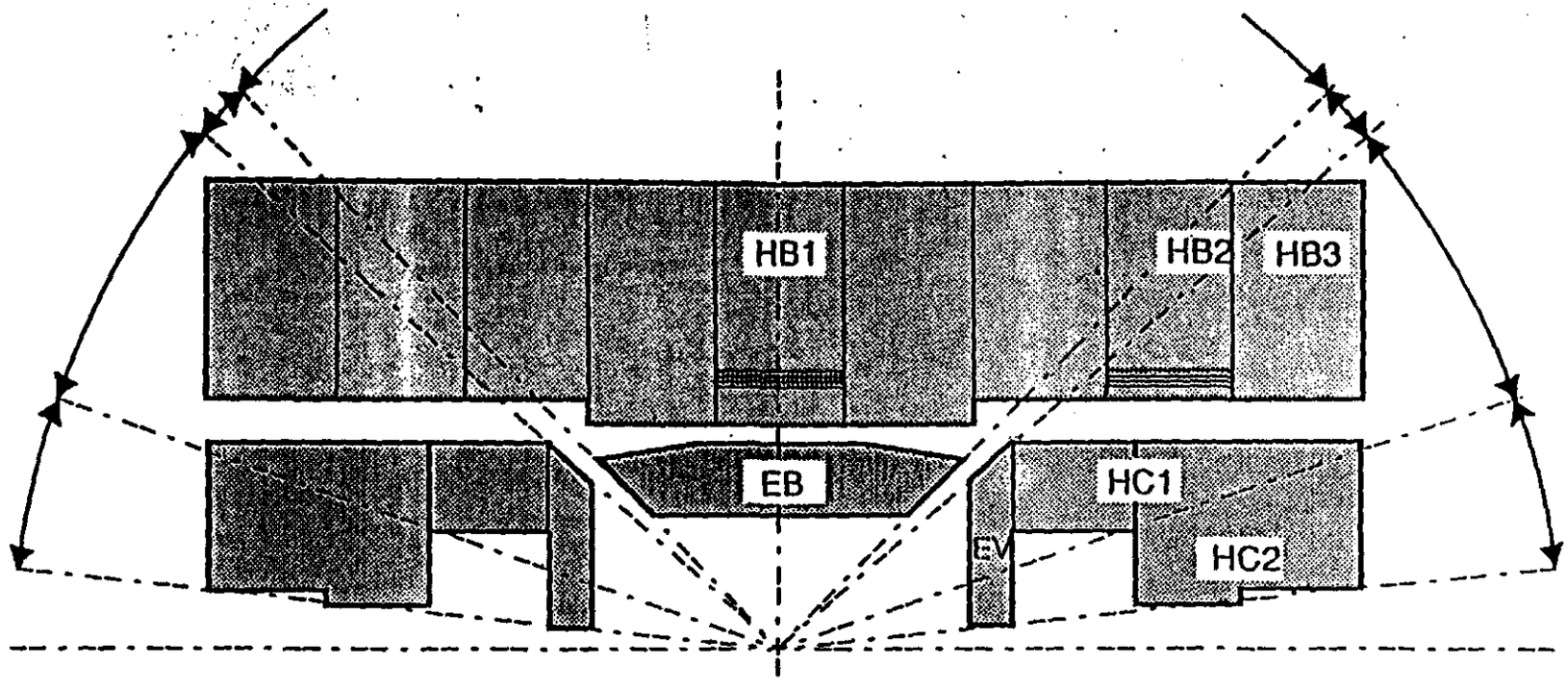

Fig. 5

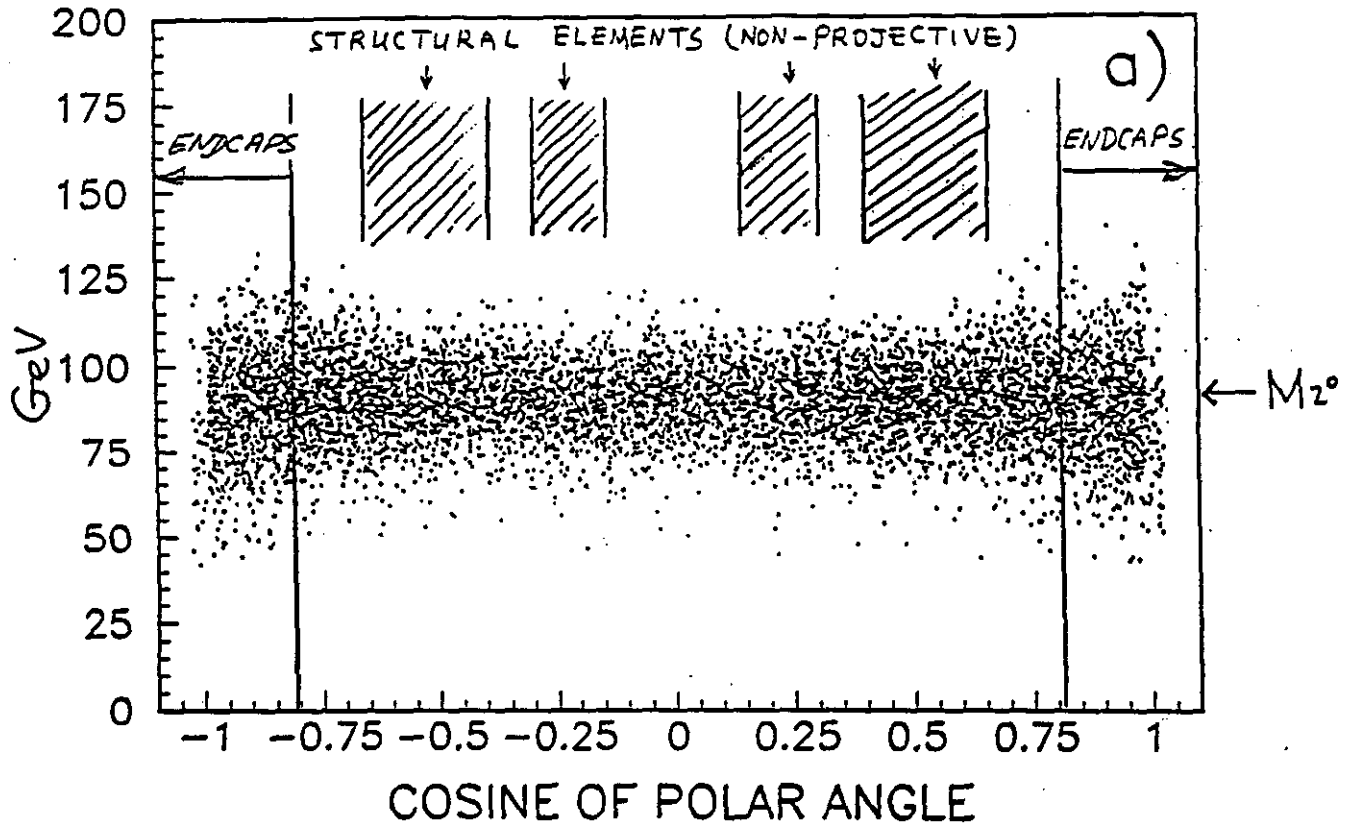
STRUCTURAL ELEMENTS (NON-PROJECTIVE)
a)
ENDCAPS
ENDCAPS
GeV
200
175
150
125
100
75
50
25
0
−1
−0.75
−0.5
−0.25
0
0.25
0.5
0.75
1
COSINE OF POLAR ANGLE
Mz°

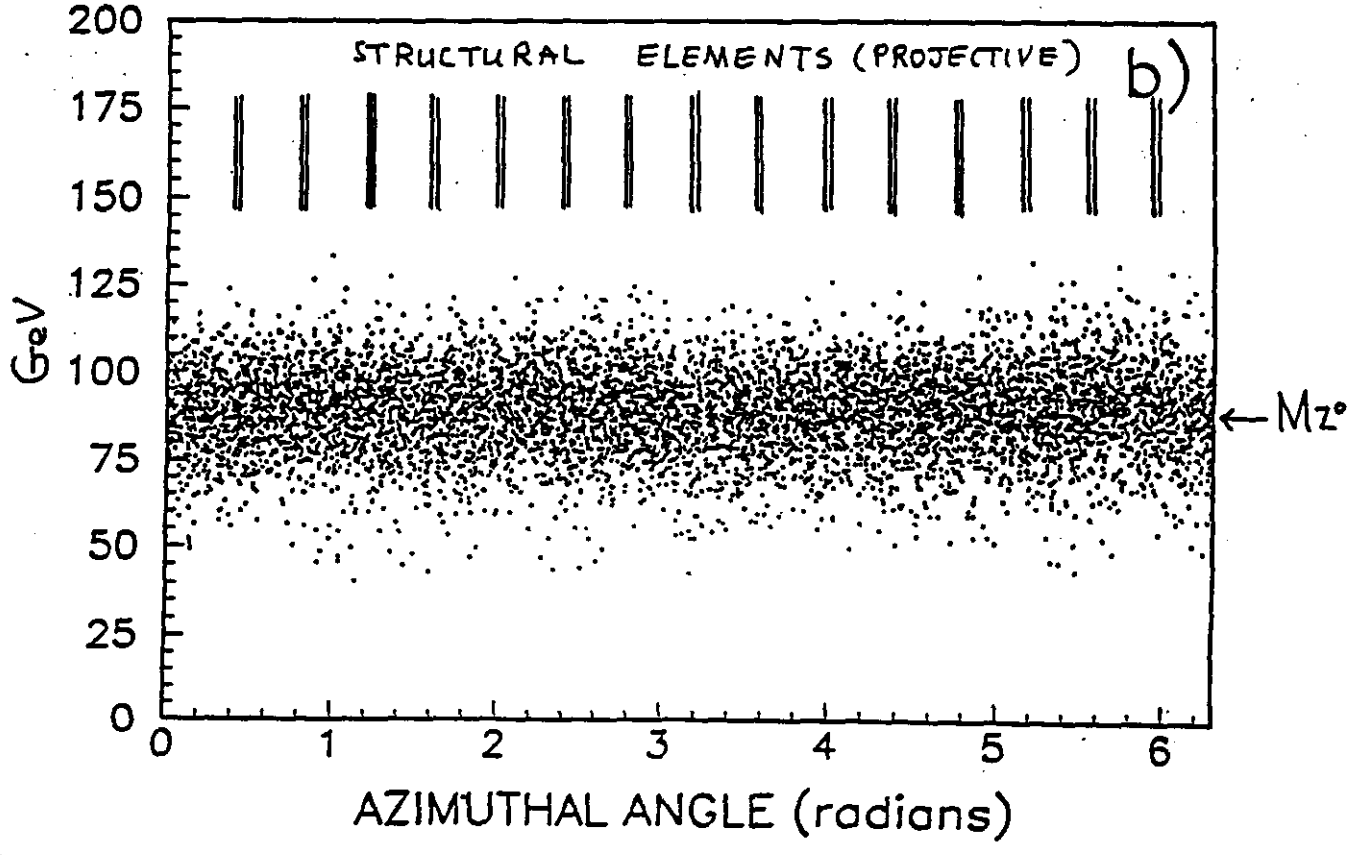
STRUCTURAL ELEMENTS (PROJECTIVE)
b)
GeV
200
175
150
125
100
75
50
25
0
0
1
2
3
4
5
6
AZIMUTHAL ANGLE (radians)
Mz°

Fig. 6

Question 2. When will there be chemically compatible scintillator and scintillating fibers?

Answer :

Chemically compatible liquid scintillator and plastic fibers are commercially available from Bicron Corporation. They are :

Liquid scintillator	: BC-517 P
Wave length shifting fibers	: BCF-91A
Clear transport fibers	: BCF-98
White reflecting paint	: BC-622A

Producer's specs for these components are shown in Figures 7-10.

Direct compatibility tests of these components show no sings for chemical attack for a time period of more than 130 days.

We have performed accelerated compatibility tests at elevated temperatures up to 65 degree C (with acceleration factor > 60) for 130 days and saw no signs of chemical attack.

By extrapolation from more chemically active liquids of the same basic composition but at different concentrations we concervatively estimate the life time of plastic fibers in liquid scintillator for the above types to be 70-450 years. These results are shown in Tables 1 and 2 below.

We have performed chemical compatibility tests under irradiation and saw no increase in the speed of chemical reactions due to irradiation. (20 MRad at 0.377 MRad/h at 32 degree C).

More details of our chemical compatibility studies can be found in [1]

Referencies :

[1] Liquid Scintillator Calorimetery (Second Year), A R$D Proposal submitted to SSCL,September 1991 (in preparation)

TABLE 1

The results of measurements of the Time of Life (TOL) for chemical compatibility of plastic fibers and Bicron scintillators.

Scintillator	BC517S	BC517H	BC517L	BC517P
TOL @ 22°C	1 hour	16 days	>150 d	>105 d
TOL @ 42°C	short	6 hours	90 days	>105 d

TABLE 2

Time of Life (TOL) of Plastic Fibers in Bicron Scintillators.

Scintillator	Pseudocumene concentration (%)	Light output (% antracene)	Flash point (°C)	H/C ratio	Time of Life @ 22°C
BC517S	< 50	66	74	1.70	1 hour
BC517H	< 40	52	81	1.89	16 days
BC517L	< 30	39	102	2.01	15 years[1]
BC517P	< 10	28	115	2.05	70-450 years[2]

[1] extrapolated from measurements at elevated temperature (42°C)
[2] extrapolated from TOL dependence on light output, flash point and H/C ratio

BICRON®

Bicron Corporation
12345 Kinsman Road
Newbury, Ohio 44065-9677
Telephone: (216) 564-2251
Telefax: (216) 564-8047
Telex: 980474 BICRON NWBY

European Office
Marktstraat 27A, P.O. Box 271
2410 AG Bodegraven, The Netherlands
Telephone: 1726-14243
Telefax: 1726-14316
Telex: 39772 BICIN NL

Nippon Bicron
Room No. 805 1-8, 1-Chome
Shinyokohama, Kohoku-Ku
Yokohama 222 Japan
Telephone: 045(474)5786
Telex: 045(474)5787

The liquid is compatible with acrylic and PVC plastics, both of which are quite useful for constructing large, low cost tanks. Bicron has supplied many thousands of gallons of this product (packaged in 55 gallon tank wagons) to the physics community.

The principal features of BC-517P are:

Exceptional light transmission

Chemical inertness

Physical Properties:

Light Output:	28% anthracene
Mean Free Path (400-500 nm):	>6 meters
Decay Time (approx.):	2.2 nsec
Wavelength of Maximum Emission:	425nm
Refractive Index:	1.47
Specific Gravity:	0.85
Flash Point (T.O.F.):	115°C (240°F)
No. of C Atoms per cm^3:	3.65×10^{22}
No. of H Atoms per cm^3:	7.50×10^{22}
No. of Electrons per cm^3:	29.4×10^{22}
Coefficient of Thermal Expansion:	0.00075/°C
Vapor Pressure, 20°C:	0.16 mm Hg
Viscosity, 20°C:	21.1 centistokes

Fig. 7

"Green" Plastic WLS Fiber

BICRON®

Bicron Corporation
12345 Kinsman Road
Newbury, Ohio 44065-9677
Telephone: (216) 564-2251
Telefax: (216) 564-8047
Telex: 980474 BICRON NWBY

European Office
Markstraat 27A, P.O. Box 271
2410 AG Bodegraven, The Netherlands
Telephone: 1726-14243
Telefax: 1726-14316
Telex: 39772 BICIN NL

Nippon Bicron
Room No. 805 1-8, 1-Chome
Shinyokohama, Kohoku-Ku
Yokohama 222 Japan
Telephone: 045(474)5786
Telex: 045(474)5787

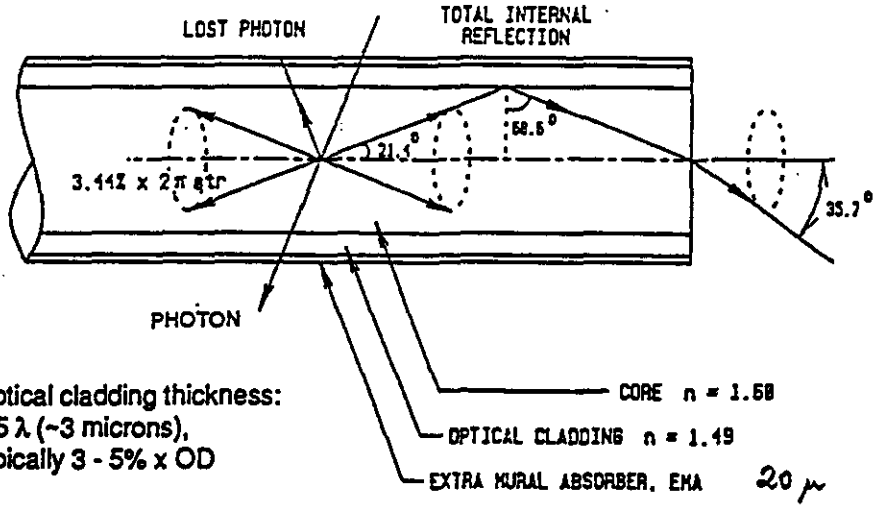

Optical cladding thickness:
> 5 λ (~3 microns),
typically 3 - 5% x OD

BCF-91A is a green, plastic, wavelength shifter (WLS) fiber having a polystyrene core and PMMA cladding. It shifts blue light in blue scintillating fibers to green so that the detector can employ such readout devices as CCDs (charged coupled devices).

The trapping efficiency is the percentage of the total light that is piped down the fiber in each direction. This is >3.4% for round fibers and <4.4% for square.

Optical and Physical Properties of BCF-91A Green WLS Fiber

Core refractive index	1.60
Cladding refractive index	1.49
Cladding thickness	
round fibers	3% of core ϕ
square fibers	4% of core side
Quantum efficiency	86%
Numerical aperture	0.58
Trapping efficiency (round fibers)	3.44% minimum
Peak emission wavelength	480 nm
Attenuation length, 1 mm ϕ	> 4 m
Vacuum compatible	yes
Operating temperature	-20°C to +50°C

May, 1991

Fig. 8

Light Transmitting, Plastic, Light Pipe Fiber

BICRON®

Bicron Corporation
12345 Kinsman Road
Newbury, Ohio 44065-9677
Telephone: (216) 564-2251
Telefax: (216) 564-8047
Telex: 980474 BICRON NWBY

European Office
Marktstraat 27A, P.O. Box 271
2410 AG Bodegraven, The Netherlands
Telephone: 1726-14243
Telefax: 1726-14316
Telex: 39772 BICIN NL

Nippon Bicron
Room No. 805 1-8, 1-Chome
Shinyokohama, Kohoku-Ku
Yokohama 222 Japan
Telephone: 045(474)5786
Telex: 045(474)5787

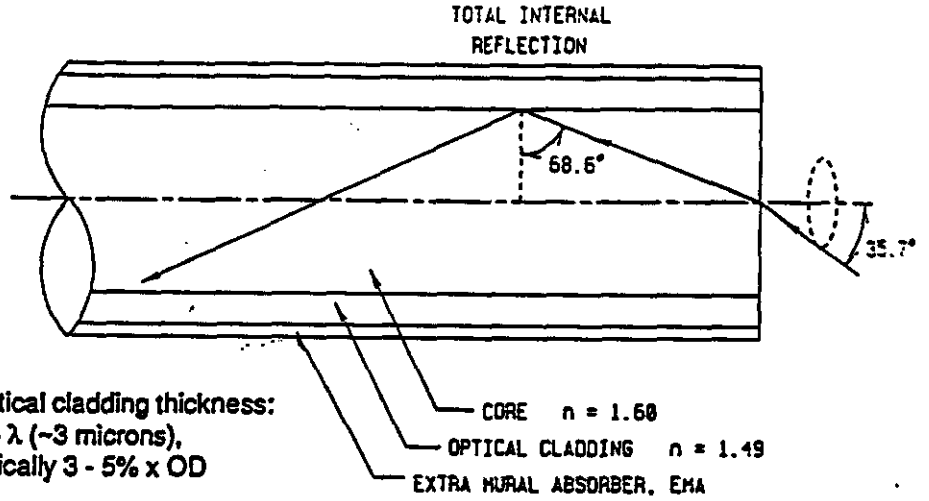

Optical cladding thickness:
> 5 λ (~3 microns),
typically 3 - 5% x OD

BCF-98 is a clear, light-transmitting, plastic fiber having a polystyrene core and PMMA cladding. It is used to transmit light from a scintillator to a readout device. Bundles of fibers form light pipes which are used to:

- Provide a PMT mounting surface
- Guide the scintillating light to the photocathode
- Back off the PMT where the scintillator is in a strong magnetic environment
- Minimize pulse height variation

Optical and Physical Properties of BCF-98 Fiber

Scintillating core refractive index	1.60
Cladding refractive index	1.49
Cladding thickness	
round fibers	3% of core ϕ
square fibers	4% of core side
Numerical aperture	0.58
Trapping efficiency (round fibers)	3.44% minimum
Attenuation length, 1/e (1 mm ϕ)	2 meters @ (400 - 500nm)
Vacuum compatible	yes
Operating temperature	-20°C to +50°C

Fig. 9

Reflector Paint for Liquid Scintillator Tanks

BICRON®

Bicron Corporation
12345 Kinsman Road
Newbury, Ohio 44065-9677
Telephone: (216) 564-2251
Telefax: (216) 564-8047
Telex: 980474 BICRON NWBY

European Office
Markstraat 27A, P.O. Box 271
2410 AG Bodegraven, The Netherlands
Telephone: 1726-14243
Telefax: 1726-14316
Telex: 39772 BICIN NL

Nippon Bicron
Room No. 805 1-8, 1-Chome
Shinyokohama, Kohoku-Ku
Yokohama 222 Japan
Telephone: 045(474)5786
Telex: 045(474)5787

BC-622A is prepared from a cross-linked polyurethane resin having exceptional chemical resistance to aromatics, which makes it highly suitable for use with liquid scintillators. It is ideal for our benzene-based BC-537 liquid scintillator.

BC-622A normally comes in 500 ml and 1 liter quantities. The paint resin and hardener are supplied in separate containers.

Application

Thoroughly clean and degrease the surfaces to be painted. Roughen with abrasive paper, if possible.

Mix only enough paint and hardener for one coat (approximately 350 ml of mix per square meter). Stir the white paint well before removing from the original can and thoroughly mix the two components in the following proportions:

Paint	2 parts by volume
Hardener	1 part by volume

The mixture has a pot life of about two hours at room temperature. Quantities of 25 ml or more will have a shorter pot life if allowed to remain in one compact mass owing to the heat generated by the exothermic reaction.

Apply with a brush and let it partially cure (about one hour) then apply the next coat. Three coats are usually required. Curing times are 4 hours at 20°C, or 1 hour at 50°C. Do not exceed 55°C.

BC-622A gives off a flammable vapor and should not be used near open flames. Skin contact should be avoided. Painting should be done in a ventilated area. For cleaning brushes, use methylene-chloride (dichloromethane) or chloroform (trichloromethane).

Fig. 10

Question 3. When will a hadronic prototype be beam tested to prove the resolution, noise, time response, uniformity, and response of the cracks where the fibers are bundled?

Answer :

Beam tests at CERN of one module hadronic prototype is scheduled for late 1992 by the LS R&D Subsystem Collaboration. In this test energy resolution, time response, and noise of single hadron calorimeter module will be measured with high energy electrons, pions and muons. We also plan to perform the calibration of the combined calorimeter system consisting of an EM BaF2 section in front of liquid scintillator module at the same beam in the spring of 1993.

Detailed study of uniformity and cracks can be done with several modules (peferably with not less than four). It is conceivable to extend the scope of our measurements to 4 or more modules + sophisticated movable support if the liquid scintillator R&D project receives sufficient financial support.

Figures 2-4 illustrate the layout of construction walls and of fiber transport gaps in the LS hadron calorimeter design. Note that both are non-projective.

Question 4. Describe the calibration system.

Answer :

The calibration is one of the basic issues of calorimeter operation. Following the ideas which have been applied realized in the construction and operation of the L3 Hadron Calorimeter [1] we choose the scheme of liquid scintillator calorimeter monitoring and calibration in which every calorimeter cell is equipped with a radioactive source. In addition the modular design of the LS Hadron Calorimeter allows to calibrate each individual module (out of 256) in the test beam using the radioactive source calibration as reference. Stable operation of SSC (fixed center of mass energy and controlled luminosity) will provide the stable source of hadron calorimeter response monitoring.

In the L3 Hadron Calorimeter the built-in source is the depleted uranium absorber which provids in every readout cell of proportional gas tube detector the counting rate of 2-40 KHz. Actual calibration in L3 HC is done with a random trigger, such that measured calibration spectra have no characteristic peaks and look like a falling exponent. Nevertheless, the accuracy of response calibration of about 2% per readout channel is achievable for ~ 30 minute run in the whole data acquisition system with over 20,000 readout channels. The same calibration system is used for the monitoring of the long term stability of the hadron calorimeter which was found to be 1.3% over a period of two years [1].

We are going to implement in every calorimeter cell a radioactive source with small activity (counting rate < 1 KHz/cell). For this purpose we have examined several source candidates U-235 (1% U-234), Sr-90, and Ru-106. Self-triggered spectra for these sources are shown in Figure 11. The U-235 source consists of 0.25 mm thick Ti disk of diameter 5 mm with high-vacuum electron-beam-evaporated enriched U-235. It provides a counting rate in the cell of about 900 Hz. This source was produced at ORNL. The cost of the source for several thousand units is estimated to be $0.25/source. This cost could be reduced by a factor two for quantities required for a full calorimeter.

In addition to the radioactive sources we are going to install an optical fiber light source on every photomultiplier, with light supplied by a green laser through a fiber distribution system. This will allow independent test of photocathode and electronics sensitivity and linearity in the full dynamic range.

Referencies

[1] S.Burov et al., L3 Collaboration, CERN-EP/88-84;
O.Adriani et al., L3 Collaboration, Hadron Calorimetry in the L3 Detector, NIM A302(1991)53-62;

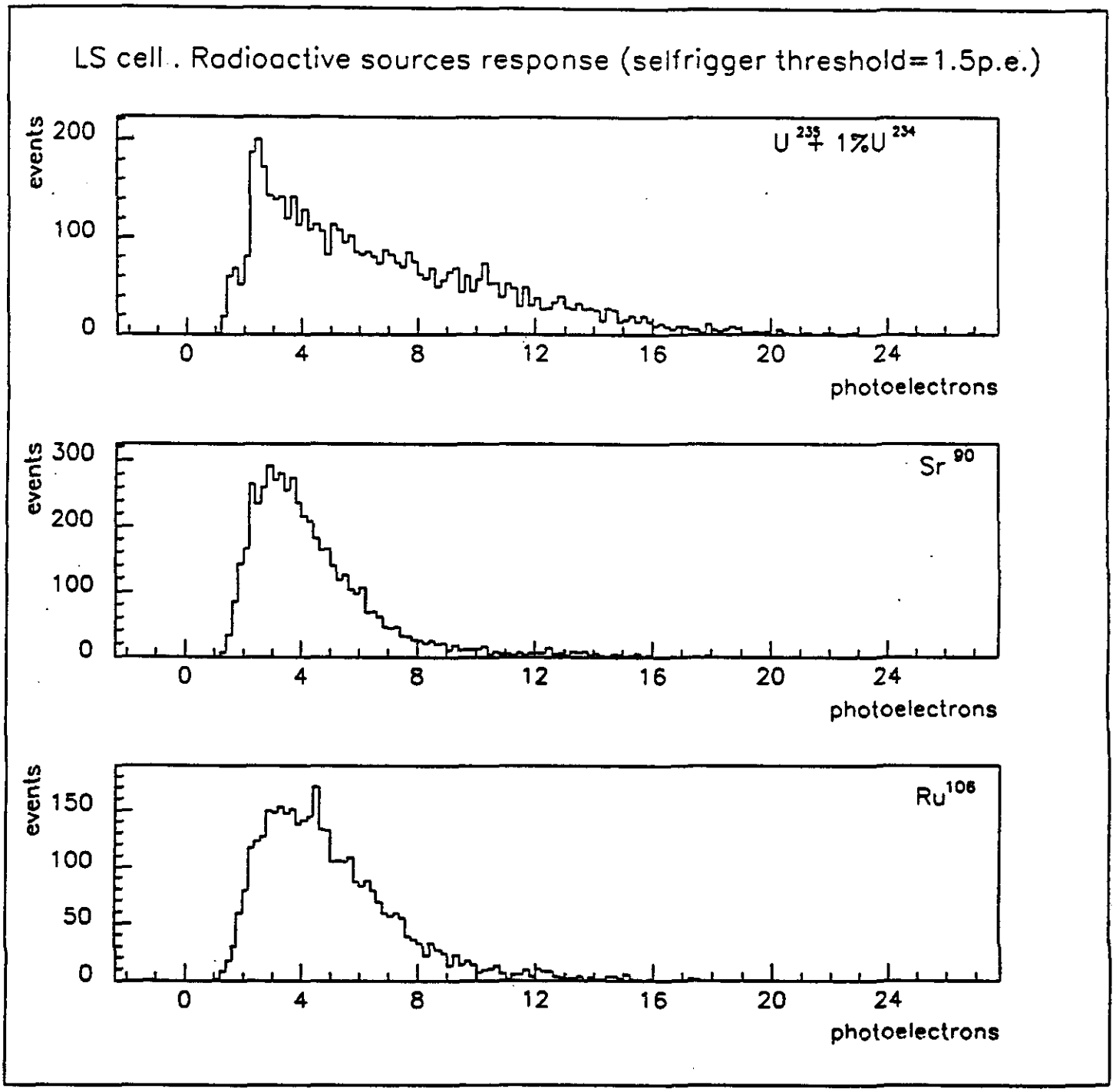
LS cell . Radioactive sources response (selfrigger threshold=1.5p.e.)
events
200
100
0
U 235 + 1%U 234
0
4
8
12
16
20
24
photoelectrons
events
300
200
100
0
Sr 90
0
4
8
12
16
20
24
photoelectrons
events
150
100
50
0
Ru106
0
4
8
12
16
20
24
photoelectrons

Fig. 11

Common questions for systems using phototubes:

Ensuring the phototubes response over the 10**5 dynamic range, finding acceptable time dispersion at 10**5 dynamic range; dealing with the tails from large pulses that are commonly found in phototubes.

Answer :

Most probable candidate for LS calorimeter light readout is proximity focusing mesh dynode multianode phototube Hamamatsu type R2490-05. This device operates with the of gain 10**4 in a longitudinal magnetic field of 0.8 T. It has a linearity of less than 1.5% for an anode current output of up to 500 mA (pulse)/anode (Figure 12.) Time response for a limited dynamic range is shown in Figure 13 (Both Figures are Hamamatsu data). We are going to have sample unit of this 16-anode photomuliplier by the end of 1991 for evaluation. This sample will be tested for linearity, time dispersion, afterpulses, stability etc. in the full dynamic range.

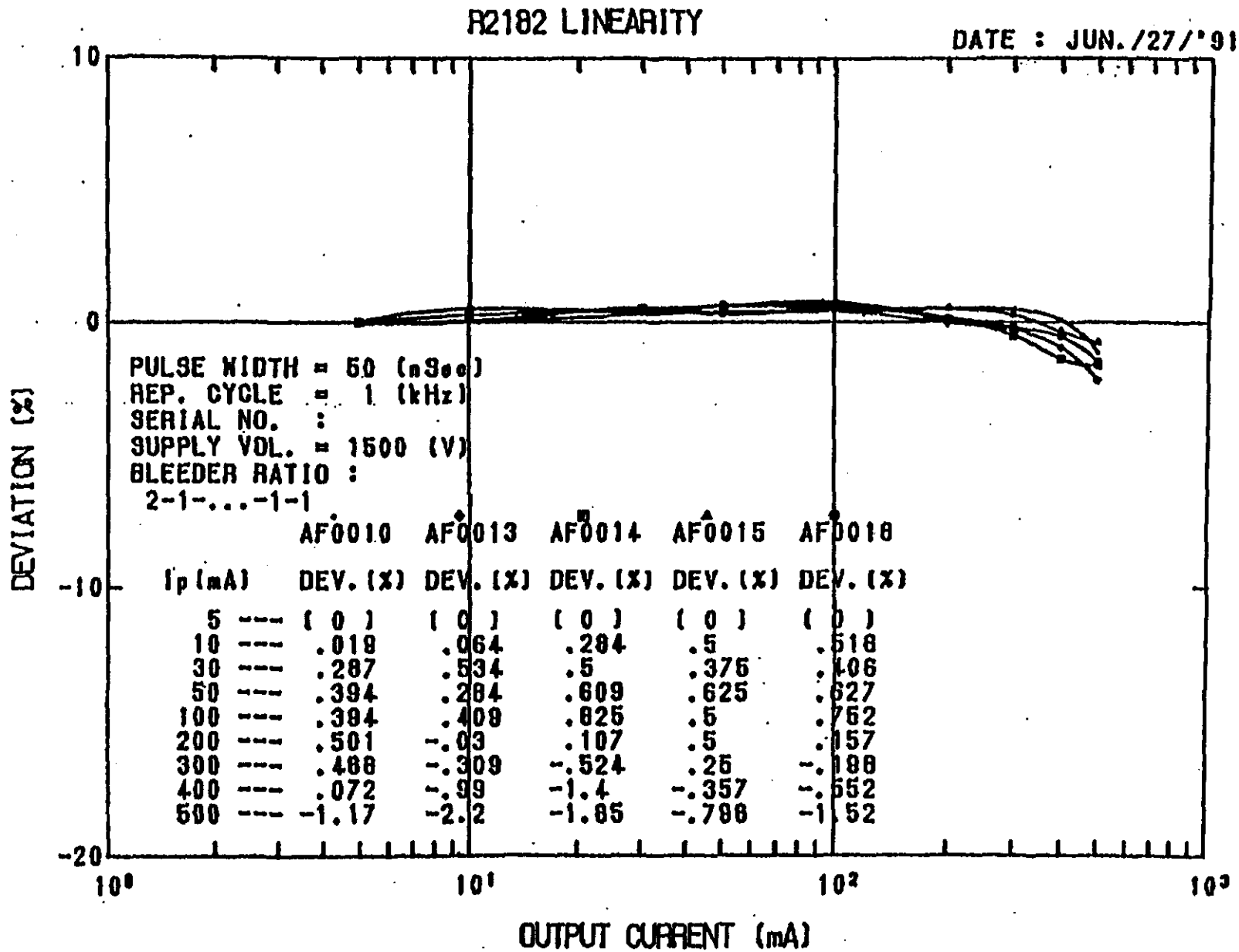
R2182 LINEARITY
DATE : JUN./27/'91
10
0
-10
-20
DEVIATION (%)
PULSE WIDTH = 50 (nSec)
REP. CYCLE = 1 (kHz)
SERIAL NO. :
SUPPLY VOL. = 1500 (V)
BLEEDER RATIO :
2-1-...-1-1
AF0010 AF0013 AF0014 AF0015 AF0016
Ip (mA) DEV. (%) DEV. (%) DEV. (%) DEV. (%) DEV. (%)
5 --- (0) (0) (0) (0) (0)
10 --- .019 .064 .284 .5 .518
30 --- .287 .534 .5 .376 .406
50 --- .394 .284 .609 .625 .627
100 --- .394 .409 .625 .5 .752
200 --- .501 -.03 .107 .5 .157
300 --- .488 -.309 -.524 .25 -.188
400 --- .072 -.99 -1.4 -.357 -.552
500 --- -1.17 -2.2 -1.85 -.788 -1.52
10^0
10^1
10^2
10^3
OUTPUT CURRENT (mA)

Fig. 12

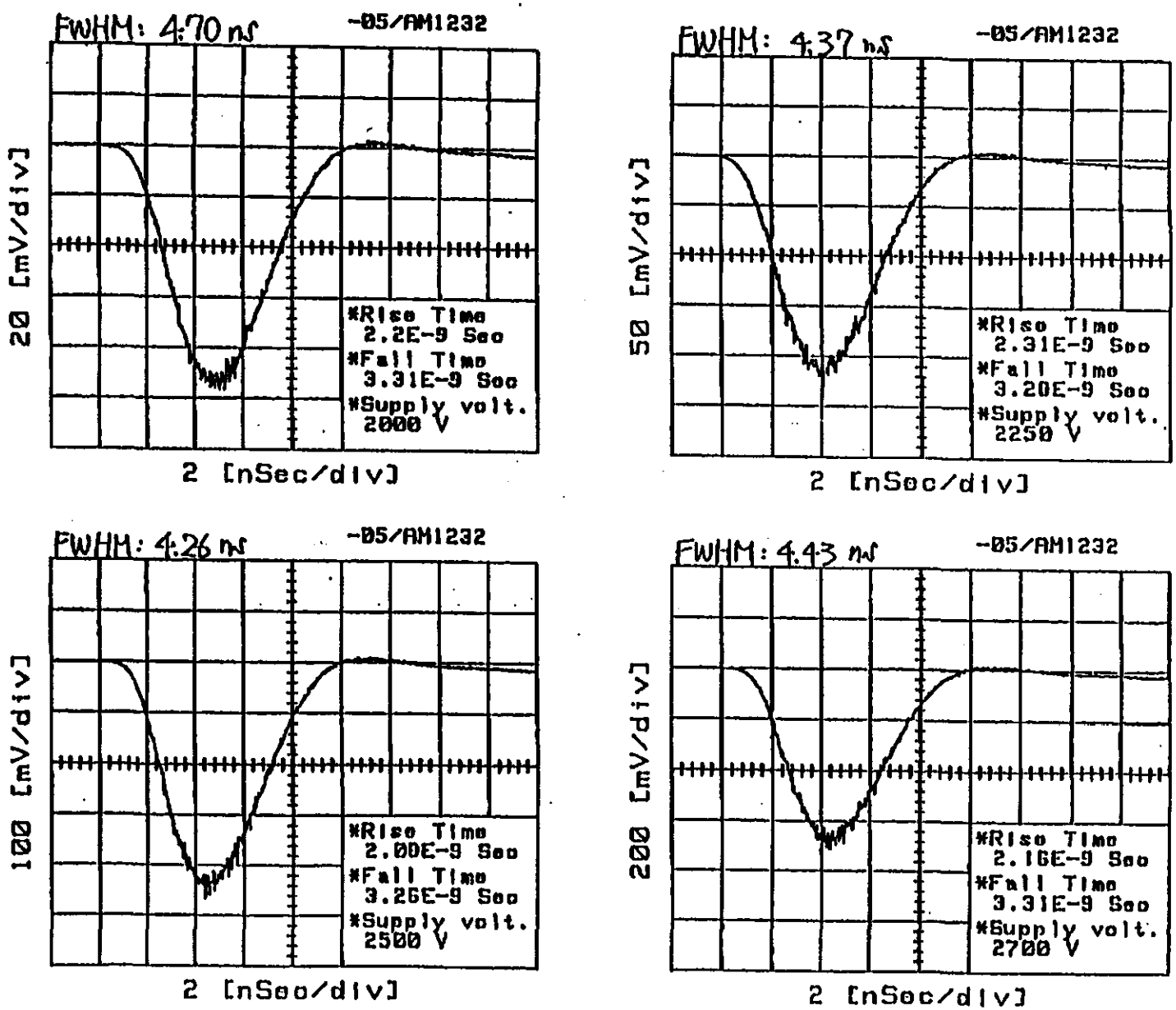

R2490-05
Time Response

Fig. 13

Answers to questions addressed by

Min Chen

IV. Liq. Scin.:

Question 1. Compensation with fast shaping?

Answer :

The time dependence of the neutron signal in a U/Sci calorimeter [1] is shown in Figure 1. Similar time development should be assumed for a Lead/Sci calorimeter. The mean energy of the neutrons in the Pb/Sci hadron calorimeter is about 1-2 MeV, the typical mean free path in the presence of a hydrogenous detector required to lose half of its energy is about 10 cm. Thus the neutron "collection" time constant is about 10 ns. Because of the fast response of the liquid scintillator calorimeter the instantaneous component of the hadronic shower and the neutron component can be resolved in time. By varying the integration or pulse shaping time the neutron component contribution to the total response signal can be reduced. On the other hand by varying the ratio of absorber to detector thickness [2], one can compensate for the loss of the neutron signal. In other words, for a 5 mm thick scintillation detector with appropriate choice of lead absorber thickness (say 5:1 instead of 4:1 for absorber:detector thickness ratio) one can achieve overcompensation, i.e. h/e>1. Since overcompensation results from the time collection of the neutron component it can be cut away by shortening the integration time (effective gate width of ADC).

We are going to test this idea in our LS single plane beam tests at ITEP in December 1991. Previously part of our group has tested U/TMS and Pb/TMS hadron calorimeters in ITEP (results shown in Figure 2 and 3) and have performed Monte Carlo simulations (based on HETC code) on the possibility of fast compensation with TMS detectors. Figure 4 shows the time development of the neutron component of a hadronic shower as calculated by Monte Carlo for two detector thicknesses in a U/TMS test calorimeter. In Figure 5 h/e ratios for two shaping times 2 microseconds and 10 nanoseconds are shown as a function of TMS detector thickness (Monte Carlo result). The solid point stands for the experimental measurement of h/e with a 2 microsecond integration time.

References :

[1] H.Bruckmann et al., Hadron sampling calorimetry, DESY 86-155 and ref. therein; H.Bruckmann et al.,"On the theoretical understanding and calculation of sampling calorimeters", DESY 87-064

[2] R.Wigmans, On the Energy Resolution of Uranium and Other Hadron Calorimeters, CERN/EP 86-141

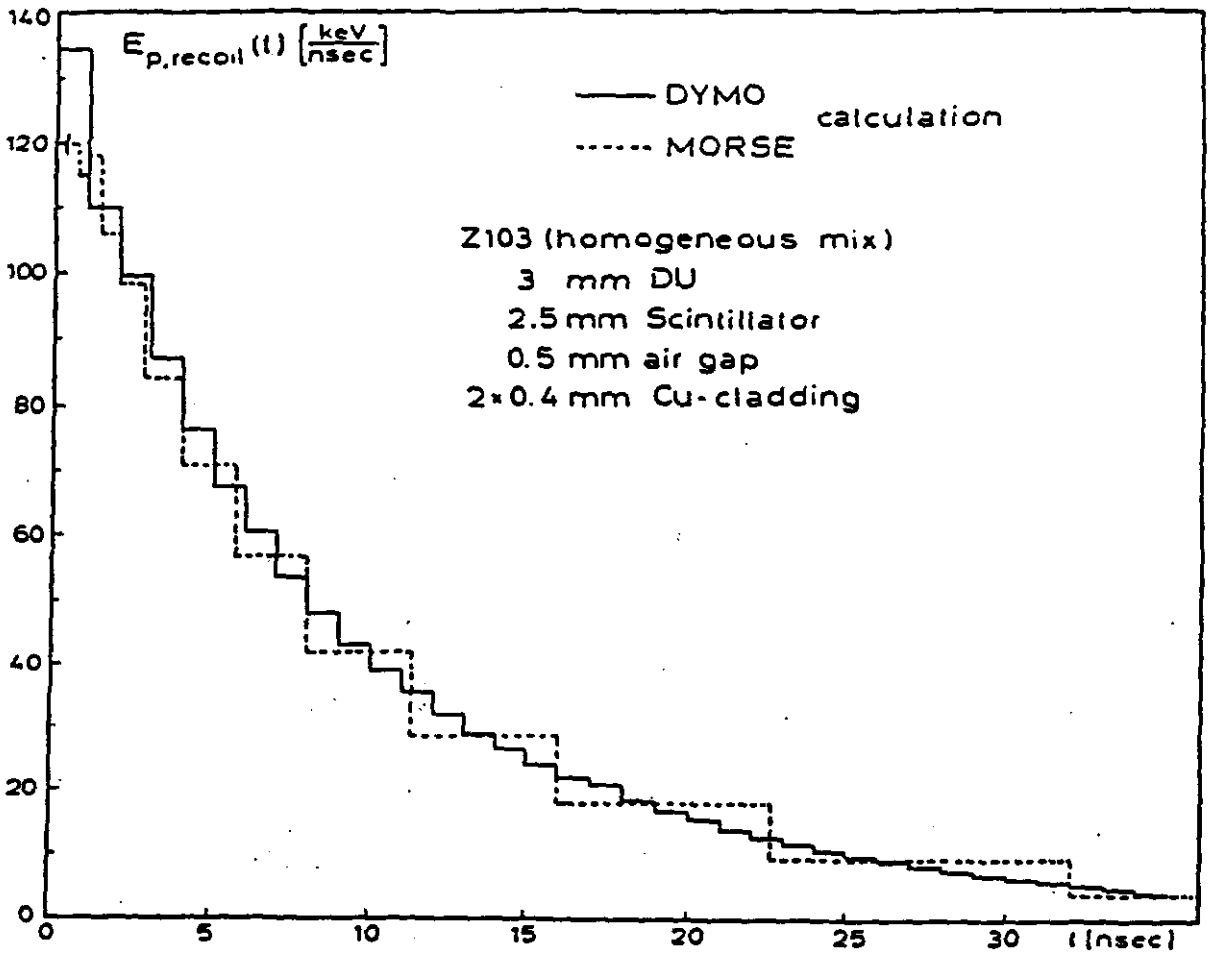

A time-dependent MORSE calculation is compared to the evaluation of dynamics with DYMO. The calorimeter contains a homogeneous mix of materials and one neutron is started at t=0 with a spectrum, normalized to one, according to Fig. 1B.

Fig. 1

U (15 mm) / TMS (7.5 mm) Calorimeter

Shaping 2.2 μs

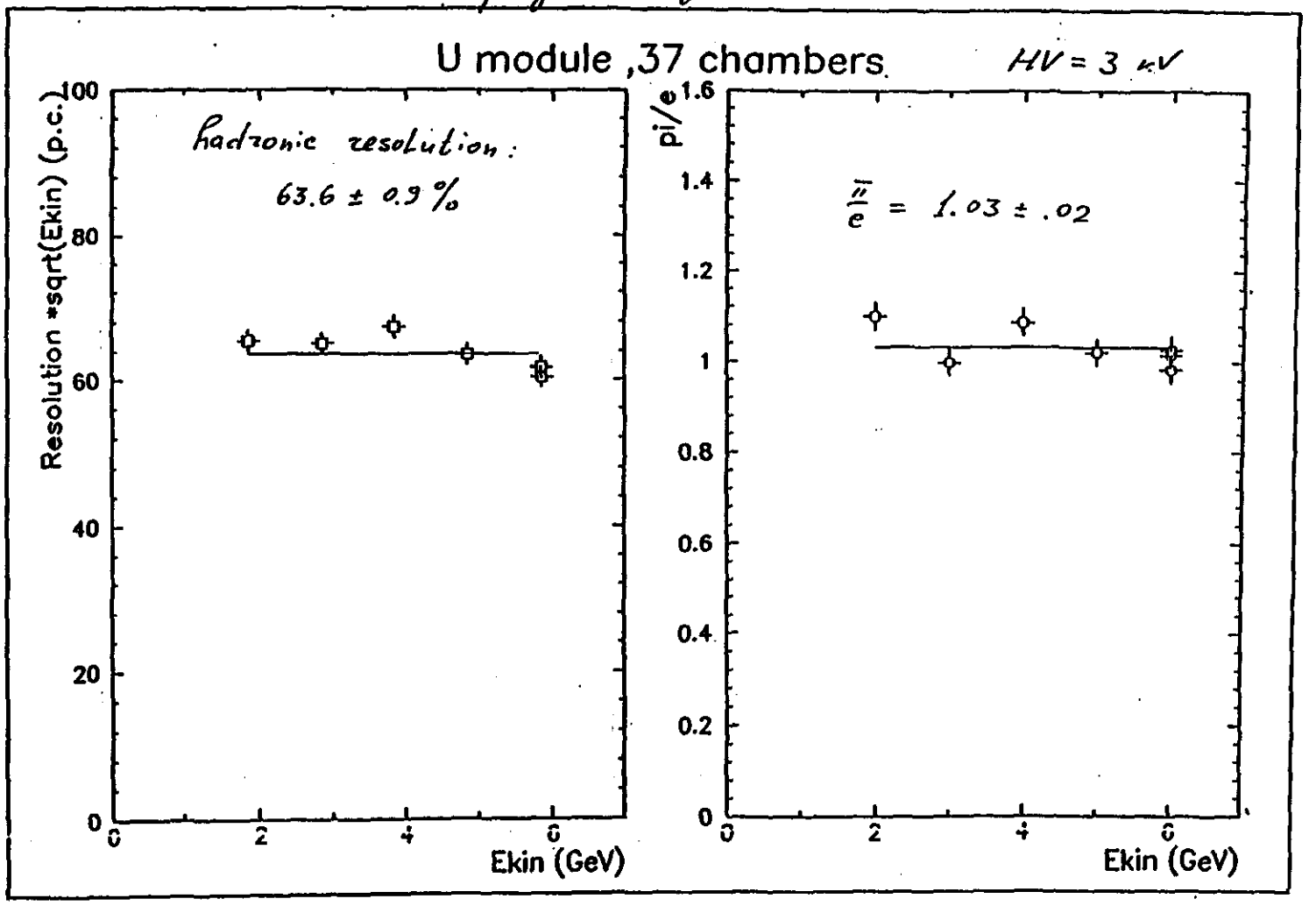

Fig. 2

PB (18 mm) / TMS (7.5 mm) Calorimeter
shaping 2.2 μs

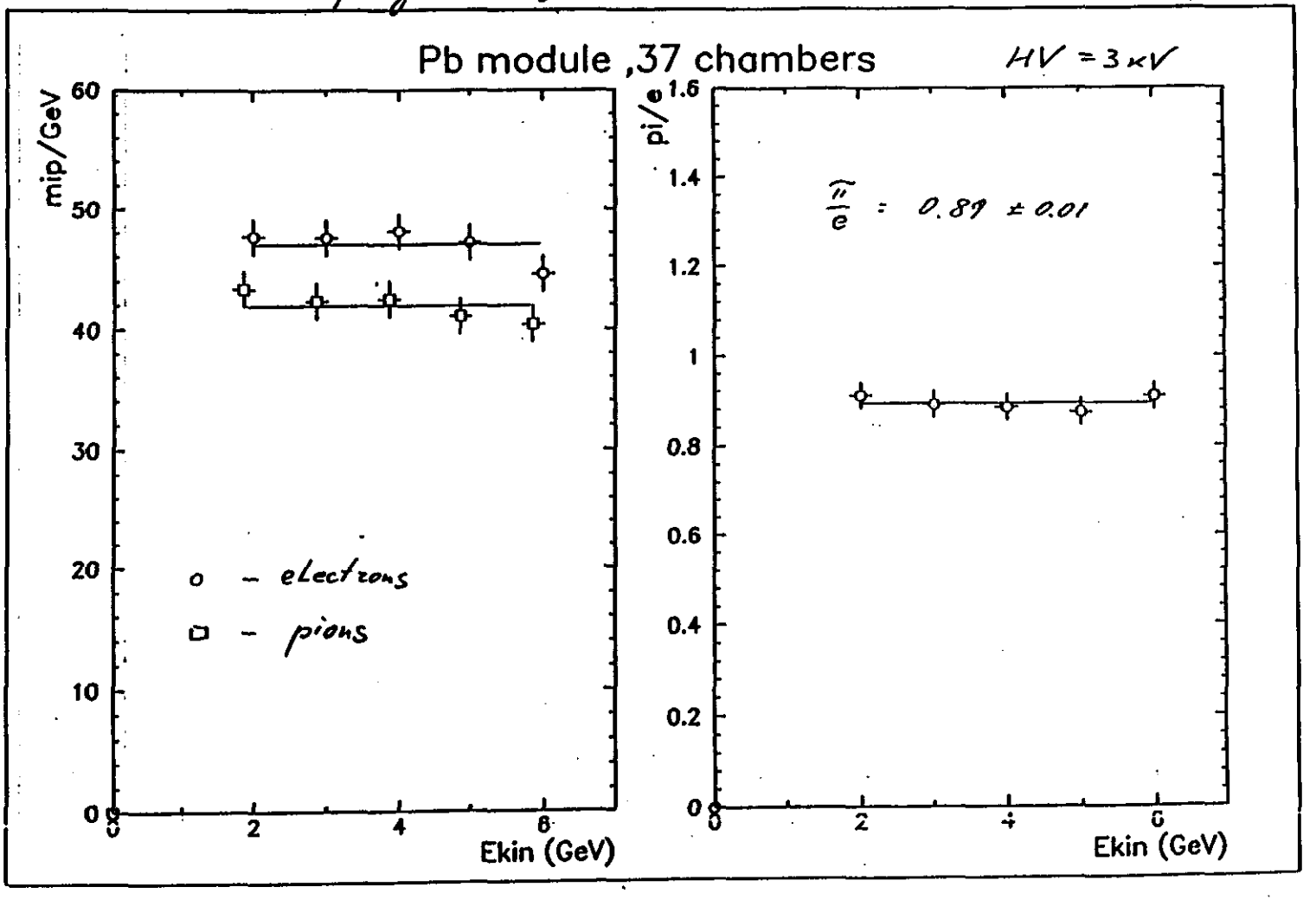

Fig. 3

Neutron response in U - TMS calorimet
(5 mm U absorber)

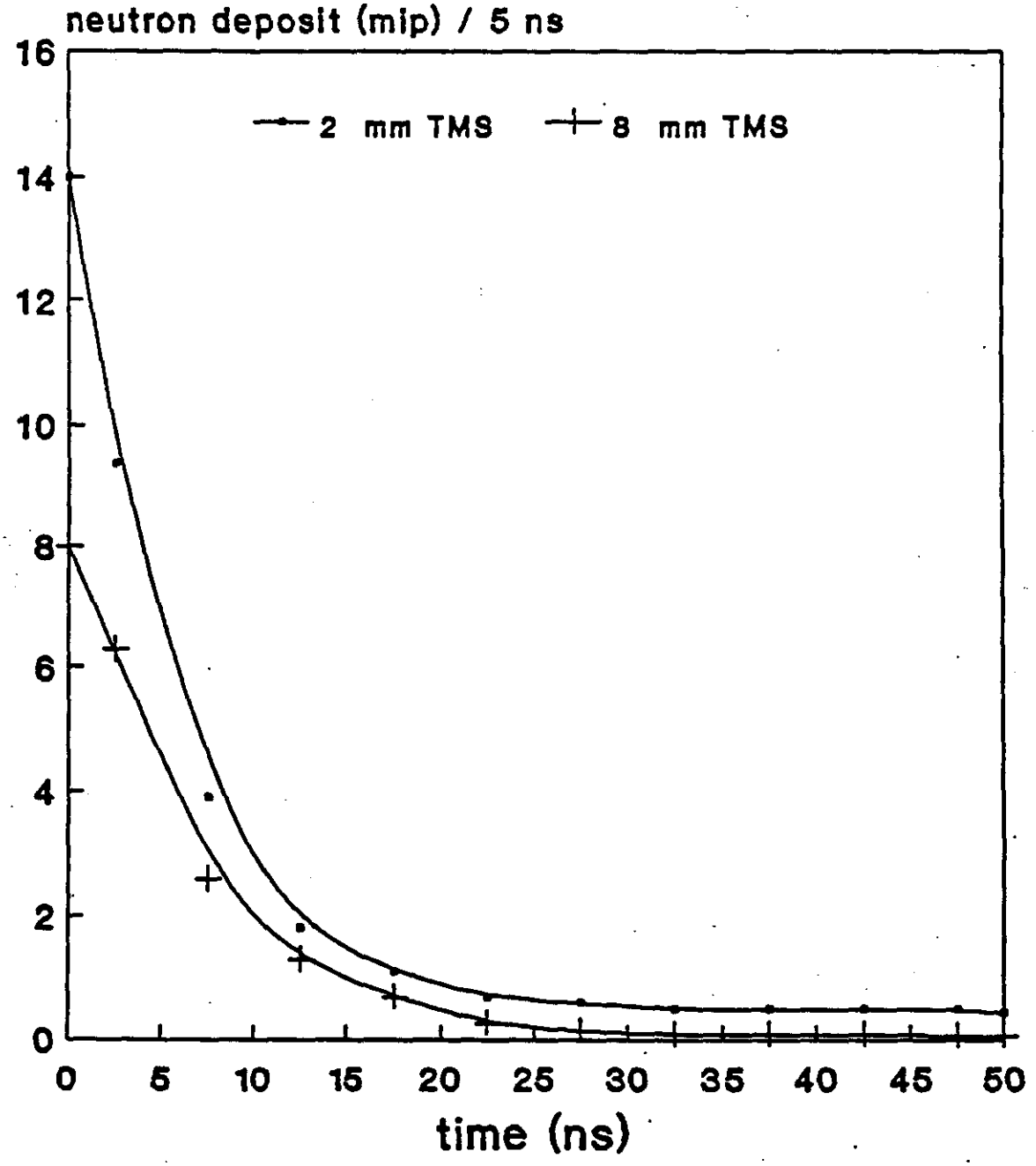

Monte Carlo

Fig. 4

h/e vs detector thickness in U(5mm) - TMS calorimeter

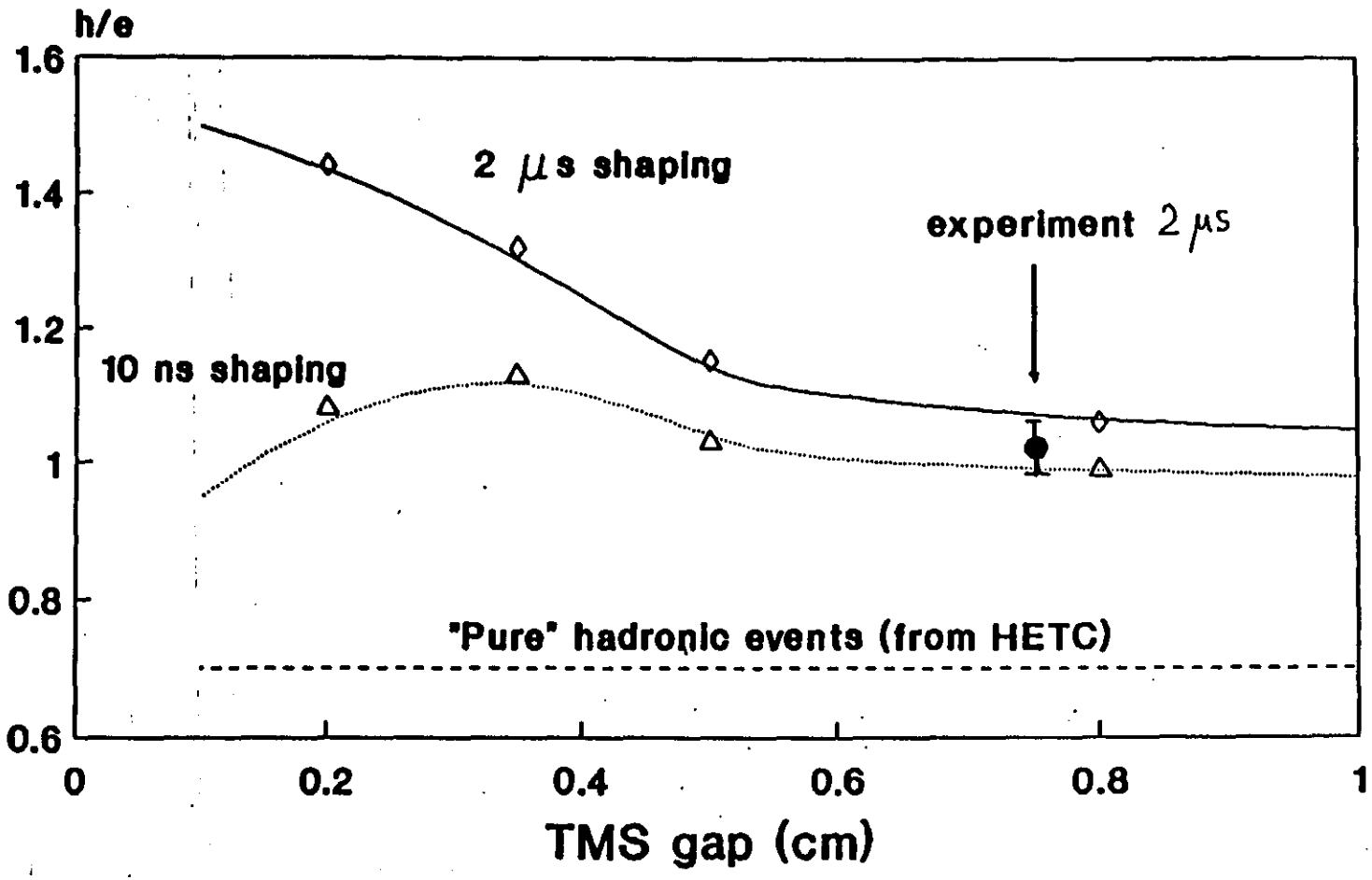

Monte-Carlo

Fig. 5

Question 2. How many m to be sealed?
Probability of leak/module/day * no. of modules.

Answer :

Liquid leaks are not desirable for proper liquid scintillator operation. Liquid scintillator saturated with oxygen reduces the light output by 20-30% as compared with one saturated with inert gas. Liquid leaks are also potentially dangerous because of liquid scintillator flammability (Flash point for BC-517P is 115 degree C).

In the LS hadron calorimeter design there are 256 sealed modules. There are several possibilities to seal these modules. The possibility which we are considering is to seal by welding.
Two tapered module sides which provide accesss to the inner assembly of the modules (Figure 6) are closed by a 1 mm membrane which is welded to the rim of the module along the full perimeter as shown in Figure 7 and then reinforced additionaly by a thick cover plate.

There are several options proposed for the sealing of light cables (fibers). In one of these options the PMT has a covar ring welded to its glass cylindrical body (Figure 8). This ring is welded with a bellow to the flange which, in its turn is welded to the top wall of the module body. Adjustment of fiber groups against the segmented photocathode is made from inside the module during module assembly. In an other option (Figure 9) the bundles of fibers coming to a single photocathode through two plates with precision holes are cast in epoxi (or other appropriate sealing material) which fills the space between the two plates. The exit surface of fibers is cut and polished after the setting of the cast. In this variation the PMT is dismountable and has to be adjusted against the fiber plane.

A whole-welded option might be considered to be more nearly leak proof. However it is likely that from cost and servicability constraints the regular (but reliable in vacuum systems) o-ring or soft metal sealing will be prefered.

Each module will also have several connections to the liquid filling system. These connections will be made with regular o-ring seal. Our present experience with a few hundred connections on the liquid scintillator test cells o-ring seal shows that once the connection is properly designed it is 100% leak proof.

Modular LS hadron calorimeter design also allows multiple checks of each module on the way between production, beam tests, transportation and final assembly. If a leak is detected, the module can be replaced before final assembly.

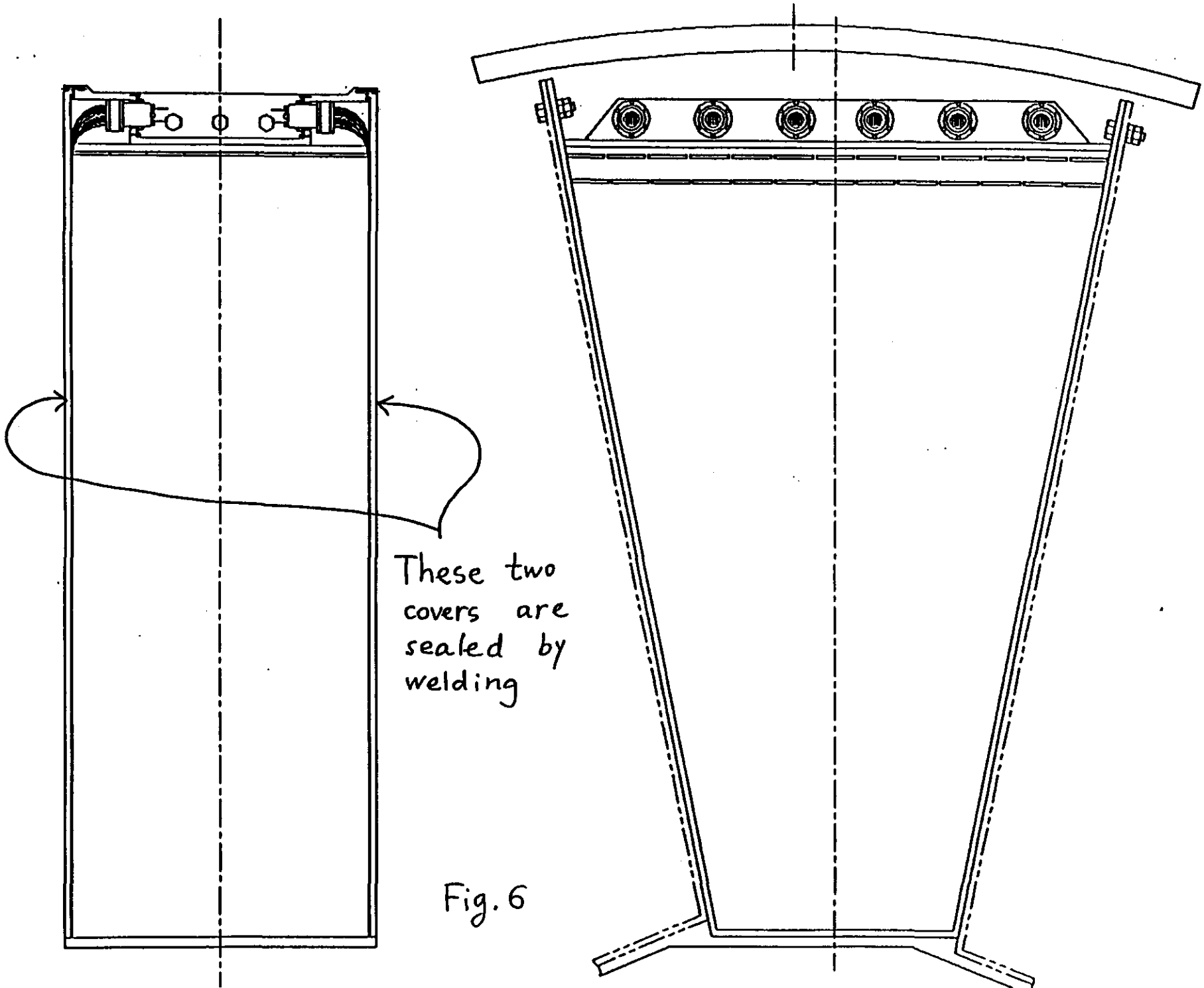

Fig. 6

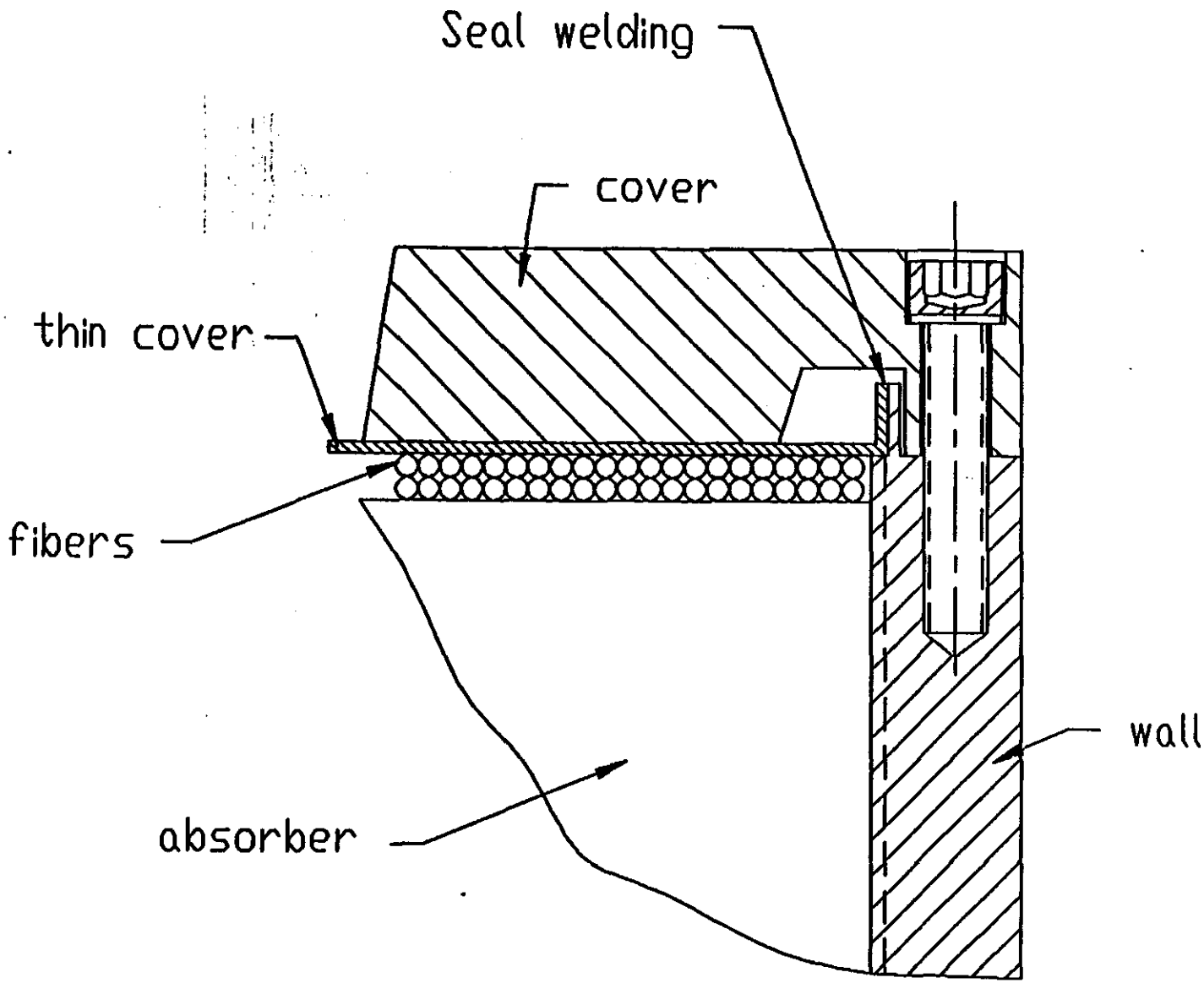

Fig.7 Sealing of the cover

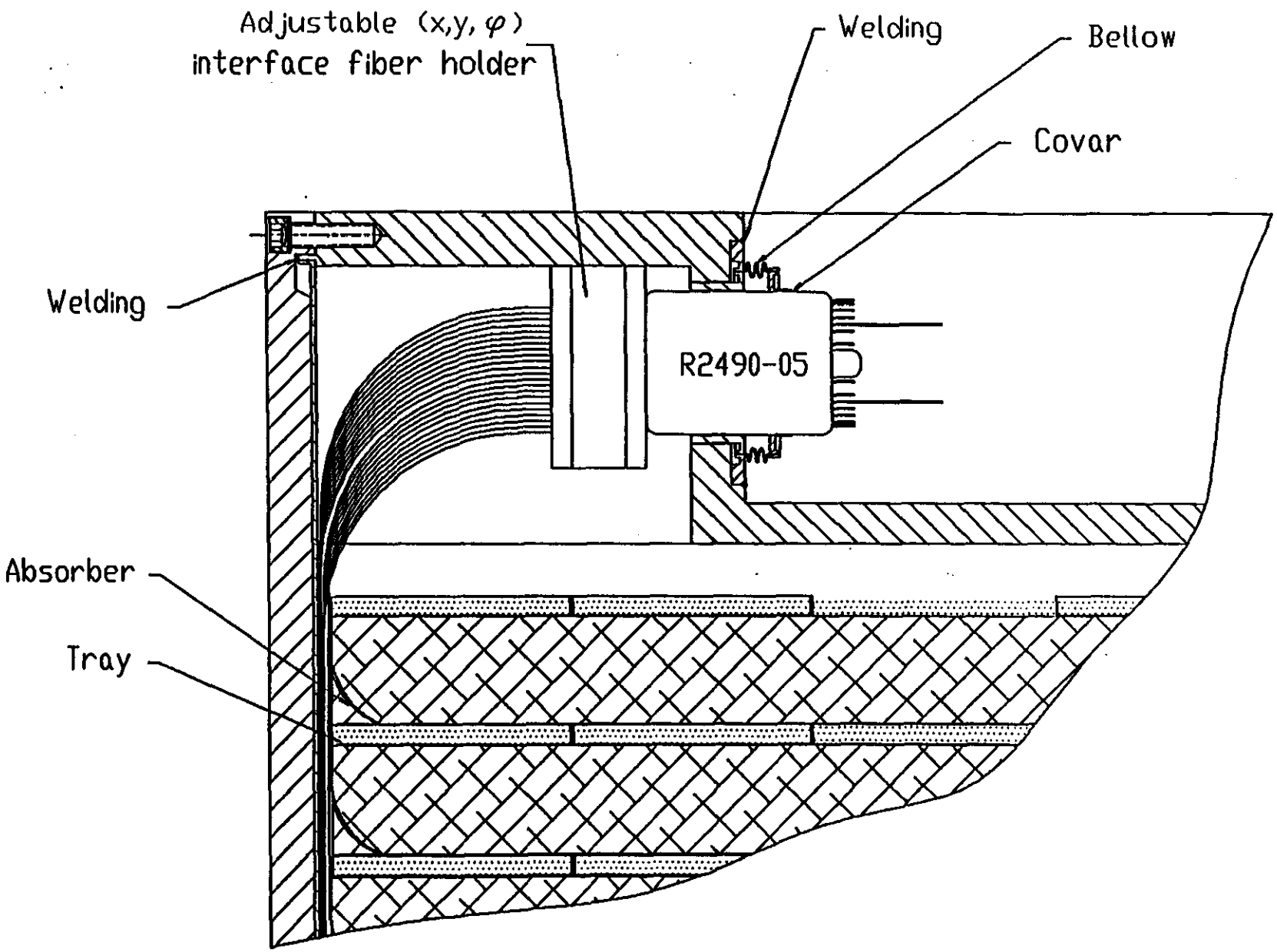

Fig. 8: Variation of fiber seal for LS HC module (sealed PMT, welded to module body)

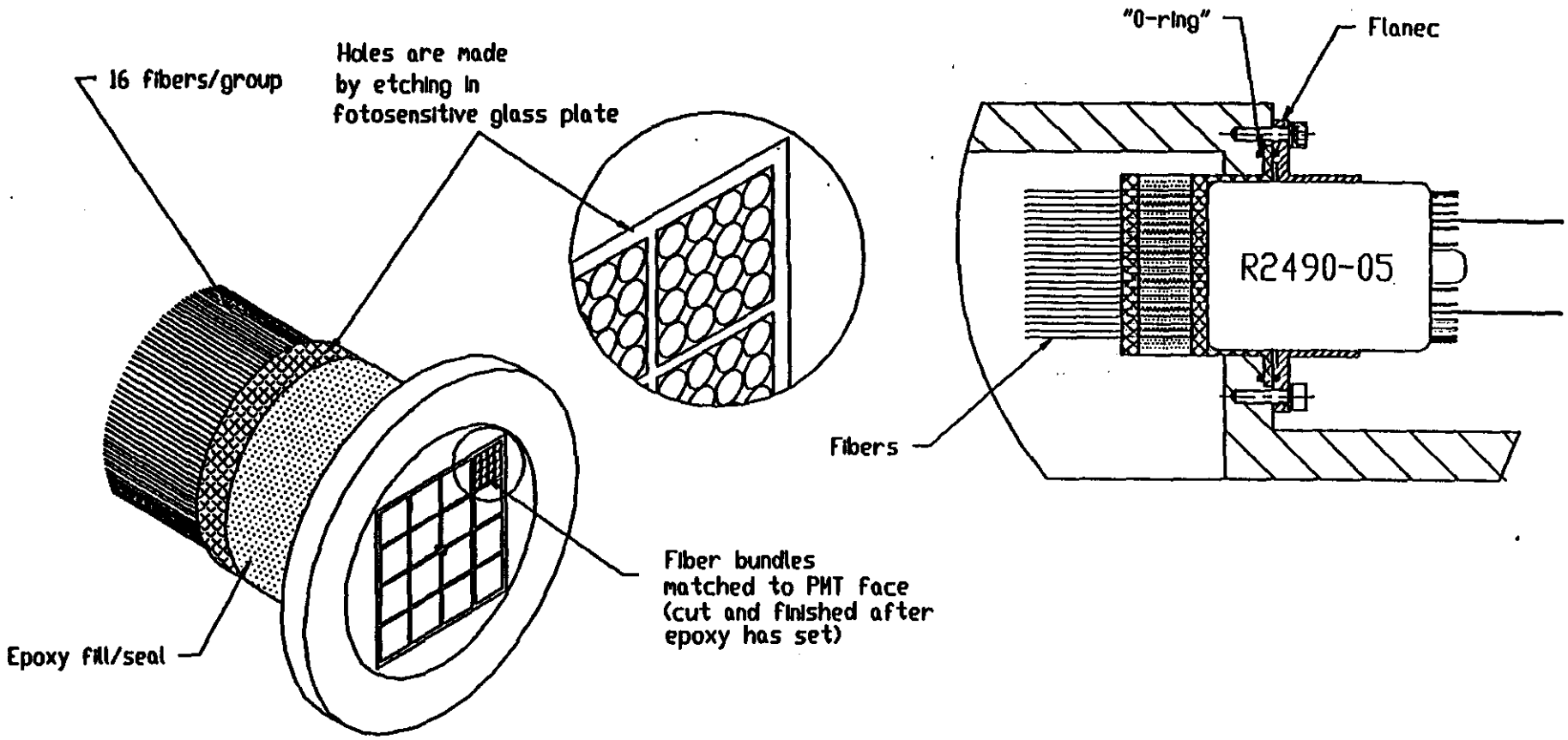

Variation of Fiber Seal
for Liquid Scintillator HC module

Fig. 9

Question 3. Not-safe: poisonous, flammable as well as container and fibre-eating.

Answer :

Material safety data sheet for BC-517P liquid scintillator together with list of LS physical properties are shown in Figures 10 and 11. Flash point for BC-517P is 115 degree C which doesn't constitute a significant hazard. From the flammability point of view it is far less dangerous than regular gasoline (flash point -43 degree C).

The containers for the liquid scintillator calorimeter modules are made of stainless steel which doesn't interact chemically with the liquid.

As we have concluded from our liquid scintillator - plastic fiber chemical compatibility tests, the first signs of fiber-eating for the chosen LS-fiber combination might appear after 70-450 years of operation. More details of chemical compatibility studies can be found in [1].

Referencies :

[1] Liquid Scintillator Calorimetery (Second Year), A R$D Proposal submitted to SSCL,September 1991 (in preparation)

BICRON

ICRON CORPORATION 12345 Kinsman Road, Newbury, Ohio 44065
(216) 564-2251 Telex 980474

MATERIAL SAFETY DATA SHEET

Product Name: BC-517P

General I.D.: Liquid Scintillator

Hazard Class: None

Hazardous Components:

Ingredient	Per Cent	TLV
Pseudocumene	<10%	TWA 25 PPM
U.S.P. Mineral Oil (or N.F.)	>90%	N/A
Pigments	0.2%	N/A

Physical Data:

Initial Boiling Point: Above 275°C at 760mm Hg

Vapor Pressure: <1 mm Hg @ 20°C

Vapor Density: approximately 4, Air=1

Specific Gravity: 0.86 @ 20°C

Per Cent Vocatile: less than 10%

Evaporation Rate: very slow >70 (Ether=1)

Fire and Explosion Data:

Flash Point: 240°F

Lower Explosive Limit: 1%

Extinguishing Media: Foam, Carbon Dioxide, or Dry Chemical

Fig. 10

BC-517P
Mineral Oil Based Liquid Scintillator

BICRON®

European Office
Marktstraat 27A, P.O. Box 271
2410 AG Bodegraven, The Netherlands
Telephone: 1726-14243
Telefax: 1726-14316
Telex: 39772 BICIN NL

Nippon Bicron
Room No. 805 1-B, 1-Chome
Shinyokohama, Kohoku-Ku
Yokohama 222 Japan
Telephone: 045(474)5786
Telex: 045(474)5787

The liquid is compatible with acrylic and PVC plastics, both of which are quite useful for constructing large, low cost tanks. Bicron has supplied many thousands of gallons of this product (packaged in 55 gallon tank wagons) to the physics community.

The principal features of BC-517P are:

Exceptional light transmission

Chemical inertness

Physical Properties:

Light Output:	28% anthracene
Mean Free Path (400-500 nm):	>6 meters
Decay Time (approx.):	2.2 nsec
Wavelength of Maximum Emission:	425nm
Refractive Index:	1.47
Specific Gravity:	0.85
Flash Point (T.O.F.):	115°C (240°F)
No. of C Atoms per cm^3:	3.65×10^{22}
No. of H Atoms per cm^3:	7.50×10^{22}
No. of Electrons per cm^3:	29.4×10^{22}
Coefficient of Thermal Expansion:	0.00075/°C
Vapor Pressure, 20°C:	0.16 mm Hg
Viscosity, 20°C:	21.1 centistokes

Fig. 11

January, 1991

Since there are many similarities between liquid scintillator and scintillating tile techniques we assume that following questions are equally addressed to liquid scintillator

V. Scint. plates:

Question 1. Dead space?

Answer :

Figures 12-14 explains the constructional walls and gaps for fibers transport. Note that there is no projected dead space.

Question 2. Wavelength shifter: Cerenkov background?

Answer :

Cerenkov light may be induced

a) in the liquid scintillator proper - useful signal;
b) in wavelength shifting fibers inside the cell - useful signal;
c) in clear transport fibers along the modules walls - this effect is small because clear fibers run non-projectively and because attenuation length of polystyrene core dramatically decreases in the UV region. If the prototype tests prove this effect to be significant, it can be removed by optical filtering on the PMT.

Question 3. Photo-tube: ustable.

Answer :

Most probable candidate for LS calorimeter light readout is proximity focusing mesh dynode multianode phototube Hamamatsu type R2490-05. Modern Mesh PMT are intrincically more stable than previous generations of PMT. To control the stability of the readout chain which includes scintillator cell, fibers, PMT, electronics, cables and ADC we forsee the monitoring/calibration system which consists of radioactive source in every calorimeter cell. In addition to that we are going to use an optical fiber light source on every photomultiplier, with light supplied by a green laser through a fiber distribution system. This will allow independent tests of photocathode and electronics.

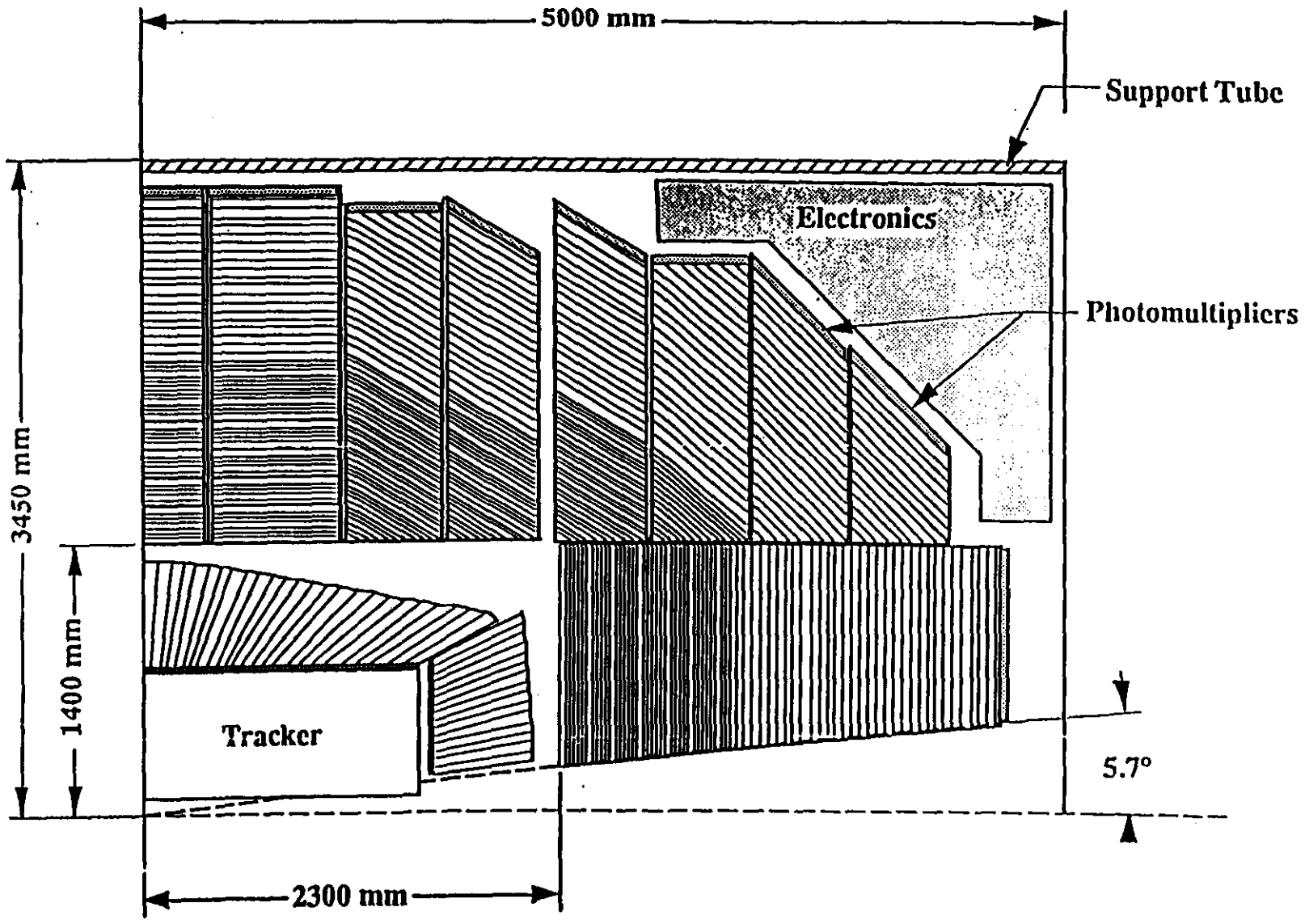

Fig. 12 **Liquid Scintillator Hadron Calorimeter**
Barium Fluoride EM Calorimeter

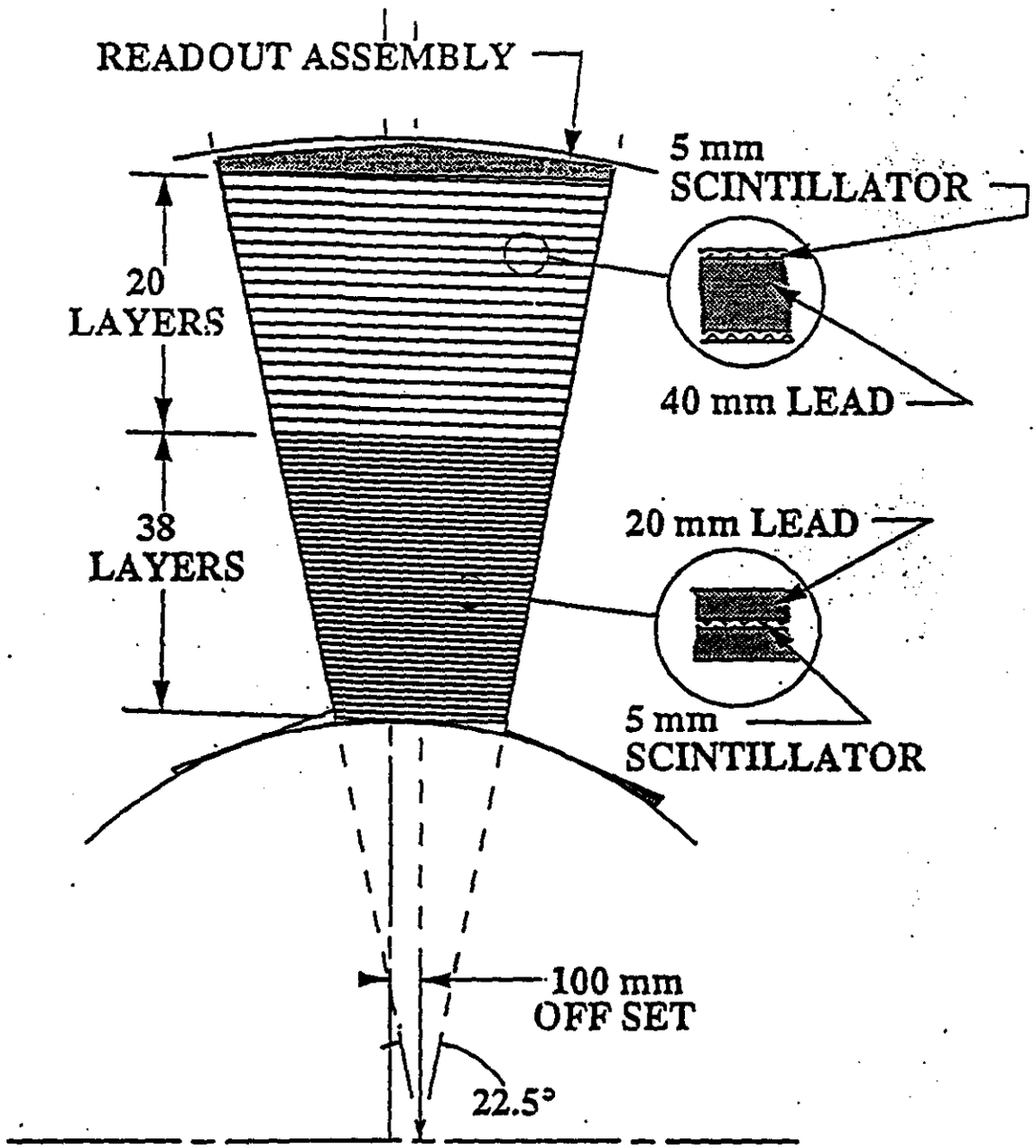

HADRON CALORIMETER
TOWER ASSEMBLY

Fig. 13

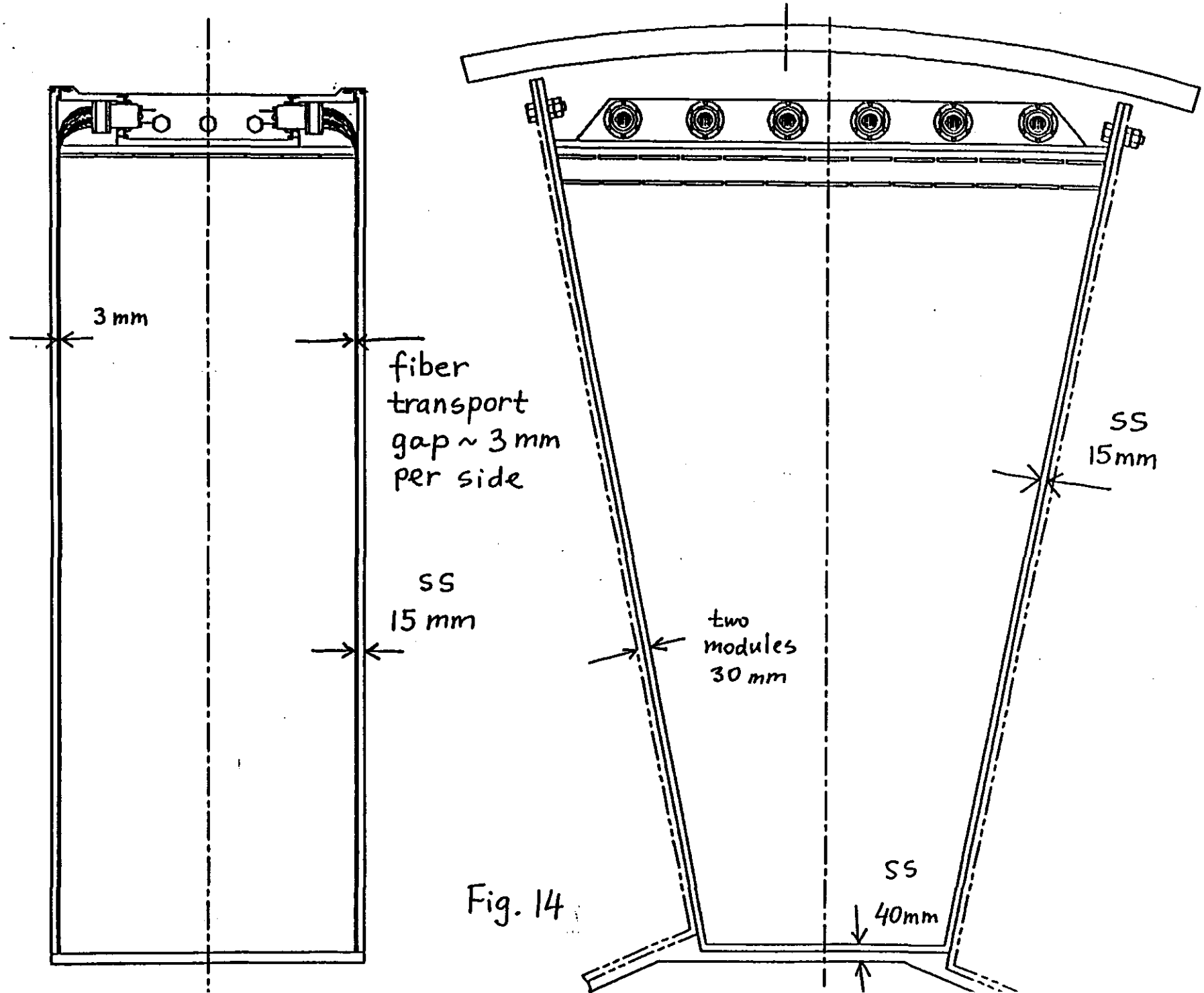
3 mm
fiber
transport
gap ~ 3 mm
per side
SS
15 mm
two
modules
30 mm
SS
15mm
SS
40mm

Fig. 14

Answers to questions addressed by

Frank Paige

HADRON CALORIMETRY
(Option A : BaF2 EM and sampling Liquid Scintillator HC)

Question 1. Delta(E)/E = a/sqrt(E) + b

Answer : Hadronic resolution a=50% ; b=2%

Question 2. Delta(E) from pileup and noise

Answer : Liquid Scintillator detector is the fastest hadron calorimeter technique which minimizes effects of event overlap from neighboring beam crossings. To quantify this conclusion we have started Monte Carlo simulation of pileup effects in LS GEM detector as well as a study of signal development and processing electronics.

Noise sources which can be presently located are :

a)induced radioactivity in calorimeter absorber (effect is being studied by us);

b)radioactive calibration source in each detector cell (counting rate 0.1-1 KHz, approx. minimum ionizing particle amplitude). Noise associated with calibration sources is presently being studied by us.

c)thermal noise of PMT. Fluctuatins of base line due to PMT noise was estimated to be no more than 30 MeV in the whole calorimeter.

Question 3. Delta(eta), Delta(phi) vs. eta

Answer : Delta(eta)=Delta(phi)=0.04 for BaF2 and 0.06 for hadron calorimeter at eta=0. Inner radius of the HC barrel 1400 mm, end caps are 2300 mm away from intersection pont. Cell size in HC is constant 90x90 mm2 in the rapidity range 0-1.6; and 45x45 in the range 1.6-3.0. (Figures 1-4)

Question 4. [time determination]

Answer : Signal arrival time spread relative to intersection moment - approx. 5 ns. Signal integration time - approx. 20 ns

Question 5. [longitudinal segmentation]

Answer : Sampling HC : 38x(20mm Pb + 5 mm LS) + 20x(40mm Pb + 5 mm LS)
6 longitudinal readout segments in HC section (Figures 3,4)

Question 6. [cracks, dead material]

Answer : Structural supports and paths for fiber readout are shown in Figure 5. Note, that there are no projected dead regions or cracks (Figures 1,2)

(Option B : both EM and HC are sampling Liquid Scintillator)

Question 1. Delta(E)/E = a/sqrt(E) + b

Answer : Hadronic resolution : a=50.% ; b=1.0%
EM resolution : a=7.6% ; b=0.6%

Question 2. Delta(E) from pileup and noise

Answer : Same as above

Question 3. Delta(eta), Delta(phi) vs. eta

Answer : Delta(eta)=Delta(phi)=0.06 both for EM and for HC sections at eta=0. HC section vs eta - same as above
EM section vs eta - 47x47 mm2 constant front cell size in the rapidity range 0-1.6, 23.5x23.5 mm2 - in the rapidity range 1.6-3.0. Projective geometry. Figure 6.

Question 4. [time determination]

Answer : Same as above

Question 5. [longitudinal segmentation]

Answer : Sampling HC : 38x(20mm Pb + 5 mm LS) + 20x(40mm Pb + 5 mm LS)
6 longitudinal readout segments in HC section
Sampling EM : 70x(2mm Pb + 4.5 mm LS),
7 segments (fibers) x 10 layers with flexible grouping;
3 longitudinal readout segments in EM section

Question 6. [cracks, dead material]

Answer : Same as above in the HC section
EM-section : 0.5 mm SS structural wall between two active towers in projective geometry

Question 7. Shower centroid determination in EM

Answer: Projective geometry, front cell size 47x47 mm2,
Effective Molier radius approx. 4 cm, 3 longitudinal readout segments

Question 8. Shower pointing to vertex in EM

Answer: Projective geometry, front cell size 47x47 mm2,
Effective Molier radius approx. 4 cm, 3 longitudinal readout segments

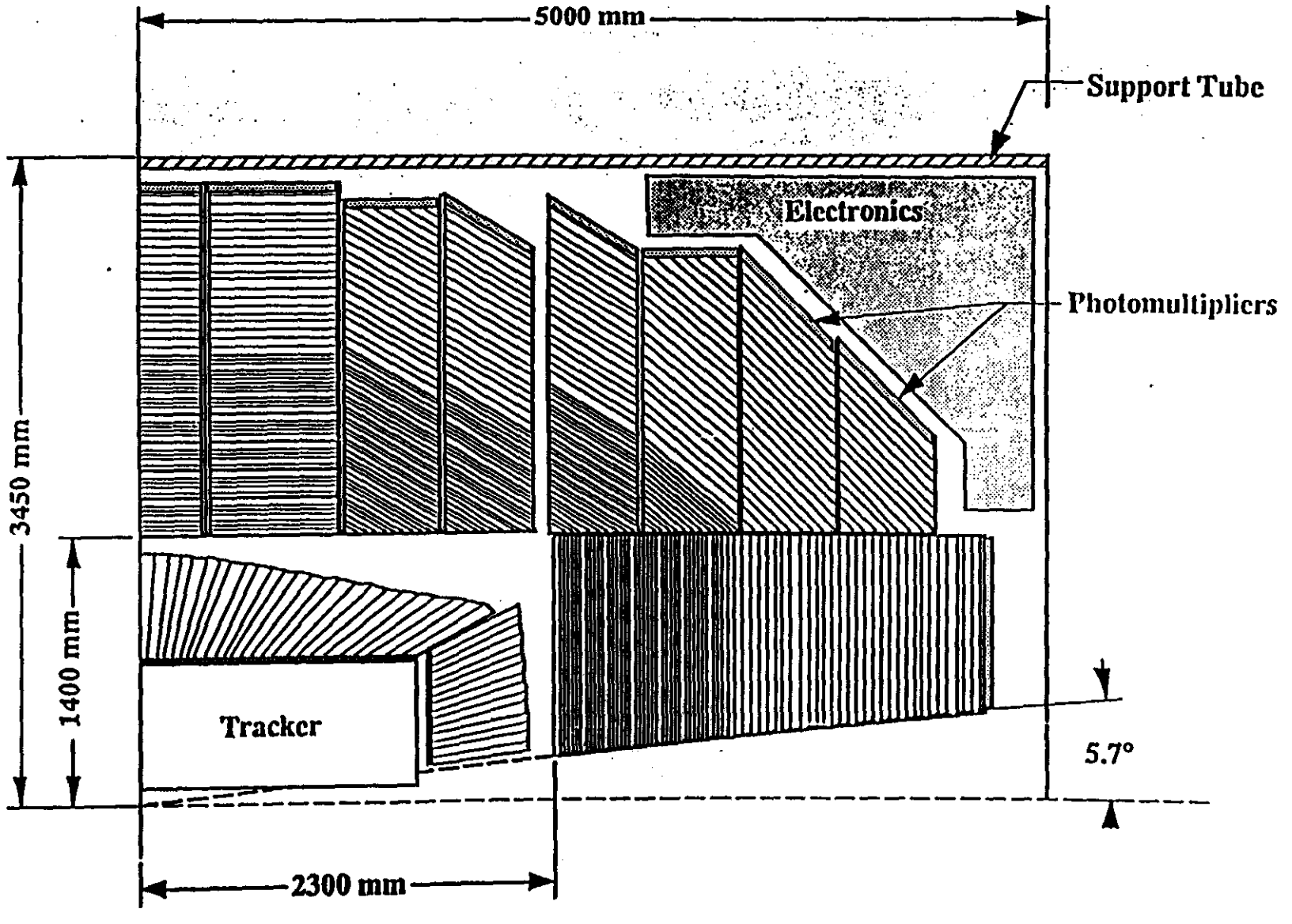

Figure 3.3-1 **Liquid Scintillator Hadron Calorimeter**
Barium Fluoride EM Calorimeter

fig. 1

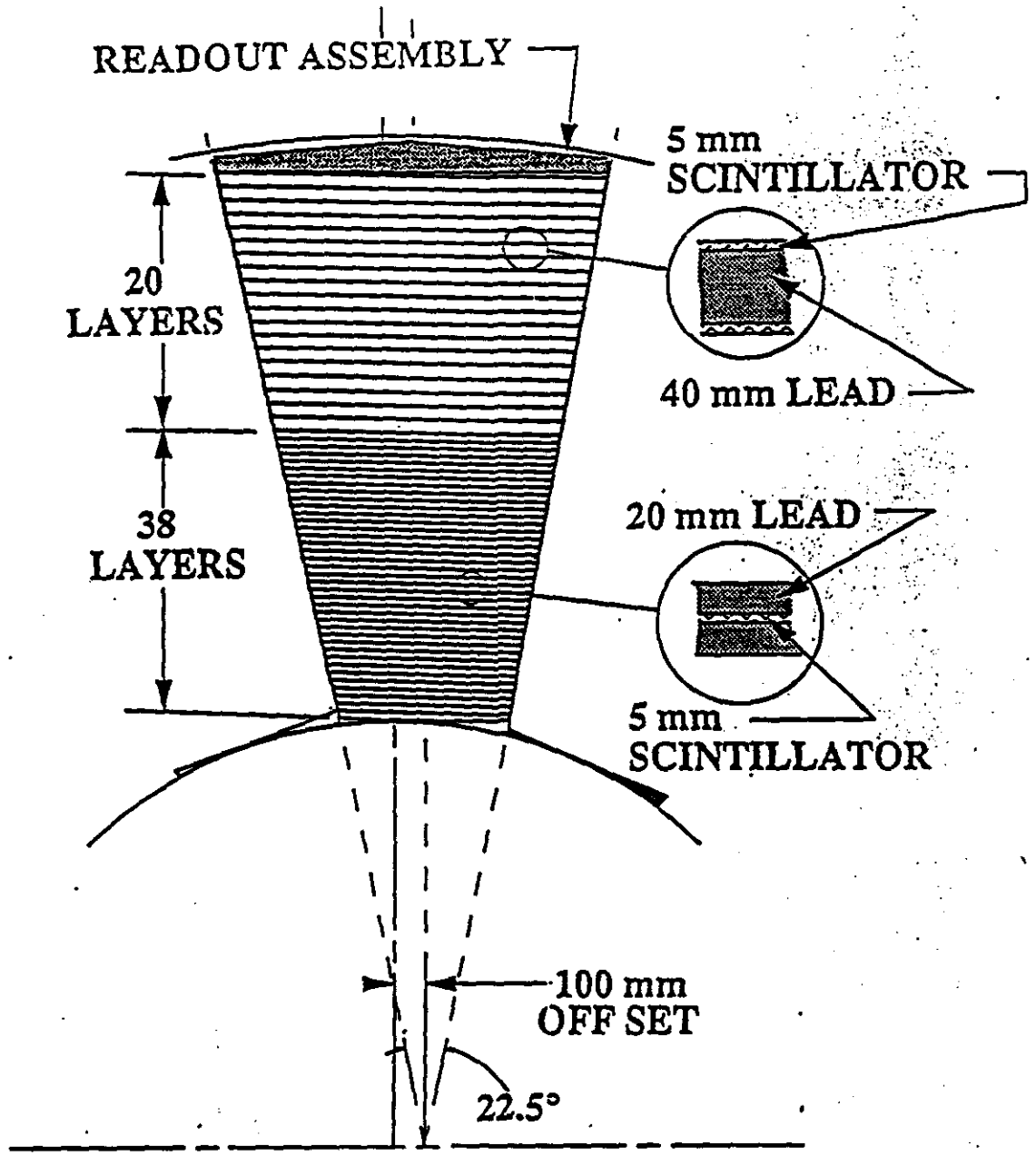

HADRON CALORIMETER
TOWER ASSEMBLY

fig. 2

Version 16-8 (192)

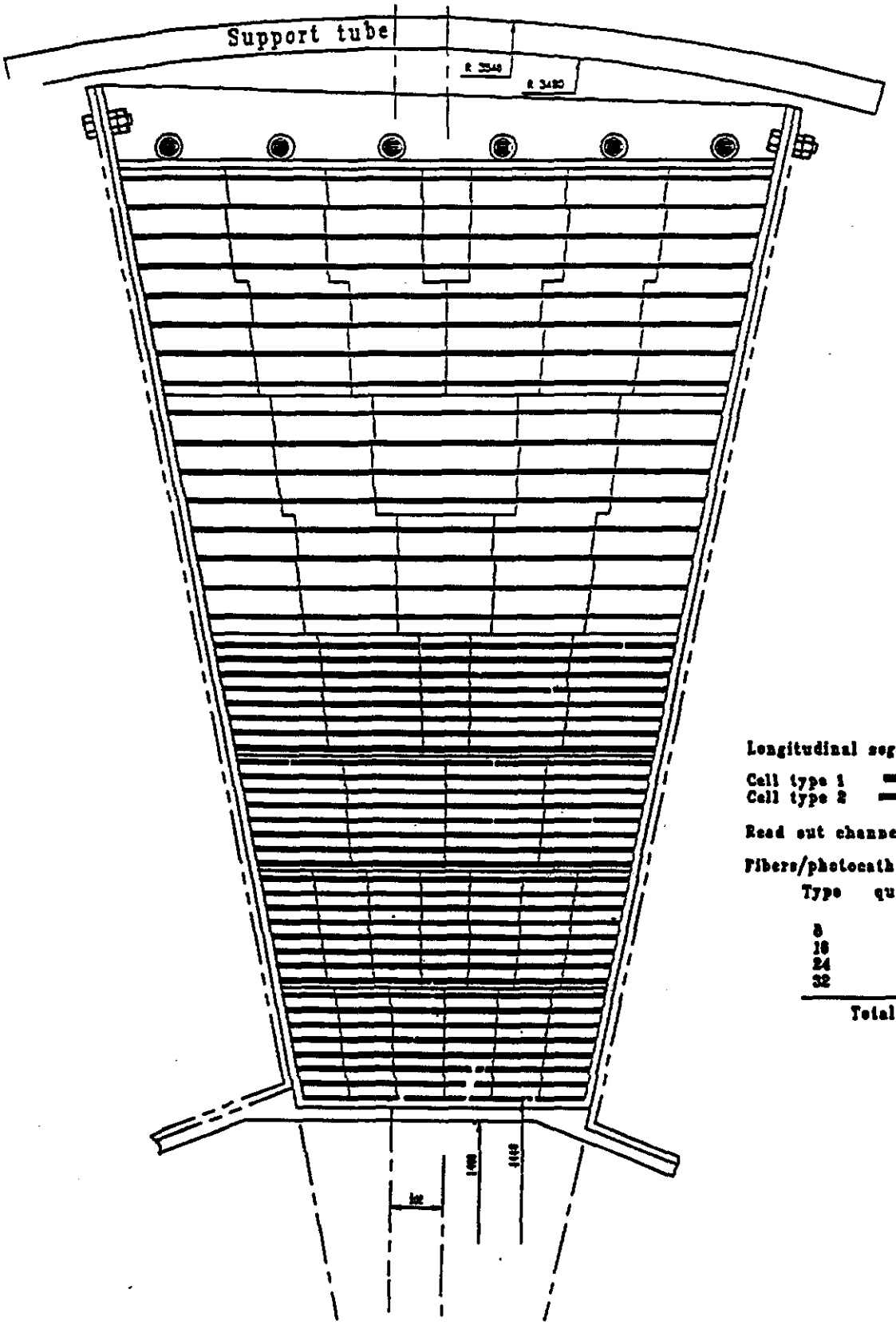

Longitudinal segments - 6

Cell type 1 ▬▬ 90.58 × 94.1 mm²
Cell type 2 ▬▬ 97.91 × 94.1 mm²

Read out channels 192

Fibers/photocathode

Type	quantity/module
8	105
16	9
24	4
32	72
Total	192

fig. 3

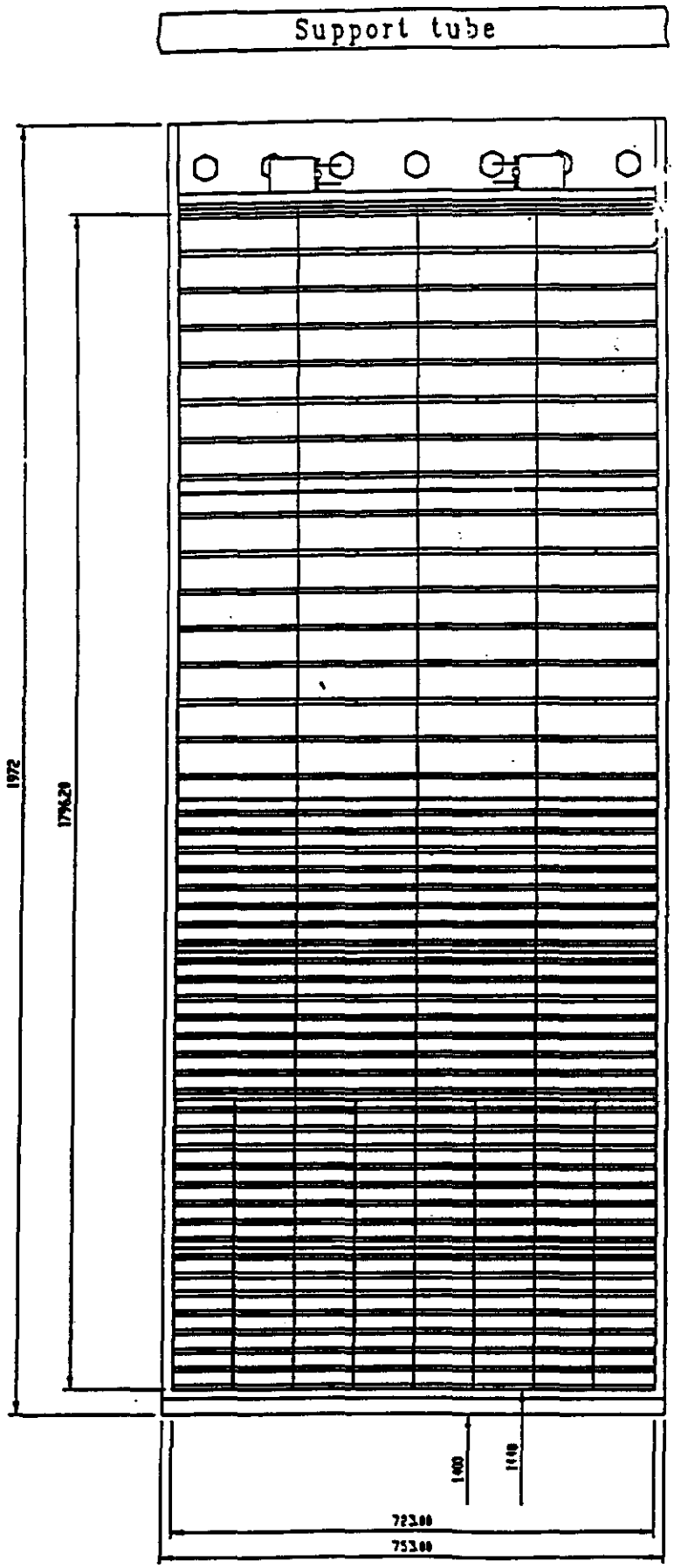

Read out channels 192

fig. 4

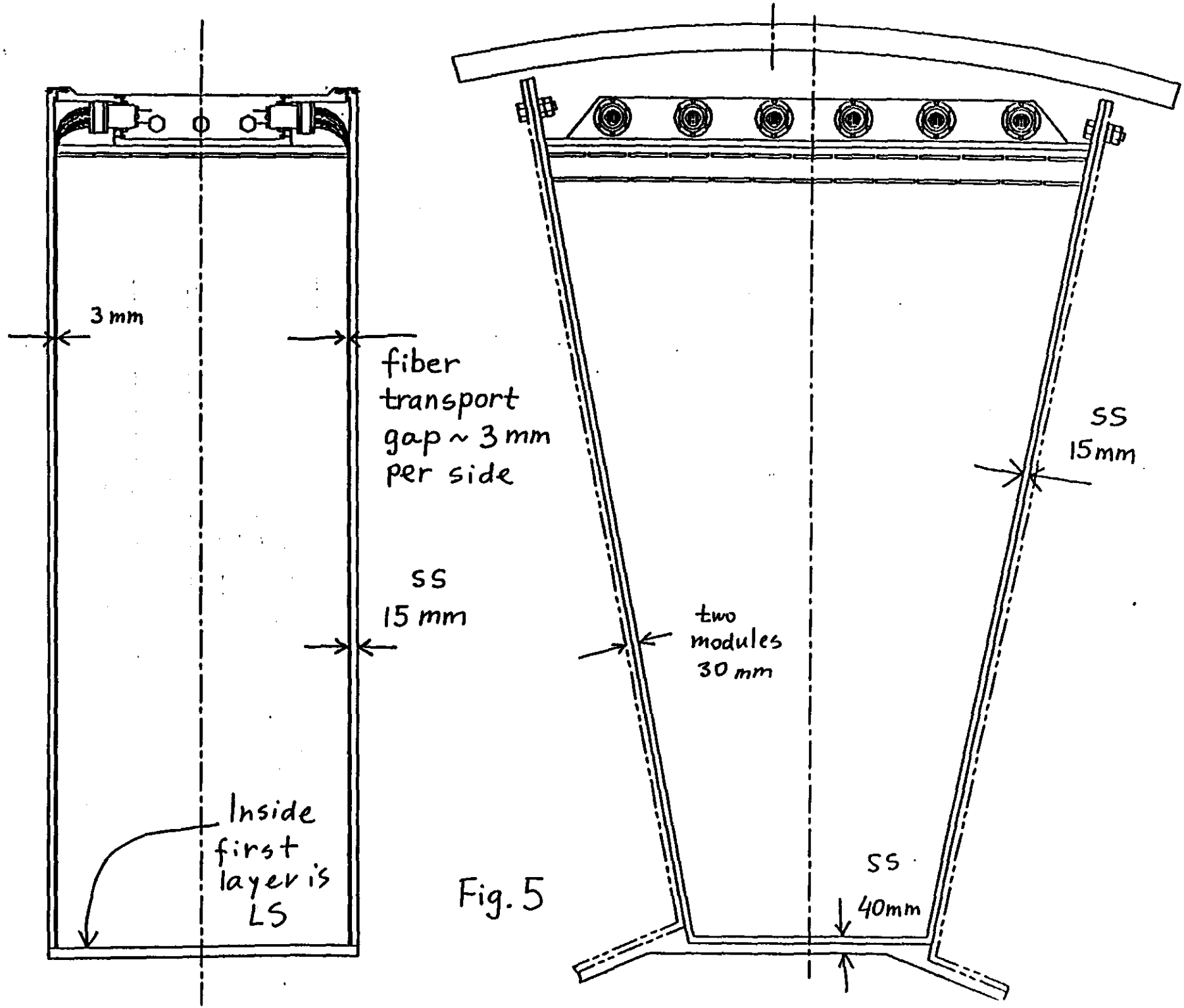
3 mm
fiber
transport
gap ~ 3 mm
per side
SS
15 mm
Inside
first
layer is
LS
SS
15mm
two
modules
30 mm
SS
40mm

Fig. 5

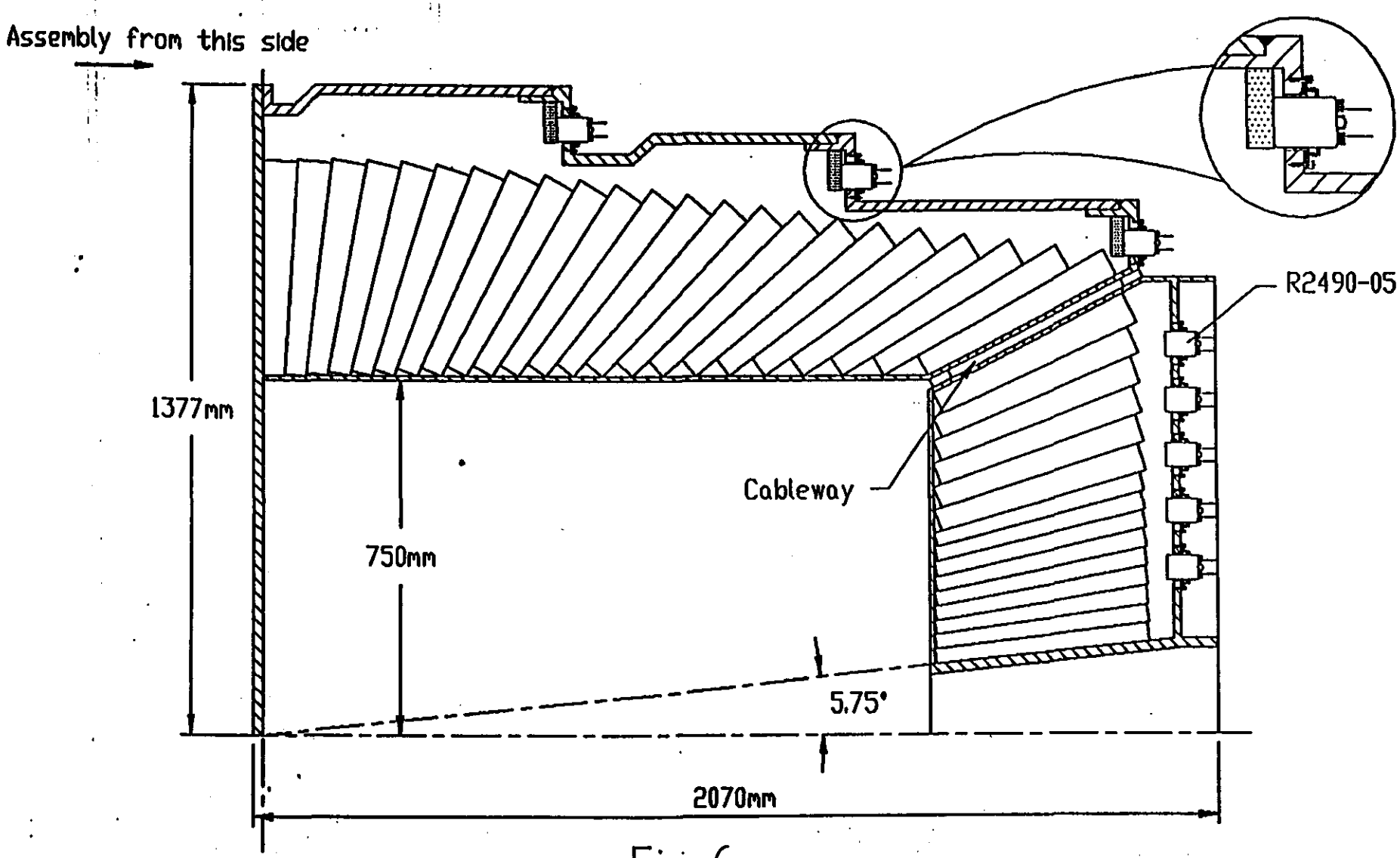

Fig. 6
Liquid Scintillator EM Calorimeter
Side View

Answers to questions addressed by

Bill Bugg

Question 1. Present a specific design for say a 25X0 EM cal followed by a 9 Lambda hadron cal with delta eta=delta phi=0.05 and starting at R= 75 cm.

Information provided should include :

1) Dimensions (radii) with details as to cell structure including walls, electronics, mechanical support structure.
2) Resolution,EM, Hadronic(for jets)
3) Electronics readout plan and layout
4) Compensation, speed, HV, magnetic field characteristics, cooling, radiation damage

Answer :

LS FINE SAMPLING EM AND HADRONIC CALORIMETER

Basic mechanical design of liquid scintillator hadron calorimeter was initially developed in L* SSC LoI [1]. Together with new idea of LS electromagnetic calorimeter this design is shown in Figures 1-13.
EM calorimeter has 25 X0 and is followed by 9.65 lambda hadronic section.

1)Dimentions

Hadronic part : Radii : 140 cm - 340 cm
Fine sampling : 38 x (20mm Pb + 5mm LS)
Coarse sampling : 20 x (40mm Pb + 5mm LS)
6 longitudinal readout section.
Cells 9x9, dead 0.3mm Fe around.
Delta(eta)=Delta(phi)=0.06
Total length - 9.65 lambda.
Electronics - outside the calorimeter body on the outer cylinder of barrel and behind endcaps.
50,000 readout channels
256 modules : 15 rings x 16 modules and 2 endcups x 8 modules.
Barrel supported on rails inside the supporting tube; endcaps - on rails inside the barrel.

EM part : Radii : 75cm - 135cm,
70 layers 2mmPb/4.5mmLS.
Calorimeter consists of 7 longitudinal segments each with individual light readout fiber flexibly combined in 3 longitudinal readout section. Cells 47x47 mm2, dead material 0.5mm SS between towers.
Projective geometry.
Total 25X0, 1.15 lambda
7,300 towers, 22,000 readout channels
Electronics - between HC and EM barrel and between HC and EM end caps.
Barrel supported on rails inside the HC barrel.

2)Resolution:

Hadronic : Delta(E)/E = 50%/sqrt(E) + 1.% (e/h=1)
EM: Delta(E)/E = 7.6%/sqrt(E) + 0.6% (EGS4 simulation)
Figure 14

3)Electonics:

Photodetector : mesh dynode proximity focusing PMT,operating gain ~10**4, 16 anodes with area about 30 mm2, capacitance <10 pF ,~ 1.5% int. linearity up to 500 mA/per anode. Amplifier/shaping : low gain, low input imp. current amplifier with 11 ns zero-pole cancellation two outputs with 1:1 and 1:100 attenuation to cover dynamic range of 10**5. Acquisition : free running time slice integrator or flash ADC (8ns), digital transmission via optical fibers (Figure 15).

4)Compensation: pi/e =1. with Pb/LS=4:1 sampling fraction in the fine sampling section of the hadronic calorimeter, proper weighting technics for EM calorimeter and coarse part of HC, fast compensation in 15-20 ns.
By reading out every 9-th layer in EM section separately one has the readout with 4:1 sampling ratio which together with 4:1 hadronic section gives e/h=1 on the trigger level. The rest is read out for purpose of EM calorimetry.

Speed : All components of LS system are fast :
LS - 2ns; ligth transport spread - 1 ns; WLS < 11 ns; phototube rise time 2 ns. Fast compensation in 15-20 ns.

HV : for PMT HAMAMATSU R2490-05 it is < 2500V. There are no electrical connections inside the modules. All PMTs circuts and electronics are on the external surfaces of the modules.

Magnetic field charact.: PMT is the only element sensitive to magnetic field. PMT candidate is HAMAMATSU R2490-05 designed to operate in fieds up to 1 Tesla (Figure 16,17).

Cooling : Heat dissipation of PMT voltage dividers is about 100 W/module, electronics 200 W/module. Total about 77 kW for hadronic and 35 kW for electromagnetic calorimeter.

Radiation : damage LS stays up to 5 Mrad and can be exchanged.
Fibers stay up to 10 Mrad with no performance degradation.
Radiation resistance of fibers beyond 10 Mrad is under study.

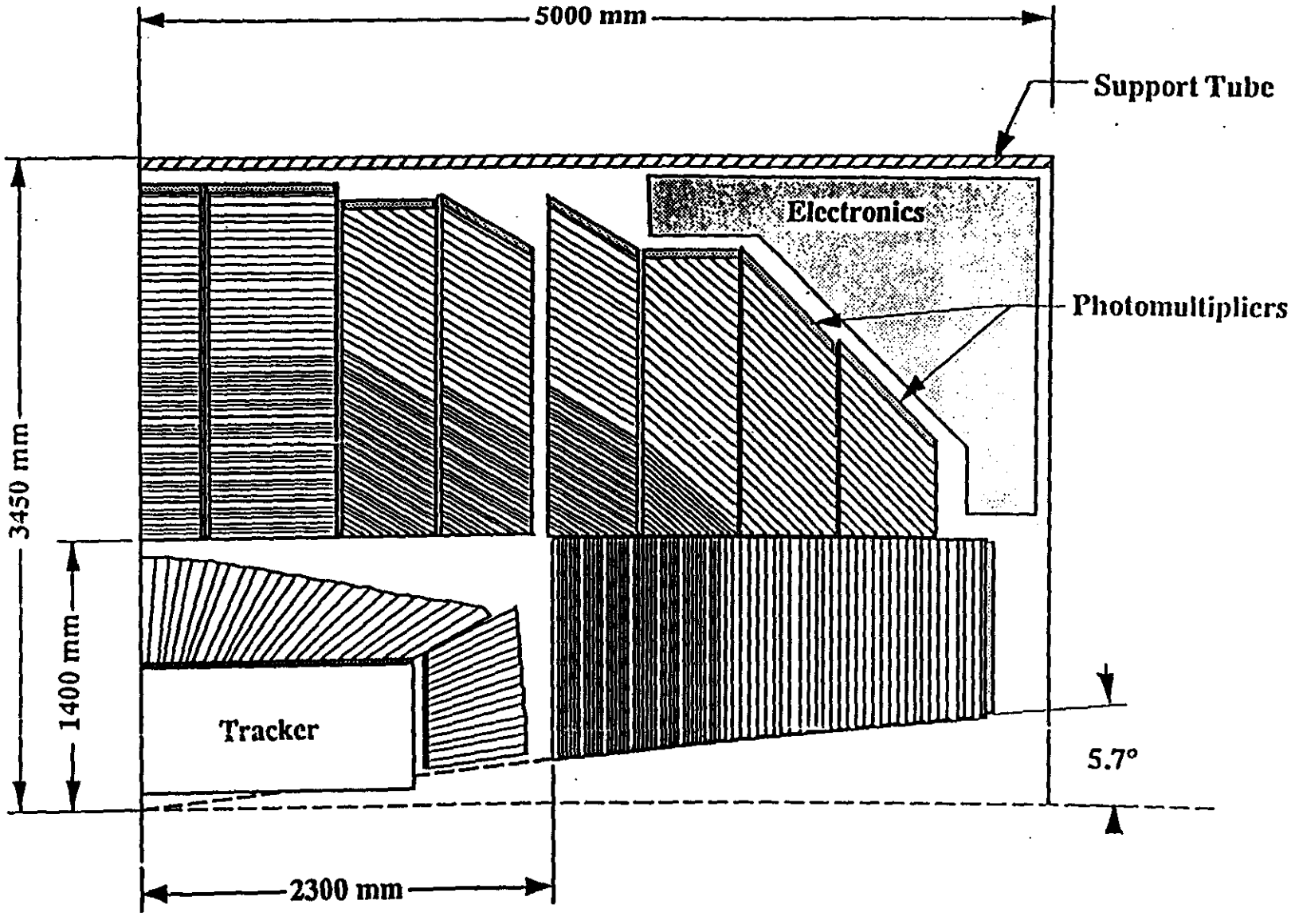

Liquid Scintillator Hadron Calorimeter
Barium Fluoride EM Calorimeter

Fig 1

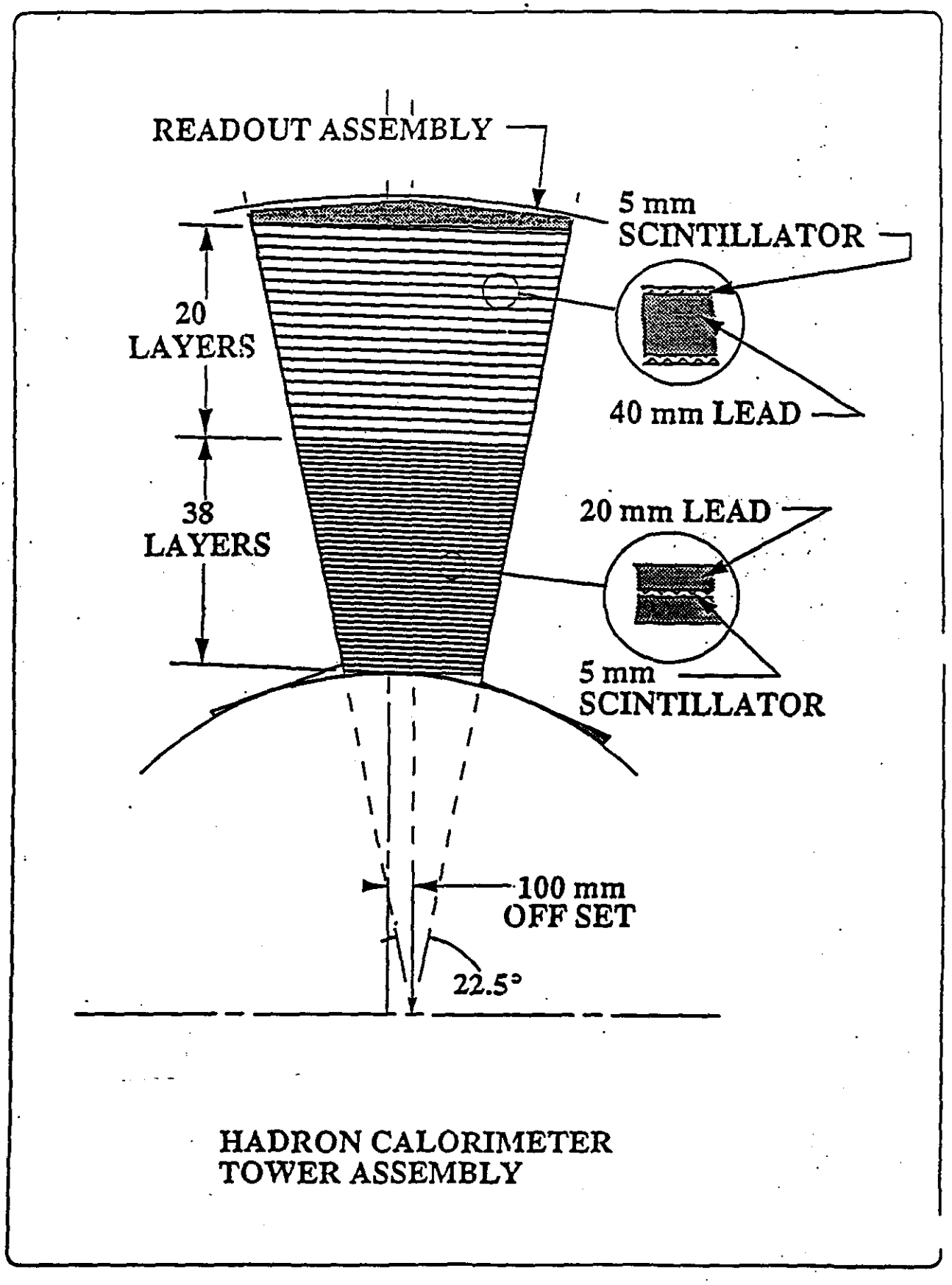
READOUT ASSEMBLY
5 mm
SCINTILLATOR
20
LAYERS
40 mm LEAD
38
LAYERS
20 mm LEAD
5 mm
SCINTILLATOR
100 mm
OFF SET
22.5°
HADRON CALORIMETER
TOWER ASSEMBLY

Fig. 2

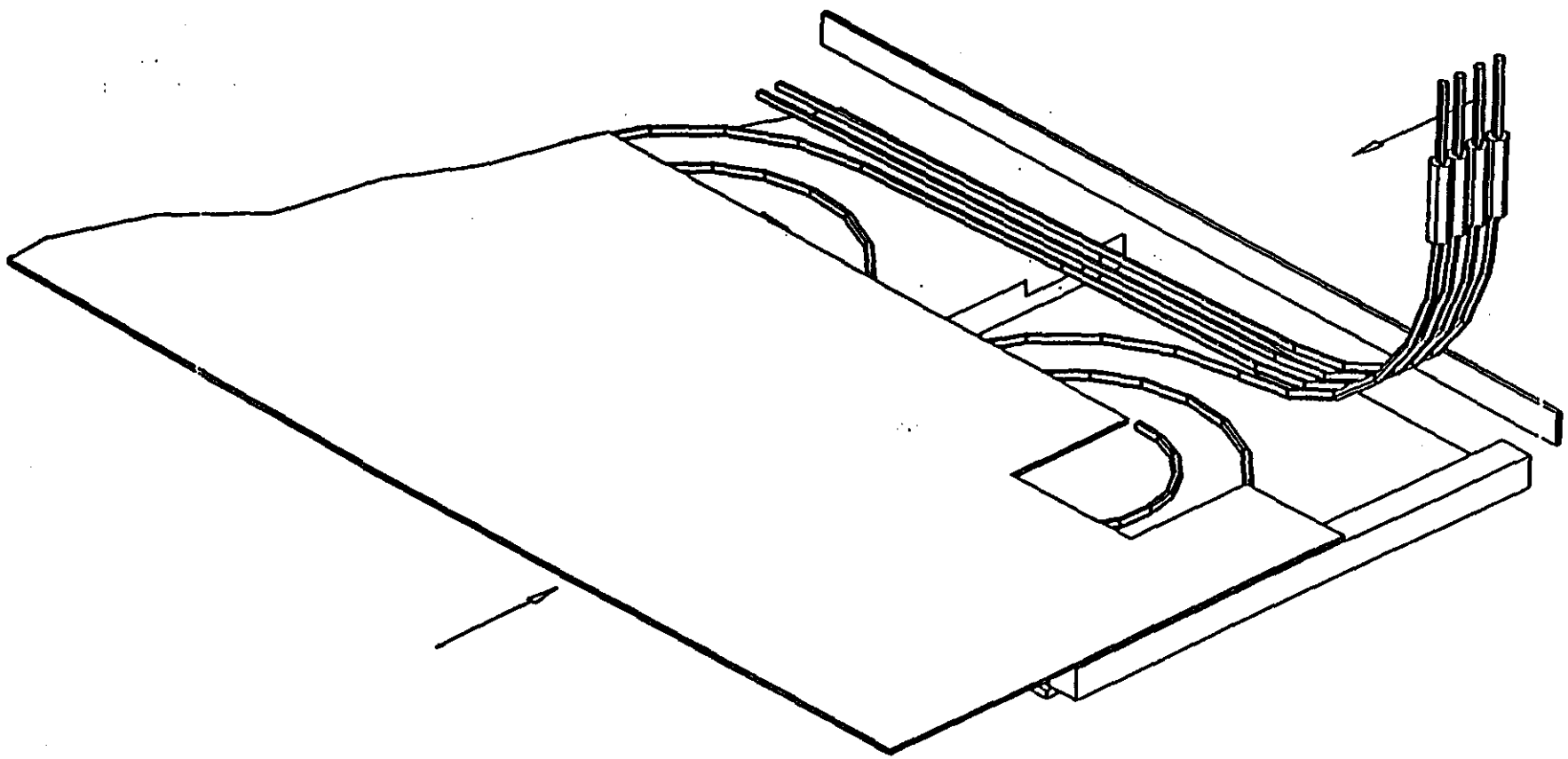

Fig. 3

LS. Detector Layer (Plane)
consists of individual trays

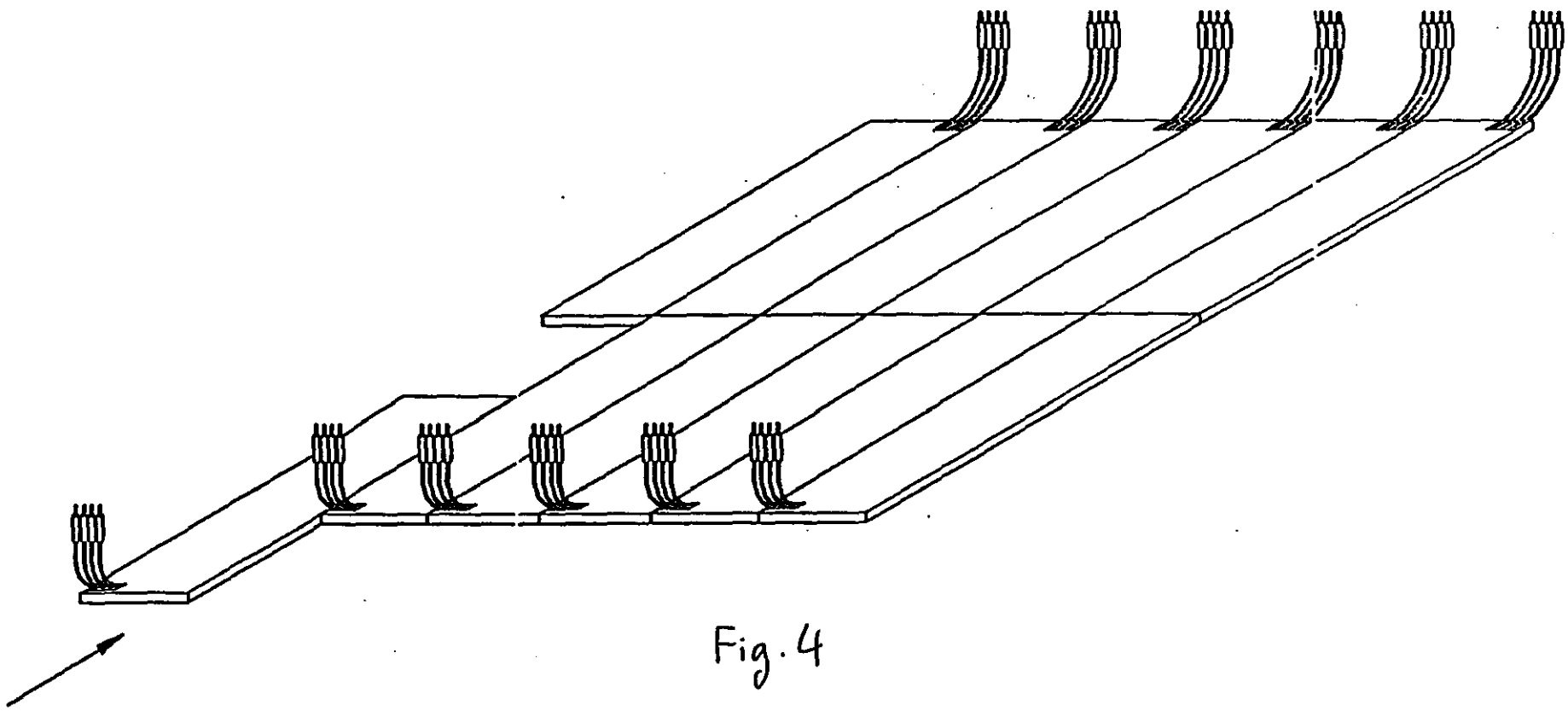

Fig. 4

LS detector tray assembly

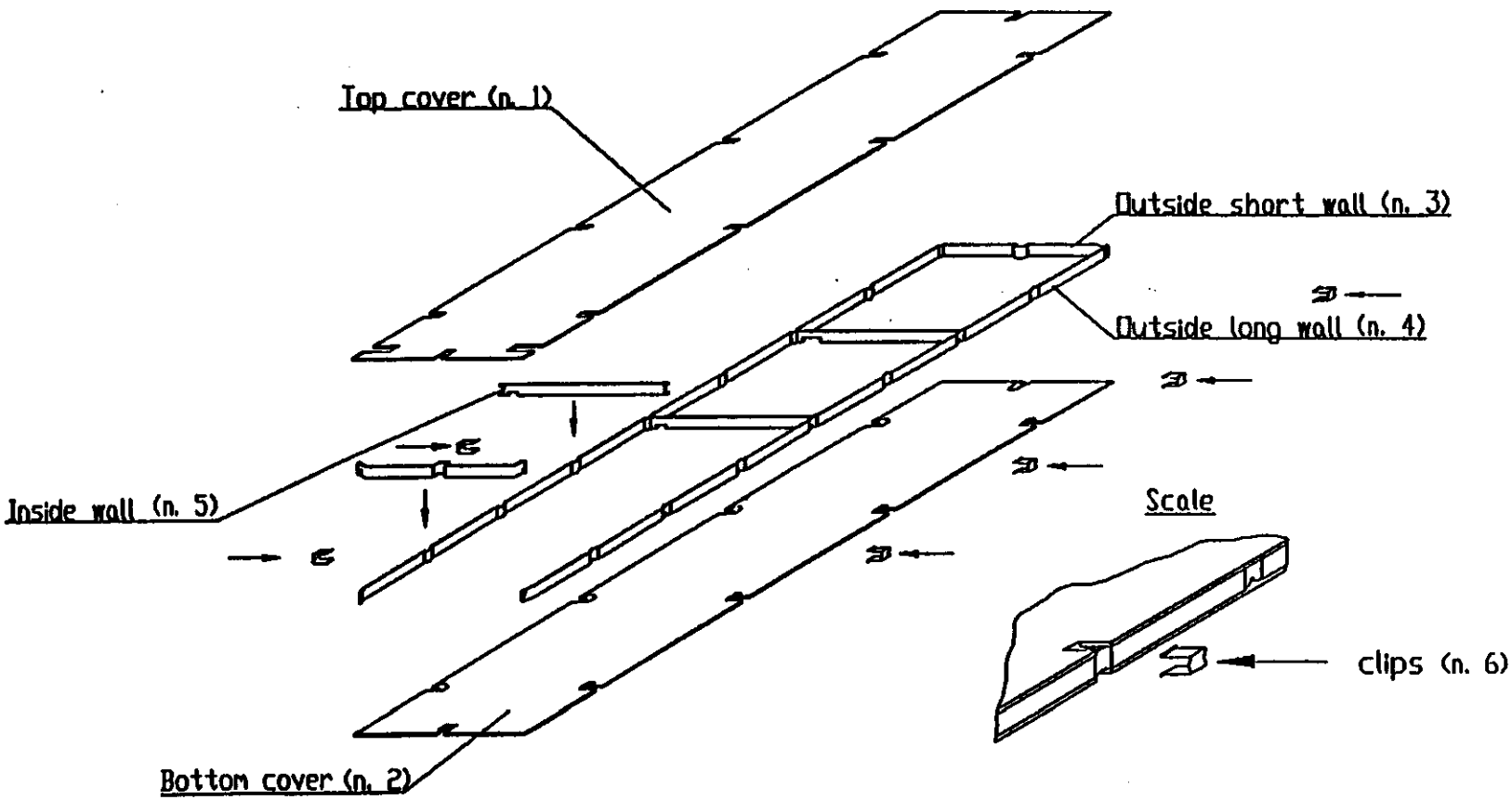

Fig. 5

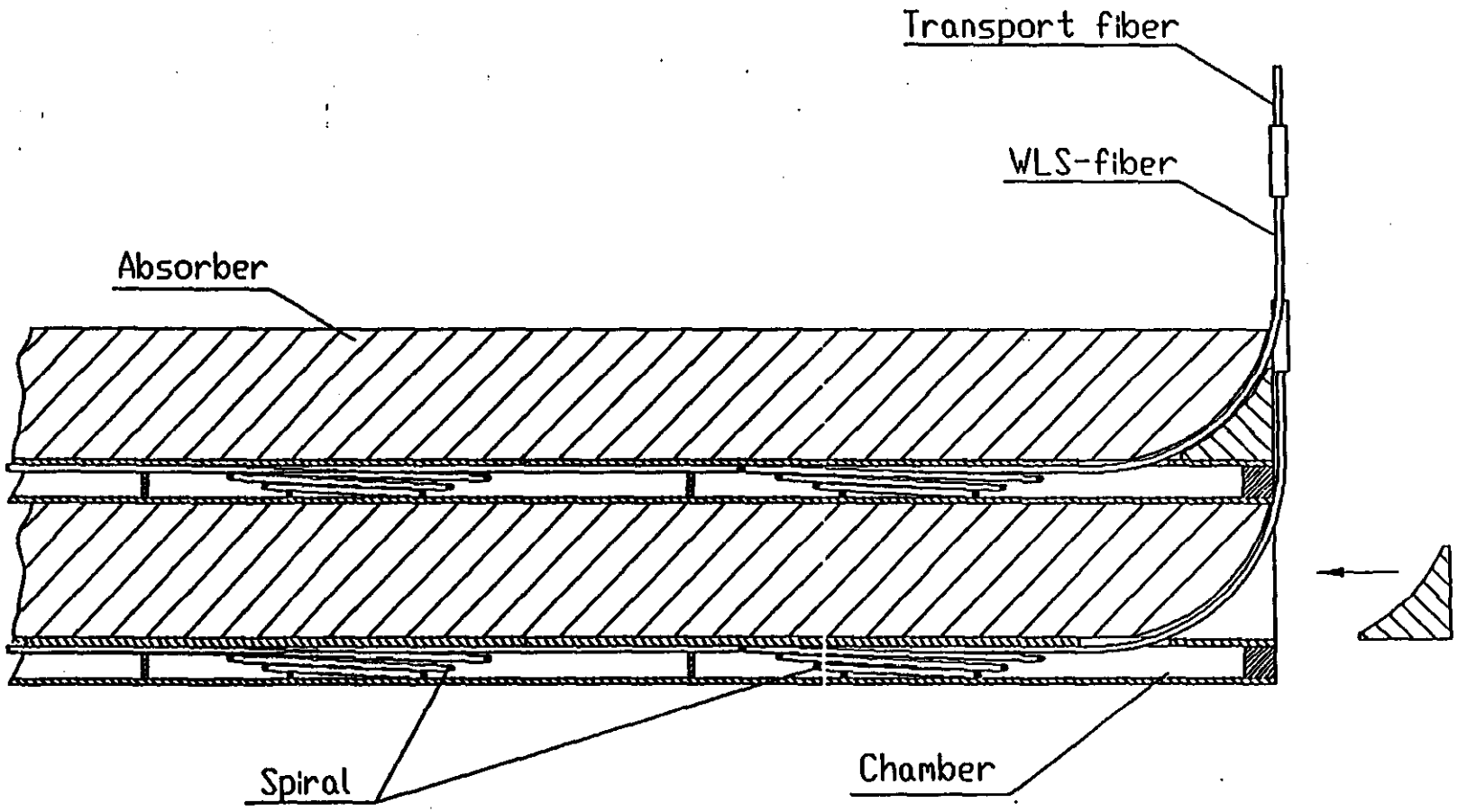

Fig. 6

Version 16-1 (192)

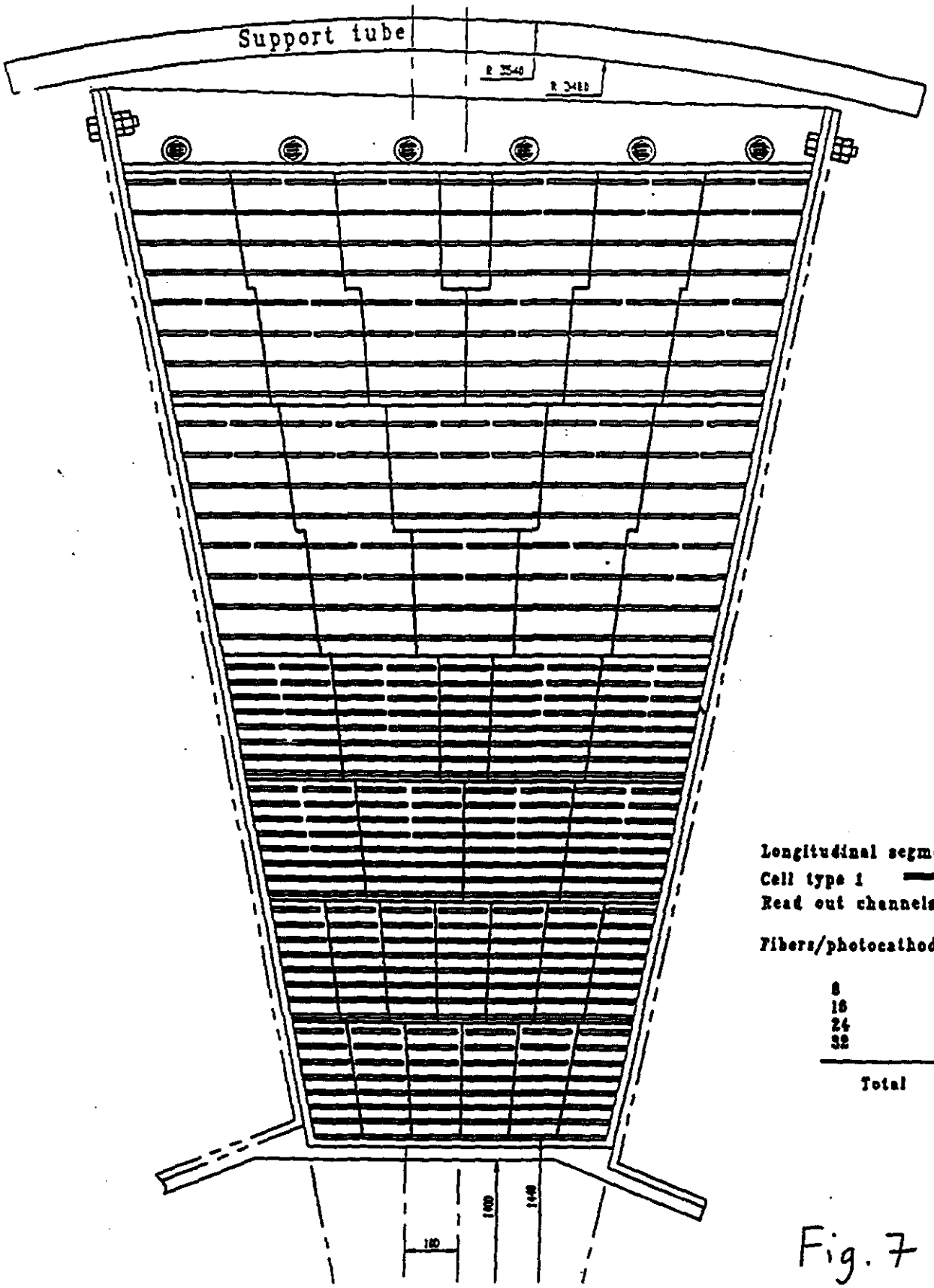

Longitudinal segmentation - 6

Cell type 1 ▬▬ 90.4 x 90.4 mm²

Read out channels 192

Fibers/photocathode

8	108
16	8
24	4
32	72
Total	192

Fig. 7

Version 16-1 (192)

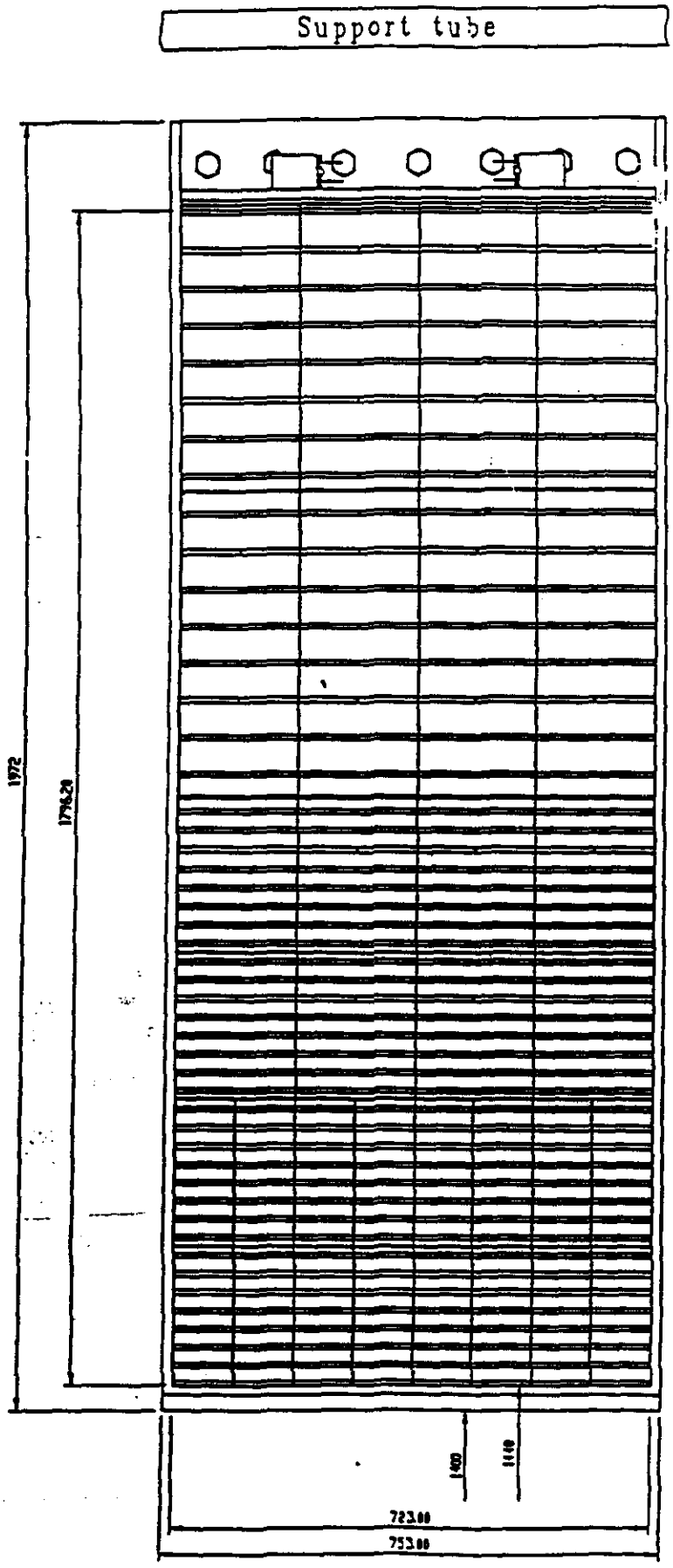

Read out channels 192

Fig. 8

LS e-m calorimeter tower

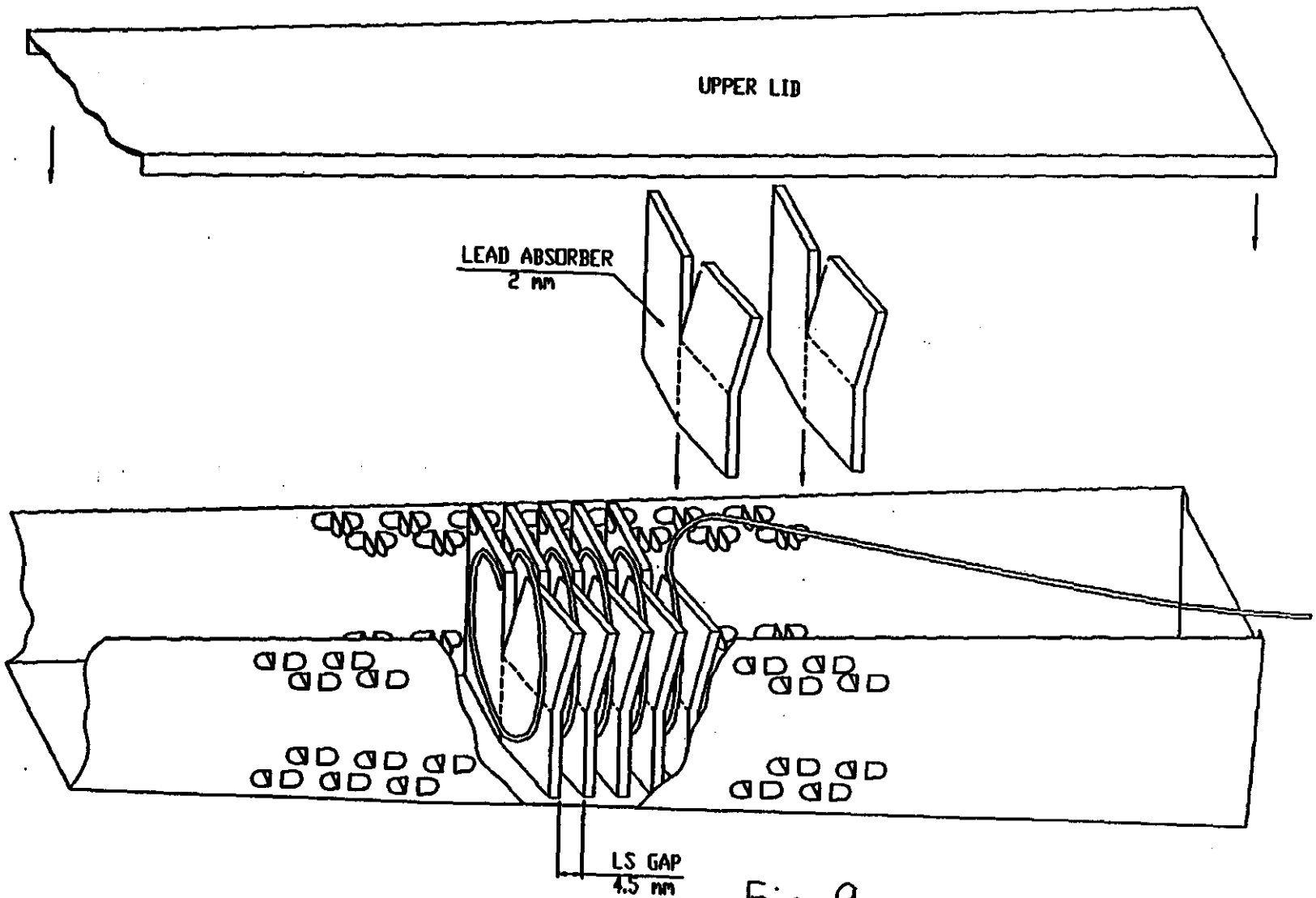

Fig. 9

Fiber routing in e-m LS calorimeter

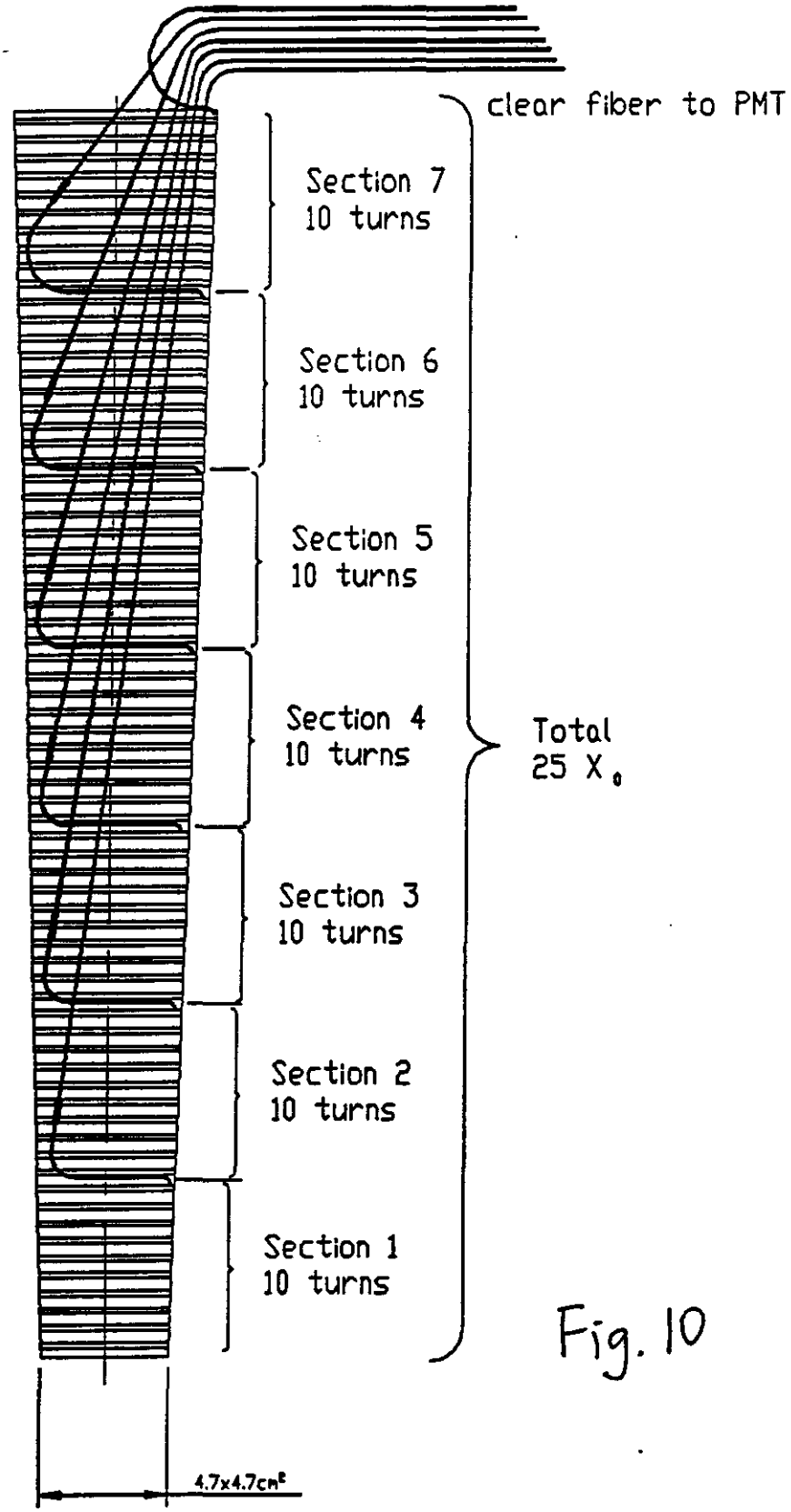

Fig. 10

e−m calorimeter assembly

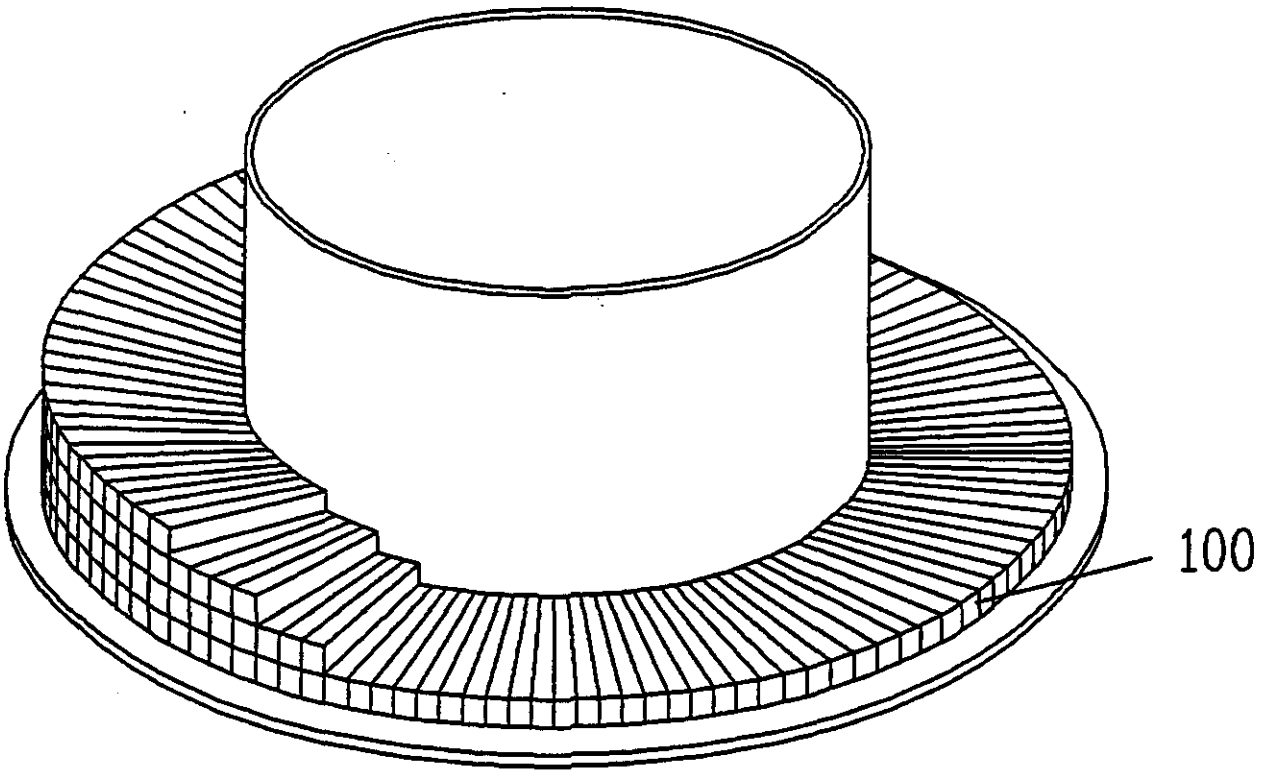

Fig. 11

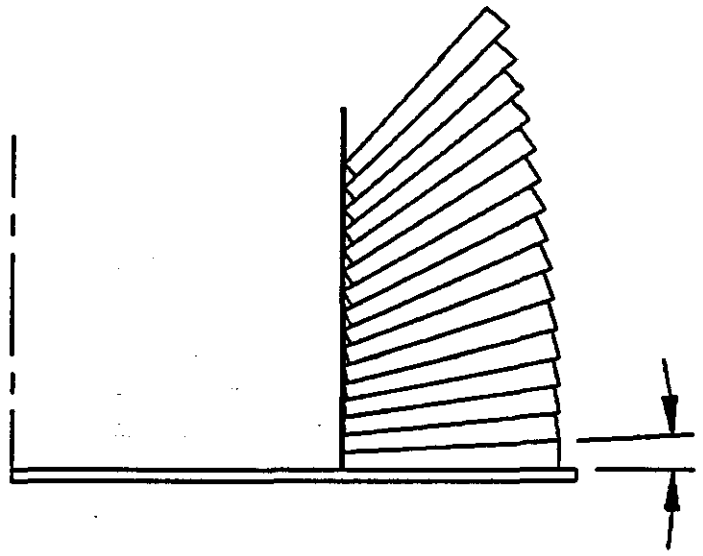

$\Delta\varphi = \Delta\eta = 0.063$

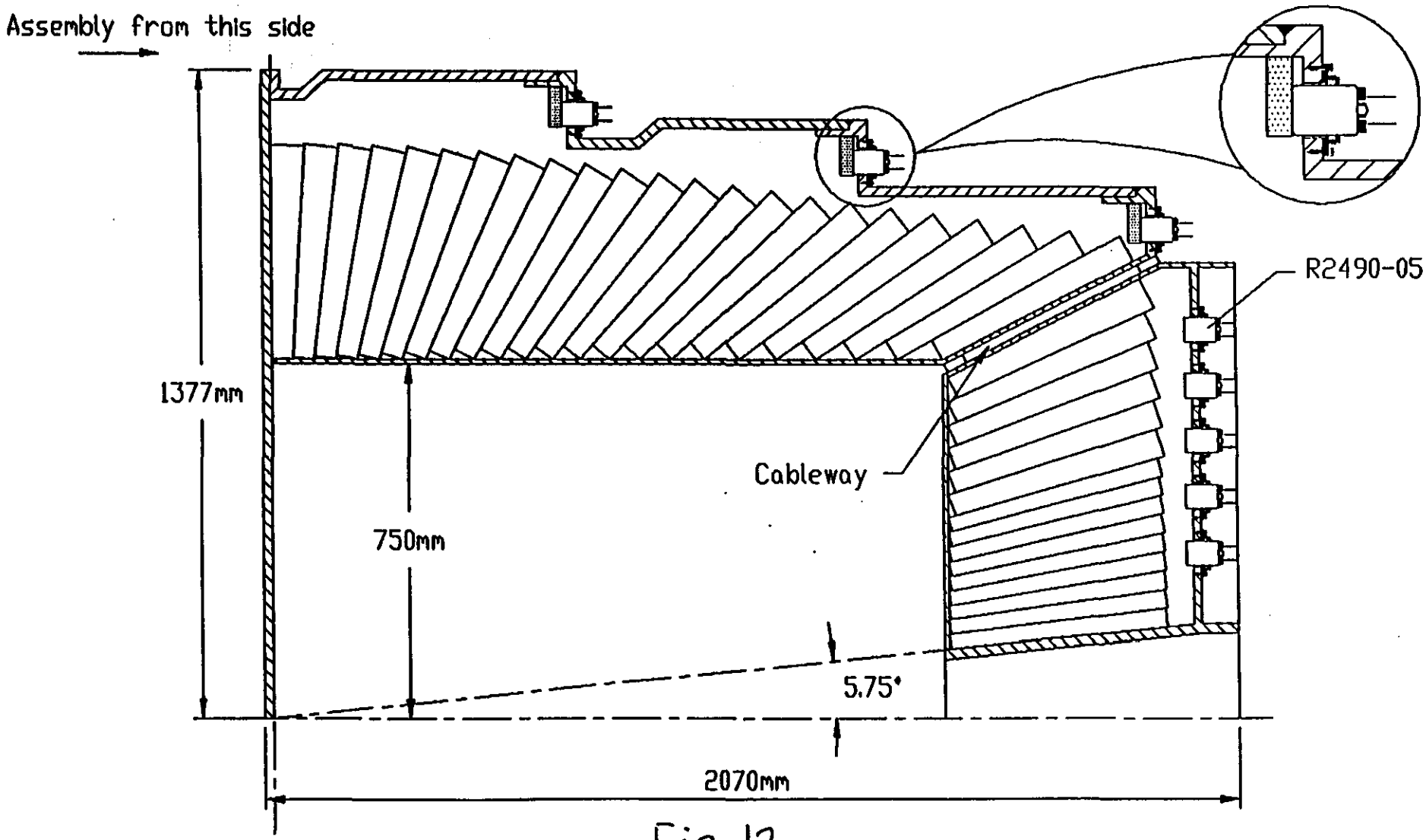

Fig. 12

Liquid ScintillatorEM Calorimeter

Side View

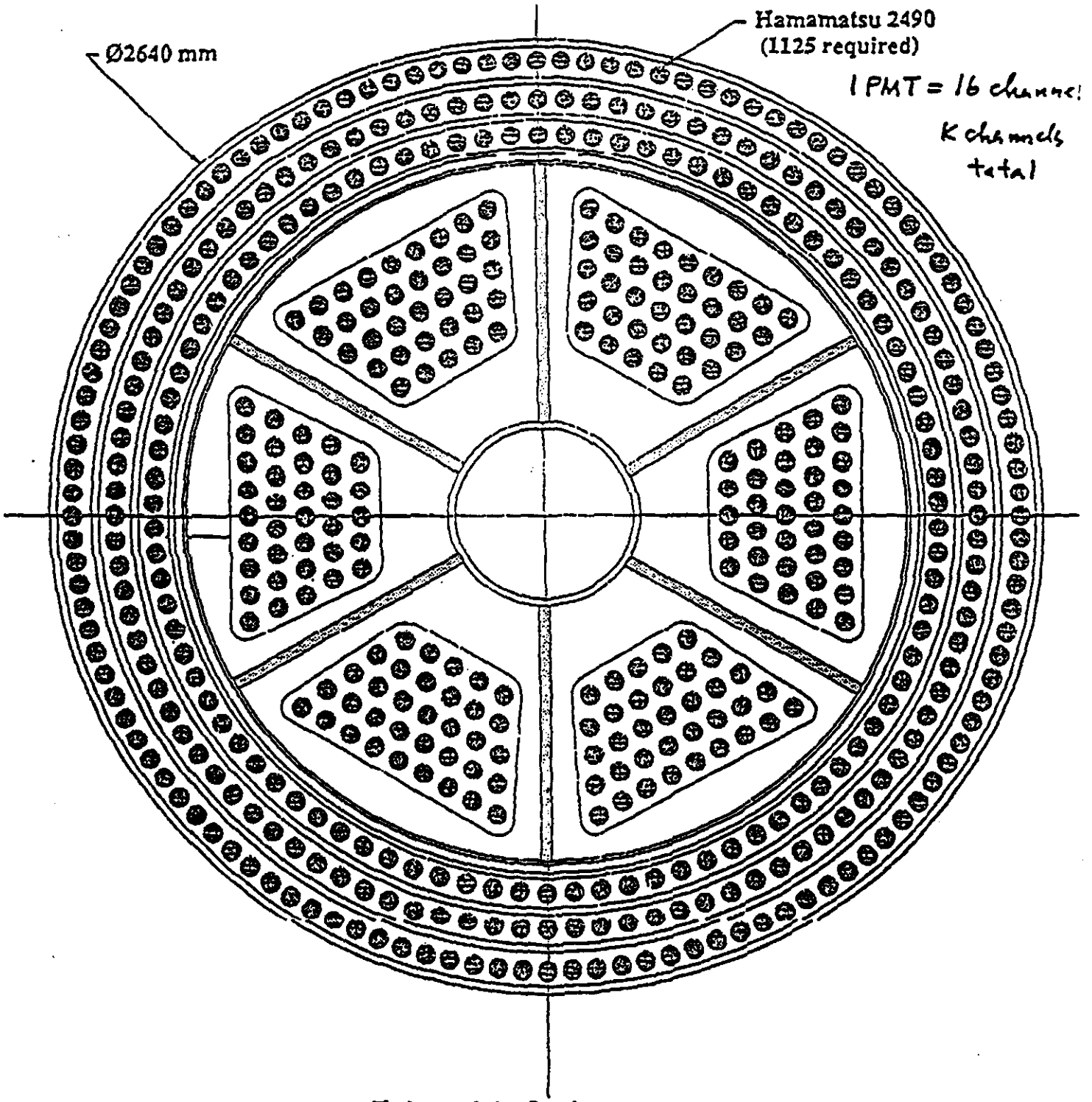

Liquid Scintillator EM Calorimeter End View

LS.03.LSEM.00010

Fig. 13

Rennich

EM

MONTE CARLO RESOLUTION (EGS4)

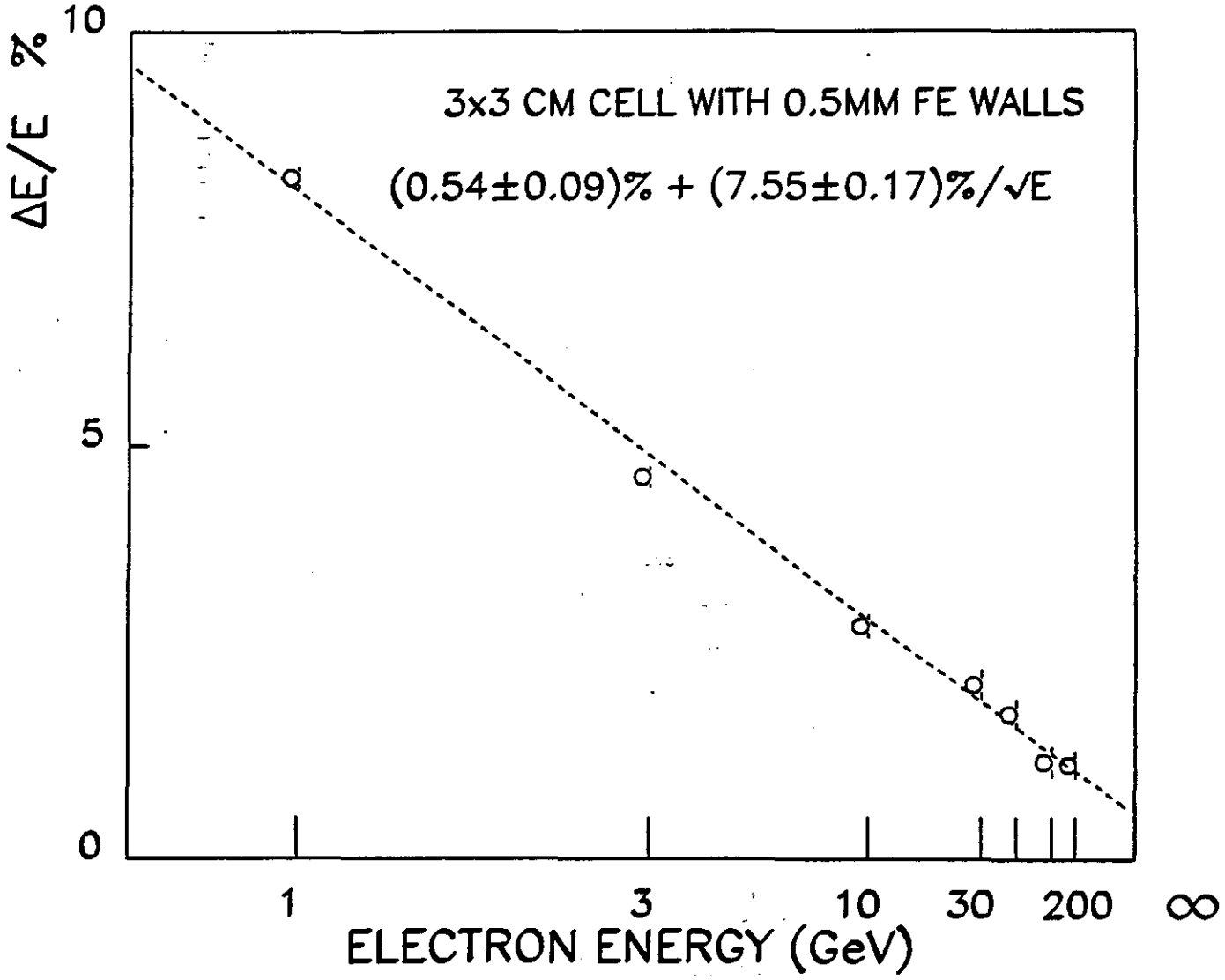

Fig. 14

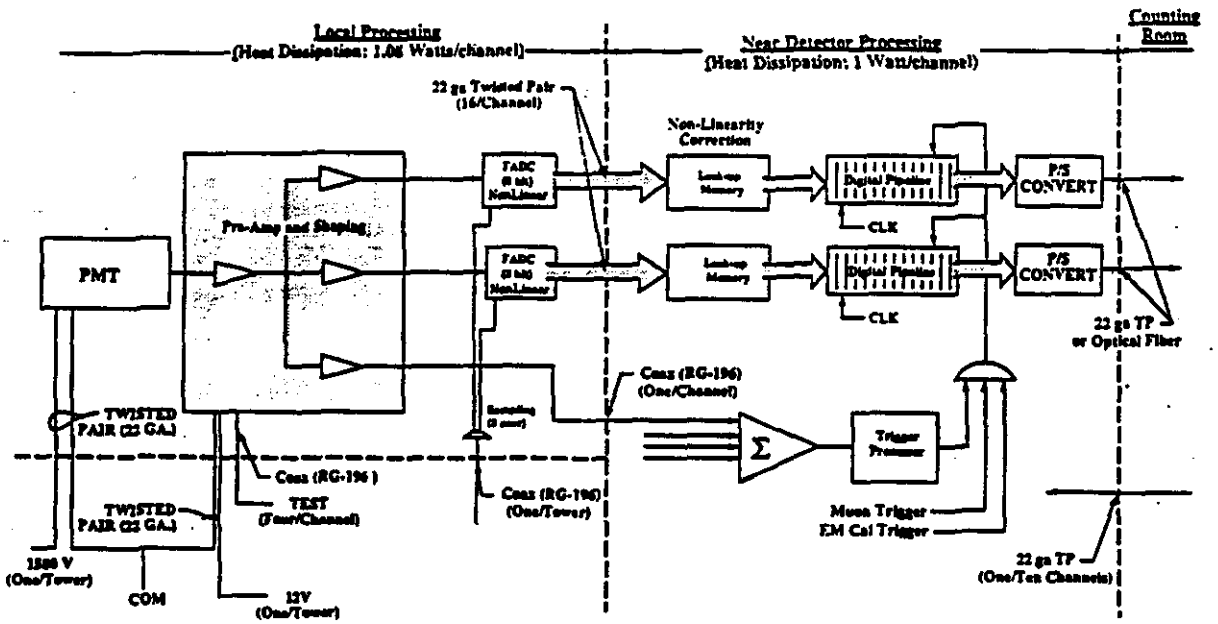

Baseline Electronics For Liquid Scintillating Hadron Calorimeter

Figure 15

HAMAMATSU

TENTATIVE DATA
June 1990

PHOTOMULTIPLIER TUBE R2490-05

FOR HIGH MAGNETIC ENVIRONMENTS

Stable Operation in High Magnetic Fields beyond 1 Tesla(Gain:2.7×10^5 at 1T.) 2 Inch Diameter, Proximity Photocathode and Mesh Dynodes Regrade of R2490-01 with Same Configuration

GENERAL

Parameters		Ratings	Units
Spectral Response		300 to 650	nm
Wavelength of Maximum Response		420 ± 50	nm
Photocathode	Material	Bialkali	–
	Minimum Useful Diameter	36	mm dia.
Window	Material	Borosilicate glass	–
	Shape	Plano-plano	–
Dynode	Secondary Emitting Surface	Bialkali	–
	Structure	Proximity mesh	–
	Number of Stages	16	–
Base		21-pin glass base	–
Suitable Socket		E678-21A (supplied)	–

MAXIMUM RATINGS (Absolute Maximum Values)

Parameters		Ratings	Units
Supply Voltage	Between Anode and Cathode	2700	Vdc
	Between Anode and Last Dynode	250	Vdc
Average Anode Current		0.1	mA
Ambient Temperature		-80 to +50	℃

CHARACTERISTICS (at 25℃)

Parameters		Min.	Typ.	Max.	Units
Cathode Sensitivity	Quantum Efficiency at 390nm	–	20	–	%
	Luminous (2856K)	50	60	–	μA/lm
	Blue (CS No.5-58 filter)	6	7	–	μA/lm-b
Anode Sensitivity	Luminous (2856K)	50	180	–	A/lm
Current Amplification	At 0 tesla	–	3.0×10^5	–	–
	At 0.5 teslas		2.2×10^5	–	–
	At 1 tesla		2.7×10^5	–	–
Anode Dark Current (after 30min. storage in darkness)		–	200	2000	nA
Time Response	Anode Pulse Rise Time	–	2.1	–	ns

VOLTAGE DISTRIBUTION RATIO AND SUPPLY VOLTAGE

Electrode	K	Dy1	Dy2	Dy3	Dy4	Dy5	Dy6	·····	Dy16	P
Ratio	2	1	1	1	1	1	·····		1	1

Supply Voltage : 2500Vdc, K : Cathode, Dy : Dynode, P : Anode

Fig. 16

Information furnished by HAMAMATSU is believed to be reliable. However, no responsibility is assumed for possible inaccuracies or ommission. Specifications are subjected to change without notice. No patient right are granted to any of the circuits described herein.

Figure 3: Typical Current Amplification and Dark Current in Magnetic Field (Parallel to Tube Axis)

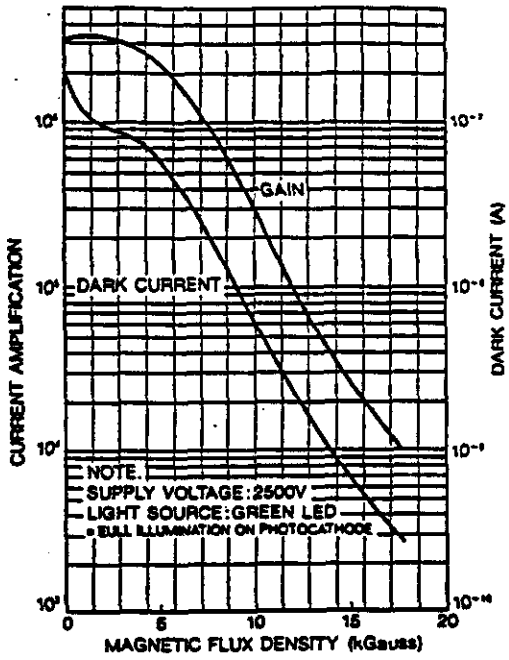

Figure 4: Typical Current Amplification vs. Magnetic Flux Direction

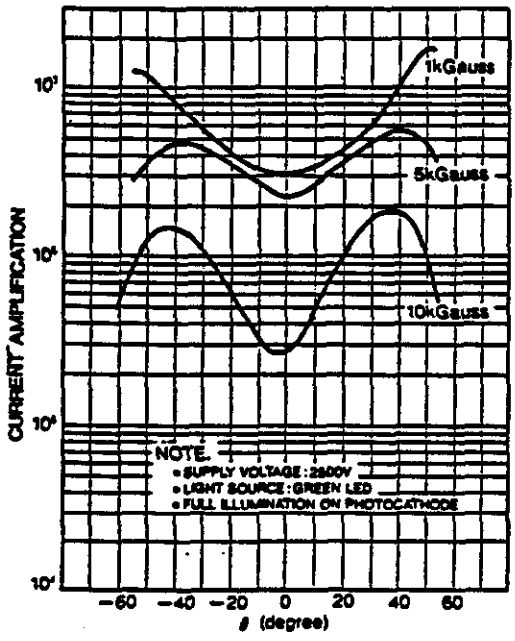

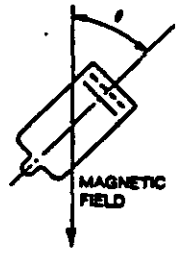

Fig. 17

Question 2. Present similar design for 9 lambda hadron calorimeter located behind BaF2 or Liquid Xenon. Results should be presented on jet resolutions,compensation etc.

a) Dimensions (radii) with details as to cell structure including walls, electronics, mechanical support structure.
b) Resolution,EM, Hadronic(for jets)
c) Electronics readout plan and layout
d) Compensation, speed, HV, magnetic field characteristics, cooling, radiation damage

Answer :

BaF2 EM CALORIMETER FOLLOWED BY 9 LAMBDA HADRONIC CALORIMETER (Pb/Sci)

1)Dimentions:
EM part: BaF2 75cm - 135cm
Hadronic part: same as in previous version

2)Resolution:
Hadronic : Delta(E)/E = 50%/sqrt(E) + 2%
(GEANT simulation for jets, Figure 18)

3)Electonics: for hadron calorimeter the same as in the previous version.
4)Compensation: e/h .NE. 1 - weighting technique should be applied to BaF2 and coarse part of the hadron calorimeter to preserve linearity at high energies.

Speed : same as in previous version

HV : same as in previous version

Magnetic field charact.: same as in previous version

Cooling : same as in previous version for HC only

Radiation damage : LS can be exchanged. The radiation stability of fibers should be extended up to 50 MRad.

HC MONTE CARLO RESOLUTION

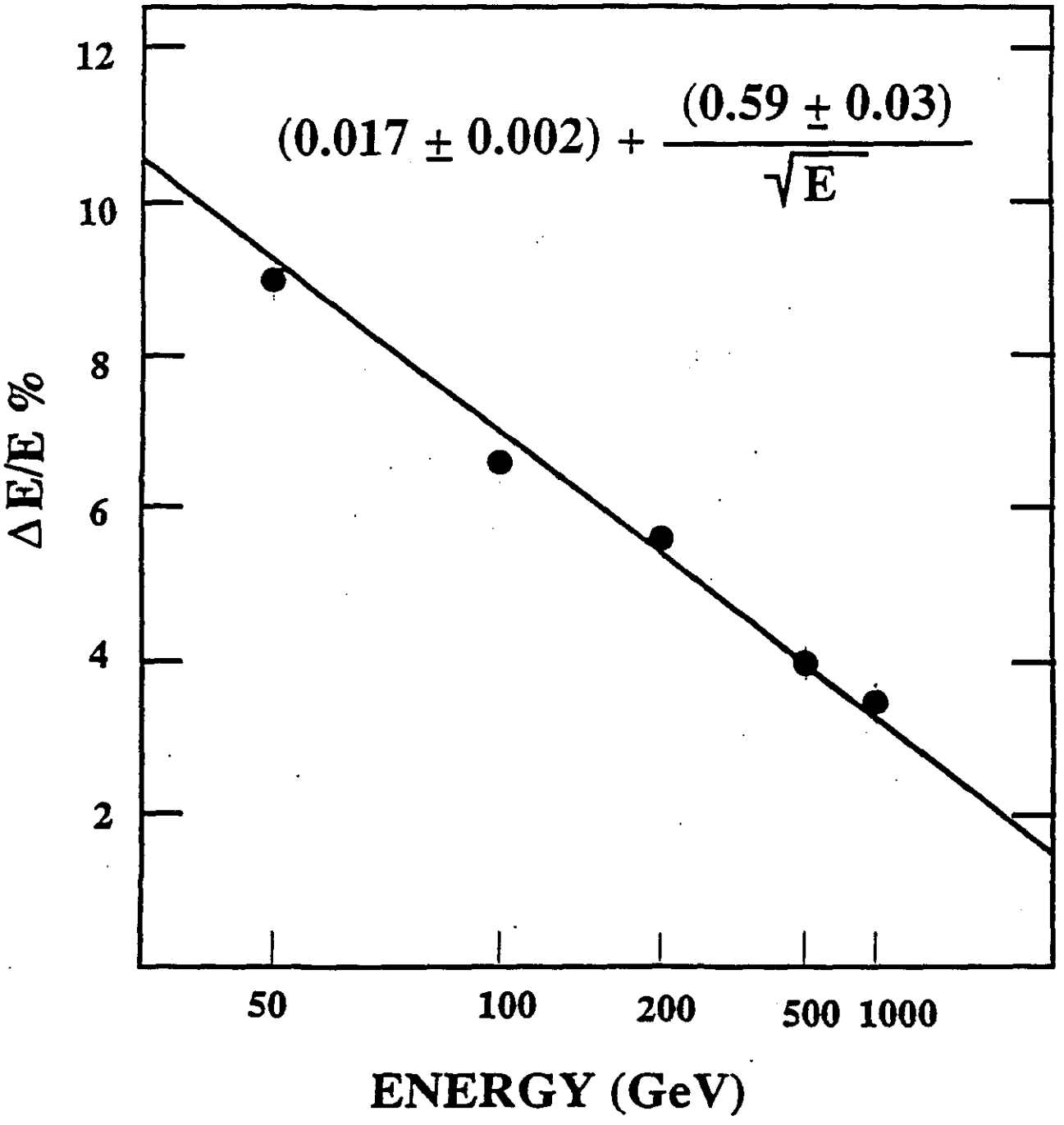

Fig. 18

Answers to questions addressed by

Peter Denes

Question 1. In order to complete a table showing signal-to-noise and pileup effects for the table discussed at the SSC next week, I would like to ask you for information on your proposed EM detector (other than LAr, LXe and BaF2). Basically, I need to know something about the signal shape (into any preamp) something about noise (unless there is a "charge sensitive preamp" in which case I can fill that in) and the details of how you would shape and acquire the pulse. For the latter, a schematic is perhaps the most useful, unless you happen to have the transfer function for all of the bits and pieces. For example, in the BaF2 case (simplest example) this information is of the form:

Signal: 50 e-/MeVwith <1 ns time constant, 30 e-/MeV with 700 ns time constant
Detector: Vacuum phototriode (1 stage, gain =4), 10 pF capacitance
Preamp: Charge sensitive preamp
Shaping: pole-zero + buffer
Acquisition: gated integrator

Answer :

The liquid Scintillator fine sampling calorimeter section consists of 7 longitudinal segments each with an individual light-readout fiber. They are grouped together at the photocathode to form three readout segments. Absorber is 2 mm Lead, and detector is 4.5 mm liquid scintillator. Each fiber or group of fibers is read out by a photocathode pad on a multianode 16 channel PMT (type Hamamatsu R2490-05). Transverse segmentation is ~0.06 and tower layout is similar to that for BaF2. Total length ~ 25 X0.

Signal : 270 MeV/GeV or 1200 p.e./GeV (full longitudinal length)
mip ~ 350 p.e. (full longitudinal length)
Timing : defined by following
- light collection processes contribute to time spread of signal with rms ~ 3 ns (from Monte Carlo)
- decay time of liquid scintillator 2.2 ns,
- decay time of reemission in wave length shifting fiber < 11 ns (single exponent only),
- PMT response time 2.1 ns

Detector : mesh dynode proximity focusing PMT,operating gain ~10**4, each of 16 anodes has an area of about 30 mm2, capacitance <10 pF (unknown), < 1.5% int. linearity up to 500 mA/per anode
Amplifier/shaping : low gain, low input impedance current amplifier with 11 ns zero-pole cancellation (not designed); two outputs with 1:1 and 1:100 attenuation to cover dynamic range of 10**5.
Acquisition : time slice integrator + free running flash ADC on the detector, digital transmission via optical fibers.

Answers to questions addressed by

Bill Worstell

LIQUID SCINTILLATOR PLATES WITH WLS READOUT:

Question 1. How can scintillator plate EM calorimeters expect to achieve a 7% stochastic term in the energy resolution and at most a 1/2% constant term in the energy resolution in the face of the following difficulties?

Question 1a) What is the best stochastic term that has been measured with a plate calorimeter in a test beam, and what was the light yield and pulse shape? Have beam tests been performed on both electromagnetic a hadronic (solid,liquid) plate calorimeter prototypes? How does the measured resolution vary with energy, and is there a linear or quadratic constant term?

Answer 1a) :

Hadron and electro-magnetic sampling scintillation calorimetry is probably the oldest calorimeter technique which has been succesfully used over the last three decades. Thus the compensation mechanism in this case is the first to have been established and understood. The best high-performance devices, such as NA-34, Argus, ZEUS and others, have been built using this technique.

The recent review of beam test results of electro-magnetic fine-sampling calorimeters has been done by J. Del Peso and E.Ros [1]. Table 3 from their work summarizes the best achieved energy resolution results using several techniques. The best stochastic terms for EM calorimeters with scintillator readout, 5%, has bean measured with PB/Sci calorimeter for sampling with 1 mm Pb and 5 mm Scint. [2] (EGS prediction 4%). For sampling with 2 mm Pb and 5 mm Scint. the measured stochastic term equals 7.5% [3], (with EGS prediction 6.3%). Our EGS4 simulations with carefully choosen low-energy cutoffs gives for the structure 2 mm Pb/4.5 mm Liq.Scint. stochastic resolution term 7.6%.

Typical light yield for plastic scintillator fine sampling EM calorimeters is 100-300 p.e./GeV . For example for 1 mm Pb/5 mm Sci calorimeter [4] light yield equals 270 p.e./GeV. Statistics of photoelectrons creates an additional stochastic term of about 6% in resolution. This term has to be added in quadrature. We couldn't find any specific information regarding the pulse shape of these devices.

For the Liquid Scintillator fine sampling calorimeter which we are proposing the expected light yield is 1200 p.e./GeV. This will contribute to the stochastic term an additional 3% (to be added in quadrature).

In recent beam tests with a fine sampling U/Sci calorimeter {180 x (3 mm U + 3 mm Sci) = 6 lambda} performed by the ZEUS Collaboration [5] hadronic resolution was found to be Sigma(E)/E = 35.7%/sqrt(E) + 1.3% with a linearly added constant term. The pi/e ratio was found to be 1.

References :

[1] J. Del Peso and E. Ross , NIM A276(1989)456-467
[2] W.Hofmann et al., NIM 195(1982)475
[3] R.Klanner et al.,ZEUS note 86-3,unpublished
[4] M.A.Schneegans et al, NIM A193(1982),445
[5] I. Kudla et al., NIM A300(1991),480-492

NIM A276
(1989) 456-467

Table 3a
Measured and calculated energy resolutions for various calorimeters employing scintillator as active material. The values given for σ are fractional energy resolutions scaled to 1 GeV showers. The contribution of photoelectron statistics has been subtracted to the measured values. Otherwise they appear in parentheses.

Absorber	t [mm]	s [mm]	σ_{exp} [%]	σ_{EGS} [%]	$\sigma_{exp}/\sigma_{EGS}$	Ref.
Pb	1.0	5.0	5.0	4.0	1.2	[20]
Pb	1.0	5.0	6.0	4.0	1.5	[24]
Pb	2.0	5.0	7.5	6.3	1.2	[25]
Pb	2.1	6.3	9.0	6.1	1.5	[15]
Pb	2.5	4.0	(10.5)	7.8	1.3	[26]
Pb	3.2	5.0	12.0	8.6	1.4	[27]
Pb	3.5	4.0	(14.0)	9.8	1.4	[28]
Pb	4.0	5.0	11.6	10.0	1.2	[29]
Pb	4.2	12.6	10.8	7.9	1.4	[15]
Pb	6.0	5.0	13.6	13.1	1.1	[30]
Pb	6.0	2.5	17.5	16.0	1.1	[31]
Pb	8.4	25.2	14.7	10.3	1.4	[15]
Pb	9.4	6.4	(18.2)	16.5	1.1	[32]
Pb	10.0	2.5	22.6	22.6	1.0	[33]
U	1.6	2.5	(11.0)	9.7	1.1	[34]
U	2.0	2.5	(13.9)	11.3	1.2	[35]
U	3.0	2.5	(16.3)	15.0	1.1	[36]
U	3.2	5.0	(14.8)	12.7	1.2	[37]
U	3.2	3.0	(15.0)	14.8	1.0	[37]
U	10.0	5.0	(28.0)	27.9	1.0	[38]
Fe	4.8	6.3	10.1	6.8	1.5	[15]
Fe	25.0	5.0	(23.0)	20.0	1.1	[7]

Table 3b
Measured and calculated energy resolutions for various calorimeters employing liquid argon as active material. The contributions of electronic noise and calibration errors have been subtracted to the measured values. Otherwise they appear in parentheses.

Absorber	t [mm]	s [mm]	σ_{exp} [%]	σ_{EGS} [%]	$\sigma_{exp}/\sigma_{EGS}$	Ref.
Pb	1.0	2.0	8.0	5.0	1.6	[39]
Pb	1.2	3.6	(8.5)	5.0	1.7	[40]
Pb	1.5	5.0	7.5	5.4	1.4	[41]
Pb	1.5	2.0	8.0	6.4	1.3	[42]
Pb	1.9	3.0	9.0	6.9	1.3	[43]
Pb	2.0	5.0	(10.0)	6.5	1.5	[44]
Pb	2.0	3.0	(10.8)	7.1	1.5	[45]
Pb	2.0	2.0	9.6	7.7	1.2	[46]
Pb	2.0	2.0	(10.3)	7.7	1.3	[47]
Pb	2.2	2.0	9.5	7.7	1.2	[48]
Pb	2.4	2.8	11.2	8.1	1.4	[43]
U	2.0	1.6	14.0	11.5	1.2	[49]
Fe	1.0	1.0	2.8	3.7	0.8	[50]
Fe	1.5	1.5	9.5	4.4	2.2	[51]
Fe	1.5	2.0	6.9	4.1	1.7	[52]
Fe	1.5	2.0	(7.4)	4.1	1.8	[53]
Fe	2.0	2.0	6.1	4.9	1.2	[46]

Table 3c
Measured and calculated energy resolutions for various calorimeters employing a gas as active material

Absorber	t [mm]	s [mm]	σ_{exp} [%]	σ_{EGS} [%]	$\sigma_{exp}/\sigma_{EGS}$	Ref.
Pb	1.1	5.0	11.2	14.0	0.8	[54]
Pb	1.3	12.7	17.0	13.0	1.3	[55]
Pb	1.4	10.0	14.0	14.0	1.0	[56]
Pb	2.0	6.0	15.0	18.4	0.8	[57]
Pb	2.0	3.2	16.0	20.5	0.8	[58]
Pb	2.8	11.6	17.0	19.5	0.9	[59]
Pb	2.8	12.4	17.5	19.3	0.9	[60]
Pb	2.8	9.5	17.0	20.2	0.8	[61]
Pb	3.0	7.0	24.0	22.0	1.1	[62]
Pb	5.0	9.0	28.0	27.4	1.0	[63]
Pb	6.0	2.0	27.0	38.8	0.7	[64]

Question 1b) What uniformity has been measured when varying the incident position of particles across the front face of a module, and across module boundaries? What mechanical tolerances are required in order to preserve the required resolution against variations in incident position and longitudinal shower fluctuations? Is there an engineering design which can meet these tolerances and/or achieve this resolution in the endcap region, as well as the barrel? What are the tolerances on the coupling uniformity across optical splices, and of the photodetector uniformity across its face?

Answer 1b) :

For our LS EM calorimeter design, Monte-Carlo simulations with EGS4 have been performed for a tower which corresponds to a transverse segmentation of 0.04 (radius 750 mm) with a front plate size of 30x30 mm2. One readout WLS spiral traversed 22 cells in this simulation. From light-transport Monte Carlo it was found that light collection nonuniformity inside this cell (in each layer) was 8% with a longitudinal increase of sensitivity from front to rear of about 25% (corresponding to a self-attenuation length in the WLS fiber of ~ 4m). This information was used in the EGS4 simulation. Stainless steel walls of 0.,0.25,0.5 and 1. mm between the towers were also simulated. Particles incident in Monte Carlo were uniformly distributed over the face of the tower. The results of these simulations are presented in Figures 1-3. They show that 7.5-7.6% stochastic term is essentially not influenced by a dead-wall thickness of up to 1 mm. The constant term is about 0.6%.

Our engeneering design for fine sampling Pb/LS calorimeter is shown in fig 4-8. Intertower walls of 0.5-1.0 mm are feasible from engineering considerations. This design applies to both the barrel EM and the endcap EM. If financial constraints are resolved, we will start production of a prototype EM calorimeter based on this design.

In our design WLS fibers are spliced with clear transport fibers which bring signals to the photocathode. The efficiency of fiber splicing was measured (relative to a reference fiber) for different combinations of fiber-end finishes and with and without optical compound between the fibers. Within 4% systematic measurement errors there is no reduction of light transmitted through optical splices. Figure 9

Photodetector cathode uniformity for Hamamatsu R2490-05 16 anode PMT will be measured by the end of the year when the test sample PMT will be received. Producer expectations are that within a 5 x 5 mm2 cathode area the non-uniformity will not exceed few percent [1]

References :

[1] K.Arisaka, Private communication

Fig. 1

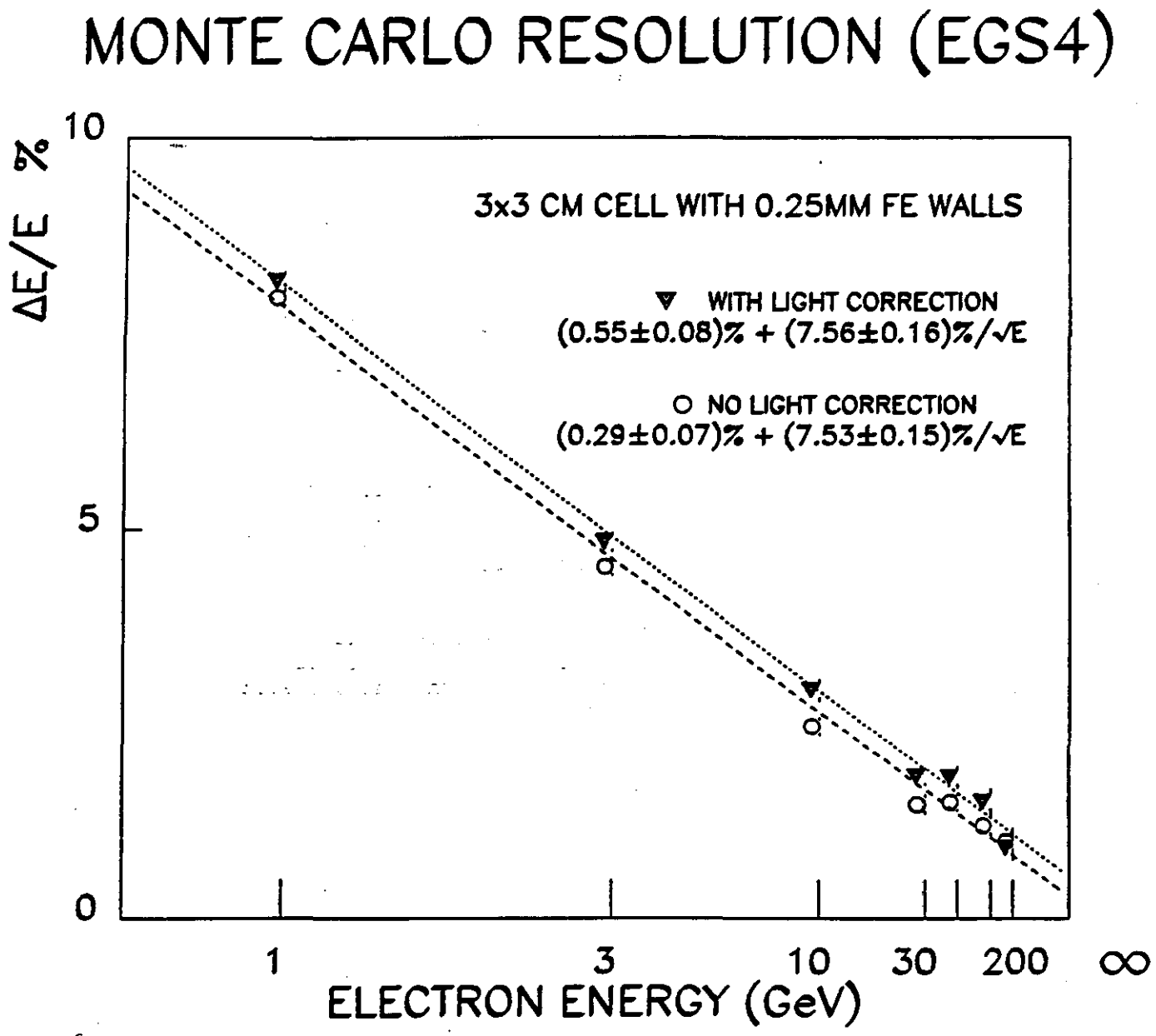
MONTE CARLO RESOLUTION (EGS4)
ΔE/E %
10
5
0
3x3 CM CELL WITH 0.25MM FE WALLS
▼ WITH LIGHT CORRECTION
(0.55±0.08)% + (7.56±0.16)%/√E
○ NO LIGHT CORRECTION
(0.29±0.07)% + (7.53±0.15)%/√E
1
3
10
30
200
∞
ELECTRON ENERGY (GeV)

Fig. 2

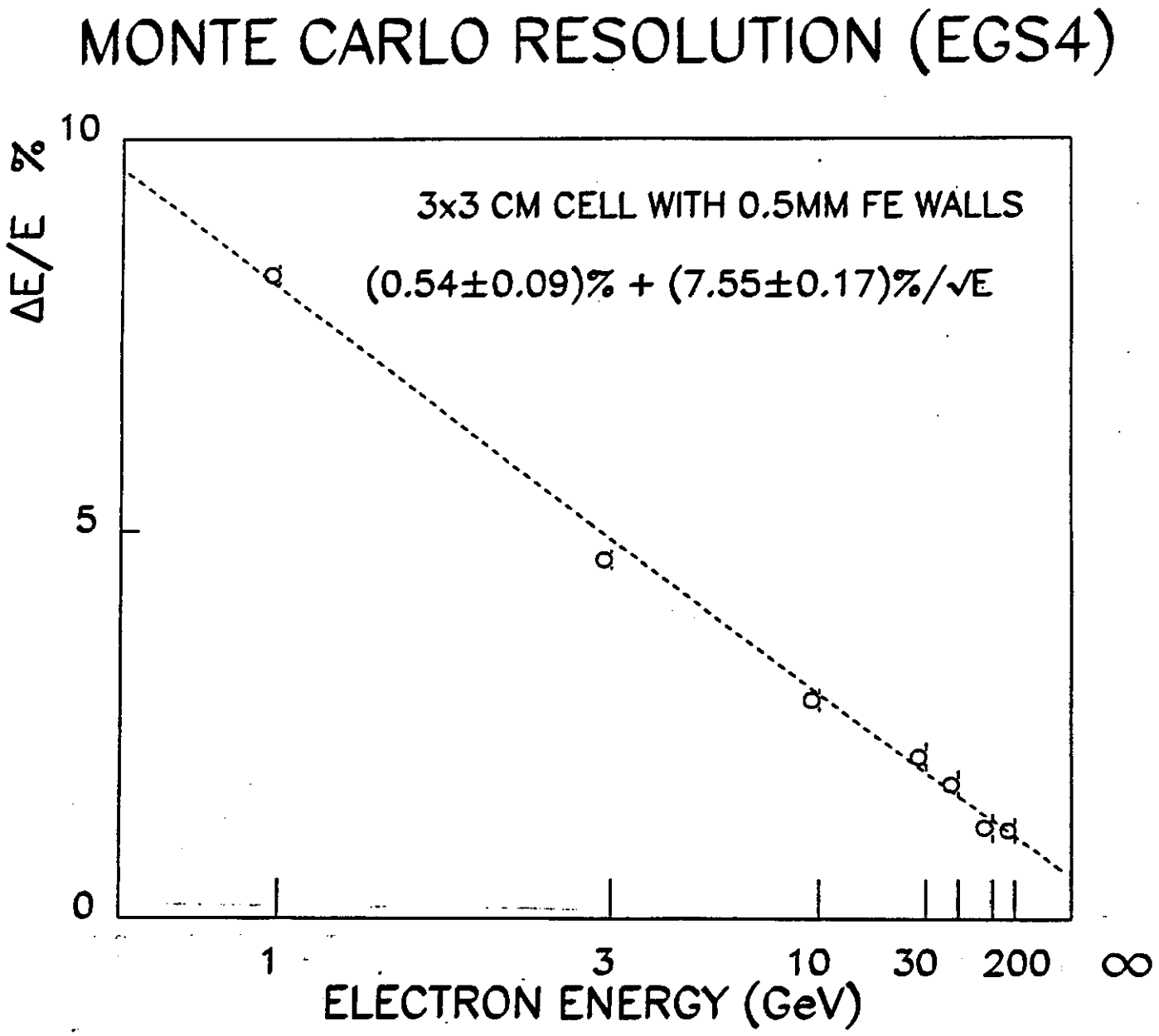
MONTE CARLO RESOLUTION (EGS4)
3x3 CM CELL WITH 0.5MM FE WALLS
(0.54±0.09)% + (7.55±0.17)%/√E
ΔE/E %
10
5
0
1
3
10
30
200
∞
ELECTRON ENERGY (GeV)

Fig. 3

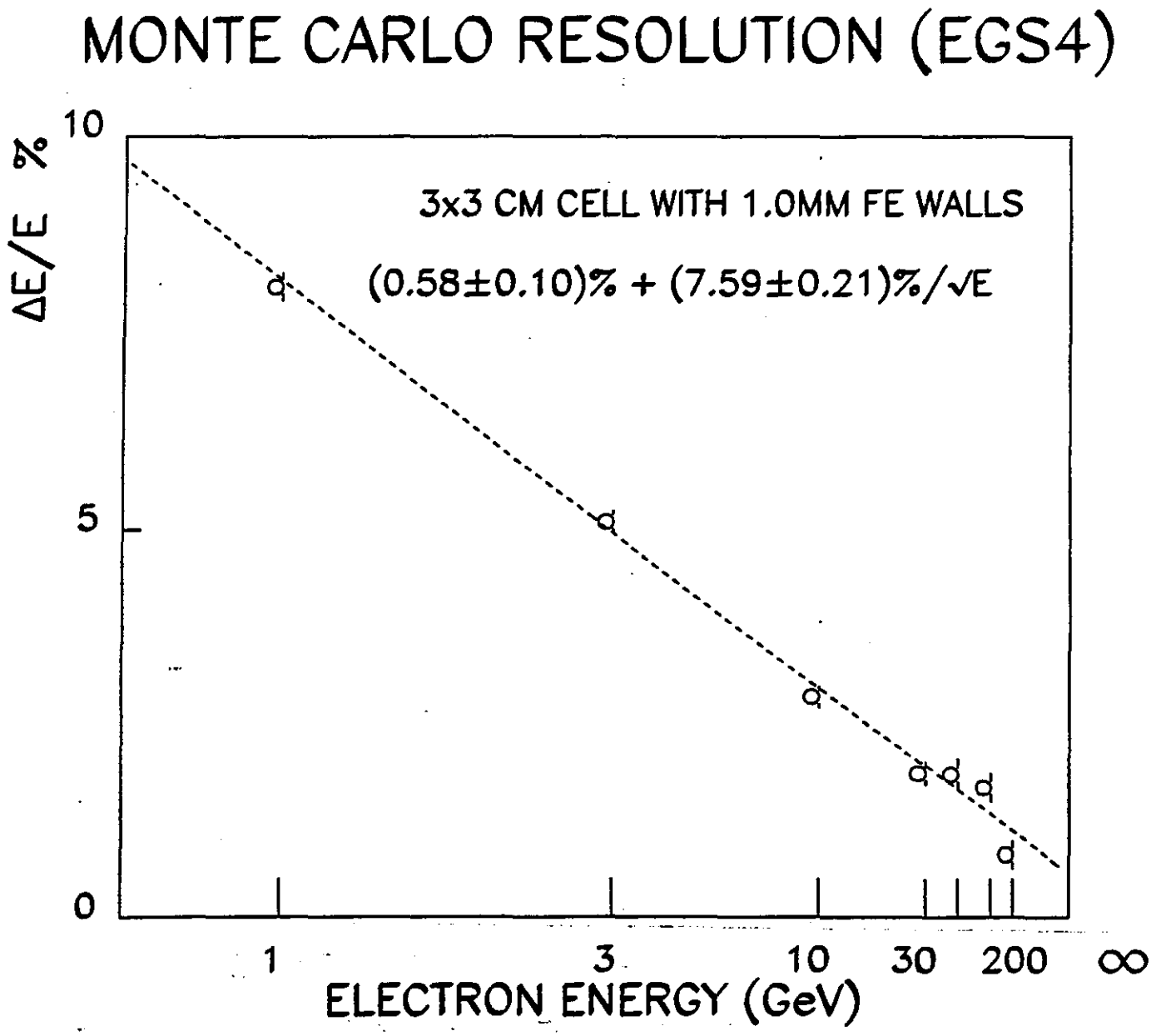
MONTE CARLO RESOLUTION (EGS4)
3x3 CM CELL WITH 1.0MM FE WALLS
(0.58±0.10)% + (7.59±0.21)%/√E
ΔE/E %
10
5
0
1
3
10
30
200
∞
ELECTRON ENERGY (GeV)

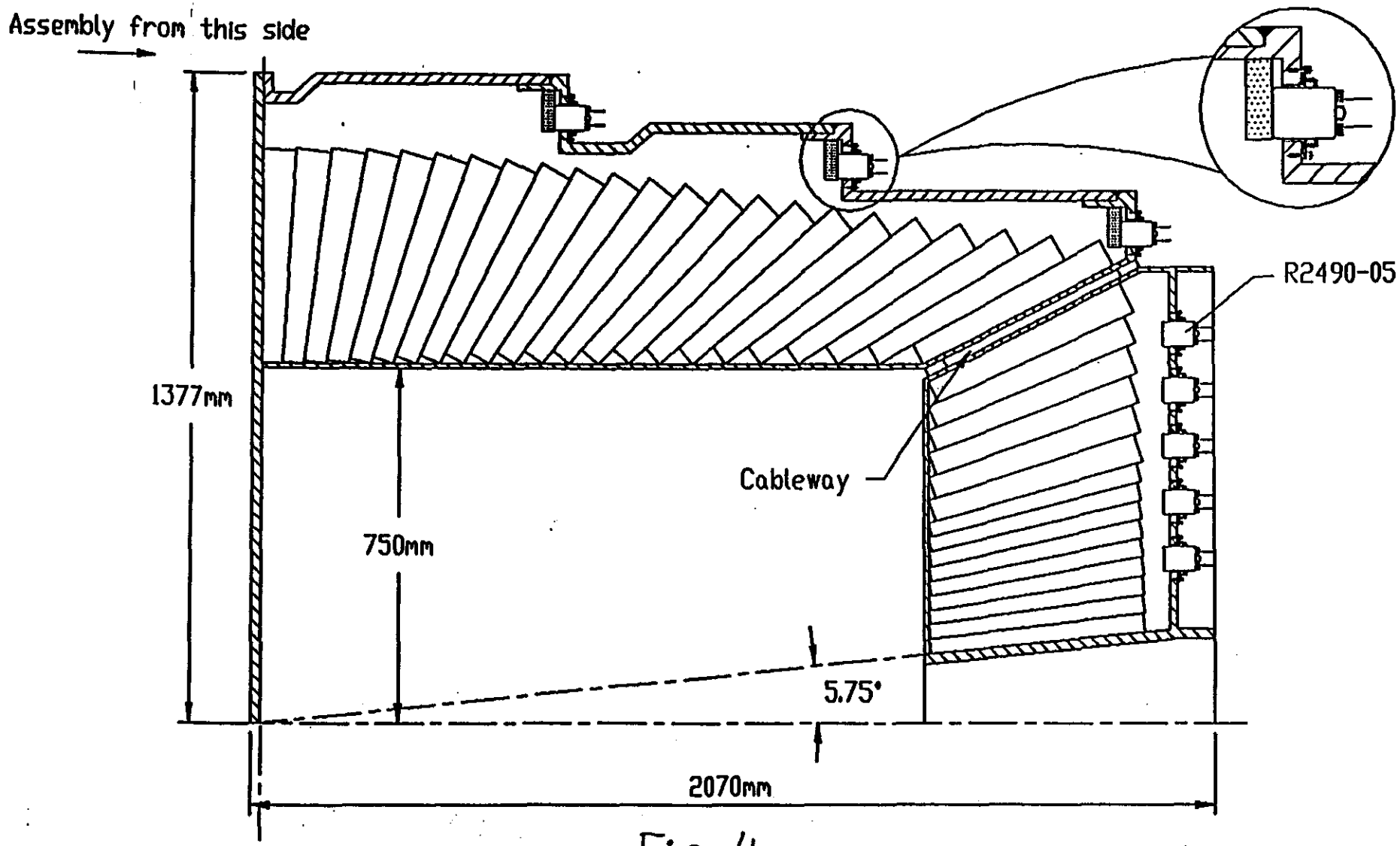

Fig. 4
Liquid ScintillatorEM Calorimeter
Side View

LS e-m calorimeter tower

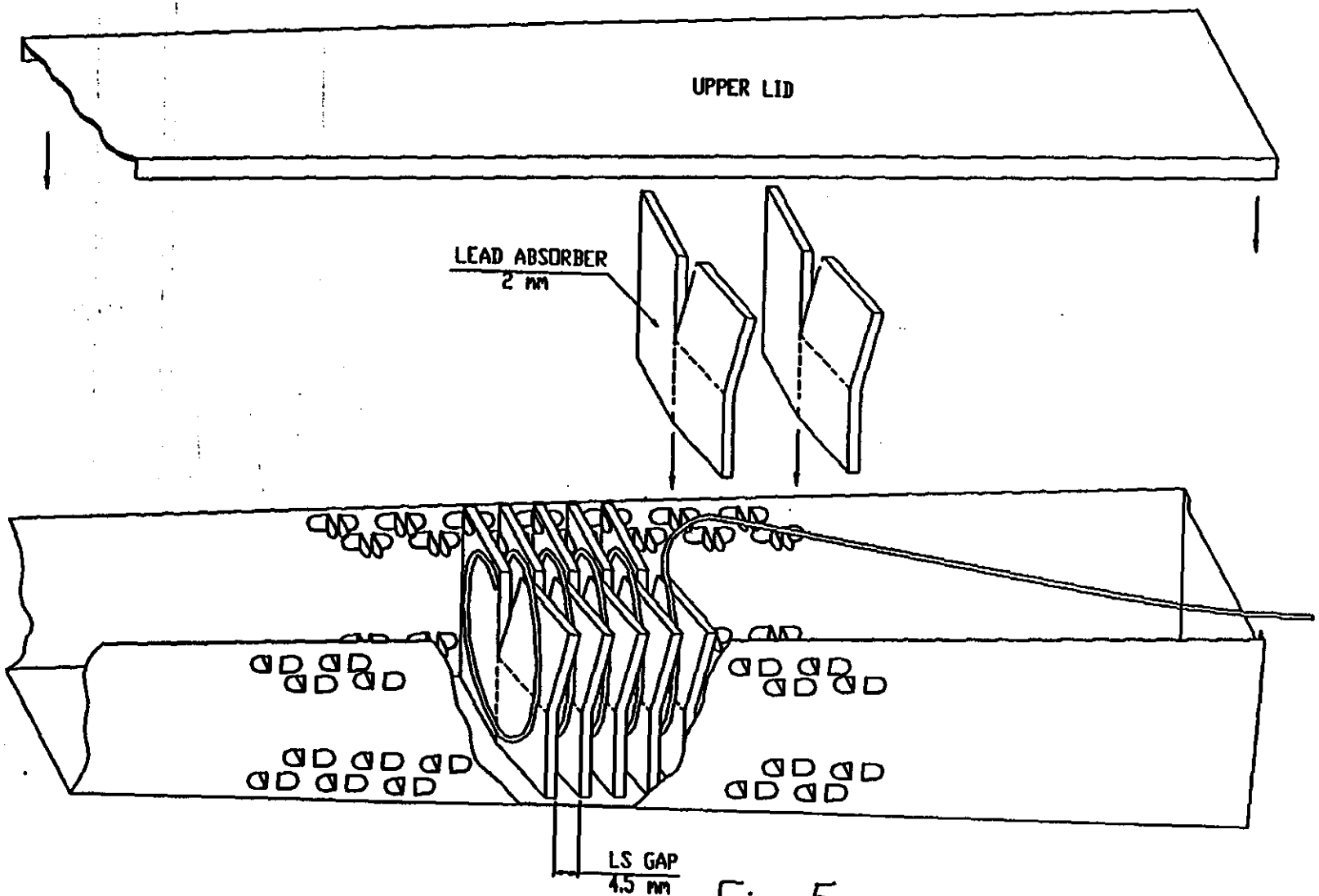

Fig. 5

Cross section of e-m calorimeter tower

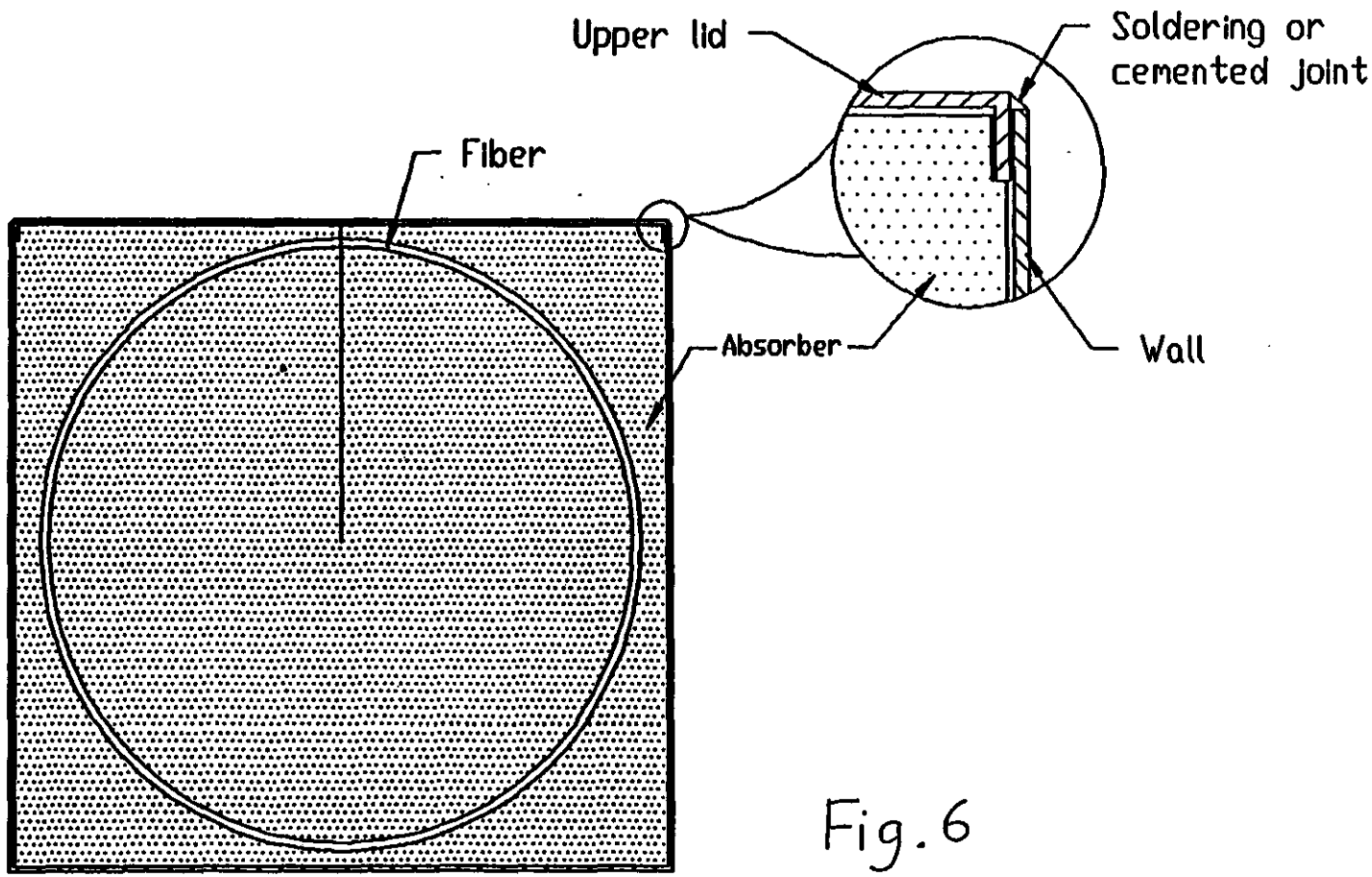

Fig. 6

Fiber routing in e-m LS calorimeter

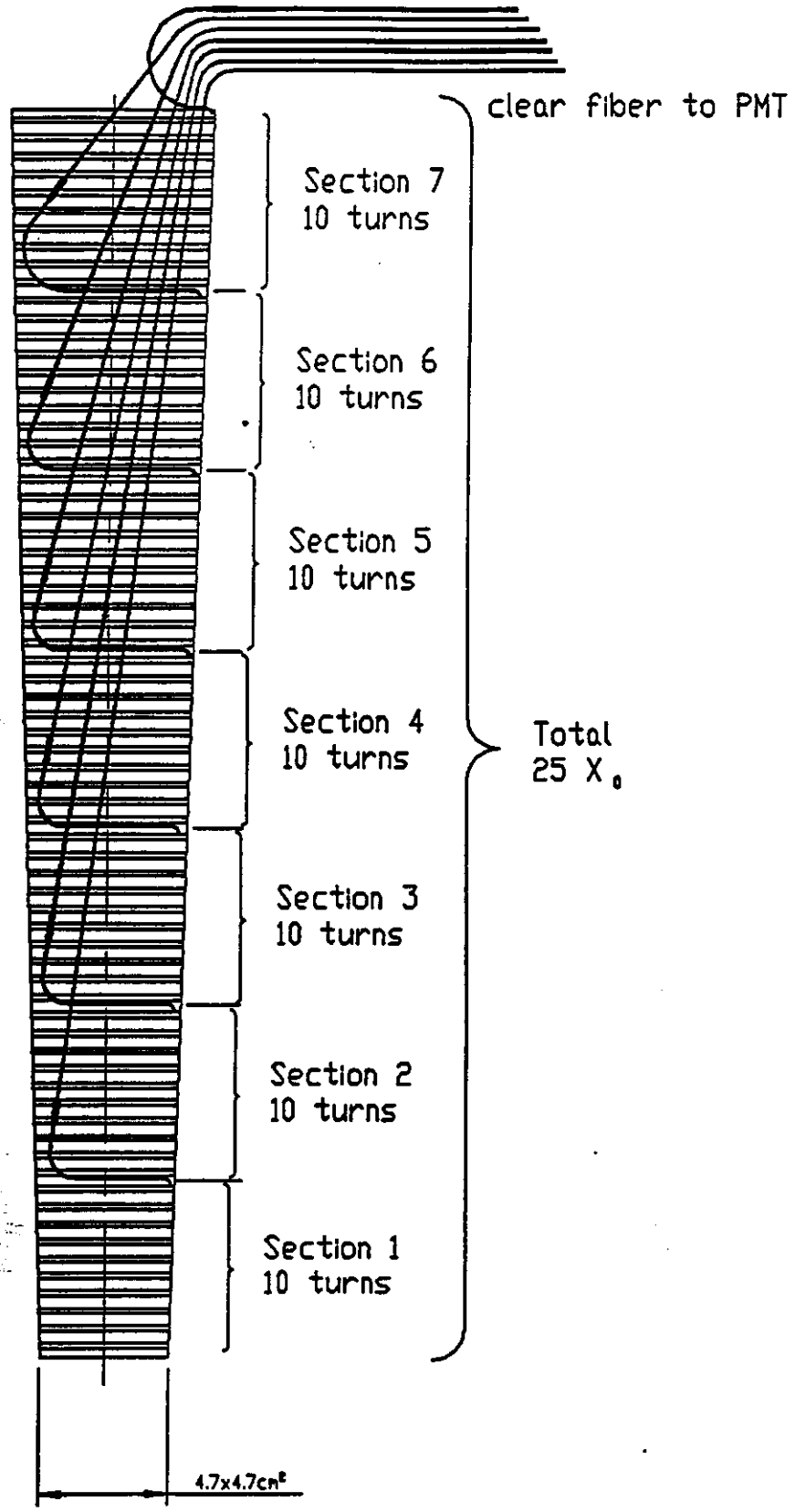

Fig. 7

e-m calorimeter assembly

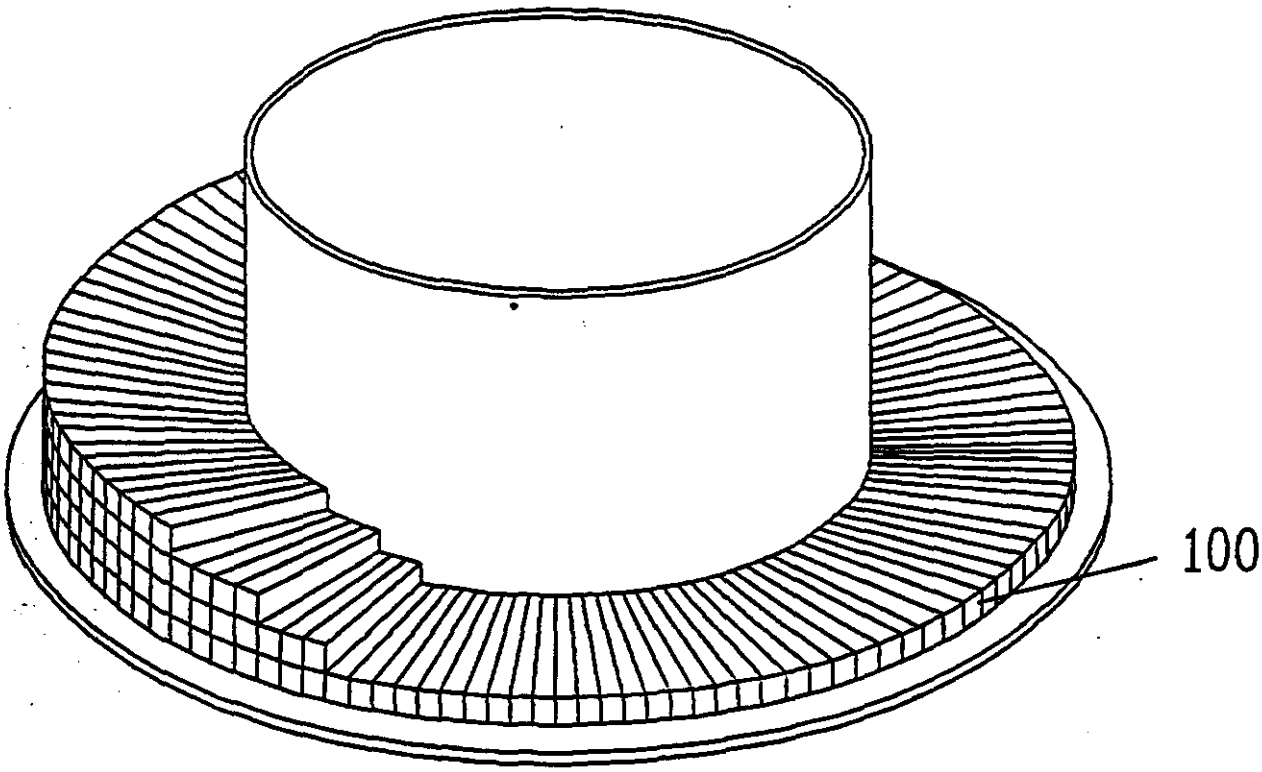

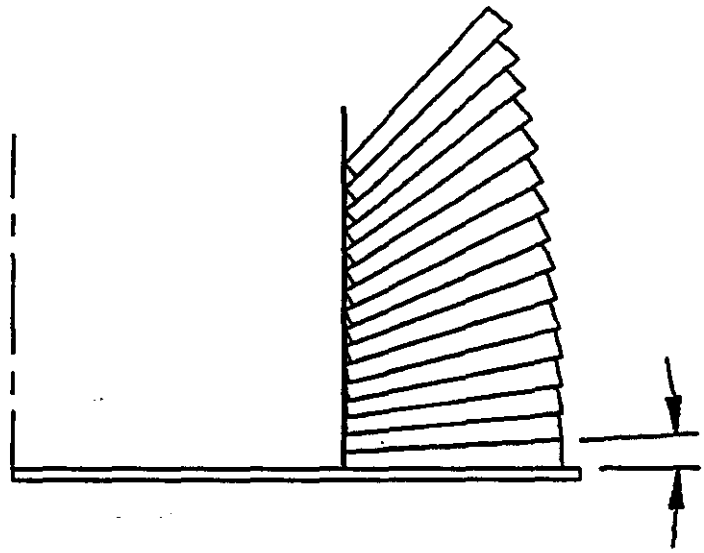

$\Delta\varphi = \Delta\eta = 0.063$

Fig. 8

Fiber Joint Tests

BCF 91 (WLS), BCF 98 (Clear) dia. 1mm

LED (550 nm) - fiber joint - Si photodiode

Transmission measurement - ~ 4% accur.

test #	fiber	ends	coupling	measured
1.	whole CF	polished	-	1.05
2.	whole WLS	polished	-	1.07
3.	WLS-WLS	polished	OC	1.07
4.	WLS-WLS	polished	OC	1.07,1.03
5.	CF - CF	polished	OC	1.06
6.	CF - CF	polished	OC	1.05
7.	WLS-WLS	polished	air	1.00
8.	whole CF	wire cut	-	1.05
9.	whole WLS	wire cut	-	1.02
10.	WLS-WLS	wire cut	OC	1.05
11.	WLS-WLS	wire cut	OC	1.05
12.	CF - CF	wire cut	OC	1.04
13.	CF - CF	wire cut	OC	1.05
14.	WLS-WLS	wire cut	air	1.00

Within 4 % error

there is no light reduction

Fig 9

Question 1c) If tail-catchers are included in the baseline hadronic design, has it been shown that longitudinal fluctuations in high-energy showers into this region will not give an unacceptably large constant term (both from decreased sampling and from lack of compensation in the tails)?

Answer 1c) :

Tail catcher in the hadron calorimeter dies not affect the electromagnetic resolution of the fine sampling EM calorimeter.

The influence of the tail catcher on the hadronic resolution was studied with GEANT Monte Carlo code for Pb/LS hadron calorimer with BaF2 in front [1]. Hadronic jets with energies 50-1000 GeV were simulated for this purpose. Produced particles went through a full hadron calorimeter detector simulation chain [GHEISHA-GEANT] and were analysed with hit-cluster-jet algorithms
[2]. In energy sums (BaF2+fine+catcher) proper weights were applied which optimized the overall energy resolution. Resolution vs jet energy values were obtained abd the extracted resolution dependences are in the following Table.

Monte Carlo LS HC resolution
BaF_2 in front, 5 mm LS gap

Fine sampling sect.	Tail catcher	Scint. nonunif. 5%	B (%)	A (%)
2 cm Pb x 90	—	—	1.1 ± 0.2	66± 3
2 cm Pb x 90	—	+	1.2 ± 0.2	66± 3
2 cm Pb x 38	4 cm Pb x 20	+	1.7 ± 0.2	59± 3
2 cm Pb x 78	—	+	1.6 ± 0.2	63± 3

References :

[1] L* LoI to SSCL, November 1990
[2] L3 software

Question 1d) If the geometry is not projective, has it been demonstrated that energy sums will give a sufficiently small constant term after allowing for lateral shower fluctuations?

Answer 1d) :

In the L3 uranium/gas calorimeter the readout in phi-view is projective and in theta view it is non-projective (brick-wall-like). Both views are interlaced in the calorimeter module and have independent readout. Distributions of theta and phi energy sums were compared and no difference in resolution was observed with and without the BGO em part added.

Both in the BaF2 (or LXe) and in the proposed LS fine-sampling EM calorimeter projective geometry is used.

Question 2. What are the measured effects of radiation damage on light yield and transmission in all stages of the optical path, for system components configured as in the baseline design? Are all readout, reflector, and support materials known to be sufficiently radiation hard? Are both scintillator plate and WLS fiber materials known to be radiation hard both alone and in combination, and have they been tested as in the proposed mechanical configuration? If WLS fibers, reflectors, or other materials have variations after radiation damage (and/or long-term mechanical stress), there may be an unacceptable constant term because of longitudinal shower fluctuations.

Answer :

Radiation damage to most commonly-used liquid scintillators have been studied in [1] In this work measurements showed that after a dose of 5 MRad (Co-60 source, dose rate 0.033 MRad/h) the scintillation yield of BC-517L and BC-517H scintillators is reduced by 35-40%. 5 MRad radiation level corresponds, for the hadron calorimeter environment (behind the EM section at angles ~6 degree in the GEM detector layout), to 5 years of SSC operation at a luminosity of 10**33. The major advantage of liquid scintillator is that it can be replaced if radiation damage occurs. In practice, during calorimeter operation, the liquid can be renewd/purified within a few days. We propose to install a radioactive source in the liquid scintillator cell (one per readout channel), such that the sensitivity of the cell can be permanently monitored (short run every 1-2 days) with an accuracy of ~1%. In this case the sensitivity degradation (down to 30-50%) can be restored by appropriate corrective action.

Radiation resistance of the whole liquid scintillator system is defined by the radiation properties of the plastic fibers, because, unlike the liquid scintillator proper, they can not be replaced in the assembled calorimeter. We have performed initial radiation damage studies of WLS and clear plastic fibers at ORNL. A Co-60 source of 0.377 MRad/hour was used to irradiate wave length shifting (BCF-91, Bicron) and clear (BCF-98, Bicron) plastic fibers in air and in BC-517P liquid scintillator. Samples of 1mm diameter and 1 m length were used for these tests. Before and after irradiation the transmission of fibers was measured relative to non-irradiated reference samples. For transmission measurements we have used a green LED (550 nm emission) and a CdS photodiode. Results of these measurements are shown in Figure 10. Test samples were extracted from the irradiator and measured several times during the total exposure dose of 26 MRad. At such high radiation dose rates (~10**4 times higher than relevant SSC dose rate) the transmission for clear fibers drops to zero after ~10 MRad. Samples irradiated to a total dose of 26 MRad were annealed at room temperature and were found to have restored their transmission level od 95% after ~100 hours. WLS fibers became opaque at much lower doses of 5-6 MRad and recover to a 50% transmission level after a total dose of 26 MRad in 250 hours at room temperature (the test was discontinued after 250 hours). We did not notice any essential difference between fibers being irradiated and annealed in air or in liquid scintillator. For the WLS fibers irradiated to the total dose of 6.4 Mrad the transmission recovered to the 90% level after ~100 hours (Figure 11). These initial measurements indicate that clear and WLS fibers can withstand doses of 5-10 MRad (and maybe even higher)

with a possible transmission degradation level of few percent, provided that annealing took place. We plan to perform a detailed program of radiation damage measurements with WLS and clear plastic fibers with dose rates which are factors 10 and 100 lower than those in the present test and then extrapolate these results to the SSC dose rate. We also plan to irradiate a totaly functional cell which most closely represents the base-line design (cell size, WLS fiber type, transport fiber length etc.) and measure the light yiel vs radiation dose, dose rate and annealing.

Radiation stability of a reflector was studied with Bicron BC-622A TiO2 paint which is prepared from cross-linked polyurethane resin. A sample of reflecting paint was irradiated to a 9 Mrad total dose over an 8 hour period using the LLNL Co-60 gamma ray source. The sample was a 2" x 2" x 1/2" piece of aluminum painted with three coats of Bicron BC622A. The irradiation was performed by enclosing the sample in an air-filled water-tight canister and lowering the canister into the Co-60 source, which is under 20 feet of water. The sample was then tested for differences in its diffuse scattering properties when compared with unirradiated samples. The result is shown in Figure 12. The effect of irradiation of reflection paint is small; it was checked via Monte Carlo [MC] simulation that the light yield of the liquid scintillator cell does not change more than 1% due to this variation.

One of the advantages of a longitudinaly-segmented calorimeter is that the effect of the longitudinal radiation damage is significantly attenuated by independent calibration of longitudinal segments. For cost constaraints reasons we have choosen a longitudinal segmentation of 6 in the HC , though more frequent readout segmentation would be more desirable.

References

[1] S.Majewski et. al, IEEE Trans.Nucl.Science,37(1990)513

1 m fiber (Ø 1 mm) transmission vs irradiation dose and annealing time

Measured with green LED (550 nm) and Si photodiode (relative to reference nonirradiated fiber)

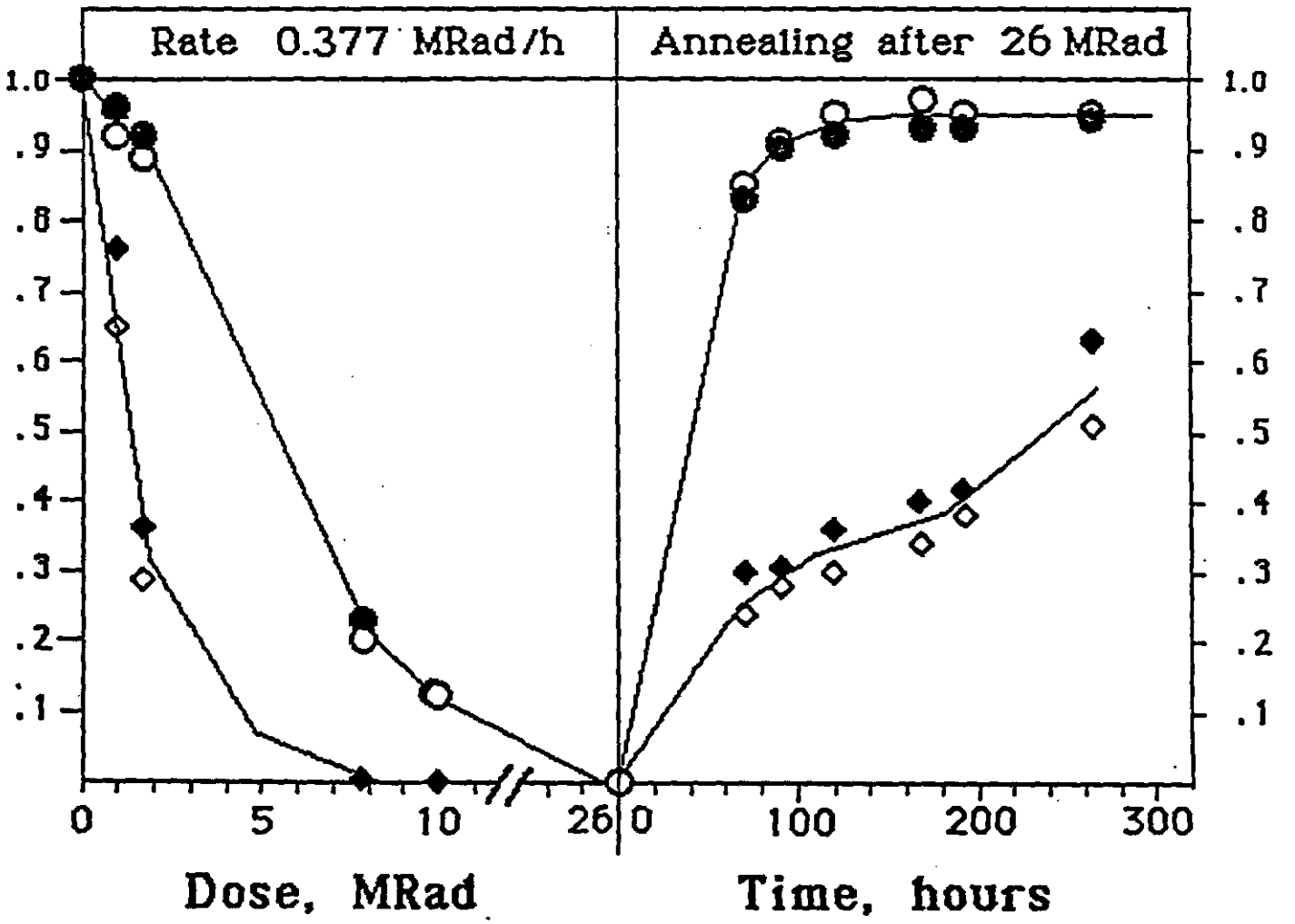

○ Clear BCF - 98

● Clear BCF - 98 + LS (BC517P)

◇ WLSF BCF - 91

◆ WLSF BCF - 91 + LS (BC517P)

Fig. 10

1 m fiber (Ø1mm) transmission

vs irradiation dose and annealing time

measured with green LED (550 nm) and Si photodiode (relative to reference nonirradiated fiber)

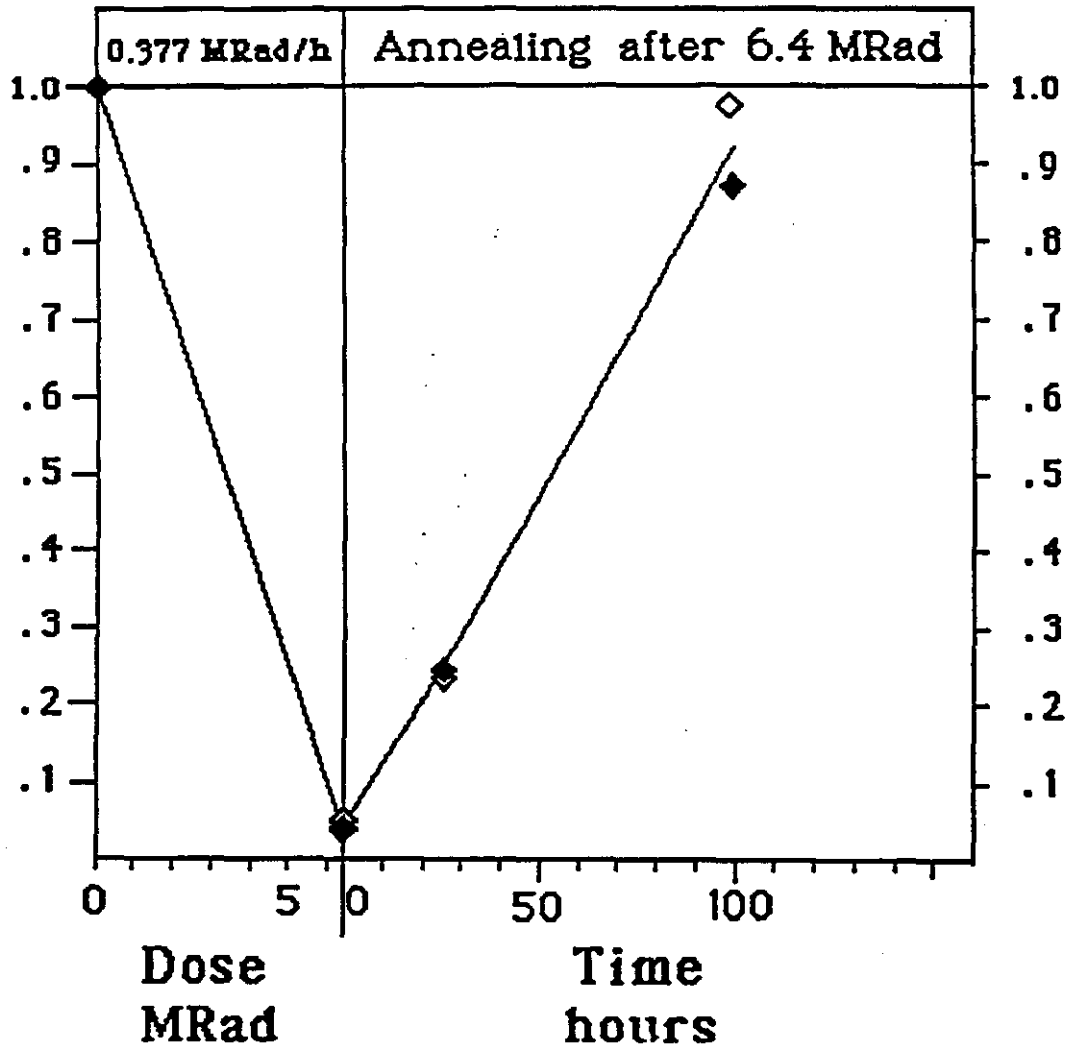

◇ WLSF BCF - 91

◆ WLSF BCF - 91 + LS (BC-517P)

Fig. 11

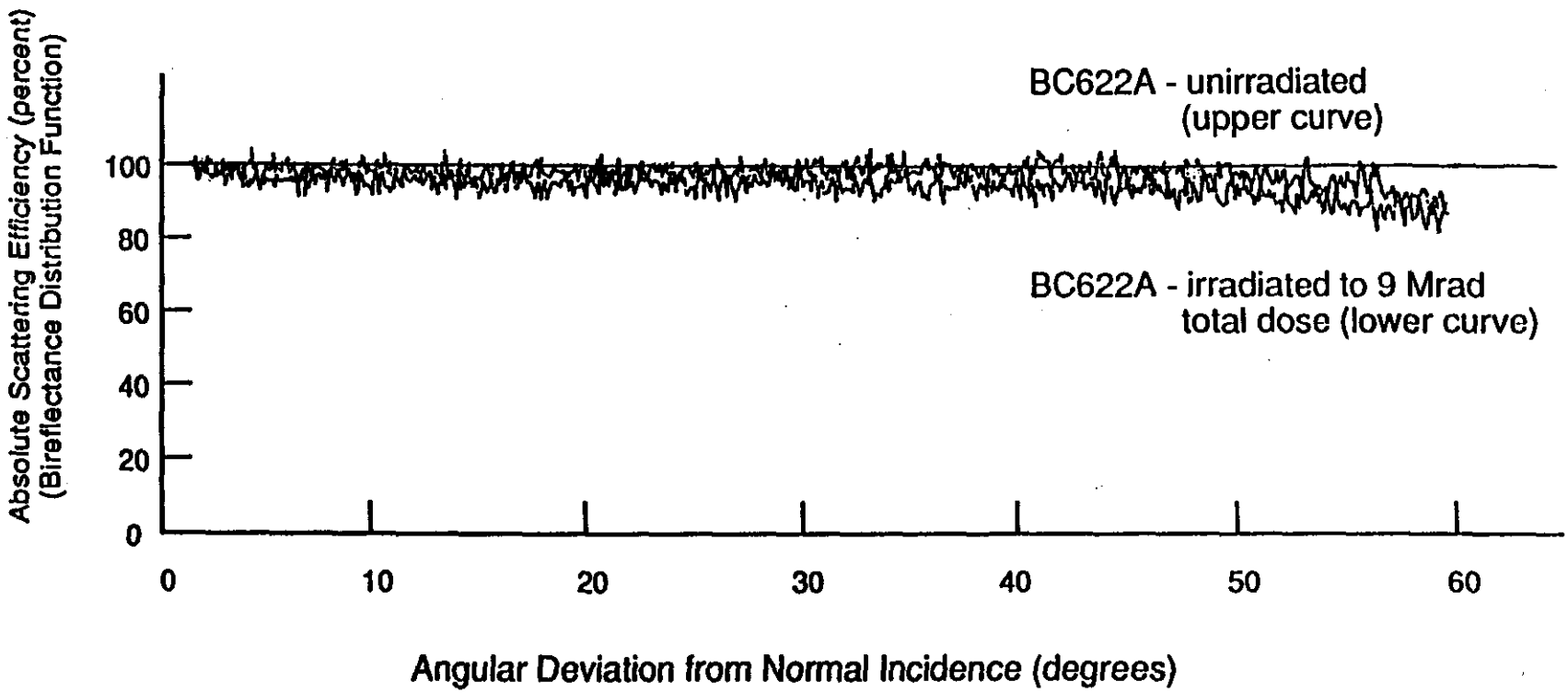
Absolute Scattering Efficiency (percent)
(Bireflectance Distribution Function)
100
80
60
40
20
0
0
10
20
30
40
50
60
Angular Deviation from Normal Incidence (degrees)
BC622A - unirradiated
(upper curve)
BC622A - irradiated to 9 Mrad
total dose (lower curve)

Fig. 12

Question 3. Is the cost of the calibration system included in the baseline? How can tower calibration be sampled in depth to assess radiation damage in situ? Can the full optical path, and the full dynamic range and linearity of the system be tested with the proposed calibration system?

Answer :

We are going to implement in every calorimeter cell the radioactive source with small activity (counting rate < 1 KHz/cell). For this purpose we have examined several source candidates U-235 (1% U-234), Sr-90, and Ru-106. Self-triggered spectra for these sources are shown in Figure 13. The uranium source is a 0.25 mm thick Ti disk of 5 mm diameter with high-vacuum electron-beam-evaporated enriched U-235. It provides a counting rate in the cell of about 900 Hz. This source was produced at ORNL. The cost of such source for several thousend units is estimated to be $0.25/source. This cost could be reduced by a factor two for quantities required for a full calorimeter. Total cost of calibration system (120K) is included in the modified cost analysis for LS HC.

Calibration with radioactive sources allows to monitor optical path and elecrtonics channel stabilitiy. To test the full dynamic range and linearity one can use a laser light source connected an with optical fiber distribution system to every photomultiplier. The cost of green laser, light distribution system and of the 3200 fibers are not included in the cost estimate.

As far as radiation damage correction to the resolutionis concerned, the usefulness of the calibration is proportional to the number of longitudinal segments. In addition to other important improvements the increase in the number of longitudinal segments will improve the longivity of the whole hadron (as well as electromagnetic) calorimeter.

Question 4. What provision has been made for the rejection of pi-zero gammas from unfavorable jet fragmentations? (The rate of such fragmentation has large uncertainties, and these may dominate the Higgs --> gamma gamma background.)

Answer :

The flexibility of the proposed LS EM calorimeter design is such that it is possible to reduce the transverse size of the EM towers at the expense of number of readout channels. With a front size of 3x3 cm3 the towers are similar to the BaF2 towers with respect to two-shower separation (Moliere radius for Pb/Sci~ 4cm).

If a preshower option is choosen to cope with pi-zeros, the size of EM towers can be compromized.

The present LS EM calorimeter design has 7 longitudinal optical sections which are grouped into 3 for readout. The front transverse size's 4.7x4.7 cm2, the total thikness is 25 X0, and the number of readout channels is 22K.

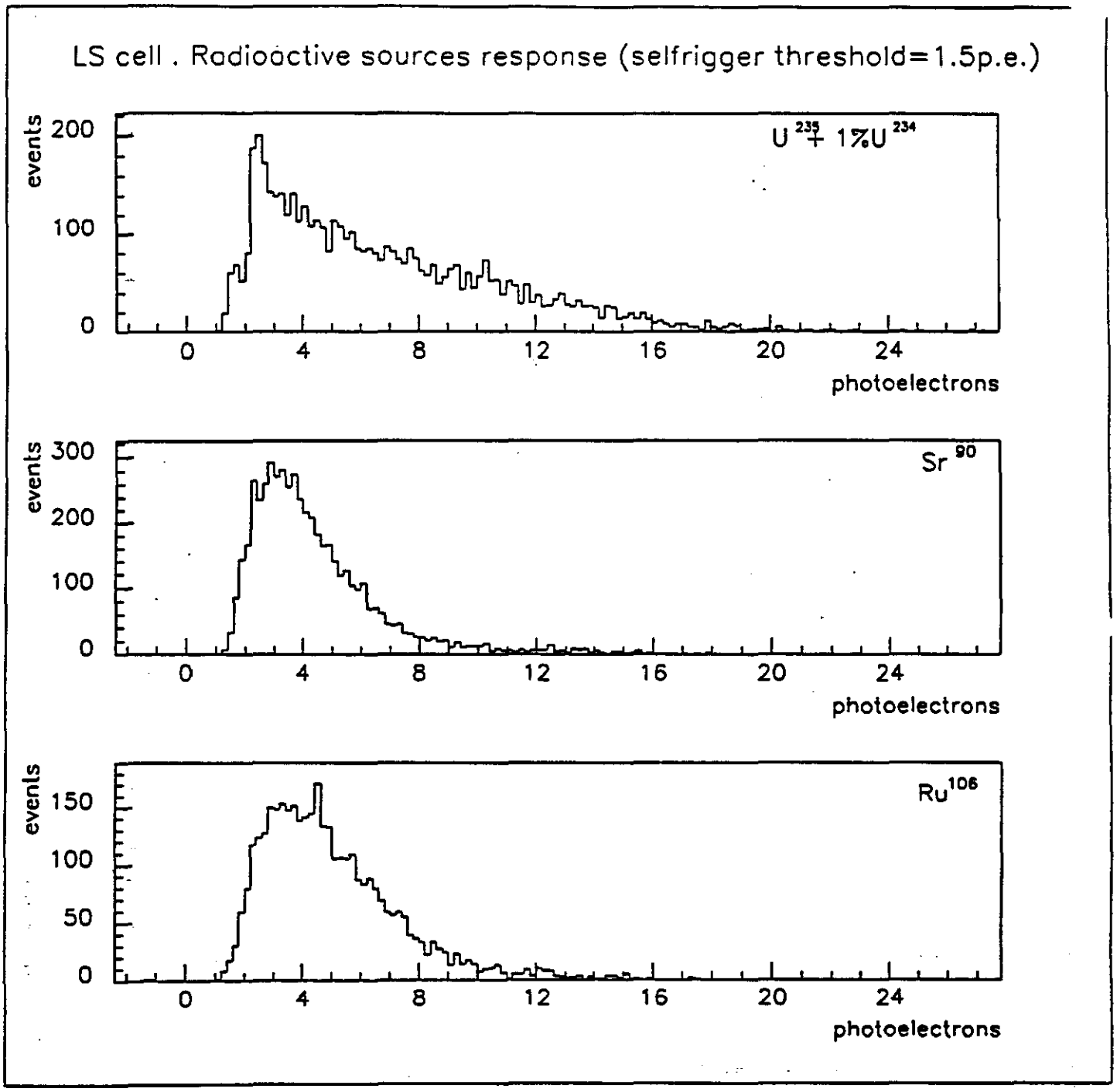
LS cell . Radioactive sources response (selfrigger threshold=1.5p.e.)
events
200
100
0
U 235 + 1%U 234
0
4
8
12
16
20
24
photoelectrons
events
300
200
100
0
Sr 90
0
4
8
12
16
20
24
photoelectrons
events
150
100
50
0
Ru106
0
4
8
12
16
20
24
photoelectrons

Fig. 13

Question 5. What is the constant term in the energy resolution for hadrons which one measures when the last 5 interaction lengths contain a non-compensating ratio of lead to scintillator? Precisely how has this been simulated, and when will it be measured?

Answer :

This question was considered in the answer 1c). The results mentioned above were obtained by Monte Carlo simulation. The conclusion is that the tail catcher in the base line design [1] doesn't degrade the resolution. It is interesting that a similar conclusion was obtained in the ZEUS calorimeter prototype tests where the tail catcher is made of noncompensating iron[2].

According to existing LS R&D plans the test of the single base line design module is scheduled for the end of 1992.

References

[1] L* LoI to SSCL, Novemebr 1990
[2] I.Kudla et al., NIM A300(1991)480-492

Question 6. What is the effect of the support structure and non-projective geometry on the hermetic containment of EM and hadronic shower energy? What are the consequences for missing Et measurement? How confident may we be that future changes in the mechanical design will not require significant increases in system size and further reductions in hermeticity?

Answer :

The proposed LS EM calorimeter has a projective geometry. The effect of structural supports for the EM calorimeter was considered in the answer to question 1b). Structural supports in BaF2 (or LXe) and hadron Pb/LS calorimeter are non-projective. The effect of structural supports on the response uniformity was discussed in detail in the answer to Question 1(3) of Howard Gordon. The key point is that in front of HC there is an EM calorimeter without any dead zones (or at least with dead zones that are not allined with the structural supports of the hadron calorimeter).

Missing Et measurements will not suffer from hadron calorimeter structural elements, provided that a calibration of response vs impact point exists. This calibration is needed for any type of calorimeter.

The confidence in the mechanical design is a function of the time this design was in development. The proposed LS hadron calorimeter design was derived from the existing design of the operating L3 calorimeter and was developed during almost two years first for the L* and later for the GEM detectors.

SILICON PAD CALORIMETRY

Answers to Questions
September 4, 1991

Summary

The major reason for wide spread use of silicon in precision electronic devices is that they are based on the planar technology developed over the last 40 years for precision spatial and energy measurements as well as integrated circuits. The full power of this technology, applied to pad detectors leads to detectors with unique advantages when applied to calorimetry particularly under the SSC conditions of speed and radiation.

A brief recount of the characteristics of silicon pad detectors for calorimeters which makes them the technique of choice from a technical viewpoint is given here.

1. With respect to speed silicon is rivaled only by scintillator systems. Typical transit times are 7 ns for electrons and 21 ns for holes for detectors of 300 μ thickness at room temperature. Lower temperature operation increases mobility and reduces transit times.

2. Silicon detectors, like those utilizing ionizing liquids, have an absolute gain of 1 which leads to the possibility of adequate calibration by a pulsed electronics system alone. However, silicon wafers with one electron-hole pair per 3.6 eV of deposited energy produce considerably more charge then other ionization devices.

3. Silicon is exceedingly linear with respect to deposited energy. Electron hole recombination is not important even for fission fragments. There is no loss of

energy sensitivity (saturation) for highly ionizing particles similar to that found in cryogenic and warm liquids. Dynamic range is limited only by electronics circuitry and not by the detector proper.

4. Transverse segmentation. Here silicon is limited only by channel count. Necessary segmentation at any level can be attained.

5. Longitudinal segmentation is similar to other sampling techniques and is dominated by channel count considerations. However, it should be pointed out that if good electromagnetic resolution is desired requiring, e.g., 1/4 X_0 sampling, silicon distinctly provides the most compact technology due to the thin layers of sampling media (3 mm/layer in present prototype and which can be reduced).

6. Silicon detectors operate well at room temperature. However, operation at -20°C decreases the leakage current by a factor of 100 and reduces the associated noise. Additionally, the electron mobility is increased by a few percent at this temperature for a given over voltage. Such operation can be attained by conductive cooling of absorber plates without the necessity of immersing detectors in a bath, although silicon detectors operate well under those conditions as well. In any case, cryogenic dead material and the complexity of cryogenic operation is avoided.

7. Silicon detectors show no sensitivity to magnetic fields nor does the signal processing circuitry.

8. Monitoring of electronics gain by radioactive sources is possible by simple, inexpensive deposition of radioactive sources on the surface of silicon. A 5

MeV alpha from, e.g., 231 Am represents the equivalent of about 50 MIP. It may be possible therefore to dispense with electronics calibration and use MIP and alphas.

9. Because silicon detector arrays can be easily attached to absorber plates, mechanical construction is particularly simple. Structural frames are almost unaffected by sampling medium and are determined primarily by mechanical and electrical considerations and cooling requirements. A silicon sampling calorimeter permits more compact construction than any other calorimetry option.

10. Only low voltages (100-200 volts) are required to bias silicon detectors which markedly simplifies design considerations and construction tolerances.

11. Radiation damage in silicon has perhaps been more extensively studied than in any other material. Much of these have concentrated on integrated circuits however. On the other hand, only recently have results become available from a number of groups in this country and in Europe on neutron damage in calorimeter type pad detectors. These results confirm that effects of leakage current increase, radiation damage induced resistivity changes and conductivity type changes, as well as charge trapping effects, are tolerable in such detectors up to levels of 5×10^{14} - 1×10^{15} n/cm^2 corresponding to 10-year SSC doses. Silicon detectors have been shown to be considerably less sensitive to electromagnetic energy damage which does not pose a threat in the SSC environment. It should be pointed out that silicon detectors are not subject to poisoning from the release of radiation induced byproducts from the absorber or other materials in the calorimeter. Parenthetically, it should be noted that these same radiation damage studies indicate that the picture for tracking

devices is not so optimistic and that for silicon drift chambers even more grim. Major work on radiation hardness may be required before satisfactory performance of these devices may be assured.

(12) Uniformity of sampling is controlled by thickness control of silicon pads which can be maintained to 1-3% level without special precautions. It is difficult to imagine how such precision can be maintained with other techniques, e.g., 100-200 μ in a 4 mm gap in a liquid ionization calorimeter.

(13) Compensation is achieved in silicon hadron calorimeters through the mechanism of suppression of electron signal as originally pointed out by Brau. Since silicon is sensitive to low energy electrons, high Z material located near the silicon surface gives a strong signal from low energy electrons which can be suppressed by interposing lower Z material. Many combinations are possible for tuning but SICAPO collaboration has reported that a 1:4 thickness ratio of Pb:Brass yields $e/\pi \approx 1$. An advantage of this mechanism is its speed. Since there is no dependence on collection of signal from delayed neutrons, the e/π ratio does not depend on the long collection times associated with the neutron signal.

SILICON PADS

Generic Questions

(1) How can silicon EM calorimeters expect to achieve a 7% stochastic term in the energy resolution and at most a 1/2% constant term in the energy resolution in the face of the following difficulties?

We support strongly the ultra high resolution option for electromagnetic

calorimetry, either BaF_2 or Liquid Xenon. The main reasons for this position are that (1) there is great intrinsic merit in achieving highest resolution possible for reasons of possible new physics and (2) that all sampling calorimeters in our opinion find the range of $7\%/\sqrt{E}$ with 0.5% stochastic term on the ragged edge of their theoretically predicted practical capability. The risks associated with trying to build a calorimeter whose performance might end up as substandard are very great. It seems that effective 1/4 X_0 sampling is required at least and possibly considerably less to ensure that resolution is achieved. This necessitates many layers of thin absorber, e.g., 100 layers of 1.5 mm Pb for a 25 X_0 calorimeter resulting in structural difficulties, increased size, loss of compensation property, greatly increased channel count, etc. However, given these caveats we believe that silicon is extremely competitive with other techniques of sampling calorimetry. The expected source of stochastic term is in uniformity of variations of absorber and sampling medium thickness, lateral and longitudinal variations in detector location, radiation induced variations in detector response, dead areas or those with reduced sensitivity or resolution and electronic cross talk. In each of these areas silicon is competitive and in most is superior to other sampling techniques although it probably cannot compete with ultra high resolution technology.

Specifically questions asked were:

(a) What is the best stochastic term that has been measured with a silicon module in a test beam, using only a fast shaped pulse within a narrow gate? How does the measured resolution vary with energy, and is there a linear or quadratic constant term? How does the measured resolution vary with pulse rate?

Answer. To our knowledge there have been no direct measurements of the stochastic term for any silicon EM calorimeter to date with fast (or slow) electronics. This is a major goal of the subsystem collaboration for silicon. We are nearing completion of a 28 X_0, EM calorimeter module (0.35 m x 0.35 m with a 1 X_0 sampling, 5 level longitudinal segmentation and expected resolution of 18-20%/$\sqrt{E}$) equipped with fast ASIC preamplifiers designed and built by ORNL. Construction was delayed considerably by the availability of FY 91 funds (released in June of this year). However, we plan to test this module at Fermilab this Fall with moderately fast (shaping time 50 ns) discrete component summing and shaping amplifiers built at ORNL. A total of ten shifts of parasitic beam use are available to us courtesy of Jim Russ of Carnegie Mellon and Fermilab E-682. Every attempt will be made to measure the stochastic term this Fall although the schedule is very tight.

The superb linearity of silicon and absence of saturation lead us to expect with some confidence linearity of energy response and well behaved resolution. For high repetition rates, we have designed, fabricated and done preliminary testing on an analog storage chip. The key components of this chip include a double correlated sampler circuit to remove preamp baseline from signal before storage and an analog memory array using straightforward voltage write charge read arrangements. This circuitry will not be used in the beam test.

(b) What uniformity has been measured when varying the incident position of particles across the front face of a module? What mechanical tolerances are required in order to preserve the required resolution against variations in incident position and longitudinal shower fluctuations? Is there an engineering design which can meet these tolerances and/or achieve this resolution in the endcap region, as well as the barrel?

Answer. These lateral effects will also be examined in the beam test at high energies. We have measured low energy results from a beam test of the SLD Luminosity Monitor using electrons of 2-7 GeV as well as muons. Two types of effects are observed. There is an almost imperceptible loss of energy when shower overlaps pad boundaries on a single wafer. In addition, edge losses in the approximately 1 mm insensitive area at the edge of a wafer can contribute up to 5% effect on energy measurement. From measured shower position, both of these effects are correctable to required accuracy.

It is straightforward to position wafers on circuit boards equipped with precision alignment pins to accuracy of 125 microns and to locate detectors on boards with comparable accuracy.

(c) If tail-catchers are included in baseline hadronic design, has it been shown that longitudinal fluctuations in high-energy showers into this region will not give an unacceptably large constant term?

Answer. We have not done a systematic study of any proposed tail-catcher designs nor have we proposed any. The question of quantitative degradation of resolution due to such a device requires careful study in the context of a particular design.

(d) Are all readout and support materials known to be sufficiently radiation hard? If preamplifiers or other materials have variations after radiation damage (or long-term mechanical stress), there may be an unacceptable constant term because of longitudinal shower fluctuations.

Answer. For silicon we claim:

- (1) Absorber O.K.
- (2) Circuit board O.K.

► (3) Wire bonds and/or conducting epoxy not yet thoroughly tested but probably O.K. No problem observed in single exposure of 3×10^{14} n/cm^2 (delivered in one month) for conducting epoxy bond.

► (4) Major problem is expected to be with preamplifiers themselves which are embedded in the detector and attached to silicon detectors. They are manufactured in the Harris radiation hard bipolar process. For these preamplifiers, gain to first order is set by feedback capacitor which is extremely radiation hard. Feedback resistor is less radiation hard but should be quite satisfactory at levels discussed. Major difficulty is with active components where deterioration could cause loss of forward loop gain which in turn would affect pulse shape and make second order change in gain. The active components have been tested to 5 m rad. These measurements have been used in the design of circuits (base bias stability, etc.). Tests on complete amplifiers are in progress.

(2) What is the effect of pile-up at 10^{33} and 10^{34} luminosity on EM and hadronic energy resolution? On the efficiency with which one can select electrons within a 0.7 rapidity unit isolation cone (5 GeV threshold)?

Effects of pile-up and thermal noise are minimal for a silicon system due to short signal duration and shaping time. Effects on resolution due to pile-up noise have been discussed by Radecka[1] and indicate noise levels to be expected. A

---

[1] SSC Detector Development R and D at BNL, BNL 52244, p. 91.

detailed analysis has not been carried out for silicon but Radecka reports pile-up noise in the ratio 3.3 (Liq A)/2.0 (scintillating plates or fibers)/1.6 (BaF_2, LXe, Silicon) at $L = 10^{33}$.

(3) Is the cost of the calibration system included in the baseline? How can a single pulse ramp simulate signals from different parts of a single module, with possibly different gap spacing, etc.?

Tests are underway at Tennessee to examine the feasibility of a calibration system consisting of alpha sources applied directly to the surface of a detector. A test of this scheme for calibration of the full EM calorimeter will be attempted in the upcoming test beam run. A full pulsed calibration system for electronic gain monitoring has not yet been costed but should be similar to the Liq A system with the exception of extra preamplifiers.

(4) What provision has been made for the rejection of pi-zero gammas from unfavorable jet fragmentations? (The rate of such fragmentation has large uncertainties, and these may dominate the Higgs → gamma gamma background.)

We remark here only that silicon calorimeters can be constructed with small Moliere radii which can improve position and overlap resolution given necessary transverse segmentation of calorimeters and can serve as useful adjunct to a preradiator which is most likely required by any sampling EM calorimeter. Pointing information is also available from the longitudinal segmentation. Silicon should be comparable to other techniques in this regard.

(5) What is the constant term in the energy resolution for hadrons which one measures after 10 interaction lengths of non-compensating silicon--with how many longitudinal segments? Precisely how has this been simulated, and when will it be measured?

A full simulation using GEANT-GHEISHA for a silicon hadron calorimeter located immediately behind BaF_2 EM calorimeter yields jet resolution of $50\%/\sqrt{E}$ + 4% as described in its L* EOI. Measurement of single particle hadron resolutions at high energy for full silicon calorimeter with various combinations of absorber is being carried out by SICAPO collaboration. Results will be available in about one year but with slow electronics. These results will, of course, not address the question of silicon hadron calorimeter behind "ultra high resolution" electromagnetic calorimeter unless such a direct test is made.

(6) How confident can we be that silicon will in fact be available in the quantities required at the anticipated cost? Are there alternative sources in case of disruption of supply from the primary source, and what would be the cost from such an alternative source?

This question is by far the most serious one with respect to use of silicon in SSC calorimetry, and if not answered satisfactorily will preclude further consideration of silicon.

We have explored commercial sources of silicon detectors and techniques for cost reduction in the detector manufacture process. While there exist numerous possibilities for cost reduction, in view of the undemanding criteria for calorimeter detectors compared to elegant properties of commercial detectors these savings do not look promising enough to warrant further consideration at this time.

We have been engaged in discussions for over 1.5 years with groups in the Soviet Union interested in use of silicon detectors at SSC, LHC and elsewhere.

A powerful consortium has been formed in the Soviet Union under the direction of Igor Golutvin of Dubna. Involved are 10 universities and institutes in

various republics of the Soviet Union with expertise in every aspect of silicon detector research from radiation damage to diagnostic of impurities in super pure materials. A major industrial participant is the ELMA corporation, one of the largest and most powerful semiconductor manufacturers in the Soviet Union. This consortium has proposed to provide silicon detectors sufficient to equip a large hadron calorimeter (up to 5×10^7 cm^2 of silicon detectors) to SSC detector in exchange for certain items of equipment necessary to produce high resistivity silicon ingots.

Initially SSC (or LHC) detector collaboration would provide the equipment at a cost of several million dollars and would also provide commercial high resistivity ingots for detector construction. While the negotiations are not complete, it is conceivable that silicon detectors for a hadron calorimeter could be provided under this arrangment for perhaps 15×10^6 dollars. As a test, the silicon subsystem collaboration has agreed to provide new silicon to ELMA sufficient for production of 16 m^2 of detectors. This is sufficient to construct a full hadron calorimeter prototype module as described in the L* EOI and LOI and the SECC subsystem proposal. The Soviet group has also entered into a similar agreement with INFN to provide silicon for the SICAPO collaboration calorimeter.

We see no likely economical source of silicon detectors if the Soviets should prove unable to deliver as promised, but estimate the probability for success as high enough to justify continued effort in this direction.

BRIEF ANSWERS TO QUESTIONS FROM SCINTILLATING FIBER SUBGROUP TO GEM CALORIMETER GROUP MEMBERS

GEM Calorimeter Working Group Meeting
SSC Laboratory
September 5, 1991

We have attempted to answer most of these questions in a consistent and relatively comprehensive manner in the document entitled "Baseline Scintillating Fiber Electromagnetic and Hadronic Calorimeters for GEM". In the interest of convenience, brief specific responses to the questions will be given below. When necessary, a more detailed description in the "Baseline" document will be referred to. Support documentation (NIM articles, etc.) are referenced in that report.

FROM HOWARD GORDON ---

1. *Describe the effects of radiation damage that will be acceptable in the barrel and end calorimeters. What will be the time scale for improving the radiation resistance of the fibers?*

This is discussed in the "Radiation Damage Effects" section. If we define "acceptable" damage as that which gives less than 1% degradation to the energy resolution at 10 GeV, and if we ignore annealing effects, currently available fibers will survive up to 7 MRad integrated dose (while losing 10% of their light production). This is 2-3 SSC Years at eta = 3 in the EM calorimeter. Projecting from the current rate of scintillating fiber development, it is not unreasonable to expect fibers with an order of magnitude greater radiation damage resistance to be available within 2 years.

2. *Describe the calibration procedure.*

This is discussed in the "Calibration System" section. It consists of absolute calibration with Z0 and other physics signals, relative and temporal calibration with laser-based light flashers, and depth calibrations with radioactive sources.

It is similar in concept to the system employed in CDF, which controlled scintillator-based EM calorimetry to better than 1% over many months.

3. *Describe the details of the design of the EM modules and the hadronic modules for the projective geometry. What is the timescale for finalizing these designs? Consider the possibility that the casting solution does not work.*

This is discussed in detail within in the "Baseline Design Parameters" section. The timescale for finalizing these designs would be to settle upon a single fully-engineered working design for the technical proposal (a little over one year), followed by another year or two of final design and fabrication experience before commencing bulk production. Our prototype construction and test beam plans are consistent with this timescale. If the casting solution does not work, we will continue to build upon SPACAL and JETSET experience with laminated construction (we may do so in any case, but will decide this issue one way or the other before the technical proposal is due).

4. *How do you deal with finite attenuation length which leads to non gaussian tails on the energy distribution on the high side?*

This is discussed in the section on "Anticipated Performance of Baseline Design". Briefly stated, we will eliminate cladding light (by painting the cladding near the PMT if necessary). If necessary, we will mirror fiber ends away from the PMT to increase the effective attenuation length, as has been done for SPACAL. Also, this effect is much smaller for jets than for single hadrons. Note that a 4 meter attenuation length is sufficient to eliminate this effect, and this is available by filtering light from existing fibers without requiring mirrored ends.

5. *What is the long term chemical stability of the fibers?*

There is no evidence for long-term chemical instability of the fluors currently used in rad-hard fibers, but this question merits further study. It will require careful tests as we move toward a choice of fiber for the experiment (in particular, tests at elevated temperatures).

Common questions for systems using phototubes:

*Ensuring the phototubes response over the 10**5 dynamic range, finding acceptable time dispersion at 10**5 dynamic range; dealing with the tails from large pulses that are commonly found in phototubes.*

This is discussed in the "Readout System" section. A dynamic range of >10^4 is readily available from magnetic field insensitive mesh-dynode PMTs. We could operate at 10^3 gain in a 1 Tesla field (requiring fewer dynode stages) followed by pulse shaping and a fast preamplifier, etc. Mesh dynode PMTs can be linear to1% to 500 mA peak anode current with the proper base and readout electronics (they dc not acquire long tails until they are saturated). Our alternative design path of hybrid photomultipliers has demonstrated linearity over a 10^5 dynamic range, but requires further development for operation in the magnetic field.

FROM HARVEY NEWMAN:

A. *What is the best expected EM resolution (statistical and constant term) that can be achieved with 0.5 mm fibers, based on GEANT or EGS simulations, and SPACAL results of Paar et al. ?*

This is discussed in the "Anticipated Performance" section. Recent SPACAL preliminary results for beam tests of 0.5mm fibers and 20% fiber packing fraction give10.4%/√E + 0.4%. JETSET beam tests give a sampling term of 6.3%/√E at low energy (1 GeV). It is not unreasonable to expect that increasing the fiber packing fraction within the SPACAL device should allow it to meet or exceed the sampling resolution of the JETSET device, while preserving or improving its constant term.

B. *If one goes to a 40% fiber fraction, what is the cost increase for the EM section ?*

The system which was costed as our baseline was similar to JETSET, with 50% fibers, 35% lead, and 15% epoxy by volume. Fabrication costs dominate.

C. *Since the Moliere radius is relatively small, will many towers be used in the EM section, or a preradiator ? In either case,*

what are the associated added costs ?

The Moliere radius of JETSET style modules, and of our baseline design, is 3.5 cm. This is very similar to BaF2, so that with 0.5 x 0.5 lateral segmentation energy-sharing can be used to give about 3mm/$\sqrt{E}$ shower centroid position resolution.

D. How are the systematics of the following effects removed, to avoid increasing the constant term ?:

(1) Uniformity of the scintillating fibers -- how non-uniform are they from lot to lot, and how difficult is it to make this average out to the required level of well-below 0.5% ?

As discussed in the "Performance" section, fiber-to-fiber light yield variations of 15% are acceptable within an EM module using either 0.5mm fibers (SPACAL)or 50% fiber packing (JETSET and our baseline). This is readily met with current fiber manufacturing techniques (current variations <10%).

(2) Uniformity of attenuation length in the clear fibers to which the scintillating fibers are bonded -- (same detailed question as in (1) above) ?

The requirement for fiber-to-fiber uniformity in the hadronic section (the only place where our baseline uses splices) is again no more than 15%, assuming that the variations are random. This last assumption is currently untested, but we have the back-up of fiber bundling for readout as in SPACAL.

(3) Light loss across the bond between the scintillating fiber and the clear fiber, where the best uniformity from bond to bond achieved so far is 4%.

See above.

E. In the presence of radiation damage to the plastic scintillating fiber, particularly near the shower maximum, what is the best

overall resolution (not just a fitted constant term) that can be obtained:

This is discussed in detail in the "Radiation Damage Effects" section, and is summarized below:

(1) As a function of dose, or as a function of Eta, at 10^33 in the EM Section ?

For the EM calorimeter, light yield loss is more important than attenuation losses. With current fibers, discounting annealing, a 7 MRad dose causes 10% light yield loss at EM shower max. This results in a 1% degradation in EM resolution at 10 GeV (the effect decreases logarithmically with energy, falling to 0.5% at 100 GeV). At 10^33 luminosity, eta = 3 towers would survive for about 2 years, while eta=2.4 towers would survive 10 years.

(2) At 10^34 in the EM Section?

Again, we consider fiber to be damaged at >7 MRad integrated dose. At 10^34 luminosity, eta=2.4 towers would survive 1 year, while eta=1.6 (barrel) towers would survive 10 years. Improvement in fiber radiation hardness (annealing effects and increased fluor concentrations at the expense of attenuation length, for example) may well extend the 10-year 10^34 region to the endcaps.

(3) Same questions as (1) and (2) for an HCAL section, behind another (non-SciFi) EM calorimeter?

Less work has been done on modelling radiation damage to hadronic scintillating fiber calorimetry than for electromagnetic. For hadronic SciFi, attenuation-length effects predominate. We estimate a dose as low as 0.2 MRad at hadronic shower maximum may cause sufficient attenuation through a 2m fiber to degrade the resolution by 1% at high energy, but this has not been properly tested. For 10^33, this means 3 years at eta=3, while for 10^34 there is damage at eta>2.5 in 1 year, and at eta>1.6 in 10 years.

(4) Referring to Para and Green's Paper Fermilab-FN-565 ("Radiation damage, Calibration and Depth Segmentation

in Calorimeters", May 1991), Figure 8, how do you propose to maintain the energy resolution in the EM section, or the HCAL section?

Para and Green propose roughly reconstructing the starting point for EM showers within the calorimeter to correct event-by-event for longitudinal shower fluctuations in and out of a damaged region. We do not propose to employ this method. We believe that the fiber light loss can be kept to less than 10% at shower maximum (f = 0.1 on their plots), in which case such measures are not necessary.

(5) If a full longitudinal monitoring scheme is proposed to correct each tower for the degradation of the resolution in the presence of radiation damage, as is suggested by the Green and Para paper:

(a) how would it be implemented?
This is discussed in the "Calibration System" section. It is essentially the CDF method, with Cs137 sources at the end of long wires which are inserted into hollow tubes and moved under stepper-motor control. This would be implemented in 4 towers at each eta, relying upon azimuthal symmetry of the radiation dose to carry this calibration to the rest. It is primarily used for gain and linearity corrections.

(b) How would a calibration be carried out, and how long would it take ?
CDF calibrates 48 modules in less than an hour, and we could calibrate 500 in an hour through parallel operation.

(c) What resolution could be foreseen to be maintained in practice ?
1% has been achieved in CDF.

(d) How much would such a system cost ?
It was included in our baseline cost estimate.

FROM MIN CHEN:

0. Show schematic design of pointing geometry with photo-tubes.

This is discussed in the "Baseline Design Parameters" section, although Fig. 1 is old and incorrect. The offset-pointing geometry is offset in azimuth rather than eta, pointing toward a circle around the beamline so that there is always at least 3 degrees between the incident electron direction and the fiber axes. Phototubes for the EM section are located before the hadron calorimeter, according to a scheme very similar to that outlined for Barium Flouride in the EOI. Phototube axes would be aligned with the field either through prism/mirrors (baseline) or with curved fiber bundles.

Stability of photo-tubes?

This is discussed in the sections on "Calibration" and "Readout". Long-term gain stability of PMTs of a few percent is typical, and with a light-flasher monitoring system correction to better than 1% has been achieved in CDF, UA2, and other large experiments.

1. 7. Show the mechanical tolerance needed for a ring of counter to fit in azmuthal direction.
i.e. What is the space needed in order for 200cm long cells to fit in rings in Phi and self supported?

As discussed under "Baseline Design Parameters" we have made provision for (and have costed) a "fitting tower" for each azimuthal ring of towers, to correct for tolerance build-up. This tower is individually cast to fit (the inside of the mold is shimmed, the preform adjusted, and the sheath modified). The support structure for towers and rings is mechanically connected to the hadronic tower "sheath", which consists of a 1/16" stainless steel sheet (or equivalent mesh) as recommended by Draper Laboratories; this sheath is cast with the tower as a unit. The entire mechanical integrity of the module is calculated from the sheath and support structure, neglecting the strength of the lead alloy and fiber matrix entirely.

2. Demonstrate a single cell which is radiation hard.

As discussed in the "Radiation Damage Effects" section, a radiation hardness of less than 10% light reduction for 7 MRad integrated dose has been achieved with existing fibers. A test calorimeter (using an earlier generation of fibers) was irradiated to the 3 MRad level and had its resolution degraded from 6.3%$\sqrt{E}$ to 8.8%$\sqrt{E}$ (D. Hertzog et. al., Proceedings of the Workshop on Radiation Hardness of Plastic Scintillator, March 1990, Florida State University, Kurtis Johnson ed.) This module in fact recovered much of this resolution through annealing over a time period of 2 months (D. Hertzog, private communication). In GEM, a 3 MRad dose is that received in 1 SSC year at eta=3; a 3 MRad dose is received at eta=2.3 in 10 SSC years. Fibers with improved radiation hardness are being developed.

3. Show how to calibrate the scintillation of the cells when different parts are radiation damaged to different and unknown degrees.

This is discussed in the "Calibration System" section. It is essentially the CDF method, with Cs137 sources at the end of long wires which are inserted into hollow tubes and moved under stepper-motor control. This would be implemented in 4 towers at each eta, relying upon azimuthal symmetry of the radiation dose to carry this calibration to the rest. It is primarily used for gain and linearity corrections.

B. Show how an RFQ would fit in GEM without destroying the 4 pi geometry of the calorimeters and muon detectors and still be properly focused.

We do not explicitly propose to use an RFQ, although calibration of front-surface system response combined with longitudinal attenuation methods could be used for attenuation corrections.

C. RFQ gammas stop at the very front of the cells. How could this be used to calibrate crystals damaged at different depth?

It can't.

4. Is the test array of crystals radiation hard, workable in a B field (up to 2 tesla) with realistic walls?

The prototype currently being constructed is built with radiation-hard fibers and other materials and will be radiation-tested after beam testing. It will also be constructed with realistic sheath walls. The initial readout will not be magnetic field-insensitive because of cost constraints, but we will test individual mesh dynode PMTs in magnetic fields to ascertain their performance.

5. How to measure the linearity of phototubes in a magnetic field up to 2 Tesla over a dynamic range of 10^5?

As discussed in the "Calibration Systems" section, we propose a Nitrogen laser-based flasher system with variable attenuation capable of delivering light signals over 10^5 dynamic range. Such a system is currently implemented in the MACRO experiment, among others.

6. Without longitudinal segments, can the cells distinguish two photon spaced say 10 cm off center (due to beam size spread) and 3 degree tilted in phi? Also how much is the determination of impact point for such off center photons deteriorated?

This would require a pre-radiator in our system, as it would for BaF2 or other systems which have not included longitudinal segmentation in their costed baseline design. We can determine the shower centroid to within 3mm/$\sqrt{E}$, as discussed in the "Anticipated Performance" section.

FROM SSCINTCAL:

1) How can scintillating fiber EM calorimeters expect to achieve a 7% stochastic term in the energy resolution and at most a 1/2% constant term in the energy resolution in the face of the following difficulties?

Below we summarize the "Anticipated Performance" section of the Baseline Design Report in response to a series of questions.

a) What is the best stochastic term that has been measured with a fiber calorimeter in a test beam, and what was the light yield and pulse shape?

As discussed in the "Anticipated Performance" section of the Baseline Design Report, $6.3\%/\sqrt{E}$ has been measured for an EM prototype, and $10.4\%/\sqrt{E} + 0.4\%$ in a compensating EM prototype. A resolution of $28\%/\sqrt{E} + 2.5\%$ has been measured with a hadronic prototype, and the origin of the constant term is well-understood and should be limited to 1% in future prototypes. The light yield, after all filtering and light losses during collection, was >1000 pe/GeV for an EM prototype and >400 pe/GeV for a hadronic prototype. EM pulses had a full width of 18ns, while hadronic pulses had a full width of 21-27 ns for 150 GeV pions.

Have beam tests been performed on both electromagnetic and hadronic fiber calorimeter prototypes?

Yes, and more beam tests are ongoing through December 1991 at FNAL.

How does the measured resolution vary with energy, and is there a linear or quadratic constant term?

The data scales as sampling fluctuations ($x/\sqrt{E}$) up to high energies, where a linear constant term fits the data slightly better than a quadratic term.

b) What uniformity has been measured when varying the incident position of particles across the front face of a module, and across module boundaries?

There is a measured < 3% variation with incident position within 2mm of the boundary of 10cm x 10cm modules. Elsewhere the prototype is uniform to <1%.

What mechanical tolerances in fiber positioning are required in order to preserve the required resolution against variations in incident position and longitudinal shower fluctuations?

Fibers randomly offset within "tubes" (or grooves) 40% larger than the fiber radius give less than 1% density variations when averaged over the size of an EM shower.

What are the requirements on fiber light attenuation so that longitudinal fluctuations not give rise to too large of a constant term?

The effective attenuation length (after filtering) must be >400 cm in the hadronic section and must be >50 cm in the EM section to keep from degrading the energy resolution by more than 1% at 10 GeV, and by more than 0.5% at 100 GeV (the effect decreases logarithmically with energy).

Is there an engineering design which can meet these tolerances and/or achieve this resolution in the endcap region, as well as the barrel?

Yes, and we are currently building prototypes according to this design for beam testing by December, 1991 at FNAL.

What are the tolerances on the coupling uniformity across optical joints, and of the photodetector uniformity across its face?

Fiber-to-fiber light variations within the EM section must be held to <15%, with slightly larger variations allowable in the hadronic section (this is determined by the number of fibers participating in the core of the shower). By using a light mixer, <20% RMS variations in PMT response across its surface (with a coherence length of 5 cm) give <1% variations in the detector sensitivity to electron incident position.

2) What are the measured effects of radiation damage on light yield and transmission in all stages of the optical path, for system components configured as in the baseline design? Are all readout, reflector,

and support materials known to be sufficiently radiation hard? What are the consequences of radiation damage for the constant term in electromagnetic and hadronic resolution?

These issues are discussed in detail in the "Radiation Damage Effects" section of the Baseline Design Report. With current fibers, ignoring annealing, a 7 MRad dose causes 10% light yield loss at EM shower max. This results in a 1% degradation in EM resolution at 10 GeV (the effect decreases logarithmically with energy, falling to 0.5% at 100 GeV). At 10^33 luminosity, eta = 3 towers would survive for about 2 years, while eta=2.4 towers would survive 10 years. Clear fibers and acrylic light pipes are rad-hard and are well away from EM shower maximum (where most of the damage is concentrated).

3) Is the cost of the calibration system included in the baseline? How can tower calibration be sampled in depth to assess radiation damage in situ? Can the full optical path, and the full dynamic range and linearity of the system be tested with the proposed calibration system?

The calibration system is included in the baseline cost estimate, and is described in the "Calibration System" section of the Baseline Design Report. It consists of absolute calibration with Z0 and other physics signals, relative and temporal calibration with laser-based light flashers, and depth calibrations with radioactive sources. It is similar in concept to the system employed in CDF, which controlled scintillator-based calorimetry to better than 1% over many months.

Longitudinal fiber response is monitored with Cs137 sources at the end of long wires which are inserted into hollow tubes and moved under stepper-motor control. This would be implemented in 4 towers at each eta, relying upon azimuthal symmetry of the radiation dose to carry this calibration to the rest. It is primarily used for gain and linearity corrections.

For PMT gain and linearity monitoring, we propose a Nitrogen laser-based flasher system with variable attenuation capable of delivering light signals over 10^5 dynamic range. Such a system is currently implemented in the MACRO experiment, among others.

4) What provision has been made for the rejection of pi-zero gammas from unfavorable jet fragmentations? (The rate of such fragmentation has large uncertainties, and these may dominate the Higgs --> gamma gamma background.)

Our design is compatible with a pre-radiator designed for this purpose. Other detectors not employing longitudinal segmentation combined with fine centroi capabilities in the EM will similarly require a pre-radiator to achieve this backgroun suppression.

5) What is the effect of the support structure and non-projective geometry on the hermetic containment of EM and hadronic shower energy? What are the consequences for missing Et measurement? How confident may we be that future changes in the mechanical design will not require significant increases in system size and further reductions in hermeticity?

EM cells are tapered pyramids with <1/16" stainless steel supports about the last 8 o radiation lengths, while hadronic towers are tapered pyramids with 1/16" stainless walls along their entire length. The steel walls are connected to a stainless steel sup structure similar to that designed for EMPACT/TEXAS (see E/T EOI) and discussed b our "Baseline Design Parameters" section. The effects of this support structure on missing Et measurement are negligible, and very small effects on the resolution coul be removed by corrections based on shower centroid position measurements. The mechanical stability of the system with sheaths has been tested through mechanical component testing and finite element analysis. Changes in the device design will if anything result in size reduction, through the introduction of more dense absorber (lead shot) if this proves feasible in full-scale prototype tests.

6) How confident can we be that scintillating fiber will in fact be available in the quantities required at the anticipated cost? Are there alternative sources in case of disruption of supply from the primary source, and what would be the cost from such an alternative source?

Fibers are currently available from 3 vendors, with a fourth potential vendor expressing interest. We have received quotes from 2 major vendors which differ by less than 10%. The market is quite competitive, and barriers to entry are low. Each vendor has expressed their capability to deliver the entire quantity of fibers needed for a hadronic calorimeter within 2 years at the cost quoted.

FROM FRANK PAIGE:

SIMULATION PARAMETERS NEEDED
Physics Simulation Group

HADRON CALORIMETRY

Delta(E)/E = 50%/sqrt(E) + 3% (if behind BaF2)
Delta(E)/E = 50%/sqrt(E) + 1% (if behind SciFi)
Delta(E) from pileup and noise = 30 MeV
Delta(eta), Delta(phi) vs. eta = .10 x .10
[time determination] = 25ns full width, 40ns integration
[longitudinal segmentation] = None
[cracks, dead material] = No projective cracks, minimal dead material

EM CALORIMETRY

Delta(E)/E = 6.5%/sqrt(E) + 0.5%
Delta(E) from pileup and noise = 30 MeV
Delta(eta), Delta(phi) vs. eta = .05 x .05
[time determination] = 15ns full width, 30ns integration
[longitudinal segmentation] = None
[cracks, dead material] = No projective cracks, minimal dead material

Shower centroid determination = 3mm/sqrt(E)
Shower pointing to vertex = 5mm with preradiator

FROM BILL BUGG:

I think it is important to compare the calorimetry options on a roughly eq ual basis. We should ask each of the techniques (liq.sci,spacal, LA, Si) to present a specific design for say a 25X0 EM cal followed by a 9Lambda hadron hadron cal with delta eta=delta phi=0.05. and starting at R= 75 cm.

These are our baseline parameters.

Information provided should include
1) Dimensions (radii)with details as to cell structure including walls electron ics, mechanical support structure.

For our baseline, the EM inner radius is 75 cm, and the calorimeter + readout require less than 75cm. The Hadronic inner radius is 150cm, and 9 interaction lengths + readout requires about 2.2 meters. EM cells are tapered pyramids with <1/16" stainless steel supports about the last 8 of 25 radiation lengths, while hadronic towers are tapered pyramids with 1/16" stainless steel walls along their entire length. The steel walls are connected to a stainless steel support structure similar to that designed for EMPACT/TEXAS (see E/T EOI) and discussed briefly in our "Baseline Design Parameters" section. The electronics is similarly based on our E/T design, developed in consultation with LeCroy Inc.

2)resolution,EM, Hadronic(for jets)

HADRON CALORIMETRY
Delta(E)/E = 50%/sqrt(E) + 3% (if behind BaF2)
Delta(E)/E = 50%/sqrt(E) + 1% (if behind SciFi)

EM CALORIMETRY
Delta(E)/E = 6.5%/sqrt(E) + 0.5%
Shower centroid determination = 3mm/sqrt(E)

3)electronics readout plan and layout
This is discussed in the "Readout Systems" section of our baseline design report

4) compensation,

A scintillating fiber EM calorimeter followed by a scintillating fiber hadronic calorimeter is the only system which has been proposed for GEM which can provide a compensated response ($e/h - 1 < 0.1$) throughout the entire calorimeter and provide high-precision electromagnetic resolution ($<6\%/\sqrt{E} + 0.5\%$ with 0.5mm fibers and 50% packing).

speed,

[Hadronic] = 25ns full width, 40ns integration
[Electromagnetic] = 15ns full width, 30ns integration

HV,magnetic field characteristics, cooling ,

Mesh dynode PMTs use <2500V, operate in up to 2 T field, and dissipate <1 Watt each.

radiation damage

Discussed in detail in the "Radiation Damage Effects" section of our Baseline Design Report.

Similar design should be presented for 9 lambda hadron calorimeter located behind BaF2 or Liquid Xenon. Results should be presented on jet resolutions, compensation etc.

Our system was designed to operate behind compensating precision EM scintillating fiber calorimetry, but the same design could be placed behind BaF2 or LXe.

In general the presentations should not only address the questions asked but should be a concise summary of the technique and permit comparison of the techniques as applied to a calorimeter of specific size and characteristics.

This is the goal of our Baseline Design Report.

BASELINE DESIGN REPORT

SCINTILLATING FIBER ELECTROMAGNETIC AND HADRONIC CALORIMETERS FOR GEM

GEM Calorimetry Workshop
SSC Laboratory
September 6, 1991

We have prepared a baseline conceptual design and cost estimate of scintillating fiber electromagnetic and hadronic calorimeters for the GEM detector. Our design has been primarily based on the demonstrated performance of existing prototypes, and our cost estimate reflects our experience in constructing these prototypes. Existing technology has been assumed in most cases, using measured performance parameters from existing devices, although we anticipate future improvements in technology and consequent future improvements in device performance. Similarly, we have not claimed significant economies of scale in the manufacture of large numbers of calorimeter modules, but rather have simply scaled manufacturing techniques which were appropriate to the construction of a relatively small number of prototypes. In light of the substantial contingencies which were nonetheless associated with both fabrication and raw materials costs, we believe that the resulting cost estimates were very conservative indeed.

Whenever possible, we have based our design and our cost estimates on demonstrated methods and measured prototype performance. We believe that the collaboration should be leery of untested designs and large extrapolations away from proven experience with existing devices.

1) BASELINE DESIGN PARAMETERS

Our baseline design consists of independent electromagnetic and hadron sections, which although well-matched for physics purposes may be considered as separate systems. Their readouts are completely separate, and either system might be chosen without requiring the other. There are, however, many common elements in their design and performance requirements, and one might expect considerable overlap in R & D and engineering between the two systems. This would particularly be the case for materials (fiber) optimization, calibration systems, optics, and readout systems. Overlap on fabrication, assembly, and systems engineering might be less substantial, but would still be significant.

For the electromagnetic calorimeter, we consider a baseline device based closely on the scintillating fiber calorimeter which has been constructed for the JETSET experiment[1] . Although this is only one possible scintillating fiber EM configuration, it has the virtue of having had 400 modules produced and used in an operating experiment (which was useful for our costing exercise). As in the JETSET device, we would construct laminates of grooved lead sheets and 1mm diameter scintillating fibers bound together with epoxy, with volume fractions of 50%, 35%, and 15% for lead, fiber, and epoxy respectively. The density of this device is 4.6 g/cm^3, its radiation length is 1.61 cm, and its Moliere radius is 3.5 cm. We assume 25 radiation lengths starting 75 cm from the beamline center. Tapered projective towers would be produced by machining rectangular blocks, again as in JETSET. Pyramidal towers of 0.05 η x 0.05 ϕ will have an offset pointing geometry (Fig. 1), with fiber axes pointing tangent to a cylinder with radius 10cm about the beam axis.

---

[1] *A High-Resolution Lead/Scintillating Fiber Electromagnetic Calorimeter* , D. W. Hertzog *et. al.* , NIM A294 (1990) 446.

In JETSET, a conically-shaped acrylic lightguide is glued to the rear face of each tower, with the trapezoidal shape of the rear face of the tower being cut into the guide (Fig. 2). The precise geometry of acrylic lightguides for a GEM EM calorimeter will be determined through further desig and testing, but our baseline design calls for a 15cm JETSET tapered section followed by a 10cm hexagonal light mixer as used with SPACAL. A mirrored surface at the junction between these two light pipes would permit alignment c the readout PMT axis with the magnetic field to within 45 degrees. An alternative to this design would be to bundle fibers at the output as in SPACAL. and to align the bundle with the magnetic field. The output of the light mixer would then be coupled to a photosensor, which in our baseline is an R1840 Hamamatsu 10-stage mesh dynode PMT. Assuming a total length for the PMT and base of 10cm, the total length of the EM is 75cm at $\eta = 0$.

Although the above baseline design is consistent and very similar to the JETSET device, it is not yet optimized for GEM. The measured and anticipated performance of the baseline EM device is described in the next section, and we believe it is well-matched to GEM requirements and physics goals. Nonetheless, we believe there is significant room for optimization by varying the fiber spacing and diameter. At the opposite end of this parameter space from JETSET (which has a sampling resolution of $6\% / \sqrt{E}$), SPACAL collaborators have recently achieved $10.4\% / \sqrt{E} + 0.4\%$ resolution with a device containing 20% 0.5mm diameter fibers (very near to a compensating mixture of lead and plastic).[2] Since the cost of the system is not dominated by the fiber, and since the assumed fabrication technique (JETSET's fiber "loom") is not very sensitive to fiber size or number, we believe there is significant room for optimization within the constraints of the baseline system cost estimate (Fig. 3).

---

[2]Preliminary result from August 1991 CERN beam tests.

For the hadronic calorimeter, we consider a baseline device based largely on the SPACAL prototypes[3]. This design was somewhat modified for the EMPACT/TEXAS letter of intent, and a prototype of the current GEM baseline design is under construction as part of the SSCintCAL subsystem effort. In particular, our baseline consists of cast projective towers containing 17% 2mm diameter fibers by volume, while the SPACAL tests were conducted on laminated hexagonal modules containing 20% 1mm diameter fibers. The GEM modifications to the SPACAL design are intended to preserve most of the physics performance of the SPACAL device while introducing substantial cost savings. These savings were estimated at 20% in an EMPACT/TEXAS cost study, and we have preserved these modifications in our baseline design despite additional experience with laminated construction since that time, in lieu of a second detailed cost study.

Our baseline design consists of 10 active interaction lengths at $\eta = 0$, although we believe this is excessive (we prefer 9 hadronic interaction lengths, in addition to 1 EM interaction length -- we were, however, informed that we were required to cost for 10 active interaction lengths). With 17% fibers cast within a low melting-point eutectic alloy, the density of this device is 8.0 g/cm^3, and its interaction length is 22.6 cm. Tapered projective towers would be cast 4 at a time in 1-tonne units, surrounded by a 1/16" thick stainless steel sheath to provide mechanical support (although we believe the eutectic alloy/fiber mixture may be self-supporting without sheaths, we treat it as having no structural strength in the baseline design). As with the EM calorimeter, we assume

---

[3]*Results of Prototype Studies for a Spaghetti Calorimeter* , D. Acosta *et. al.* , NIM A294 (1990) 193.

Electron, Pion and Multiparticle Detection with a Lead/Scintillating Fiber Calorimeter , D. Acosta *et. al.* , NIM A302 (1991) 36.

Localizing Particles Showering in a Spaghetti Calorimeter , D. Acosta *et. al.* , NIM A294 (1990) 193.

On Muon Production and other Leakage Aspects of Pion Absorption in a Lead/Scintillating-Fiber Calorimeter , D. Acosta *et. al.* , CERN-PPE/91-107, 24 June 1991.

pyramidal towers of 0.05 η x 0.05 ϕ with an offset pointing geometry, with fiber axes pointing tangent to a cylinder with radius 10cm about the beam axis. Both ends of the cast pyramidal towers would be machined prior to their assembly into rings as in the EMPACT/TEXAS LOI design, and provision has been made for a special "fitted tower" at each η in both the EM and hadronic systems to allow for tolerance build-up during assembly.

Although it is possible to bundle fibers at the readout end (as in SPACAL) for readout through a concentrating lightguide/mixer as in the EM section, this is not our baseline readout method. Instead, we mass-splice from 2mm scintillating fibers to 1mm clear fibers and bundle these, as in the EMPACT/TEXAS LOI design and the SSCintCAL GEM prototype. As discussed in the next section, the splice-to-splice uniformity required is only 15%, and prototypes of this mass fiber splice have been constructed. The fiber bundle would be bent to permit alignment of the readout PMT axis with the magnetic field to within 45 degrees, then epoxied to an acrylic light mixer. As in the EM section, the output of the light mixer would then be coupled to a R1840 Hamamatsu 10-stage mesh dynode PMT.

Our assembly plan and mechical support structure have been adapted for GEM from our earlier EMPACT/TEXAS design. Each hadronic supertower (4 physics towers) is surrounded by a 1/16" stainless steel sheath which mechanically couples each supertower to the outer support structure independently. The EM towers are internally self-supporting and have thin sheaths for only about their last 8 radiation lengths. The hermeticity loss from non-projective cracks at the boundaries between calorimeters is thus negligible for both the EM and hadronic calorimeters. For both the EM and hadron calorimeters, towers are bolted together by their sheaths into "superrings", with specially machined "fitting towers" providing for tolerance build-up in both η and ϕ (Fig. 4). The load from the EM and hadron calorimeters will be transferred separately to the septum and the support tube (or directly to support struts rather than the latter, which may not be needed in this design).

Although we advocate a pre-radiator for the rejection of π^0 gammas, this device should be considered independently from the EM scintillating fiber calorimeter. The performance which we anticipate from our baseline design (detailed below) has been assessed in the absence of such a

pre-radiator. The EM calorimeter performance is, however, consistent with the existence of such a pre-radiator, as has been demonstrated by SPACAL. With a 1.7 X_0 thick preshower detector, adding the preshower signals to the calorimeter signals event-by-event gave 0.1% improvement in the resolution at 5 GeV. This is as expected, since the preshower detector absorbs at maximum only a few percent of the shower energy, and only the fluctuations in these few percent affect the energy resolution. The linearity of response is however improved at low energy when the energy loss in the pre-shower detector is taken into account.

2) ANTICIPATED PERFORMANCE OF BASELINE DESIGN

We have based our performance expectations on experience with existing prototypes in most cases, and on detailed computer simulations when extrapolating from these prototypes to baseline variants. For the scintillating fiber electromagnetic calorimeter, we use test beam results obtained with JETSET and SPACAL calorimeters, while for the hadronic calorimeter we rely exclusively on SPACAL experience. While these prototypes are not precisely those proposed for GEM (the JETSET modules were designed for lower energies, while the first SPACAL prototypes provided both electromagnetic and hadronic measurements and were not projective), they form a sound basis from which to extrapolate to the GEM design. Within the SSCintCAL SSC Subsystem effort, we have constructed and are testing a number of variants on these designs: projective SPACAL, high-resolution (finer sampling) SPACAL, high-energy projective JETSET, and cast course-sampling hadronic modules. These last two are identical to our present baseline design, and this year's beam test data (from both CERN and FNAL) on all the new variants will be rapidly incorporated into our evolving design.

For the JETSET experiment, electromagnetic calorimeters were constructed from laminates of grooved lead sheets and 1mm diameter scintillating fibers bound together with epoxy, with respective fractions of 50%, 35%, and 15% by volume. Blocks 10 x 10 x 22 cm^3 (14 X_0 length) were machined into projective geometry and tested with electrons at the CERN-PS. The energy resolution obtained for energies with array of 9 such modules was 6.3%/ $\sqrt{E}$ for energies up to 5 GeV (Fig. 2b). The light yield was 970 pe/GeV, including losses in the lightguide system and

attenuation losses in the fiber. The position resolution on the shower centroid was 3mm/ $\sqrt{E}$, measured from energy-sharing within a 9-tower prototype.

While our hadronic calorimeter design is mechanically compatible with a non-compensating EM calorimeter such as Barium Flouride, we would anticipate some degradation of the calorimeter performance in this case. In particular, the constant term in the energy resolution will be increased by longitudinal fluctuations in hadronic shower development across the EM/hadronic boundary. This effect arises from neutron pion production within the non-compensated 1.7 interaction lengths of BaF2. We estimate e/h = 2 for BaF2, and would be much lower with our baseline design. Despite attempts at energy-dependent weighting of EM and hadronic signals within jets, we estimate a constant term of several percent from this effect. Since our baseline design contains a non-compensating fraction of scintillating fibers, this effect requires further study for us as well. For a scintillating fiber EM calorimeter, however, one has parameters to vary with which to effect a compromise between resolution and compensation -- specifically, the fiber packing fraction and the fiber diameter. The recent SPACAL measurement of 10.4% / $\sqrt{E}$ + 0.4% with 0.5mm diameter fibers and a 20% packing fraction (very nearly compensating) gives a great deal of promise to this approach.(Fig 5)

The SPACAL group has conducted extensive tests on a 13-ton non-projective prototype, both with electrons and with pions. This device contained 20% 1mm-diameter fibers by volume, and was made up of 155 towers with hexagonal cross-sections (86 mm apex-to-apex) and 200 cm length (Fig. 6). It obtained an energy resolution of 13%/ $\sqrt{E}$ + 1.2% for electrons, and a (filtered) light yield of about 400 pe/GeV (Fig. 7). Provided th an angle of at least 3 degrees was maintained between the particle incident direction and that of the fiber axes, there were no significant deviations from a Gaussian signal distribution on either the high-energy or the low-energy side of the peak (Fig. 8), for any energy measured (these range from 5 GeV to 150 GeV). With this same 3 degree incident angle, signals from muons were well-resolved from pedestal and muon energy losses well-measured.(Fig. 9) The device was linear with beam energy across the entire energy range, except for the 150 GeV point which was 3% low due to saturation of the PMT. Measurements were made of signal uniformity across modules anc across module boundaries, both for non-projective and for projective (machine modules. The latter gave less than 3% variation in response within 0.5cm of a

module boundary, and less than 1% variation within a module. The measured signal speed, using a 6-stage 2" PMT for readout, was 2.7ns rise time (10% to 90%), 15ns fall time (90% to 10%), and a FWHM of 6.3ns, for 150 GeV electrons (Figs. 10-11). Both the high light yield and the fast response are provided by avoiding tertiary wavelength-shifters in the readout chain (to be contrasted wi liquid scintillator read out with WLS fibers).

Several effects can give rise to a constant term in the energy resolution of a scintillating fiber EM calorimeter. These include fiber-to-fiber variations in the light yield, and in the optical coupling of each fiber to the later stages in the readout chain. In our baseline design, the number of fibers participating in a high-energy electromagnetic shower is >2000/Moliere radius, and simulations indicate that 15% random variations in fiber light yield and coupling will give rise to less than 1% variations in EM shower response. Random variations in the local sampling fraction must be similarly limited to 15%, and systematic variations in local fiber density and light yield must of course be held to <1%. The aspect ratio of a hexagonal light mixer can be chosen to provide less than 1% variation in PM response over the full light guide surface covered by fibers, as demonstrated by SPACAL (Fig. 12). Finally, light attenuation in the fibers can couple to longitudinal variations in shower development to give signal nonlinearity and to degrade resolution. For fiber effective attenuation lengths >400 cm (as with fibers in current prototypes) nonlinearity is <1% between 10GeV and 150 GeV; resolution degradation at 10 GeV is also <1%. (Fig. 13) Since shower depth increases only logarithmically with energy, the nonlinearity stays small at very high energy and the resolution degradatior is not a "constant term". Both effects could be further minimized by applying a reflective coating to the upstream fiber ends as has been done with the SPACAL prototypes.

Single pions were detected with the SPACAL prototype with an energy resolution of $28\% / \sqrt{E} + 2.5\%$. Detailed studies of the origin of the constant term ascribed 1.5% to the effect of fiber attenuation coupling to longitudinal fluctuations, and 1.0% to device non-uniformity and under-compensation. For the SPACAL prototype, tests gave a fitted $e/h = 1.15 \pm 0.02$ (Fig. 14), with a measured $e/\pi = 1.1$ at 10 GeV (which is consistent with a 1% constant term). The effect of light attenuation within the fibers coupling to longitudinal shower fluctuations for single pions was to degrade the energy resolution (from 3.7% to 4.8% at 150

GeV), introduce nonlinearity, and create a non-Gaussian signal distribution (high energy tail). The short attenuation-length component (77 cm) observed with SPACAL arises from light which is piped down the fiber cladding. Fiber attenuation effects are greatly decreased for jets, since a jet ma be considered as a hadronic shower with a fixed starting point, i.e. the interaction vertex. Jets were simulated in beam tests by measuring response to the reaction products of pions interacting in a block of paraffin upstream of the calorimeter. The resolution obtained for "jets" exceeded that obtained for single pions; there is less longitudinal fluctuation int the cladding-light region at lower energies (Fig. 15) For "jets" with 11 or more particles, we find only 2 events out of 10,000 jets from 150 GeV pions that have anomalously high energy. This is consistent with the calculated accidenta rate for piled-up events from our beam.

The fractional energy deposition for single pions (shower profile up to the effect of finite module size) was fitted to a "core" plus "wings" form of $r\ f(r) = A\exp(-r^2/c^2) + B\exp(-r/w)$, with A=15., c = 3.9 cm, B = 2.8, w = 14.5 cm (Fig. 16); 90% of the hadronic shower energy was contained within a 30cm radius. (Fig. 17) With the fine lateral segmentation of the SPACAL prototype, pairs of pions were spatially resolved 95% of the time at a separation of 10cm, and single incident pion positions were determined to within $2.4 + 31\sqrt{E}$ mm. Finally, measurements were made of hadronic pulses widths for 150 GeV pions within a smaller (50cm x 50 cm) prototype; these yielded a rise time of 3ns, a fall time of 21±3ns, and a FWHM=9±3ns. This is consistent with 1 MeV evaporation neutrons travelling at 10^9 cm/s, with a mean free path of 5-10cm, transferring their energy to recoil protons with a time constant of 5-10ns.

Our baseline hadronic calorimeter design differs in several important respects from the SPACAL prototype. It uses 3mm fibers rather than 1mm, uses projective geometry and a rectangular rather than hexagonal cross-section, contains 17% fibers by volume rather than 20%, and uses cast eutectic bismuth-lead alloy rather than lead/antimony alloy as its absorber material. Since EM energy resolution scales like the square root of the fiber radius, the energy resolution of the hadronic calorimeter is degraded from $30\% / \sqrt{E}$ to at most $42\% / \sqrt{E}$. The number of fibers sampling a hadronic shower is larger than for an EM shower by an order of magnitude, so the constant term in the energy resolution is not increased by this change. The change in packing fraction from 20% to17% is specifically designed to correct fo

the "undercompensation" observed with the SPACAL prototype. Since the fibe cladding will be in direct contact with the eutectic alloy, we should avoid the cladding light which contributed to SPACAL's hadronic constant term. The use eutectic alloy has been tested with EM prototypes, which perform identically with those constructed from grooved lead sheets, and in agreement with EGS/GEANT. We are currently constructing 4 tonnes of cast projective hadronic calorimeter with 2mm fibers and 17% packing for tests in high-energy beams at FNAL this fall.

3) RADIATION DAMAGE EFFECTS

A high-resolution EM or hadronic calorimeter must retain its resolution when subjected to the intense radiation of the SSC environment; preferably the device will remain effectively unchanged, but failing this it must change in a manner which can be corrected for through calibration. The SSC radiation field at EM shower maximum (r = 1m) may be approximated by D_EM(rads) = $10^4 + 10^{3 + \eta * 1.2}$ per SSC year (10^{40} $cm^{-2}sr^{-1}$ integrated luminosity). (Fig. 18) The radiation dose received by the hadronic calorimeter decreased by $1/r^2$, which for hadronic shower maximum (r=2m) gives a reduction by a factor of 4. The electromagnetic component of the dose (photon from π^0 decay) carry half as much energy as the hadronic component at a give angle, and the dose profile is spread by a factor of roughly 10. We therefore take as the hadronic dose: D_HAD(rads) = $200 + 10^{1.4 + \eta * 1.2}$ per SSC year. We also note in passing that a lead/scintillator calorimeter produces a factor of 3 less neutron flux within the detector cavity than does a lead/liquid argon calorimeter.[4]

The very different dose profile in the EM and hadronic calorimeters gives rise to very different radiation damage effects in the two devices. (Fig. 1 Within the electromagnetic calorimeter, the predominant effect is the

[4]*Radiation Levels in the SSC Interaction Regions* , D. Groom *et. al.*, SSC-SR-1033 (1988) and Erratum SSCL-285, July 1990.

local loss in scintillation light yield in the vicinity of EM shower maximum. This degrades the EM energy resolution through longitudinal fluctuations in and out of the damaged region, and contributes to the detector nonlinearity. Given the fact that the shape of the shower profile changes only logarithmically with energy while the damage profile is fixed, these effects decrease logarithmically with energy. Several studies have agreed that a 10% reduction in light yield in the vicinity of EM shower maximum gives rise to a 1% change in the resolution at 20 GeV, (Fig. 20 and a 2% nonlinearity between 1 GeV and 100 GeV.[5] Studies of currently available radiation-hard scintillating fibers indicate that such a 10% loss in local light yield occurs for a radiation dose of about 7 MRad. In these studies and in their application below we assume no "annealing" of damaged fibers over time, although this is observed in practice.

For a given integrated luminosity, we can divide the calorimeter by η into four regions: 1) an "unaffected" region where the gain decreases by less than 1% at 10 GeV (D<0.5 MRad), 2) an "affected" region where the gain changes by >1% (D > 0.5 MRad), 3) a "nonlinear" region where the linearity is degraded by >1% between 1 and 150 GeV (D > 2 MRad), and 4) a "damaged" region where the resolution is degraded by >1% (D>7 MRad). For 1 SSC year at 10^{33} luminosity, $\eta > 2.3$ is affected, $\eta > 2.7$ nonlinear, and none of the calorimeter (which extends to $\eta = 3.0$) is damaged. For 10 years at standard luminosity or 1 year at 10^{34} luminosity, $\eta > 1.5$ is affected, $\eta > 1.9$ is nonlinear, and $\eta > 2.4$ is damaged. This corresponds to a very small part of the EM calorimeter: a ring with inner radius 15cm and outer radius 27cm. For 5 years at 10^{34} luminosity, the entire calorimeter is affected, $\eta > 1.1$ is nonlinear, and

---

[5] *Effects of Radiation Damage on Scintillating Fibre Calorimetry*, D. Acosta *et. al.* , CERN-PPE/91-45, 6 March 1991.

Radiation Damage and Resolution Loss in Scintillating Fiber Calorimeters , Proceedings ECFA Large Hadron Collider Workshop, CERN 90-10, ECFA 90-133, Vol. III, 661.

Radiation damage, Calibration, and Depth Segmentation in Calorimeters , A. Para and D. Green, FNAL-FN-565, May 1991.

$\eta > 1.7$ is damaged. The region of $\eta > 1.6$ corresponds to the endcap EM calorimeter, which could be replaced. (Fig. 21)

For the hadron calorimeter, the effects of radiation damage on light attenuation in the fiber dominate over the effects of local light yield reduction. This is because the dose is distributed over a much larger area within the hadron calorimeter, corresponding to the ratio between interaction lengths and radiation lengths. For the same reason, the effect of fiber attenuation length on compact EM showers is much less pronounced than on extended hadronic showers. In fact, for existing fibers, the effects of fiber attenuation are completely dominated by fiber light yield reduction in an EM calorimeter, while within a hadronic calorimeter the reverse is true. With independent scintillating fiber EM and hadronic calorimeters, fibers could be optimized to stress light yield constancy for the former and light attenuation constancy for the latter.
Fiber-to-fiber uniformity requirements in radiation damage are the same as the requirements for resolution: <15% variation in the light output (from both reduction in local light yield and increased light attenuation). This is certainly within the range of radiation damage characteristics among fibers within a single production batch.

For the purposes of our baseline, we treat light attenuation as linear with dose for small doses, and treat the fiber attenuation length as if it were everywhere as short as at hadron shower maximum. Since attenuation is cumulative over the entire fiber, we ignore the difference between interaction lengths and radiation lengths in looking at the total dose, but we preserve 1/4 from $1/r^2$ and a factor of 2 from $\pi\pm/\pi 0$ doses. As with the EM calorimeter, we can then divide the hadron calorimeter by η into four regions: 1) an "unaffected" region where the gain decreases by less than 1% at 10 GeV (D<0.1 MRad, L > 400 cm), 2) an "affected" region where the gain changes by >1% (D > 0.1 MRad, L < 400 cm), 3) a "nonlinear" region where the linearity is degraded by >1% between 1 and 150 GeV (D>0.5 MRad, L < 300 cm), and 4) a "damaged" region where the resolution is degraded by >1% (D>5 MRad, L < 100cm.). For 1 SSC year at 10^{33} luminosity, $\eta > 2.1$ is affected, $\eta > 2.5$ nonlinear, and none of the calorimeter (which extends to $\eta = 3.0$) is damaged. For 10 years at standard luminosity or 1 year at 10^{34} luminosity, $\eta > 1.3$ is affected, $\eta > 1.7$ is nonlinear, and $\eta > 2.5$ is damaged. For 5 years at 10^{34}

luminosity, the entire calorimeter is affected, $\eta > 0.9$ is nonlinear, and $\eta > 1.8$ is damaged. As with the EM calorimeter the region of $\eta > 1.6$ corresponds to the endcap, and could be replaced.

It should be stressed that the above results are for existing fibers, with no allowance for annealing. Annealing is most pronounced in recovery of long fiber attenuation lengths, and thus will have its most dramatic effect on the hadron calorimeter (Fig. 22). The results for the hadronic calorimeter are already a worst-case estimate, since light attenuation in the fibers will be concentrated around hadron shower maximum. Based on the rap progress which has been made in improving the radiation-hardness of scintillating fibers within the last 2 years, there is reason to believe that this progress will continue, and by 2 years from now scintillating fibers able to withstand an order of magnitude greater dose in either EM or hadronic calorimeters may well become available. For the EM fibers, it is known that increasing the concentration of the scintillation fluor (such as 3HF) within the fiber greatly increases its resistance to local light yield loss, at the expense of increased pre-irradiation attenuation (Fig. 23); the latter is not a problem for the EM device.[6]

There is no evidence for any long-term chemical instability of scintillating fibers, although this and questions of slow radiation exposure will require long-term R & D efforts. Similarly, questions of annealing in the presence or absence of oxygen require further detailed study, although such atmospheres appear less important than originally thought. Finally, we note that the excellent radiation hardness of scintillating fibers arises in part from the short distance which UV light travels before being wavelength-shifted to visible light -- a characteristic which is not shared by scintillating plate calorimeters. Similarly, the high light yield of a scintillating fiber calorimeter allows one to filter out the short-wavelength components which are most prone to increased attenuation after radiation damage.

---

[6]*Proceedings of the Workshop on Radiation Hardness of Plastic Scintillator* , Tallahassee, FL, March 1990.

4) CALIBRATION SYSTEM

Calibration of time-dependent variations of scintillating fiber calorimetry could be accomplished through three basic methods: (1) radioactive sources, (2) UV and visible light sources, and (3) beam signals. CDF and FNAL E687 have demonstrated that this combination can give calibration of scintillators with a precision of better than 1%.[7] (Fig. 24) Moveab radioactive sources are provided for 4 towers at each η in our baseline design, in order to monitor the longitudinal dependence of fiber attenuation and any radiation damage effects. CDF used 3 mCi ^{137}Cs source and drive hardware permanently attached to a drive system and an individual calorimeter module (i.e. the source is the tip of a "sword" within a "sheath"). In CDF, simultaneous calibration of 48 modules required less than an hour, with a data rate of 5 Hz (DC current measurement). We are building 4 channels of the CDF source calibration system into our upcoming GEM hadron calorimeter prototype.

For short-term calibration and monitoring, our baseline design employs nitrogen lasers coupled through UV-transmitting quartz fibers to diffusing splitters, and then to the front and back of individual calorimeter towers (both EM and hadronic) (Fig. 25). At the front of this monitors attenuation through an entire calorimeter, while at the back it monitors the response and

---

[7]*Calibration Systems for the CDF Central Electromagnetic Calorimeter* , S. Hahn *et. al.* , NIM A267, 1988, 351.

Y. Kubota and C. O'Grady, NIM A279, 73 (1989); and J. Berger *et. al.* , NIM A279, 343(1989).

The Photomultiplier Gain Monitoring System for the E687 Electromagnetic Calorimeter at Fermilab , S. Bianco *et. al.* , NIM A305 (1991) 48.

linearity of the photoconverter and data acquisition electronics. The intrinsic laser pulse-to-pulse stability is about 10%, and by monitoring the laser light yield with a reference photodiode one can reduce this further and monitor long-term laser drift (a few percent per month). This system tests the performance of all the optical components in the readout chain, including PMT gains, light transmission, and time offsets. The optical stability required has been achieve in other large experiments, so that with proper care the systematic error requirements of the EM section are manageable. Given 300 laser pulses per data point, and a maximum 1Hz laser trigger rate, we could monitor the system response every 10 minutes (probably limited by DAQ rates).

A calibration beam at the SSCL will be used to obtain absolute calibration of some of the completed calorimeter modules in the 2-3 years before pp operation commences. This calibration will be used as a measurement of the variation between towers and to provide an initial calibration. For relative calibration of towers at the same η, we plan to employ techniques such as the simulated annealing algorithm (e.g. take the average minimum bias response for N-1 towers, and adjust the Nth to fit the average, etc.) The EM sections of the calorimeter will be calibrated in situ by using Z -> ee decays from pp interactions. Inclusive Z production rates are sufficient to give over 10^6 dielectrons per SSC year in the barrel calorimeter alone ($\eta < 1.5$). With cell size 0.05 x 0.05, this is about 500 e's per cell. The Z mass should then be determined with a precision of about 100 MeV per cell per year, well under the 0.5% requirements. All EM cells will be calibrated this way and with the absolute scale fixed using M_Z. The beam-calibrated modules will be a reference and starting point. Another intriguing possibility which has been explored by SPACAL collaborators is the use of minimum-bias gammas from p-p interactions to hourly calibrate EM towers.[8]

The absolute calibration requirements for the hadron calorimeter are not as stringent as for the EM device. We plan to calibrate some of the modules in a test beam and to cross-calibrate the remainder by E_T balance and energy flow uniformity. The calibration will be fixed with

---

[8] *On the Calibration of the Electromagnetic part of a Spaghetti Calorimeter at a multi-TeV Hadron Collider* , A. Contin *et. al.* , CERN Preprint.

respect to the EM section by using QCD events with a single photon recoiling against a hadronic jet. This technique has been demonstrated to be effective by CDF.[9] In addition, one might use hadronic signals from well-tracked single pions, and from isolated muons and cosmic rays, to provide a redundant check on hadron calorimeter calibration and uniformity of response.

5) READOUT SYSTEM

Our baseline design calls for readout with mesh dynode photomultiplier tubes. A dynamic range of >10^4 is readily available from magnetic field insensitive mesh-dynode PMTs. We coul operate at 10^3 gain in a 1 Tesla field (requiring fewer dynode stages) followed by pulse shaping and a fast preamplifier, etc. Mesh dynode PMTs can be linear to1% up to 500 mA peak anode current with the proper base and readout electronics (they do not acquire long tails until they are saturated). Pulse shaping electronics coupled to the mesh dynode PMT outputs require further study. Pulses of up to 25 Volts into 50 ohms are available, and correction for PMT nonlinearity above 2.5 V is possible through the laser-based calibration system.

We are also considering hybrid photomultipliers consisting of a vacuum diode containing a semiconductor diode. The photocathode and the diode at the anod are separated by a vacuum gap and held at a voltage difference of a few kilovolts. An incoming photon is converted on the photocathode into a photoelectron, swhich is then accelerated and focussed towards the silicon diod by an electrostatic focussing system. The semiconductor diode is then placed near the spot where accelerated photo-electrons are focussed. These devices have demonstrated linearity over a 10^5 dynamic range, (Fig. 26) but requires further development for operation in the magnetic field.[10]

---

[9] *Jet Energy Measurement-CDF Experience*, Proceedings of the Workshop on Calorimetry for the SSC, Tuscaloosa, Alabama, 1989.

[10] *First Results on the Hybrid Photodiode Tube* , R. DeSalvo *et. al.* , CERN Preprir

Figures:

1) Schematic illustration of Fiber Calorimeter (From the EOI). This should be modified to illustrate PMTs coupled to EM modules at the boundary between th EM and hadronic sections, as in Figure 2.

2) The JETSET scintillating fiber electromagnetic calorimeter and its measured performance.

3) Schematic illustration of laminated tower fabrication method for JETSET, and illustration of SPACAL projective electromagnetic calorimeter modules.

4) Schematic illustration of the assembly method for constructing rings of hadron calorimeter modules. From the EMPACT/TEXAS EOI.

5) Monte Carlo study of energy resolution for compensating mixtures of lead and scintillating fibers, with SPACAL data points.

6) Schematic illustration of SPACAL laminated construction and 155-module hadronic shower-containing prototype.

7) Measured energy resolution of SPACAL prototype to electrons (old data) and of recent projective SPACAL prototype (new data).

8) SPACAL measured response to 80 GeV electrons.

9) SPACAL measured response to 150 GeV muons.

10) SPACAL pulse shapes for 150 GeV electrons and pions.

11) SPACAL pulse rise and falls times for 150 GeV electrons and pions.

12) SPACAL module uniformity and module boundary scans with 40 GeV electrons, for projective and non-projective towers.

13) Monte Carlo analysis of sensitivity of constant term in energy resolution to longitudinal shower fluctuations as a function of fiber attenuation length, for electromagnetic and hadronic modules.

14) Measured e/π and e/h in SPACAL, with and without correction for fiber attenuation (cladding light).

15) Measured attenuation in SPACAL prototype (note cladding light at <0.5m from PM gives short attenuation-length component) and consequent non-Gaussian high-energy tail on response to 150 GeV pions. Note that response to "jets" (secondaries from hadronic interaction in upstream target) give a Gaussian response, since they result in several hadron showers which develop farther from the PM.

16) Measured lateral spread in SPACAL of hadronic energy deposition (modulated by detector granularity) for 150 GeV pions.

17) Measured fraction of hadronic energy deposition in SPACAL as a function of radius of cylinder about shower core over which energy is summed

18) Monte Carlo calculation of radiation dose at EM shower maximum within GEM (from D. Groom's revised calculation).

19) Profile of radiation damage from electromagnetic and hadronic showers (T. Gabriel, ORNL).

20) Monte Carlo calculations of the effect of radiation damage on EM calorime resolution. The top curve is parametrized by fiber attenuation length at EM shower maximum (abscissa) and local light yield reduction at EM shower maximum (f = 0.1 --> 10% reduction). The bottom curve shows the resolution degradation as a function of electron energy for the case of 10%, 30%, and 50% light yield reduction at EM shower maximum (from Green and Para).

21) Illustration of the "Unaffected", "Affected", and "Damaged" portions of a scintillating fiber calorimeter after 1 SSC Year and after 10 SSC Years (see text).

22) Radiation damage and annealing of light attenuation in scintillating fiber.

23) Radiation damage to scintillating fibers as a function of 3HF fluor concentration. Note the middle plot, where a fiber with 20 times the 3HF (bottom curve) of another fiber (top curve) suffered a 40% decrease in light yield, while the top fiber suffered a 90% decrease at 100 MRad integrated dose.

24) Reproducibility of radioactive source and light flasher calibrations within the CDF electromagnetic calorimeter.

25) An example of a simple and inexpensive laser-based calibration system (in this case, from E687 at FNAL).

26) Schematic illustration of hybrid photomultiplier tube, and measured linearity of response.

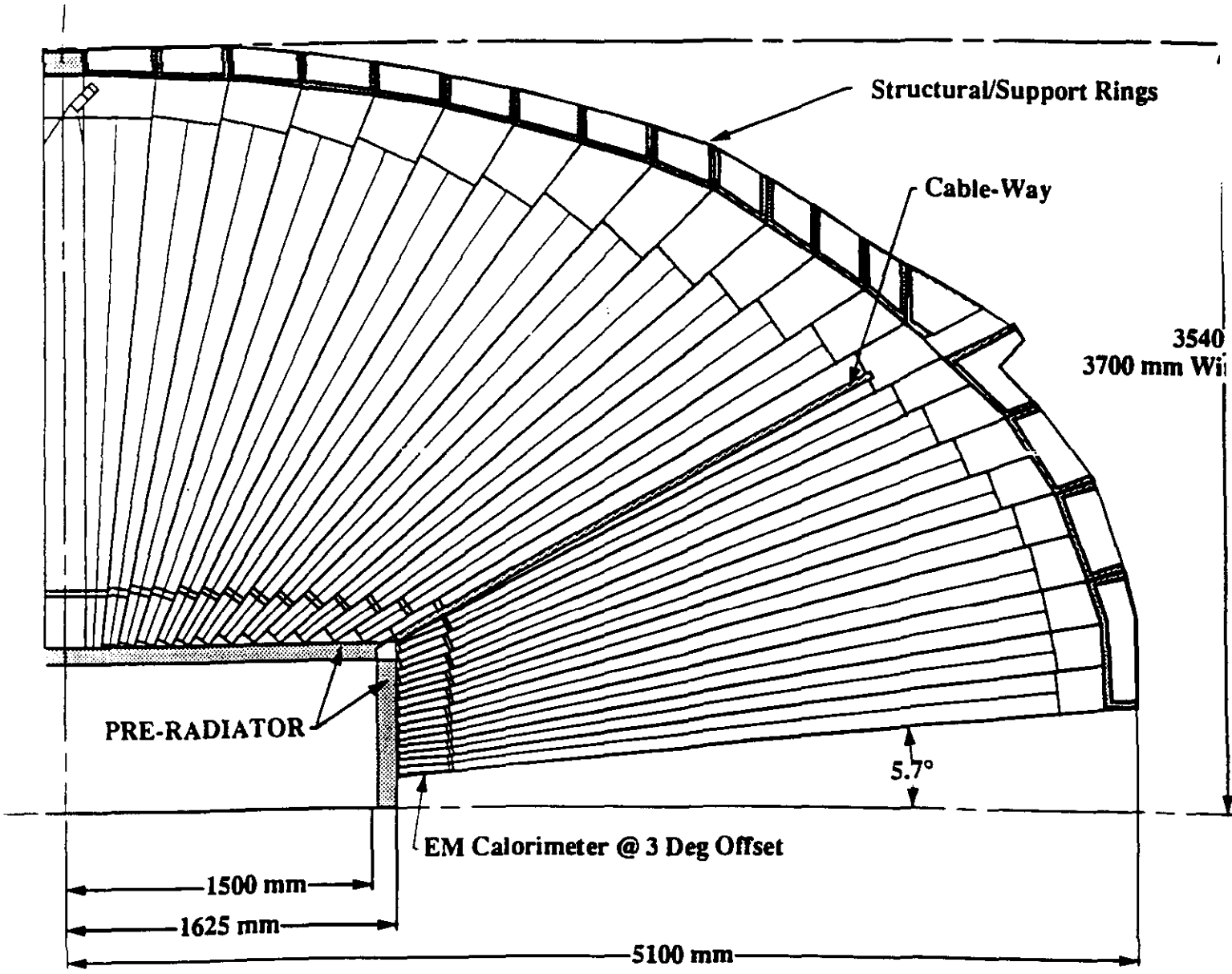

Figure 3.3-3 Spaghetti Calorimeter

Fig 1

Fig 2

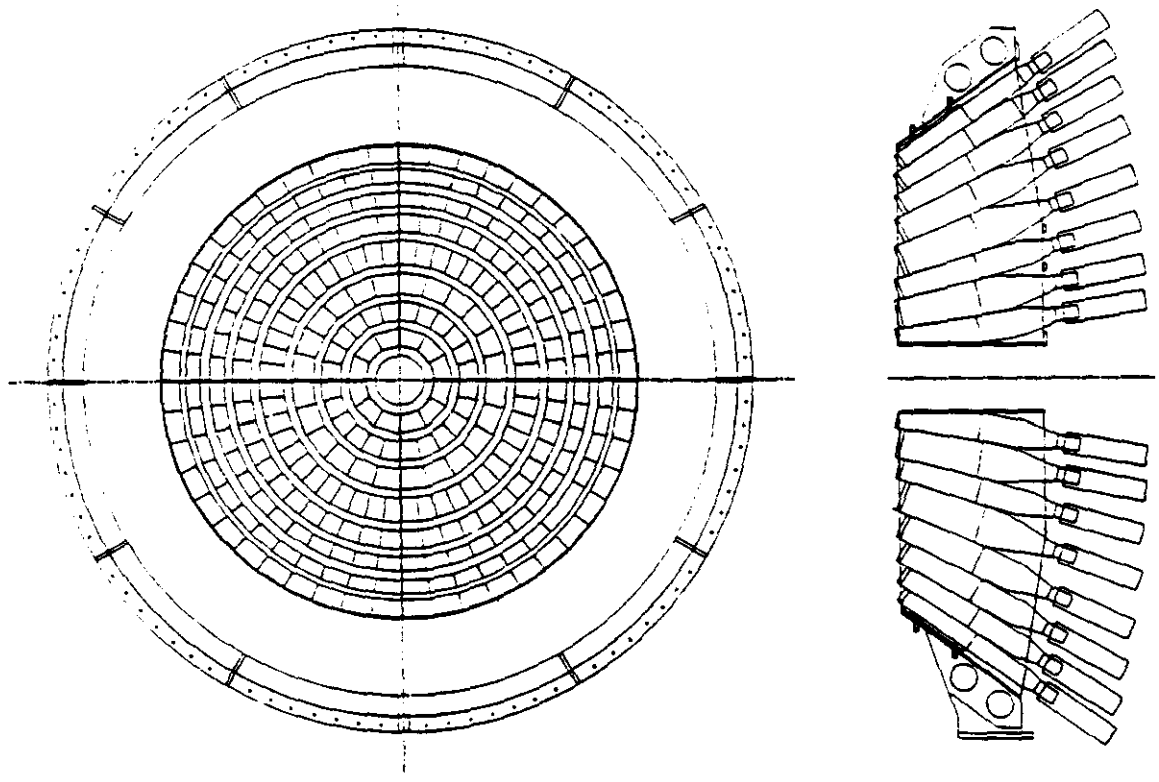

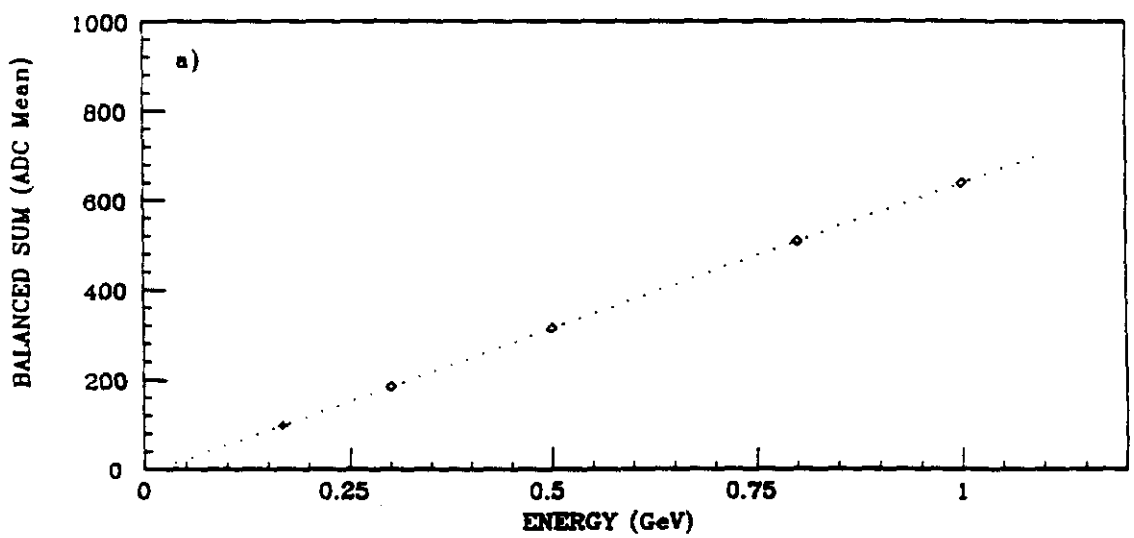

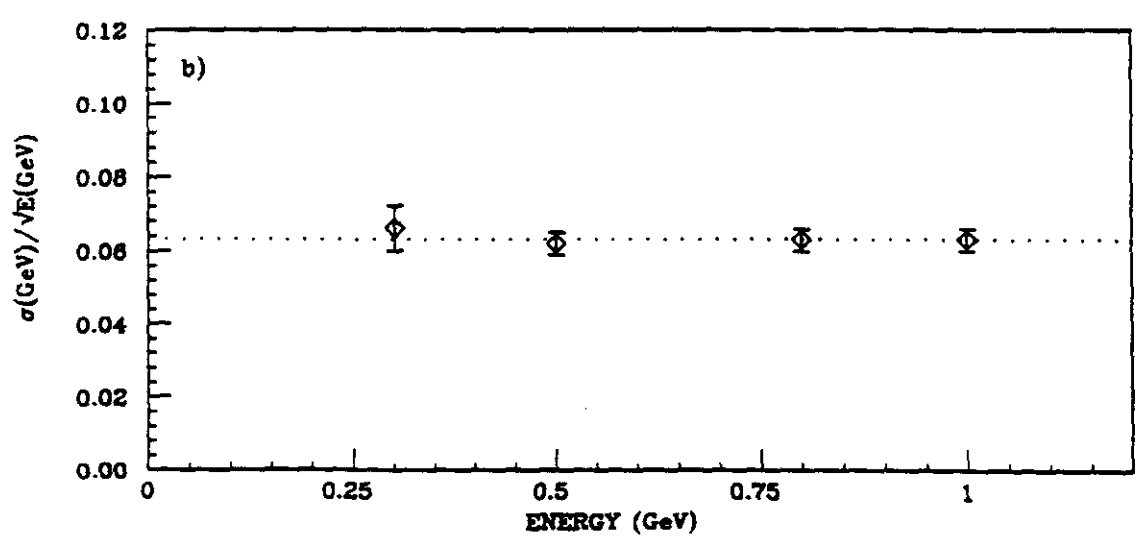

g. 8. (a) Total energy in the array of nine towers versus energy and (b) energy resolution of the sum versus energ
btained with the beam incident in the center of the central

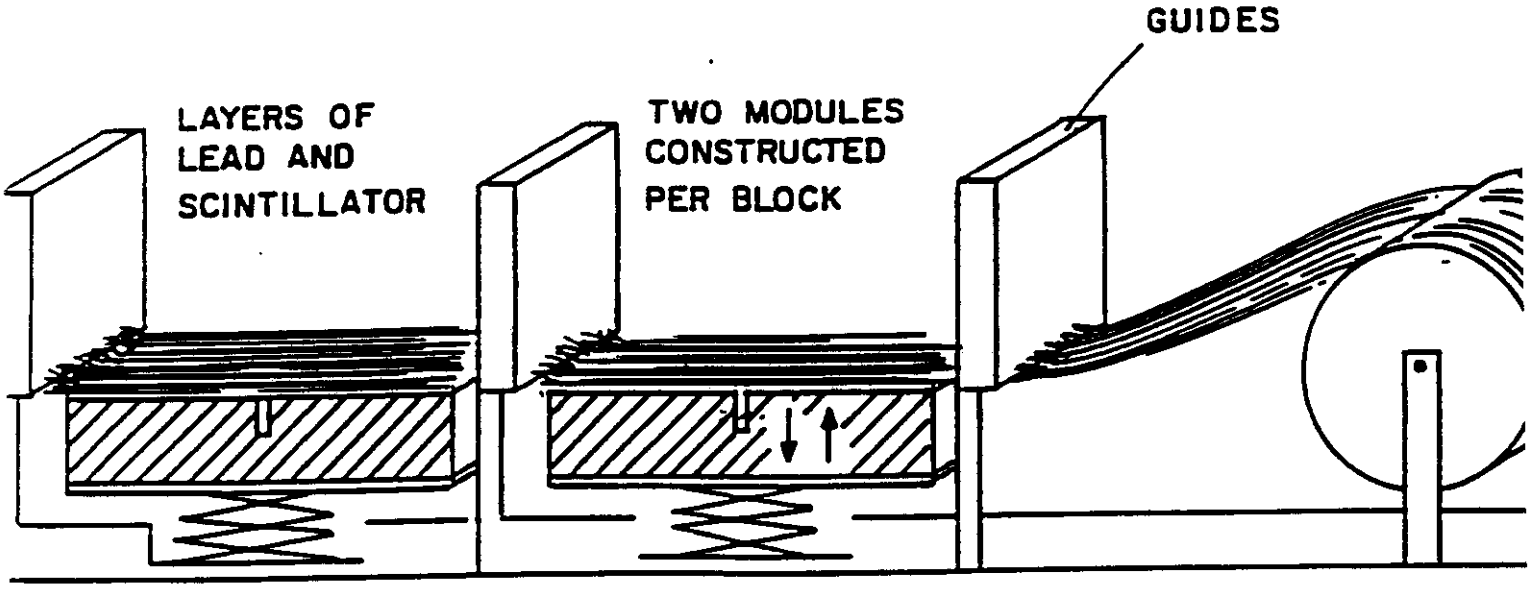

Schematic view of the calorimeter module manufacturing technique.

SPOOLS OF
SCINTILLATI
FIBER

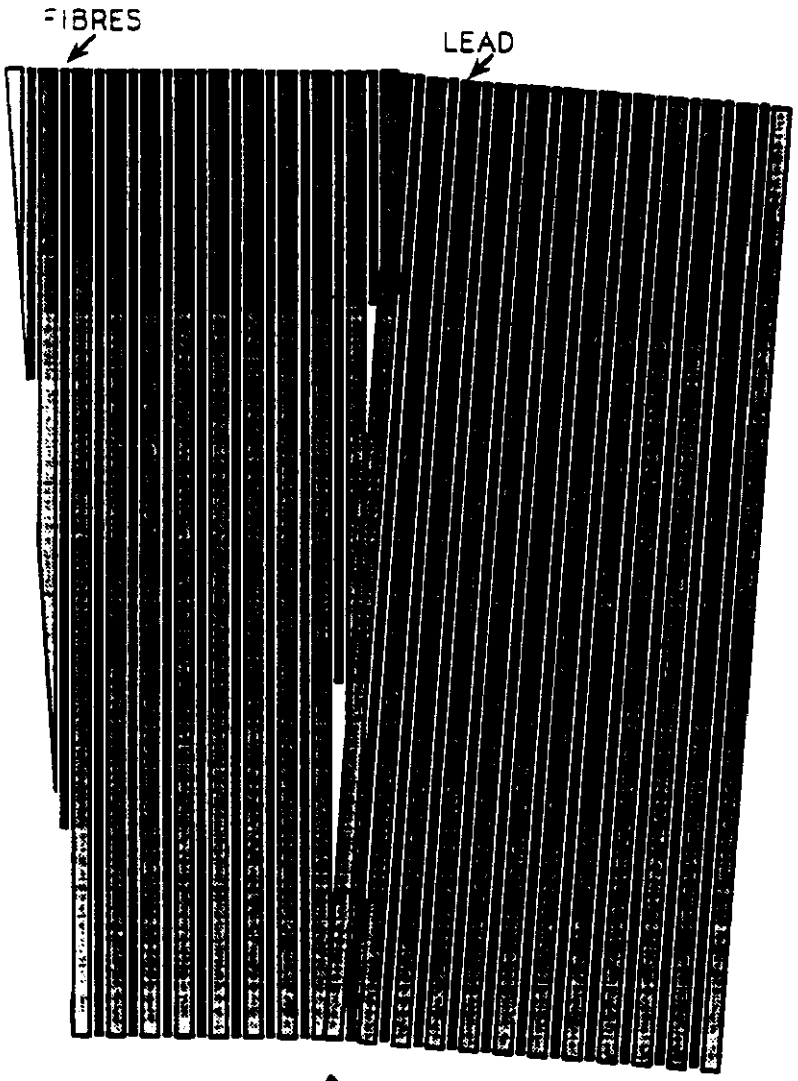

PARTICLES

Fig 3

Fig. 10. Longitudinal cross section of the pyramidal module.

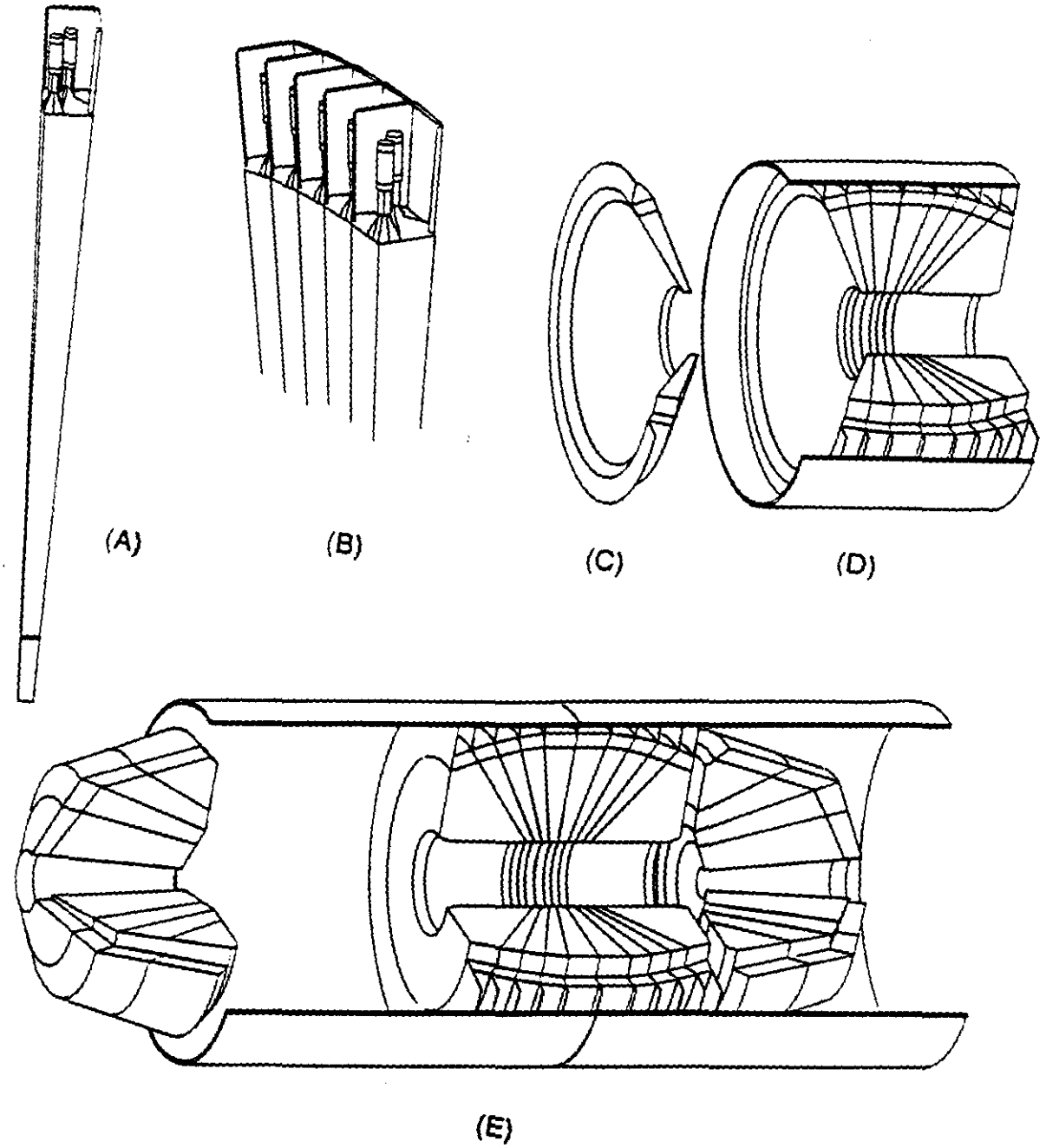

Figure 2. Construction Details of the SPACAL Calorimeter: (A) Single Tower; (B) Ring; (C) Super Ring; (D) Assembly of Super Rings in Barrel Section; (E) Full Calorimeter Showing Removable Endcap Assembly.

Fig 4

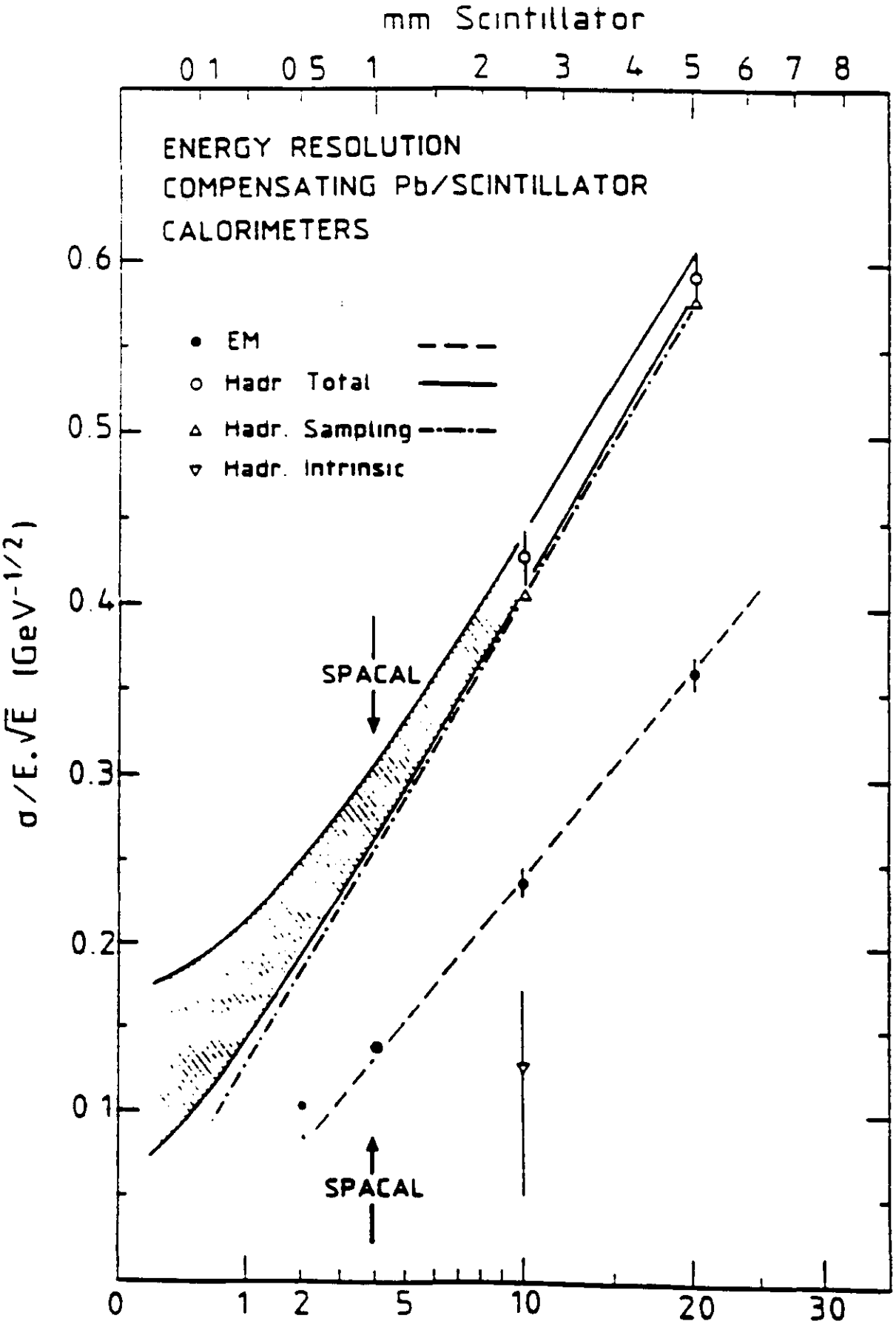
mm Scintillator
0 1
0 5
1
2
3
4
5
6
7
8
ENERGY RESOLUTION
COMPENSATING Pb/SCINTILLATOR
CALORIMETERS
EM
Hadr Total
Hadr. Sampling
Hadr. Intrinsic
SPACAL
SPACAL
σ/E.√E (GeV^-1/2)
0.6
0.5
0.4
0.3
0.2
0 1
0
1
2
5
10
20
30

Fig 5

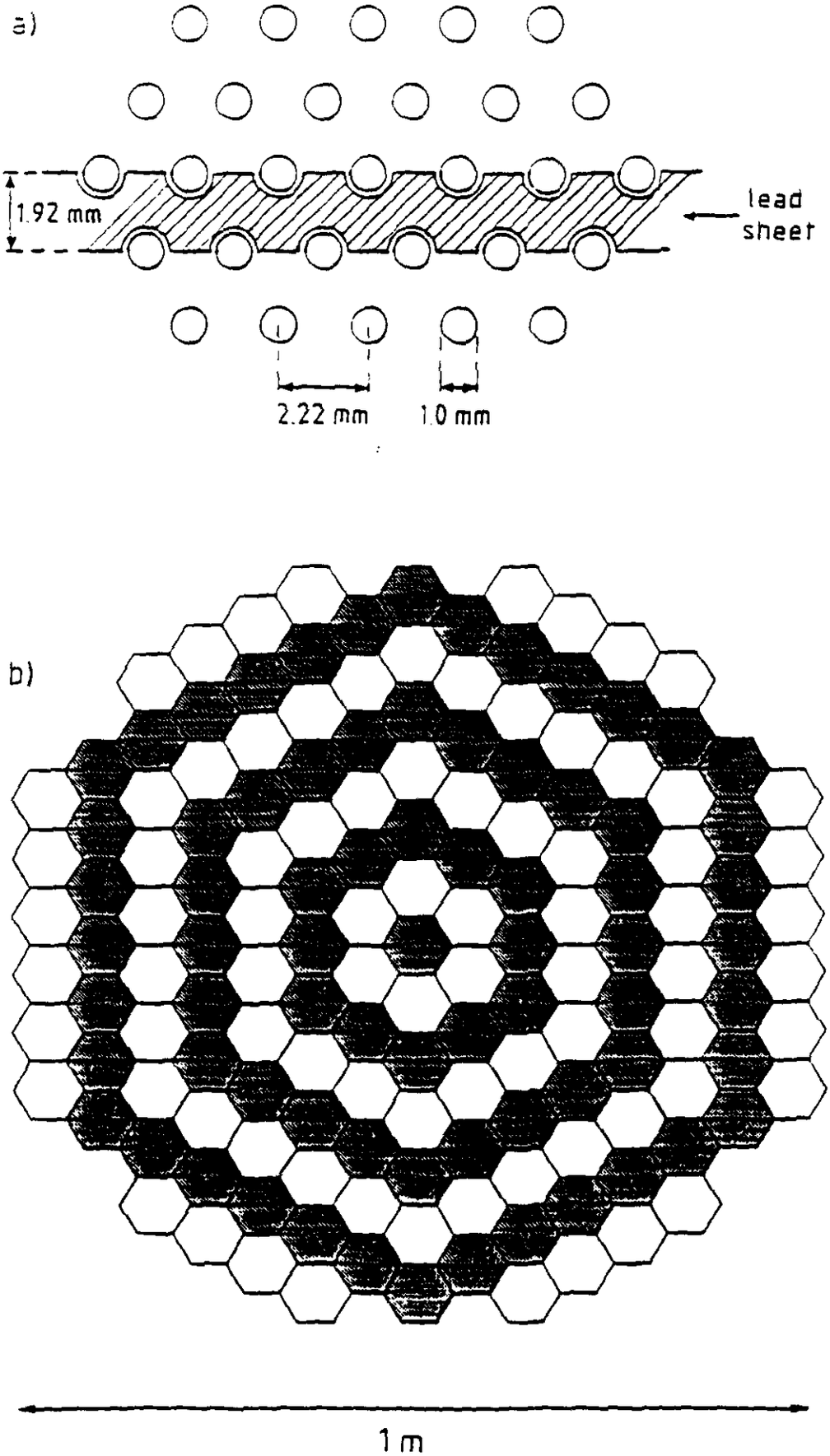

Figure 1 Fig 6

Energy resolution electrons

θ_y=1.5°, θ_x=1.5°

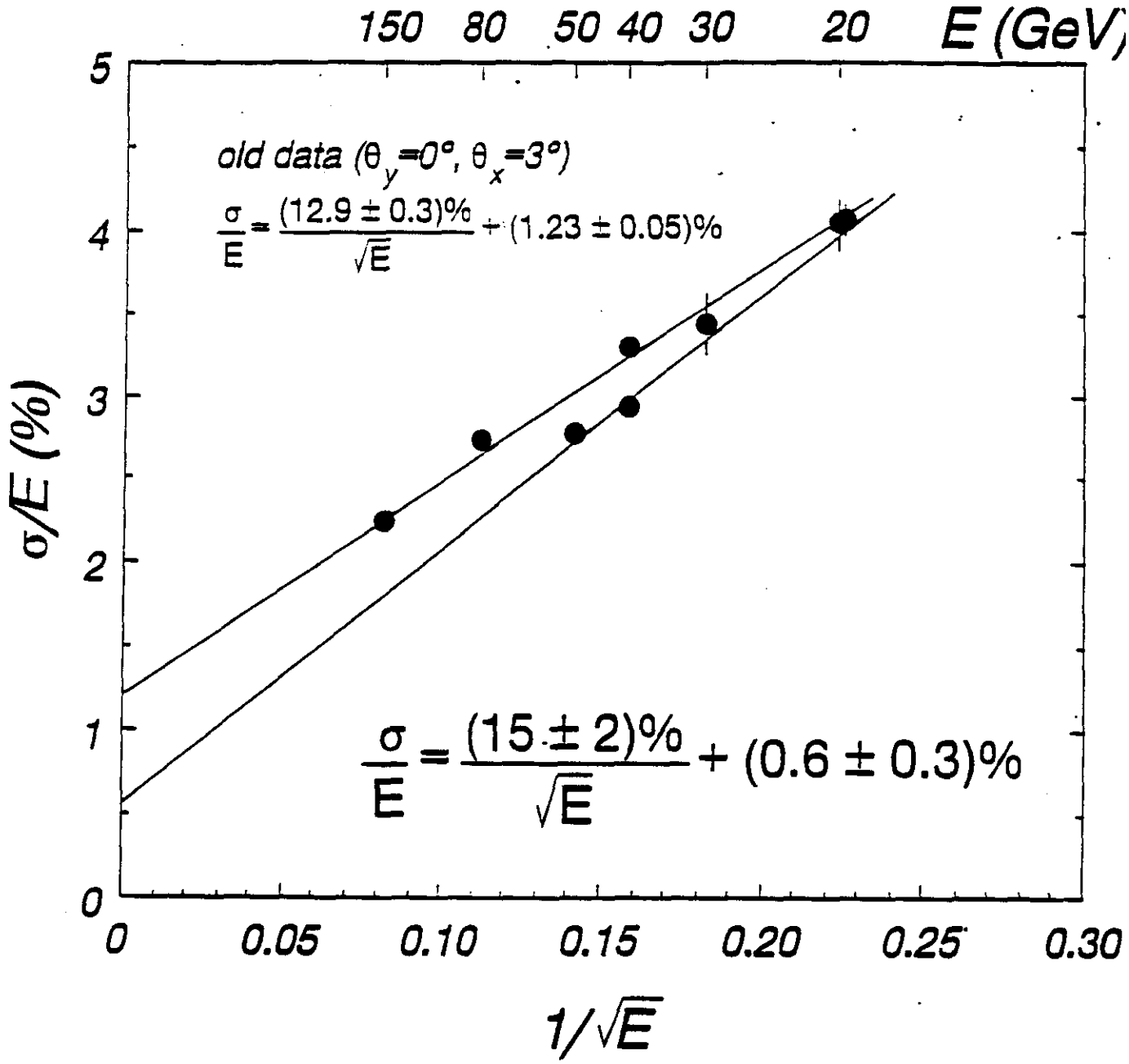

Fig 7

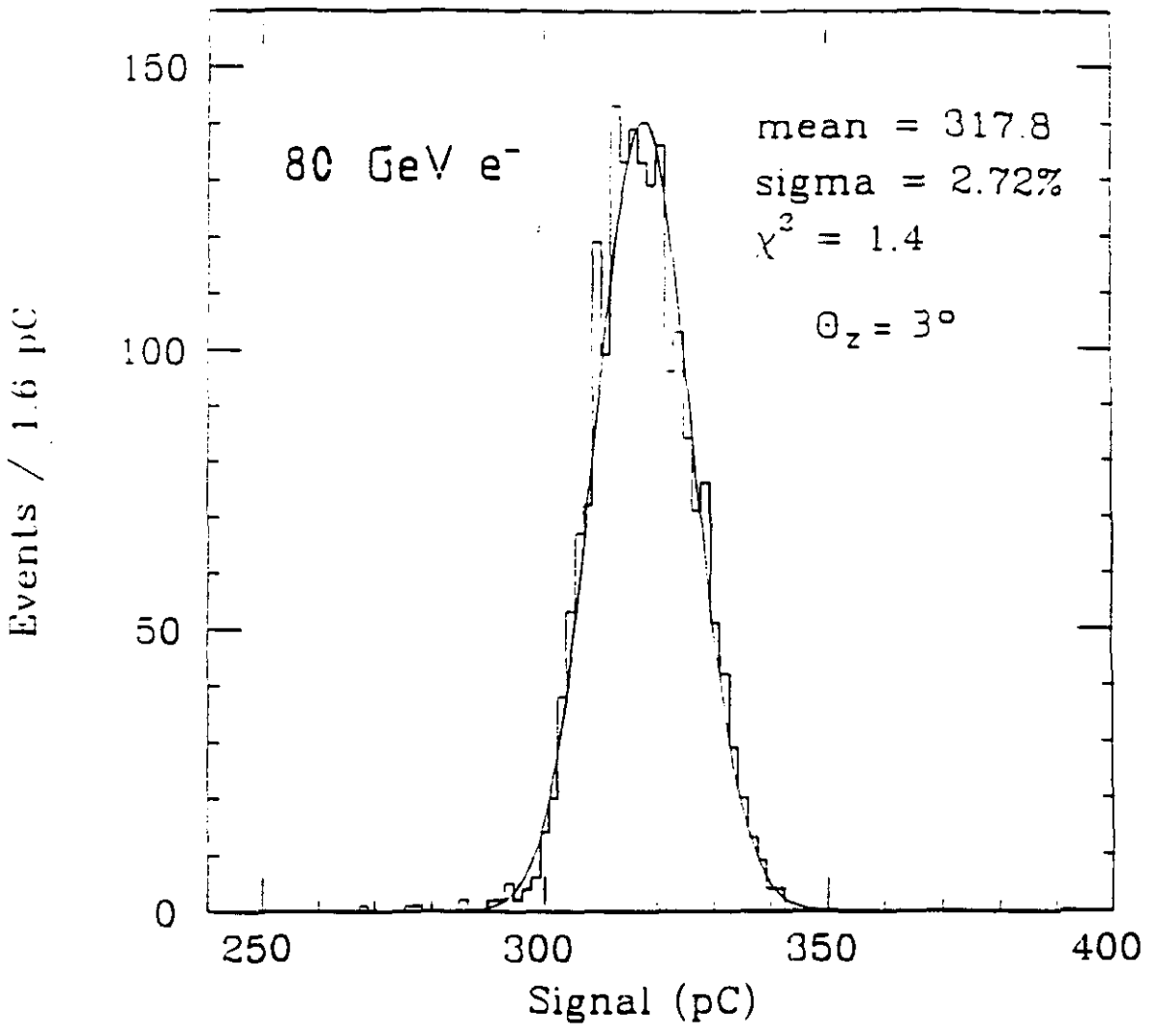

Figure 5

Fig 8

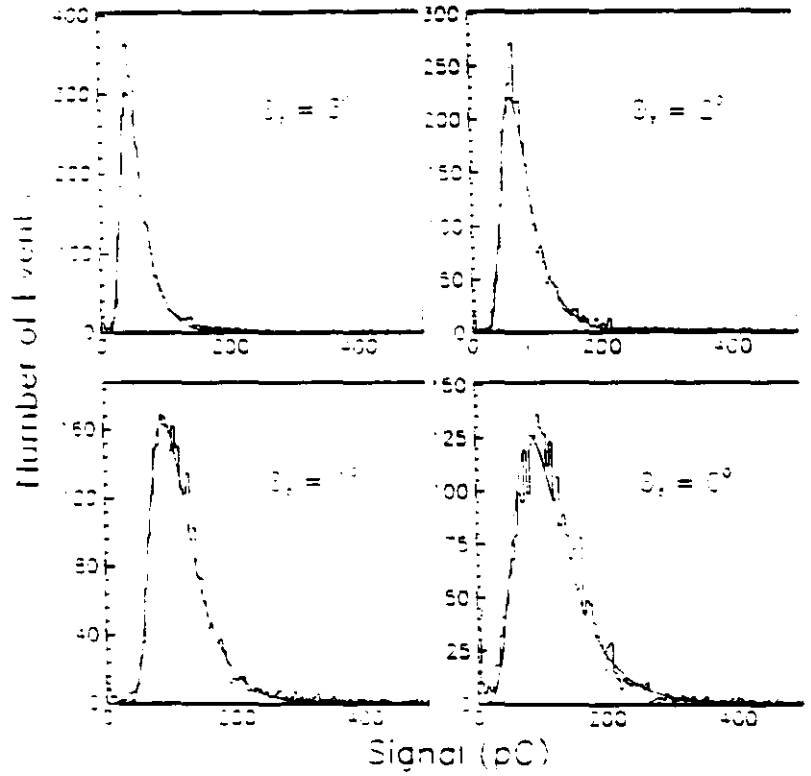

Fig. 16. Signal distribution for 150 GeV muons in a 2 m long module, for different angles θ_z.

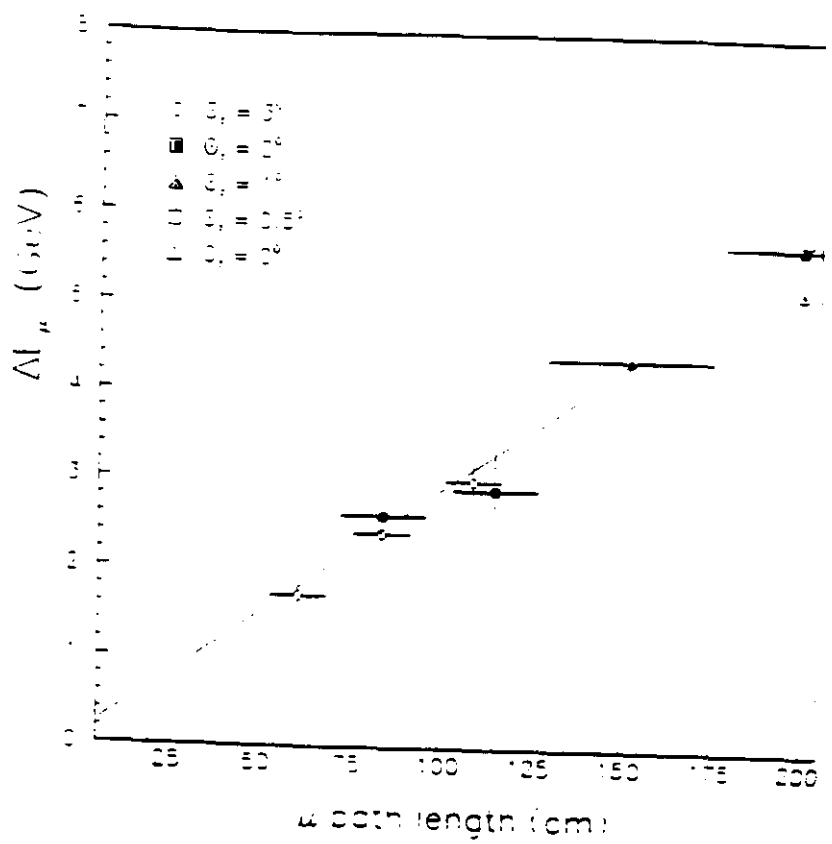

Fig. 17. The path length of 150 GeV muons in a 2 m long fibre detector module vs the resulting signal, for various values of the angle θ_z.

Fig 9

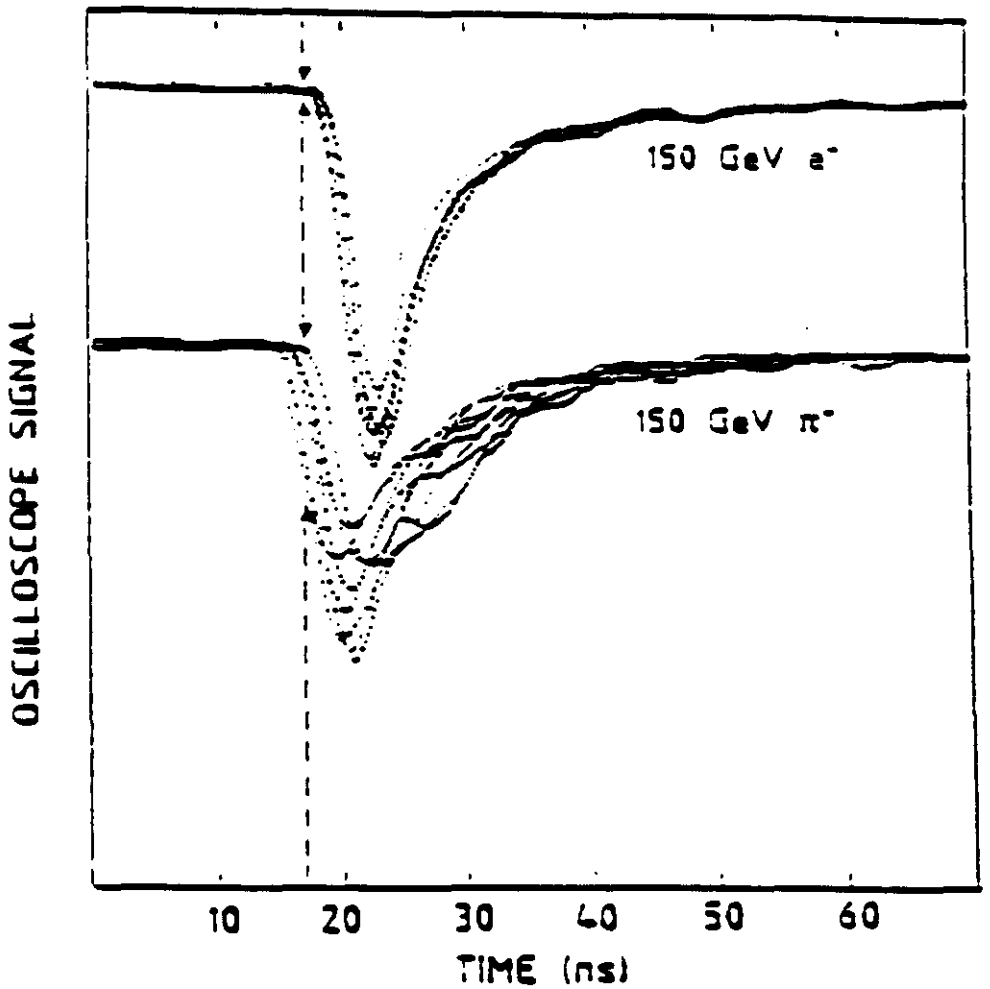

Fig. 2. Examples of pulses from the photomultiplier for 150 GeV electr
ıd pions. Data are from the July 1988 beamtests with an earlier 2 m long ver
the LJ module.

Fig 10

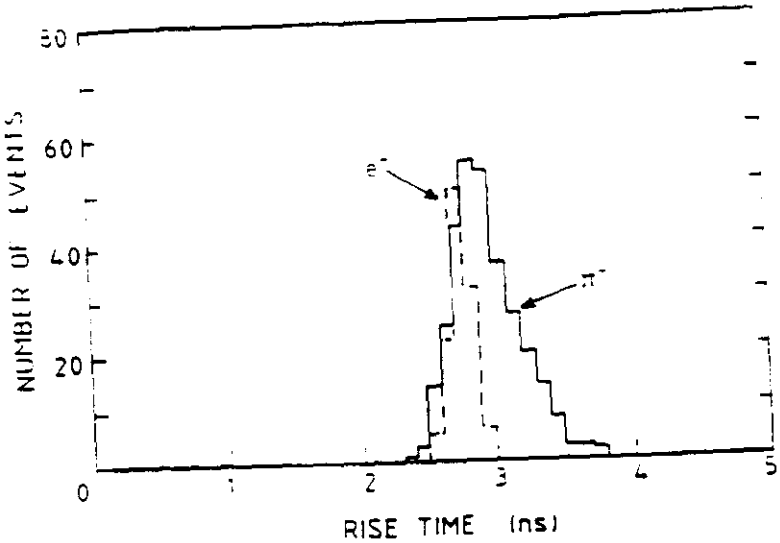

Fig. 7. Distribution of the rise time, defined as the time interval over which the signal rises from 10% to 90% of the peak value, for 150 GeV electron and pion pulses from the spaghetti calorimeter.

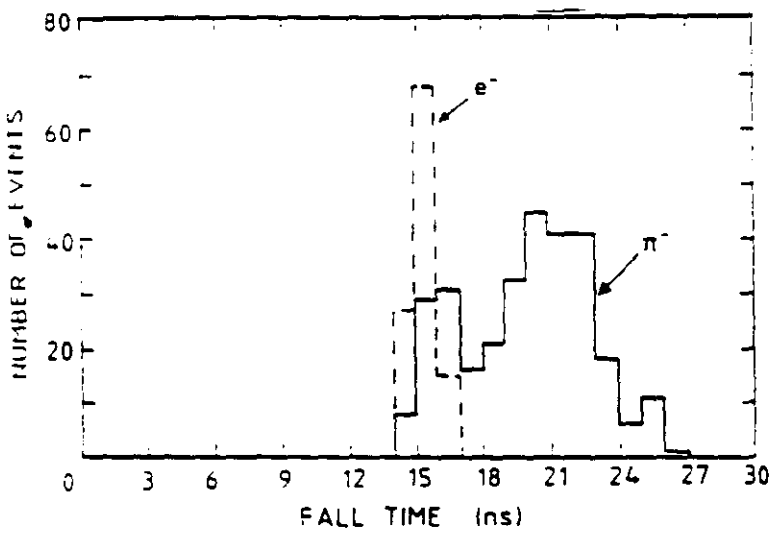

Fig. 5. Distribution of the fall time, defined as the time interval over which the signal drops from 90% to 10% of the peak value, for 150 GeV electron and pion pulses from the spaghetti calorimeter.

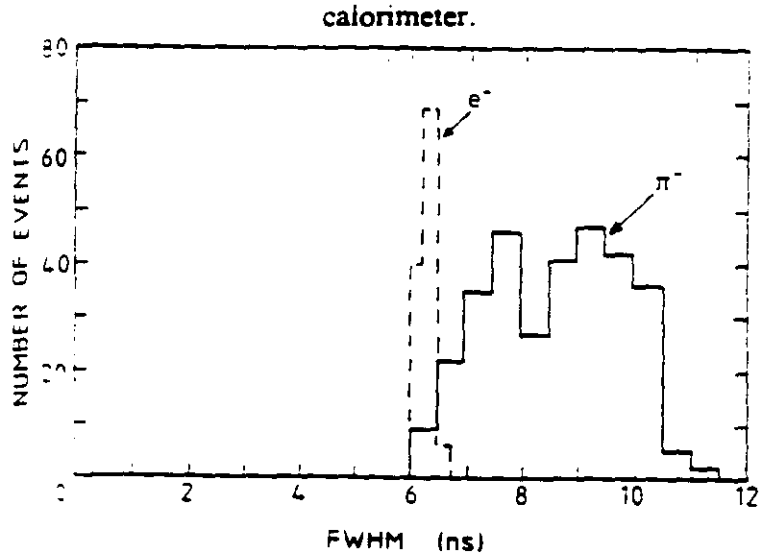

Fig. 4. Distribution of the fulll width at half maximum for 150 GeV electron and hadron pulses from the spaghetti calorime-

Fig 11

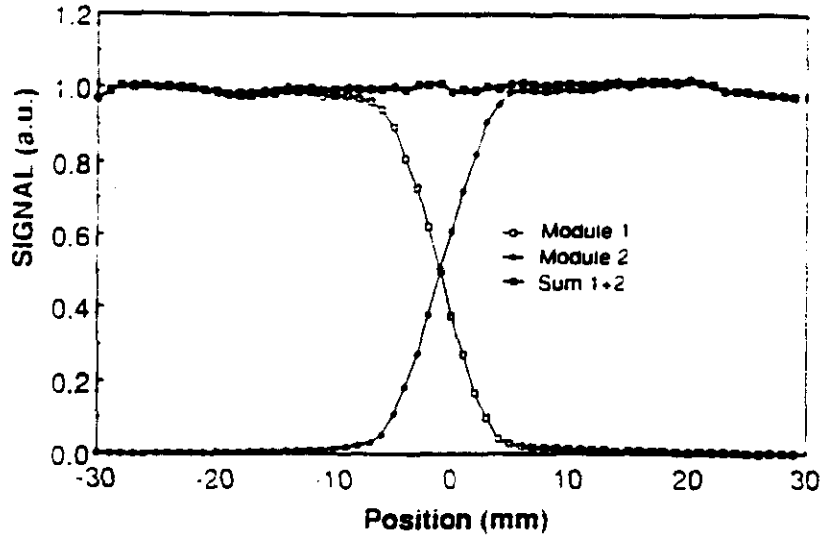

Fig. 8. Calorimeter response to a collimated β-source scanning the boundary between two SPACAL modules.

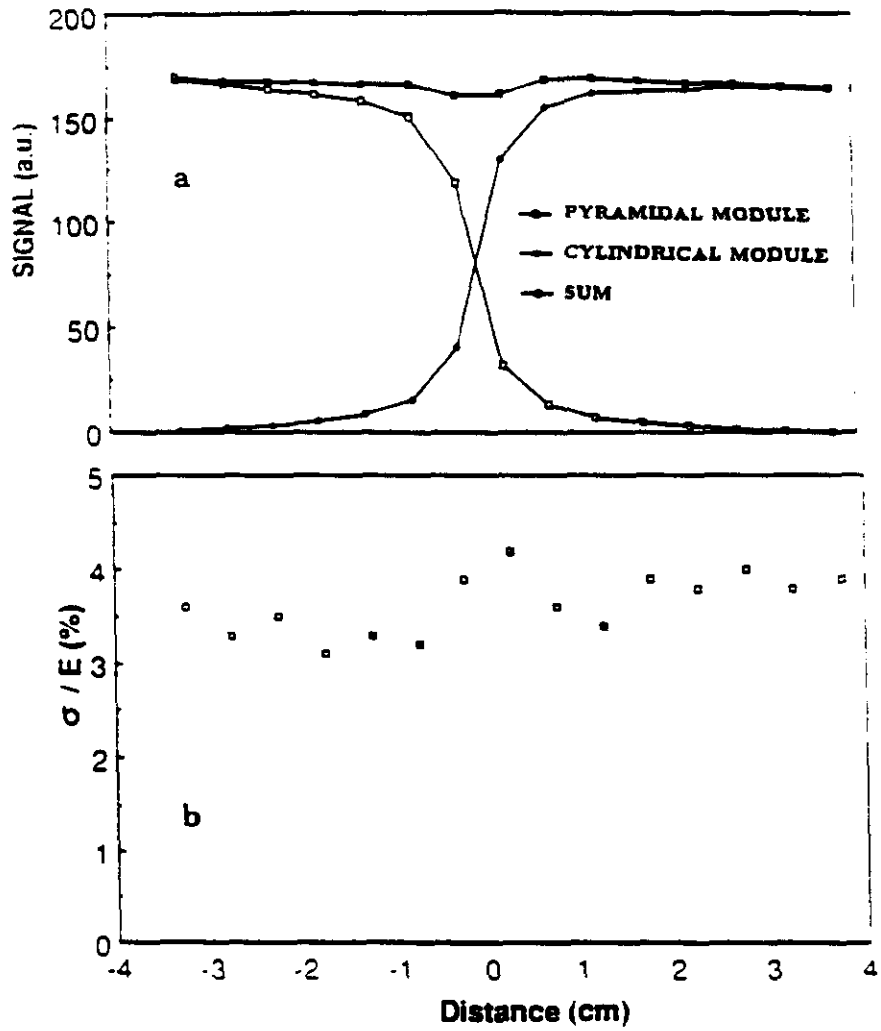

Fig. 23. Results of a scan with 40 GeV electrons between the centers of two adjacent modules with small or no sampling fraction fluctuations. One of the modules is cylindrical, the other pyramidal, with a projective geometry. In (a) is plotted the average signal in both modules and their sum, as a function of the beam position. In (b), the energy resolution with which the electrons are detected is given.

Fig 12

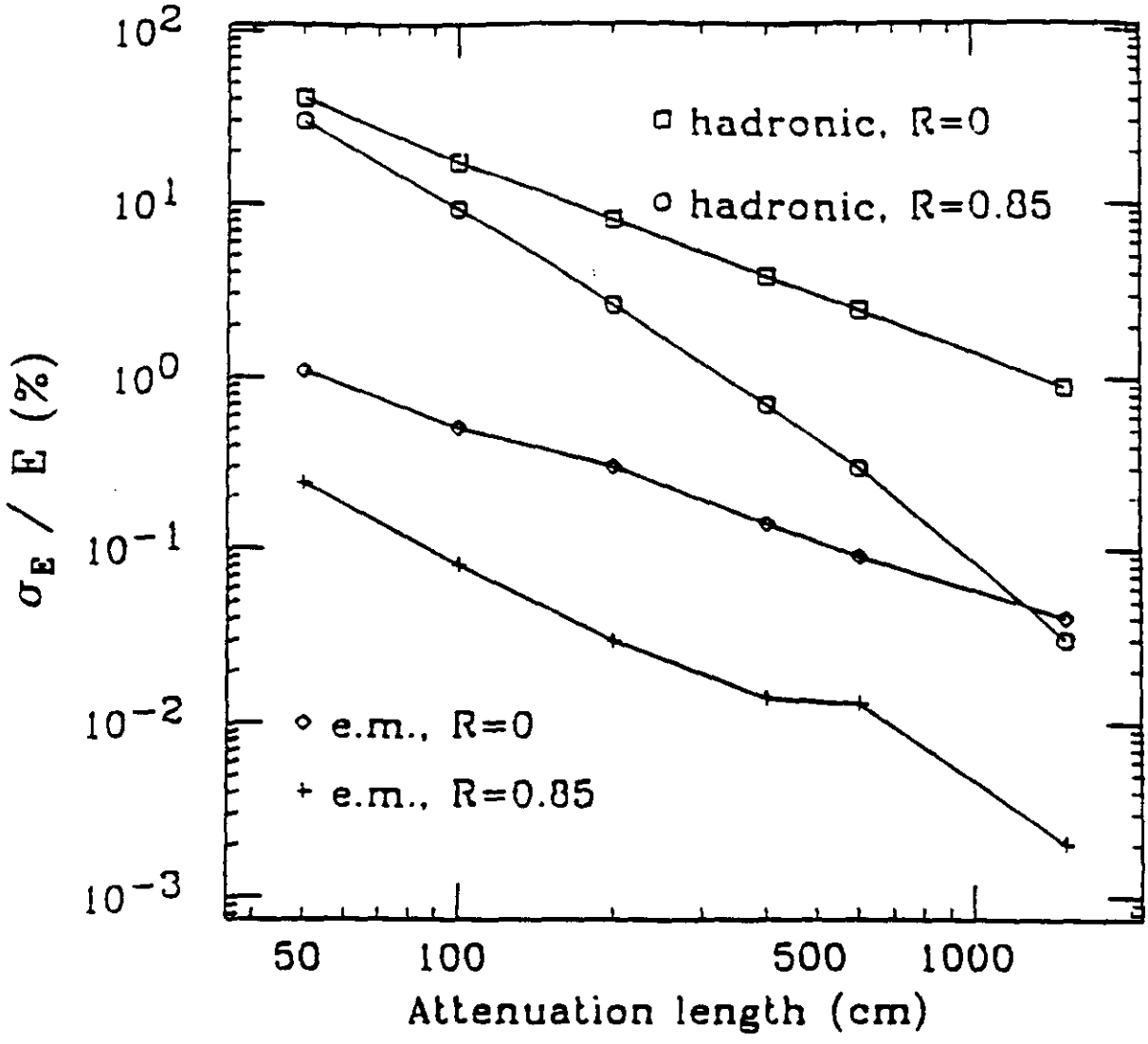

Fig. 1. Calculated contribution of the finite attenuation length λ to energy resolution σ_E/E for electromagnetic and hadronic showers.

Fig 13

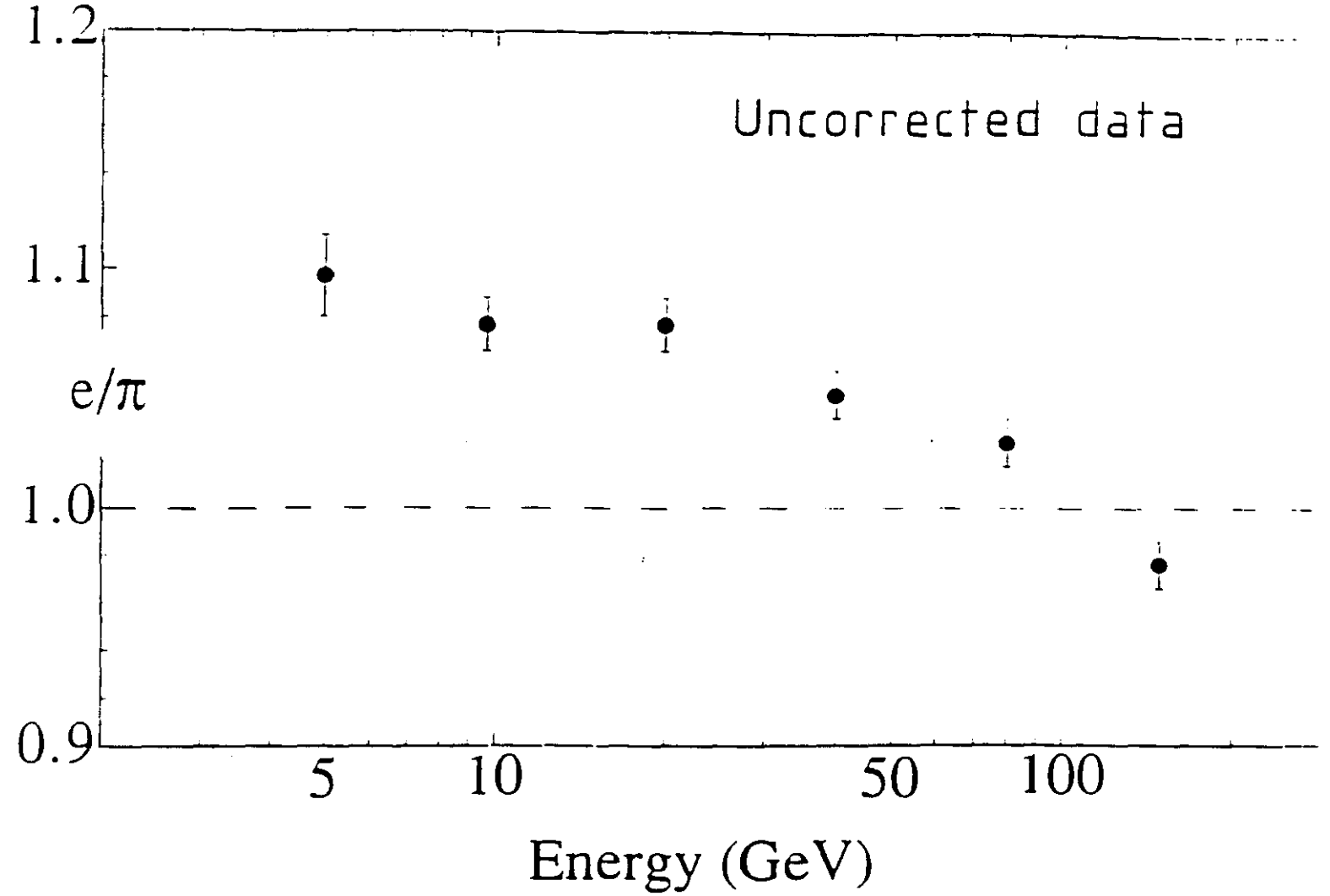
Uncorrected data
1.2
1.1
1.0
0.9
e/π
5
10
50
100
Energy (GeV)

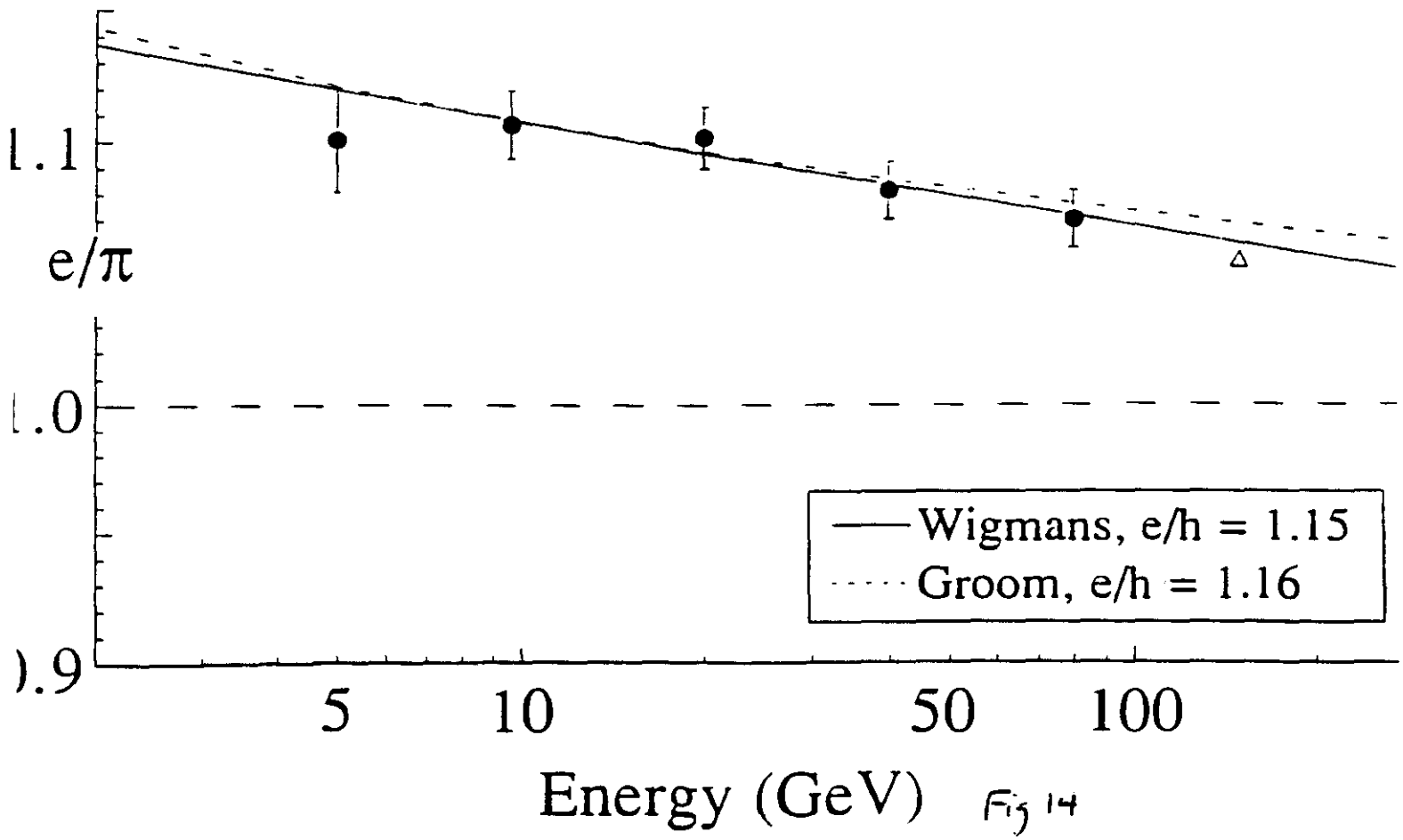
1.1
1.0
0.9
e/π
Wigmans, e/h = 1.15
Groom, e/h = 1.16
5
10
50
100
Energy (GeV)

Fig 14

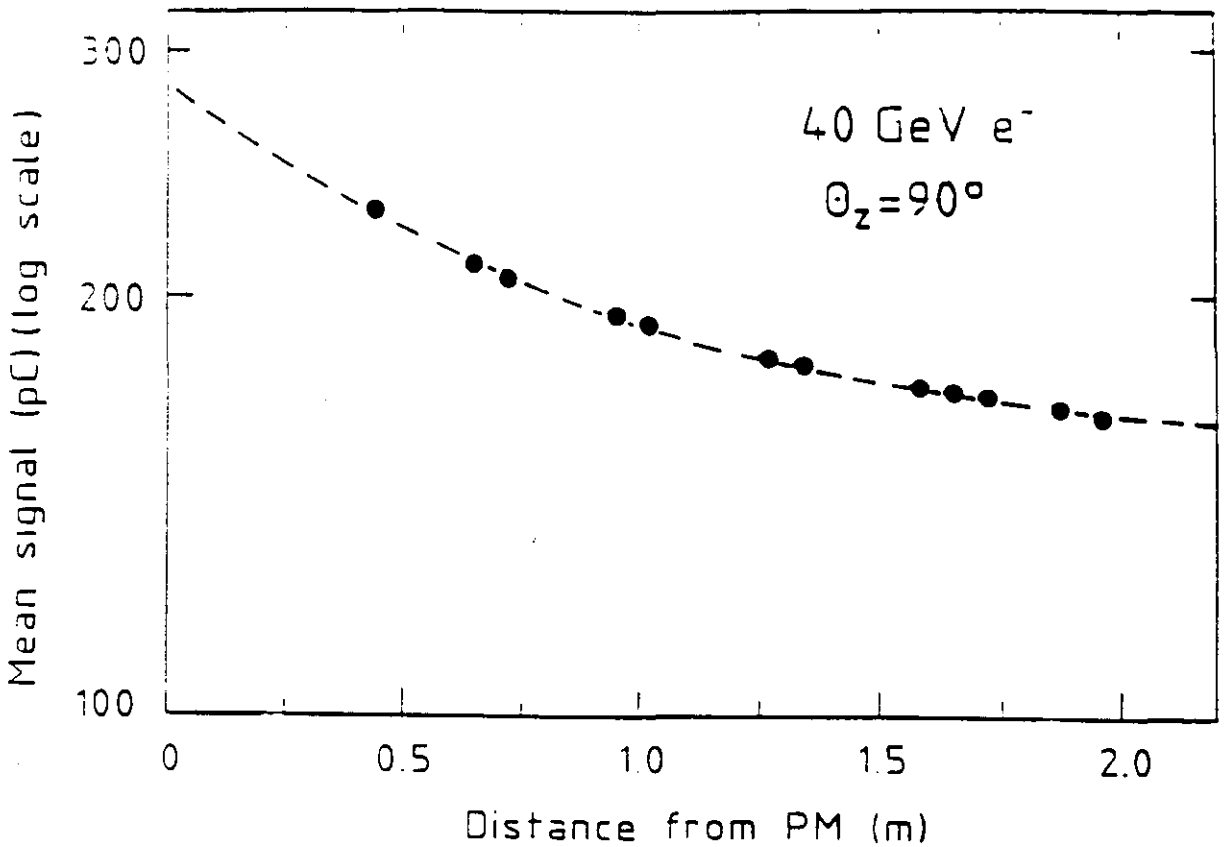
40 GeV e⁻
θz=90°
Mean signal (pC) (log scale)
300
200
100
0
0.5
1.0
1.5
2.0
Distance from PM (m)

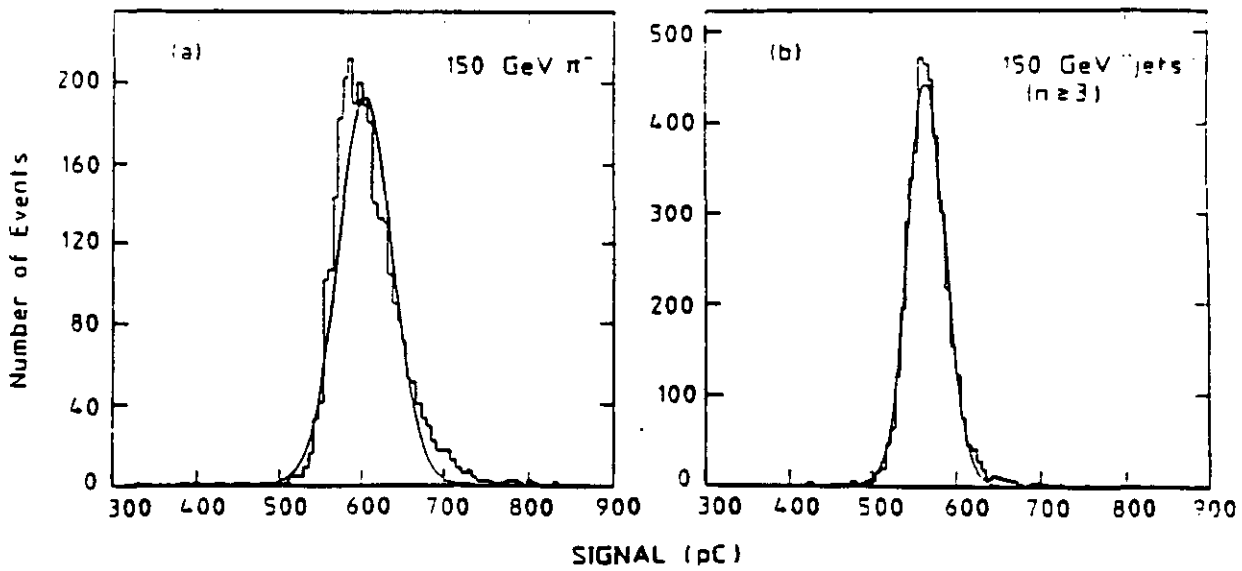
(a)
150 GeV π⁻
(b)
150 GeV "jets"
(n ≥ 3)
Number of Events
200
160
120
80
40
0
500
400
300
200
100
300
400
500
600
700
800
900
SIGNAL (pC)

Fig 15

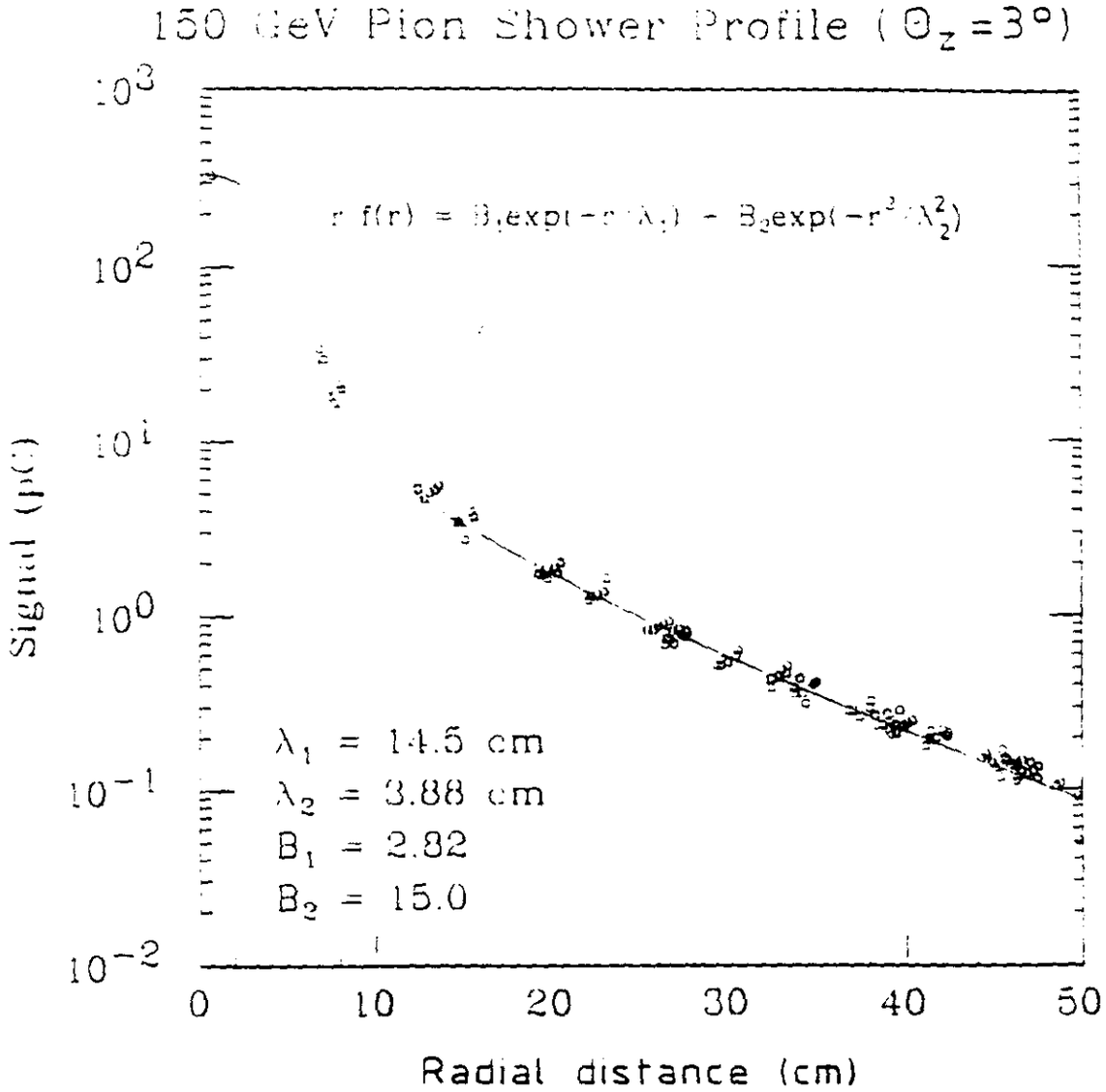

Fig 16

Figure 27

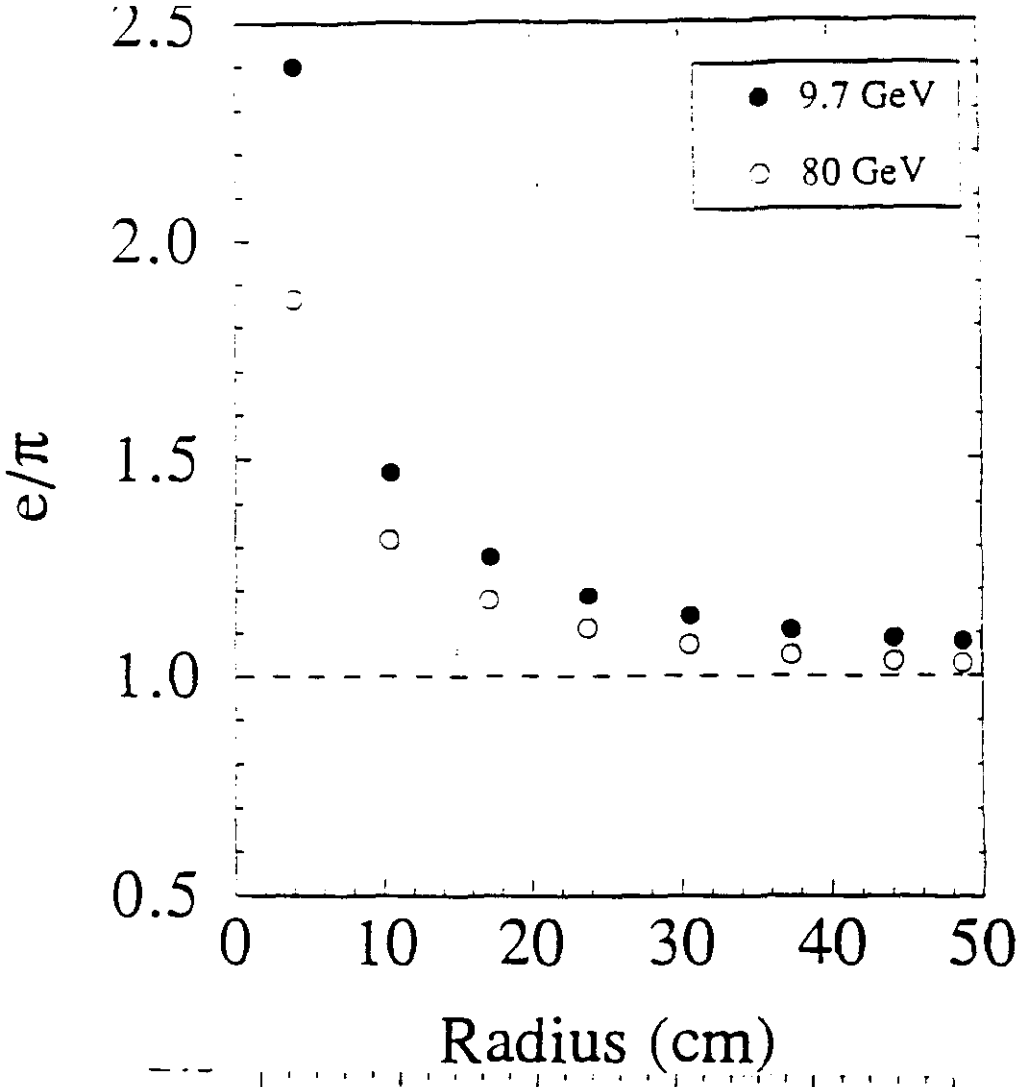
2.5
2.0
1.5
1.0
0.5
e/π
9.7 GeV
80 GeV
0
10
20
30
40
50
Radius (cm)

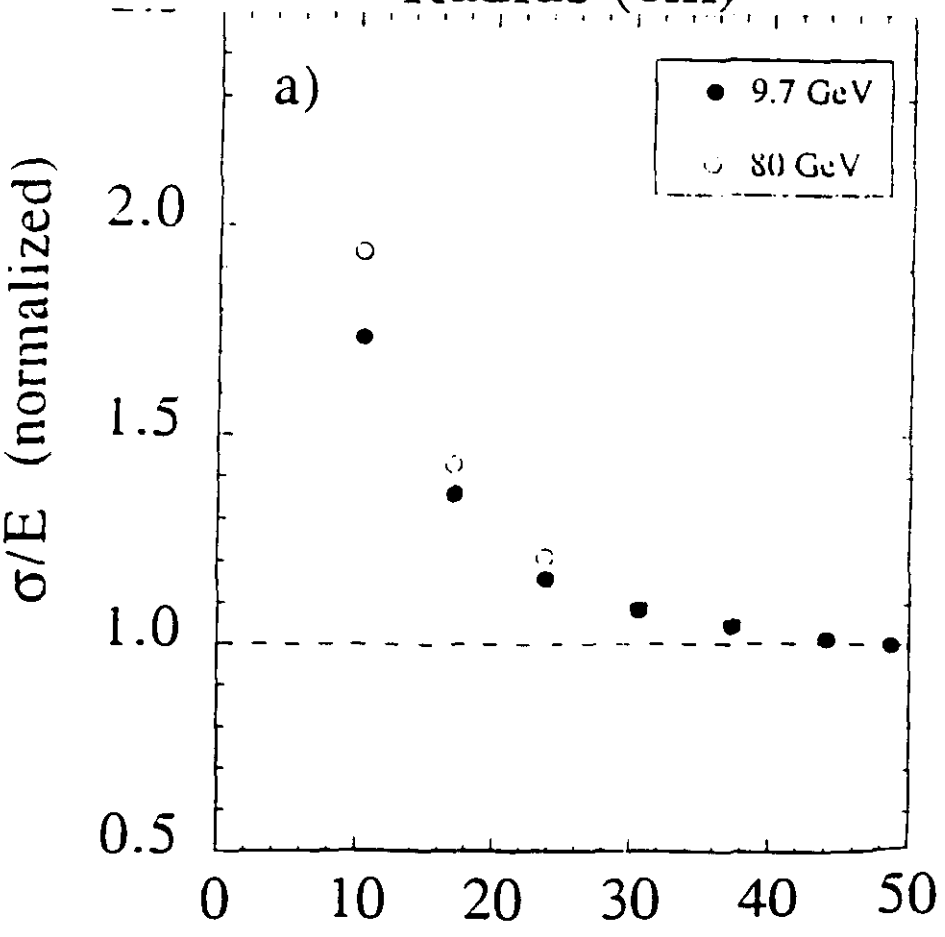
a)
9.7 GeV
80 GeV
2.0
1.5
1.0
0.5
σ/E (normalized)
0
10
20
30
40
50

Fig. 17

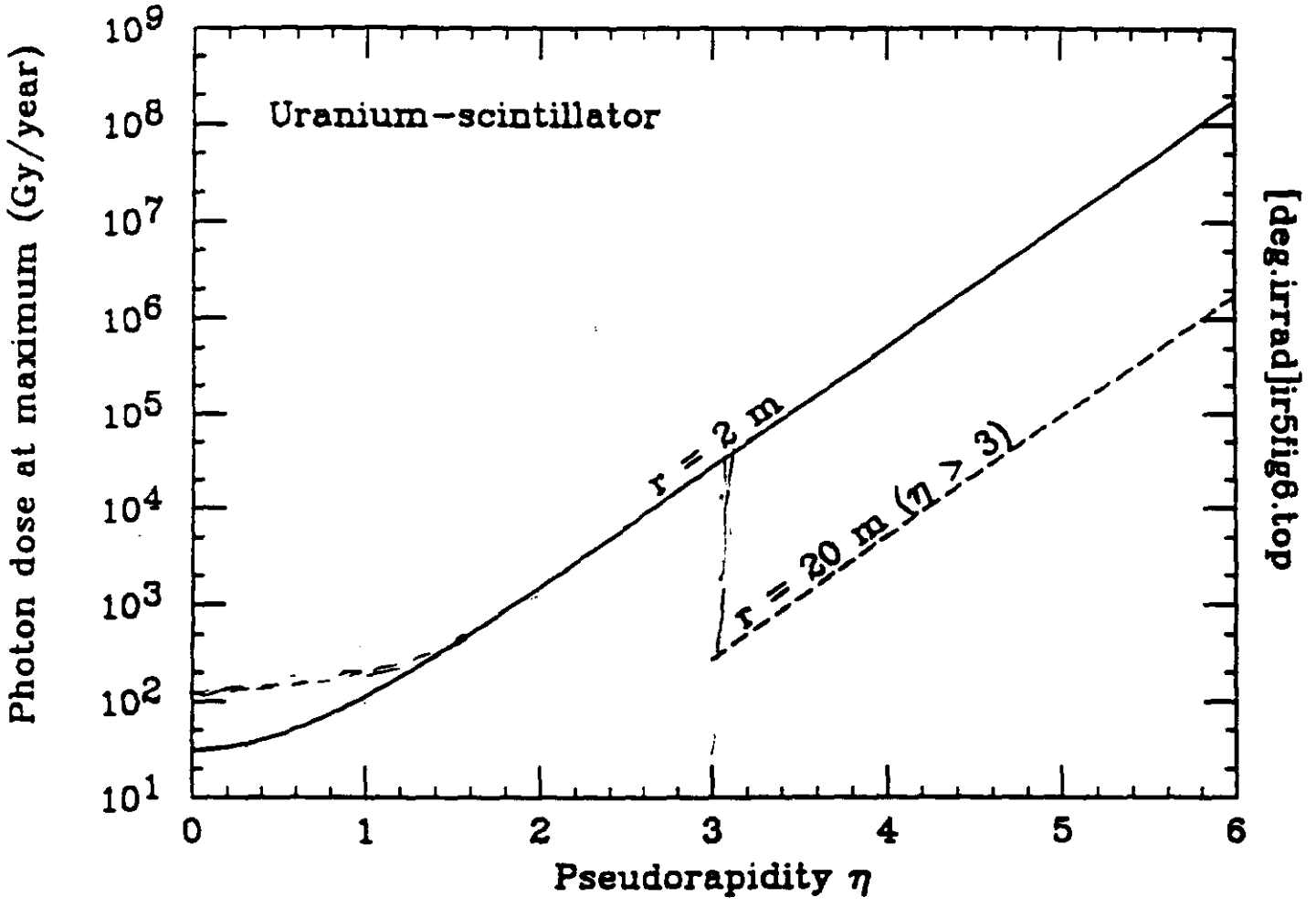

FIG. 5-6 *Revised.* The maximum dose from incident photons. The solid curve assumes the maximum occurs at 200 cm. The other curve is calculated for 20 m, typical of forward detectors.

FIG. 4. Revised Fig. 5-6 from SSC-SR-1033. Maximum dose is for lead (or uranium) plat the calorimeter, and may be somewhat higher in the lower-Z sensitive material.

Fig 18

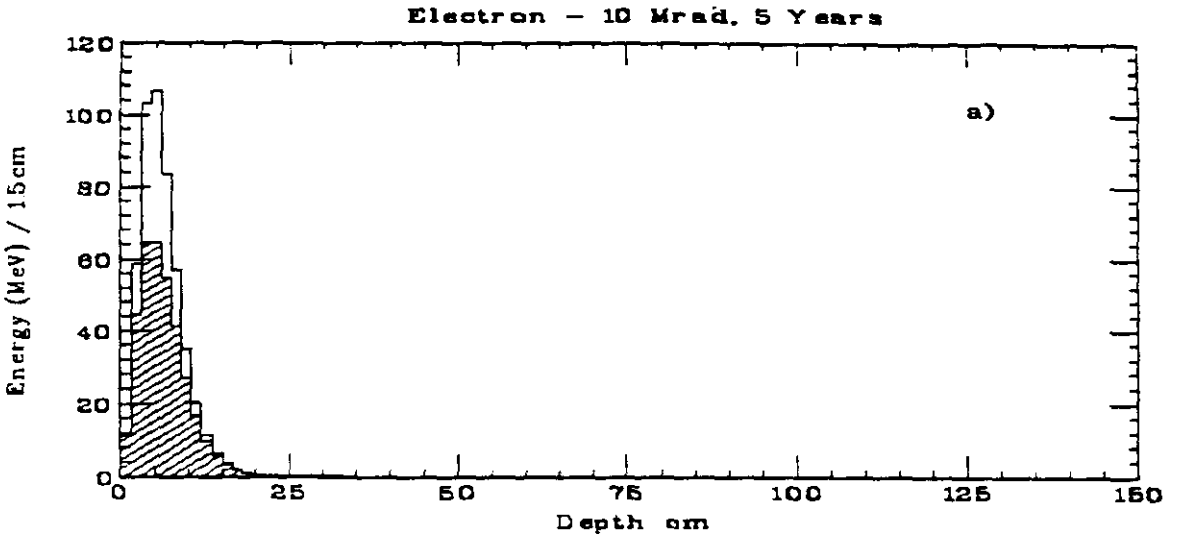

Fig 2a. Electron shower depth profile. The unshaded histogram is the original profile, while the shaded histogram is the resultant profile after 5 years at 10 Megarads/year at 1% signal loss/Megarad/year done geometrically(see text).

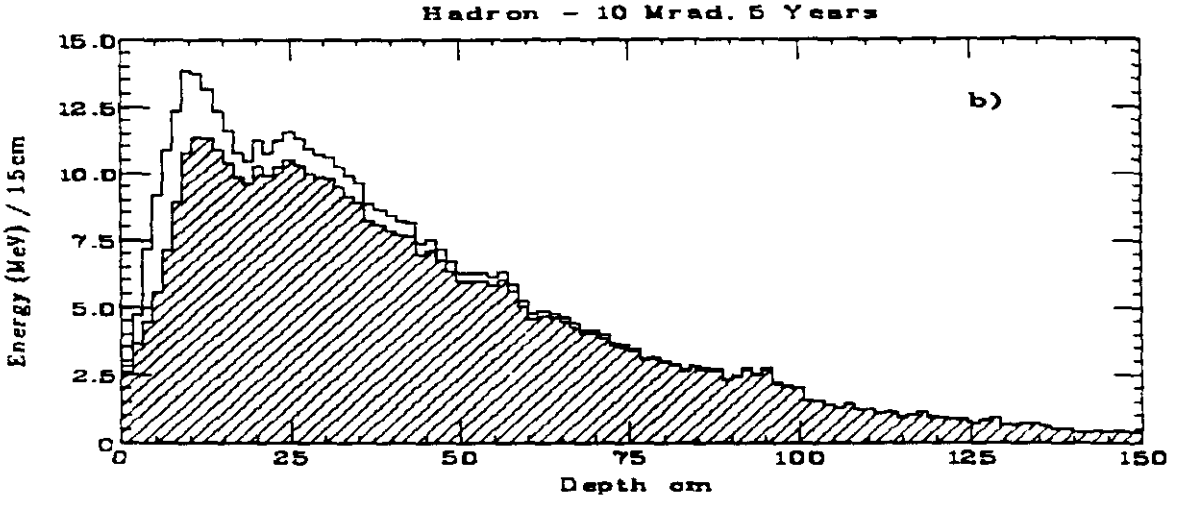

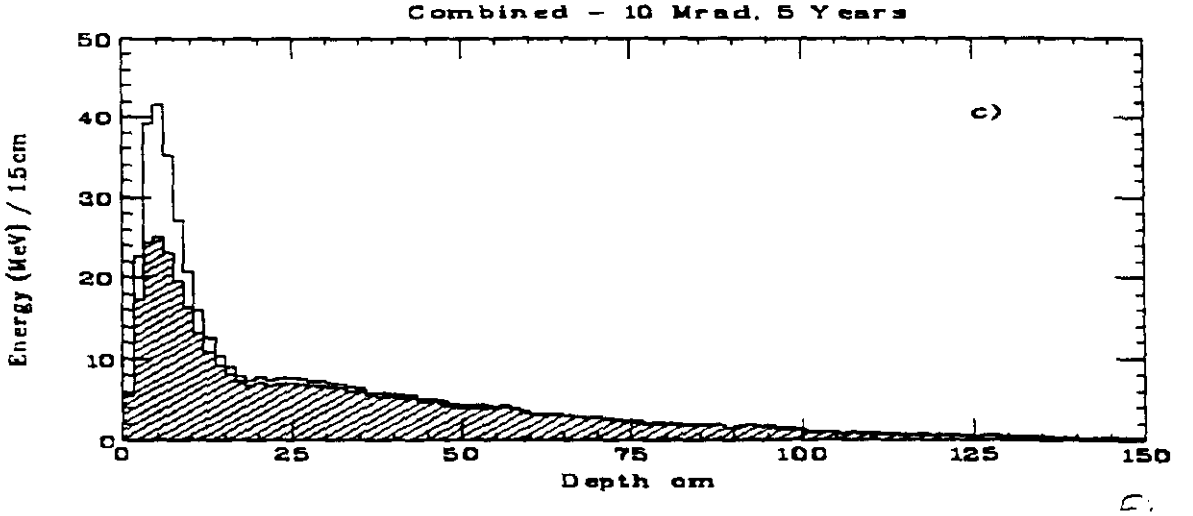

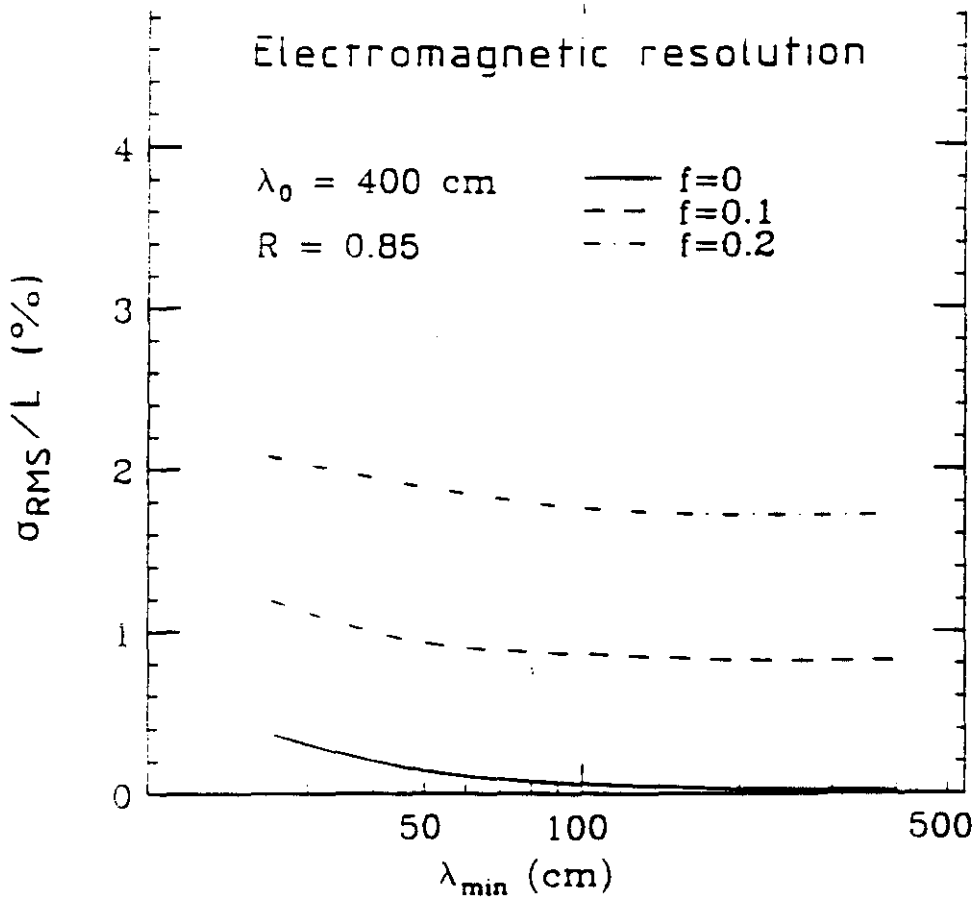
Electromagnetic resolution
λ0 = 400 cm
R = 0.85
f=0
f=0.1
f=0.2
σRMS/L (%)
0
1
2
3
4
50
100
500
λmin (cm)

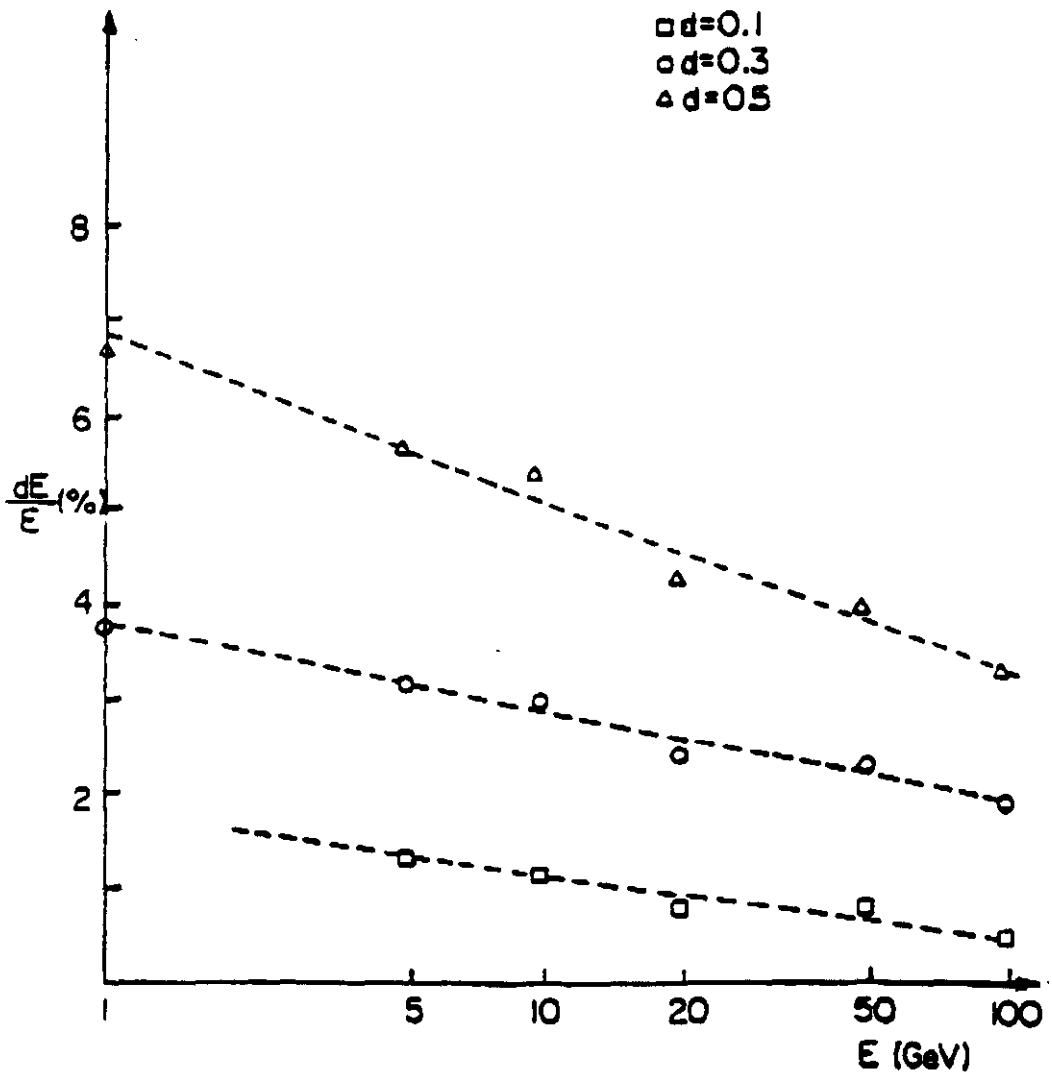
d=0.1
d=0.3
d=0.5
dE/E (%)
2
4
6
8
1
5
10
20
50
100
E (GeV)

Fig 20

Radiation Damage with current fibers

1 Year at 10^{33} luminosity

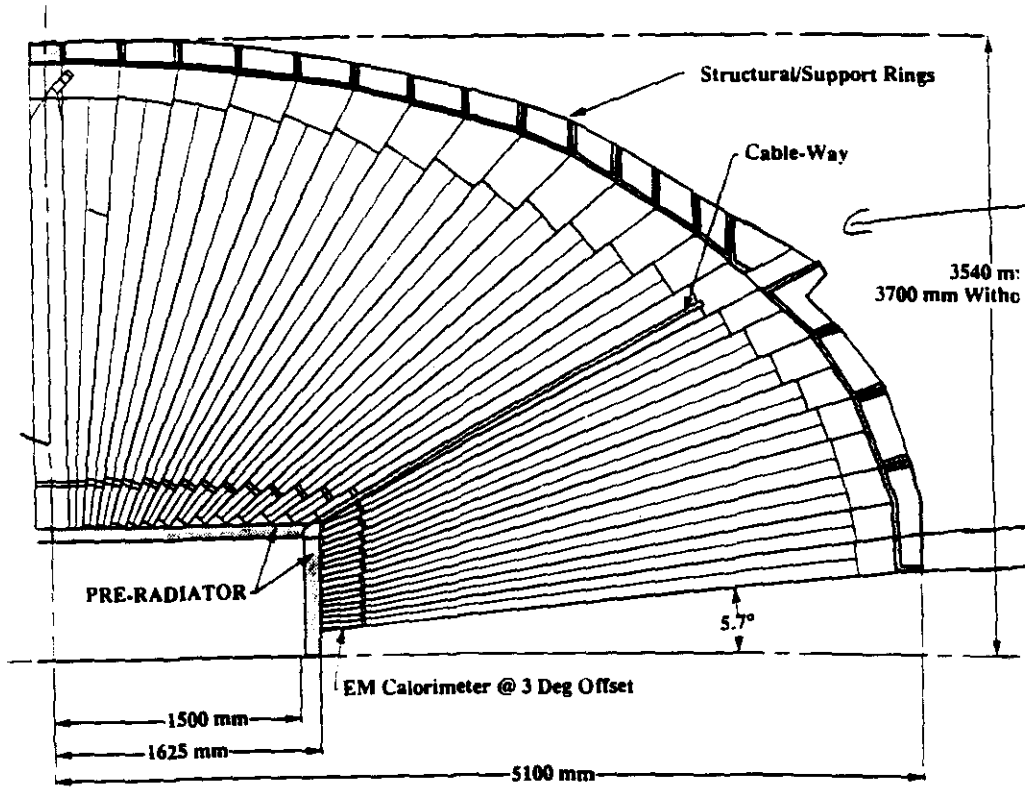

Not Affected

Calibrated gain + linearity shifts

Figure 3.3-3 Spaghetti Calorimeter

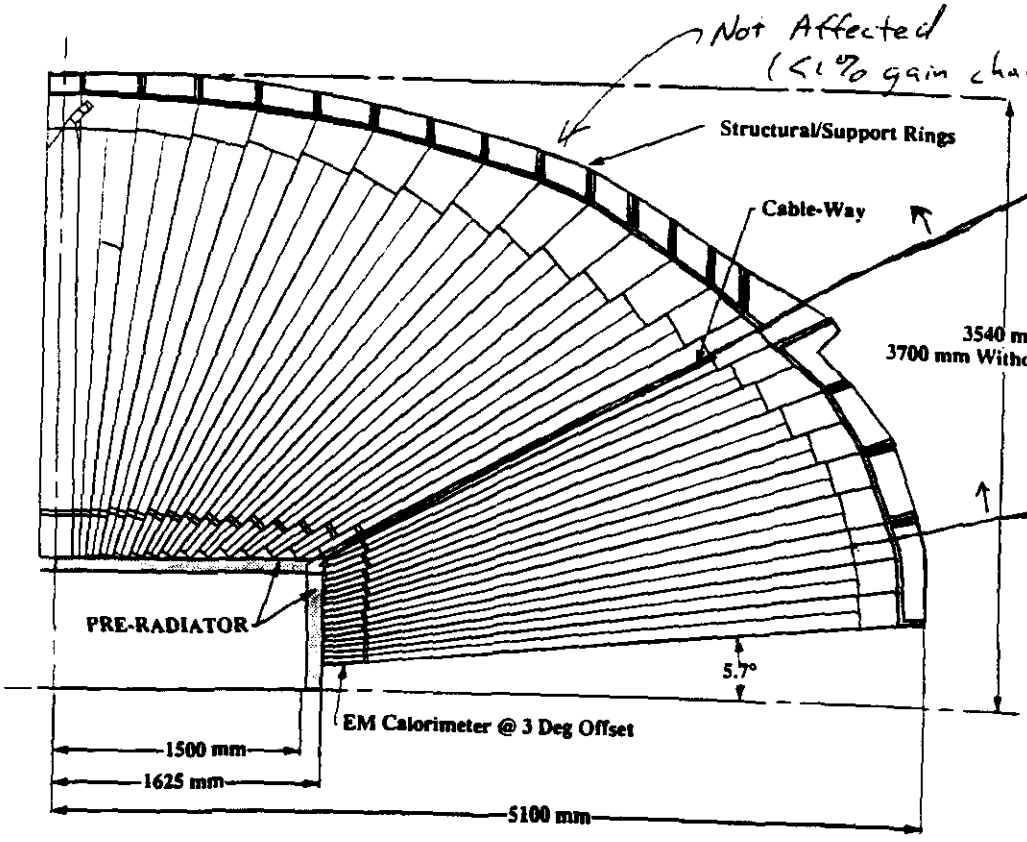

Not Affected (<1% gain change)

10 Years at 10^{33} luminosity

Calibrateable gain + linearity shifts

≥1% non-correctable energy resolution degradation

Figure 3.3-3 Spaghetti Calorimeter

Fig 21

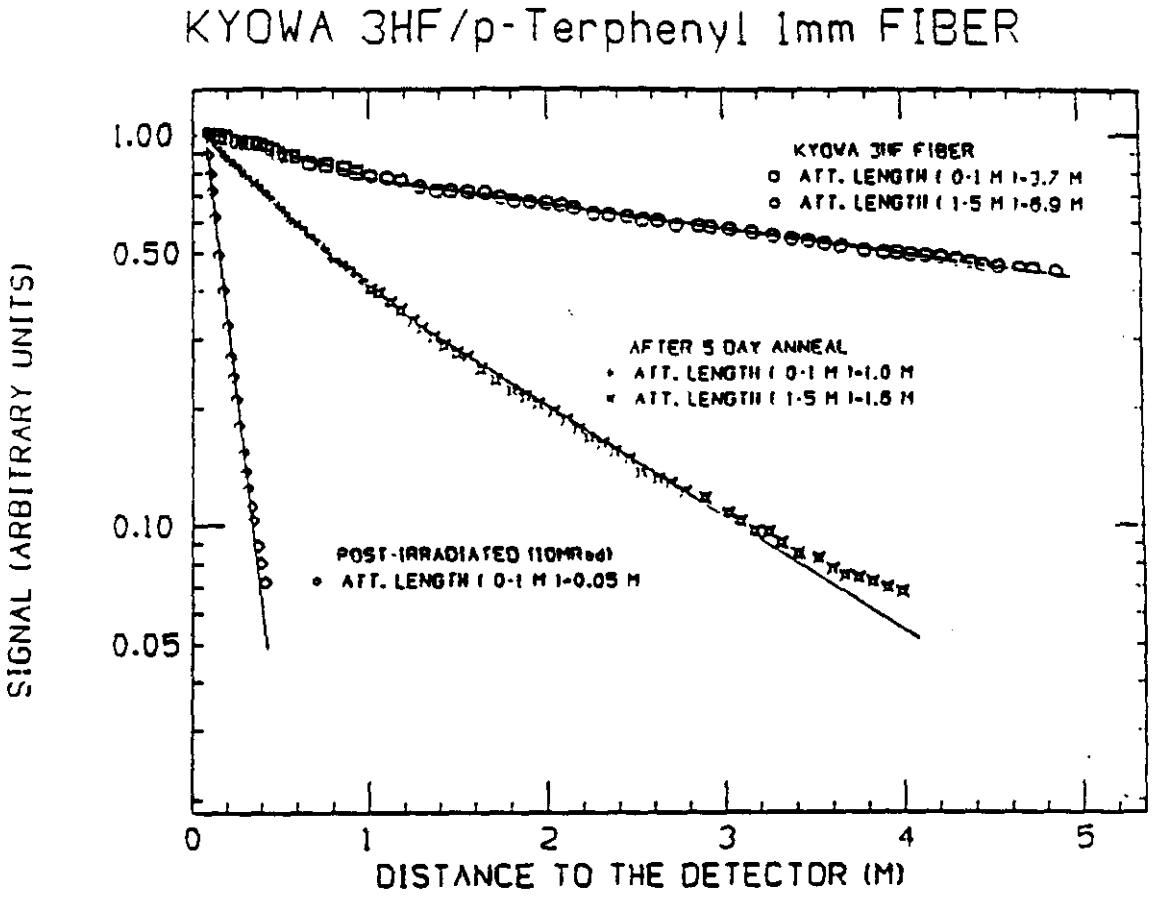

Fig. 12. Attenuation curves measured for polystyrene fibers doped with 3-HF, before and after irradiation with 10 MRad, and after 5 days annealing. Data are from Ref. 7.

Fig 22

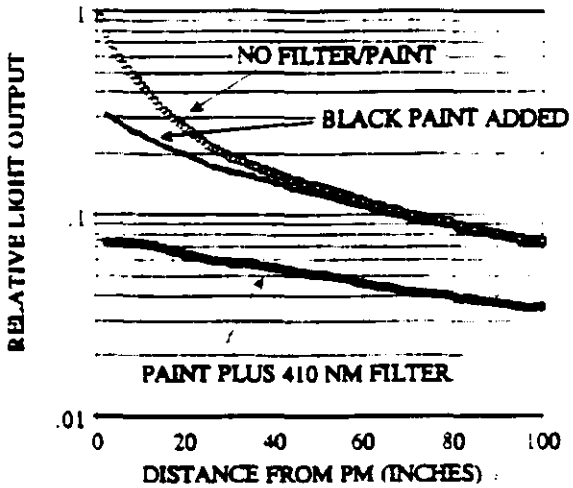

Figure 6: The effect of cladding light upon the attenuation curve can be eliminated by applying an extramural absorber (in this case, a one-inch long layer of black paint one cm from the PMT end of the fiber). An appropriate filter can eliminate the remaining effect due to short-wavelength absorption by the plastic.

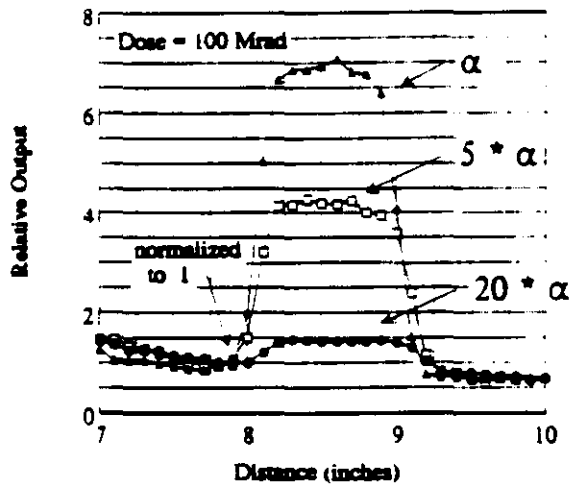

Figure 7: The effect of the concentration α of the fluor 3HF upon the loss in intrinsic scintillation yield after irradiation (and recovery). A portion of the fiber was protected from irradiation by use of a lead shield. The size of the step between the irradiated and virgin section of the fiber gives a figure of merit: the larger the step, the larger the loss in intrinsic scintillation yield.

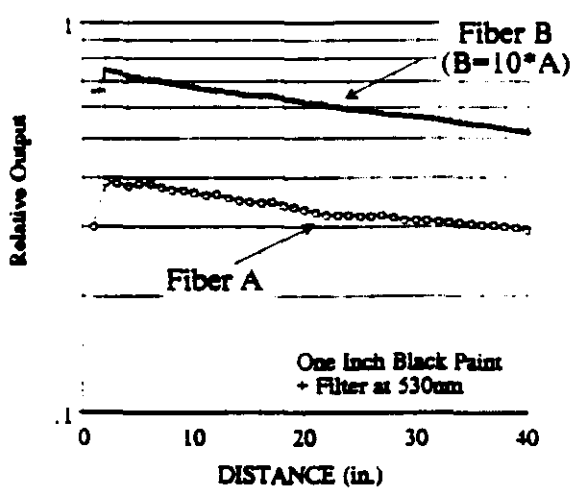

Figure 8: The effect of 3HF concentration upon the attenuation curve of the fiber. Fiber B uses 10 times the concentration of 3HF doped in fiber A.

Fig 23

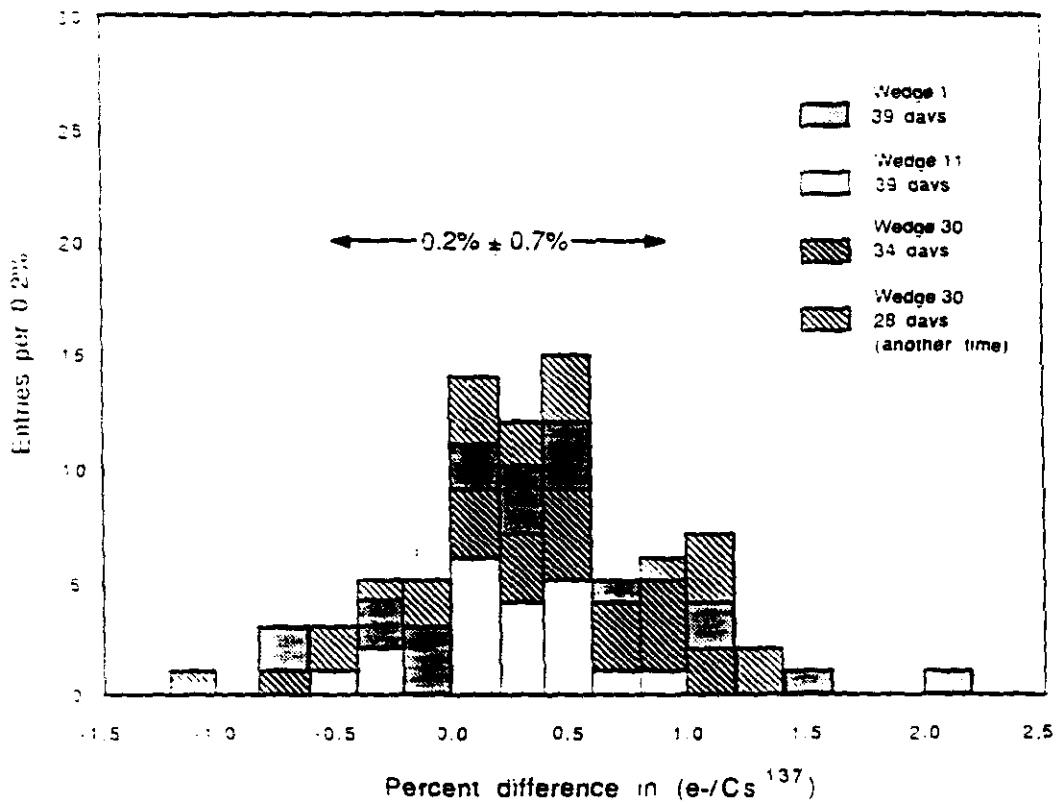

Fig. 16. Calibration reproducibility. The difference in beam to ^{137}Cs source ratio for each tube is plotted for successive calibration procedures, about 5 weeks apart, for three modules. The deviation of the centroid from zero corresponds accurately to the source decay.

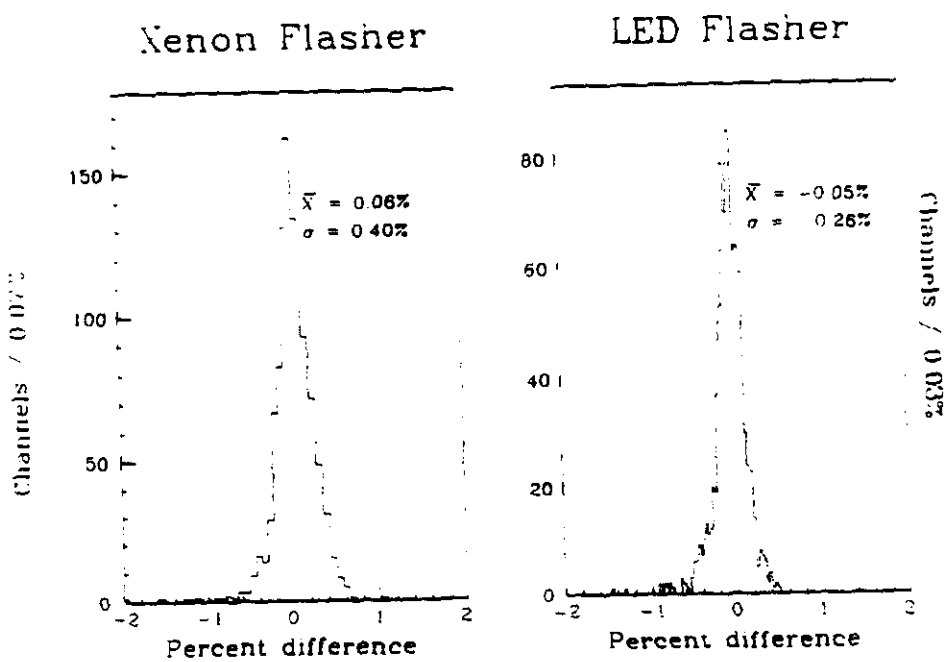

Fig. 12. Comparisons of two xenon flash and LED runs separated by about a day. For the xenon flash, the ratio of raw phototube signal to Pin diode signal was compared; while for the LED's, the raw phototube signal was used.

Fig 24

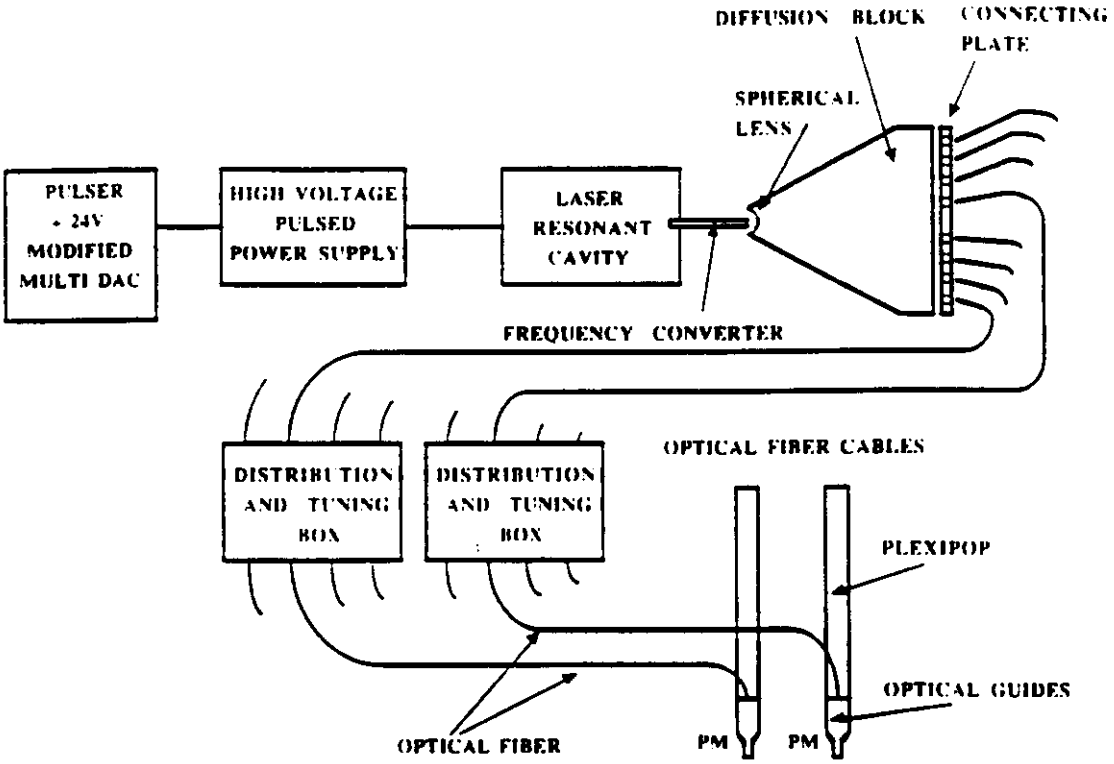

Fig. 1. Hardware schematics of the monitoring system.

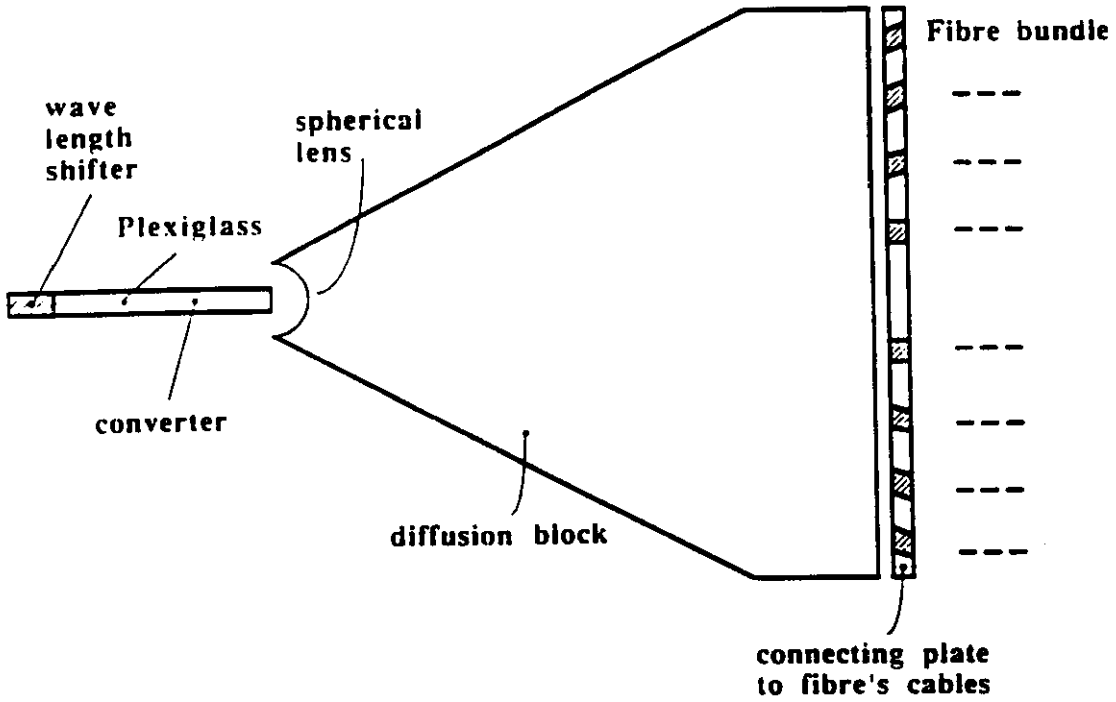

Fig. 4. Converter and light diffusion block.

Fig 25

a)

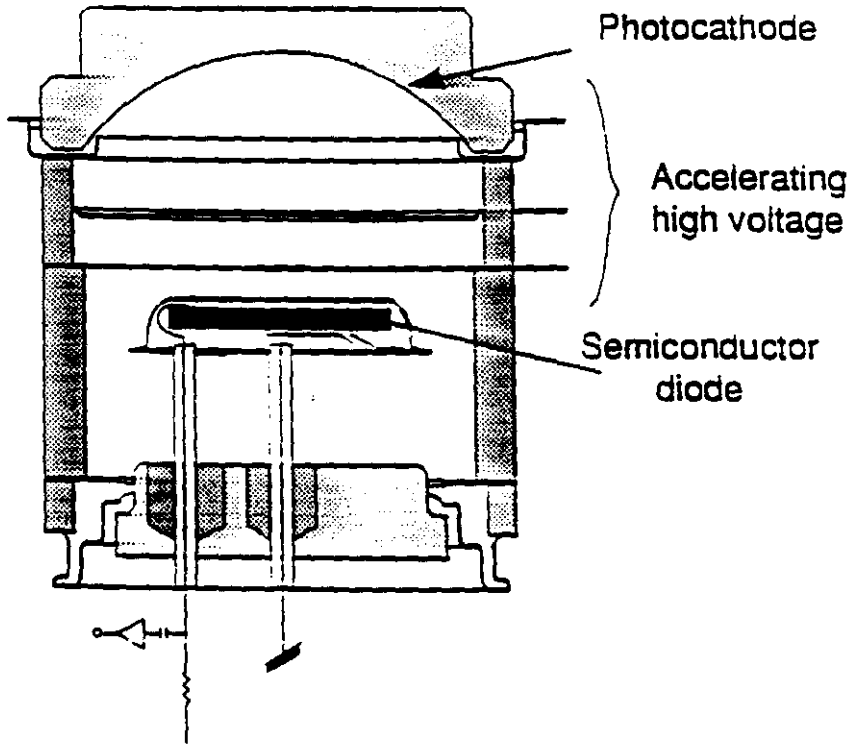

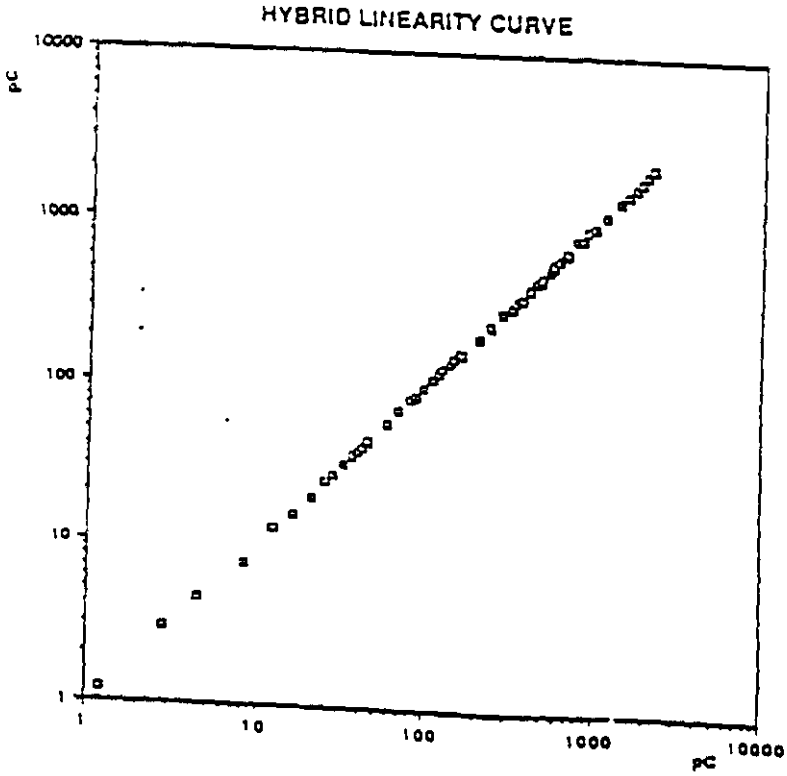

Figure G2.4

Fig 26

H. Gordon, P. Mockett, V. Radeka, J. Rutherfoord

Sept. 5, 1991

GEM Calorimetry

Answers to the questions for Liquid Argon

II. For Liquid Argon (Harvey Newman)–

A. What is the ideal resolution that can obtained, as shown with a GEANT simulation including a reasonable cryostat and particles incident up to the maximum relevant angle wrt the normal, for the EM part ?

• Answer: NA31 is an example of a large detector using liquid argon. They have a resolution of $7.5\%/\sqrt{(E)} \oplus 0.5\%$ in an real experimental environment[1]. They have also measured a stability of the system of less than 0.5% over months of operation as well as a uniformity of 0.5% versus position over the entire detector. GEANT simulation of the EMPACT EM calorimeter and cryostat (4 cm of Al[2]) showed a resolution of $7\%/\sqrt{(E)}$. We are planning to construct a test calorimeter that will provide $6.5\%/\sqrt{(E)}$ resolution. This appears to be quite feasible given the extensive experience in liquid argon calorimetry that has been achieved over the years. An attractive new structure for liquid argon calorimetry has been developed recently in the RD3 collaboration in which BNL is a collaborator. This is referred to as the accordion calorimeter. It appears that this technique will provide an easier system to build and could be more hermetic in azimuth than the well established parallel plate design. The tests of this calorimeter gave $9.6\%/\sqrt{(E)}$ with 100 ns peaking time. There has been a full GEANT (EGS) simulation of the accordion structure with 2 mm lead/stainless steel plates for particles incident at 90°.[3] The result is $8.7\%/\sqrt{(E)}$. We are proposing to continue R&D in FY92 to design and test a prototype accordion calorimeter with 1 mm lead plates. The GEANT simulation predicts a resolution of $\approx 7\%/\sqrt{(E)}$. GEANT also predicts that an accordion system with 1.5 mm lead plates and with the substitution of krypton for the argon would produce a resolution of $6\%/\sqrt{(E)}$. Because of the higher risk in the accordion design, we are also pursuing a more conventional parallel plate structure that meets the requirements of signal speed and provides a resolution of $6.5\%/\sqrt{(E)}$.

B. What is realistic for the accordion design in a 4Pi Detector ? (1) Can 1mm plates be used in a reasonable mechanical design. What are the limitations on acceptance and resolution from internal spacers, support structures, etc. ?

- Answer: Our collaborators at CERN are pursuing the design with 2 mm plates which looks quite solid. The dead material in the barrel is quite minimal. The biggest problem is the transition region between the barrel and the end calorimeter. We are pursuing several ideas on how to minimize the dead material there. A full engineering design must be done for the 1 mm plates before these questions can be answered.

(2) What is the effect of liquid argon gap thickness variations on the resolution, given the readout sheets of Kapton and copper traces that are not negligibly thick compared to the liquid argon gap ? (A simple simulation is needed to answer this question, but systematic variations over a tower must average out to the few micron level to avoid degrading the resolution).

- Answer:

It is easy to show that the peak current I_m in a LAr chamber for minimum ionizing particles is independent of the gap. The induced signal charge Q $=I_m t_p(1-t_p/2t_d)$, where t_p is the integration time and t_d is the electron drift time, see Fig. 2. The ratio of the relative variation in the signal charge and the relative variation in the electron drift time (the gap) is simply $t_p/2t_d$. For a 40 nsec integration time this ratio is 1 over 20. So for example a 20% gap variation would result in only a 1% signal change.

This answers both the questions raised. An advantage of fast calorimetry with LAr is that the effect of gap variations on the measured signal is attenuated by a large factor (there is an additional effect of the electric field variation, but of the opposite sign). It is also obvious that one has to calibrate with a defined peak current and not with a charge defined for the long pulse (as assumed by Denes). Then the calibration is also insensitive to gap variations, and to the calibration pulse width.

Also there is empirical data from the 1991 accordion beam test with 100 ns peaking time. The beam was uniformly distributed over an entire tower. The energy resolution was measured to be $9.6\%/\sqrt{(E)}+0.0\%$. This prototype did not have the type of micron precision suggested in the question. In a sampling calorimeter of this sort, there are compensating effects when for example one gap is a little too thick, the next one will be

thinner by the same amount. Mechanical tolerances on the absorber are very important, however, for a systematic error of 0.5%, the pieces need to be controlled to $\approx 100\mu m$. Also even in D0 where the total charge is important we achieve better than 1% sampling variations.citemd Fig. 3B shows the variation in sampling fraction in the 32 modules X 48 towers in the D0 Central Calorimeter.[4] The sigma of the distribution is less than 1%. Fig. 4 shows the linearity of the D0 End Calorimeter with electrons from 10 to 150 GeV. The deviation from linearity is less than 0.5%.

(3) Is it possible to build accordion endcaps ? Can the gap sizes, radii of curvatures of the plates, and projective geometry be achieved in any real design. If so, will the construction cost be reasonable ? What is the tradeoff between the accuracy of the gap width, accuracy of the radius of curvature, resolution, and cost ? (4) Is it possible to build an HCAL accordion ? Again, what is the tradeoff between gap width accuracy, and radius of curvature accuracy ? Can one arrange to have projective towers ? What is the cost of tooling, machines, and measurement tools to build and verify the accuracy of the HCAL accordion ?

• Answer: There are several designs for accordion endcaps that we have heard about and even invented as a result of our trip to CERN in August, 1991. These ideas need to be worked out. In particular we show some of them in Fig. 1. There is a natural design for the endcap with a domed head that solves the problem of projective geometry. We assume for the baseline design only accordion EM sections with parallel plate structures for the hadron calorimeter. However, the RD3 is committed to testing an accordion hadronic module in 1992. We will keep close watch of their progress.

(5) Wherever an accordion cannot be used, what are speed limitations due to capacitance per tower – or will the number of towers have to be increased substantially ? If the number of towers are increased, what is the cost increase ?

• Answer: We propose to develop a parallel plate design for the hadronic calorimeter with some synthesis of the D0, SLD, H1 and RD3 designs. The speed would be achieved through the use of wide strip lines with no compromise in speed of the signal relative to the accordion. The electrostatic transformer concept[5] would be used to reduce the capacitance seen by the preamps.

B. What is the effect on EM and HCAL resolution and acceptance of the cryostat walls between the barrel part and the endcap part, whether we have accordion modules or not ? This requires a full simulation of at least a strawman-design.

• Answer: We have not been able to get the engineering to do the strawman design yet, however we refer to our published work[6] which shows that the cryostat walls and support structure need not affect the physics. The crucial design goal is to reduce the thickness of the walls so there are not more than a few radiation lengths of dead material. This probably will require stays.

C. Overall Mechanical Design –

Will the overall detector radius be increased ? If so, what is the extra cost of this ?

• Answer: There is no need to increase the radius of the detector. The number of absorption lengths appears to be adequate for the muon detector. Compared to those techniques which do not require a cryostat, however, the strengths of liquid argon have not been demonstrated in any other technique: uniformity, ease of calibration, radiation hardness, etc. We also will consider the use of uranium which will increase the density by about 20%.

D. Electronics –

As shown by Denes, high occupancy as well as high rate is part of the problem of readout. With shaped signals that integrate to zero, and may therefore (as in the pulse used in the accordion test this year) include a long flat negative baseline shift, how accurately can one actually pick off the signal from the shifting baseline:

• Answer: This is not a baseline shift - pileup with bipolar shaping does not change the baseline as shown in NA34 and at BNL at rates up to 2×10^6 in one spot. We have always included the contribution of the negative lobe of the bipolar shape as the pileup contribution to the energy resolution(as did Peter Denes), therefore, no special treatment is needed. Specifically in Table 1 are some calculations based on the measured values of noise from the 1991 accordion beam tests and pileup as calculated by Cleland et al.[7]

You can see that the optimum for 10^{33} is between 40 and 20 ns but the total noise would not degrade the energy resolution of a calorimeter with intrinsic resolution of $7\%/\sqrt{(E)} \oplus 0.5\%$.

Table 1: Noise in Accordion EM

		5 X 5 cells	3 X 3 cells	
peaking time	40 ns	20 ns	40 ns	20 ns
$\sigma_{thermal}$	62 MeV	170 MeV	37 MeV	102 MeV
σ_{pileup}	166	114	98	67
(10^{33}) σ_{total}	177	205	105	122

(1) How many points are needed to pick off the signal to an accuracy of 1% ? of 0.5 % at a luminosity of 10^{33}.

- Answer: Optimally 1.

(2) At a luminosity of 10^{34} ?

- Answer: Optimally 1.

(3) How much data must be stored before and after each significant "peak" in the output data stream, to be able to pick off the signals to the desired accuracy ?

(4) What is the size of the resolution tails generated by baseline shifts which are imperfectly corrected, in a given (realistic) sheme of following the baseline ?

(5) How much does it cost to shape the signal, store the history, and pick off the signal to high accuracy – per channel, compared to the fast (single beam crossing) readout of a homogeneous calorimeter ?

- Answer: As pointed out in the article by Cleland et al.[7], there is a method called adaptive filtering which can optimize the signal to noise for luminosities other than that designed for. Four samples around the peak are a minimum. Hopefully the cost of this would be included in the system cost. This is to be compared with 2 points even for BaF_2.

LIQUID ARGON(Scint Cal - Bill Worstell):

1) How can liquid argon EM calorimeters expect to achieve a 7% stochastic term in the energy resolution and at most a 1/2% constant term in the energy resolution in the face of the following difficulties?

a) What is the best stochastic term that has been measured with a liquid argon module in a test beam, using only the a fast shaped pulse within a narrow gate? How does the measured resolution vary with energy, and is there a linear or quadratic constant term?

How does the measured resolution vary with pulse rate? What is the anticipated resolution as a function of eta (is it variable?)

- Answer: NA31 has demonstrated 7.5improves the stochastic term. The stochastic term from the accordion test in 1991 with 100 ns shaping time is $9.6\%/\sqrt{(E)}+0.0\%$. This is the result of a fit to the data from 29 to 146 GeV. The stochastic term and the constant term do not depend on shaping time as far as we know for electromagnetic showers. Only the pedestal width depends on shaping time. We propose to use 40 ns for the SSC. We will try to improve the stochastic term by using 1 mm lead sheets, but this requires more R&D. For the resolution vs. η see the answer to Newman IIa above.

b) What uniformity has been measured when varying the incident position of particles across the front face of a module? What mechanical tolerances are required in order to preserve the required resolution against variations in incident position and longitudinal shower fluctuations? Is there an engineering design which can meet these tolerances and/or achieve this resolution in the endcap region, as well as the barrel?

- Answer: The uniformity of the accordion across 1 cell is $\approx 1/2\%$. The NA31 calorimeter published a $\approx 1/2\%$ variation for a large device [1] We feel that with attention to tolerances of $\approx$ 0.1mm, this precision can be achieved both in the barrel and endcap (which is just a rotation of the barrel design).

c) If tail-catchers are included in the baseline hadronic design, has it been shown that longitudinal fluctuations in high-energy showers into this region will not give an unacceptably large constant term?

- Answer: There are GEANT simulations of liquid argon EM + a) liquid argon/lead; b)liquid argon/stainless steel; and c) 1 mm scintillating fiber/lead which give the following results: a) $(63\pm4)\%/\sqrt{(E)}+(1.6\pm0.4)\%$; b)$(62\pm5)\%/\sqrt{(E)}+(2.5\pm0.5)\%$; c) $50\%/\sqrt{(E)}+0.02$.[8]

d) Are all readout and support materials known to be sufficiently radiation hard? If preamplifiers or other materials have variations after radiation damage (or long-term mechanical stress), there may be an unacceptable constant term because of longitudinal shower fluctuations.

- Answer: Yes. Radiation damage to preamplifiers will not affect longitudinal fluctuations - just a broadening of the pedestal. No gain variations in JFET's have been

seen up to 10^{15} neutrons/cm^2. Noise increases at $10^{14}/cm^2$ were less than 25%. Ionizing radiation up to 200 MR shows no increase of noise with fast shaping (40 ns) as shown in Fig. 5.

e) What is the response of the hadron calorimeter when high energy pions (100 GeV and above) scan across a preamp location? If the magnet crashes, what happens to the LArgon preamps from eddy currents, induced voltages, etc?

• Answer: Why should that matter??? Particles have hit preamps in NA34 without being detected. Eddy currents are not imagined to cause problems.

2) What is the effect of pile-up at 10^{33} and 10^{34} luminosity on EM and hadronic energy resolution? On the efficiency with which one can select electrons within a 0.7 rapidity unit isolation cone (5 GeV threshold)? A calorimeter will trigger preferentially on pileup events. What is the liquid Argon calorimeter trigger rate for 100 GeV p_T jets and 100 GeV missing p_T events?

• Answer: From Table 1 the total EM noise in a cone of 0.6 is 1.1 GeV at 10^{33} (3.3 GeV at 10^{34}). The hadronic resolution would be 4.3 GeV at 10^{33} (8.6 GeV at 10^{34}). One may question whether such a large isolation cone is the best way to isolate the signal. For example one may not require the entire depth of the hadron calorimeter (a reduction of noise of at least 2). One may use towers only about a threshold energy - say 1 GeV. The role of the preshower detector that distinquished γ's from π^0's would help significantly. This quoted noise should not bias the jet trigger which would use a smaller cone - eg. 0.2. Cleland et al.[5] studied missing E_T and within their statistics found no events beyond 100 GeV.

3) Is the cost of the calibration system included in the baseline? How can a single pulse ramp simulate signals from different parts of a single module, with possibly different gap spacing, etc?

• Answer: Calibration is required for all systems and so must be included in the cost. As mentioned above, the peak current is what is important not the charge - this needs to be distributed accurately to all channels.

4) What provision has been made for the rejection of pi-zero gammas from unfavorable jet fragmentations? (The rate of such fragmentation has large uncertainties, and these may dominate the Higgs $\rightarrow \gamma\gamma$ background.)

• Answer: There are 3 options being considered: a) Strips of electrodes 2 mm in width inside the cryostat measuring the first 3-4X_o as shown in Fig. 6. These have been tested at CERN in the beam in the RD3 collaboration. The main problem is how to multiplex the multitude of channels. b) The use of the silicon drift detector(SDD) after $3-4X_o$ inside the cryostat. The main problems are whether the SDD will withstand the radiation damage (tests are underway), to what extent this one longitudinal sample with perhaps 50μm precision will separate π^0's from γ's, and what to use to sample the first 3-4 X_o. c) The use of a silicon or scintillating fiber preradiator outside of the cryostat. Here the main problem will be the effect of the cyrostat and the magnetic field.

5) What is the constant term in the energy resolution for hadrons which one measures after 10 interaction lengths of non-compensating liquid argon ($e/h = 1.5 - -3\%$ constant term)? Precisely how has this been simulated, and when will it be measured?

• Answer: It will be measured in 1992 in RD3 at CERN. It has been simulated(see 1c above).

6) What is the effect of the cryostat and support structure on the hermetic containment of EM and hadronic shower energy? What are the consequences for missing Et measurement? How confident may we be that future changes in the mechanical design will not require significant increases in system size and further reductions in hermeticity? How many fasteners are needed to construct the full LArgon calorimeter subsystem?

• Answer: See answer to Newman B above. What relevance is the question of fasteners???

——————————————— III. LAr(Min Chen):

1. Uniformity of the pre-radiator.

• Answer: What does this mean? The preradiator can be as uniform as any other part of the liquid argon system.

2. Design of Accodion endcap.

• Answer: See answer to Newman B3 above.

3. 20 ns shaping.

• Answer: We propose to use 40 ns peaking time. This should be sufficient for 10^{33} and beyond - see answer to Worstell 2 above.

QUESTIONS AND CRITICISMS ON LAR-ACCORDION OPTIONS FOR GEM —

Hans P. Paar and Richard Wigmans

1. Cryostat.

How thick would the cryostat have to be for a full scale barrel LAr calorimeter? In which eta- area would the calorimeter performance suffer from this cryostat and how badly?

- Answer: (See answer to Newman IIa above)

2. Projective accordeon.

Can degradation of the electromagnetic resolution due to a projective accordeon structure be avoided (sampling fraction is a function of depth)! Are there Monte Carlo results available on this subject?

- Answer: See answer to Newman IIb2 above. There are beam tests of a projective accordion module now going on at CERN. There are plans for a more elaborate module for CERN for 1992. M. Lefbvre has a full GEANT simulation of the projective structure but has not finished the work.

3. Endcap.

How does one want to construct the endcap calorimeter with LAr technology? Which eta-area is covered by the endcap?

- Answer: See above.

4. Radiation hardness.

How does the measured radiation hardness of the cold electronics relate to the neutron fluxes expected at the position where this electronics will be installed?

- Answer: See above.

5. High voltage breakdown.

Although bipolar pulse shaping techniques allow to extract fast signals, LAr remains an intrinsically slow technology. Charge collection will continue for a long time after the event happened. In particular thousands of pp interactions will occur during the time needed to collect all the slowly drifting positive ions created in one event. As a consequence there may be considerable buildup of charge carriers in the gaps between the electrodes. Especially at high luminosities and large eta this may eventually lead to high voltage breakdown.

At which η will this become a problem for 10^{33} and for 10^{34}, or inversely, up to which luminosity will it be no problem for $\eta = 3$ and 5?

• Answer: The magnitude of the problem is a function of the gap width, voltage, and positive ion mobility as well as the ionization rate in the gap. To discuss the problem in a coherent manner it is useful to define a critical ionization rate and refer all ionization rates relative to this critical value. The critical ionization rate is defined on Fig. 7. It increases with the square of the voltage, linearly with the positive ion mobility and decreases with the fourth power of the gap width. Alternatively it increases with the square of the average electric field, linearly with the positive ion mobility and decreases with the square of the gap width. At electromagnetic shower maximum, where the problem is at its most extreme, the relative ionization rate is plotted versus η in Fig. 8. This is at the nominal luminosity for the SSC. For 10 times the nominal, the curve moves up by one order of magnitude. Fig. 9 shows what happens to the electric field in the gap for different values of the relative ionization rate. When the relative ionization rate is unity, a case which is only reached in the forward calorimeter at nominal luminosity, the maximum value of the electric field is twice the average value. At ionization rates above the critical value the maximum electric field rises with the one fourth power of the relative ionization rate. We have assumed a somewhat pessimistic value of the rather poorly known positive ion mobility. Also we have not chosen calorimeter design parameters which acknowledge this effect. Raising the voltage and/or decreasing the gap width actually reduce the problem (for relative ionization rates of order unity and larger), contrary to naive intuition. (I don't really know where breakdown will be a problem. We ran the Blazey cell up to 7 kV or so before we blew it out. I suspect the actual limit comes from the care required to manufacture a calorimeter without limits due to sharp edges, slivers, dust, etc. On the other hand I found in the literature a value of the dielectric breakdown constant that would have liquid argon arcing at the electric fields we routinely use??? I never understood this.)

6. Stability.

The positive ions buildup mentioned in 5 may also lead to changes in electric field and thus signal charge collection. The result may be that the calibration constant of a gap depends upon the luminosity. At what eta and luminosities is this a problem?

Does the accordeon prototype's analysis support the advertised stability of LAr? Are all gaps assigned the same calibration constant or are they adjusted individually? Does this mean that all cells need calibration in a testbeam?

Up to relative ionization rates of unity the signal is hardly affected at all. (This assumes the signal is defined as the total charge collected. This statement must be modified for short clipping times but I haven't worked this out yet.) This is because the charge collected is rather insensitive to the electric field as long as the electric field is large enough to prevent recombination. For reasonably pure liquid argon this electric field is quite low. Fig. 10 shows what happens to the signal for ionization rates above the critical value. A range of possibilities fall between the two curves. The range comes from my lack of understanding of recombination rates at very low electric fields. So except for eta very near 3.0 and at higher than nominal luminosities the signal is not at all sensitive to the charge buildup. All this discussion assumes that the calorimetry under discussion is the barrel and endcaps. The conclusions are quite different for forward calorimetry where positive ion buildup will be a major concern.

If liquid argon proves unworkable in the forward calorimeter, we propose using high pressure argon gas (30-40 atmospheres).

7. Uniformity.

Fig. 8 of the accordeon paper (CERN-PPE/91-73) shows the uniformity of the accordeon over a cell. We also need to know about the uniformity over a much larger region that encompasses different amplifiers and different regions of the detector.

- Answer: See quoted results from NA31 above.

8. Prototype tests.

We are extremely interested in the preliminary results of the ongoing BNL beamtests of Pb/Lar. Could these be provided in written form for evaluation by interested parties?

- Answer: Appended is a preliminary report from the BNL tests similar to the presentation given recently at the DPF meeting in Vancouver in Aug. 1991.

References

1. H. Burkhardt, NIM, A268, 116, (1988).

2. T. Adams et al., Design of the Liquid Argon Calorimeter, EMPACT/TEXAS Technical Note 351(1990)..

3. M. Lefebvre, M. Pepe, G. Polesello, LAr Accordion Calorimeter Simulation, LAR Note 1 (May, 1990).

4. M. Demarteau and H. A. Neal, Sampling Fractions of CCEM Modules, D0 note 912, Dec., 1989.

5. J. Colas and W.A. Wenzel, Electrostatic Transformers for Large Towers, Proceedings of the Workshop on Calorimetry for the Superconducting Super Collider, March 13-17, 1989, Tuscaloosa, Alabama..

6. T. Adams, et al., AN ENGINEERING DESIGN STUDY OF A HERMETIC LIQUID ARGON CALORIMETER FOR THE SSC, Nucl. Instru. and Meth. A306,128(1991)..

7. W. Cleland et al., Proceedings of the Symposium on Detector Research and Development for the Superconducting Super Collider, Oct. 15-18, 1990, Fort Worth, Texas, 382(1991)..

8. M. Nessi et al., "Comparison between few hadronic calorimeter scenarios", CAL-TR-037, Feb. 1991..

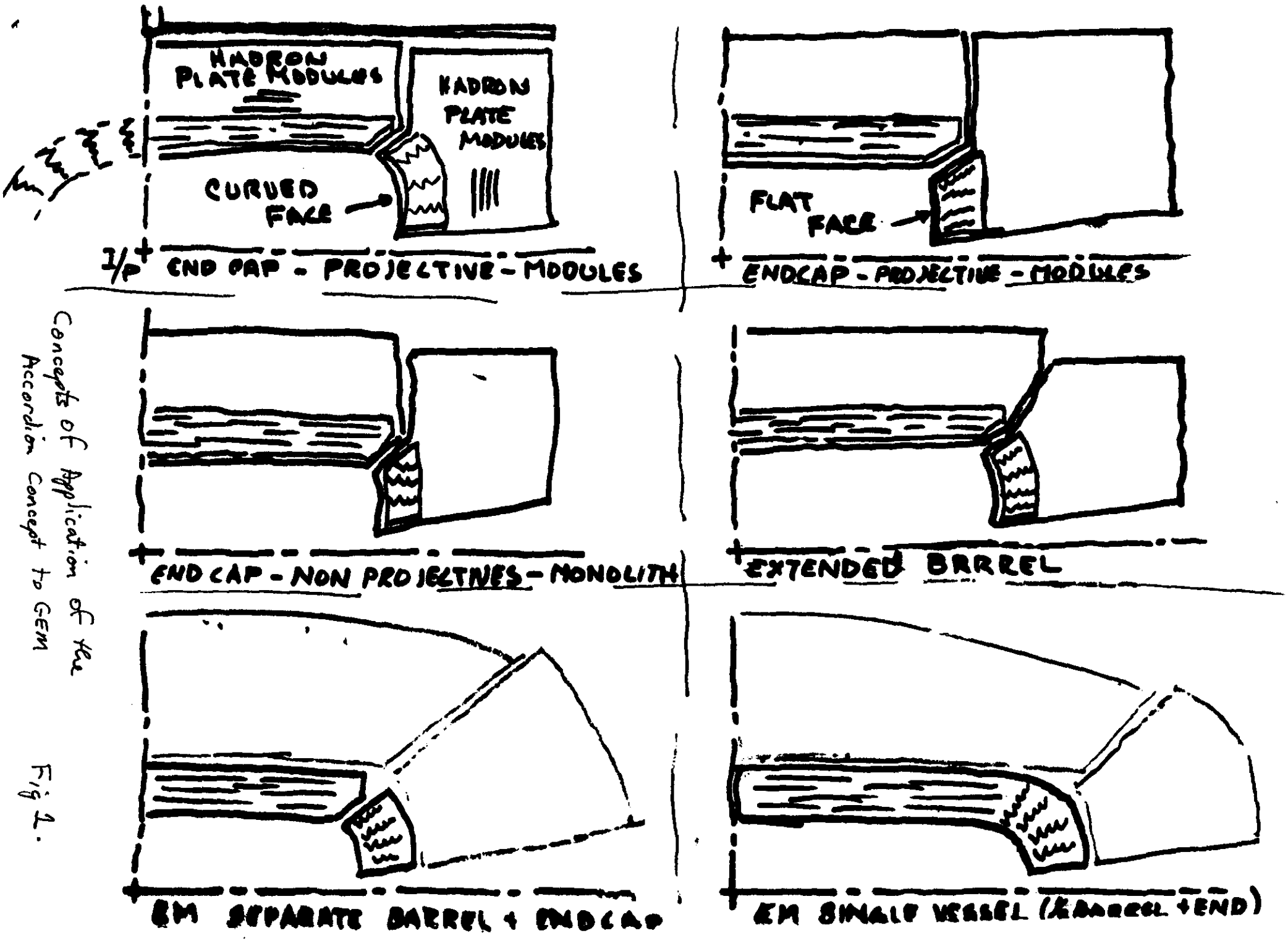

Concepts of Application of the Accordion Concept to GEM

Fig 1.

Pulse width

single carrier:

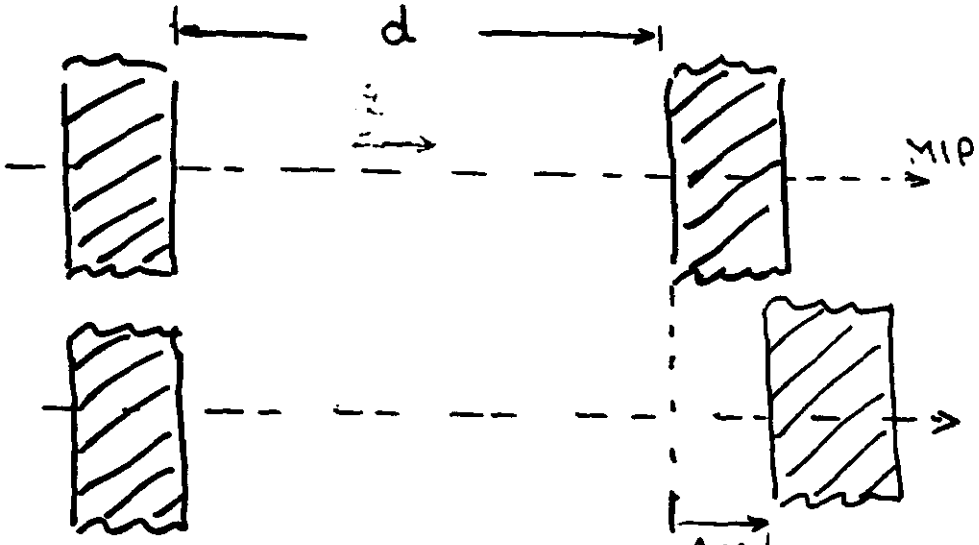

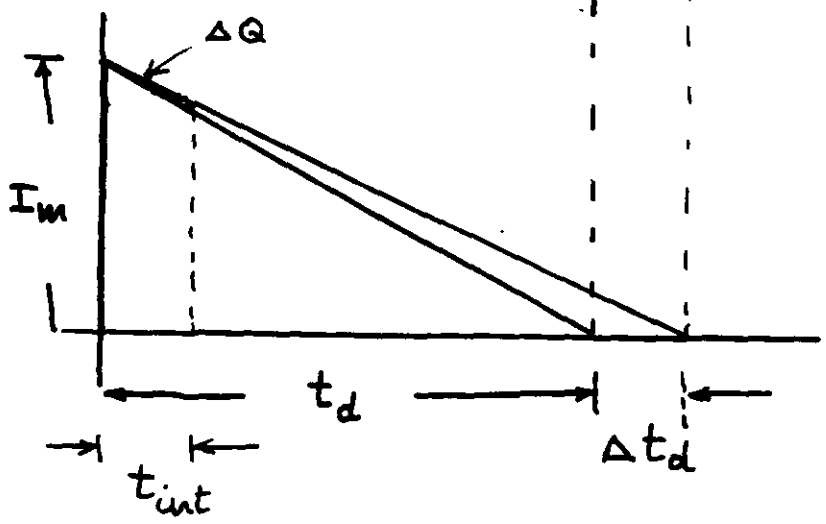

MIP responce:

$$I_m = e \frac{du_e}{dx} \frac{d}{t_d}$$

$$= e \frac{du_e}{dx} v_e$$

I_m is independent of d!

Long integration: $t_{int} > t_d$ $\quad Q_s = \frac{1}{2} I_m t_d$

Short integration: $t_{int} \ll t_d$ $\quad Q_s = I_m t_{int} \left(1 - \frac{1}{2} \frac{t_{int}}{t_d}\right)$

$$\frac{\Delta Q_s / I_m t_{int}}{\Delta t_d / t_d} = \frac{1}{2} \frac{t_{int}}{t_d} \approx \frac{1}{20}$$

for $d = 2$ mm (400
$t_{int} = 40$ use

∴ 20% gap variation results in 1% signal variation.

Calibration should be by I_m and not by $Q = \frac{1}{2} I_m t_d$

Fig. 2

M. Demarteau and H. Neal

DØ

SAMPLING FRACTION VERSUS MOD. NO. (INTERPOLATED)

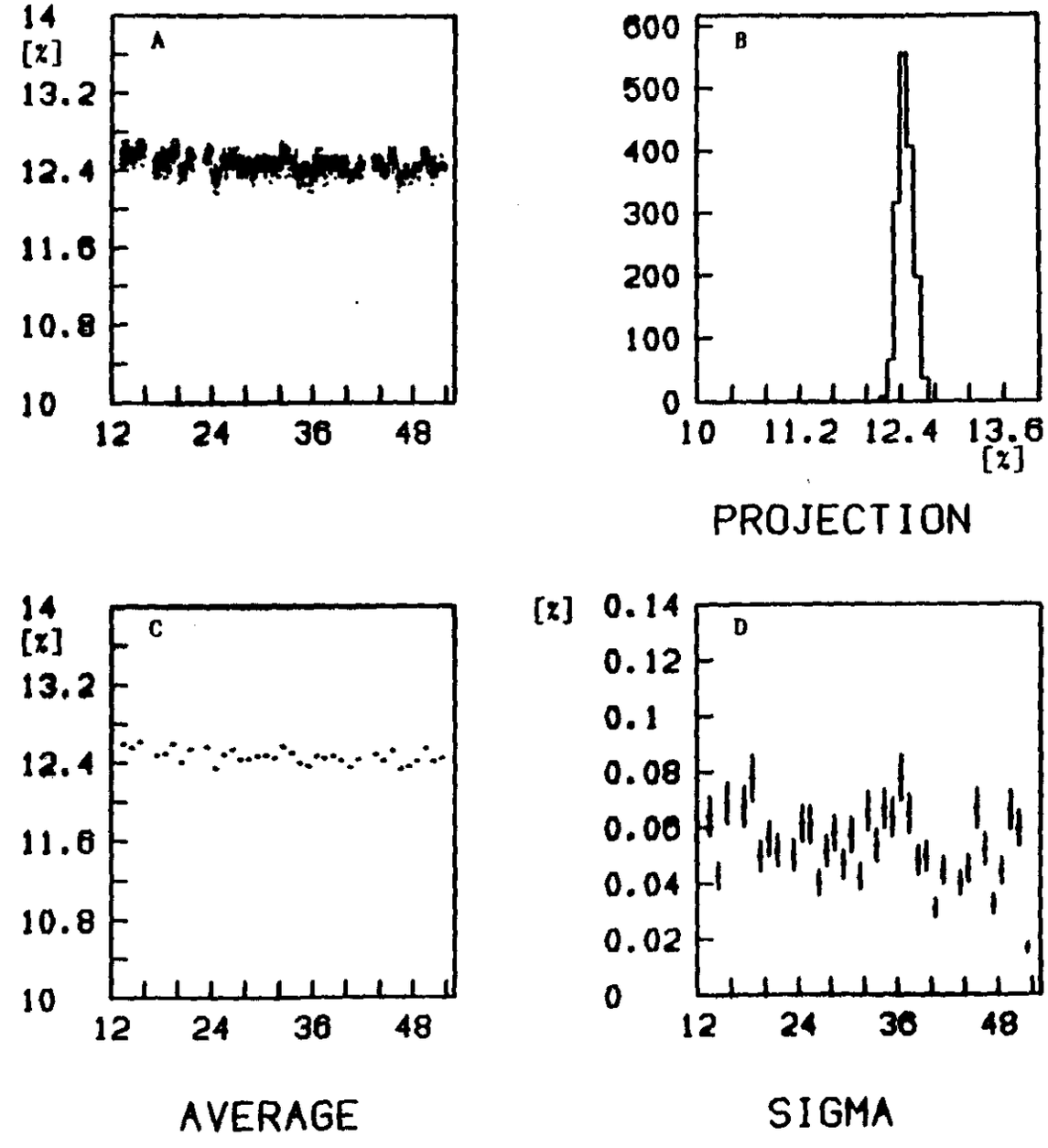

32 EM modules each of 48 tower.

Fig. 3

ECEM LINEARITY OF RESPONSE

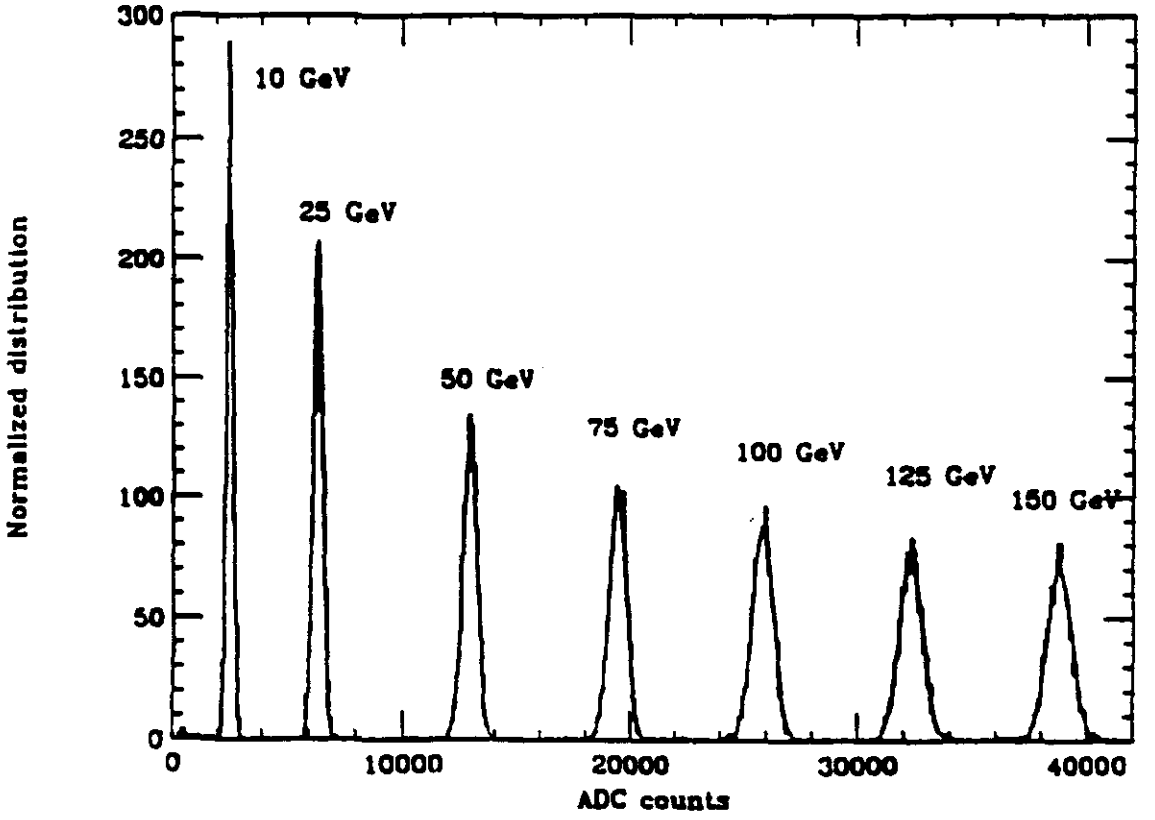

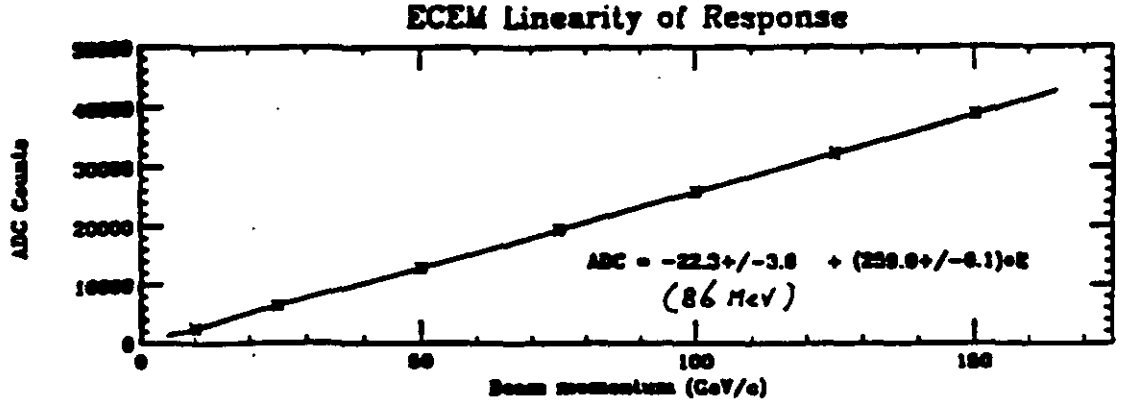

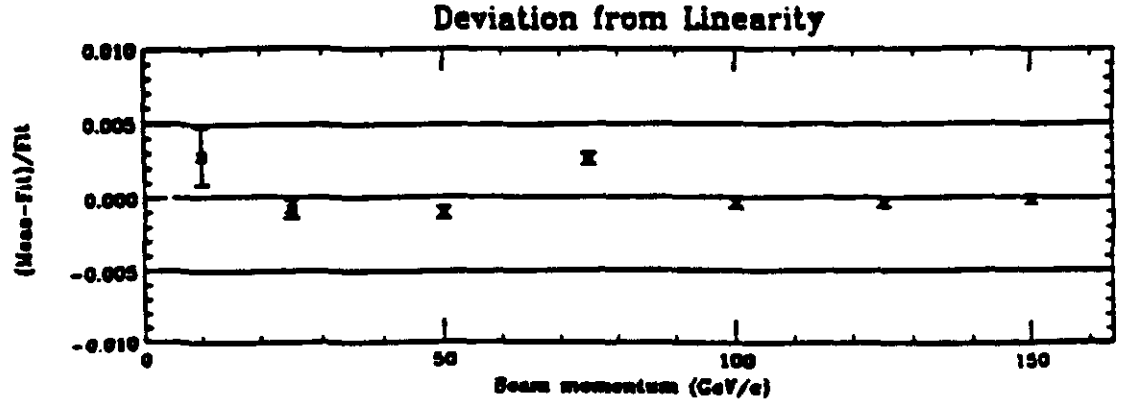

± 0.5 %

Fig. 4

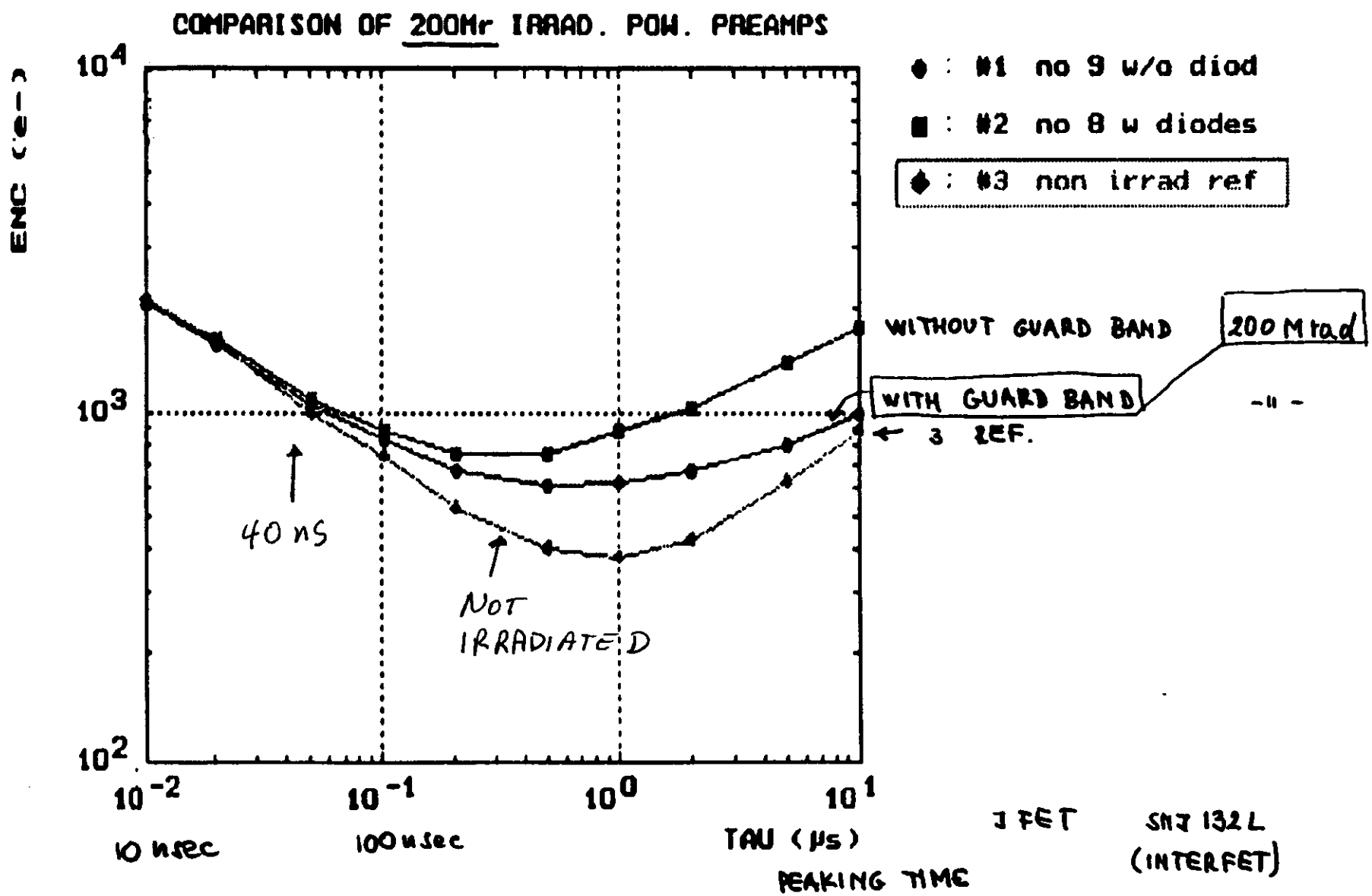
COMPARISON OF 200Mr IRRAD. POW. PREAMPS
ENC (e-)
10^4
10^3
10^2
10^{-2}
10^{-1}
10^0
10^1
10 nsec
100 nsec
TAU (µs)
PEAKING TIME
♦ : #1 no 9 w/o diod
■ : #2 no 8 w diodes
♦ : #3 non irrad ref
WITHOUT GUARD BAND
WITH GUARD BAND
200 Mrad
← 3 REF.
40 nS
NOT IRRADIATED
JFET
SNJ 132L
(INTERFET)

Fig. 5

PRESAMPLER | First look

* Correction for dead material in front of calorimeter [cryostat, coil]

* "high granularity"
  → e/π separation
  → π^0/γ identification

* 2 layers of "ministrips" behind 1cm Pb (+ Al)

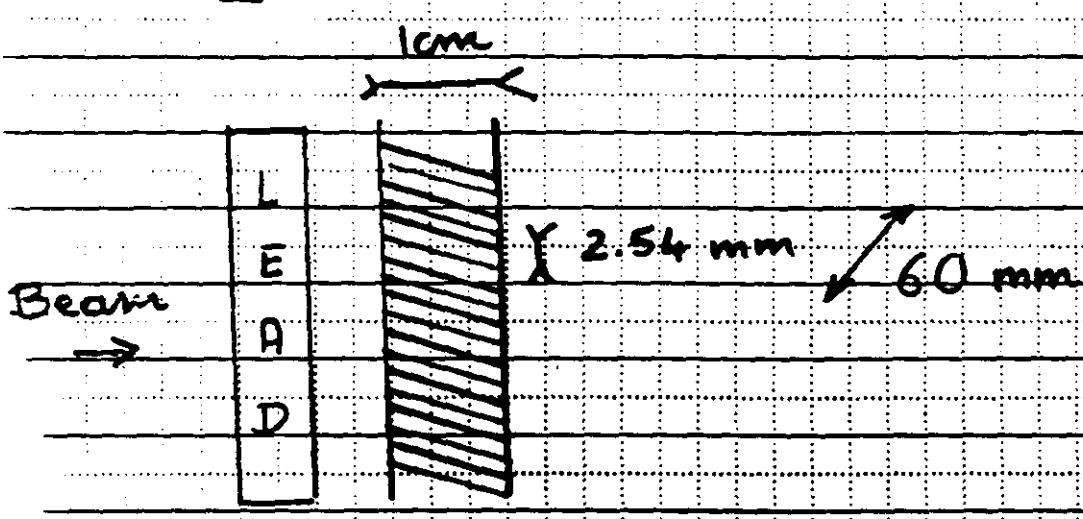

– signal
– ground

$C \simeq 15\,pF$

minionizing collected charge $\approx 8000\,e$

noise: presently ≈ 4000
using cato p.amp

Fig. 6

DEFINING EQUATIONS

Critical charge density: Charge in gap equals charge on plates

$$\rho_c \equiv e n_c = 2\sigma/a = 2V_o\epsilon/a^2$$

Ionization Rate: Units of ions/mm^3/sec

$$D_c = \frac{n_c}{\tau} = \frac{4V_o^2\epsilon\mu_+}{ea^4}$$

Associated critical current density

$$J_c = eaD_c = \frac{4V_o^2\epsilon\mu_+}{a^3} = \frac{2V_0\mu_+}{a}\rho_c = 2v_+\rho_c$$

Full ionization rate with recombination

$$D(z) = D_i - \mathcal{R}(D_c/n_c^2)n_+n_-$$

Relative Ionization Rate

$$r \equiv \frac{D_i}{D_c}$$

Fig. 7

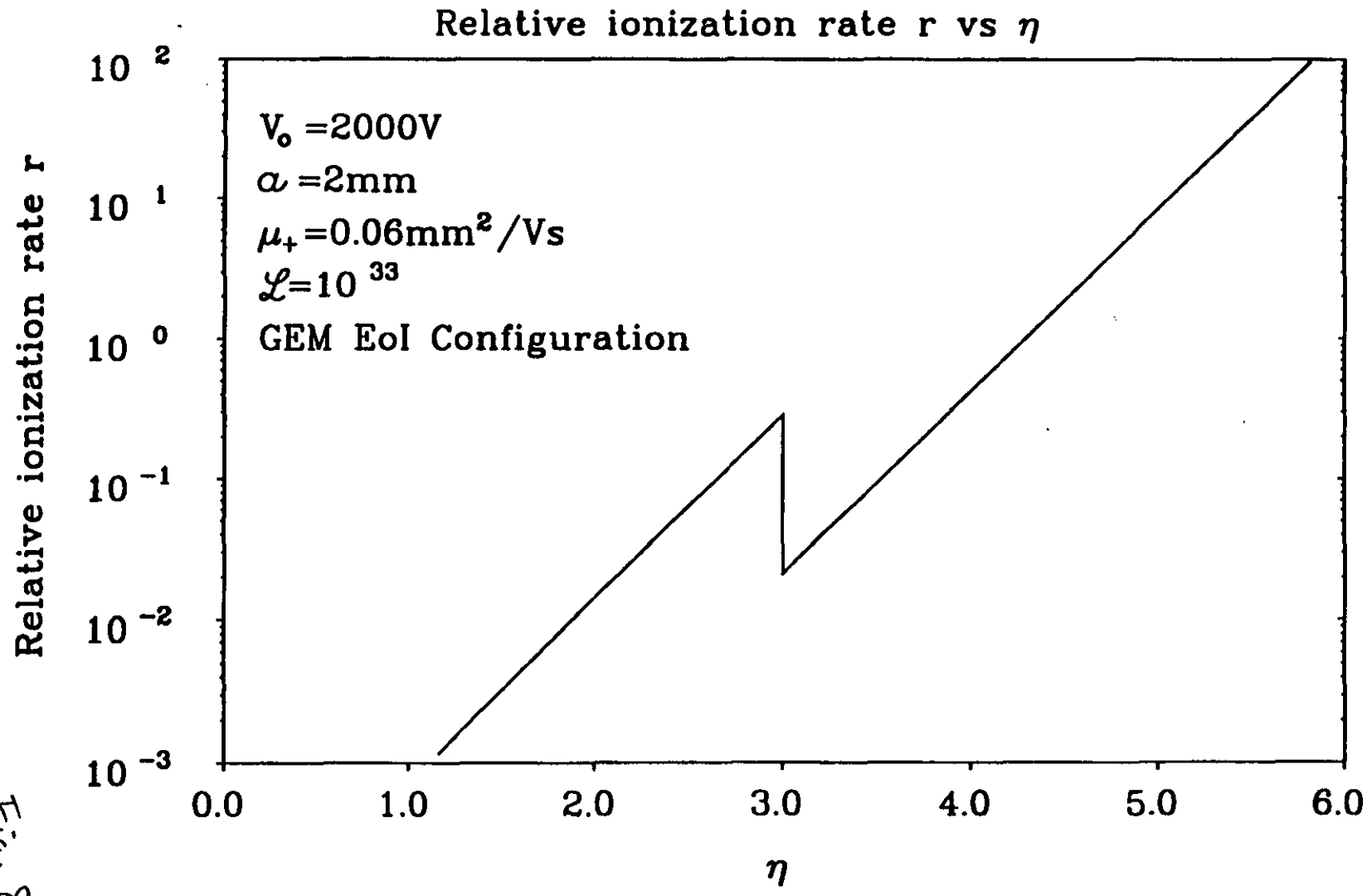
Relative ionization rate r vs η
V_o =2000V
a =2mm
μ_+=0.06mm^2/Vs
$\mathcal{L}$=10^{33}
GEM EoI Configuration
Relative ionization rate r
10^{2}
10^{1}
10^{0}
10^{-1}
10^{-2}
10^{-3}
0.0
1.0
2.0
3.0
4.0
5.0
6.0
η

Fig. 8

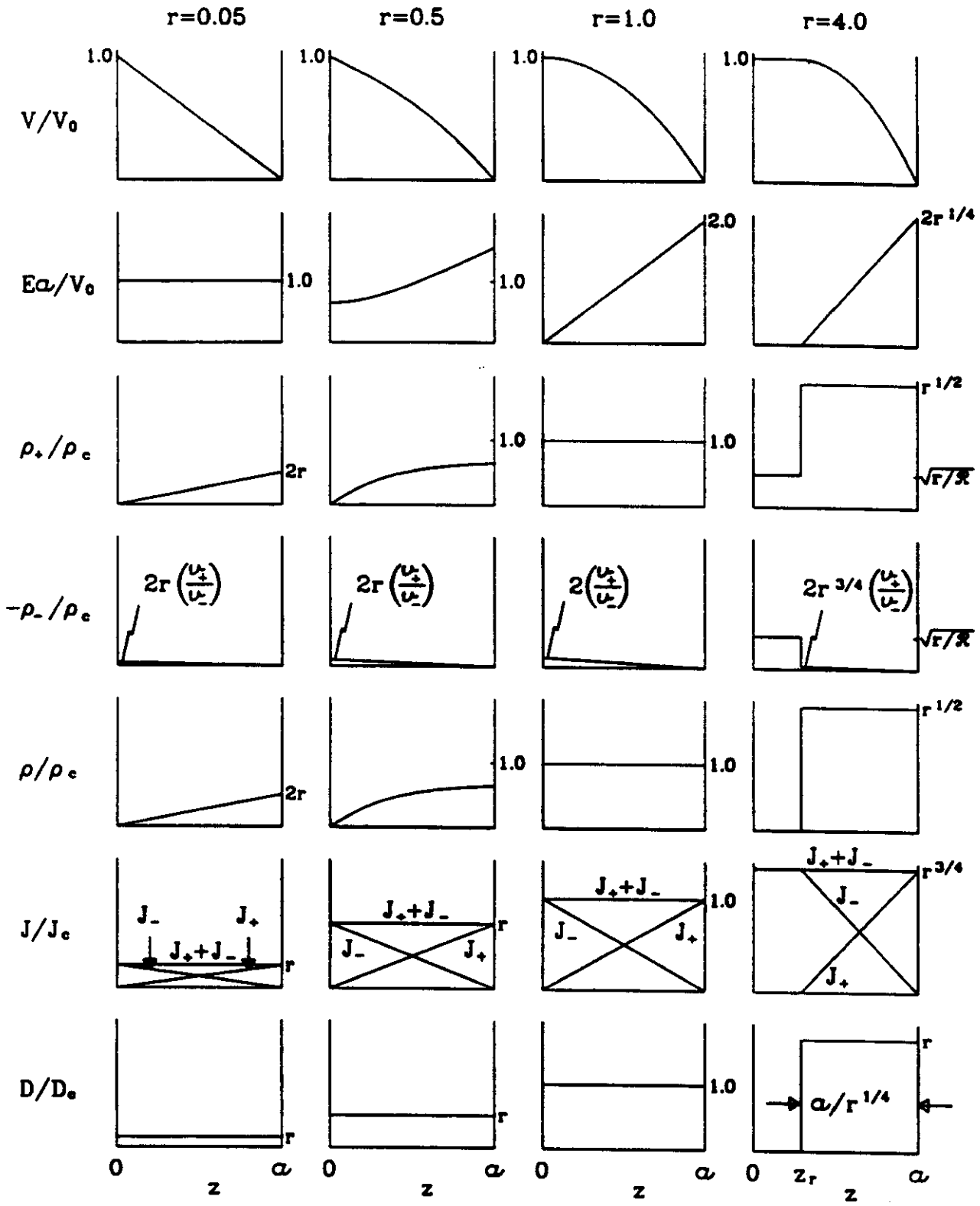
r=0.05
r=0.5
r=1.0
r=4.0
V/V₀
Ea/V₀
ρ₊/ρ_c
−ρ₋/ρ_c
ρ/ρ_c
J/J_c
D/D_e
1.0
2r
2.0
2r 1/4
r 1/2
√r/π
2r (υ₊/υ₋)
2r 3/4 (υ₊/υ₋)
2 (υ₊/υ₋)
J₋
J₊
J₊+J₋
r
r 3/4
a/r 1/4
0
z
a
z_r

Fig. 9

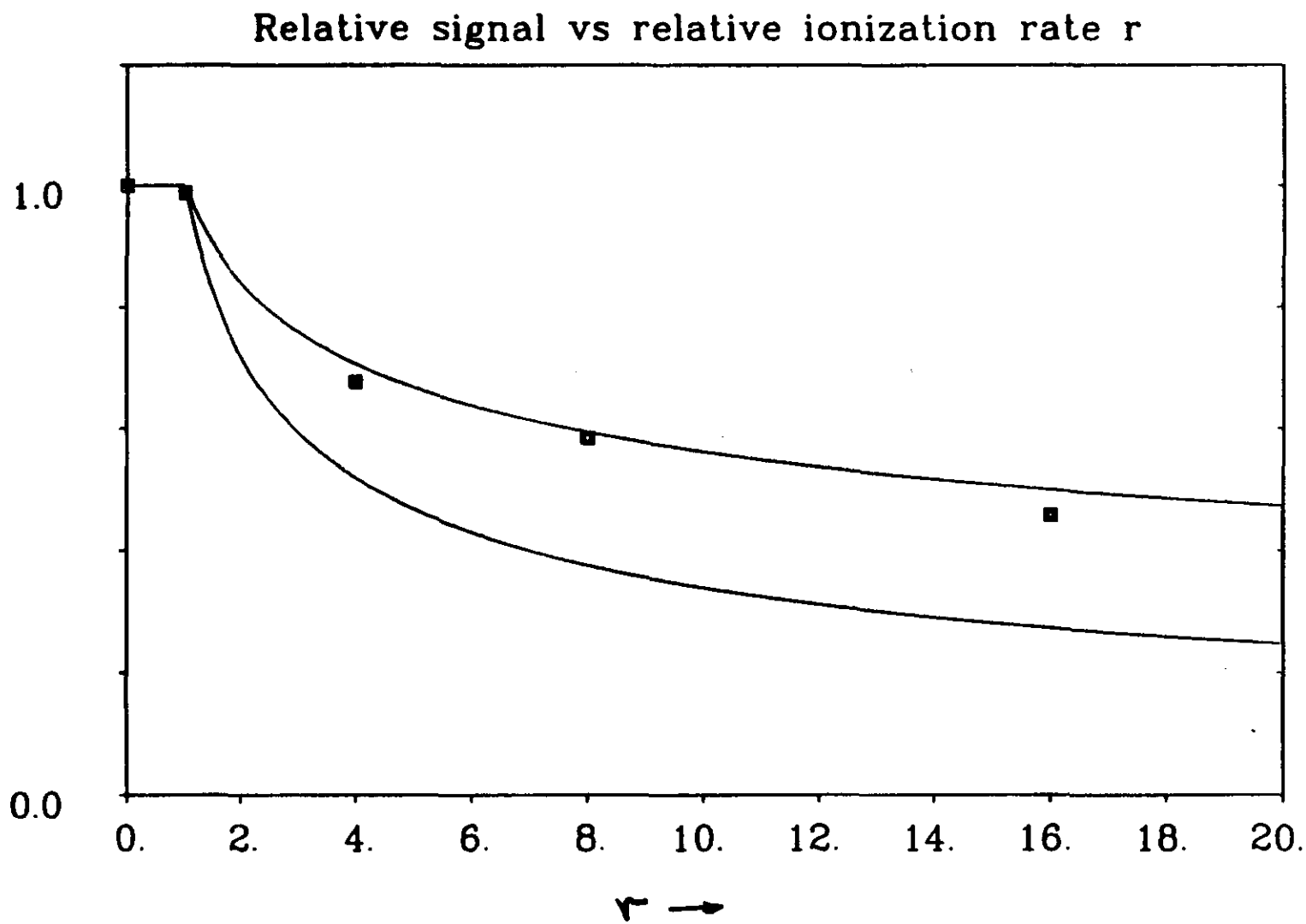
Relative signal vs relative ionization rate r
1.0
0.0
0.
2.
4.
6.
8.
10.
12.
14.
16.
18.
20.
r

Fig. 10

AGS TEST BEAM RESULTS FOR LIQUID ARGON CALORIMETRY WITH FAST SHAPING

The Liquid Argon Collaboration
R. Steiner
Adelphi University
G.Forden, J. Rutherfoord, M. Shupe, T. Bowen, A.Nelson
The University of Arizona
H.A.Gordon, E. Kistenev, P. Kroon,
H. Ma, D. Makowiecki, V. Radeka, D. Rahm, S. Rescia
Brookhaven National Laboratory
J. Womersley
Florida State University
S. DeBoer, J. Hauptman, M. Pang, A. Zinchenko
Iowa State University
S. Inaba, H. Iwasaki, N. Kanematsu, T. Kondo, Y. Sakai, Y. Unno
KEK, National Laboratory for High Energy Physics
K. Kaneyuki, L. Soso, Y. Watanabe
Tokyo Institute of Technology
G.S. Abrams, D.E.Groom, C. Hearty, M. Levi
The Lawrence Berkeley Laboratory
R. Black, C. Chang H. Deng, J. Goodman, D. Fong, N. Hadley, G. Long
The University of Maryland
N. DiGiacomo
Martin Marietta Astronautics
H. Weerts
Michigan State University
L. Cremaldi, B. Moore, J. Reidy
The University of Mississippi
R.G. Alsmiller, P. Fu, T.A. Gabriel
Oak Ridge National Laboratory
F. Lobkowicz, J. Ftacnik, I. Horvath, G. Diloretto
The University of Rochester
J.Siegrist, M. Turcotte, L. Villasenor,J. Yarba
The SSC Laboratory
T. Handler
The University of Tennessee
T. Burnett, V. Cook, J. Eisenberg, P. Mockett, R.W. Williams
The University of Washington

ABSTRACT

We have measured the response of a lead liquid argon calorimeter with fast shaping to both electrons and pions with momentum between 500 MeV/c and 20 GeV/c in the A3 beam line at the AGS. The shaping times used were 50 ns, 100 ns and 200 ns. We have preliminary results on e/π, linearity, pileup, and electron and hadron resolutions.

1. Introduction

Liquid argon calorimetry has many advantages for use at the SSC or LHC. These include unity gain which leads to relatively easy calibration; linear response over a large ($\geq 10^5$) dynamic range; uniformity; good energy resolution; minimal systematic variations; ease in segmentation; hermeticity; and radiation hardness. It is a mature technology where there is now considerable experience with large systems. A typical drift velocity in liquid argon of 5 mm/μsec implies that for reasonable readout gaps of 2 mm one cannot collect all the charge in less than 400 ns. However, since the current peaks at t=0 and the pulse shape is triangular, one can collect 44% of the charge in 100 ns. The effective signal to noise is, therefore, reduced, if the integration time is shorter. This can be quite adequate, particularly at high energies where the total amount of charge is large. Also, since one can measure the arrival time of the pulse to a fraction of its rise time, the energy of an electron or jet can easily be associated with the correct 16 ns bucket at the SSC.

We have built a lead liquid argon calorimeter to measure its response to π's and electrons with fast time shaping. Such fast shaping liquid argon calorimeters have been made using uranium plates (eg HELIOS[1]), but as uranium is costly and difficult to work with, we used 12 mm lead as the absorbing medium based on calculations[2] showing that such a thick plate might lead to an e/π closer to 1.0 than using thinner plates. We have made systematic studies of the calorimeter's resolution, relative response to electrons and pions (e/π) and response in high rate environments so that the performance of liquid argon calorimeters for the SSC or LHC could be evaluated.

2. Calorimeter Construction

The calorimeter as built was 1 meter by 1 meter wide and 7.5 interaction lengths deep. The calorimeter unit cell consisted of a 12 mm lead sheet, a 2 mm argon gap, a readout board, and another 2 mm argon gap. The readout boards are three layer printed circuit boards with readout strips on the inner layer and high voltage strips on the outer two layers. Both the high voltage and the readout strips were 2.5 cm wide. The readout strips were oriented in both the X and Y directions with X and Y cells interleaved. In depth, 16 X or Y readout cells were ganged together so that the calorimeter was divided into three identical modules, each 2.5 interaction lengths deep, and each having 40 X and 40 Y readout channels.

The calorimeter electronics were designed to be fast and to have low noise. It was similar to that used in the Helios Experiment (NA 34). See Fig. 1 for a block diagram of the electronics. The preamplifiers were placed inside the cryostat in the liquid to optimize the charge transfer time from the calorimeter to the preamp. The charge transfer time is determined by electrode capacitance and inductance of connections to the preamp.[3] The analog summing circuit could be readout with three different shaping times: 50 ns, 100 ns, and 200 ns. The effective shaping time for the digital outputs is about 125 ns.

Fig. 1. Electronics Block Diagram

An electromagnetic module with finer sampling was placed in front of the above stack during the last part of the 1991 beam run. It was designed to measure the noise and resolution of an electromagnetic module and to study the cracks between such modules.

3. Test Beam

The Liquid Argon calorimeter was placed in the A3 line at the Brookhaven National Laboratory. This beam line had been used for many years as a K_L^0 beam. The last two quadrupoles were replaced with quadrupoles with larger aperature. The beam was a secondary beam at 0° from the interaction of 24 GeV protons on a one interaction length target. There are usable fluxes of pions and electrons from 500 MeV/c to 20 GeV/c. The electron fraction in the beam varied with energy and was about 1% at 10 GeV. Particle identification was done by two Cerenkov counters each three meters long. An X-Y hodoscope of 1 mm diameter scintillating fibers defined the beam position near the calorimeter. $\bar{p}$'s were identified by time of flight. Fig. 2 shows the layout of the beam defining elements and the cryostat containing the calorimeter. The maximum beam intensity was 2×10^6 particles in a spill of approximately one second.

Fig. 2. Experimental setup showing (from lower right to upper left) the Cerenkov counters, veto array, cryostat and cryogenic piping.

Fig. 3. Response to electrons and pions as a function of momentum

Fig. 4. e/π as a function of momentum

4. Results

4.1. Resolution and e/π

Note that all following results are preliminary(eg. corrections for the dead material in front of the calorimeter have not yet been made). In Fig. 3, we show a plot of the mean response of the calorimeter to electrons and pions with momenta between 500 MeV/c and 20 GeV/c for the digital output. The data points are described by a straight line as our the results for 50 ns, 100 ns and 200 ns shaping times. The sampling term in the resolution was $(0.22 \pm 0.02)/\sqrt{E(GeV)}$ for electrons and $(0.65 \pm 0.05)/\sqrt{E(GeV)}$ for pions. Note that this resolution is for two radiation length sampling with a 5% sampling fraction. The noise on each of the 240 channels was about 100 MeV for the digital output. The observed noise was inversely proportional to shaping time.

In Fig. 4 we show a plot of the ratio of the response of the calorimeter to electrons and pions, (e/π) for momenta from 500 MeV/c to 20 GeV/c. This plot is for the digital output. e/π is the same within errors for shaping times of 50 ns, 100 ns and 200 ns and agrees with the data given in Fig. 4.

4.2. *Pileup*

We observed the response of the calorimeter at 10 GeV/c with up to 2×10^6 particles per 1 second pulse corresponding roughly to the energy that would be deposited in the calorimeter at the SSC at a luminosity of 10^{35}. The response of the calorimeter is as expected from Campbell's theorem[3] and the effect on the resolution for electrons is small for luminosities less than 10^{34} for shaping times of 125 ns or less.

5. Acknowledements

We gratefully acknowledge the contributions to the success of this experiment by the staff and management of the Brookhaven National Laboratory, the University of Washington physics shop, and the Fermilab Online Computing Department. The Liquid Argon Collaboration was funded by the US Department of Energy SSC Major Subsystem R& D program. This work was also supported by the US Department of Energy, the US National Science Foundation and the Ministry of Science, Culture and Education of Japan.

References

1. HELIOS(NA34) Data, **Detector R &D at BNL,** BNL Report 52244, 14(1990).
2. P.M. Mockett and M. Boulware, *Proceedings of the Symposium on Detector Research and Development for the Superconducting Super Collider,* Oct. 15-18, 1990, Fort Worth, Texas, 382(1991).
3. V. Radeka and S. Rescia, *Nucl. Instru. & Meth.,* **A265,** 228(1988) and references therein.

Liquid Argon Calorimeter

Electronics Chain Block Diagram

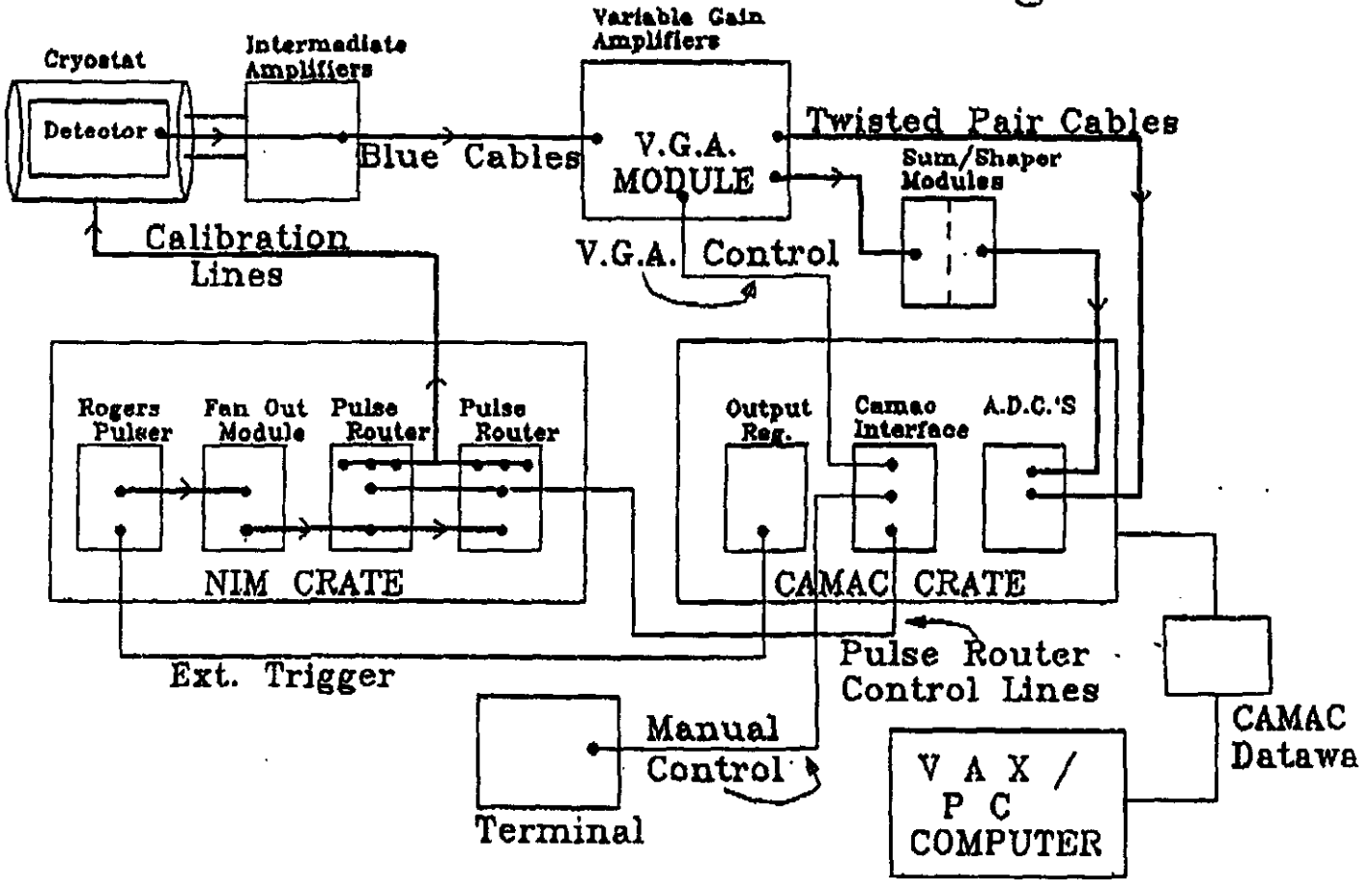

-Bold lines indicate signal path.

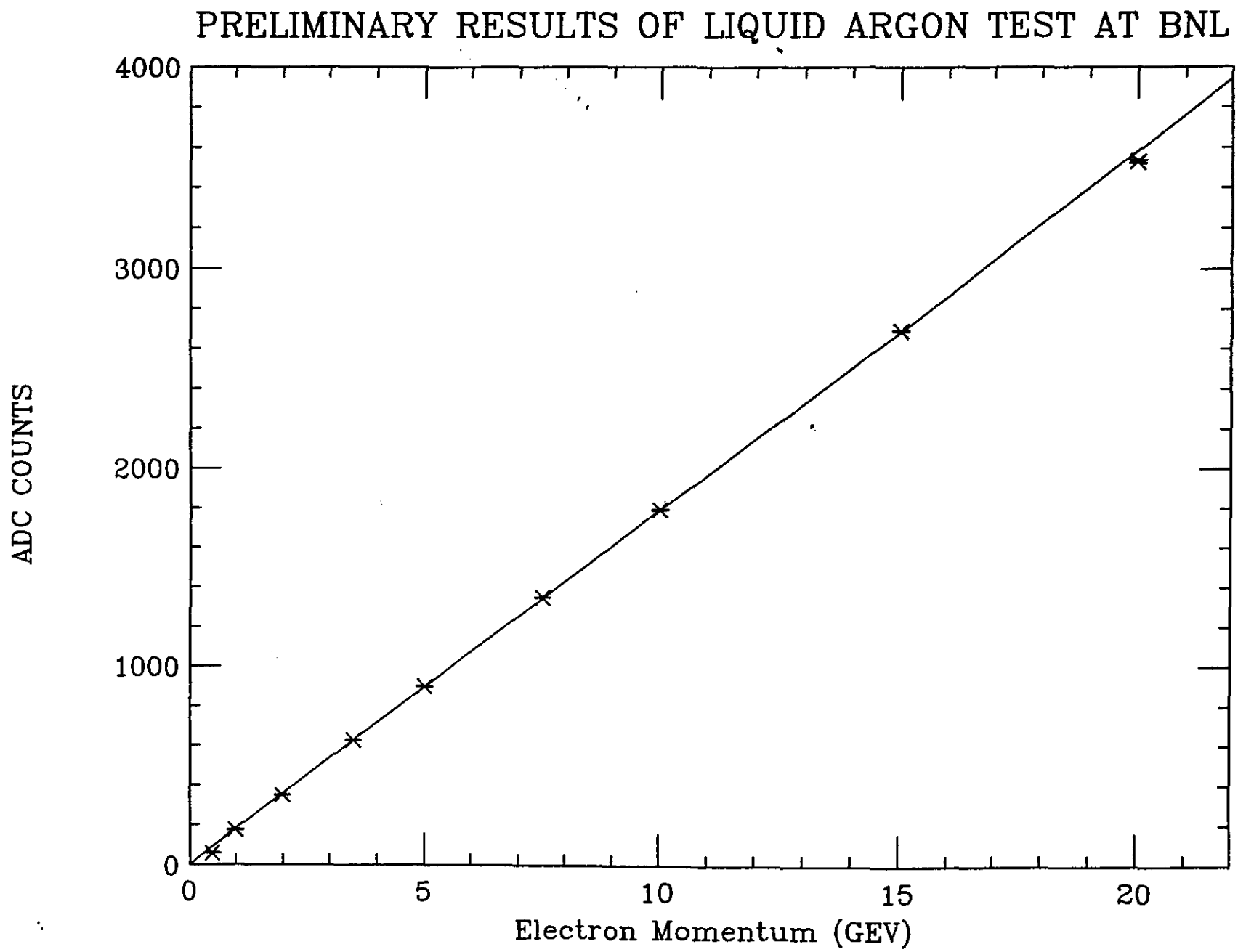
PRELIMINARY RESULTS OF LIQUID ARGON TEST AT BNL
ADC COUNTS
4000
3000
2000
1000
0
0
5
10
15
20
Electron Momentum (GEV)

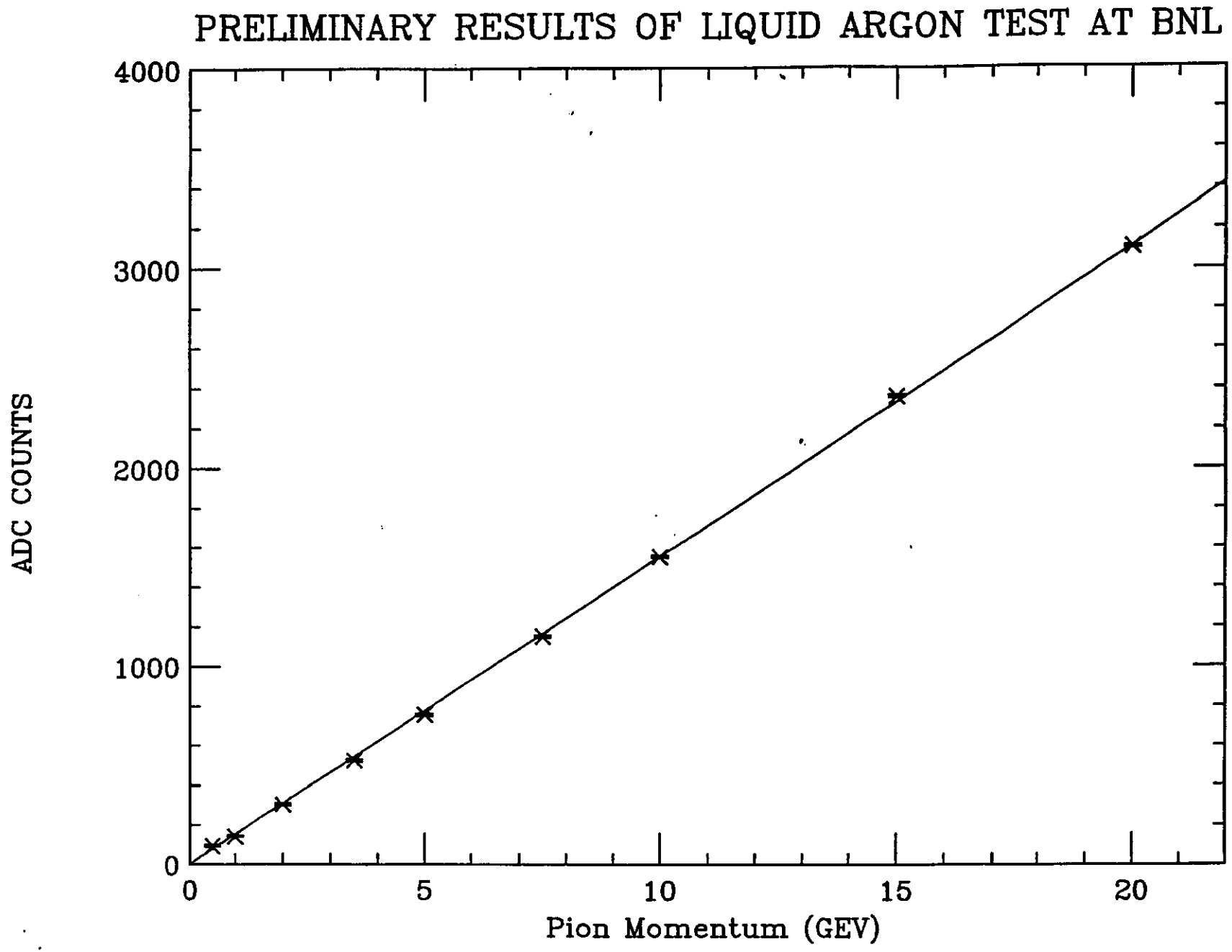
PRELIMINARY RESULTS OF LIQUID ARGON TEST AT BNL
ADC COUNTS
4000
3000
2000
1000
0
0
5
10
15
20
Pion Momentum (GEV)

Preliminary Results of Liquid Argon Test at BNL

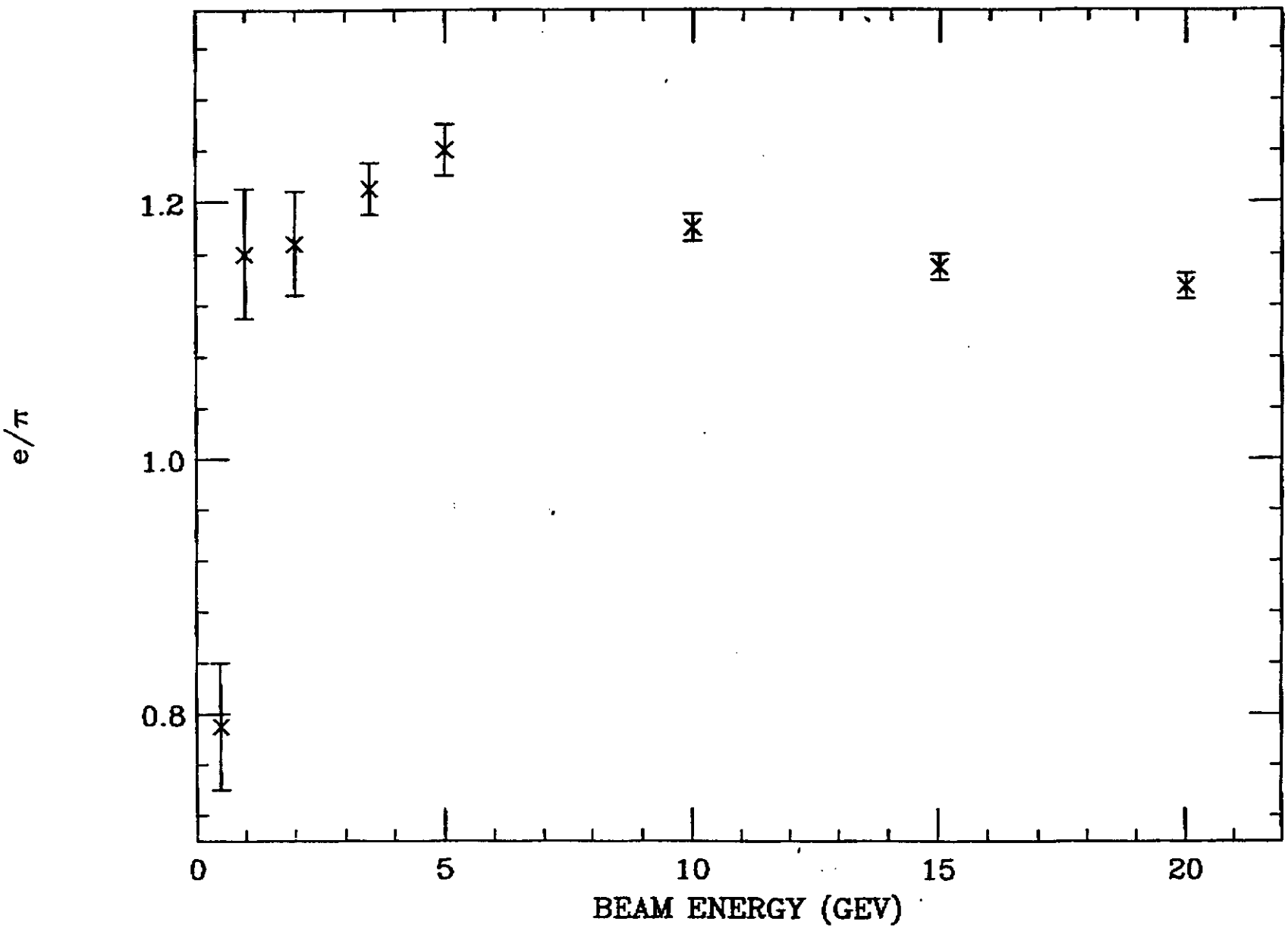

HIGH RESOLUTION BARIUM FLUORIDE CRYSTAL CALORIMETER

RESPONSE TO CONCERNS AND QUESTIONS By GEM COLLABORATORS

H. Newman
On Behalf of the Members of
The BaF_2 Collaboration

PART I

September 1991

Insitutions in the BaF_2 Collaboration:

- **UNITED STATES**
  - Caltech
  - Univ. of California, San Diego
  - Princeton University
  - Carnegie Mellon University
  - Oak Ridge National Lab
  - Brookhaven National Lab
  - Los Alamos National Lab
- **CHINA**
  - Shanghai Institute of Ceramics
  - Beijing Glass Research Institute
  - Institute of High Energy Physics, Beijing
  - University of Science and Technology, Hefei
  - Tongji University
- **INDIA**
  - Tata Institute of Fundamental Research

1 Production of Radiation Hard Crystals

Question (1) (Gordon): Solving the radiation damage problem depends on knowing more about the effects of impurities. How long should we wait for the specifications to be met?

Answer:

SIC and BGRI have undertaken a large-scale technical collaboration to develop the production of radiation-hard crystals meeting our specifications at \$ 2.5/cc (Appendix A). Their confidence in undertaking, and recently expanding this project at great expense, and our confidence in their success, is based on:

- Their long experience with the development and production of crystals, for many applications, over the last 30 years.
- Their experience and knowledge of BaF_2 , at BGRI since 1985, and at SIC in collaboration with Caltech since 1989.
- The studies and successful production of the L3 BGO crystals at SIC, including finding a dopant to increase the radiation hardness of the crystals used in the inner rings of the luminosity monitor.
- The demonstration of small radiation hard crystals on several occasions over the last six years. Examples include Majewski *et al.* [1], Y. Zhu *et al.* at IHEP, and Woody (BNL),
- Recent detailed studies which have established that the damage is impurity-related,
- Progress towards the understanding of the basic radiation damage at SIC, including which impurities are critical and the role of dissolved Oxygen in the crystals, as summarized in Appendix C.

The target date for production of radiation-hard crystals is mid-1992. Note that SIC and BGRI have invested approximately \$ 1.3 M in hard currency up until now, with an additional \$ 1.5 M of investments planned in 1992. These amounts do not include the labor costs of 49 faculty members, technicians and workers, for whom BaF_2 development and production is their principal activity.

Note that studies of the radiation effects of Co^{60} γ-rays we well as neutrons are also underway at SIC, BGRI, BNL, CMU, TIFR (Bombay) and Caltech (see Appendix C); as well as at Merck.

Given the scale of the research program, and the investments in the U.S. as well as China and India, it would be prudent to allow them to proceed up the end of 1992 to demonstrate the production of full-sized crystals with the required radiation hardness.

Question (2) (Worstell): How confident can we be that crystals will in fact be available in the quantities required at the anticipated cost ? Are there alternative sources in case of disruption of supply from the primary source, and what would be the cost from an alternative source ?

Answer:

The cost of the crystals has been fixed at $ 2.5/cc for large quantities, in a Memoranum of Understanding signed between Caltech, SIC and BGRI (see Appendix A.2) on May 29, 1991 in Shanghai. The production time for 32,000 crystal pieces at the full production rate would be 40 months, or four years including the time to ramp up the production. As discussed in Section A.3, production will be expanded (with funding provided by China) to 130 full-sized pieces in 1992.

We are thus quite confident that SIC and BGRI can meet our production needs, at the specified price, once the radiation damage problem is solved.

The SIC and BGRI project, and the signing of the MoU, were strongly supported by the Chinese Academy of Sciences. In his welcoming address at a specialized conference on BaF_2 held in China a few days prior to the signing of the MoU, Prof. Yan Don-Sheng, Vice President of the Academy of Sciences, mentioned that he expected that SIC and BGRI would be able to carry out the project successfully. He added that Shandong University – which is known throughout China for its expertise on crystals – could assist in the production if necessary, as an alternative source. The price would be the same – $ 2.5/cc – from this alternative source.

2 Background Rejection in the $H^0 \rightarrow \gamma\gamma$ Search

Question (3a) (Worstell): What provision has been made for the rejection of pi-zero gammas from unfavorable jet fragmentations? Has the jet fragmentation into 2 or more leading pi-zeros been taken into account for Higgs to 2 gamma studies for BaF_2 ?

Answer:

The procedure used to reject the QCD background has been presented by R. Zhu at the GEM Meeting on June 12, 1991. The procedure is summarized below. All of the effects mentioned in the question, and more, are included in the background computation.

The simulated events were produced using the PYTHIA 5.4 program. The fragmentation of jets in this program includes the production of multiple pi-zeros, η^0's and the full complement of known neutral and charged mesons. This fragmentation scheme has been shown to give an accurate description of jet production at present-day $e^+e^-$and $p\bar{p}$ colliders.

Photon candidates were selected with the following selection cuts on the photon rapidity (η_γ), photon transverse energy (E_T^γ), rapidity of the 2 photon system ($\eta_{\gamma\gamma}$) and $\cos\theta_\gamma^*$, where θ_γ^* is the polar angle of photons in the $\gamma\gamma$ rest frame:

- $|\eta_\gamma| < 2.5$ (The region covered by the proposed BaF_2 calorimeter);
- $E_T^\gamma > 20$ GeV;
- $|\eta_{\gamma\gamma}| < 3$ ($\Rightarrow$ to reduce $qq \rightarrow \gamma\gamma$).
- $|\cos\theta_\gamma^*| < 0.8$ ($\Rightarrow$ to reduce $gg \rightarrow \gamma\gamma$).

These selection cuts reduce the so-called *"irreducible background"* background, which is from direct photon production: $q\bar{q} \rightarrow \gamma\gamma$ (78 pb) and $gg \rightarrow \gamma\gamma$ via a box diagram (199 pb) [3]. After selection cuts the direct photon background is reduced to a cross section of 27 pb.

The QCD background is suppressed by an isolation cut, which is implemented as follows:

- Generate QCD jets;
- Search through BaF_2 cells ($\Delta\eta \times \Delta\phi$=0.04 $\times$ 0.04) to identify all cells hit by photons only. Define the sum of the transverse energy of all photons hitting one cell (ΣE_T^{γ}) as E_T^{cell};
- **Charge Veto**: Starting with the largest E_T^{cell}, if there is a charged track hitting the 3 $\times$ 3 cells centered on this cell, the cell is rejected;
- Define the sum of E_T^{cell}'s of these 9 cells ($\sum_{3\times 3cells} E_T^{cell}$) as the E_T^{photon}.
- **Energy Veto:** Require that the sum of the transverse energies in a cone of radius R=0.6 (R=$\sqrt{\Delta\eta^2 + \Delta\phi^2}$), excluding the E_T^{photon}, is less than 10% of the E_T^{photon} plus an isolation energy parameter (E_T^{cut}):

$$\sum_{R<0.6} E_T - E_T^{photon} > (E_T^{cut} + 0.1 E_T^{photon}) \Rightarrow Reject.$$

- Continue this process for all identified cells which were hit by photons only;
- Define the probability (F) of a jet faking an isolated photon as the number of photons passing all above cuts normalized to the number of jets generated.

By using this isolation cut, the rate of a jet faking an isolated photon is reduced by a factor of F. The rate of two isolated photons from two jets is thus reduced by a factor of F^2, assuming that the two jets are statistically independent. Similarly, the rate of qg $\rightarrow q\gamma$ or qq $\rightarrow g\gamma$ faking two photons is reduced by a factor of F. After these cuts, the background is reduced to:

- QCD: 12 pb[1];
- $qg \rightarrow q\gamma$: 12 pb;
- $qq \rightarrow g\gamma$: 0.6 pb.

[1]This was the status as of June, 1991. The analysis of the QCD background, including the effects of jet-jet correlations and the difference between the probability of a quark jet versus a gluon jet producing a photon, is being continued by R. Zhu at Caltech. As discussed in Part II of our Response, detailed shower shape analysis will be used to suppress this background.

Table 1: $H^0 \rightarrow \gamma\gamma$ detection in one SSC-year with BaF_2 resolution: signal versus irreducible background.

M_H(GeV)	$\sigma_{H\rightarrow\gamma\gamma}$(fb)	$\delta_{M_{\gamma\gamma}}$(GeV)	N_B(k)	N_S	$N_S/\sqrt{N_B}$
80	102	0.36	6.2	352	4.6
90	124	0.39	7.68	427	6.0
100	153	0.44	5.94	526	8.2
120	193	0.53	3.67	664	13
140	204	0.60	1.98	581	15
150	171	0.66	1.64	423	13
160	48	0.73	1.40	168	5.6

As a systematic check, we computed the background rate from b-quark jets, and found it to be no larger than the background produced by light-quark jets.

Note that the ability to make a clean isolation cut, with low noise in the isolation cone, is most important.

A summary of the results for a calorimeter with BaF_2 resolution is given in Table 1. computed with PYTHIA 5.5.

Question (3b) (Worstell): Why does the ELMUD proposal show very little signal for a 90 GeV Higgs, in the 2γ decay mode ?

Answer:

In the proposed ELMUD detector [4], the acceptance as well as the resolution are significantly lower. In particular, the physics cuts:

- $|\eta_\gamma| < 1.5$ (The region covered by the ELMUD EM calorimeter);
- $E_T^\gamma > 40$ GeV;

reduce the $H^0 \rightarrow \gamma\gamma$ signal to a level which is not compatible with Higgs detection (with 5σ significance) in one SSC year of $10^4 pb^{-1}$. The figures shown in Ref. [4] for a 90 GeV Higgs thus do not show a substantial visible peak for any resolution (although there is an indication of a peak for GEM-BaF_2 -like resolution) due to the smaller rapidity coverage, and the larger E_T^γ cuts of ELMUD, compared to GEM.

It is important to note in general that the ELMUD proposal does not state that it would be able to find the Higgs below $\sim$ 140 GeV. The reduced ELMUD acceptance combined with its resolution appears to make this impossible. Table II.3 in Ref. [4] discusses the detection of a 150 GeV through the two-photon decay channel, but Figure II.2 (the $M_{2\gamma}$ distribution after cuts) shows no signal at all with ELMUD's resolution. In addition, the figure shows that there is a clear difference, even at 150 GeV, between $7/\sqrt{E} \oplus 0.5\%$ and BaF_2 resolution. With $7/\sqrt{E} \oplus 1\%$, their analysis shows no visible peak at all, even at 150 GeV (where the 4-lepton channel provides an additional signal for the Higgs in any case).

It should be further noted that the ELMUD studies (as of Feb. 1991) used the obsolete version PYTHIA 4.9 for the simulation studies. Use of PYTHIA 5.4 or 5.5 (or the equivalent) is needed for correct computation of Higgs production at the lower end of the Intermediate Mass range, as discussed between L* and Texas/EMPACT last year.

3 Radiation Effects in BaF_2

Question (4a) (Worstell and Chen): If BaF2 shows significant light yield at low radiation doses before "saturating", will this reduction be uniform throughout the crystal ?

Answer:

The radiation hardness specification is that the crystals shall show a change in the fast-component light collected of 25% or less, after doses of several Megarads. (see Appendix A). This will limit the degree of radiation-induced non-uniformity which is acceptable. Within the specifications, the additonal non-uniformity which could result from radiation damage can be corrected, by methods which already have been used on our crystal prototype, as described below.

Note that (as discussed in Section 9.1 and Appendix D) the scintillation light rays are focused along the long axis of the crystal, due to the crystal's tapered shape, as they travel through the crystal towards the phototube. This tends to enhance the relative response to the part of the shower originating at the end far from the phototube, in a clear crystal. This effect is counterbalanced by bulk attenuation of the light in the crystal, and by light losses at the crystal surfaces and at the UV reflectors. We achieve overall light collection uniformity by wrapping and/or coating techniques. If the radiation damage causes a non-uniform local absorbance, this changes the balance between these effects. Within the specifications, the effect of this extra variation of local transmittance will be corrected with the following procedure:

- Pre-irradiate the crystals, up to saturation.
- Measure the post-irradiated uniformity curve.
- By applying our wrapping or coating techniques, restore light collection uniformity to within the specifications, i.e. within the level of several percent which is required to maintain the resolution (see Section 9.1 for details).

If the damage is controlled by a metallic impurity controlling the damage, as verified by SIC (see Appendix C), the local absorption tends to increase monotonically as the impurity concentration increases along the crystal. This is caused by

impurities being carried along, as the solid-liquid phase boundary layer advances along the crystal during the growth process. Once the principal metallic impurities are removed, the residual effect of dissolved Oxygen in the crystals is expected to be uniform.

Note that because the crystals are grown from the small end to the big end, there is a tendency for the local absorbance to increase near the phototube, after irradiation (for the 'metallic-impurity' case). As demonstrated by our recent preparations of our prototype crystal matrix, one naturally gets better uniformity if one increases the local absorbance (e.g. with black-painted mylar) near the phototube, to counteract the effect of direct light. For the 'dissolved oxygen' case, the decrease in attentuation length can also be corrected by using a wrapping or coating with higher UV-reflectance.

Note that a complete simulation of light propagation, surface reflection and diffusion has been written by students D. Kirkby and G. He (Caltech) to help address these problems, by assisting in the design of the wrapping and coating process.

Question (4b) (Worstell) What are the measured effects of radiation damage on light yield and transmission of the short-wavelength fast component?

Answer:

This is discussed in detail in Appendix C.

4 Detector Calibration (I)

Question (5a) (Worstell): Is the cost of the calibration system included in the baseline?

Answer:

Yes. The baseline calibration system costs, listed as \$ 3.3M, include a conservative estimate of the cost (new) of a complete RFQ system (\$ 1.5 M for a few μsec pulse; \$ 0.6 M additional to compress the pulse to 100 nsec), and of a UV-light monitoring system.

Question (5b) (Worstell): How can a UV monitoring system with 220nm light be provided?

Answer:

CMU has designed, and is developing a UV laser light monitoring system for the BaF_2 calorimeter. This will monitor the crystal transmission and photodetector response, in a way which is analogous to the Xenon lamp + light fiber system used in L3. The CMU system uses laser light pulsed at a rate of several tens of Hertz and several nsec pulselength, to monitor the transmission of the crystals and the photodetector response. The laser light will be transported through pipes filled with inert gas to minimize transmission loss, to a point near the calorimeter. The light will then be fanned out to UV-transmitting fibers which will transmit the light to the individual crystals. For test purposes CMU is using a Spectra Physics pulsed laser system which provides 532 nm light, combined with a frequency doubler (to obtain 266 nm). Tests with this laser, couplings to the fiber fanout and a BaF_2 crystal mounted on a R4406 phototriode are in progress.

In the longer term, excimer lasers in the 190 - 220 nm range could also be used, which are available at moderate cost. Argon-Chloride (193 nm) lasers, for example, have recently come into widespread use for medical applications, with systems in the price range of \$ 50 - 100 k. The use of noble gas-halogen lasers in the appropriate frequency range would provide light up to the TeV-equivalent range in a pulse, compared to the L3 Xenon lamp system which is in the GeV-equivalent range.

In addition, where precise matching to the BaF_2 light spectrum is a concern, one

could indeed choose a Xenon lamp system, coupled to a narrow-band interference filter composed of multiple dielectric layers. A filter of this type manufactured by Twardy, Inc. was tested at Caltech in 1988. The filter had an acceptance of 230 ± 30 nm (with zero acceptance for wavelengths longer than 280 nm) and 30% peak transmission.

Among these choices, the pulsed laser system is preferred, and will be pursued by CMU, with assistance from Caltech.

Question (5c) (Worstell): Can a MIP be used for calibration?

Answer:

The outlook for use of a MIP calibration is very good, as summarized below. Preliminary tests of MIP calibration are already available: from hadronic Z^0 decays measured in L3, and from a test with a BaF_2 crystal pair at UCSD. A further test, to determine the realistic MIP resolution, will be done in our Fermilab test beam by October 1991, in an area behind the first section of the backup (Barish-Sciulli) HCAL, where a clean muon flux is available.

More details on the test beam plans are presented in Appendix E.

A MIP passing through a BaF_2 crystal longitudinally would approximately 0.33 GeV energy in the crystal, which would be read out by the crystal with a few percent resolution. With a statistics of a few hundreds tracks, the peak position or the calibration point can be determined to 0.4%. According to simulation studies by R. Zhu, the multiplicity of charged hadrons at SSC is large enough to provide a calibration within 12 hours during SSC running.

In L3, where the minimum ionizing peak signal measured in 22 radiation length BGO crystals was cleanly extracted with a simple cut on the energy in neighboring crystals, the MIP signal was observed to have a resolution $\sigma = 6\%$ (summed over all crystals). For the LEP data, one event contributing to the minimum ionizing peak was obtained for approximately every 10 hadron events. Tests with cosmic rays at UCSD, using a BaF_2 crystal pair 50 cm in length showed a resolution of 3%.

5 Detector Calibration (II): The RFQ System

Question (6a) (Gordon): Describe the RFQ calibration system completely.

Answer:

The RFQ technique is uses a 3.9 MeV proton beam from a Radiofrequency Quadrupole accelerator. For the SSC, the intense burst of photons produced by radiative capture of the beam in a Fluoride target may be used to provide a relative calibration of all the crystals at once – within a few minutes. Depending on the beam intensity on target, the equivalent energy per pulse can be adjusted from tens to hundreds of TeV of energy (composed of 6 MeV photons) over the sphere. More details on the RFQ system concept, and the initial test run, may be found in [5]. The status of the accelerator systems, and the plan to make a fast pulse (100 nsec) and transport it into the GEM detector is detailed in AccSys Technology, Inc. final report to DoE/SBIR [6].

The basic RFQ technique, and the results of the initial tests, are summarized below.

Depending on the type of target, this calibration scheme can be run in two different modes.

The first mode, developed for an absolute calibration in L3, uses a lithium target: the reaction $^{7}Li(p,\gamma)^{8}Be$ produces a flux of 17.6 MeV photons which can be used to calibrate the thousands of electromagnetic calorimeter cells at once, with an absolute accuracy of better than 1% in 1–2 hours. The feasibility of this calibration mode has been proven in an experimental test of a 4×5 L3 BGO crystal array [5]. An absolute calibration precision of 0.7% was achieved in the test. This low energy photon calibration, however, is not directly relevant to an SSC electromagnetic calorimeter.

The second mode [6], developed for SSC and LHC as well as for higher energy relative calibrations in L3, uses a fluoride target. The reaction $^{19}F(p,\alpha)^{16}O^{*}$ and the subsequent decay of the excited oxygen nucleus $^{16}O^{*}$, produces hundreds to thousands of 6 MeV photons per millisteradian per beam pulse. These photons, functioning as a synchronised "equivalent high energy photon" of up to 30 GeV per calorimeter cell, would serve as a calibration source for SSC electromagnetic

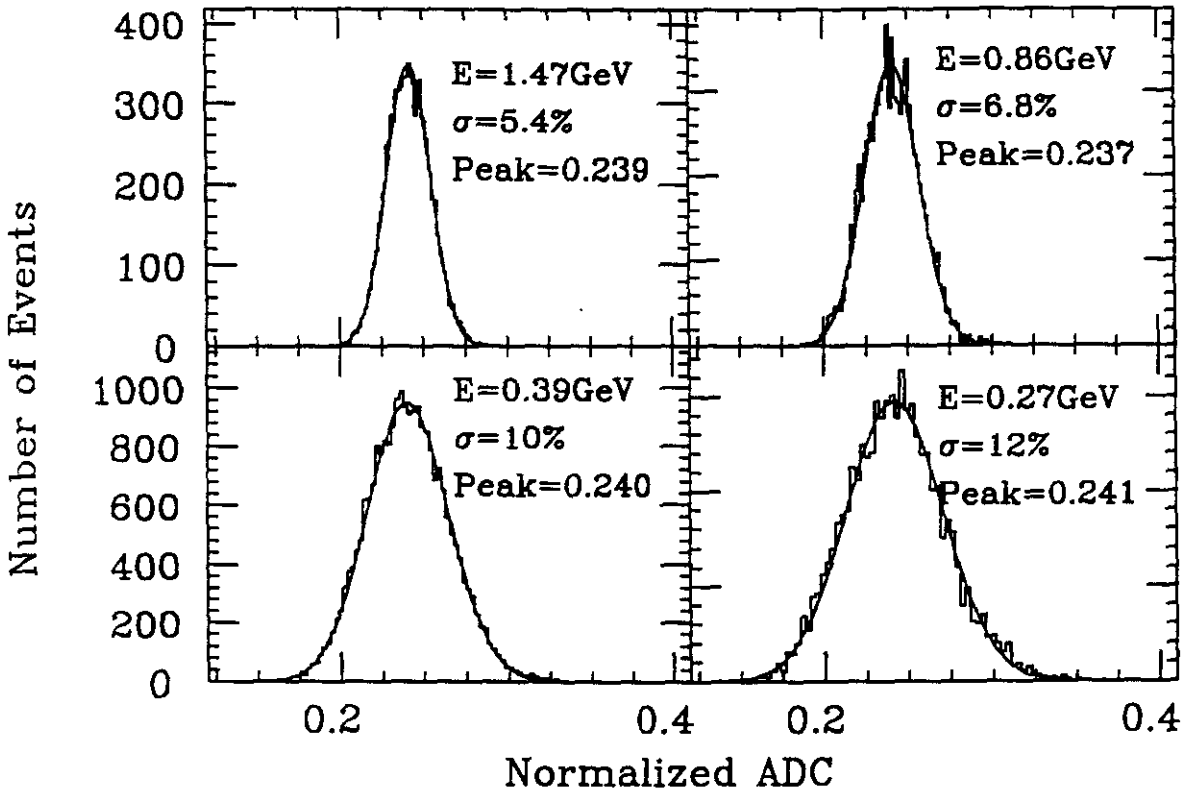

Figure 1: Normalized ADC distribution of a crystal at different energies.

calorimeters. With a proper normalization, this technique provides a relative calibration with precision of 0.4% in a few minutes. The feasibility of this calibration mode has been proven in another experimental test with 4 BaF_2 counters and a 7 × 7 L3 BGO crystal array [5]. Figure 1 shows the normalized ADC distributions of a crystal for runs with different beam intensities. The perfect Gaussian distribution and the correlation between the r.m.s. width and the total energy deposited in the crystal is clearly seen.

Figure 2 shows that the deviation of the peaks of 49 BGO distributions, normalized to the sum of BGO energy in the 7 × 7 matrix, for several runs. This distribution has a gaussian shape with a standard deviation of 0.34%. It is therefore evident that a stability of 0.4% may be achieved.

The equivalent photon energy (EPE), defined as the sum of the energies of photons from one beam pulse hitting one crystal detector, was measured at AccSys with a LiF target. Up to 2.38 GeV/0.1μCoulomb/1.6msrad was observed for a

Table 2: Measured and Calculated Equivalent Photon Energy.

Proton Energy (MeV)	2.0	2.5	3.0	3.5	3.85
EPE_{meas} (GeV)	1.5	13	22	30	37
EPE_{cal} (GeV)	2.6	14	24	33	38

1.92 MeV beam. There are much stronger fluorine resonances between 2.0 and 4.0 MeV [7], beyond the 1.92 MeV beam energy used in the test. By using a 3.85 MeV RFQ and a CaF_2 target, which would have no neutron production as a by-product below 4.05 MeV [7], an EPE of 30 GeV/0.1μCoulomb/1.6msrad or more is expected. Table 2 lists EPE's measured with a CaF_2 target bombarded with a proton beam from a Van de Graaff at Kellogg Lab at Caltech. The expected equivalent photon energies, calculated with an integration of the resonances [7], are also listed in the table. It is clear that with a 3.85 MeV proton beam up to 40 GeV/1.6 msrad/0.1 μCoulomb is achievable.

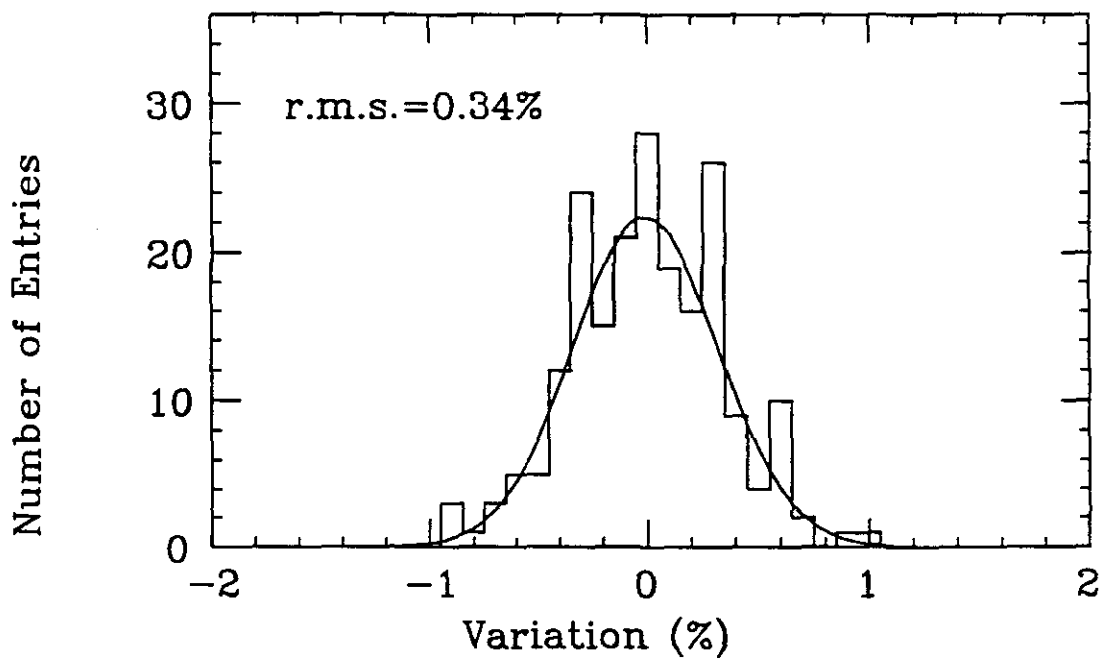

Figure 2: Variation of the normalized peak positions from BGO crystals.

Question (6b) (Gordon): Indicate when each of the parts of the RFQ system will be available to be tested.

Answer:

- **RFQ Systems:**
  The RFQ technique has been fully tested at 1.9 MeV RFQ beam energies in 1988, and the cross sections used to extrapolate to the higher RFQ energy, to achieve 30-40 GeV per crystal have been experimentally checked at Caltech, as discussed above. Two RFQ systems with exactly the specifications required for our calibration system are currently under construction at AccSys Technology, Inc. for the U.S. Navy (for a different application). One of the accelerators is expected to be available by mid-1992 for a full scale test of our technique at 3.85 MeV, using a BaF_2 prototype matrix. At least one of the accelerators could be purchased (used) at very low cost by 1995, once the Navy's test program is completed.

- **Pulse Compressor Storage Ring:** If production of the full charge on target (0.1 μCoul) in a 100 nsec pulse is required, a design of a compact H^- storage ring [6], using charge-exchange 50 turn injection (1 Ampere stored), and single turn extraction onto a Fluoride target, has been developed by P. Meade (a synchroton expert) for AccSys, as shown in Figure 3. The design includes the injection and extraction method for the ring.

The time required to complete, test and deliver the system, including the storage ring and a 3.85 MeV RFQ, is estimated in Ref. [6] to be two years, once the first 3.85 MeV RFQ (for the Navy) is completed. This means the system could be available by mid-1994.

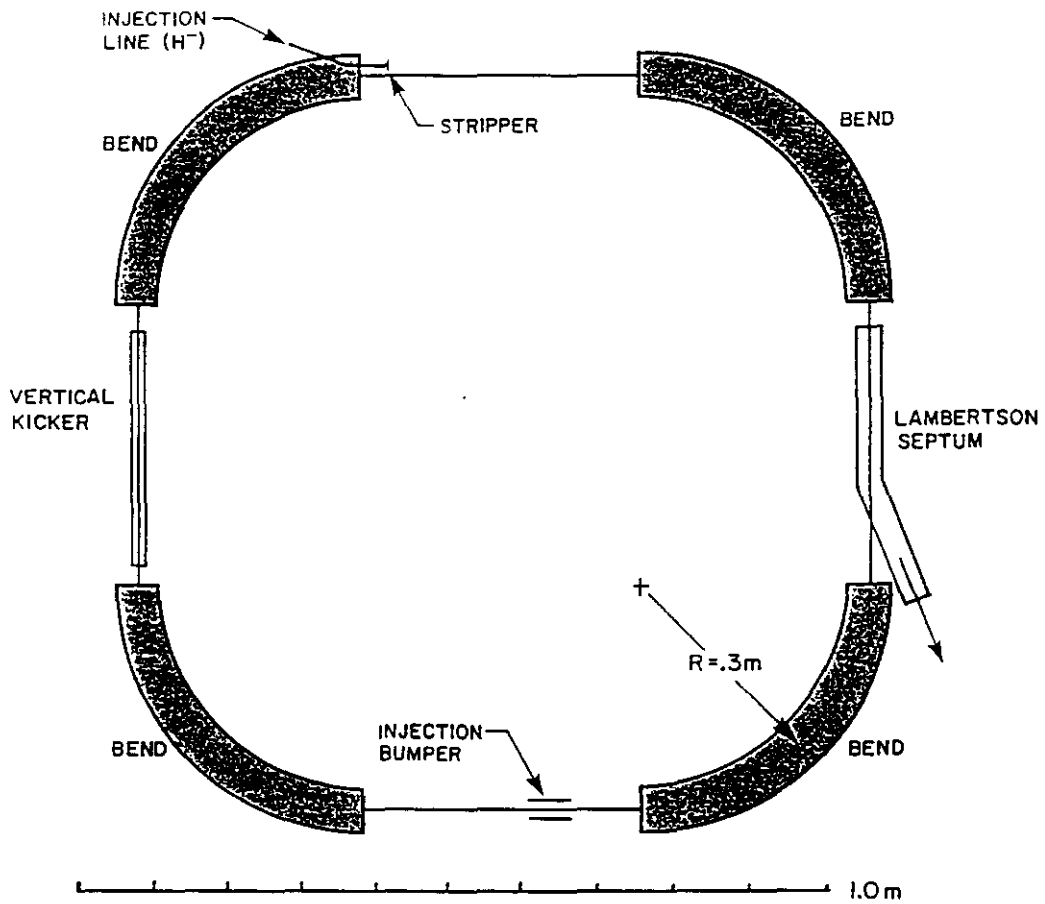

Figure 3: Compact layout of the storage ring designed for the SSC RFQ calorimeter calibration system.

Question (6c) (Chen): RFQ gammas stop at the very front of the crystals. How could this be used to calibrate crystals damaged at different depth?

Answer:

The question of non-uniform damage, the radiation hardness specifications, and the way to obtain light-collection uniformity prior to installation was covered in the answer to a previous question.

The 6.1 and 7 MeV photons, produced by the RFQ when used in the "Equivalent High Energy Photon" mode, do not stop at the front of the BaF2 crystals. As shown in the Particle Properties Data Booklet (4/90 Edition) p. 121, the minimum

of the absorption cross section in a medium-Z material such as BaF_2 is precisely at these energies. From the Particle Data Book graph, the attenuation length of the photons in BaF_2 is $\approx 6cm$ (3 radiation lengths). This is in excellent agreement with the EGS result for BGO, computed by Hong Ma in 1985, where the mean depth of energy deposition was computed to be 3.1 cm (2.8 radiation lengths), for 17 MeV photons used in a "one at a time" mode for absolute calibration [5]. (Note that the Particle Data Book shows that 17 MeV photons have a very similar absorption length to 6-7 MeV photons.)

Extensive simulation studies of showering and light collection were performed by R. Zhu in 8/85 - 12/85, for the L3 BGO case, using single 17 MeV photons. These studies, which were presented at L3 meetings in 9/85 and 12/85 [8], showed that the RFQ photons were surprisingly useful in providing a calibration that tracked the overall gain shift due to radiation, with an accuracy of 1% or better, up to gain shifts $\sim 20\%$[1].

The RFQ system thus is able to detect radiation-induced gain shifts. The energy deposition profile is close enough to high energy showers that a first order correction can be made, up to damage levels which are well beyond our radiation damage specifications.

[1]In the extreme scenarios considered in the L3 BGO study, a gain shift of 20% corresponded to such severe local darkening of the crystal that the resolution would be degraded, and it would thus be imperative to remove the crystals, and anneal them (e.g. by heating).

6 Readout Electronics

Question (7) (Gordon): When will fast shaping electronics be tested ?

Answer:

Work at ORNL

ORNL has provided the integrated front-end electronics for the BaF_2 matrix at Fermilab, including a fast preamplifier and a shaper. The peaking time of the circuit designed at Oak Ridge, approximately 22 nsec, is determined by the gate width and dynamic range of a standard Fastbus ADC. Faster shapers and special digital readout will be implemented starting later this year.

ORNL has reported [9] their intention to modify the present generation of RHIC CMOS pad chips, and to use them in our 1992 beam test as a proof of a fully integrated front end. This chip presently is designed to contain the preamplifier, shaper, correlated sampler, pipeline storage, and ADC. It is designed for the 100 ns RHIC clock. While this will not get us to the 16 ns SSC clock rate by next Summer, ORNL will thus be able to prove an evolutionary step along the way.

ORNL also intends to carry out the following steps in time for the Summer 1992 beam tests [9]:

- Develop and design shaping circuitry for optimal return-to-baseline and signal-to-noise response.
- Address other shaping algorithms. These include delay-line shaping, tapped delay-line shaping, other triangular and trapezoidal shaping schemes, and correlated sample shaping. Test chips will be built in CMOS through the MOSIS fabrication system.
- Examine DAC issues - pipe-lining/analog vs digital, etc. In particular, ORNL wishes to examine correlated sampling techniques, and its association with capacitor pipeline storage. Test chips will be fabricated in CMOS through MOSIS.

It is clear that much of the above work overlaps with the interests of the Princeton group, and with the development of specific items for the GEM trigger and data

acquisition systems which is under the leadership of Dan Marlow. A collaboration on these items is suggested.

The above information indicates that the first adequate front end readout with the SSC 16 ns clock, and significant parts of the higher level readout in association with this front end, could be available by 1993.

Work by Princeton

In order to study future (much faster) preamp designs, the Princeton group has used a cascoded grounded Gallium Arsenide FET, and has developed a preamp with a 2 nsec risetime and a voltage swing of 2 Volts, followed by an output buffer able to drive 50 Ohms. The general design of this circuit follows Princeton's long experience with reading out Silicon photodiodes on L3's BGO calorimeter. Figure 4a shows the response of the preamp (top trace) to a test pulse with a 1 nsec rise time(bottom trace). Figure 4b illustrates the response expanded to 1 nsec/cm, showing the risetime of less than 2 nsec. A shaper fast enough to follow this preamp is under development by the Princeton group.

The response to a 25 GeV positron beam, measured with a 25 cm BaF_2 crystal equipped with a Hammamatsu R4406 phototriode and a GaAs Princeton preamp, is shown in Figure 5. The fall time of the preamp shown in the figure is determined by a bleeding resistor, so that the pulse returns rapidly to baseline.

Work at Los Alamos

Work on radiation-hard electronics using GaAs technology is underway at Los Alamos (LANL) by Dave Lee *et al.*, in collaboration with Sandia. LANL has specified the design, and has obtained quotes from four vendors who are able to produce a Gallium Arsenide pulse amplifier (preamp and shaper) which will meet our needs for a final BaF_2 readout at the SSC. The specifications include: rise and fall time of 1 nsec, 6 nsec pulse FWHM, dynamic range of 10^5, linearity 0.1%, two output ranges to cover the energy range of 50 MeV to 5 TeV, return to baseline (0.2 mV) from a 2 Volt maximum pulse within 32 nsec, and less than 10% gain change after a radiation dose of 5×10^{14} neutrons/cm^2 or 10 MegaRads. The costs indicated in the quotes were in the range under $ 100 per channel, for large quantities.

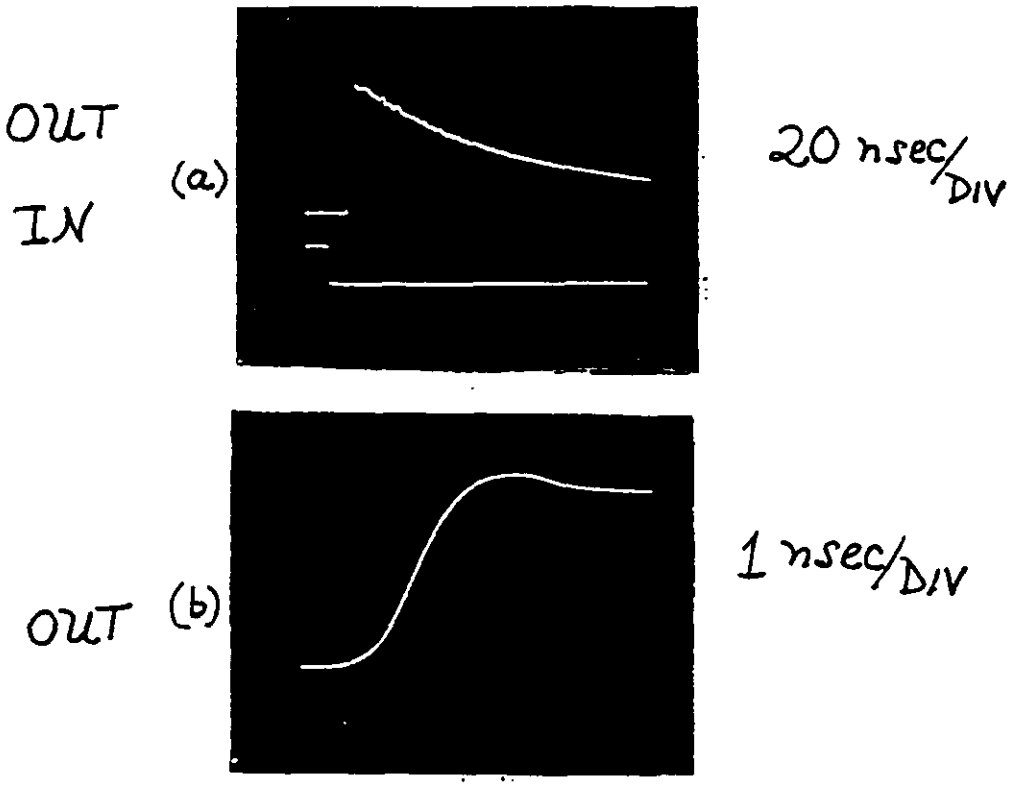

Figure 4: (a) GaAs Preamp Response to a Step Input (b) Leading Edge of Response, Showing Rise Time Less than 2 nsec

As an alternative to a commercial effort, in order to obtain the maximum speed and radiation resistance at a low cost, LANL has been working on the design and understanding of an amplifier using individual MESFET transistors. A variety of GaAs transistor suppliers were investigated, and MESFET transistor arrays from Gigabit (Model 16G020) have been purchased for the first round tests. Each 16G020 FET package consists of 11 single gate depletion MESFET's, and costs ≈$ 29 each, in quantities of 1000. The rated radiation resistance of the MESFET is typically 10^{15} neutrons/cm^2 and 10^8 rads, which is adequate for our purposes.

LANL is investigating the performance of the MESFETs by considering each transistor as a building block from which we will come up with suitable amplifier. This approach is important because they need to know the various parameters of the transistors, so that they can be used in various design models. As the experience of the physicists at LANL with GaAs technology is still limited, they have enlisted the help of their RF engineers, as well as a very knowledgable physicist (at very modest cost).

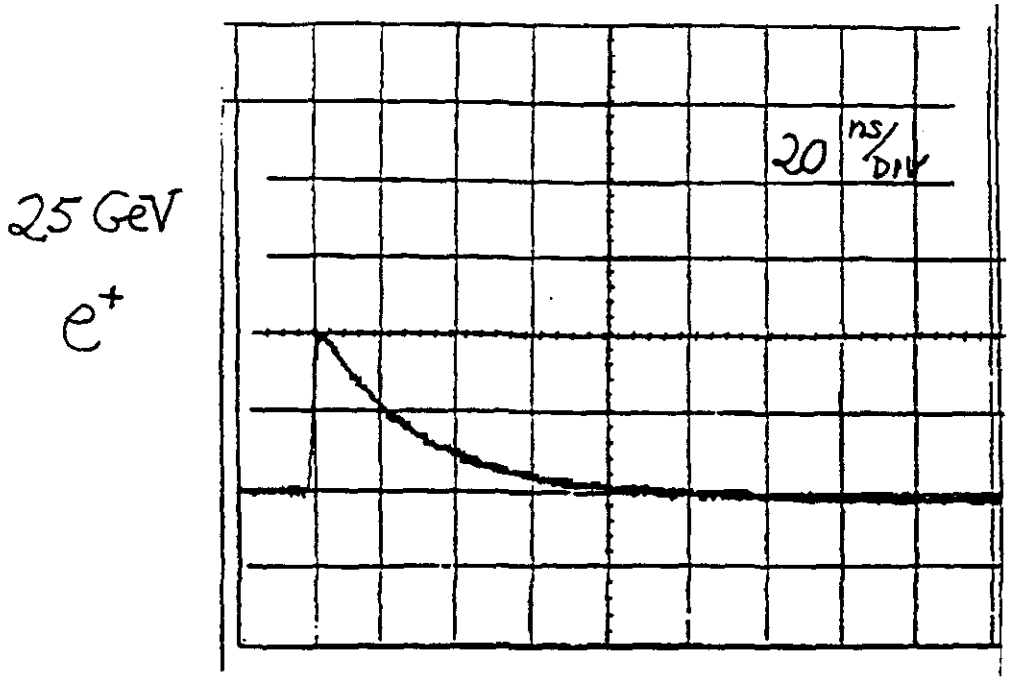

Figure 5: Response of a 25 cm BaF_2 Crystal, Equipped with a Vacuum Phototriode and a GaAs Preamp, to a 25 GeV Positron Beam

The results of their initial studies, and their plans for the next several months are:

- The open loop gain is limited by the internal shunt resistance to 7 (they had hoped for 10). This is a common limitation of all GaAs devices.
- The speed of the chosen transistors is limited to 128 Mhz. The bandwidth is believed to be limited by the Miller effect.
- Because of the Miller effect limitations, they will now look at two transistors in a cascode configuration that will allow them to get a frequency response of > 500Mhz at an open loop gain of 7.
- Once the operating parameters of the two-transistor model with open loop gain are understood, they will design an amplifier that includes feedback.

Table 3: π/e Separation of the BaF_2 Calorimeter.

E (GeV)	10	100	1000
After Lateral Shower Cut:			
π acceptance (10^{-2})	32.6 ± 0.4	34.7 ± 0.5	39.4 ± 0.7
e acceptance (%)	99.3	99.5	99.5
After E_{BaF_2} and P_{trk} match (10° - 90°):			
π acceptance (10^{-3})	< 0.1	12.3 ± 0.9	388 ± 7
e acceptance (%)	97.3	99.2	99.5
After HCAL Veto:			
π acceptance (10^{-4})	< 1	2.0 ± 1.4	< 2.2
e acceptance (%)	97.3	96.4	95.0

7 Depth Segmentation

Question (8) (Gordon): Describe the justification of no depth segmentation which compromises the ability to get the photon direction, the photon/pi0 separation, and degrades the electron/pion separation.

Answer:

The principal justifications for no depth segmentation are cost, detector layout, and studies [10] which have shown that e/π separation and γ/jet separation at the level of 10^{-4} may be achieved without longitudinal segmentation.

Electron - Pion Separation

As an example we show the results of our e/π separation study in Table 3. The table is the result of a complete a complete GEANT simulation of an array of crystals, carbon fiber support, and an appropriate amount of material in front, combined with parametrizations of the (L*) tracker resolution and the HCAL response (simulated in a separate GEANT study). As seen in the table, the detector is be able to separate isolated electrons and pions with a rejection ratio of $\sim 10^{-4}$.

After these cuts, longitudinal segmentation was found to improve the electron-pion separation by a factor of at most two. More details are available on pp. 82-86

of Ref. [10].

Cost

The base price of a crystal channel is \$ 550 for the photodevice and electronics readout, or approximately \$ 1,000 per channel including contingency, EDIA, and R&D (using the standard Theriot factors). If the crystal were in two segments, the additional cost would thus be \$ 16 M. Note that if less expensive, compact UV-selective photodevices become available, then the cost of the overall BaF_2 detector might go down, and the use of two longitudinal segments could then be within our budget.

For a photodevice with a base cost of \$ 50 per channel, the total base channel cost would be \$ 300, instead of \$ 550. The cost of reading out the front and back of the crystal separately would then be only $\sim$ \$1.5M more than the cost of the current design.

As an example Los Alamos has also been investigating the possible use of metal semiconductor junctions based on $Al_xGa_{1-x}N$, which are being developed by Honeywell as UV-selective fast photosensors. These devices are "tunable", in that one can vary the long wavelength cutoff by varying the fraction x. Materials have been grown at Honeywell with cutoffs varying across the whole range from 200 to 360 nm, with sensitivity decreasing by a factor of 100 to $>$ 1000 over a 40 to 90 nm range. Honeywell estimates the cost for 16,000 pieces to be \$ 50 per piece. These devices are thus extremely interesting because of their speed, higher quantum efficiency, compactness, and potentially low cost.

Detector Layout

Apart from cost, a design which has a short forward part read out from the front, and a back part read out from the back, is feasible. The original L* (internal) design by H. Newman had a front piece a few radiation lengths long. If the front piece is short, then we could still bond two crystal pieces together for the back element, using the highly UV-transparent, strong KE-103 RTV which we have used in our prototype test matrix [11].

If the decision were taken to have two readout layers, following the appearance of a reliable device at low enough cost, we would have to consider the following

factors:

- The light collection is assisted by having the photosensor on the large end of the crystal. One could consider having the photosensor in front of the front crystal section of each pair, but the length of the front segment would then have to be limited. More tests – including a series of destructive tests where we would have to cut up some of our large crystal pieces – would be needed to establish the maximum crystal length over which light collection uniformity could be achieved, reading out from the small end. In the endcaps, where the crystals are less tapered, it may be possible to achieve uniform light collection over longer pieces.

- The decision would have to be taken early enough so that the crystal piece sizes could be set, prior to the start of mass-production.

A design with more than one longitudinal segment has the disadvantage of greater complexity in the calibration – and with 32,000 channels instead of 16,000.

8 BaF_2 Calorimeter Design

Question (9) (Chen): Show the design of the mechanical supporting wall, thickness of BaF2 coating or Al foil, and the space needed in order for 50cm long crystals to fit in rings in Phi and self supported.

Answer:

The BaF_2 calorimeter mechanical design, which is based on the L3 BGO design, has been studied in depth over the last year. As summarized in Appendix B, a complete design concept has been developed by engineers M. LeBeau (Chief engineer for the L3 BGO), Mark Rennich (ORNL) and Jim Moore (ORNL). A complete set of drawings for the final calorimeter prototype carbon fiber composite support and enclosure has been finished, and has been sent to the Italian manufacturer. A finite element stress analysis has been done for the entire BaF_2 calorimeter on a supercomputer at ORNL, and it has been found that the structure is extremely safe. As an example (see Appendix B), the safety factor on the maximum shear stress is $\approx$10, in spite of using composite walls 300 μm thick.

Following the L3 experience, and after review by SIC and BGRI, the space between crystals includes 50 μm for wrapping or coating, 100 μm of clearance, the 300 μm carbon fiber-epoxy composite wall, 100 μm of clearance, and 50 μm for wrapping or coating. This gives a typical distance between crystals of 700 μm, compared to 900 μm for BGO. Note that:

- These cracks do not point to the intersection point, and the effect on the BaF_2 resolution is extremely small.
- Because the front surface area of the BaF_2 calorimeter is typically twice as large as the BGO calorimeter, the effect of the structure on the statistical term is expected to be smaller than the (already small) effect in the BGO case.

Our demand for the use of tighter tolerances for the BaF_2 calorimeter than for the L3 BGO is simply based on experience (and agreed to by SIC and BGRI). SIC had just learned to do the necessary cutting and polishing operations for BGO, using technology developed by engineer LeBeau, at the time of setting the L3

specifications. The crystals delivered to L3 were actually measured to be within $+0 \; - 100$ μm of the specified dimensions[2].

In order to extend these tolerances to the 50 cm long crystal-pairs, it was decided by the engineers, in consultation with SIC and BGRI during the May 1991 conference in China, to make one long crystal face perpendicular to the critical faces where the two crystals are joined. While the flatness of a typical face is specified to be within 50 microns or better, the critical faces to be joined will be machined flat and parallel to within 10 microns with a precision jig. One of the senior technicians at SIC then demonstrated (with Newton's rings) how he had done better than this critical tolerance, with a BGO crystal.

[2]Measured to an accuracy, using the instruments developed at LAPP(Annecy) by LeBeau, of $\pm 5\mu$m.

9 BaF_2 Calorimeter Design and Prototype Details

Question (10a) (Chen): How do you achieve sufficient light collection uniformity, and light output (p.e./MeV) to maintain the resolution ?

Answer:

9.1 Light Uniformity Measurements

For a tapered crystal with its 6 faces polished, there are two complementary factors which affect the light uniformity along the crystal axis: the attenuation and the optical focusing. While the first factor causes a decrease of the response with the increase of the distance to the light-sensitive device, the second factor causes an increase of the response. For a BGO crystal, the second factor dominates: a strong increase of light response to the small end was observed for the L3 crystals [25]. Only after extensive studies of controlled depolishing of the surface, was light uniformity and high light collection efficiency achieved by coating the polished BGO crystals with a 40 to 50μm thick layer of high reflective NE560 paint.

Figure 6a shows the light uniformity curves with and without the NE560 coating, measured with a ^{137}Cs source. The parameter R in Fig. 6a is the relative light output difference for the source at 21 cm and 3 cm from the photodiode. The crosses correspond to aluminized mylar wrapping and the diamonds to NE560 coating.

The optical focusing effect, however, is less important for the BaF_2 because of its smaller refractive index. The light collection uniformity of BaF_2 crystals measured with a collimated ^{137}Cs source is shown in Fig. 6b. The photodetector used in this measurement is a photomultiplier (PMT) with a Cs-Te solar-blind photocathode (Hamamatsu R3197). With simple aluminum wrapping, the measured response of the fast scintillation component shows a uniformity within $\sim$2% in a 25 cm crystal piece. Because of a longer light attenuation length, the response of the slow scintillation component shows an increase with an increasing distance from the PMT, as shown in Fig. 6b.

In order to extend these results to the 50 cm long crystal-pairs which make up the prototype BaF_2 detector, we required:

(1) A grease of very high viscosity, or preferably a glue that bonds to BaF_2 , with good UV transmission down to at least 200 nm. This is needed to optically couple the two crystal pieces together, as well as to couple the crystal-pair to the photodevice.

(2) A technique of wrapping, or UV-reflective coating to combine good light collection efficiency with overall uniformity.

Extensive spectrophotometric transmission tests at Caltech, CMU and Fermilab over the last three years, up through July 1991, found that the best UV-transmitting optical coupling material (down to 190 nm) is Dow Corning 200 Silicone fluid. The best viscous grease, which can be used for good long-term joints if set up and used with care, is GE Silicone based UISC600M. Although greases of this type have been used successfully on large BaF_2 crystals in experiments: by

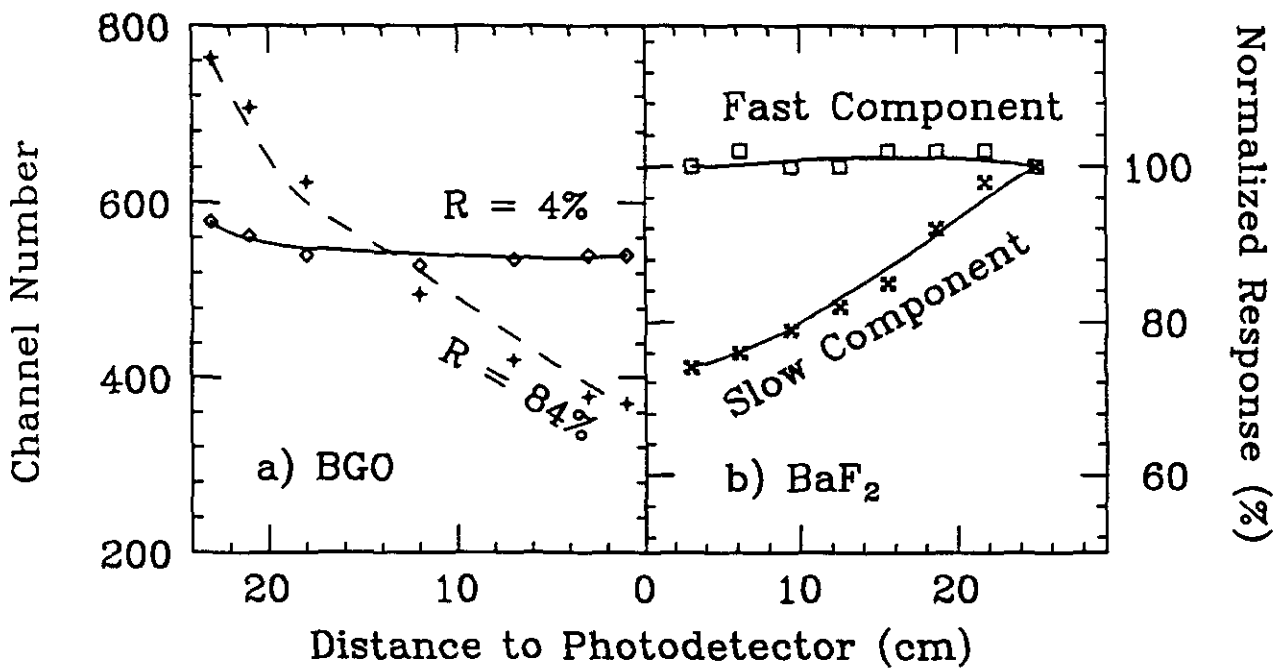

Figure 6: The light collection responses of L3 BGO crystals (a) and BaF_2 crystals (b), measured with a collimated ^{137}Cs source running along the axis of the crystals.

Table 4: UV transmission measurements for thin layers of KE - 103 RTV, and GE UISC600M grease. Results are expressed in percent, relative to Dow Corning 200 fluid.

Wavelength (nm)	190	195	200	205	210	215	220	225	230
KE - 103/1	97.2	87.6	90.5	94.6	97.8	98.3	99.9	99.4	99.4
KE - 103/2	83.7	88.5	95.3	97.6	98.8	99.8	99.4	99.9	99.8
UISC600M		90.0	94.4	96.4	96.2	97.5	97.3	97.5	97.7

Woody at BNL, and by the TAPS Collaboration [26], there is no doubt that a glue is more secure.

Up until August 1991, no suitable glue was found: indications in the literature of suitable UV-transmitting elastomers by Doering *et al.* [26] were not confirmed in our tests at Fermilab, or at Caltech.

Recently, measurements by Kobayashi *et al.* at KEK [11] indicated that KE - 103[3] — an RTV glue — could be suitable for our purposes. KE - 103 was also shown to be radiation hard, up to a level beyond 10^7 Rads [11]. The transmission results were verified in August 1991 with hard-cured samples of KE - 103, as summarized in Table 4 below. Thin joints of KE - 103 were made by pressing two pieces of quartz together, and the UV transmittance was measured, normalized to the results obtained with Dow Corning 200 fluid between two similar pieces of quartz. The results for the GE grease UISC 600M are shown for comparison. As shown in the table, the transmission of KE - 103 adhesive is nearly as good as the Dow Corning fluid down to 200-205 nm, and it shows good transmission down to 190 nm.

The actual crystal-pairs in our first test matrix have therefore been glued together with a thin layer of KE-103. Tests with these pairs show that neither the UV transmittance, or the light uniformity is disturbed by this bond (note that the fast BaF_2 light peaks at 220 nm). The thin layer bond is quite strong, and the two crystals cannot be separated with 'normal' force. By breaking the crystals apart (by unusual force) it has been found that one can clean up the surfaces afterward

[3]Manufactured by Shin-etsu Chemical Co., Japan.

completely, so that the crystals can be reglued.

A special wrapping technique, in which the region near the phototube is covered in black paper to suppress direct light, has been developed by Z. Wei at Caltech[4]. By adjusting the wrapping, uniformity at the required level of $\approx$ 10% or better over the length of the crystal can be obtained. A result with a typical 50 cm long crystal pair is shown in Figure 7, corresponding to a variation over the region from 4 to 18 radiation lengths of 6.8%.

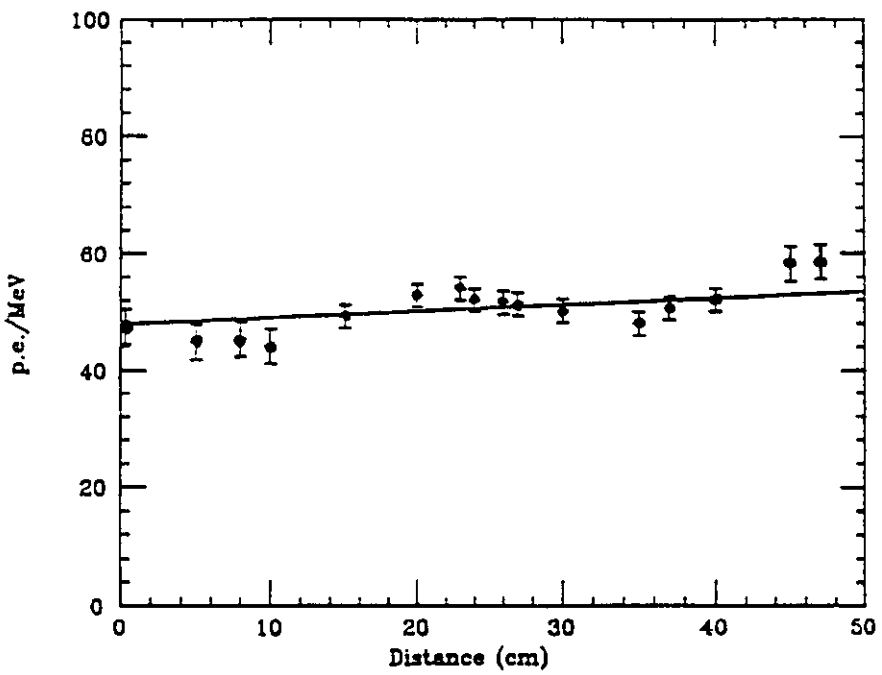

Figure 7: Photoelectrons/MeV obtained with a 50 cm crystal pair measured with a Cs^{137} source. x = 50 cm is near the phototube.

L3 experience during construction and testing of the BGO calorimeter has shown that uniformity at this level is sufficient to maintain the resolution. Recent simulation studies by CMU and Caltech on BaF_2 light collection uniformity are discussed in Appendix D. As discussed in Appendix E, the uniformity of each crystal will be checked against the initial laboratory tests with a Cs^{137} source, at

[4]Similar techniques have been used to obtain excellent light uniformity in BaF_2 crystals by B. Winstein *et al.*at Fermilab.

our Fermilab test beam by October 1991.

Note that the above results were obtained in spite of the fact that there were substantial variations in the light output of the very first crystal batches produced in 1990. It is also known that Aluminum foil in contact with air is not a high-efficiency reflector for UV light.

CMU has recently investigated the use of new radiation-hard Teflon wrappings [5]. The pulse height obtained (with small BaF_2 pieces) was 25% higher than Al foil, with no significant change in light output up to the maximum locally-available Co^{60} dose of 1.3×10^5 Rads. Tests with doses up to 10^7 Rads are planned at Caltech or BNL.

For the final BaF_2 system, we are investigating the use of a UV-reflecting coating, such as MgF_2 (used routinely for RICH Counter mirrors at 170 nm). The MgF_2 would be applied in a vacuum tank, immediately followed by a sealing layer of quartz. A masked pattern of reflector would be used to achieve the uniformity. This technique, which is not available during small-scale prototyping at moderate cost, would increase our light collection efficiency as well as the uniformity during mass production.

Note that the original question requested a result with a prism, in order for Prof. Chen to be convinced to join the BaF_2 effort. The effects of prisms of quartz and of BaF_2 will be tested by the end of the 1992 beam test. Phototubes with integrated wedges may also be available from Hammamatsu by that time, (see the Answer to Question 10(c)). Note that the wedges are needed only for the crystals near $\eta = 0$.

The next question also addresses the use of wedges.

[5] Interlocking meshes of silicone rubber and PTFE manufactured by Tetratec.

Question (10b) (Worstell): If BaF2 prisms are included in the baseline design, has it been shown that longitudinal fluctuations in high-energy showers into this prism will not give an unacceptably large constant term? If a UV quartz prism is proposed, what constant term will it introduce?

Answer:

The energy leakage out the back of a 24.5 radiation length crystal-pair is very small: typically 0.5% at 10 GeV, 0.8% at 100 GeV, and $\approx$ 1.8% at 1 TeV. This result has been computed in our electron/pion separation study, using GEANT.

In order to calculate the effect of having an additional piece in the back of the crystal which is 0 to 2 radiation lengths thick, corresponding to a 4 cm diameter phototriode equipped with a BaF_2 wedge (typically covering 50% of the back face) of the crystal, we used the following properties of electromagnetic showers:

- The shower can be modeled as having a fixed profile, relative to a point of conversion that fluctuates by approximately one radiation length.
- The attenuation length of the shower tail is approximately 4 radiation lengths, which is the result of the shower tail consisting largely of photons with an energy of 1 to a few MeV (i.e. near the minimum absorption cross section).

As a typical example result, the leakage energy is expected to fluctuate up and down by a factor of ($e^{1/4}$), or 1.28, when the shower goes through one radiation length of extra material after 24.5 radiation lengths. After taking into account that the tube only covers 50% of the rear face of a crystal this leads to a typical fluctuations of 0.07%, 0.10% and 0.23% for 10, 100, and 1000 GeV respectively. This will not significantly degrade the resolution.

Note that this effect can be corrected as part of the position correction which is used in the reconstruction, using the energy sharing between crystals.

For a quartz prism, this effect is much smaller; this will not affect the resolution.

Question (10c) (Chen): How to you obtain phototubes with sufficient linearity, working in a magnetic field over a dynamic range of of 10^5 ?

Answer:

Components and Tests in 1991

We have decided to use a Hammamatsu R4406 Phototriode with a K-Cs-Te photocathode as the photosensitive device for our first round beam test. The R4406 has been shown to have very high radiation resistance against photon and neutron doses [12], and it provides a fast/slow ratio of 2 or better. The triode also has a gain of more than 50% of its nominal value when operating in a 1 Tesla magnetic field with an angle of 45° or less to its axis [13].

The R4406 tubes have been specified by Hammamatsu as being linear to 2% up to 100 mA, with their standard diode chain, where 100 mA corresponds to the TeV range (for our typical 50 p.e./MeV). Hammamatsu has tested higher-gain versions of this tube, the 10 stage R4480 (typical gain $\sim 5,000$) and found that the deviation from linearity was -2% at 40 mA, -5% at 100 mA, -9% at 150 mA, and -17% at 200 mA.

Improved linearity is expected from the low gain R4406's, and from linearity-optimized transistorized bases which are being built now at UCSD.

The linearity will be tested this year at the Fermilab test beam, at least up to 150 GeV. Tests with a strong 200 nm pulsed light source, and beam tests with a tube in a magnetic field, are planned for 1992.

Future Developments

For future developments, Hammamatsu has proposed to develop a proximity-focused few stage mesh dynode phototube for mass production, following our specifications. The objective of the proposal (presented to us with several design options) is to:

- Improve the processing yield, quantum efficiency and cathode uniformity, by using a manipulator in a large vacuum system[6].

[6]The prototype series of tubes are constructed individually at Hammamatsu by evaporating

- Improve the ratio of sensitivity between 220 nm and 310 nm, up to a ratio of quantum efficiencies of 160.
- Provide increased gain, and improve the magnetic field immunity, by closer spacing of the electrodes.

One of the design options, for a 5-stage tube incorporating a BaF_2 wedge (for use near $\eta = 0$) is shown in Figure 8.

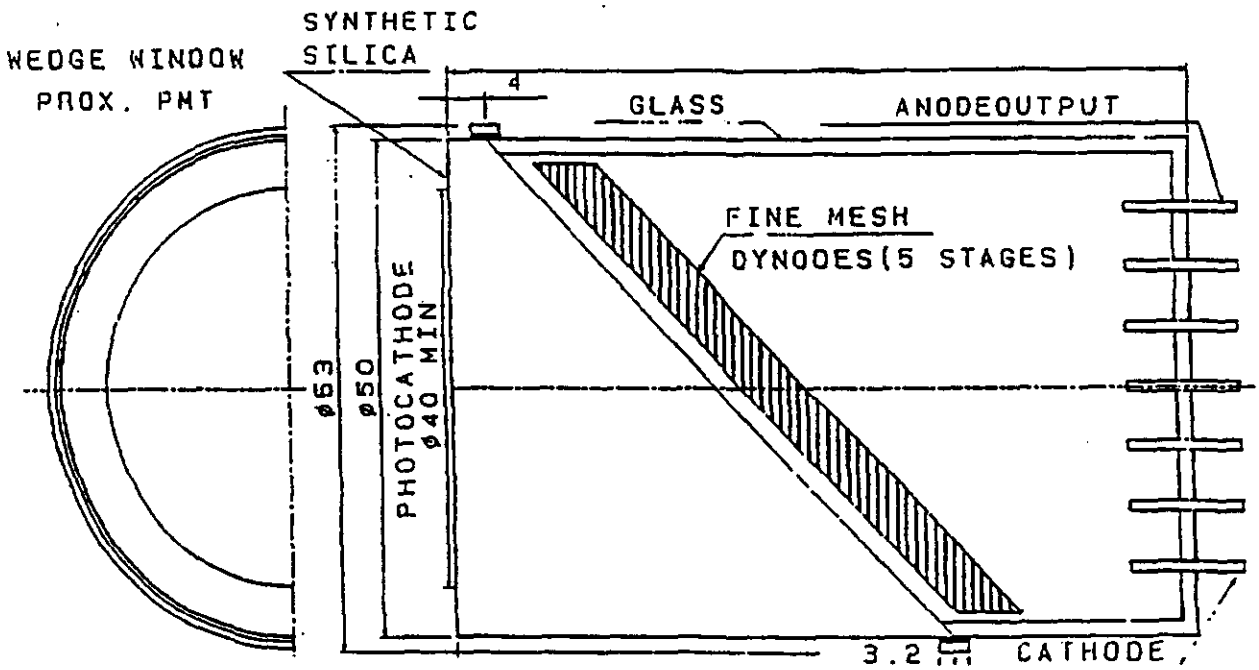

Figure 8: Hammamatsu Option for a 5 Stage Proximity Focused UV-Selective Phototube

As mentioned above, Los Alamos has also been investigating the possible use of metal semiconductor junctions based on $Al_xGa_{1-x}N$, which are being developed by Honeywell as UV-selective solid state photosensors. These devices are expected to have magnetic field immunity similar to silicon photodiodes.

the photocathode material onto the quarts front face of the tube, after sealing the glass envelope.

APPENDICES

- **Mass Production of BaF_2 Crystals in China**
  - UV Transmittance of the Crystals
  - Memorandum of Understanding Between Caltech, SIC and BGRI for BaF_2 Crystal Mass Production in China
  - Production Capacity and Investments in China
- **Structural Design of the BaF_2 Calorimeter, and the Final Prototype**
  - Design Concept
  - Carbon Fiber Structure
  - Structure for the Final Prototype
  - Materials Study for the Structure
  - Other Design Aspects: Electronics Placement, Cable Routing and Thermal Control
- **BaF_2 Radiation Resistance**
  - Measurements of BaF_2 Radiation Damage Phenomena in the BaF_2 Collaboration
  - Studies of Doped Crystals, and Correlation of Radiation Damage With Impurities
  - Studies of Radiation Damage Effects on Transmission and Light Output at BNL

- Studies of the BaF_2 Radiation Damage Mechanism at SIC

- **Light Collection Uniformity**
  - EGS Study of Light Uniformity Requirements in Coupled Crystals

- **Test Beams**
  - Beam Requirements
  - Test Beam Status at Fermilab

- **BaF_2 Calorimeter Performance**
  - Position Resolution
  - Energy Resolution

- **R&D Budget**

- **Attachment: Progress Report on BaF_2 R&D at BNL**

A Mass Production of BaF_2 Crystals in China

The Shanghai Institute of Ceramics (SIC) is specialized in inorganic, non-metallic materials and materials science. The total work force of SIC consists of 200 professors, associate professors and senior engineers, 500 researchers and technicians and 300 skilled workers. SIC's research field includes synthetic crystals, advanced ceramics, special glasses and ceramic coatings, compositional analysis, structure analysis, instrumental design, and other related topics.

Studies of synthetic crystals started at SIC in 1960, including crystal growth, crystal physics, crystal chemistry and crystal devices. About 50 kinds of crystals have been studied so far, such as electro-optical crystals, acoustic-optical crystals, piezoelectric crystals and crystal scintillators. SIC has successfully studied the BGO crystals for L3, and established an R&D Center with a production capacity of 400 BGO crystals per month. By June 1990, 11,000 high-quality BGO crystals, meeting the specifications required for L3, were delivered to the L3 Collaboration.

BGRI has been working on synthetic crystal growth technology for many years. BaF_2 crystals were first developed at BGRI for infrared applications, and as crystal scintillators starting in 1985. During 1986-1988 BGRI and SIC collaborated on producing BaF_2 scintillators, with radiation hardness up to the level of 10^7 Rads. By 1987, BGRI had grown a crystal 30 cm in length and 10 cm in diameter, using a modified Bridgeman method in vacuum. The technique has since been successfully adapted, at SIC as well as BGRI, to produce large BaF_2 crystal boules with the characteristic long truncated-pyramid shape required for our EM calorimeter, with a boule size up to 45 cm in length. Using these boules, BGRI has agreed to produce demonstration crystal-pieces 35 cm in length.

The research and development program for BaF_2 crystal mass production at SIC and BGRI began in January 1991, as a natural continuation of the generic research carried out by SIC and Caltech since 1989. The studies, which are focused on the development of a reliable method of growing large size, highly transparent and radiation resistant BaF_2 crystals at low cost, include:

- Micro-compositional chemical analyses of impurities in raw materials and crystals;

- The effect of impurities on UV transmittance and radiation resistance; determination of critical and non-critical impurities.
- A determination of the basic process responsible for radiation damage in BaF_2 .
- The effect of doping on properties of crystals;
- Research on pre-processing of the raw materials;
- Optimization of crystal growth technology on large crystals;
- Improvement of growth equipment for large crystals;
- Systematic studies of mechanical processing of BaF_2 crystals;
- Methods of eliminating internal stresses in large BaF_2 crystals;
- Crystal structure and defects studies;
- Exploration of new scintillation crystals, especially rare-earth fluoride crystals[7].

The first year of the development program has focused on the growth and mechanical processing of the first prototype matrix (now completed), using raw materials of standard industrial quality in China (typical impurity levels up to 100 ppm). The final prototype will be produced from materials with a purity level which is sufficient to achieve the radiation hardness specified below.

Studies on the breaking stress of BaF_2 crystals, in compression and bending, and on crack formation and propagation, showed that BaF_2 is much more difficult to machine and polish – while maintaining a high yield of finished crystals, than BGO. Nevertheless, by adapting the diamond wheel cutting (using lower cutting speeds), lapping, polishing and dimensional control and measurement techniques developed for the L3 BGO calorimeter, under the guidance of engineer M. LeBeau[8], SIC and BGRI were able to produce the full complement of 98 crystal pieces need for the first prototype beam test, and a number of spares, up until now. By the time of producing the final array of 81 crystal-pairs, by mid-1992, SIC and BGRI

[7]Most of the work on alternative crystals at SIC, such as CeF_3, has been done in relation to the Crystal Clear Collaboration.

[8]Chief engineer for the development of the L3 BGO.

are confident of reaching an overall yield of 70% or more (compared to a typical yield of $\approx$ 80% for BGO after two to three years of production).

A.1 UV Transmittance of the Crystals

Good UV light transmittance through the crystal is vital, so that we can achieve uniform response, and thus maintain the intrinsically high resolution of the BaF_2 calorimeter. We have specified the transmittance requirement in terms of the minimum fraction of the light passing through a 25 cm long BaF_2 crystal at specified wavelengths:

- $\geq$ 75% at $\lambda = 200$ nm
- $\geq$ 80% at $\lambda = 220$ nm
- $\geq$ 88% at $\lambda = 550$ nm

For simplicity, these specifications include ~8% loss at two interfaces between air and BaF_2. Figure 9 shows transmittance curves of four 25 cm long BaF_2 crystals from SIC and BGRI, together with our specifications shown as crosses. These transmittances have met the specifications quoted above. The impurities of the raw materials used for crystal growth have been analyzed. The small dip around 288 nm is attributed to Ce^{3+} contamination (see Appendix C.5).

All of the 98 crystal pieces in the first prototype matrix have met or exceeded these transparency requirements. This is illustrated by Figure 9 where the results measured at Caltech for four of the crystals from the first batches are shown.

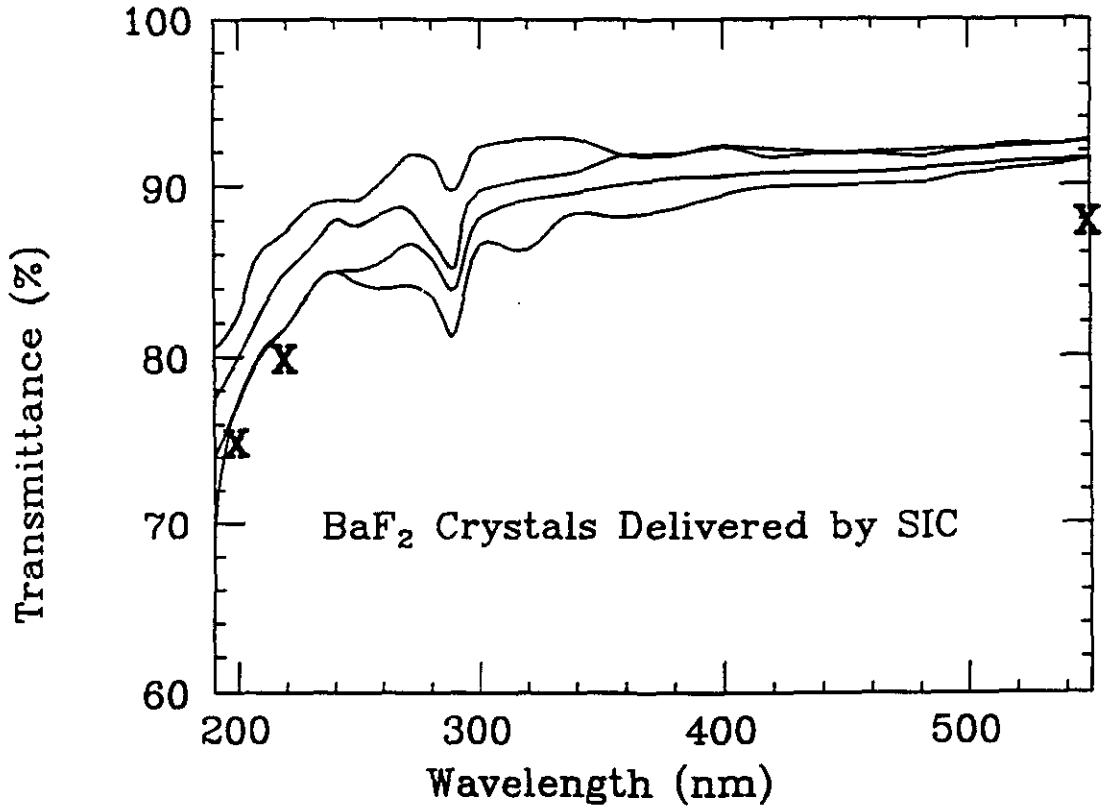

Figure 9: Optical transmission of four 25 cm long crystals delivered by SIC and BGRI. The crosses represent the transmission specifications required.

A.2 Memorandum of Understanding Between Caltech, SIC and BGRI for BaF_2 Crystal Mass Production in China

At the time of completion of the production for the first prototype array, a specialized conference was held in Shanghai and Beijing, together with site visits to the production facilities at SIC and BGRI. Following the site visits, a Memorandum of Understanding (MoU) between Caltech, BGRI and SIC was signed on May 29 in China. The principal terms of the agreement, and recent actions resulting from it, are summarized below:

1. CRYSTAL PRODUCTION and QUALITY

- The crystal price will be fixed at \$ 2.5/cc, for mass production of a total of approximately 16,000 crystal-pairs. The production of the full calorimeter would proceed at a full production rate of 800 crystals per month.

- SIC and BGRI agree to demonstrate radiation-hard crystal pairs with a target date of mid-1992 or earlier. The radiation hardness specification is that the crystals shall show a change in transmission of 25% or less, following a dose of several Megarads of Co^{60}, or a dose of 10^{13} neutrons/cm^2. As measured at Caltech and BNL, the damage effect is expected to be saturated, such that further doses up to 10^7 Rads (Co^{60}) or 10^{14} neutrons/cm^2 do not lead to any further changes in the crystals.

- In concert with its production of radiation hard crystals, SIC and BGRI will complete the final prototype crystal array of 81 crystal pairs with a target date of 6/92. The price for these prototype crystals will be fixed at the originally foreseen price for small quantities of \$ 3.5/cc.

- Studies of radiation damage in BaF_2 crystals indicate that the damage may be associated with an absorption peak at 288 nm (see Appendix C). This peak has been correlated with Cerium or O_2 in the crystals, according to tests at SIC. SIC and BGRI are now pursuing a systematic series of studies to eliminate this absorption peak; they will also specifically determine the source of the Cerium as a trace element, and eliminate it from further crystal batches.

- SIC and BGRI also will continue to pursue tests that will determine the effect of Oxygen(O_2) dissolved in the crystals. SIC, BGRI, Caltech, engineers from ORNL, and engineer M. LeBeau will work together to improve the growing conditions, so as to remove O_2 down to a level where it does not lead to significant absorption in the UV following irradiation. In order to achieve this, the vacuum systems of the ovens, which have been manufactured in China, may be improved. A production oven with improved pumping, to achieve a vacuum in the 10^{-6} to 10^{-7} Torr range, will be set up with the assistance of Caltech and the engineers by the end of 1991.

- Following up on their measurements of impurities in the crystals. SIC and BGRI will investigate the use, and necessity of the use, of very pure raw materials in the crystal growth.

- BGRI agrees to carry out a production demonstration of a crystal-pair of full size, consisting of two crystal pieces approximately 35 cm and 15 cm long. The crystals will have the trapezoidal shape characteristic of the final calorimeter. The crystal pair will also be required to meet the usual transmission requirements before irradiation of production quality crystals. At a later stage, following the successful demonstration of 35 cm finished crystals, SIC and BGRI will try to meet the radiation damage specifications given above, with the larger crystal pieces.

- SIC and BGRI will investigate the effect on the final crystal quality of:

  - Growth Speed, and its relation to the final impurity content.
  - Annealing Time, for release of trapped stresses.
  - Growth Initiation Conditions, as related to the polycrystallinity and impurity content of the final crystals.

2. CRYSTAL PROTOTYPE MATRICES

- An SIC staff member (who was formerly principally responsible for lapping and polishing the BGO crystals for L3) has been assigned to work with Z. Wei at Caltech, to carry out the post-production treatment of the crystals in the prototype, to obtain uniform light collection in the 50 cm long crystal-pairs [9].

- Engineers M. LeBeau (LAPP/Annecy) and M. Rennich (ORNL) have provided specifications of dimensional tolerances and flatness for the 81 crystal pairs for the final prototype matrix. Particular attention to the critical end surfaces where the two pieces of each crystal pair are joined is required, in order to mount each crystal within the carbon fiber structure with a clearance between the crystals and the structure of approximately 100μm.

- M. LeBeau is providing consulting help for the development and installation of new machines for the mechanical processing of the crystals, as required

[9] This operation has just been completed, at the time of this report.

for handling the larger crystal pieces of $(4 \times 4) \times (5 \times 5) \times 25$ cm^3. The European companies which produced the diamond cutting machines, and the lapping and polishing machines for the L3 BGO have been visited by LeBeau, together with engineers from the BGRI factory, to develop plans for mechanical processing of the crystals in the final prototype, and mass production processing for the full calorimeter.

- The engineers will work with SIC and BGRI to develop a full estimate of the processing requirements, in terms of the number of machines, cutting and polishing speeds, time, and labor, for:
  - Production of the crystals for the second prototype within a time period of approximately 6 months.
  - Mass production of the required 32,000 crystal pieces for the full calorimeter within a time period of 48 months. Production is forseen to start in 1993.

A.3 Production Capacity and Investments in China

Using their own funds, SIC and BGRI have installed a total of six crystal furnaces (as of June, 1991). Three additional furnaces are currently being installed in Shanghai, which will bring the total production capacity to 90 crystal boules per month. The first computer-controlled mass production furnace with a production capacity of 40 crystals per month is now under construction in BGRI. By the end of 1991, the crystal production capacity will be 130 boules per month.

In setting up this production, and associated R&D, SIC and BGRI have invested the equivalent of approximately $ 1.3M U.S. in hard currency[10]. This does not include the labor costs for 28 full time persons at SIC, and 21 full time persons at BGRI.

As specified in a letter by Dr. Wen Ou, Director of BGRI (June 6, 1991), SIC and BGRI will each invest an additional $ 750,000, to increase the BaF_2 production capacity to 2×2.5 metric tons per year (0.5 m^3 at SIC and 0.5 m^3 at BGRI) during 1992, in support of this project.

[10]The installation of a similar facility in the U.S. would cost several million dollars.

B Structural Design of the BaF_2 Calorimeter, and the Final Prototype

Engineer J. Moore (ORNL) has developed the full specification of the final prototype matrix support, including a carbon fiber-epoxy cell structure structure housing the crystals, and an aluminum enclosure housing the cell-array. In order to ensure that the performance of the final prototype will be truly representative of the full-size calorimeter, engineering design of the full detector has proceeded along with the engineering of the prototype.

B.1 Design Concept

Because of the density of the crystals, their brittleness, and the constraint of having to minimize the dead material in the calorimeter to maintain the best resolution, the BaF_2 calorimeter design follows the safe, proven design concept of the L3 BGO calorimeter. Each crystal is located in a cavity composed of thin walls made of carbon fiber-epoxy composite. The carbon fiber cavities are bonded together to form a rigid honeycomb with a wall thickness of approximately 300 μm. The carbon fiber cells in the barrel are bonded to an inner cylindrical shell (composed of an acrylic foam core and thin carbon fiber composite skins). The inner tube is attached to a conical funnel at each end, to transmit the load to roller-bearing pads.

Note that the crystals are not in contact with the thin carbon fiber walls: there is a clearance between the crystals and the enclosing cell of approximately 100 μm. Each crystal-pair is mounted under compression, with a force approximately equal to twice its weight. As in L3, the mechanical stability of the assembly is increased by using a spring loaded fixture at the back face of each crystal to push the crystals against the inner shell, so that the crystals remain under compression and the cell walls are under tension. The inner shell thus takes the weight of the crystals and transmits it to the end-flanges.

B.2 Carbon Fiber Structure

During the last year, engineers Moore, Rennich and LeBeau have worked with Italcompositi, the company which manufactured the L3 BGO, and have verified that the larger structure and greater crystal weight to be supported are well within the capability of the manufacturer. The cell walls will consist of two of their standard layers of composite cloth (0.12 mm and 0.18 mm) with a total thickness tolerance of ± 10 μm.

Based on the manufacturer's experience, the BaF_2 carbon fiber cells will be produced in standard groups, making the structure more modular, and hence less costly per unit weight. The modularity also has the advantage that the overall tolerances of the structure can be better controlled. Because the molds used to form and cure the components are adjustable, the dimensions of subsequent components can be arranged to offset the tolerance of previously manufactured components. This leads to an overall positional tolerance of the structure within ± 20 μm.

The entire structure will be coated with nickel, in order to provide a good electrical ground, and to eliminate the problem of electronic noise pickup. The nickel will be applied by an electrodeless chemical deposition process which is available from several companies in the U.S., in Europe, and at two plants at ORNL. (A similar process was used in the course of manufacturing the L3 RFQ accelerator).

B.3 Structure for the Final Prototype

The overall assembly of the Prototype Array support structure[11] is illustrated in Figure 10. The prototype represents a section of the calorimeter barrel near $\eta = 0$.

The prototype support structure includes three main components:

- An 11×11 Array of 121 carbon fiber-epoxy composite cells, in which the crystals are mounted[12].

[11] The carbon fiber structure for the final BaF_2 prototype is being funded by INFN Rome.

[12] The array is large enough to accommodate additional crystals beyond the 81 pairs forseen for 1992, in case a joint test with a hadron calorimeter is carried out in 1993, as discussed in Section E.

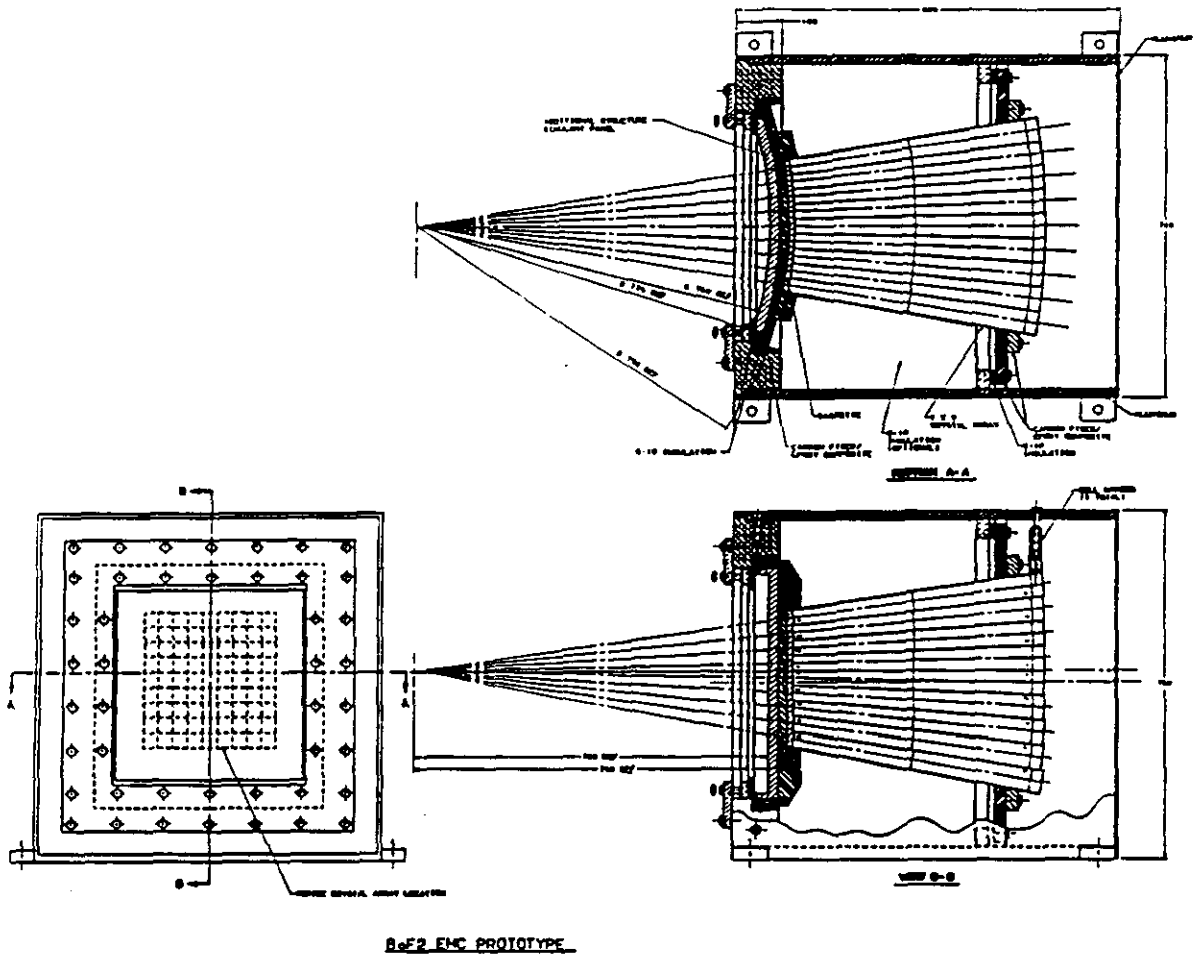

Figure 10: Overall Assembly of the BaF_2 EM Calorimeter Prototype Array.

- A "Barrette" consisting of a cylindrical shaped segment of carbon fiber composite, to which the Array is mounted. The Barrette has flat reference faces (steps) that are perpendicular to the axis of each crystal.
- An aluminum enclosure box, to provide optical and electrical isolation of the assembly.

The prototype includes a cylindrical plate, composed of carbon fiber 50 mm thick mounted in the front of the Array, to simulate the inner shell of the full EM calorimeter barrel structure. Provision is made for mounting additional layers of material in the front, for test purposes.

The carbon fiber structure is a long lead time item, because of the complex

tooling and preparation of the precision molds for manufacturing the carbon fiber modules. The manufacturer estimates 9 months to complete the structure, including tooling, and dimensional, mechanical and radiation tests of specimen modules. The completed specifications and drawings are now being delivered to the manufacturer. The progress of the manufacture will be closely monitored by physicists from the University of Rome starting this Summer, to ensure that the structure is ready in time for the 1992 beam test.

B.4 Materials Study for the Structure

The mechanical strength and radiation resistance of various composite materials were studied, and it was found that a standard carbon fiber-epoxy composite would be sufficient for our needs. Figure 11 shows that the ultimate strength of carbon fiber composite is maintained up to doses of more than 10^{10} Rads. Similarly, the shear modulus is nearly unaffected by doses of this magnitude. These doses are far in excess of the maximum 20-year dose that would be encountered at the SSC, so that radiation damage of the structure is not expected to be an issue.

The stresses on the entire calorimeter structure, including the weight of the crystals and the tensile and shear forces caused by compressing the crystals against the inner shell, were computed using a supercomputer at ORNL. A sample of the results is shown in Figure 12. While not obvious without a color drawing, the results show that the maximum shear stress occurs at a point on the inner shell. The maximum stress is 10% of the ultimate shear stress of the composite material. A cutaway of a cell, shown in the figure, shows that the stresses inside the cells are very low.

B.5 Other Design Aspects: Electronics Placement, Cable Routing and Thermal Control

A detailed study of electronics, cable and cooling tube layout for the full calorimeter was carried out by M. Rennich [13]. Two readout options – with signal digitization locally at the crystals, or "nearby" within a few meters of the detector – are shown

[13] Work performed in the context of integrating the BaF_2 calorimeter into the L* experiment.

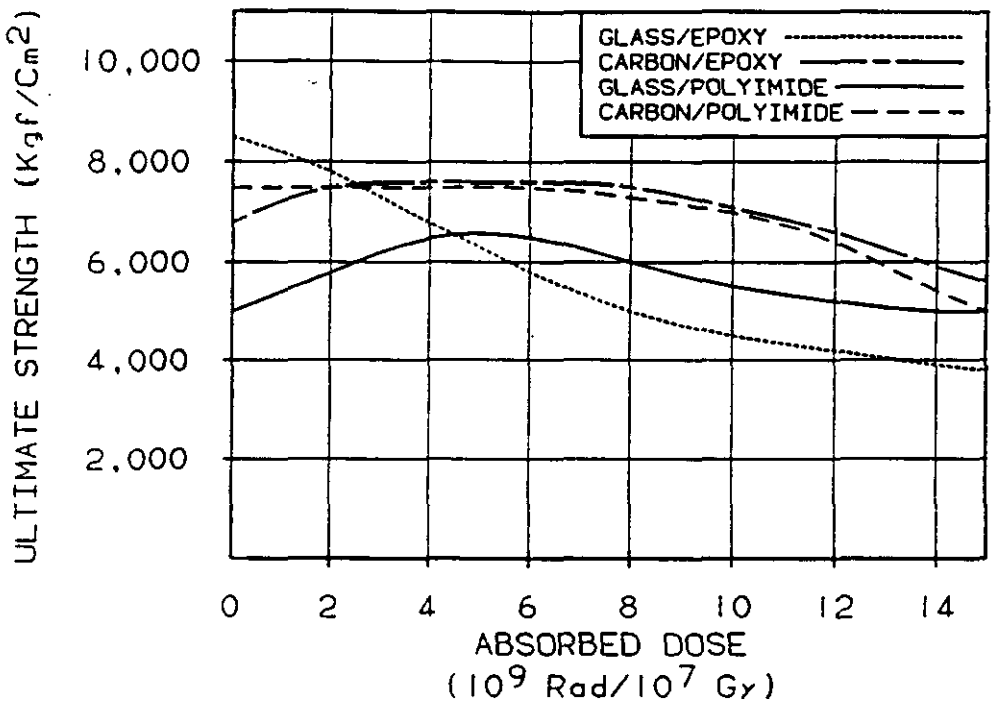

Figure 11: Ultimate strength versus absorbed dose for composite materials

in Figure 13. More complete on-crystal signal processing may be doable with sufficient reliability in the future.

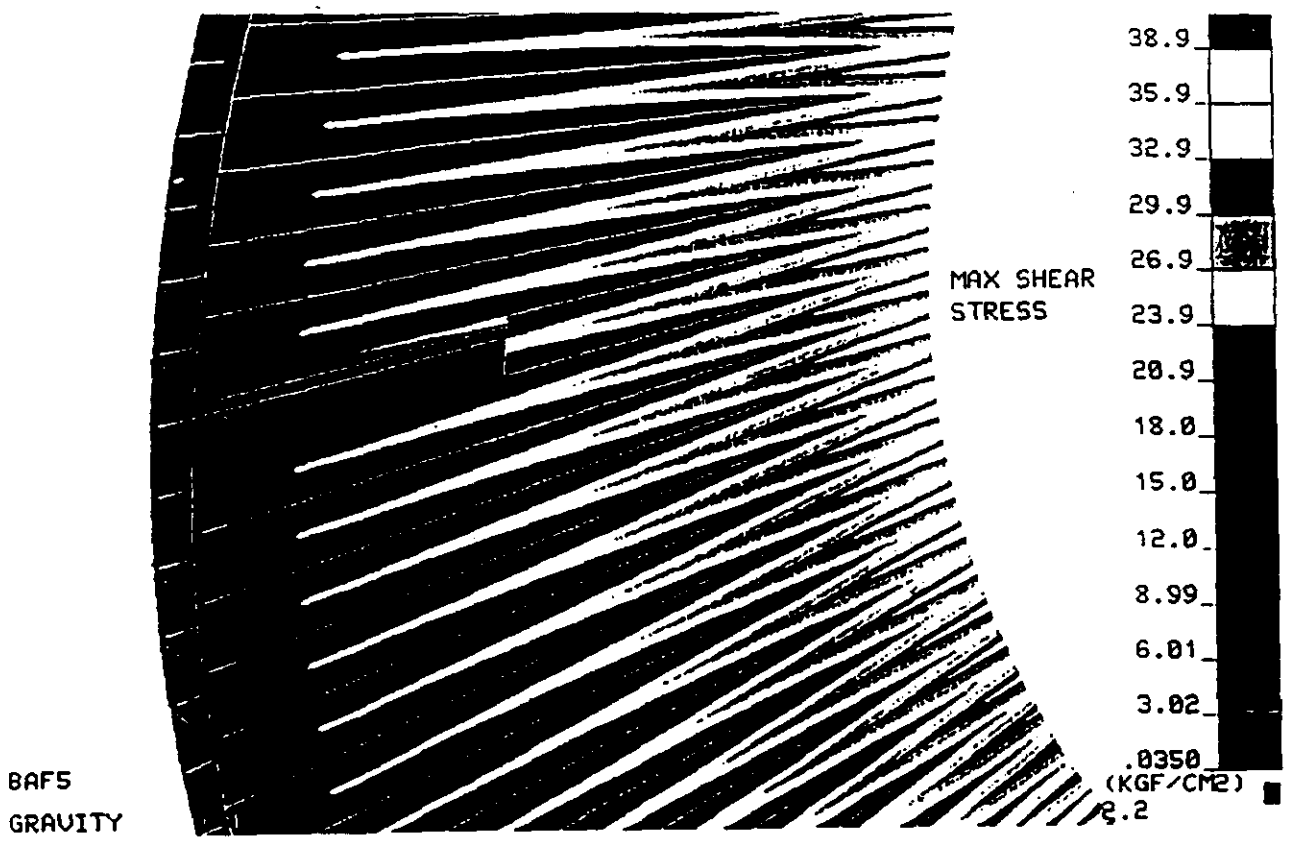

Figure 12: Sample result from a finite element analysis of the shear stresses on the full BaF_2 calorimeter structure.

C BaF_2 Radiation Resistance

C.1 Introduction

BaF_2 is one of the most radiation resistant crystals known, for crystals of sufficient purity. It is understood that the fast component in BaF_2 is produced by the "cross scintillation" mechanism [14]. Studies on other fluoride crystals have shown that this mechanism occurs in crystals with very high radiation resistance, and that it produces scintillation light with only a weak temperature dependence [14].

Early work done by S. Majewski and D. Anderson [1] showed that no color centers were formed in BaF_2 up to a dose of 1.3×10^7 Rads in an 800 GeV proton beam. The crystals tested were from Harshaw. Many other works [1] confirmed this early observation for irradiations from either charged particles or photons. It is also known that impurities in the crystal will cause radiation damage. An absorption

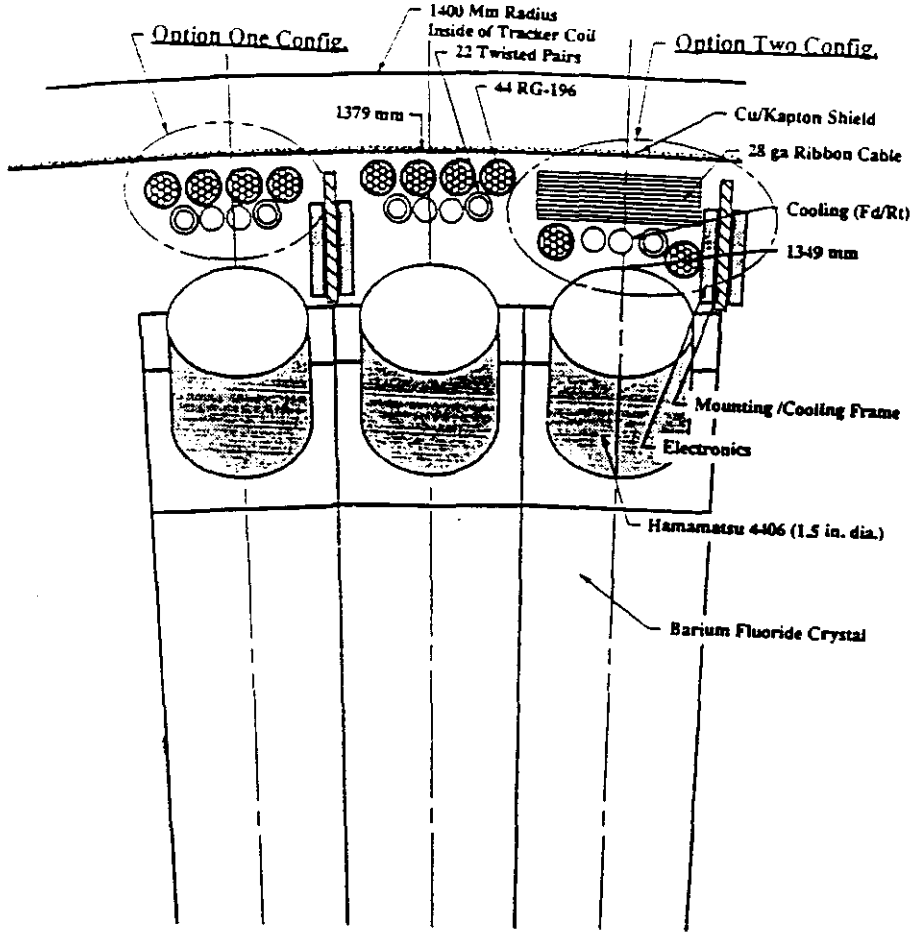

Figure 13: Cross section of BaF_2 central calorimeter barrel (example at η=0.4): two options for grouping and layout of cables, cooling and front-end electronics.

band around 205 nm was identified as originating from Pb contamination [15], and this was correlated with the susceptibility to radiation damage.

C.2 Measurements of BaF_2 Radiation Damage Phenomena in the BaF_2 Collaboration

Systematic studies of radiation damage in BaF_2 have been performed at SIC, BGRI, BNL, CMU, TIFR (Bombay), and Caltech. Tests at Caltech have shown that the radiation damage BaF_2 caused by either γ-ray or neutron irradiation is completely recoverable by annealing the crystal at 500°C for 3 hours [16]. Figure 14a shows the light transmittances before and after 10^{14} neutrons/cm^2 irradiation. Also shown in the figure is the full recovery after annealing. This measurement indicates that neutrons, as well as photons, do not cause permanent damage to BaF_2 crystals.

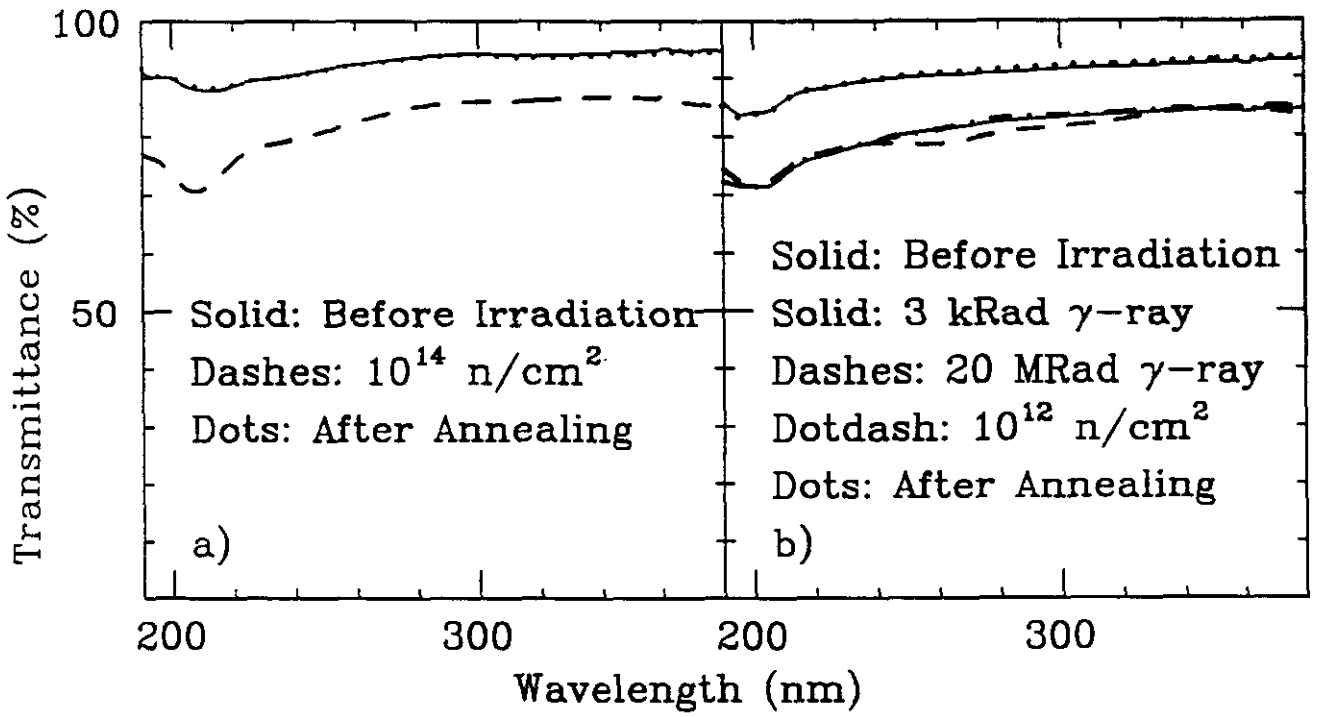

Figure 14: Transmittances before and after irradiation showing a) recovery from neutron damage; and b) typical saturation effect.

Studies at Caltech, BNL, SIC and IHEP(Beijing) have also demonstrated that BaF_2 undergoes a striking recovery after a few hours' exposure to a UV lamp. The spectral component of the UV light in the 200 nm range required to break up the UV color-centers appears to be very low. A recent study by J.T. He (IHEP Beijing) for example, showed complete recovery after two hours' exposure to sunlight.

BaF_2 crystals irradiated with γ-ray doses up to 20 MRad, and at the UC Irvine reactor with doses up to 10^{14} neutrons/cm^2, show that a small initial damage occurs after the first 100 kRads, and no further damage follows. This saturation effect indicates that the radiation damage in BaF_2 is not caused by an intrinsic color center in the bulk material of crystal, such as O^{--} vacancies in BGO [17], but by externally-introduced impurities.

The consequence of this initial damage has also been investigated. Figure 15 shows that the transmittance of a 2.5 cm long BaF_2 crystal decreased by ~1% after 2 MRad dose of ^{60}Co γ-rays [18]. This indicates a ~20% loss in transmittance for a 50 cm long crystal with existing quality. This loss will be further reduced by determining the critical impurities, and by removing them from the raw materials

used to grow the crystals.

During the measurements of new radiation-hard Teflon wrappings by CMU (mentioned in Section 9.1), the radiation hardness of a small BaF_2 crystal was tested. No change was observed up to 130,000 Rads. Tests with larger samples (and larger doses, using facilities at JPL and BNL) are planned

Studies of radiation damage effects are also underway at TIFR Bombay, using Mev neutrons at their swimming pool reactor, as well as Co^{60} γ-rays [19]. In order to proceed with their tests, they will acquire several large sample crystals, and UV-selective phototubes (such as the R4480) this Fall.

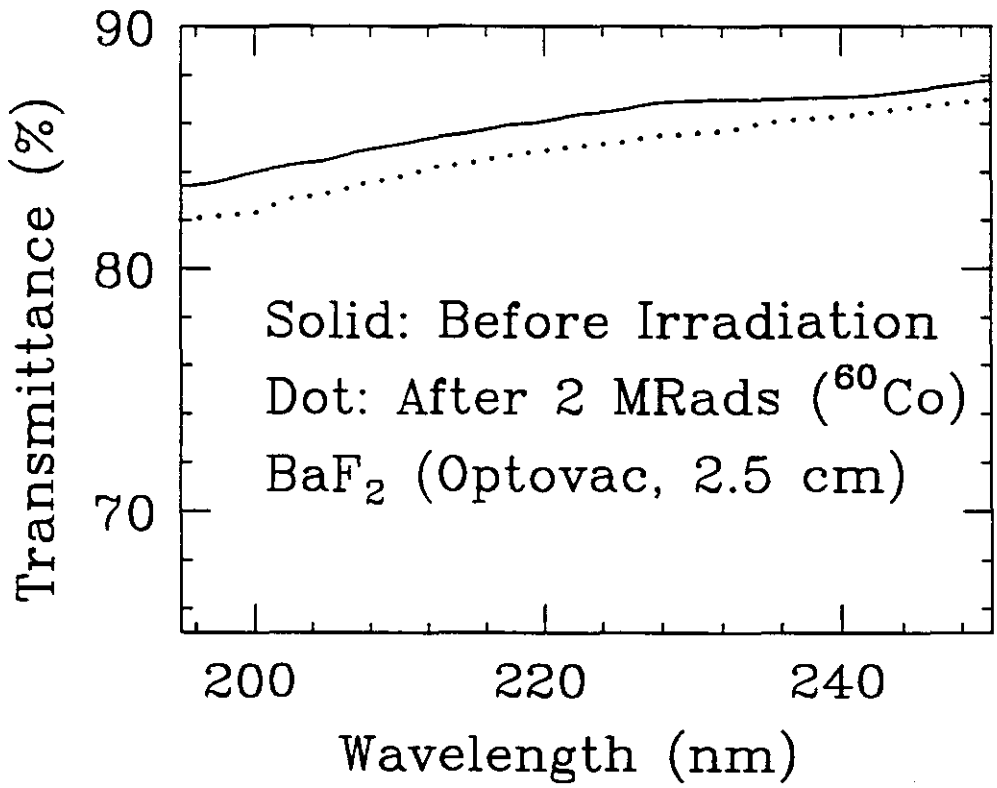

Figure 15: The transmittance of a 2.5 cm long BaF_2 crystal, as a function of wavelength, before and after 2 MRad dose measured by Woody *et al.*

C.3 Studies of Doped Crystals, and Correlation of Radiation Damage With Impurities

J.T. He *et al.* have studied the radiation damage of BaF_2 at IHEP (Beijing), including pure BaF_2 crystals, and crystals doped with 1 PPM, 10 PPM, 1% ,and 10Cerium. A series of Dysprosium-doped BaF_2 crystalswas also studied. The crystal samples were grown at SIC and BGRI. This group is now in the process of analysing the impurities of each BaF_2 crystal, and correlating it with the measured radiation damage effects. The impurities ahve been measured with neutron activation analysis (NAA), and they have been cross-checked using Inductively Coupled Plasma spectroscopy (ICP).

This group also studied the "cycling" of radiation damage and recovery. In each cycle, the BaF_2 crystal was irradiated by 10^6 of γ-rays, then the damaged crystal was put into sunlight for 2 hours. After three cycles, it was found that there was complete recovery on each cycle, and the damage level after each irradiation was the same.

He *et al.* are continuing to study the relation of radiation damage and impurities in the crystals, to identify the critical impurities. As found at SIC, some trace contaminants, such as Fe and La, are not harmful.

C.4 Studies of Radiation Damage Effects on Transmission and Light Output at BNL

Many of the above studies, with many different crystal samples, have shown that the effect of radiation damage causes a change in light transmission, but no change in the actual emission of scintillation.

One series of tests at BNL by Woody *et al.* [20] however, showed some apparent effect on the scintillation light, in particular crystal samples. Other tests done in the same time period by them, at an irradiation facility where the actual light during irradiation can be measured, showed no effect on the scintillation spectrum at all. This is summarized in Ref. [20], a copy of which is attached as Appendix H to this report.

Woody states that their results are indicative of damage caused by impurities or defects in the crystal, implying that radiation hardness can be increased by improving the purity of the raw material and better control of the growth conditions. Moreover, their observation (also seen at IHEP, SIC, BGRI and Caltech) that the radiation induced damage, both in the UV transmission and light output, could be mostly recovered by a short ($\sim$ 15 minute) exposure to a mercury lamp, also implies that the damage is impurity or defect related rather than intrinsic to the crystal.

C.5 Studies of the BaF_2 Radiation Damage Mechanism at SIC

In depth investigations of the role of impurities, and dissolved Oxygen in the radiation damage of BaF_2 crystals have been carried out at SIC and BGRI in China. The results of investigations by Prof. Z. Y. Yin, who is the scientific leader of the BaF_2 production project, and who was in charge of the L3 BGO project, are summarized below. Preliminary conclusions of the study are also given.

The results of the tests and studies at SIC (through August, 1991) are:

- Slices taken from a 30 cm long crystal boule at SIC show that the radiation damage rate increases as one moves away from the growth initiation point. Since the impurities tend to concentrate at the end of a long boule, this shows that the degree of damage is correlated directly with the impurity concentration.

- SIC has also shown that the dips in the transmission spectrum observed in the crystals of the first prototype matrix – a primary peak at 288 nm and a secondary rounded peak at $\approx$ 200 nm, are due to Cerium (Ce^{+++} in the crystals). This was verified by 1 ppm and 10 ppm doping of some BaF_2 crystal samples with Cerium.

- A sharp absorption band at $\approx$ 190 nm has been observed in a few of the first prototype matrix crystals. Based on the knowledge of other similar fluoride (and oxide) crystals, and tests in which the pretreatment process (where water and oxygen are removed) was varied, SIC has correlated the absorption in the 190-200 nm region with the oxygen content in the crystals. Measurements of the transmission of the crystals in the infrared show no evidence of the very sharp absorption peak at 3630 cm^{-1} which is characteristic of OH^-.

- Diffraction studies with an electron beam with a diameter of 1000 Angstroms focused on a crystal verified the presence of dissolved Oxygen. As shown in Figure 16a, the crystal shows a perfect diffraction pattern, just after the start of bombardment. This perfect pattern can be found nearly everywhere in the crystal, indicating a low density of dislocations. After a few minutes, however, diffraction rings appear, as shown in Figure 16b. These rings have

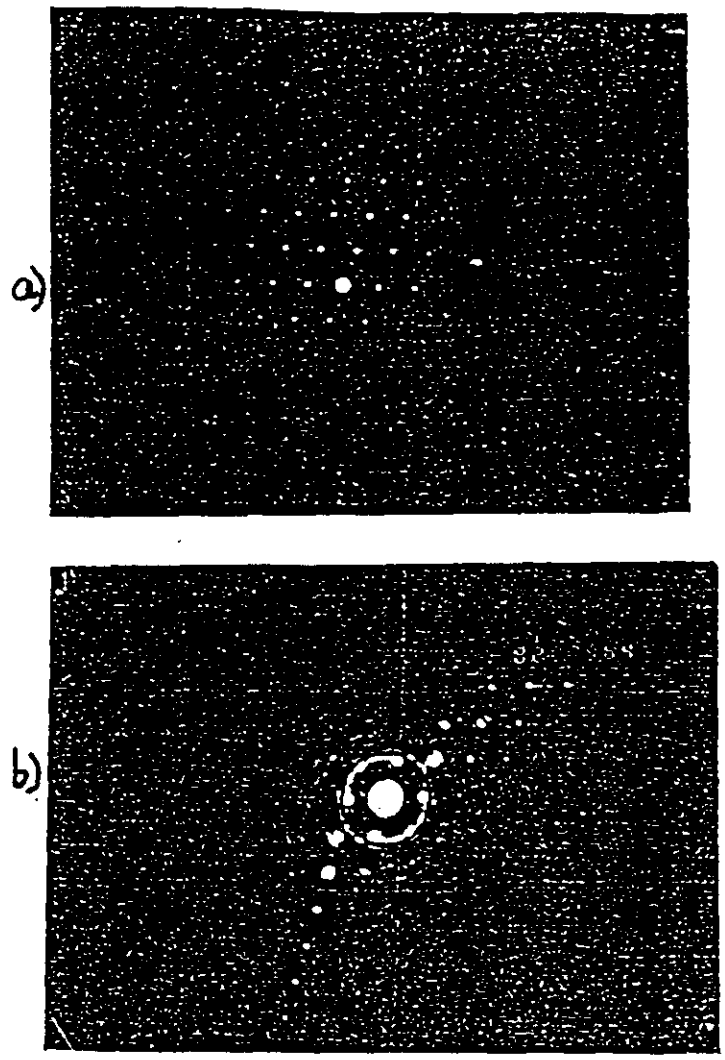

Figure 16: Electron diffraction patterns of a BaF_2 crystal a) just after the start of electron beam bombardment b) a few minutes later, showing the characteristic pattern of BaO rings.

been identified as BaO, which is formed when a fluorine atom (relatively loosely bound in the BaF_2 lattice.) is displaced from a lattice site, and is replaced by an Oxygen ion.

The preliminary understanding of the radiation damage mechanism, based on the above results in addition to SIC's experience with many other fluoride crystals is:

- Radiation damage is associated with some particular cationic impurities,

including Pb and Ce. Many other metallic impurities which are important in BGO, such as Fe, do not have a harmful effect in BaF_2 .

- When Oxygen is absorbed in the crystals, during the pretreatment or growing process, $O^{2-}F^{+}$ dipoles are formed[14].

- If the crystal is then irradiated, the $O^{2-}F^{+}$ dipoles are decomposed. This increases the concentration of lone O^{2-} ions, and O^{2-} pairs, which are responsible for increased absorption in the 190-250 nm region. The formation of more lone fluorine vacancies leads immediately to the formation of the well-known 'F-centers' when electrons are captured at the F^{+} vacancy site. The F-centers are responsible for absorption bands in the visible.

- When a radiation damaged crystal is illuminated with UV light, the electrons trapped in the F-centers escape, so that the F-centers are destroyed. The resulting F^{+} vacancies are then free to associate again with O^{2-} ions. The decreased concentration of F-centers, lone O^{2-} ions, and O^{2-} pairs leads to decreased absorption both in the UV, and in the visible.

Note that the studies above are done on crystals grown from industrial raw materials, with typical impurities of metal oxides in the 10 - 100 ppm range. Tests with higher purity crystals, and with more tightly controlled pretreatment of the raw materials to remove oxygen – to meet the specifications presented in Section A, are now underway. As mentioned earlier, the target date for completion of this study is early 1992, with production of large radiation-hard crystals in mass production by mid-1992.

[14]Where F^{+} denotes a fluorine vacancy in the lattice.

D Light Collection Uniformity

Experience with the L3 BGO, and other precision crystal calorimeters, has shown that light collection uniformity at the level of several percent over the length of the crystal (except for the first few and the last few radiation lengths), is important to maintain the resolution. This uniformity is also needed to maintain good linearity over a large dynamic range, e.g. from ~ 10 GeV up to the TeV range at the SSC.

D.1 EGS Study of Light Uniformity Requirements in Coupled Crystals

Simulation studies of the light-uniformity requirements have been carried out independently at CMU and Caltech. A light-transport simulation package that allows us to relate variations both in the bulk and surface properties of the crystals to the overall light collection efficiency also has been written by D. Kirkby, and has been used in the Caltech study.

The CMU group, for example, has used EGS to simulate optically coupled BaF_2 crystals (25 + 25 cm), to estimate the degree of deterioration of the energy resolution as a function of the relative fraction of light collected from the front vs the back crystal. They simulated incident electrons of 20, 40, 80, and 120 GeV, and found that an optical mismatch as large as 10% could be tolerated without destroying the intrinsic resolution at a level above 0.5%.

E Test Beams

We require the use of an electron/pion beam to test the pre-production prototype crystal matrix this Fall (starting now), and the first production-quality crystal matrix (with carbon fiber structure) in the Summer of 1992. We are also considering a combined test of a 121 crystal prototype with a suitable hadron calorimeter module in the Spring of 1993.

E.1 Beam Requirements

The characteristics of the beam are given in the Table E.1.

TEST BEAM SPECIFICATIONS

Momentum range:	10 GeV/c - 180 GeV/c
Intensity:	100 - 1000 tagged particles/second
Momentum resolution	0.5 %
Space resolution	0.1 cm
Electron misidentification	$\leq 0.1\%$
Pion misidentification	$\leq 1\%$

E.2 Test Beam Status at Fermilab

For the first test beam run, we have been approved to share the N-T beam line at Fermilab. This beam line has been commissioned by Sciulli *et al.* for the calibration of the ZEUS calorimeter for HERA (experiment E790). E790 has now been completed, and (as of this report) dedicated running for BaF_2 is about to begin.

Electrons and pions in the beam are separated with online triggers and analysis using two Pruss-type Cherenkovs and a Xenon TRD, combined with a drift chamber spectrometer. Scintillator veto-walls are installed between the bending magnets in the spectrometer, to help suppress beam halo. A part of the Barish-Sciulli hadron calorimeter (4 inch steel plates) is situated at the back of the user

area behind the movable stand where the ZEUS modules under test are currently mounted. This 'Backup Calorimeter' may be used to further separate electrons from pions, and to test the fraction of energy deposited in the crystal array.

Behind the first section of the Backup Calorimeter is an area that can be used, together with a trigger instrumented by E790, to provide a clean muon flux. Immediately following its arrival at Fermilab, the first prototype array will be measured with muons: transversely to cross-check the uniformity of light-collection measured on a test bench at Caltech, and longitudinally to test the idea of calibration of the crystals with minimum-ionizing particles.

A test beam group headed by H. Kobrak (UCSD) and X. Shi (Caltech), including several full time physicists, is now installing the trigger, readout, data acquisition and offline analysis (IBM RS6000/32H) facilities for the BaF_2 run. We are replacing the drift chamber spectrometer TDC's to improve the beam resolution, and are working on improvements to the Xenon TRD electron trigger. This work should enable us to meet the beam specifications listed above.

We estimate that the first round of tests will require two dedicated "beam on" periods of at least one month each, separated by a data analysis period of about one month.

The volume of the first prototype test-box is less than one 0.1 cubic meter, with a weight of less than 250 Kg. The large movable stand used by E790, in conjunction with a support designed and built at CMU to mount the BaF_2 matrix box in the beam, will allow us to illuminate the prototype with particles over a wide range of impact points.

A GEANT simulation of the matrix has now been prepared, and is ready for the dedicated BaF_2 run. The simulation includes the material between the crystals as well as in front of them (a minor effect). A light uniformity curve, as measured, will be applied to each crystal. The effect of non-uniformities of light collection will be studied with the simulation combined with the real data.

The second round of tests will require two periods of up to 3 months of dedicated beam time, separated by data analysis periods totaling 6-8 weeks during the second half of 1992[15]. The beam parameters listed in the table above will be sufficient

[15] As there will be no test beam available at Fermilab in 1992, we intend to apply for test beam

for the final prototype test, but a beam with a larger range of energies (below 10 GeV and above 100 GeV), and with pion misidentification at or below the 0.1% level is desirable. A beam momentum resolution of $\Delta p/p = 0.5\%$ will be just sufficient, but a momentum resolution of 0.3% or better at the higher energies is highly desirable. A study of the beam spectrometer at Fermilab is now getting underway, to minimize the $\Delta p/p$ of the beam spectrometer.

An additional test period of 2-3 months, foreseen for the Spring of 1993, will be needed if we are to carry out the combined test of a 121 crystal array with a hadron calorimeter. The larger crystal array size, approaching the size originally proposed to SSC Lab in September 1990, is needed to provide sufficient transverse containment of most hadronic showers that result from primary hadrons interacting in the Barium Fluoride (1.7 Lambda deep).

E.3 Test Beam Program Outline

A brief outline of the test beam program is given below.

time at CERN in 1992, and possibly in 1993.

FIRST ROUND TEST:
7×7 ARRAY (9/91 - 12/91)

- **ELECTRON RESOLUTION**
  To Demonstrate $\sigma_E/E = (2.0/\sqrt{E} \oplus 0.5)\%$
  With Electrons from 10 GeV to $\geq$ 100 GeV
  - Calibrate the gain for each crystal + phototube.
  - Scan the beam across the central crystal to establish the (position corrected) uniformity of response.
  - Check the stability of a period of weeks.
  - Compare to GEANT predictions for resolution, energy sharing distributions, and position reconstruction accuracy as a function of the impact point.
- **PION RESPONSE**
  From 10 GeV to $\geq$ 100 GeV
  - Using data taken at the same time as for the electrons above.
- **ELECTRON-PION SEPARATION**
  Note: because of the limited transverse size of the first round crystal array, we will be able to test our electron selection criteria, but we will not have a complete test of e/π separation.
  - Test (Sum of 25)/(Sum of 49)
    Note: This is like (Sum of 9)/(Sum of 25) with the final crystal sizes.
  - E (electromagnetic energy) versus p (Momentum),
    using the drift chamber spectrometer.
  - Possibly: Veto on the energy in the backup calorimeter.
    Note: This may or may not be possible given the thickness of the calorimeter plates. A better HCAL module is needed.
- **MIPs CALIBRATION TEST**
  - Calibrate the crystals using minimum ionizing particles (MIPs) going along the long axis of a crystal. The mean energy for a MIP is expected to be 330 MeV.

- **ELECTRONICS DEVELOPMENT**
  - Test the resolution without a large electronic-noise contribution (with Rb-Te PMT's).
  - Isolate the contribution of noise using vacuum phototriodes and a first-round preamp and shaper matched to standard FASTBUS ADC's.
  - Develop mounting, shielding and grounding techniques to reach an acceptable noise level.
  - Possibly: Test a second-round of preamps and shapers with a shaping time $\sim$ 10 nsec or less, lower noise, and higher rate capability, used together with custom ADC's.
  - Test a Switched Capacitor Array readout module.

SECOND ROUND TEST:
9×9 ARRAY (Summer 1992)

- **ELECTRON RESOLUTION**
  Demonstrate $\sigma_E/E = (2.0/\sqrt{E} \oplus 0.5)\%$
  With Electrons from 10 GeV to > 100 GeV
  - Calibrate the gain for each crystal + phototube.
  - Scan the beam across the central crystal to establish the (position corrected) uniformity of response, with the carbon fiber prototype structure, and full-size crystals.
  - Check the stability of a period of weeks.
  - Check the resolution, and the absolute response, as a function of the rate.
  - Compare to GEANT predictions for resolution, energy sharing distributions, and position reconstruction accuracy as a function of the impact point.
- **PION RESPONSE** From 10 GeV to > 100 GeV
  - Using data taken at the same time as for the electrons above.
- **ELECTRON-PION SEPARATION**
  - Test (Sum of 9)/(Sum of 25): Transverse shower shape.
  - E (electromagnetic energy) versus p (Momentum), using the drift chamber spectrometer.
  - Veto using an HCAL module from our Collaboration, placed behind the crystal array.
- **ELECTRONICS DEVELOPMENT**
  - Use proximity-focused few-stage tube from Hammamatsu. Cross check against a separate run with high gain tubes or the previously-used phototriodes.

- Use monolithic preamp + shaper circuits, with lower noise than in 1991 tests; speed compatible with complete separation of signals from each SSC beam crossing.
- Develop mounting, shielding and grounding techniques to reach an acceptable noise level for the full-scale calorimeter.
- Test SCA or other higher level (e.g. FADC) trigger and readout modules.

THIRD ROUND TEST (OPTION): 11×11 CRYSTAL ARRAY and HCAL MODULES (Spring 1993

Note: This test will include further developments along the lines specified in the second-round test above, plus the following.

- **ELECTRON-PION SEPARATION**
  - Test (Sum of 9)/(Sum of 25), and other algorithms to fit jointly for the energy and position (analogous to a test of γ/π° separation.
  - Check simulated results on side and rear leakage from the crystal array.
- **ELECTRONICS DEVELOPMENT**
  - Use latest UV-selective photodevice. Cross check against runs with previous devices.
  - Use monolithic preamp + shaper circuits, with final noise and pulse-spacing capability, corresponding to separation of signals from each SSC beam crossing.
  - Test trigger and digital readout modules.
- **COMPENSATION**
  - Measure the constant term in the resolution.
  - Develop optimized weighting methods, to minimize the constant term.
  - Check results on the energy distributions in the crystals and the HCAL, and their correaltions, against GEANT (GHEISHA) simulations. Check against other simulations (e.g. HETC) if necessary.

F BaF_2 Calorimeter Performance

An analysis of the expected performance of the full-size BaF_2 calorimeter is summarized in the following sections.

F.1 Position Resolution

The position of an electromagnetic shower, i.e. the coordinate of the impact point of an electron or a photon on the front surface of an electromagnetic calorimeter, is usually measured by using the center of gravity method. The position resolution of a calorimeter thus depends on its structure, especially the lateral cell size. For a calorimeter organized in pointing towers, the position resolution as a function of energy can be parametrized as:

$$\delta x(mm) = \frac{3}{\sqrt{E}} e^{0.4D} \tag{1}$$

where E is the energy of the particle being measured in GeV, and D is the cell size in radiation lengths. The position resolution of the BaF_2 calorimeter, calculated according to Eq. 1 for a 20 GeV electron or photon, is 1.2 mm, which is comparable with what has been measured with L3 BGO calorimeter [25]. This position resolution will not compromise the discovery potential of the BaF_2 calorimeter [27].

F.2 Energy Resolution

The energy resolution of an electromagnetic calorimeter can be parametrized as:

$$(\frac{\delta E}{E})^2 = (\frac{\mathbf{a_0}}{E})^2 + (\frac{\mathbf{a_1}}{\sqrt{E}})^2 + \mathbf{b}^2 \tag{2}$$

The contributions of each term to the resolution are:

- $\mathbf{a_0}$ is the contribution from electrical noise, summed over a few Moliere radii around the maximum of the lateral shower distribution;
- $\mathbf{a_1}$ is the contribution from the photoelectron statistics;
- the systematic term $\mathbf{b}$ has three contributions:

$$\mathbf{b}^2 = \mathbf{b_n}^2 + \mathbf{b_G}^2 + \mathbf{b_C}^2 \tag{3}$$

- b_n represents physics noise, including fluctuations of the shower and uniformity of light response etc.;
- b_G represents the geometry effect, including shower leakage at the front, side and back of the detector and inactive material between cells;
- b_C represents intercalibration error.

At low energy, the dominant contribution to the energy resolution is the noise term (a_0), which decreases quickly with increasing energy. The sampling term (a_1) dominates in the range of medium to high energies until a high energy limit is reached, where the systematic term (b) dominant.

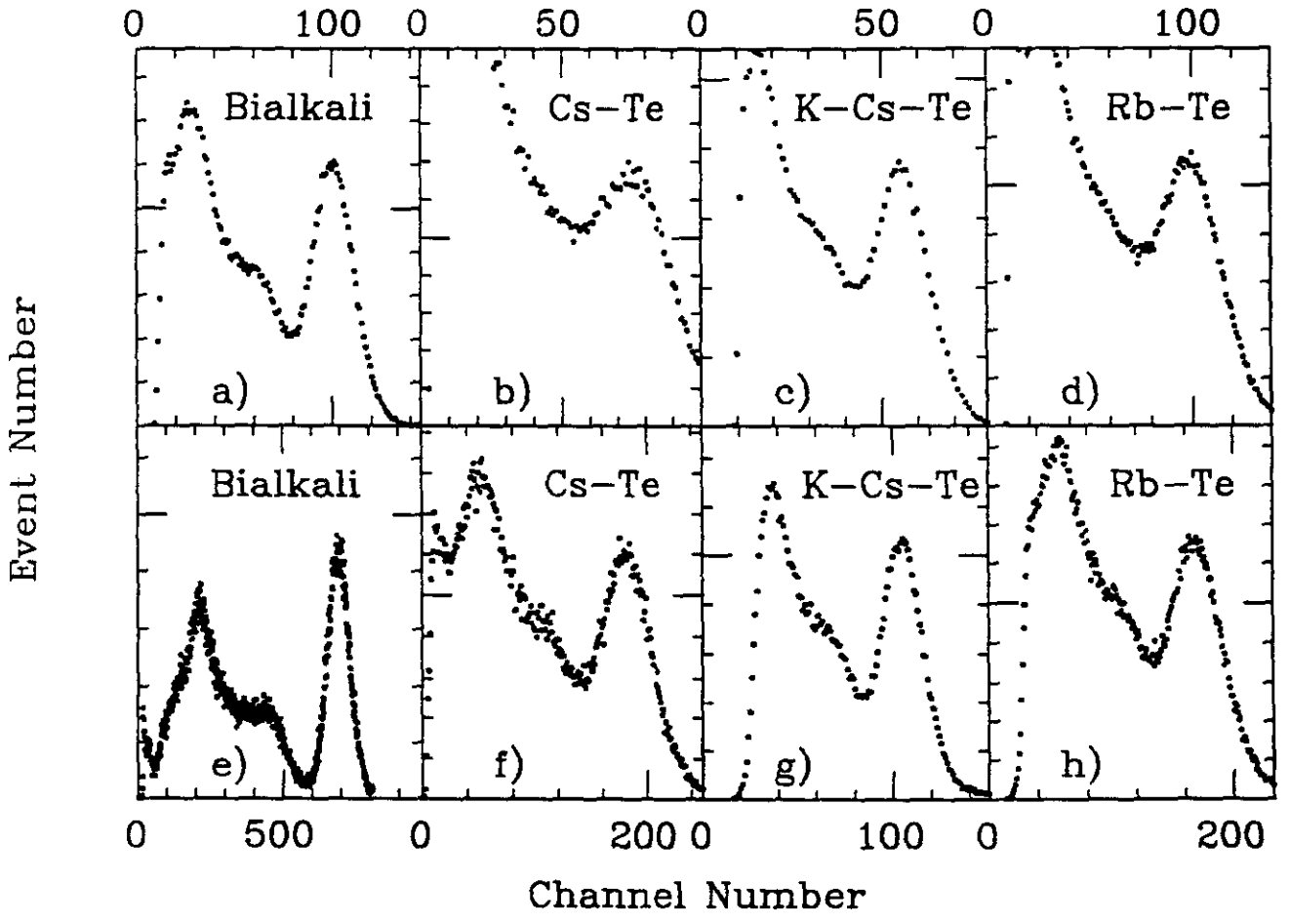

Figure 17: ^{137}Cs spectra measured with 4 PMTs with different photocathodes for two different gate widths: 55 ns (a–d) and 2 μs (e–h).

F.2.1 Light Yield: a_1

It is not very difficult to build a homogeneous electromagnetic calorimeter with a small a_1 term. A photoelectron (p.e.) yield better than 10 p.e./MeV would be enough to provide an a_1=1%. Figure 17 shows the measured ^{137}Cs spectra obtained from the same BaF_2 sample by using four PMTs with different photocathodes (bialkali, Cs-Te, K-Cs-Te and Rb-Te) for two different gate widths (55 ns and 2 μs). By comparing the spectra, it is clear that the K-Cs-Te cathode has good quantum efficiency (better than Cs-Te and Rb-Te) in detecting the fast components from BaF_2. A detailed analysis showed that more than 50 p.e./MeV has been obtained from typical 25 cm long BaF_2 crystals by using the K-Cs-Te photocathodes. This light yield would contribute an a_1 term of about 0.45% or better.

F.2.2 Electrical Noise: a_0

Because of its small capacitance (10 pf) and small dark current (0.1 nA), it is not difficult for the R4406 vacuum phototriode and the front electronics described in previous section to provide an electrical noise level of 2000 electrons per channel [28]. In reality, one needs to sum over a few Moliere radii to reconstruct an electromagnetic shower. In the case of using 3 × 3 crystals, which contains more than 95% of shower energy according to GEANT simulations [29], the intrinsic electrical noise is 6000 electrons without channel-to-channel correlations. Assuming the minimum gain of the R4406 phototube is 6, i.e. 50% of its nominal gain of 12 in the worst magnetic field situation[30], the signal corresponds to 300,000 electrons/GeV with a K-Cs-Te photocathode. This means an a_0 term of 2% for 3 × 3 crystal readout. The electrical noice introduced by channel-to-channel correlations, however, must be reduced by carefully implementing the electrical isolation between the readout channels.

F.2.3 Physics Noise: b_n

As discussed in Section D, good light collection uniformity longitudinally along the crystal axis (within several percent) is important to maintain the high resolution, and the linearity over a wide energy range, for a precision crystal calorimeter.

F.2.4 Geometry Effect: b_G

To reduce the systematic effects caused by shower leakage and inactive material, a precision electromagnetic calorimeter must be designed to contain nearly the complete electromagnetic shower, over the whole energy range. A GEANT simulation shows that an electromagnetic calorimeter designed for the SSC/LHC must have more than 24 radiation lengths. It must have minimum dead material in the front, between cells and, especially inside the calorimeter[16].

A proper lateral cell dimension is very important. The choice of the lateral cell dimension is usually a compromise between good position resolution, shower containment in a 'tower' consisting of a moderate number of lateral cells, and the total number of readout channels (which is reflected in the cost). Good position resolution as well as a good knowledge of the transverse shower shape (important for e/π resolution) favor a small cell size, while shower containment in a few cells favors a larger size. A cell dimension in the neighborhood of approximately one Moliere radius — or more — is usually taken, corresponding to $\approx 75\%$ of shower energy deposited in the center cell[17].

The need to reduce the pile-up noise within the 'tower' used to reconstruct an electromagnetic shower is also important, and is a dominant factor at the LHC.

All of these factors taken together have led to a technical consensus that the optimum lateral segmentation is $\approx 0.04 \times 0.04$ ($\Delta\eta \times \Delta\phi$) at the SSC (as in the BaF_2 design), or 0.02×0.02 at the LHC [31][18].

F.2.5 Summary of the Energy Resolution

To predict the overall performance of BaF_2 calorimeter, a GEANT simulation with the exact design was carried out. The simulation was calculated for an array composed of 121 (11×11) BaF_2 crystals with the proposed size: 3×3 cm^2 at the

[16]The carbon fiber structure described in an earlier section meets these criteria.

[17]The front face of a BaF_2 crystal in our calorimeter has a typical tranverse dimension of 0.9 Moliere radii.

[18]The lateral segmentation, combined with considerations of the Moliere radius, the requirements of other subdectors in the experiment, and the need to reduce the cost, also put limits on the inner radius of the calorimeter.

front, 5×5 cm^2 at the back and 50 cm long. Effects included in the simulation are:

- the carbon fiber wall between crystals;
- shower leakage because of summing a limited number (3×3) of crystals; and
- 0.30 radiation lengths of dead material, representing the beam pipe, tracker, and carbon fiber mechanical support, at the front of the BaF_2 array.

The result of this simulation is listed in Table 5.

Table 5: Energy Resolution (%)

E (GeV)	5	10	100	500
Electrical Noise	0.4	0.2	0.02	0.004
Photoelectrons	0.2	0.14	0.045	0.02
GEANT	0.67	0.56	0.42	0.36
Intercalibration	0.40	0.40	0.40	0.40
Total	0.90	0.73	0.58	0.54

Table 5 summarizes the BaF_2 resolution, including the contributions from electrical noise, photoelectron statistics, intrinsic resolution from GEANT simulation and the intercalibration. A precision of intercalibration of 0.4% is assumed, which is discussed in the next section. The result of the energy resolution is shown in Fig. 18b. It can be parametrized as $2\%/\sqrt{E} \oplus 0.5\%$, which is also shown in Fig. 18b as a solid line.

As a comparison, Fig. 18a shows the energy resolution measured with 4000 BGO crystals in a CERN test beam [25]. In the energy range beyond 20 GeV, the dominant contribution to the energy resolution is the systematic intercalibration term. The resolution of the L3 BGO calorimeter can also be parametrized as $2\%/\sqrt{E} \oplus 0.5\%$, which is also shown in the Fig. 18a as a solid line.

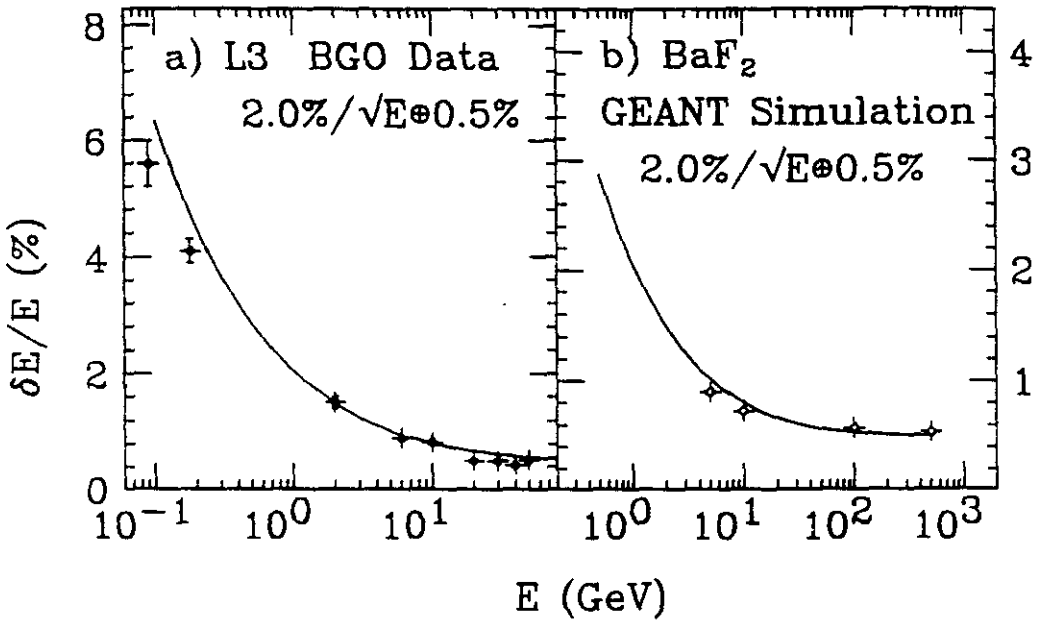

Figure 18: Energy Resolution of L3 BGO calorimeter (a), measured at CERN test beams with 4000 crystals, and BaF_2 calorimeter (b), calculated with GEANT simulation. The solid curves represent a simple parametrization of $2\%/\sqrt{E} \oplus 0.5\%$.

G R&D Budget

In this section we specify the funding requests for the continuation of the R&D program beyond October 1991. This includes all of the DoE-supported research tasks which are now underway, and the ongoing test beam program. Note that the proposed FY 1993 funds do not include the costs of mounting hadron calorimeter modules (developed in a separate R&D effort) in a test beam together with the BaF_2 crystal prototype matrix.

Table 6: Budget of BaF_2 R&D Program (k$).

Item	FY92	FY93
BaF_2 Crystal Array Components:	**407**	**429**
BaF_2 Crystals ($3.5/cm^3)	122	188
Hammamatsu Photodevices	49	38
Analog Readout Circuits for Matrix	86	68
Rad Hard Proto. Circuits	25	25
Digital Readout Channels	55	30
Support Structures and Mounting	70	80
Materials and Services:	**249**	**156**
Electronics Test Supplies	32	24
Crystal Materials Analysis	26	18
UV Reflector; Optical Coupling	25	10
Temperature Control and Monitoring	16	4
BaF_2 Radiation Damage Tests and Runs	55	25
BaF_2 Test Beam Setup and Runs	95	75
Equipment:	**72**	**43**
High and Low Voltage Power Supplies	20	16
Dimensional Measurement System	25	15
UV Monitoring System	27	12
Personnel:	**414**	**246**
Engineers ($ 150 k Per FTE)	270	150
Technical Staff ($ 80 k Per FTE)	144	96
Travel	**30**	**30**
ANNUAL TOTALS	**1172**	**904**

H Progress Report on BaF_2 R&D at BNL

C.L.Woody, J.A.Kierstead, P.W.Levy
Physics Department
Brookhaven National Laboratory
August 23, 1991

The present R&D effort at BNL on the BaF_2 Subsystem Proposal has concentrated on the study of radiation damage in BaF_2 crystals, with related studies on light output, uniformity and optical couplings. We have also been involved in the early stages of the design of the front end readout electronics and investigations of new photocathde materials. Our main purpose at the present time is to study radiation induced effects, such as changes in the uv transmission and scintillation light output, in material which is currently available from different manufacturers, including SIC and Merck. It is hoped that a better understanding of these effects will lead to improved radiation hardness in the crystals which will used at the SSC.

The radiation studies have been carried out using two facilities at BNL. One, the Physics Department's Gamma Ray Radiation Facility [1], consists of a multipurpose uv spectrophotometer used in conjunction with a high intensity ($\sim$ 20KCi) ^{60}Co source. This system can be used to carry out optical measurements on crystals before, *during* and after irradiation, as well as being used simply as an irradiation source for non-optical samples such as electronic components. Another facility, HIRDL [2], consists of a collection of ^{60}Co sources totaling $\sim$ 90KCi arranged in a pool of water containing long exposure tubes which provide uniform doses for samples up to 30 cm in length. We have up until now only used the Gamma Ray Facility to irradiate small samples and measure the optical transmission before and immediately after irradiation. Due to the strong scintillation emission of BaF_2, it is not presently possible to make transmission measurements during irradiation, but a planned upgrade of the system will soon allow this. However, transmission measurements can be made within a few minutes after interrupting the exposure, as is shown in in Fig.1., and permits the study of any short lived absorption effects in the crystals.

We have recently used the HIRDL facility to irradiate several small samples at a time in preparation for radiation studies on larger crystals. The uv transmission and

scintillation light output was measured before irradiation and subsequently after doses of 10^3, 10^4, $6x10^4$, $2.6x10^5$, $9.0x10^5$ and $4.6x10^6$ rad. For this study, the uv transmission was measured within a few hours after irradiation on another uv spectrophotometer (Hitachi 3210) and the light output was measured with a Hamamatsu H3197 phototube having a Cs-Te solar blind photocathode. The samples were handled with a minimal exposure to external light to mimimize any optically induced recovery in the material. Figure 2 shows the transmission spectrum for various doses for one of the samples. We observed a relatively small change, typically a few percent or less, in light transmission in the region of the fast component, along with the production of several absorption bands at longer wavelengths. This behavior was typical of all the samples measured. The light output, however, showed a somewhat larger change, as shown in Figure 3, decreasing by roughly 30% after a dose of 10^4 rad and then leveling off. This leveling off, or saturation behavior, can also be seen in the transmission spectra, and has been reported previously for other samples [3]. It is indicative of the type of damage caused by impurities or defects in the crystal, implying that radiation hardness can be increased by improving the purity of the raw material and better control of the growth conditions. Moreover, we observed that the radiation induced damage, both in the uv transmission and light output, could be mostly recovered by a short ($\sim$ 15 minute) exposure to a mercury lamp. This again indicates implies that the damage is impurity or defect related rather than intrinsic to the crystal.

A measurement of the scintillation light output was also carried out at the Gamma Ray Facility in which the actual scintillation emission spectrum was measured *during* irradiation. In this case, shown in Fig. 4, the sample showed essentially no change in the scintillation emission intensity up to a dose of 1 Mrad. These results show that in this sample, the intrinsic scintillation efficiency of the crystal is not altered by the radiation. We are now in the process of making a more detailed study to correlate the effects of changes in scintillation intensity, light output as measured with the photomultiplier and uv transmission in various samples.

We also observed a strong phosphorescense in virtually all of the samples we tested, although this effect has not been observed in some of the samples grown at SIC [4]. The emission spectrum of the phosphorescense, measured at the Gamma Ray Facility, is shown in Fig. 5. The peak occurs at a wavelength of around 330 nm, roughly in the region of

the slow component. This is fortuitous, since it is therefore undetected by the solar blind photocathode which is to be used in the final readout. The intensity of the phosphorescense is, however, quite strong, and indicates a large amount of activity in the crystal. The time dependence of the emission can be characterized by at least one component with a very short decay time, decaying away significantly within 10-20 seconds after irradiation, with additional components which persist for weeks or even months. The phosphorscense can also be optically reactivated by exposure to roomlight, giving rise to an increase in the total observed activity, until such a point where the exposure to external light has caused significant recovery and the phosphorescense essentually disappears.

We plan now to continue our studies of radiation effects in larger variety of samples, concentrating on larger crystals of the type that will be used in the actual detector, and on material with improved radiation hardness being developed at SIC and Merck. Our studies will rely heavily on the two radiation facilities here at BNL, both in their present form and with planned future improvements. We intend to request support for this effort from the SSC lab as part of the R&D request for the development of the BaF_2 electromagnetic calorimeter for the GEM detector.

References

1. *Facilities for Studying Radiation Damage in Nonmetals During Irradiation, P.W.Levy, Society for the Advancement of Material and Process Engineering Journal, 21 (1985) 35.*
2. *The High Intensity Radiation Development Laboratory at BNL.*
3. *R.Y.Zhu, Contribution to Symposium on Detector Research and Development at the SSC, Oct. 15-18, 1990, Ft.Worth, Texas, pp.340-348.*
4. *Z.Y.Wei et.al., A Study on Radiation Damge of Barium Fluoride Crystals, Cal Tech Internal Report (unpubished).*

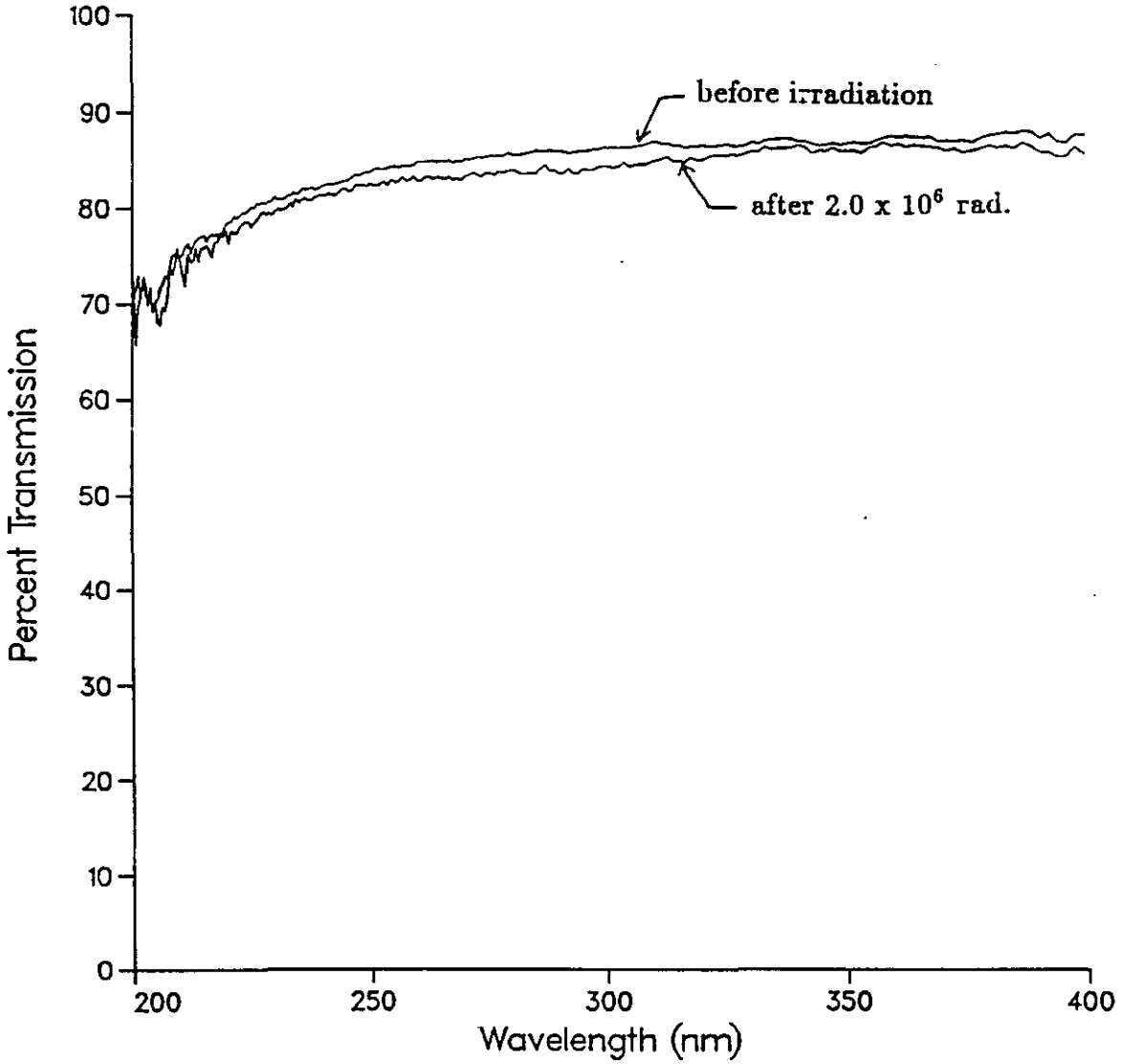

Fig.1 Transmission spectrum for a 1"diameter x 1"long BaF_2 crystal measured before irradiation and several minutes after a dose of 2.0 x 10^6 rad.

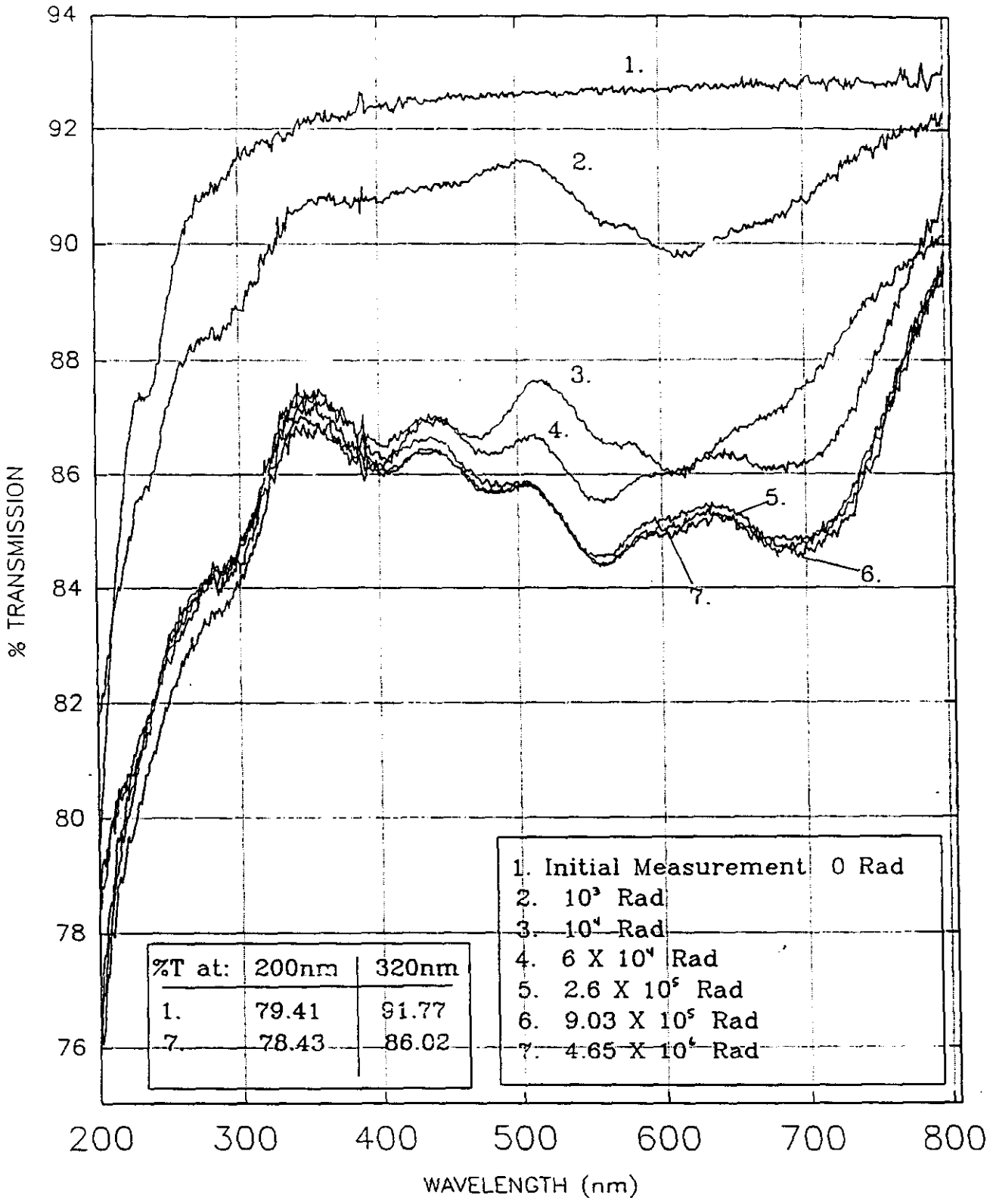

Fig.2 Transmission spectra as a function of dose for a 1" diameter x 1" long BaF_2 crystal measured within approximately 1 hour after irradiation.

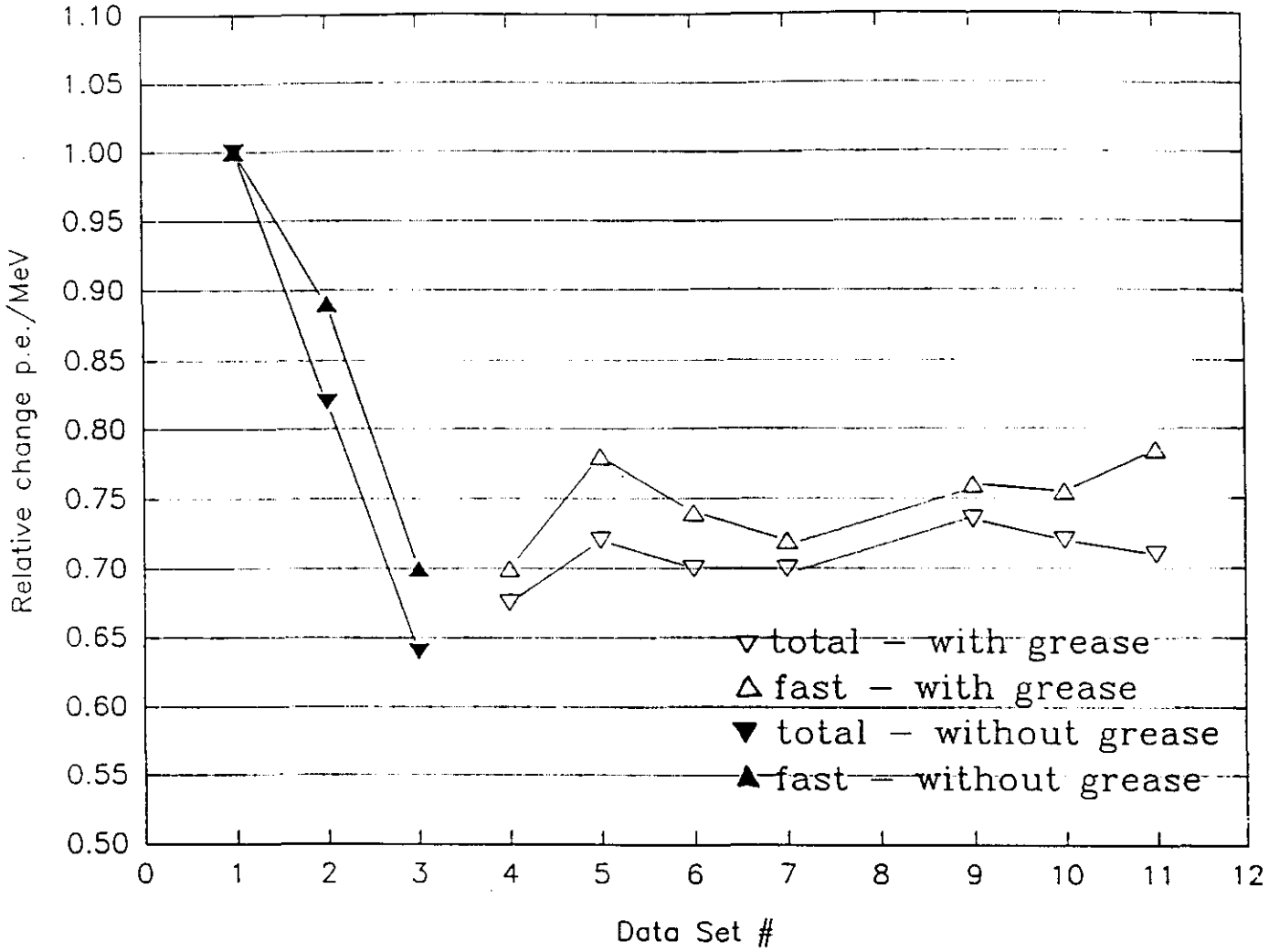

1. 7/2 Initial Measurements 0 Rad.
2. 7/8 10^3 Rad.
3. 7/8 10^4 Rad.
4. 7/9 6 x 10^4 Rad.
5. 7/9 2.65 x 10^5 Rad
6. 7/10. 9.03 x 10^5 Rad
7. 7/15 4.65 x 10^6 Rad.
8. 7/15 4.65 x 10^6 Rad.
9. 7/16 no additional radiation exposure
10. 7/17
11. 7/22

Fig.3 Relative light output vs. dose for a 1"diameter x 1" long BaF_2 crystal.

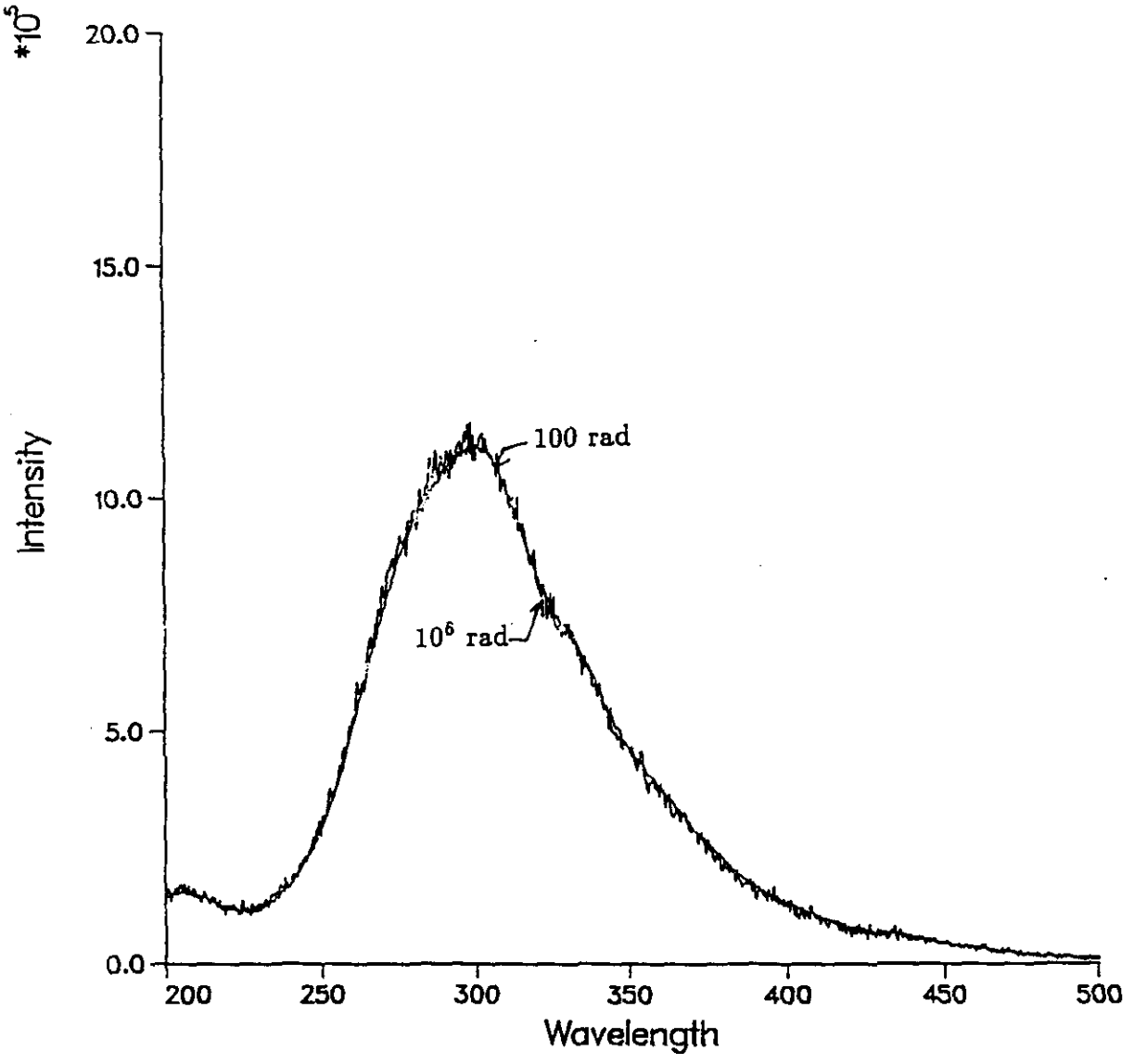

Fig.4 Scintillation emission spectrum for a 1"diameter x 1" long BaF_2 crystal measured *during* irradiation (100 rad and 10^6 rad).

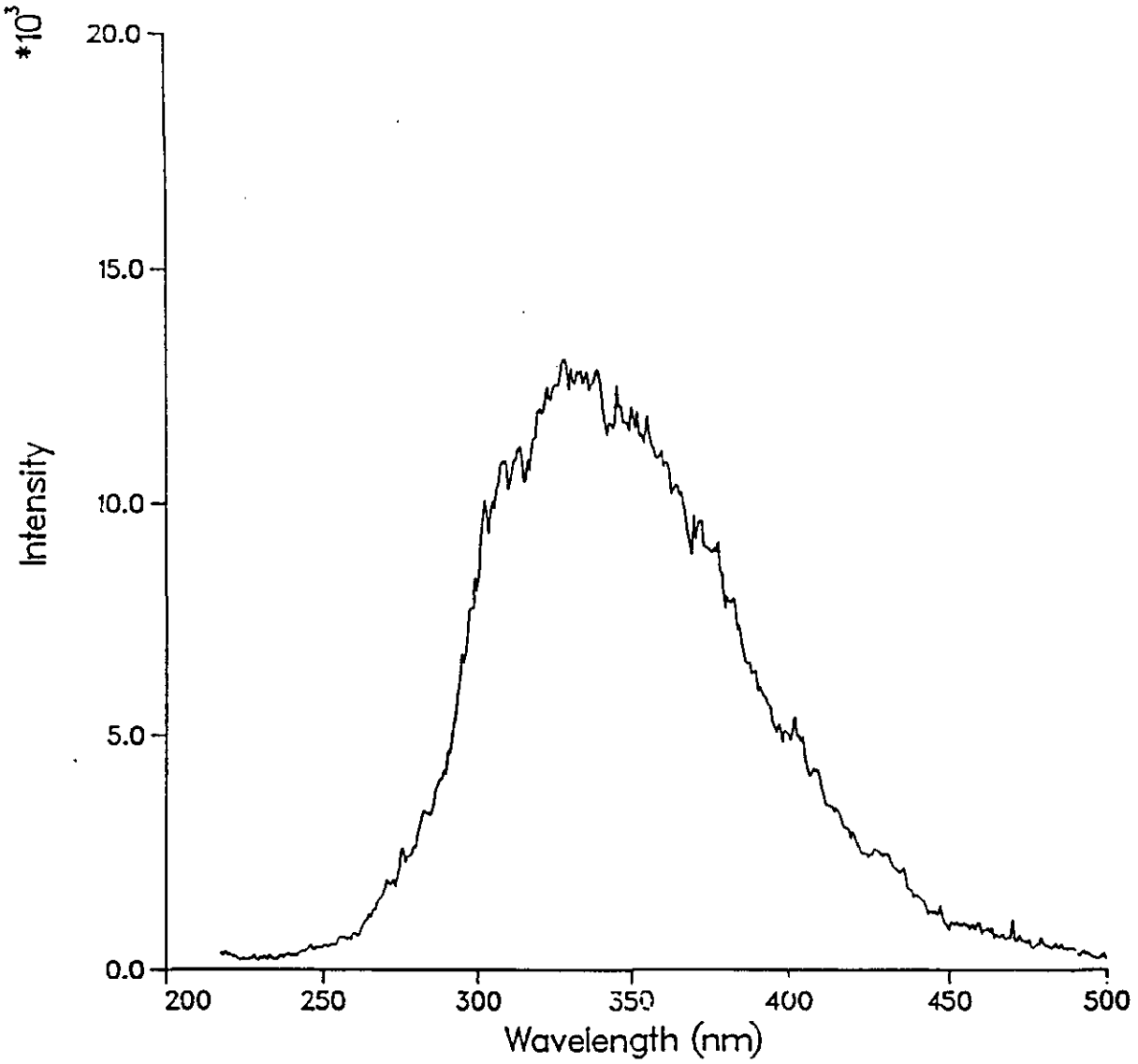

Fig.5 Phosphorescense emission spectrum for a 1"diameter x 1" long BaF_2 crystal measured after irradiation to 10^6 rad.

References

[1] S. Majewski and D. Anderson *et al.*, *Nucl. Instr. and Meth.* **A241** (1985) 76; A. J. Caffrey *et al.*, *IEEE Trans. Nucl. Sci.* **NS-33** (1986) 230; and S. Majewski *et al.*, *Nucl. Instr. and Meth.* **A260** (1987) 373.

[2] R. Zhu, talk given in *Second Detector Worksshop*, SSCL, June 12, 1991.

[3] D. Dicus and S. Willenbrock, Phys. Rev. **D37** (1988) 1801.

[4] ELMUD Study, S. Linn et al., Florida State Univeristy Supercomputer Computations Research Institute Report FSU-SCRI-91T-15, Feb 1991.

[5] R.Y. Zhu *et al.*, *Super Collider I*, Plenum Press, ed. McAshan, (1989) 587; H. Ma *et al.*, *Nucl. Instr. and Meth.* **A274** (1989) 113; and *Nucl. Instr. and Meth.* **A281** (1989) 469.

[6] R. Hamm *et al.*, *An SSC Electromagnetic Calorimeter Calibration Source*, Final SBIR Project Report to the Dept. of Energy, AccSys Technology Inc., Pleasanton, California, August, 1991.

[7] F. Ajzenberg-Selove, *Nucl. Phys.* **A475** (1987) 1; and H. B. Willard *et al.* *Phys. Rev.* **85** (1952) 849.

[8] R. Zhu and H. Newman, talks given at the September and December, 1985 L3 General Meetings on the RFQ status. L3 Notes No.380 and 397.

[9] M. Bauer *et al.*, *ORNL Status Report for BaF_2 Calorimeter*, BaF_2 Collaboration Internal Note, August, 1991.

[10] Caltech *et al.*, *A Precision BaF_2 Crystal Calorimeter for the Superconducting Supercollider*, Subsystem R&D Proposal to the SSC Laboratory, September, 1990.

[11] M. Kobayashi *et al. Transmittance and Radiation - Resistivity of Optical Glues*, KEK Preprint, 1991; Also see M. Kobabyashi *et al.*, KEK Preprint 90-130, October, 1990.

[12] S. Suzuki, in *Symposium on Detector Research and Development for the SSC*, Fort Worth, Texas, October 15–18 (1990).

[13] Hamamatsu Photonics K.K., *R4406 specification.*

[14] See for example, P. LeCoq *et al.*, in *ECFA LHC Workshop*, Aachen, October, 1990.

[15] P. Schotanus *et al.*, *Nucl. Instr. and Meth.* **A272** (1987) 917 and *Technical Univ. at Delft Preprint* **88-1**.

[16] Z. Wei *et al.*, **CALT-68-1659**, will be published in *Nucl. Instr. and Meth.*

[17] Z. Wei *et al.*, *Nucl. Instr. and Meth.* **A297** (1990) 163;
R.Y. Zhu *et al.*, *Nucl. Instr. and Meth.* **A302** (1991) 69;
T.Q. Zhou *et al.*, *Nucl. Instr. and Meth.* **A258** (1987) 464.

[18] C. Woody *et al.*, in *Symposium on Detector Research and Development for the SSC*, Fort Worth, Texas, October 15–18 (1990).

[19] S. Banerjee *et al.Radiation Study of* BaF_2 , Tata Institute of Fundamental Research Preprint TIFR/EHEP 91-11, August, 1991.

[20] C. L. Woody, J. A. Kierstead, and P. W. Levy, *Progress Report on* BaF_2 *R&D at BNL*, BaF_2 Collaboration Internal Note, August 24, 1991.

[21] P. Levy, *Facilities for Studying Radiation Damage in Nonmetals During Irradiation*, Society for the Advancement of Material and Process Engineering Journal, **21** (1985) 35.

[22] **HIRDL**, The High Intensity Radiation Development Laboratory at BNL.

[23] R.Y.Zhu, Contribution to Symposium on Detector Research and Development at the SSC, Oct. 15-18, 1990, Fort Worth, Texas, pp.340-348.

[24] Z. Y. Wei *et al.*, *A Study on Radiation Damage of Barium Fluoride Crystals*, Cal Tech Internal Report (unpubished).

[25] L3 Collaboration, *Nucl. Instr. and Meth.* **A289** (1990) 35.

[26] W. Doering *et al.*, Total Absorption Photon Spectrometer (TAPS) Collaboration Report No. 3, March, 1988.

[27] For a detailed discussion, see R.Y. Zhu, **CALT-68-1707**, in *International Conference on Calorimetry in High Energy Physics*, Fermi Lab, October 1990.

[28] The ATT preamplifier has 1200 electron noise for an input capacitance of 10 pf. See M. Levi, in *Symposium on Detector Research and Development for the SSC*, Fort Worth, Texas, October 15–18 (1990).

[29] R.Y. Zhu, **CALT-68-1693**, in *ECFA LHC Workshop* Volume III, Aachen (1990) 411.

[30] The nominal gain of R4406 is 4 in the Hammamatsu specification. The reason of its lower gain, compared to the gain of 12 of Hammamatsu's standard R2148 triode, is due to the processing technology used. At present, the K-Cs-Te cathode has been eveporated inside the closed triode envelope. This contaminates the dynode. The lower gain of R4406 is due to the lower efficiency of the secondary electron emission from the K-Cs-Te contamined dynode. By using a remote transfer technology in a large vacuum tank, this contamination will be eliminated. It is therefore expected (as indicated by Hammamatsu themselves) that R4406 triodes produced in future, under standard production conditions, will have a nominal gain of 12.

[31] C. Seez and J. Virdee, in *ECFA LHC Workshop*, Aachen, October, 1990.

HIGH RESOLUTION BARIUM FLUORIDE CRYSTAL CALORIMETER

RESPONSE TO CONCERNS AND QUESTIONS By GEM COLLABORATORS

H. Newman
On Behalf of the Members of
The BaF_2 Collaboration

PART II

September 1991

1 BaF_2 Versus A "High Z Sampling Calorimeter"

Question (11a) (Paar and Wigmans): How will e/π separation, e/Jet separation, and γ/Jet separation compare to a "High Z Sampling Calorimeter" (HZSC) ?

Answer:

1.1 Definition of a High Z Sampling Calorimeter (HZSC); Input Parameters

To answer this question, it is first necessary to precisely define the High Z Sampling Calorimeter. We keep the basic assumption that GEM remains a **precision lepton and photon detector**. We therefore assume that in order to reach the minimum quoted resolution of $7.5\%/\sqrt{E} \oplus 0.5\%$ the HZSC is a Pb/Scintillating Fiber calorimeter, whose EM section is composed of Pb plus $\approx 45\%$ of low Z materials (principally fibers).

We first review some physics examples related to electron and photon identification, as well as associated questions of the transverse shower spread in the L3 BGO and (by direct extension) in the GEM BaF_2 EM calorimeter. We then return to the comparison with the HZSC[1].

1.2 Level of e/Jet, e/Jet, and γ/Jet Separation Achieved with the BaF_2 Calorimeter

As discussed in the answer to Question (8) of Part 1 (p. 24ff) of our Response, we have been able to achieve a level of e/π, e/Jet, and γ/Jet separation at a level $\sim 10^{-4}$, for isolated electrons and photons. Since related concerns were raised by Worstell and Gordon, we attach our calculation of Electron-Hadron Separation in Response the PAC's L* Question 7 (July 1990) as Appendix 3.

[1]The level of detail of our response to the comparison proposed by Paar and Wigmans is limited mainly by a lack of our knowledge of any detailed studies of the shower spread in an HZSC. Such a study should include a complete conceptual design of an HZSC as a GEM Subsystem.

The studies summarized in this appendix, and follow up studies (by D. Kirkby and R. Zhu), showed that e/π separation at or below a level of 1×10^{-4} is most difficult. The strong cuts available from the BaF_2 , namely:

- A precision cut on the lateral shower shape,
- Energy-momentum matching with the inner tracker[2], and
- A veto on the energy with the hadron calorimeter

are illustrated in Figures 1-3 of Appendix 3. Once these cuts are made, the follow-up study showed that longitudinal sampling could improve the e/π separation by at best a factor of two, at the price of some additional loss of electron efficiency (from 95% to $\approx$ 90%). The conclusion of this study was thus that the precision measurement of the transverse shower shape, combined with the other cuts, had largely offset the potential advantages of longitudinal sampling.

Studies on γ/Jet separation, using the latest QCD and direct photon-production cross sections at SSC energies, are under continual review by R. Zhu *et al.*at Caltech, as presented at several GEM meetings. In particular, we are beginning to specifically use the detailed information of the transverse shower shape in the BaF_2 calorimeter to further suppress the QCD background. This analysis is based on the work of G. Gratta, D. Kirkby *et al.* using the L3 BGO calorimeter at CERN, to extract a clean sample of hadronic Z^0 decays containing hard isolated final-state photons – as a signal for quark bremsstrahlung, and to a search for excited quarks q^*[3]. Based on the L3 experiece, we also expect to be able to (at least partially) separate out single isolated pizeros from η's, η''s, and multiple pizeros.

Since the BGO crystal size, inner calorimeter radius and Moliere radius are all 2/3 of the corresponding parameters for the BaF_2 calorimeter, the transverse shower containment in $\Delta\eta$ and $\Delta\phi$ is essentially identical for the two calorimeters.

[2]It has been noted by Willis that electron bremsstrahlung in the material in front of the tracker could degrade this matching. Given that (a) the material in front is a fraction of a radiation length, (b) the bremsstrahlung spectrum peaks sharply at low photon energy, and (c) that the momentum resolution of the compact tracker is modest, the main function of the tracker is to reject low momentum overlapping charged particles. Bremsstrahlung is thus not expected to significantly affect our results. A study on this point is being completed at Caltech by R. Zhu.

[3]This analysis was in a preliminary state at the time of the L* response to the PAC's physics questions, in July 1990.

The comparison of BaF_2 and BGO properties is summarized[4] in Figure 1. Cuts developed for L3 can thus be applied with little or no modification. In this way we are confident of keeping the background level down to the 1 to 2 $\times 10^{-4}$ range.

Crystal	Density	Radiation length cm	Moliere radius cm	Decay time nsec	Peak emission nm
BGO	7.13	1.11	2.33	300	480
BaF2	4.89	2.06	3.39	0.6 620	210 310
CeF3	6.16	1.68	2.63	5 20	300 340
YAP:Ce	5.35	2.83	2.82	35	390
GSO:0.5%Ce	6.71	1.39	2.42	55	435
GSO:2.5%Ce	6.71	1.39	2.42	31	450
ThF4	6.32	1.18	2.71	≤ 25	315,330,450
BaLiF3	5.24	2.13	3.13	≤ 25	435
LiYbF4	6.09	1.56	2.70	≤ 25	≈ 450
PbF2	7.66	.94	2.24	-	-

Figure 1: Characteristics of Crystals for Calorimeters.

[4]The properties of BGO, BaF_2 and several other crystals under study by the Crystal Clear Collaboration at CERN, are shown here in a compilation provided by P. LeCoq.

1.3 Isolation Cuts, Shower Spread, and the Identification of Interesting Inclusive Photon and Lepton Signals

Question (11b) (Paar and Wigmans): Won't the identification of electrons (or photons) in or near a jet be much worse in a BaF_2 calorimeter than in an HZSC ?

Answer:

It is extremely important to keep in mind that most interesting "new" physics signals involve *isolated* photons and leptons. Potential signals which involve leptons or photons within jets tend to be overwhelmed by "irreducible" backgrounds - either from from light mesons if one is looking for a photon signal, or from charm (and bottom) quark decays if one is looking for leptons. As an example, consider the isolation cut for the L3 hard-photon analysis mentioned above. Here the photons were in the range of 10 - 45 GeV, and the typical isolation cut was 20°. This isolation cut was set by the intrinsic width of hadron jets, and has nothing to do with shower spread in the EM calorimeter, as illustated below.

We consider two examples from L3, where nearby particles could lead to background, and thus reduced sensitivity to an interesting physics signal:

- The L3 photon identification studies have shown that single γ's may be separated from π^0's with good efficiency up to the 30 GeV range. This indicates that one can cut on isolated photons, where the nearest additional photon is within a few milliradians.
- Consider the study of inclusive electrons in hadron events, as a means of extracting a clean signal from b-decays[5]. One can achieve a purity of 90% using a momentum cut of 3 GeV, a modest p_T cut of 1.5 GeV, and an isolation cut of just 10 milliradians on the nearest charge track in ϕ. The measured p and p_T spectra for electrons resulting from this analysis (and the corresponding spectra for muons) are shown in Figure 2 below. Note that the success of this analysis comes from the fact the showers in the BGO have a sufficiently limited shower spread, combined with the precise measurement of the transverse shower profile to identify the electrons cleanly.

[5]Note that this physics example, while interesting today at LEP, may be of second-rank importance for physics with GEM at the SSC several years from now.

As discussed above, the BaF_2 calorimeter will have very similar properties to the L3 BGO, in its ability to separate leptons and photons in angular space. Combined with precision vertex measurements in GEM, the BaF_2 calorimeter would thus give the GEM experiment the ability to tag b-quarks with high efficiency. In conclusion, we have presented a few physics examples, based on real and simulated data, and naturally including the effects of the supports and other dead material in our studies. We would like to request in turn that for fair comparisons, that groups claiming that sufficient resolution can be achieved with other technologies simulate – or extrapolate their test data to construct a simulation – of a subsystem in the GEM experiment, with a similar level of realism. We have been unable to perform the simulations now on behalf of the groups working on HZSC due to lack of time.

In addition, where there is no time for detailed simulations or extrapolations from real data, it is essential to get the input parameters correct when making simple arguments. This is treated in the answer to the next question.

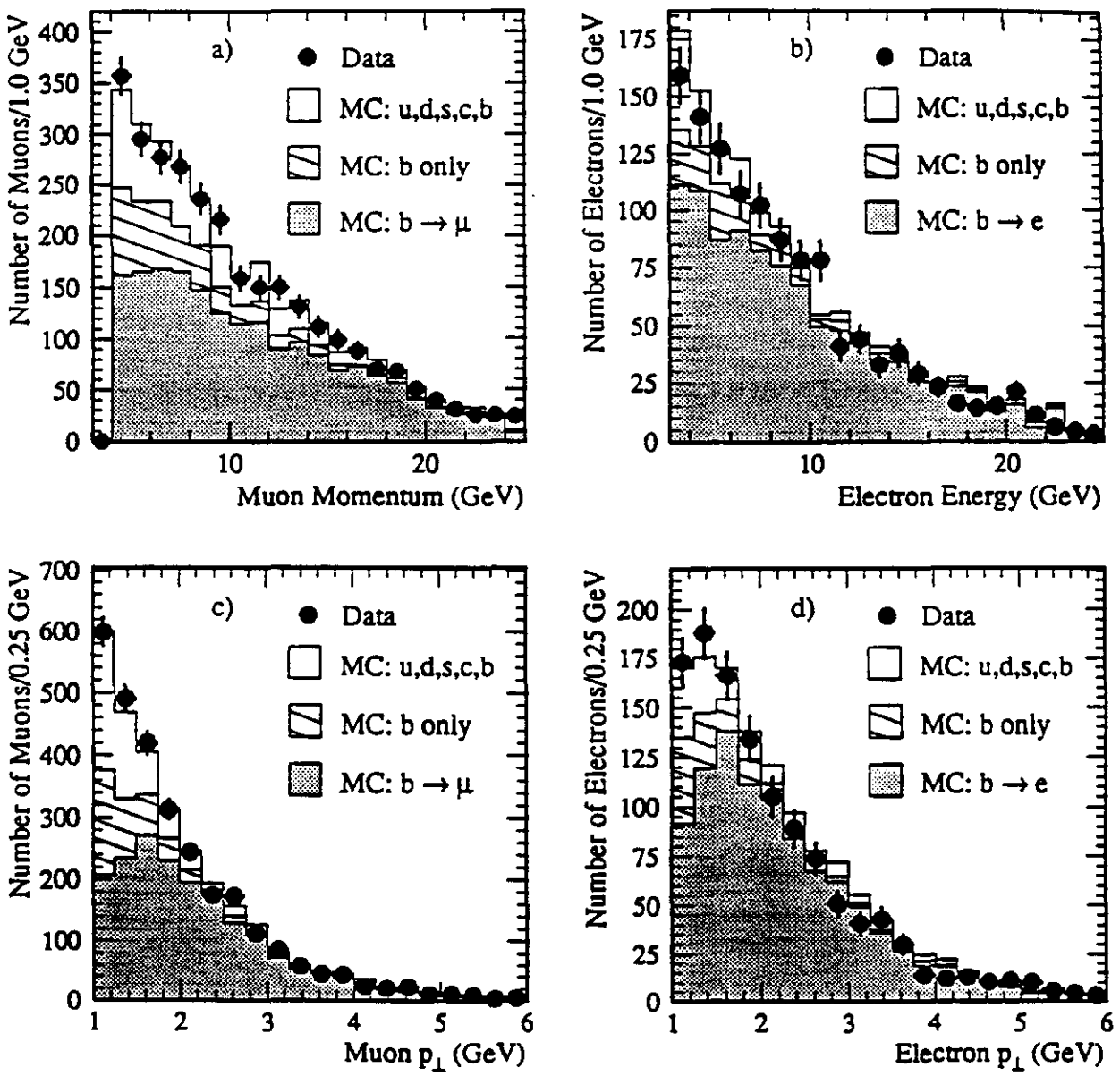

Figure 2: Measured lepton p and p_T spectra in semileptonic decays in L3 at LEP

1.4 Shower Spread and Occupancy in BaF_2 Versus an HZSC

Question (11c) (Paar and Wigmans): Won't the $\Delta\eta \times \Delta\phi$ area occupied by a hadron shower be about 4 times larger in a BaF_2 calorimeter than in an HZSC ? Won't the area occupied by an electromagnetic shower be 10 times larger ?

Answer:

No in both cases, as explained below.

The HZSC with sufficient resolution to do the physics required by GEM (as defined in the answer to Question 11(a)) has a Moliere radius of ≈ 2.2 cm[6]. This may be compared to 3.55 cm for BaF_2 calorimeter, including the effect of the carbon fiber support (see Figure 1, and p. 27 ff and Appendix B. of Part I of our Response.).

Apart from rough estimates based on the Moliere radius, the transverse electromagnetic shower spread in a BaF_2 calorimeter is very well understood (1) from GEANT studies, and (2) from a beam test with high energy electrons incident on an L3-sized BaF_2 crystal, which confirmed the GEANT results. Typically, 75% of a shower is contained in a cone with a half opening angle of one Moliere radius; 93.5% (97%) of the shower is contained in a subarray of 3×3 (5×5) BaF_2 crystals. As shown above from L3 experience and our simulations studies, this sort of transverse containment is sufficient to do the interesting physics.

The shower spread in angle in the HZSC thus will be no better than a factor of $\sim$ 1.6 in angle, compared to the BaF_2 calorimeter. The corresponding spread in area is ≈ 2.6 (although angular separation in each dimension is the relevant parameter in most analyses). Paar's and Wigmans' estimate that the electromagnetic shower spreads more in the BaF_2 , by a factor of 10 in area, is thus incorrect.

Similarly, Paar and Wigmans state that the spread of a hadron shower in the HZSC will be 4 times less (in area) than in the BaF_2 calorimeter. Based on the interaction length in BaF_2 (31.3 cm; with support) versus the HZSC ($\approx$ 26.6

[6]See p. 112 of the Particle Data Booklet, April 1990. Also note that this is not much different from BGO (2.33 cm).

cm), this leads to a difference in the spread of hadron showers in the EM section, expressed in terms of the area, of a factor of 1.40. In the more appropriate terms of angular spread, the difference is a factor of 1.18. Again, the quoted difference in spread for hadron showers (twice in angle; 4 times in area) is not correct.

1.5 Possible Radial Space Savings

Question (11d) (Paar and Wigmans): Wouldn't the use of an HZSC save more than 30 cm in the radius, compared to the BaF_2 Calorimeter ? Would we not then be able to substantially increase the tracker volume ?

Answer:

There might be some savings of radial space, but nowhere near as much as stated in the question. We consider the case of a separate EM section, as emphasized at the July meeting by Barry Barish:

- The HZSC will have a radiation length of 1.0 cm, or 24.5 cm for the active material versus 50 cm for BaF_2 .
- The readout will very likely be a vacuum phototriode (VPT) with a 4 cm diameter. The radial space for a triode with an incorporated wedge (near $\eta = 0$ only) is $\approx 8cm$. Without the wedge, over most of the η range, the tube will be 4 to 5 cm in length[7].
- Because the light yield per MeV for the HZSC is two orders of magnitude less per MeV than for the 50 cm BaF_2 crystal pairs, higher gain, larger diameter tubes will have to be used. The fibers will have to be brought out to these tubes. The tubes will have to be stacked up behind the EM section, turned at an angle close to parallel with the magnetic field.

Because of the above factors, we doubt that the net savings would exceed 10 cm in practice. A detailed design is needed to see if any space could be saved relative to the BaF_2 design, where radial space is given high priority in both designs.

It is not clear that GEM could utilize a larger tracking volume – independent of whether or not the use of an HZSC results in a net space savings. The principal factor here is cost. This part of the question thus cannot be answered by the Calorimetry Subgroup on its own.

[7]This may be further reduced if one of the options for a proximity focused tube phototriode is developed by Hammamatsu; see p.35ff of Part I of our Response.

2 Higgs Mass Reconstruction, Vertex Selection and Charge Multiplicity

Question (12) (Paar and Wigmans): The need for measuring gamma directions in a sophisticated pre-radiator will significantly increase the complexity and require extra space relative to a simpler pre-radiator that does not measure directions. The suggestion is to use the multiplicity of a Higgs event as a flag as to which vertex to use in the gamma-gamma effective mass calculation if there is more than one. How can this be done, since the multiplicity distribution of a Higgs event does not differ that much however from a background QCD event ?.

Answer:

As shown in Figures 3 and 4 the number of charged particles in a Higgs event, where the Higgs decays into two photons, and in a QCD event can be substantially different. This is particularly true if one makes a cut on the p_T of the charged particles counted in the event at about 0.5 GeV (see Figures 3b and 4b for example). A preliminary analysis of the distributions with different p_T and η cuts indicates that by making a maximum likelihood decision on the vertex choice, using the charge-multiplicity associated with each of several sets of kinematic cuts as input, we estimate that we will be able to maintain the efficiency for selecting the correct vertex at the level of 90% or above. Further study is required to determine the optimum efficiency.

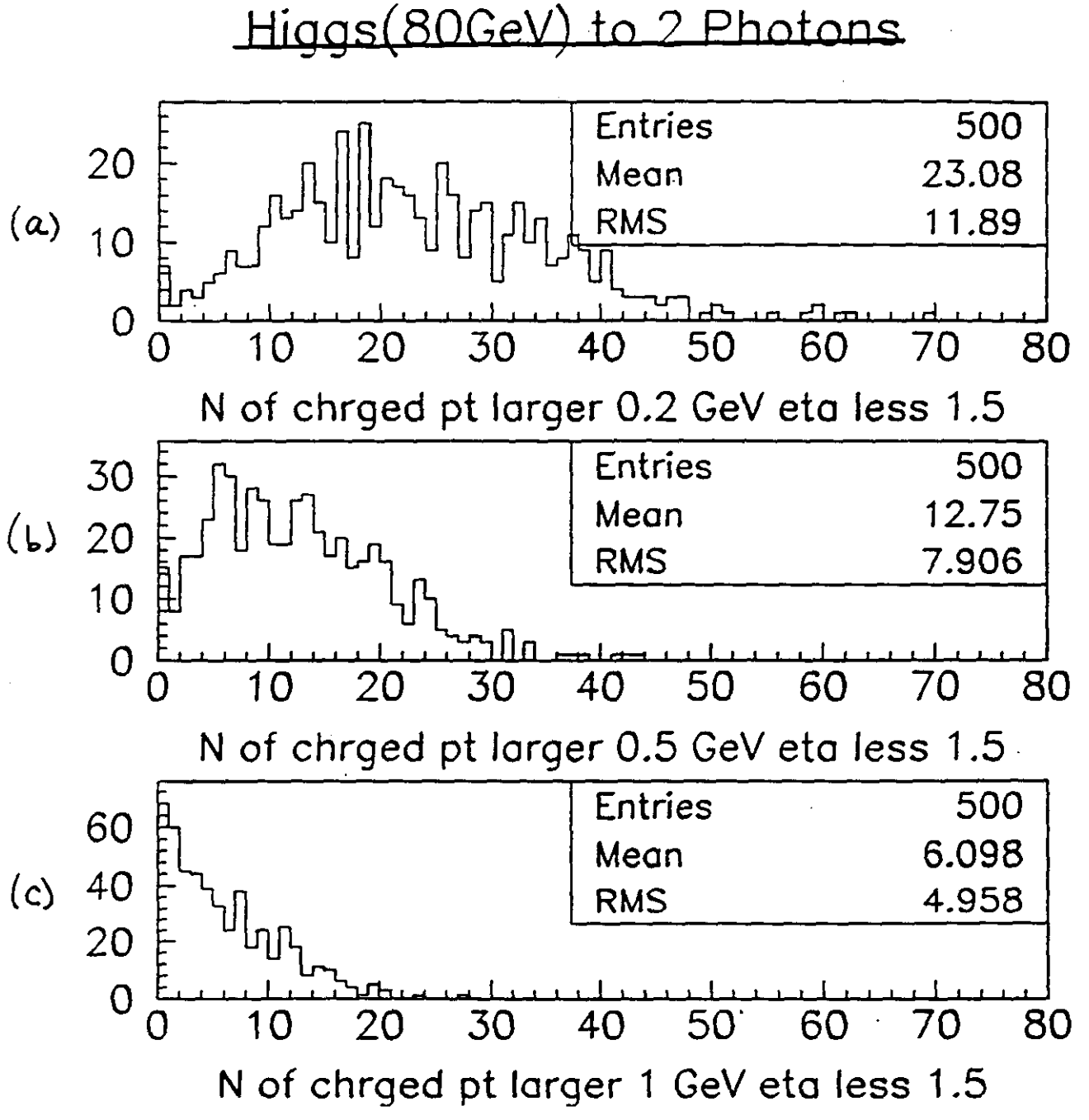

Figure 3: The charged multiplicity distribution for events containing a $H^0 \rightarrow \gamma\gamma$ decay, for a Higgs mass of 80 GeV, with different sets of cuts indicated in the figure.

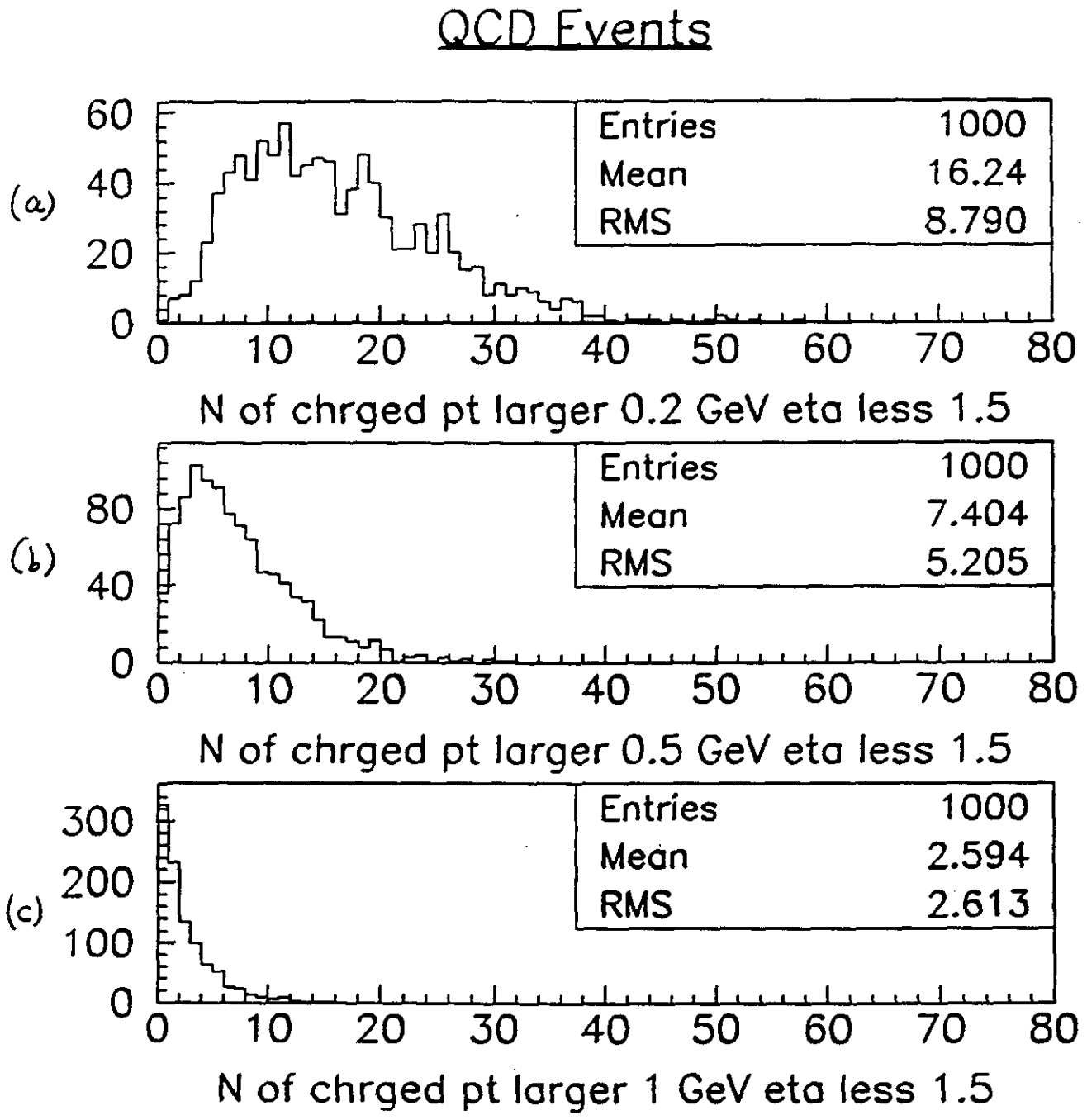

Figure 4: The charged multiplicity distribution for QCD events, with different sets of cuts indicated in the figure.

3 Hadronic Energy Resolution

Question (13a) (Paar and Wigmans): Because of the relatively poor efficiency for detecting the kinetic energy carried by neutrons in hadron showers in a homogeneous scintillation calorimeter, wont the ratio of electron to hadron response (e/h) for the BaF_2 calorimeter be very high ? Wigmans estimates that this ratio will be 2.0.

Answer:

The measured e/h ratio for BGO has been measured to be in the range 1.8 - 2. The ratio for NaI(Tl) is ≈ 1.4. Given the properties of BaF_2 relative to BGO and NaI, we estimate the ratio will be 1.6 to 1.7.

Question (13b) (Paar and Wigmans):

Won't this greatly reduce the sensitivity for supersymmetric particle searches because there will be a higher level of apparent E_T imbalance in events where there is none ?.

Answer:

The ability to search for supersymmetric particles by using a missing energy tag will depend on the energy resolution for hadron jets. Extensive resolution studies of hadron calorimeters with different designs, behind a BaF_2 electromagnetic calorimeter, were carried out by Harm Fesefeldt using his GHEISHA simulation code in the second quarter of 1990. The results are illustrated in Figures 5 and 6. From Figure 5 we see for example that the resolution for a BaF_2 EM calorimeter followed by a hadron calorimeter composed of 2 cm Pb plates interleaved with 0.5 cm scintillator layers has a calculated resolution of:

$$\sigma_E/E = (53 \pm 5)/\sqrt{E} + (1.6 \pm 0.5)\ \%$$

. Note that the constant terms in the cases studied are relatively small. According to the calculations, this is due to the fact that if the hadron calorimeter contains a sufficient fraction of hydrogenous material, then the neutrons escaping from the BaF_2 section are detected in the hadron calorimeter section behind it.

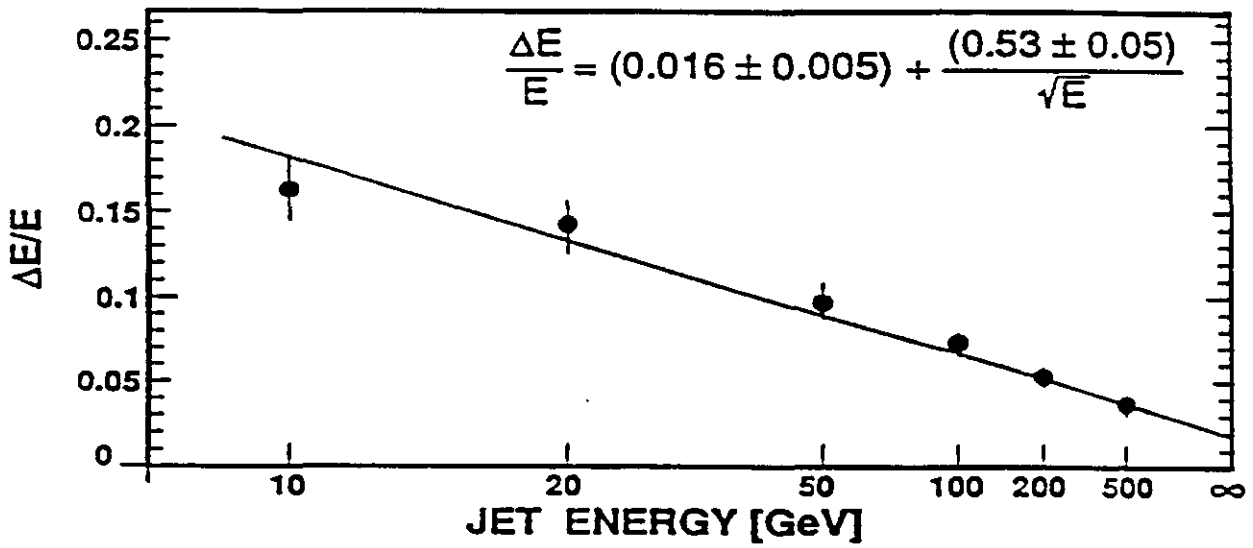

Jet energy resolution of BaF_2 (1.7λ) followed by 10.7λ of 2 cm Pb/0.5 cm scintillator.

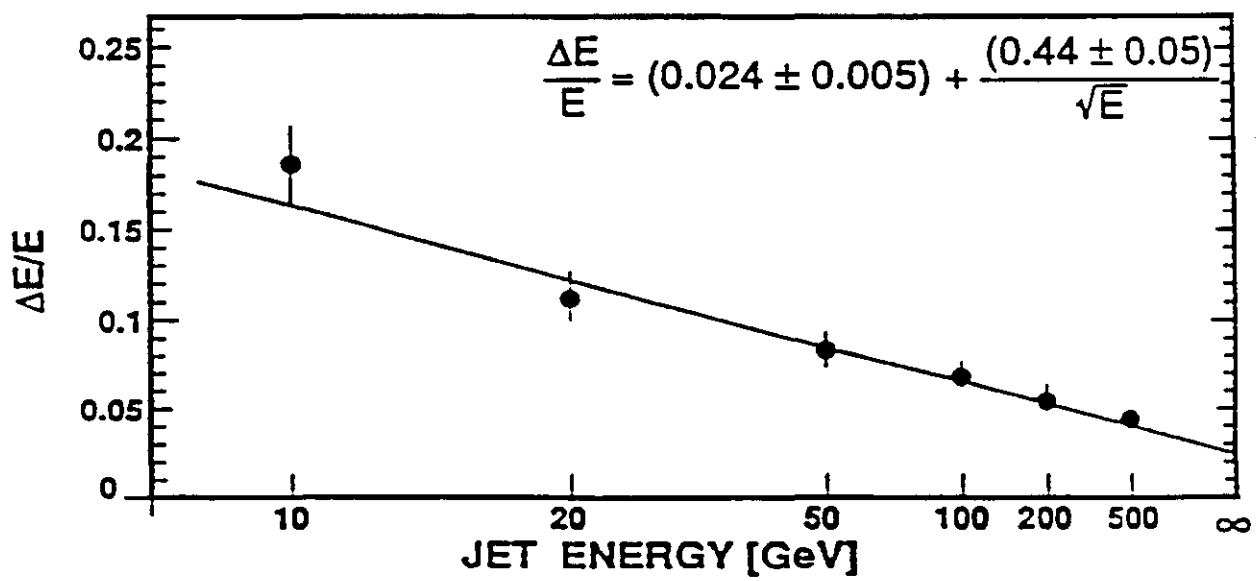

Jet energy resolution of BaF_2 (1.7λ) followed by 10.7λ of 1 cm Pb/0.5 cm scintillator.

Figure 5: Energy resolution, for jets of 10 to 500 GeV, incident on a BaF_2 EM calorimeter followed by a Pb/Scintillator hadron plate calorimeter (two example HCAL designs).

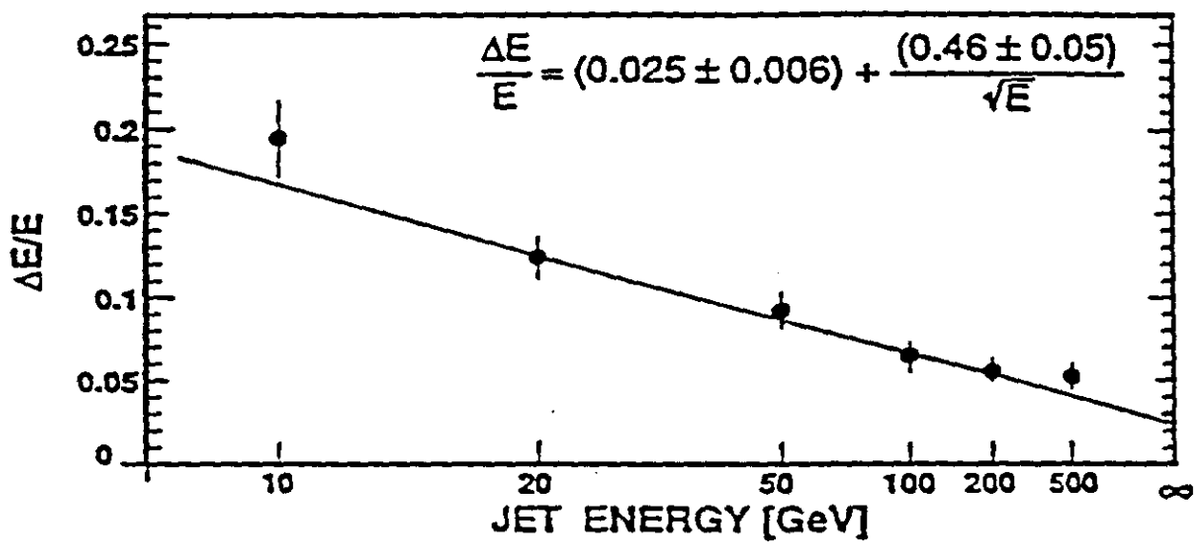

Jet energy resolution of BaF_2 (1.7λ) followed by 12λ of 0.5cm U/0.5 cm scintillator.

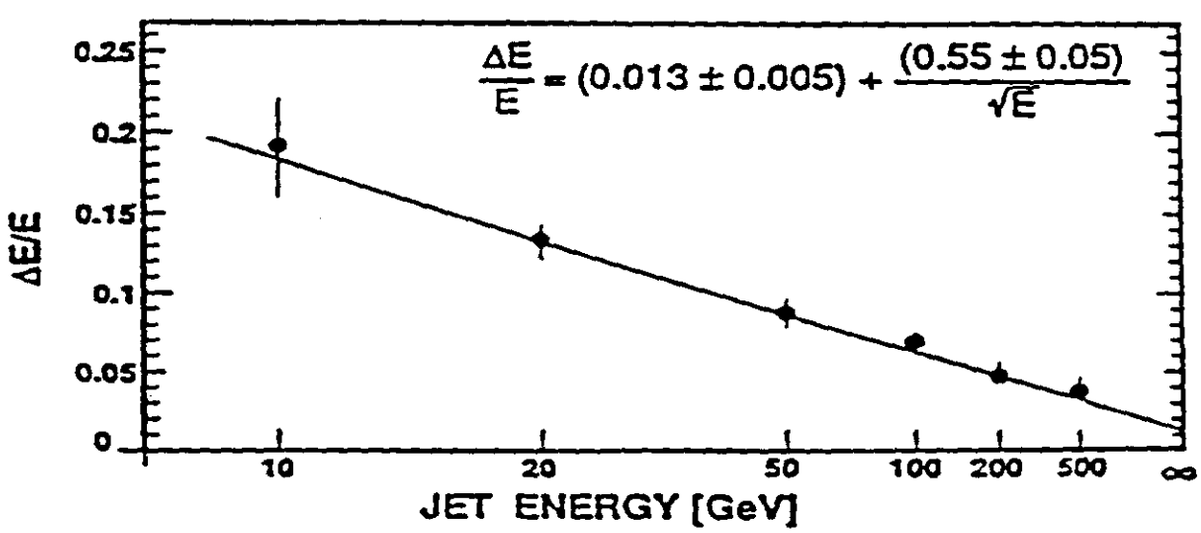

Jet energy resolution of BaF_2 (1.7λ) followed by 10.7λ of 0.4 cm U/0.5 cm scintillator with 1 mm Fe vessel walls.

Figure 6: Energy resolution, for jets of 10 to 500 GeV, incident on a BaF_2 EM calorimeter followed by a U/Scintillator hadron plate calorimeter (two example HCAL designs).

Studies by Y. Kamyshkov *et al.* for L* also have shown that the weight given to the EM section, and to the hadron section of the calorimeter could be adjusted in the energy reconstruction, such that it was possible to obtain a smaller constant term, in exchange for a somewhat larger statistical term, in the overall resolution. This could be useful in the search for supersymmetric in the very high energy range (several hundred GeV jets), where the constant term in the resolution is very important.

Independent of these studies, it is important to note that the L3 calorimeter has acheived a resolution of $55\%/\sqrt{E} + 5\ \%$, using real jets in Z^0 decays at LEP. In this case the hadron calorimeter has a gas chamber readout, and the BGO e/h ratio is worse than what we will have for BaF_2 . We thus expect a constant term of no worse than 4% and more likely $\approx 2\%$ for design combinations such as those shown in Figure 5.

As summarized on p. 67 of Part I of our Response, we intend to test the "effective compensation effect" described above, and the size of the constant term in the resolution, in a Spring, 1993 beam test using a BaF_2 EM prototype of 121 crystal-pairs (just large enough for sufficient transverse containment of hadron showers), combined with an appropriate HCAL section.

It is interesting to note that studies by Groom[1] have shown that a detector with a large tracker, such as SDC, will have additional systematic effects due to the bending away, and hence the loss of association of low momentum ($z < 0.01$) charged particles due to jets. The resulting constant term is exepcted to be $\sim 2\%$ in the resolution, from this source alone.

In summary, the existing calculations show that the missing energy resolution of a BaF_2 + "Hydrogenous" HCAL will not be substantially worse, and in many cases it will be better than alternative EM + HCAL designs. The discovery potential for SUSY particles will thus not be compromised, relative to most of the other designs being considered for GEM[8].

[8]We have assumed that a forward-backward hadron calorimeter with at least moderately good resolution will be included in the overall GEM design – at some stage – to make searches of this type possible.

APPENDIX

A On Electron-Hadron Separation in L* With a BaF_2 EM Calorimeter

Response to the PAC, July 1990

Submitted to the P.A.C. in Response to L* Question 7

7 Electron-Hadron Separation;

As emphasized in our "Expression of Interest" (EoI) to the SSCL, the L* experiment will explore new physics through high resolution measurements of electrons, muons and photons. In order to achieve this goal, we must separate out the interesting physics signals, such as Higgs decays, from backgrounds due to misidentified hadrons. In the part of this report on the Higgs Search (Generic Question 1) we have discussed L*'s ability to distinguish isolated photons from π^0's. By using an isolation cut, the probability of a jet faking an isolated photon, because of the fluctuations of jet fragmentation, is $\sim 10^{-4}$.

In general, many interesting physics processes, resulting from the decays of heavy particles, lead to distinctive signatures involving isolated leptons or photons. Conversely, the usefulness of searching for leptons within jets, or in the vicinity of jets is limited, because of the copious production of "background" leptons from charm and bottom decays. The use of isolation cuts is thus an important part of this analysis.

In this section we show L*'s π/e separation ability. We will first discuss L*'s ability to distinguish isolated electrons from single charged hadrons, and then discuss the probability of a hadron jet faking an isolated electron.

7.1 Isolated π/e Separation;

Since the L* electromagnetic calorimeter is finely segmented in η and ϕ, we can use the detailed transverse shower information, and the energy in the first layers

of the hadron calorimeter, to distinguish an electron from a charged pion. The ability to match the momentum measured in the central track detector with the energy measured in the electromagnetic calorimeter provides powerful rejection in addition.

The main mechanism of a charged pion faking an electron in the electromagnetic calorimeter is the charge exchange process, which produces an energetic π^0 from an incident charged pion. The charge exchange cross-section, however, decreases with increasing energy. In the energy region relevant to the SSC, i.e. > 5 GeV, rejection against pions at the level of $\sim 10^4$ can be obtained with the L* detector by the following method:

- Since the shower from a hadron which interacts in the electromagnetic calorimeter tends to spread more laterally than an electron shower (which is relatively narrow), we use a lateral shower development cut to reject hadrons:

  $$\frac{\sum_{3\times3} E_{EM}^{cell}}{\sum_{5\times5} E_{EM}^{cell}} > \mathrm{S_{cut}} \Rightarrow \textbf{ Reject}$$

  where the we sum over the 3×3 and 5×5 group of cells centered on each cell in the electromagnetic calorimeter (EM). S_{cut} is slightly energy dependent, and was determined using a GEANT simulation (see below): $S_{cut} = 0.95$, 0.96, 0.965 for $E_{EM} = 10$, 100, and 1000 GeV respectively.

  The tight cut applied here is only possible, as in the L3 detector, because of the high energy resolution of the electromagnetic calorimeter. In particular, the part of the energy away from the center of shower, in the surrounding 8 cells also is well measured. This results in a distribution of $\sum_{3\times3} E_{EM}^{cell} / \sum_{5\times5} E_{EM}^{cell}$ which is a narrow peak.

- Matching the energy measured in electromagnetic calorimeter (E_{EM}) and the momentum measured in central tracking detector (P_{trk}):

  $$|E_{EM} - P_{trk}| > 3\sigma \Rightarrow \ Reject$$

  where

  $$\sigma = \sqrt{\sigma^2_{E_{EM}} + \sigma^2_{P_{trk}}},$$

$$(\sigma_E/E)_{EM} = 1.3\%/\sqrt{E_{EM}} + 0.5\%, \text{ and}$$

$\sigma_{P_{trk}}$ is parametrized as a function of polar angle (θ):

$$\sigma_{P_{trk}}/P_{trk} = X\% \; sin\theta \; P_{trk} \; (in \; GeV)$$

with X = 0.13, 0.22, 0.29, and 0.65 for θ in the range $(26°, 154°)$, $(22°, 26°)$ or $(154°, 158°)$, $(17°, 22°)$ or $(158°, 163°)$, and $< 17°$ or $> 163°$ respectively.

- Since a hadron shower usually penetrates much deeper than an electron shower, we apply a veto on the energy in the hadron calorimeter (HCAL):

$$E_{HCAL} > E_{EM} \times \mathrm{H_{cut}} \Rightarrow \textbf{Reject}$$

where H_{cut} is slightly energy dependent, and was determined using a GEANT simulation: H_{cut} = 0.025, 0.025, 0.040 for E_{EM} = 10, 100, and 1000 GeV respectively.

A GEANT (full shower) simulation was carried out to obtain the π/e rejection ratio as a function of energy. The simulation was done by injecting electrons and pions uniformly at the front surface of the center crystal of a Barium Fluoride (BaF_2) matrix composed with 13 × 13 crystals with the proposed L* size. A layer of aluminum 0.12 radiation length thick in front of the BaF_2 array, and the 250 μm thick carbon fiber walls between crystals were included in the simulation. The energies deposited in each crystal, in the carbon fiber walls between crystals, in the aluminum sheet, and leaking out sideways were recorded. The full resolution of the electromagnetic calorimeter in measuring electromagnetic energy ($1.3\%/\sqrt{E} + 0.5\%$), the resolution of the hadron calorimeter by itself in measuring hadronic energy, and the momentum resolution of the tracker as a function of angle, were taken into account in the simulation.

The rejection power of each cut is illustrated in Figures 1, 2, and 3. Figure 1 shows that the rejection power of the cut on $\sum_{3\times3} E_{EM}^{cell}/\sum_{5\times5} E_{EM}^{cell}$ stems from the fact that this ratio is a narrow peak in a high resolution calorimeter, as explained above, coupled with the fact that many of the surviving pions do not interact in

the electromagnetic calorimeter. Figure 2 shows that after the cut on the lateral shower shape, no pions at 10 GeV, and few at 100 GeV, have enough energy deposited in the electromagnetic calorimeter to match the momentum measured in the tracker. Figure 3 shows that all of the remaining pions (down to the 10^{-4} level deposit a large part of their energy in the hadron calorimeter. The rejection power of the HCAL veto cut (Figure 3) increases with increasing energy.

The results of the simulation are summarized in Table 1[1]. As seen in the table, the L* detector will be able to separate isolated electrons and pions with a rejection ratio[2] of $\sim 10^{-4}$.

Table 1: π/e Separation of L* BaF_2 Calorimeter

E (GeV)	10	100	1000
After Lateral Shower Cut:			
π acceptance (10^{-2})	32.6 ± 0.4	34.7 ± 0.5	39.4 ± 0.7
e acceptance (%)	99.3	99.5	99.5
After E_{BaF_2} and P_{trk} match (10° - 90°):			
π acceptance (10^{-3})	< 0.1	12.3 ± 0.9	388 ± 7
e acceptance (%)	97.3	99.2	99.5
After HCAL Veto:			
π acceptance (10^{-4})	< 1	2.0 ± 1.4	< 2.2
e acceptance (%)	97.3	96.4	95.0

[1]The 10 GeV, 100 GeV and 1000 GeV runs consisted of 1000, 500, and 200 electrons and 13000, 10000, and 4560 pions respectively. The higher energy runs required vast amounts of computer time. For the 10 GeV case, no π^+'s or π^-'s (out of 13000) survived the matching cut. For the 1 TeV case, no π^+'s or π^-'s (out of 4560) survived the hadron calorimeter veto cut.

[2]The use of longitudinal sampling in the electromagnetic calorimeter, such as a BAF_2 preshower counter or three longitudinal cells in liquid Xenon, could result in pion rejection below the 10^{-4} level. Realistic shower simulations with large enough statistics, to determine this added suppression at high energies precisely, are beyond the capability of our largest computers within the time available.

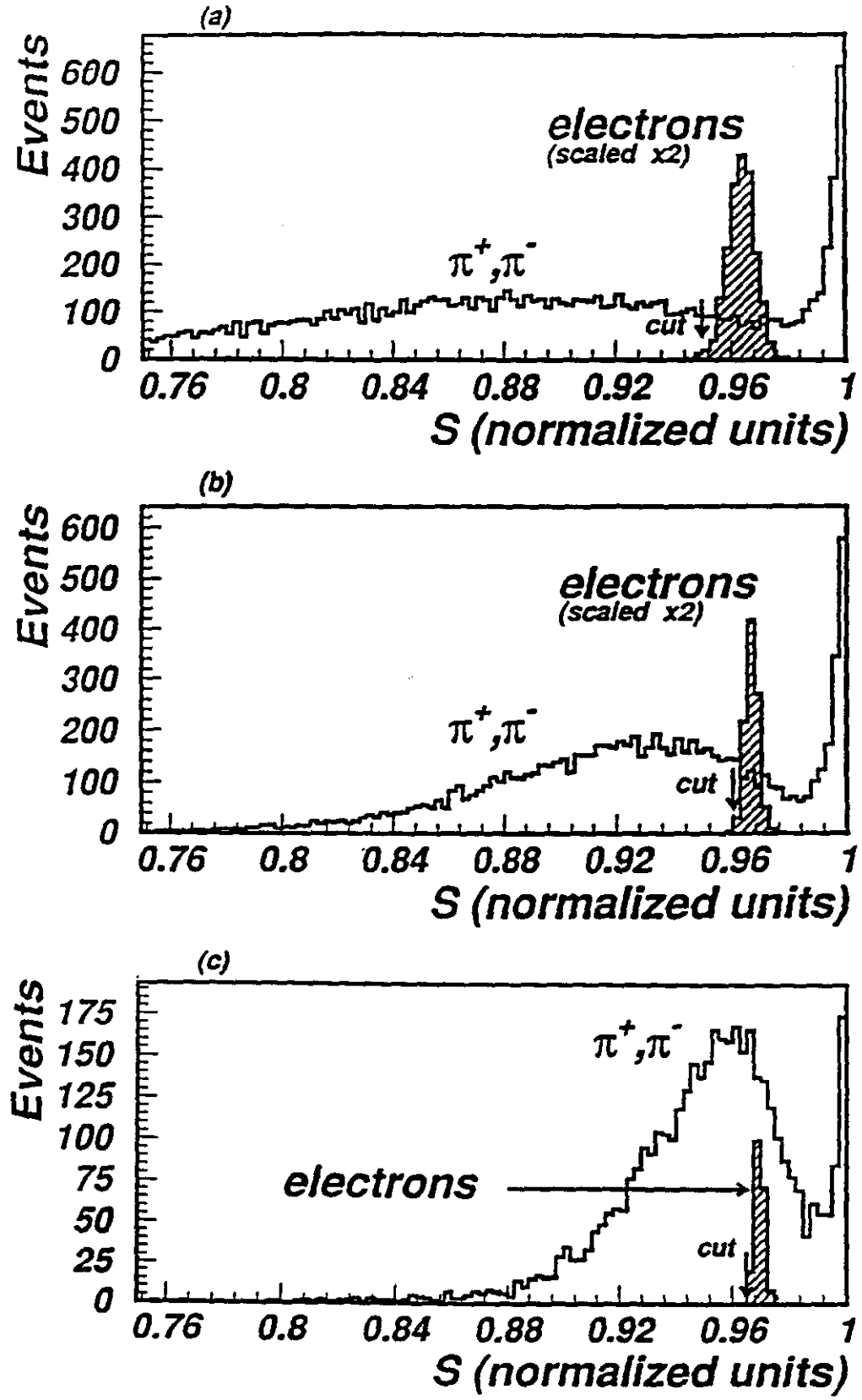

Figure 1: The transverse shower shape distribution in $S \equiv \sum_{3\times3} E_{EM}^{cell} / \sum_{5\times5} E_{EM}^{cell}$, for electrons and charged pions at (a) 10 GeV, (b) 100 GeV, and (c) 1 TeV.

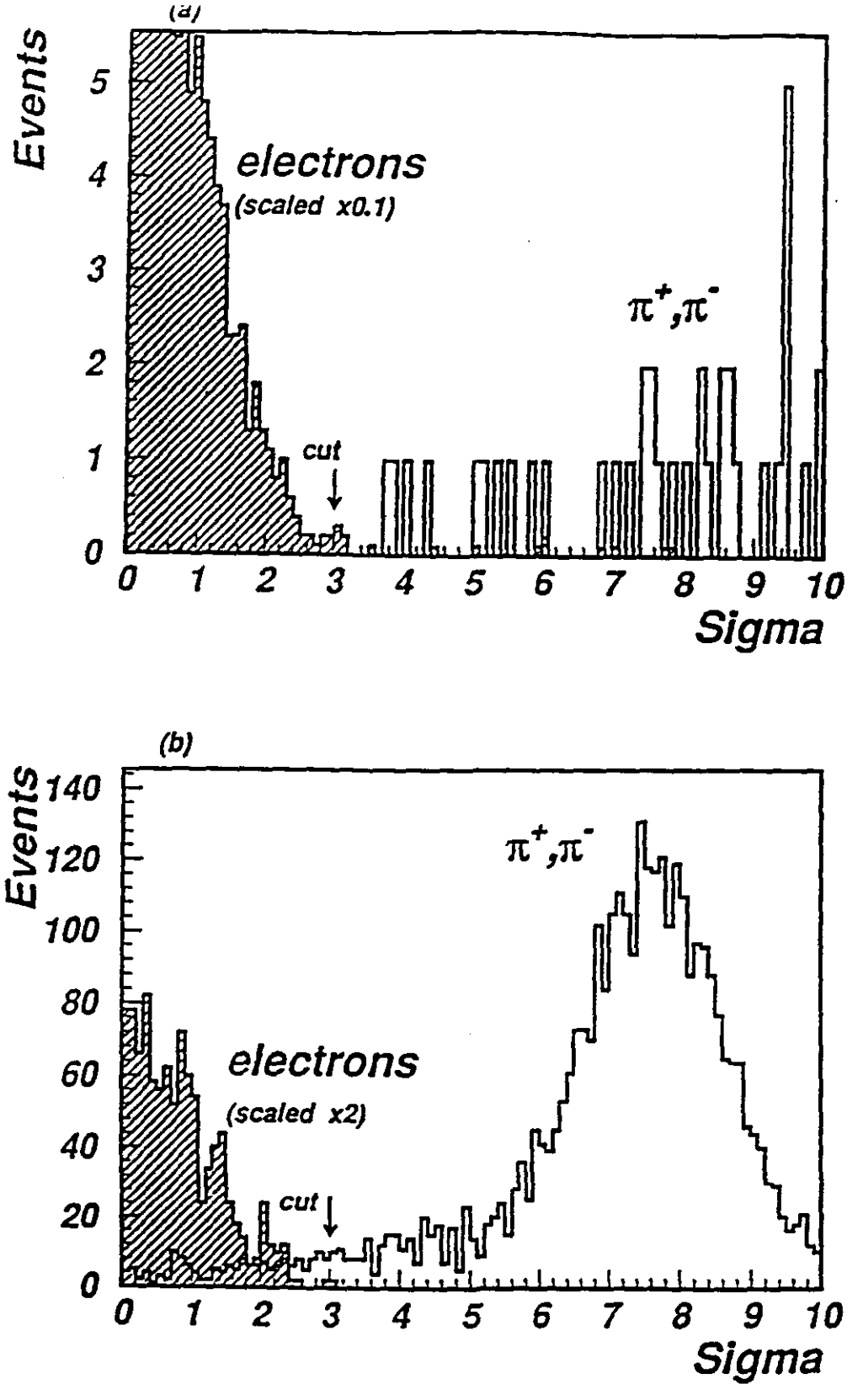

Figure 2: The distribution in $|E_{EM} - P_{trk}|$ (in units of σ) which is used in matching the energy in the electromagnetic calorimeter and the momentum in the tracker, after the transverse shower shape cut, for electrons and charged pions at (a) 10 GeV (b) 100 GeV.

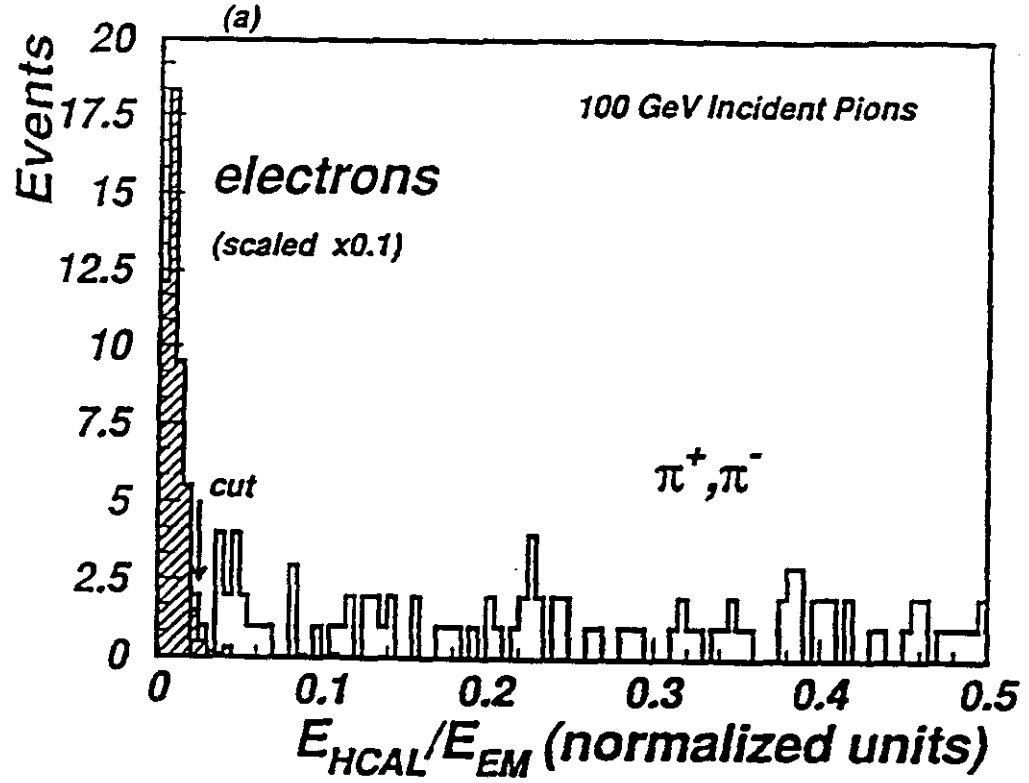

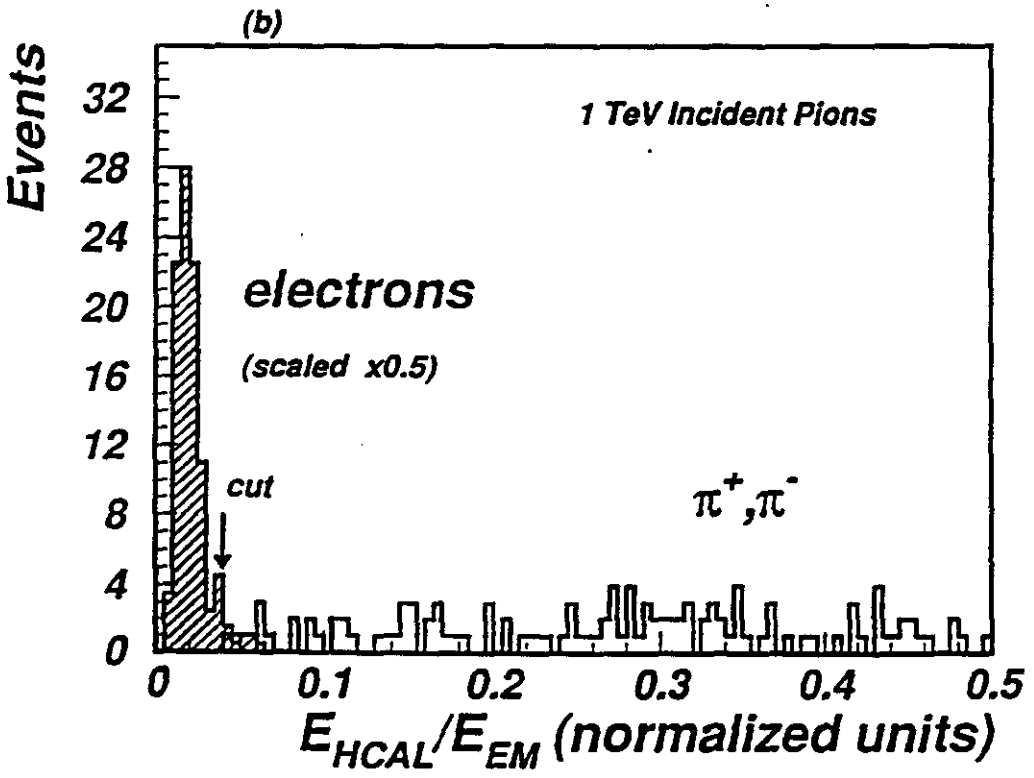

Figure 3: The distribution in E_{HCAL}/E_{EM} which is used for the hadron calorimeter energy veto, after the other cuts, for electrons and charged pions at (a) 100 GeV (b) 1 TeV. None of the pions survived the first two cuts in our simulations at 10 GeV.

7.2 Probability of a Jet Faking an Isolated Electron

The identification of isolated electrons is important for many physics processes, such as $H^0 \rightarrow e^+e^-e^+e^-$, $Z' \rightarrow e^+e^-$and $W' \rightarrow e+X$. A QCD jet, however, may fake an isolated electron for the following reasons:

- genuine electrons may be produced by heavy quark decays and π^0 Dalitz decays: $\pi^0 \rightarrow \gamma e^+e^-$;
- charged pions may fake an electron, with the probability calculated in the previous section;
- a photon from π^0 decay and a charged particle may both hit a single calorimeter cell.

Simulation shows that the dominant background which produces a fake 'electron' is from a photon overlapping with a charged particle. To eliminate a jet faking an isolated electron, we employ an isolation cut with a reduced radius of R=0.3 ($R=\sqrt{\Delta\eta^2 + \Delta\phi^2}$), and we require that the electron criteria described in the previous section are satisfied.

Following process were used in our analysis to implement the isolation cut:

- Generate QCD 2 jets using the PYTHIA 5.4 program [1];
- Assume electrons and photons deposit all their energies in BaF_2 calorimeter, and assume that charged hadrons deposit their energy in BaF_2 according to a distribution generated with a GEANT (full shower) simulation.
- Define the sum of the transverse energy in BaF_2 from all particles hitting one cell (ΣE_T) as E_T^{cell};
- Starting with the largest E_T^{cell}, if there is no charged track hitting the cell or more than one charged track hits the 3×3 cells centered on this cell, the central cell is rejected;

- Define the sum of E_T^{cell}'s in the 3×3 set of cells centered on each cell surviving the above cuts as $E_T^{electron} = \sum_{3x3Cells} E_T^{cell}$.

- Require that the sum of the transverse energy in a cone of radius R=0.3, excluding all energy in the 3×3 matching cells in both BaF_2 and hadron calorimeter, is less than 10% of the $E_T^{electron}$ plus an isolation energy cut (E_T^{cut}):

$$\sum_{R<0.3} E_T - \sum_{3x3cells} E_T > E_T^{cut} + 0.1 E_T^{electron} \Rightarrow Reject,$$

- If a charged pion passed above cuts, we weight it by its probability of faking an electron, i.e. by 2×10^{-4} as shown in the previous section;

- Continue this process for all cells;

- Define the probability (F) of a jet faking an isolated electron as the sum of the weights of all cells passing all above cuts, normalized to the number of jets generated.

Table 2 lists the probability of a jet faking an isolated electron (F) as a function of the electron P_T. It is clear that a 10^{-4} jet/electron rejection ratio may be obtained by using the isolation cut described in this section.

Table 2: Probability (10^{-4}) of a Jet Faking an Isolated Electron

E_T^{cut} (GeV)	5	10	15	20
$E_T^{electron} > 10$ GeV	1	3.8	6.5	9.0
$E_T^{electron} > 20$ GeV	0.25	0.5	1.3	1.5

References

[1] H. Benson and T. Sjostrand, *"A Manual to the Lund Monte Carlo for Hadronic Processes"*, PYTHIA version 5.4, June 1990.

[2] J. Gunion et al., *"The Higgs Hunter's Guide"*, UCD Preprint, 89-4 (1989).

[3] The cross-section of $H^0 \rightarrow \gamma\gamma$ is scaled up by a factor of two according to J. Stirling, a talk given in a recent *"ECFA-LHC meeting"* at CERN. An argument was given that one should use a running b quark mass (in the spirit of perturbative QCD) in evaluating the $H^0 \rightarrow b\bar{b}$ coupling. Since the b quark mass is smaller than the scale of the Higgs mass, the width for this channel is reduced by almost a factor of two. Also other quark channels are reduced by the same argument. Since the effective width into $\gamma\gamma$ is unchanged, the actual branching ratio thus is increased. See also [2].

[4] CERN Green Book, *"ECFA Workshop on LEP 200"*, Aachen, September 1986.

[5] D. Dicus and S. Willenbrock, Phys. Rev. **D37** (1988) 1801.

[6] T. Sjo strand, private communication.

[7] D. Froidevaux, summary talk on Higgs serach given in *"LHC ECFA Study Workshop"*, CERN, June 1990.

[8] F. Paige and S.D. Protopopescu, *"ISAJET 6.28 A Monte Carlo Event Generator for P-P and $\bar{P}$-P Reactions"*, April 1990.

[9] M.D.G. Gilchriese, in *"Proceedings of the 1984 Summer Study on the Design and Utilization of the Superconducting Super Collider"*, edited by R. Donaldson and J.G. Morfin, Snowmass, Co.(1984) 607; H.H. Williams, in *"Proceedings of the 1986 Summer Study on the Physics of the Superconducting Super Collider"*, edited by R. Donaldson and J. Marx, Snowmass, Co.(1986) 327; SSC Central Design Group, *"Report of the Task Force on Detector Research Development for the Superconducting Super Collider"*, SSC-SR-1021 (1986).

References

[1] D. Groom, *Jet Response of a Homogeneous Calorimeter*, Contribution to the ECFA LHC Workshop, Aachen, October, 1990.

LIQUID XENON/KRYPTON

Report to Technical Questions from GEM

Question (1) When will a fully developed Liquid Xe unit cell be beam tested and tested for radiation damage?

To keep the cost of R&D to the minimum, we build only once and re-use > 90% equipment, including media, cryostats, purification system, diodes, UV-mirrors, and amplifiers for all of the following tests:

1. **Components: xenon, MgF_2 mirrors and diodes to be tested for radiation damage:**
   Oct., 1991

2. **1x1 full length, fully developed Liquid Xe unit cell to be α, heavy ion, and cosmic ray tested in Sept., 1991 and tested for radiation damage: Oct./Nov., 1991**

3. **7x7 full length, with half the mirrors and diodes, be**
   α and cosmic ray tested: Dec., 1991
   beam tested: Mar., 1992 at BNL

4. **7x7 full length, with all the mirrors and diodes, be beam tested:**
   Fall, 1992 at BNL/CERN

5. **7x7 full length, with all the mirrors and diodes, be beam tested:**
   Fall/Winter with H1 hadron calorimeter, 1992 at BNL/CERN

Question 2). Describe the calibration procedure for high energy - i.e. between 1 GeV and 5 TeV.

The complete Signal Processing Diagram is:

Emitter(Xe/Kr)-Transmitter(reflector)-Receiver(diode)-Amp–ADC

to be calibrated by α's and electronically simulated by

Generator————Capacitor————————————Amp–ADC

1. **To monitor the stability and linearity of the electronic channels, we use vacuum α's as well as a pulse generator to put signal through very stable calibration (1/10,000) capacitor.**

   - **Generator (5k$);**
   - **Fanout (4500 vac. relay at 5$ each, multiplex=25k);**
   - **Capacitor(1$) x 45k**
   - **Total cost: 5 + 25 + 45k = 75k$ x 2 (safety factor) = 150 k$**

2. **LXe/Kr: keeping impurities < 0.01 ppm by externally monitoring with (liquids are homogeneous):**

- **a. Ionization chamber to detect impurities > 1ppb:**

  Using Bi^{207}'s two γ rays in 2 and 5 cm drift gaps, we determine the electron drift attenuation length > 1m or a sensitivity on H_2O, O_2, CO_2, CO, and Halocarbons = 1 ppb;

- **b. Infrared spectrometer to ID impurity:**

  Sensitivity on CO_2(0.01 ppm), Halocarbons(1 ppb), and CO(0.4ppm), etc.

- **c. Xe_2 laser simulating scintillation with adjustable intensity, checks both transparency of liquid and uniformity of reflectors.**

- **d. Resonance spectroscopy (RS):**

  Laser beam with proper wave length passing through the liquid excites impurity molecules; photosensor detects luminescence of deexcited molecules in perpendicular direction to the incident laser beam, during purification of Xe gas.

2. **LXe/Kr: keeping impurities < 0.01 ppm by externally monitoring with (liquids are homogeneous).**

- **a. Ionization chamber to detect impurities > 1ppb:**
  Using Bi^{207}'s two γ rays in 2 and 5 cm drift gaps, we determine the electron drift attenuation length > 1m or a sensitivity on H_2O, O_2, CO_2, CO, and Halocarbons = 1 ppb;

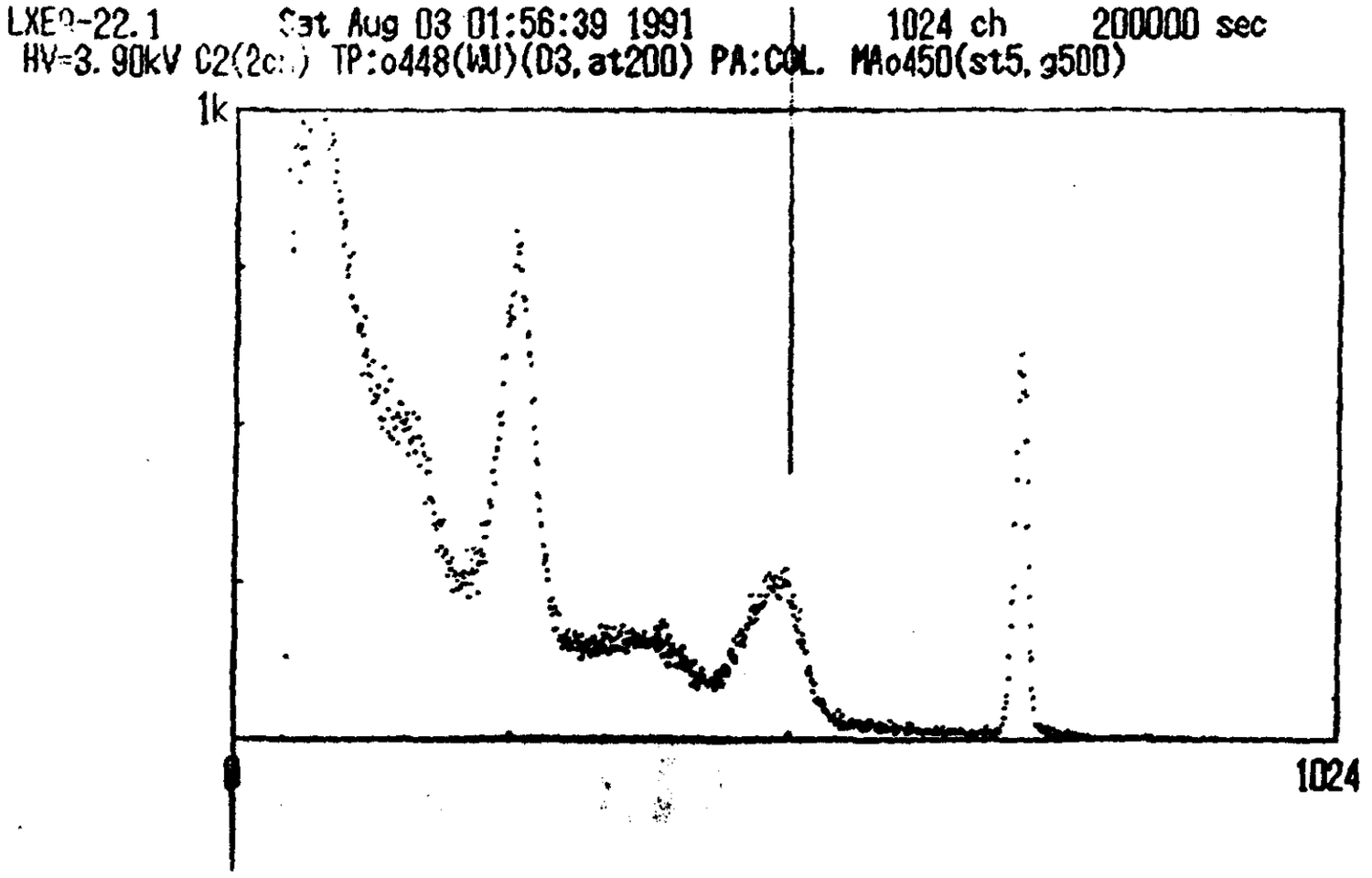

LXE9-12.1 Fri Aug 02 22:17:01 1991 1024 ch 200000 sec
HV=8.4kV C1(5cm) PA:Col TP:o448(WU)(D3,At200) MA:o450(st5,g500)

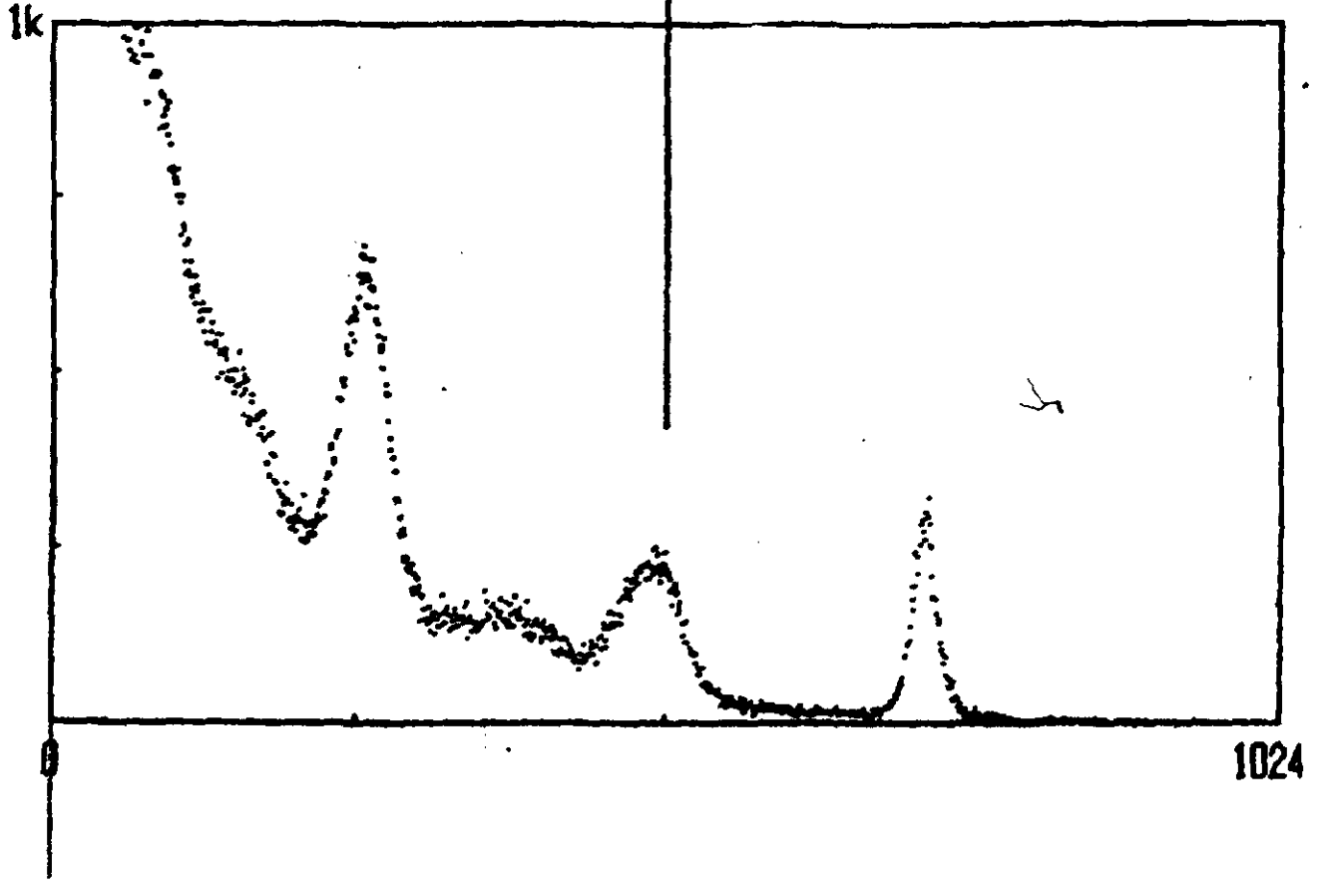

$E = 1.5\ kV/cm$

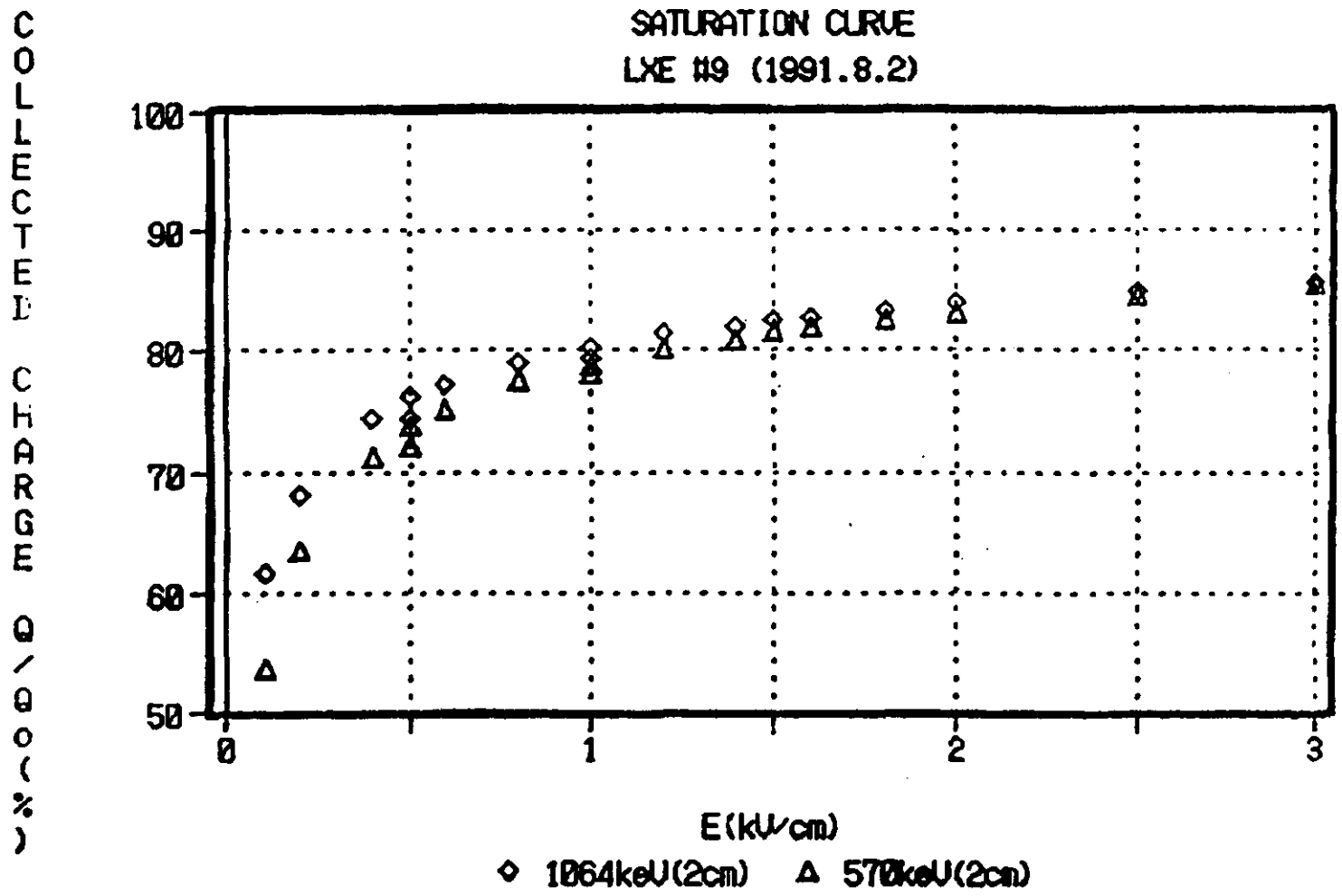
SATURATION CURVE
LXE #9 (1991.8.2)
COLLECTED CHARGE Q/Qo(%)
100
90
80
70
60
50
0
1
2
3
E(kV/cm)
1064keV(2cm)
570keV(2cm)

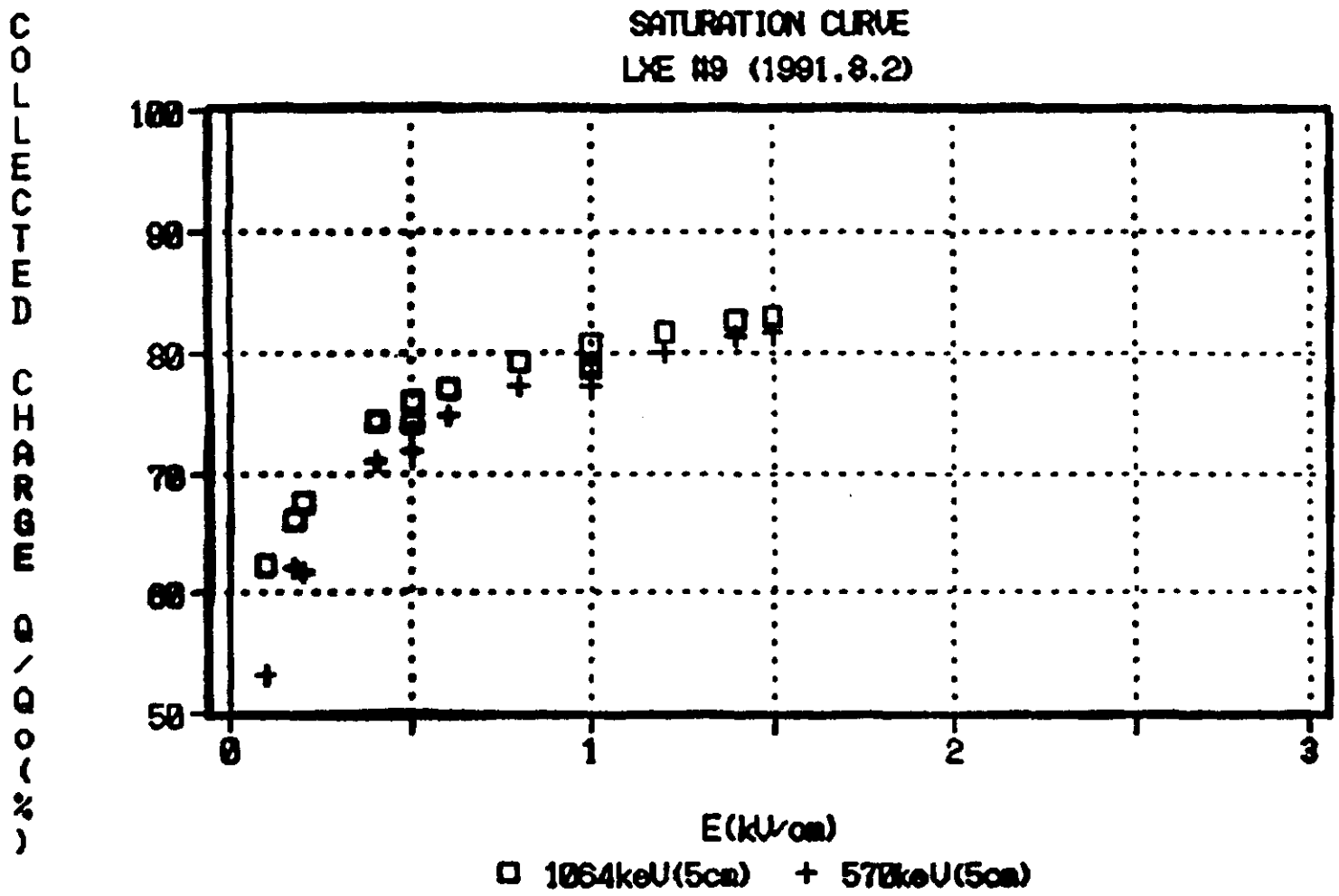
SATURATION CURVE
LXE #9 (1991.8.2)
COLLECTED CHARGE Q/Qo(%)
100
90
80
70
60
50
0
1
2
3
E(kV/cm)
1064keV(5cm)
570keV(5cm)

- b. **Infrared spectrometer to ID impurity:**
  Sensitivity on CO_2(0.01 ppm), Halocarbons(1 ppb), and CO(0.4ppm), etc.

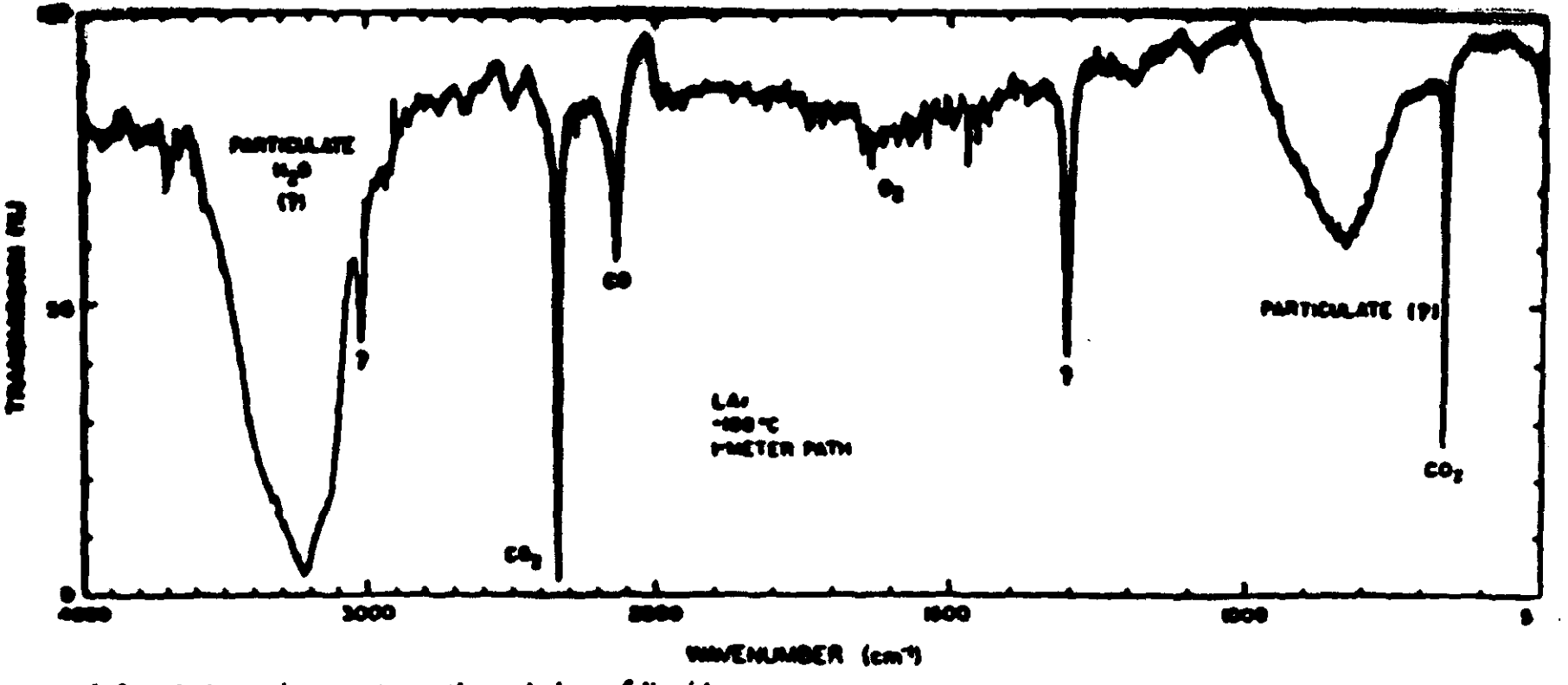

- Infrared absorption spectrum through 1 m of liquid argon.

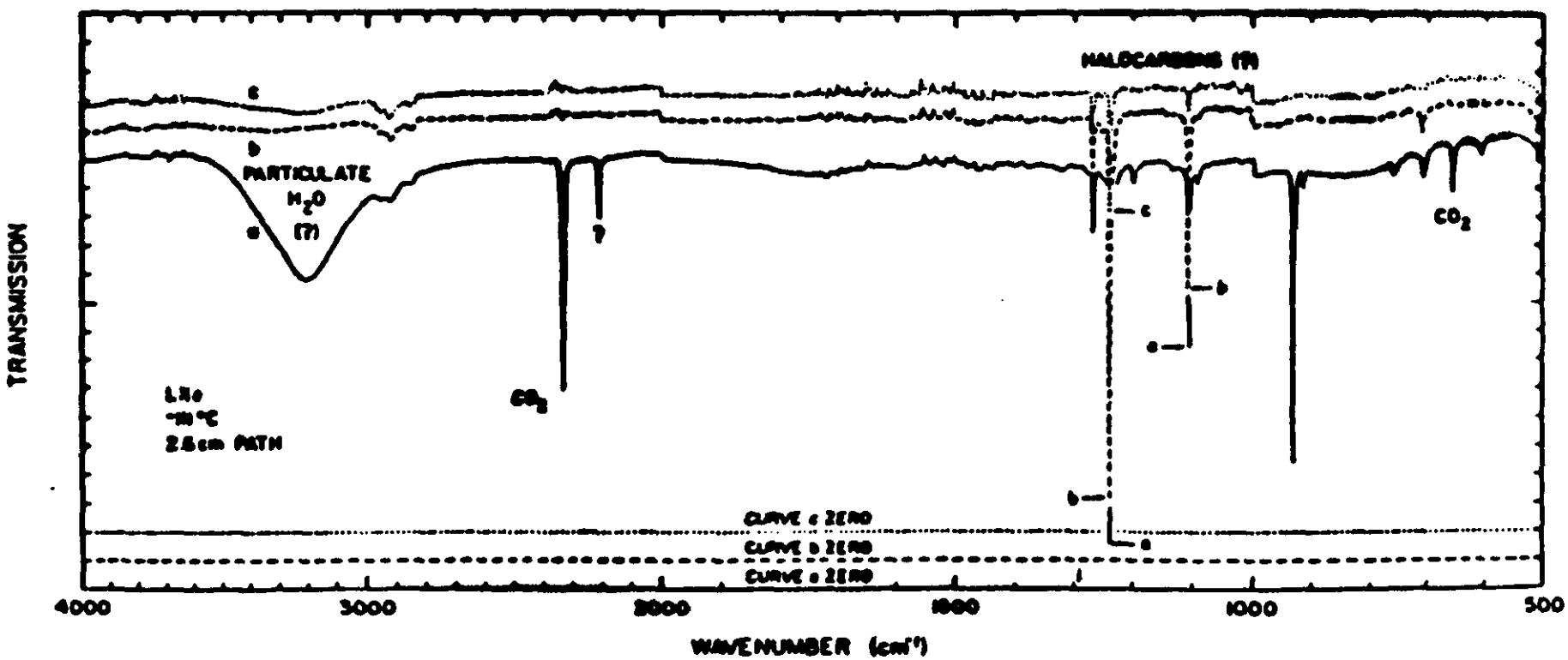

Effect of flow rate through a hydrox purifier on the removal of impurities in xenon. The instrumental resolution is $\sim 4\ cm^{-1}$.

- e. 48 special cells (20cm long) for calibration, connected to the LXe/Xi cells from outside in the empty space of the cryostat, with one triode and one diode at the two ends of each cell. A point-like α source, situated at 5cm from the diode and 10cm from the triode. The solid angle is about 0.1 for the triode. For the diode, the signal is about 8000 γ_e, and S/N is around 7. For the triode., the signal is about 1800 γ_e and S/N is around 18. The attenuation length for LXe has been determined to be greater than 200 cm.

  It is easy to achieve 0.5% accuracy, since the mean peak position can be monitored to 1/1000.

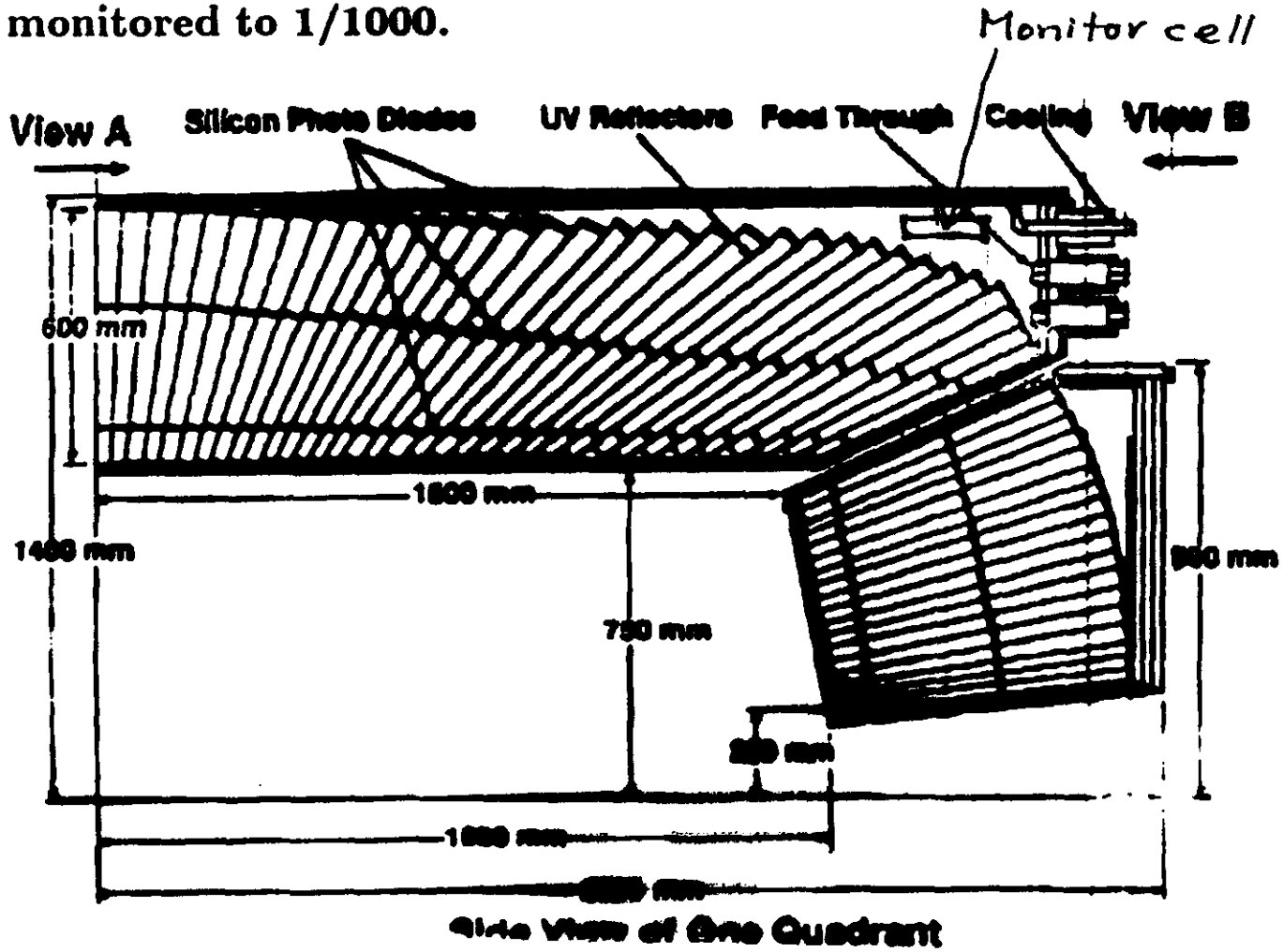

3. Calibrating Quantum efficiency of diodes under high radiation,

- Peak position of α in vacuum has a resolution of 0.2%. and a mean peak position accurate to 0.02%.
- We also measure peak position of α in liquid with a signal of 5 σ effect or a mean peak position accurate to 0.5% in minutes (2000 events).
- Cost/channel: discriminator(10$) + vac. relay (5$) for MUX = 15$
- Total cost for 48k ch = 700 k$ x 2 (safety factor) = 1.5 M$.
- Xe_2 laser: 75k$.
- Auto VUV spectrometer with Xe_2 laser: 225 k$.
- Grand total = 1.8 M$.

α Calibration Spectrum

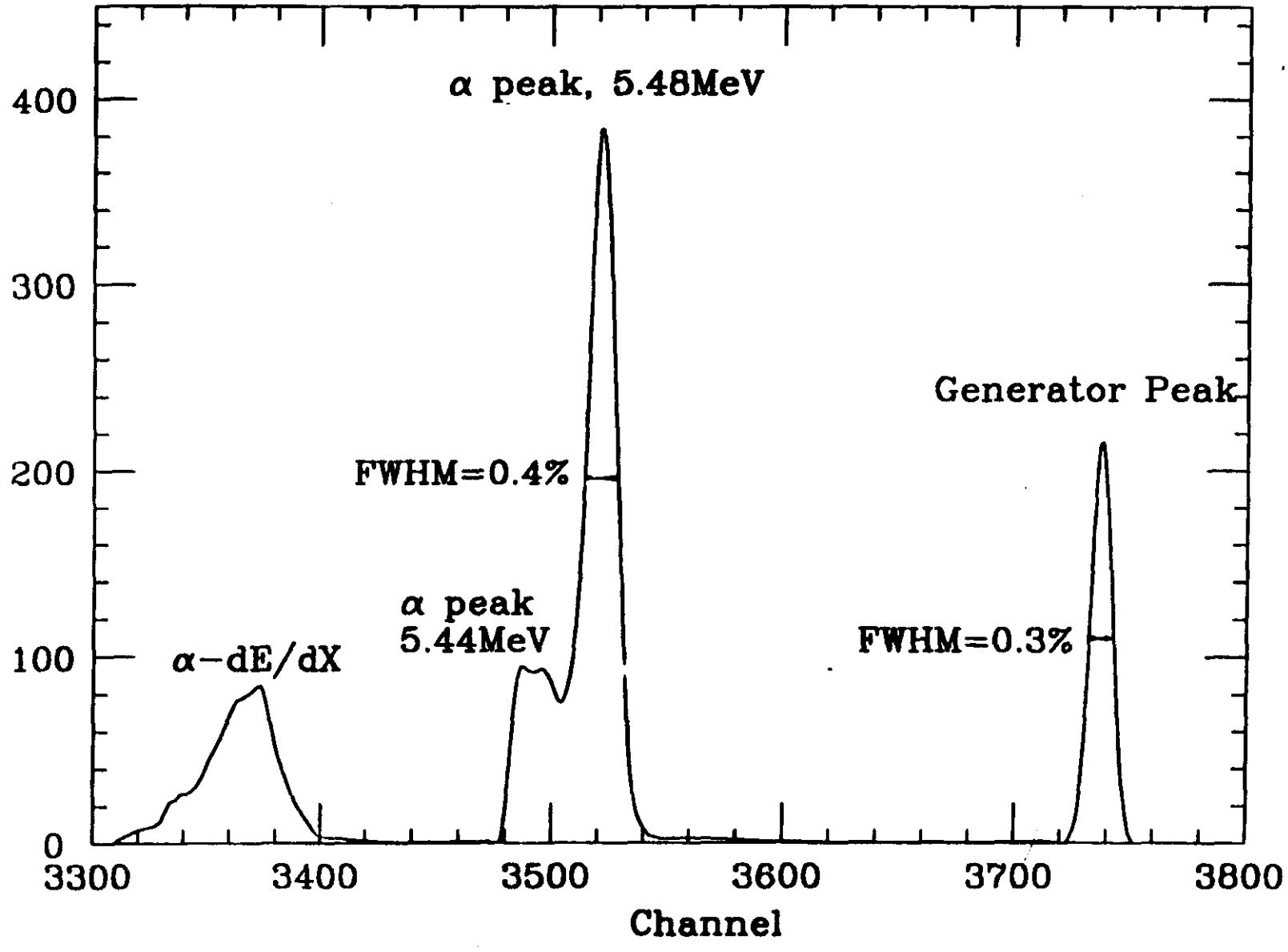

Hamamatsu Diode K2, Thickness: 500μm, Vacuum, −110°C

α Calibration Stability

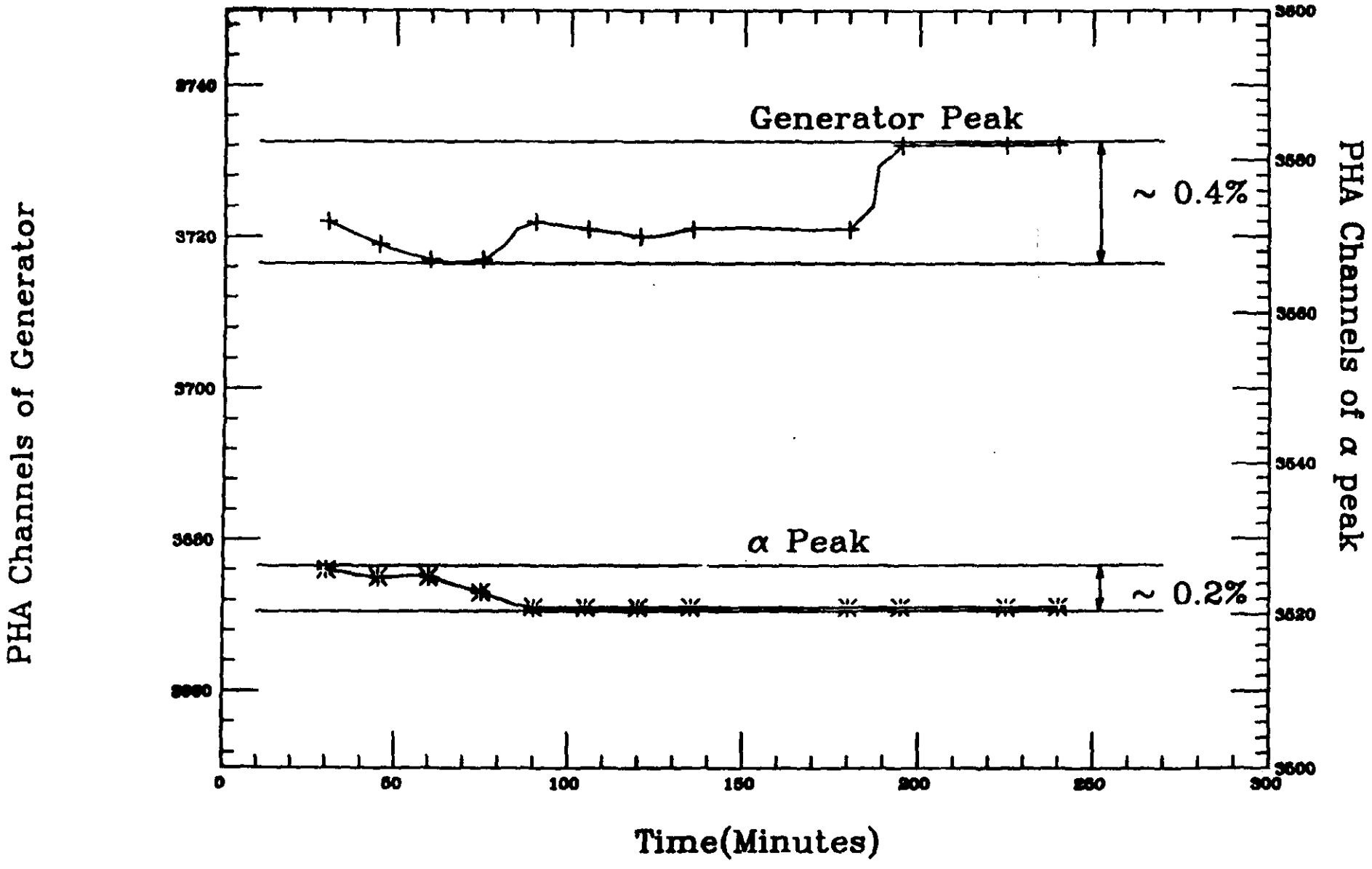

Hamamatsu Diode K2, Thickness: 500μm, Vacuum, −110°C

Scintillating Liquid Xenon Calibration

Xenon scintillation light

from 5.5 MeV α's (^{241}Am)

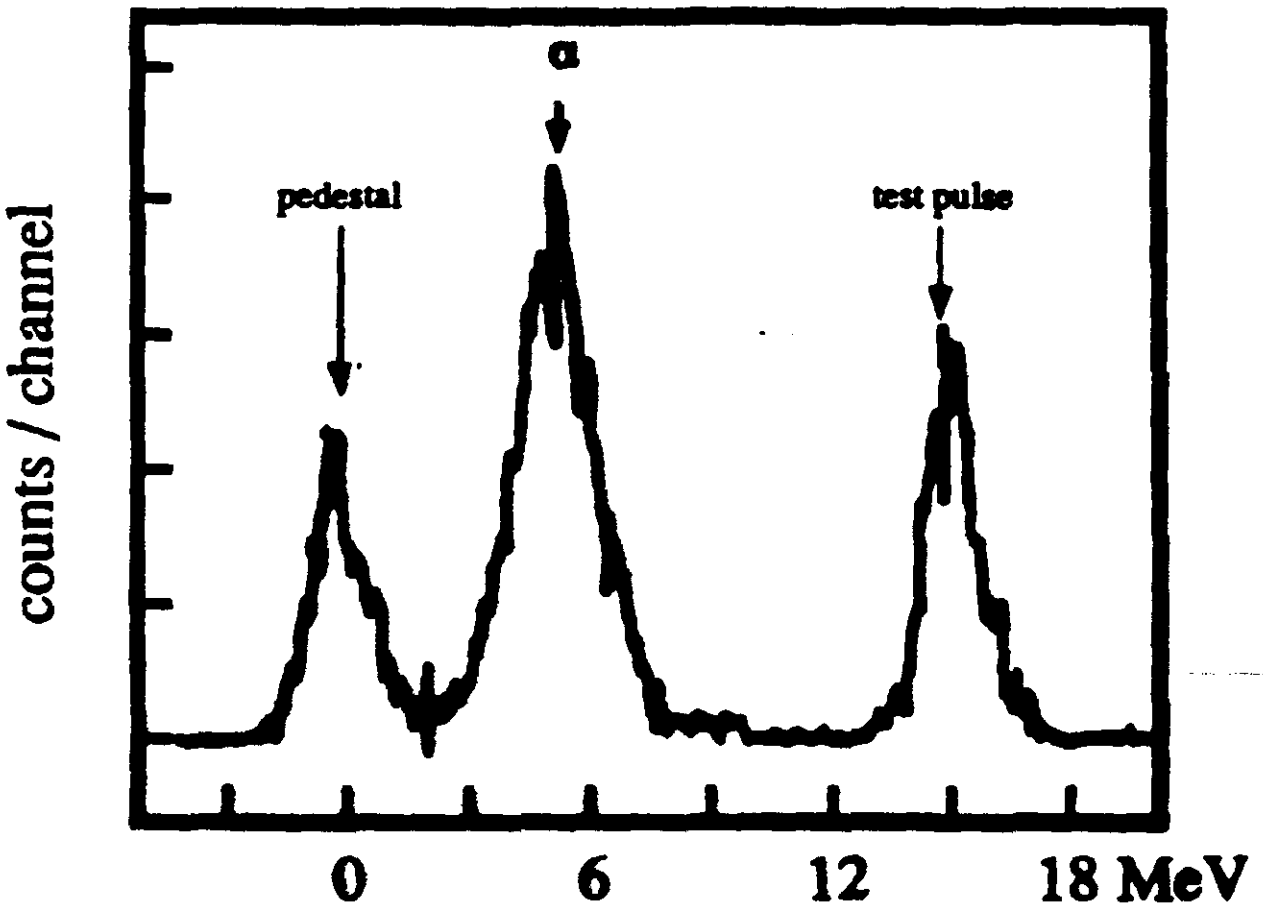

PH.calibration.2

we baked the diode until Q.E. reduced by 0.5
calibrated using α's
Repeat the measurement:

0.5% for 2.47 GeV ^{27}Al,
with 40 ns gate,
corresponding to 1.36×10^7 electrons.
Q.E. = (1.36 /2.47) / (2.91/2.65) = 0.50.

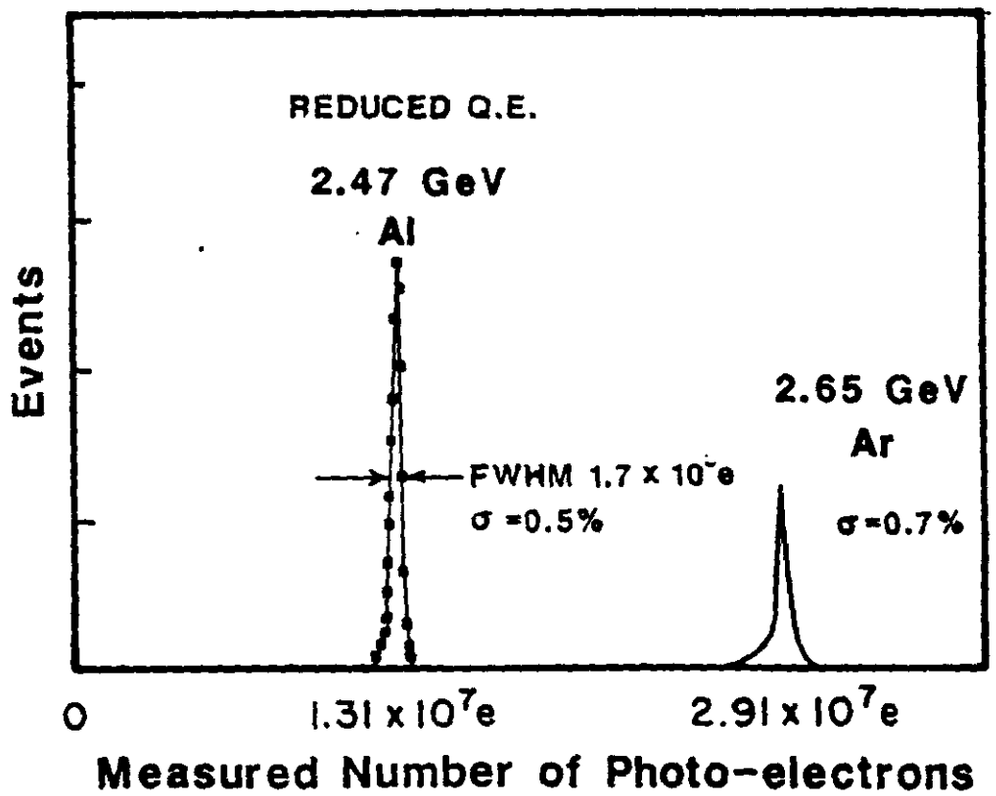

These results demonstrate that:

The calibration method with α's does work;
Resolution is due to beam energy spread, not electronics or photon statistics: the actual energy resolution of LXe detectors is much better.

4. Our amplifier/diodes are linear to 10^{-} from 1 to 100,000 MeV and will be further improved to reach higher energies. So the calibration of α in liquid and vacuum α can be extrapolated to 100 GeV for now.

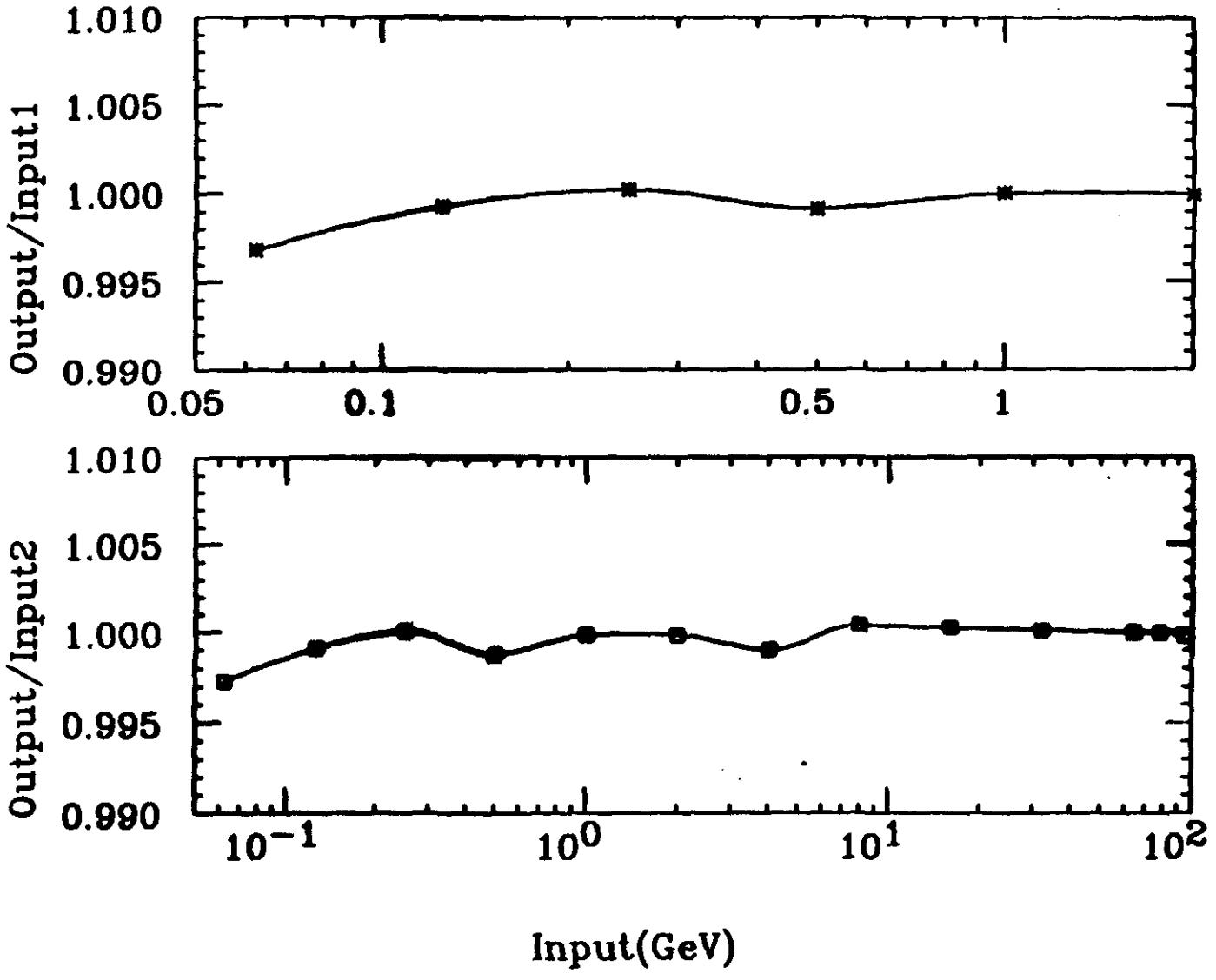

5. To check the linearity at TeV, we must accumulate high p_t Z0–> 2e events over long periods.

Calibration of liquid xenon detector
using α particle in LXe and
direct on the diodes, cosmic μ's,
based on our measurements,
and monitored by
$Z \rightarrow ee$ events
expected at the SSC.

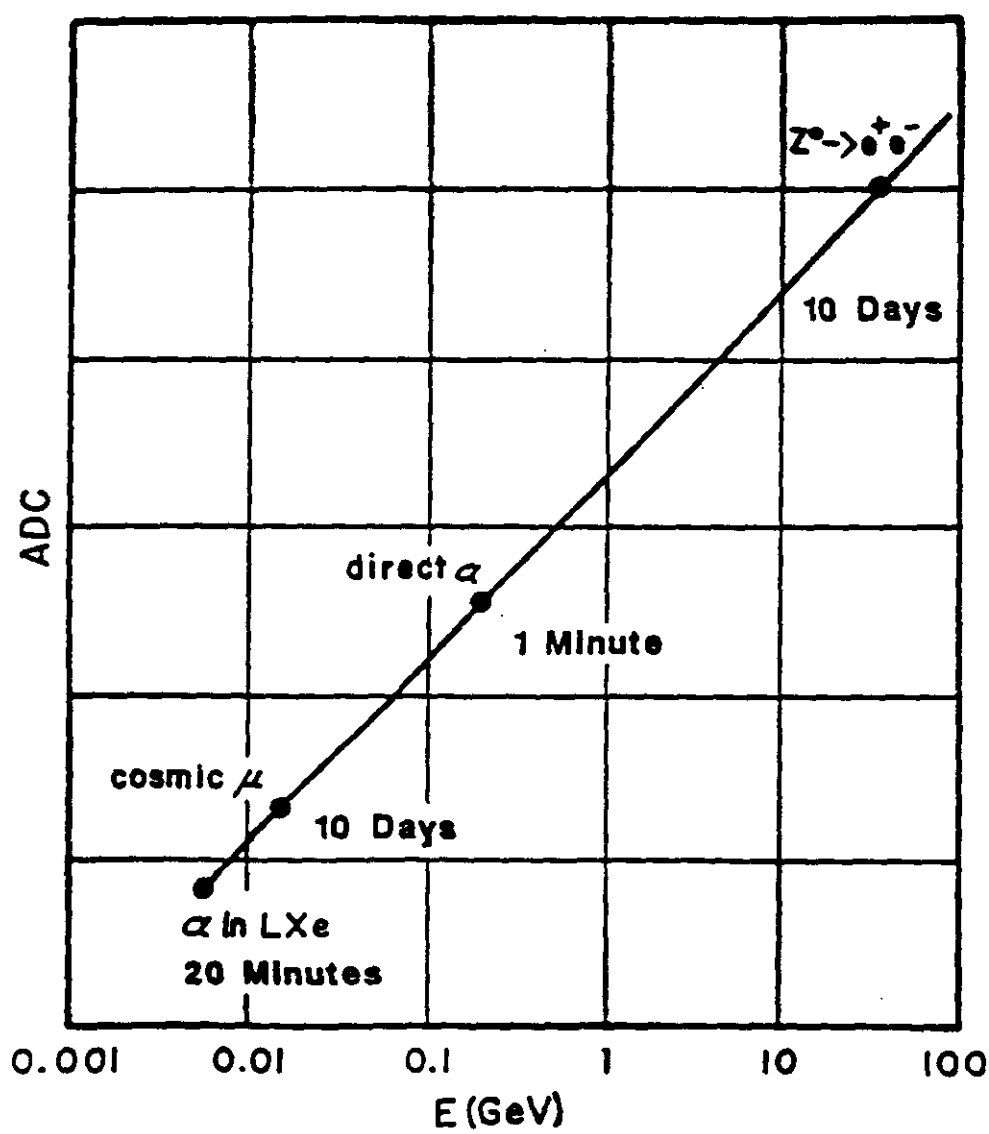

The time needed
to achieve 0.5% accuracy of calibrati

Question (3) How can a Xe/Kr, SANDI EM calorimeter expect to achieve a 2% stochastic term in the energy resolution and at most a 1/2% constant term in the energy resolution in the face of the following difficulties?

Question (3a) What is the best stochastic term that has been measured for electrons with a Xe/Kr device in a test beam, using only the fast component within a narrow gate? How does the measured resolution vary with energy, and is there a linear or quadratic constant term?

Expected energy resolution:

- LXe/LAr/LKr achieved $\delta E/E < 0.5\%$ at 1.5 GeV heavy ion beams with zero electric field.
- For electrons, Ypsilantis obtain 1.4% at 7000 photo-electron or 1 MeV with the fast component within a narrow gate using photo-tube.
- All these show that a stochastic term < 1% and a constant term < 0.5%.
- We will be the 1st one to measure the energy resolution for high energy electrons with a Xe or Kr device next March, using only the fast component within a narrow gate. See Q.1.

High energy electrons differ from heavy ions in longitudinal shower distributions. This has been studied with Monte Carlo simulation. See below.

1. Nonuniformity of reflectors.

   Xe2-laser can simulate scintillating light to scan reflectors and measure the reflectivities.

Summary
of
Xenon R&D work

absorption length	> 200 cm
light yield	$4 \cdot 10^7$ photons GeV^{-1}
calibration with α's	5.5 MeV is at 6 σ from pedestal
signal peaking time for full size photo detector	10 ns for 50 mm ø diode

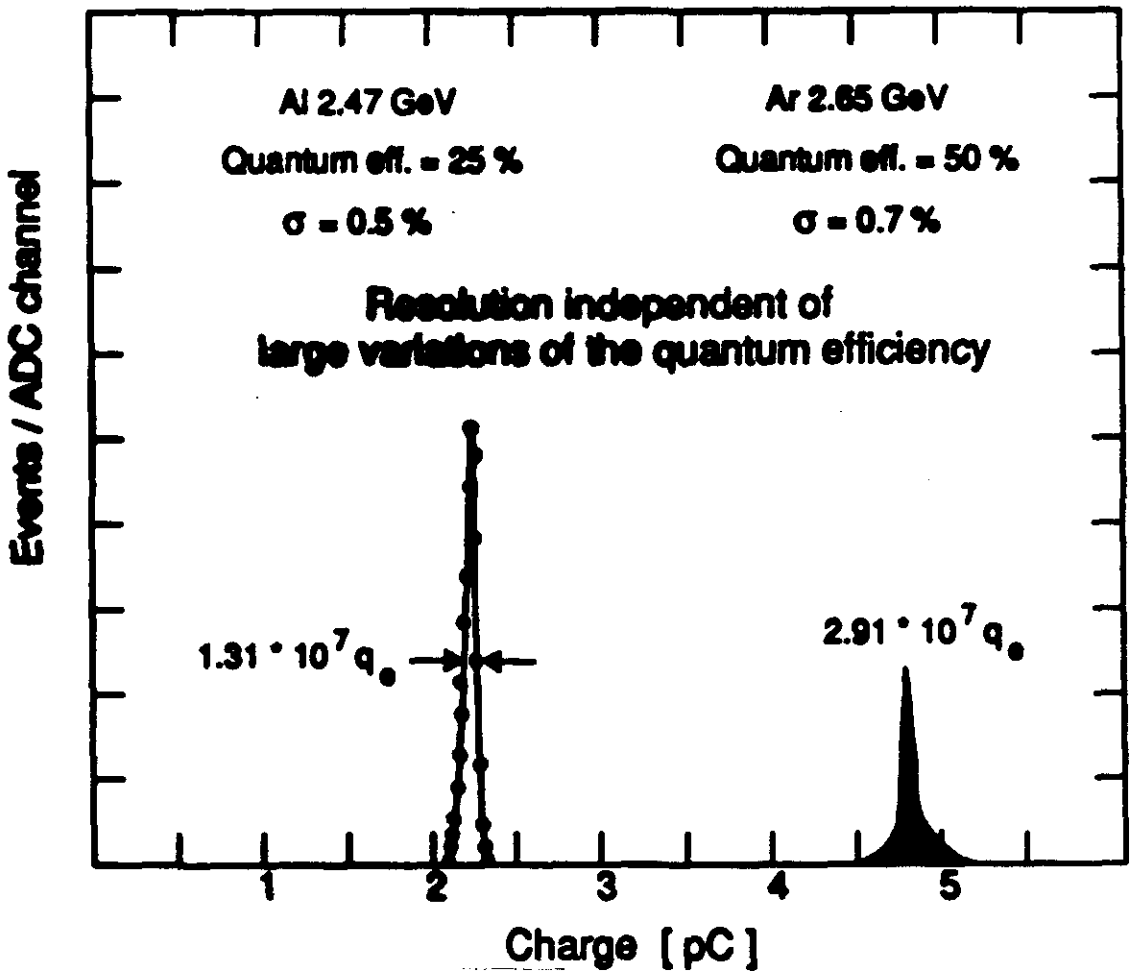

Figure 13: Measured numbers of photoelectrons for 2.65 GeV Ar ions (solid); and 2.47 GeV Al ions with 50% reduced quantum efficiency (points), showing that the resolutions are not limited by photoelectron statistics.

Energy Resolution

$$\delta E/E = (A/\sqrt{E} + B + C)\%$$

- A < 1 for LXe;
  = 1.3 for BGO; and
  = 6–10 for Fibre or LAr.
- B depends on systematics, e.g., BGO achieved 0.5.

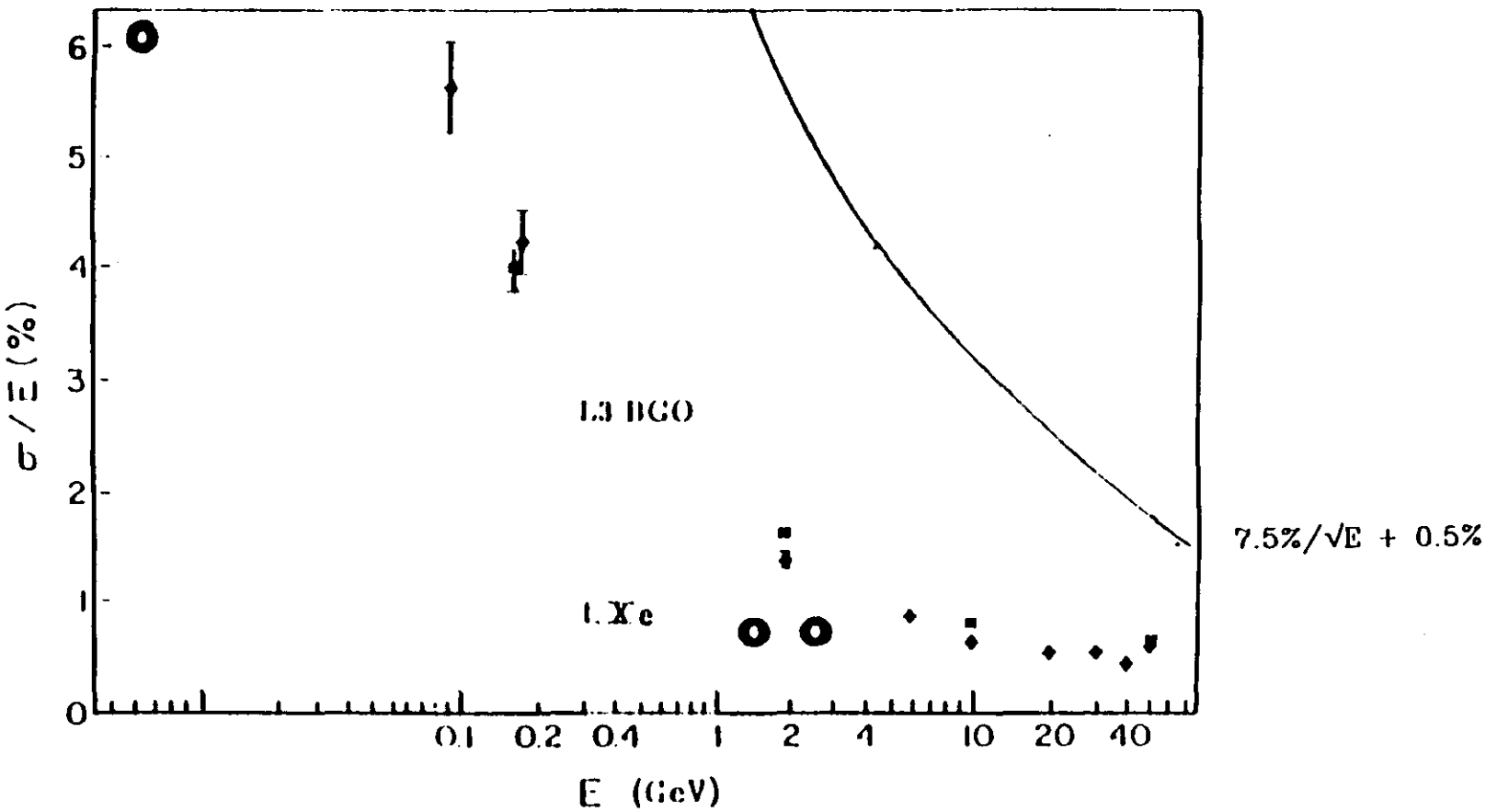

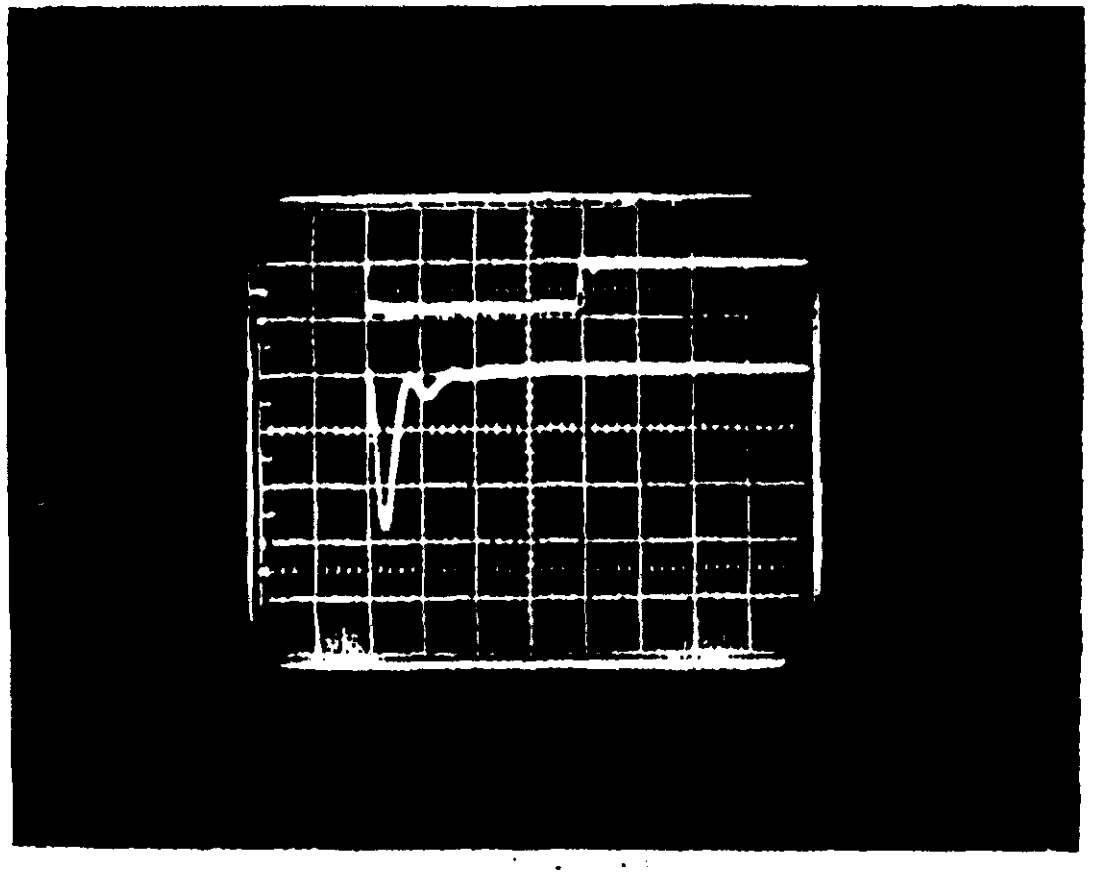

Bias 200 V
Fast amp w/ gate width 200 ns

Upper: Gate pulse
1 V/div

Lower: PD signal (fast amp out)
0.1 V/div

Al-27 ion 100 MeV/n 2.47 GeV
Liq.Xe scintillation

Horizontal: 50 ns/div

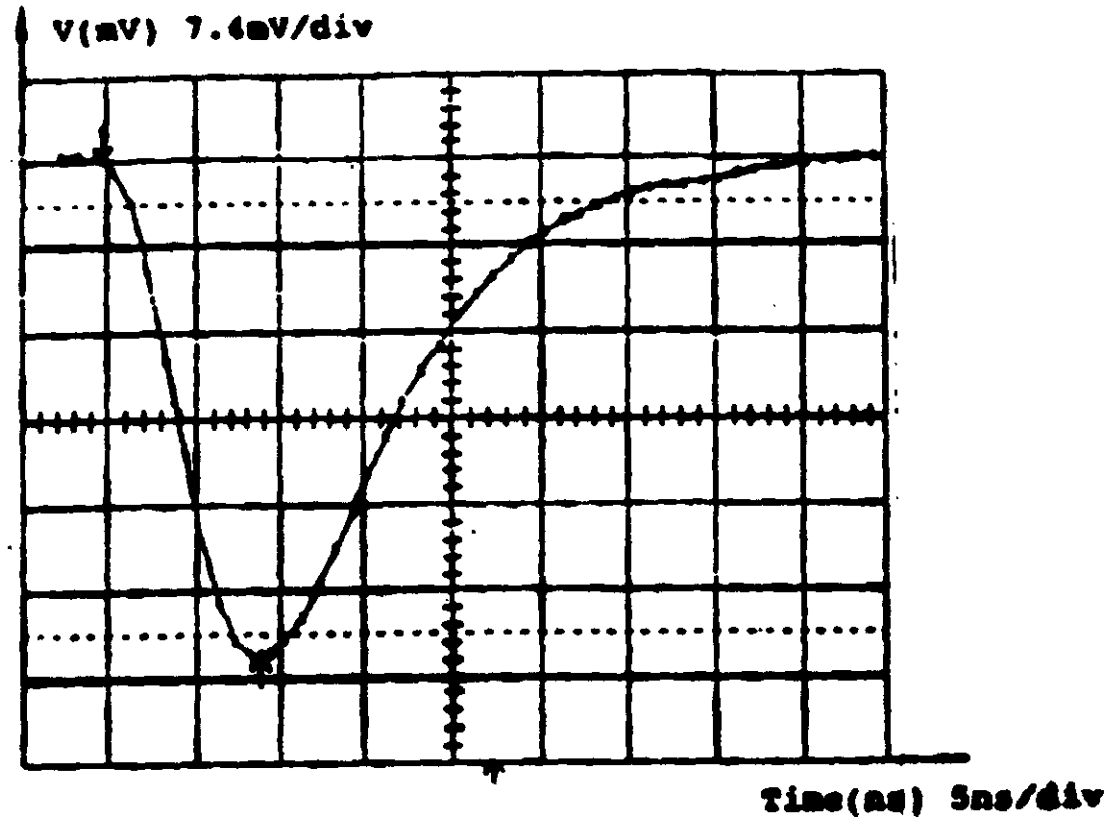

α Signal Diode W2

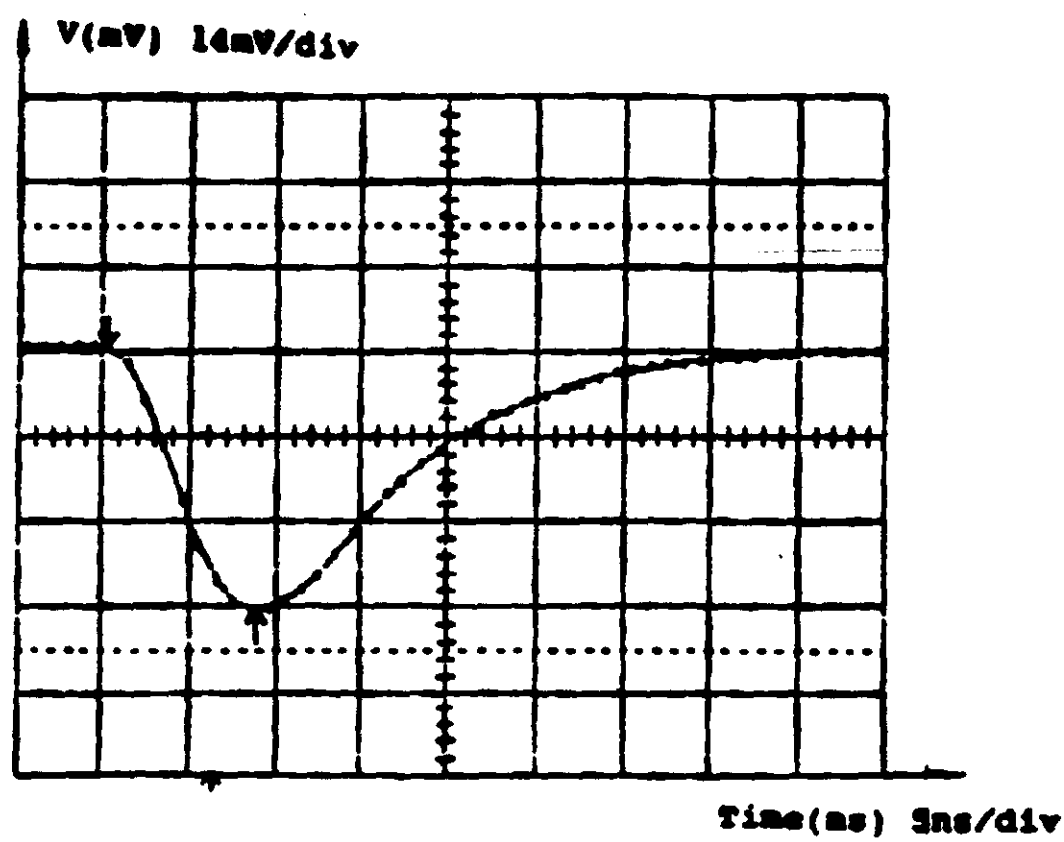

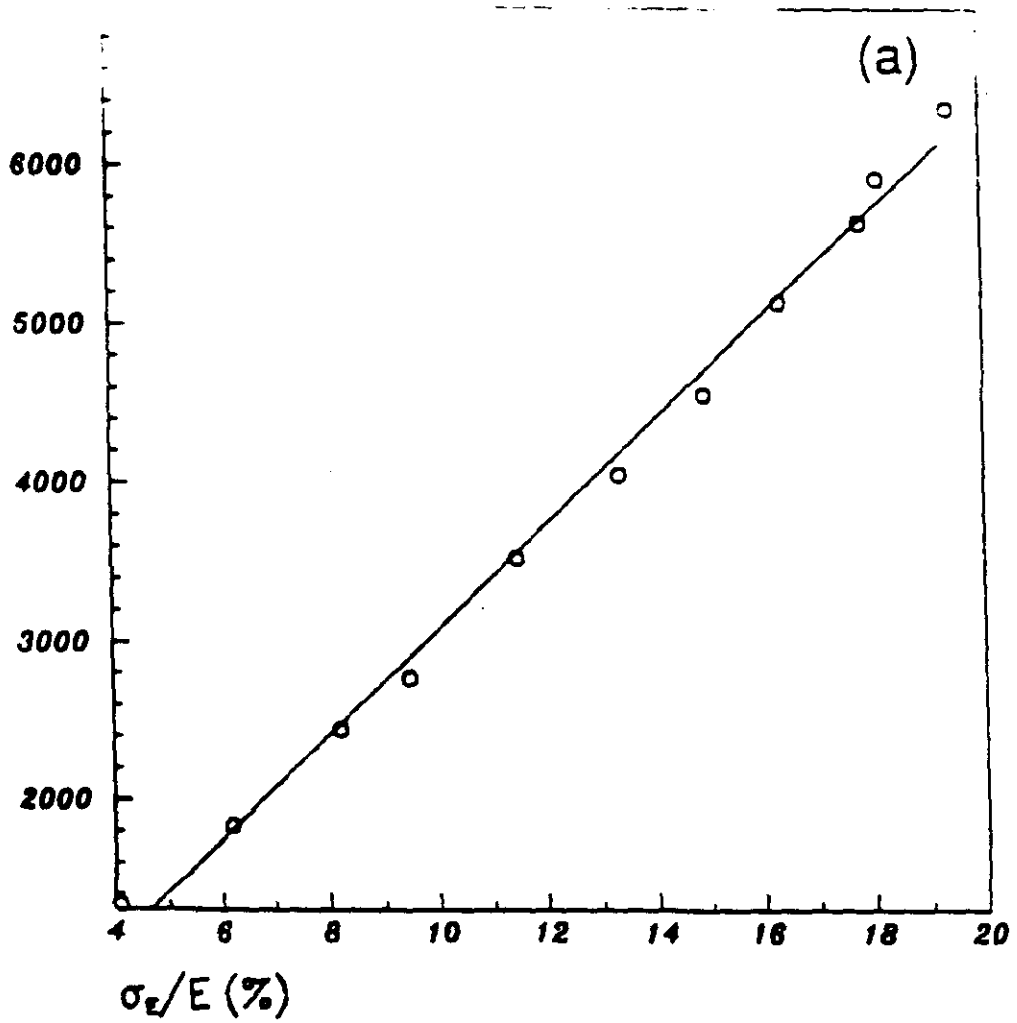
(a)
6000
5000
4000
3000
2000
4
6
8
10
12
14
16
18
20
σE/E (%)

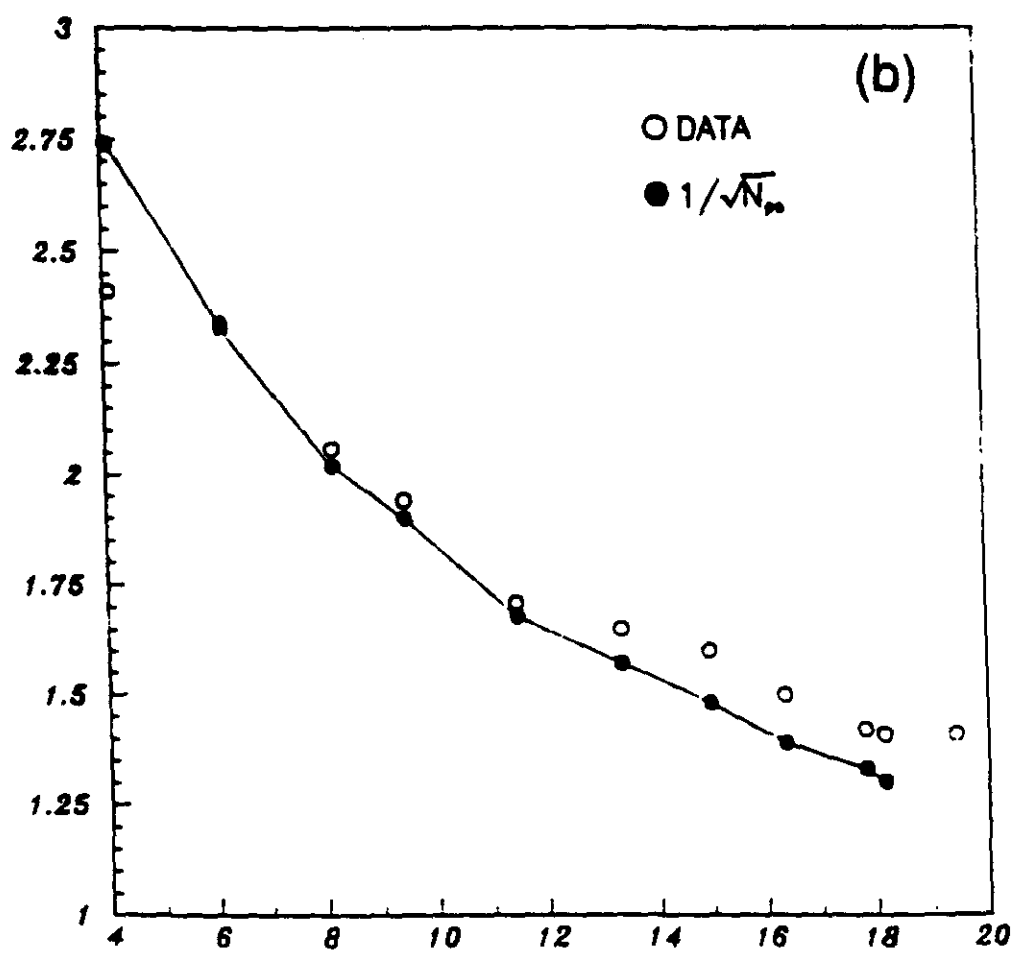
(b)
O DATA
● 1/√Npe
3
2.75
2.5
2.25
2
1.75
1.5
1.25
1
4
6
8
10
12
14
16
18
20

Liquid Xenon (LXe)
is radiation hard and
its scintillation light for e/γ
is fast (decay time 20 ns) and

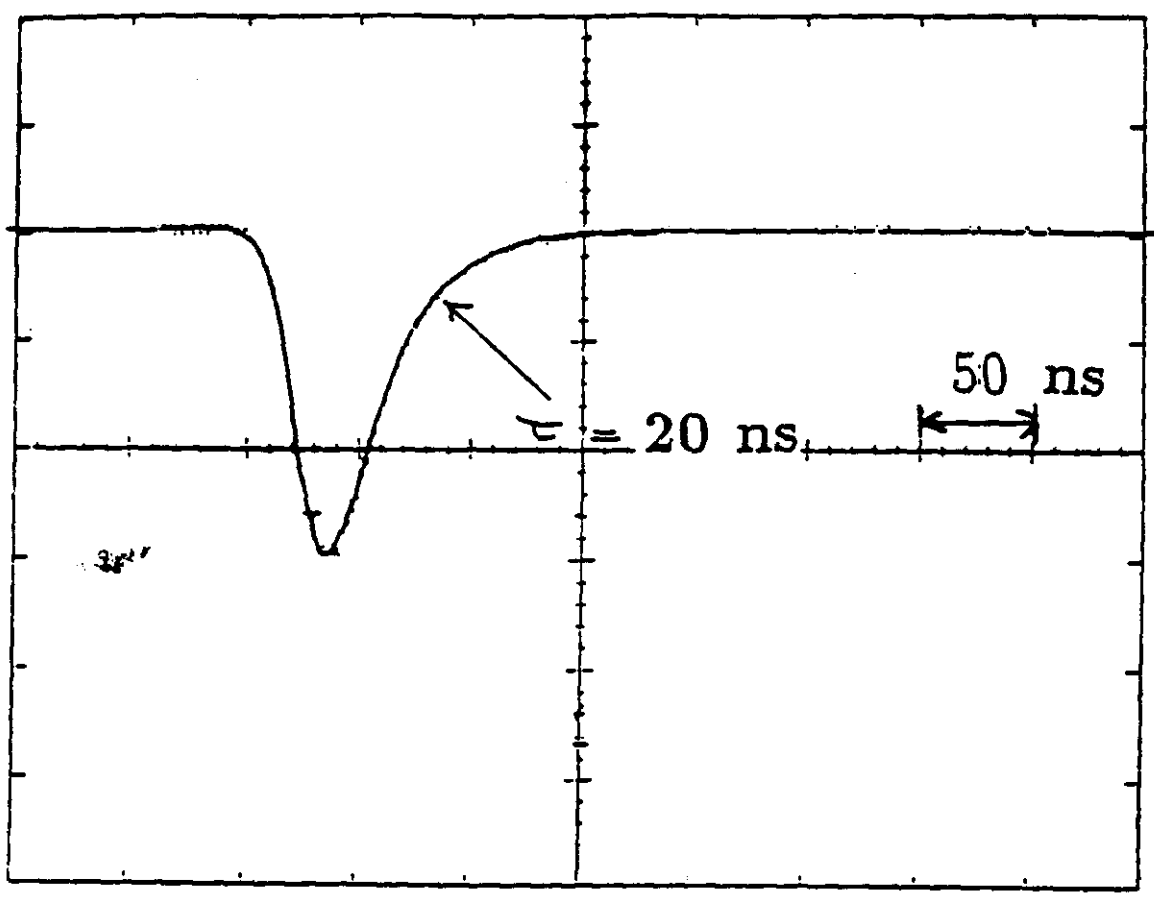

intense ($4 \times 10^7 \gamma$/GeV at 170 nm)
which naturally results in $\sigma(E)/E < 0.5\%$
and excellent dE/dX measurement.

Comparison between Three Kr- and Xe Calorimeters

	Kr-Calorimeter	Xe-Calorimeter	
	[USSR-Italy]	[USSR]	[Japan]
Gap	20 mm	12.0 mm	3.5 mm
Thickness of Electrodes	0.5 mm G-10 + 2.35 μm Cu	50μm Al	125 μm Kapton + 2 x 18μm Cu
Length of Calorimeter	76 cm(16.4 X_0)	50 cm(17.7 X_0)	70 cm(25.4 X_0)
Diameter of Calorimeter	42 cm(9.5 X_0)	25 cm(9.0 X_0)	30 cm(10.8 X_0)
Number of Readouts	19	1	20
Thickness of Entrance Window	2 mm Fe(0.13 X_0)	?	1 mm Fe(0.06 X_0)
Energy Resolution	1.7 % for 1.2 GeV positrons	3.4 %/$\sqrt{E(GeV)}$	0.80 % for 1 GeV 0.38 % for 5 GeV 0.30 % for10 GeV

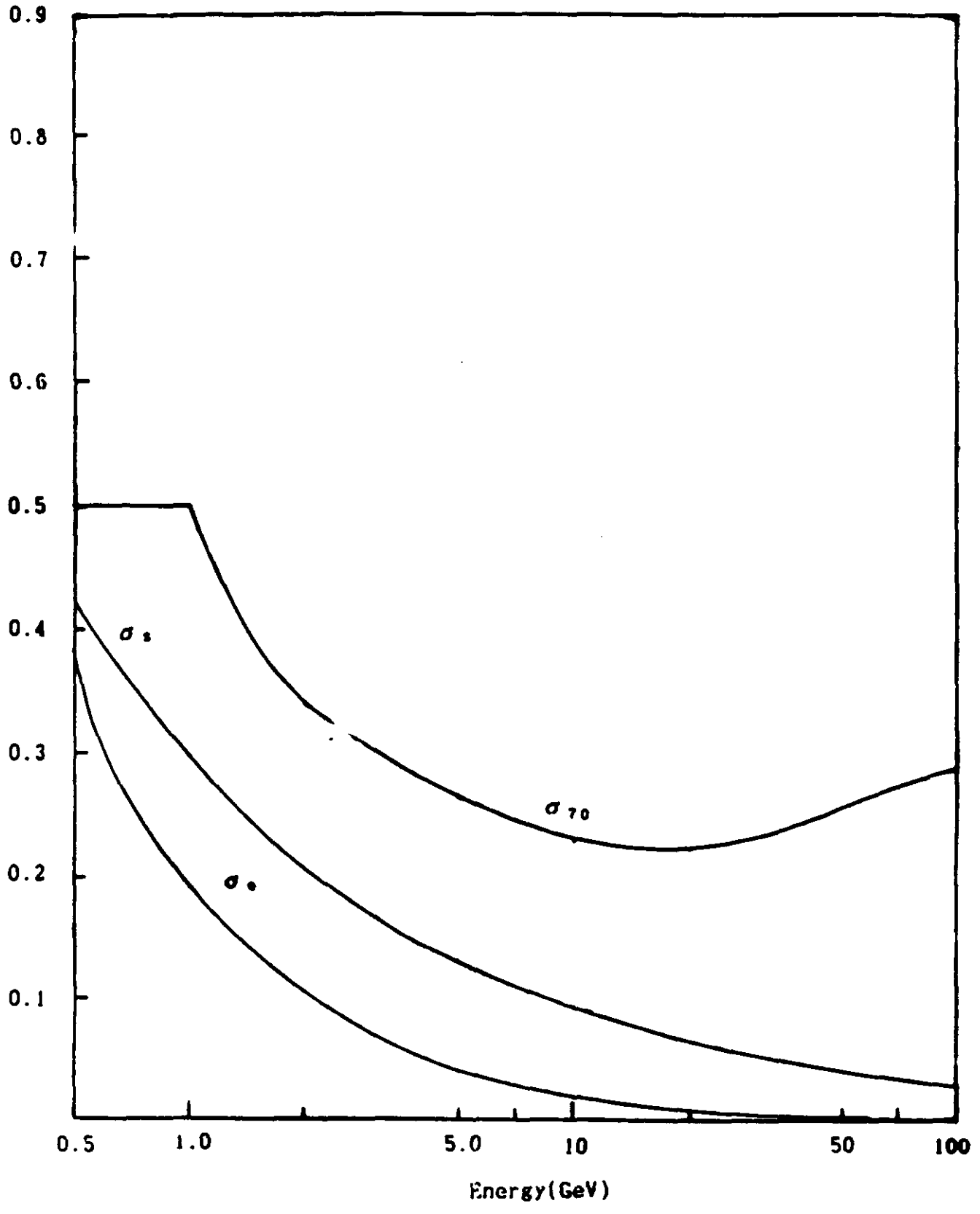
0.9
0.8
0.7
0.6
0.5
0.4
0.3
0.2
0.1
σ s
σ 70
σ e
0.5
1.0
5.0
10
50
100
Energy(GeV)

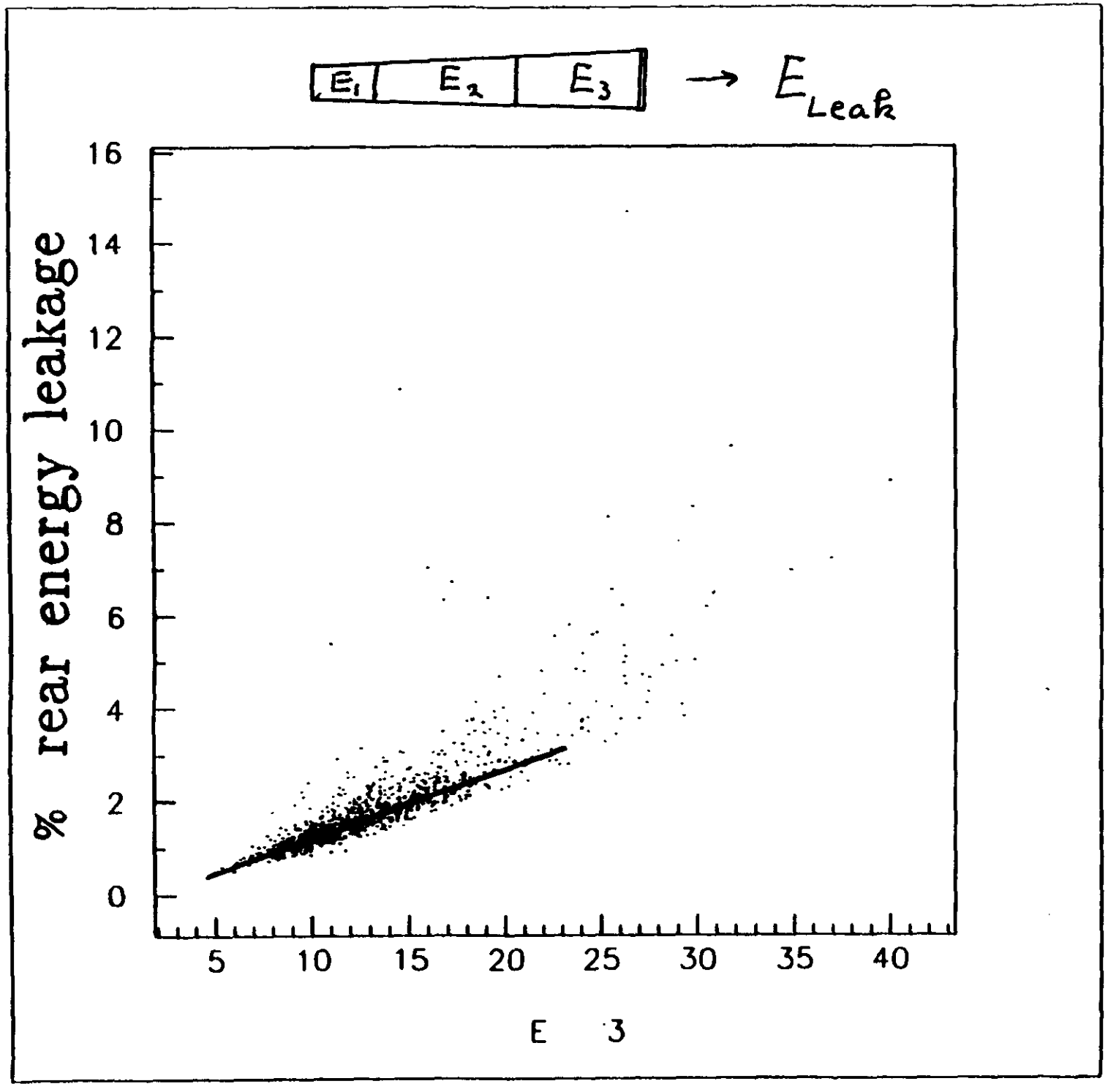
E1
E2
E3
→ E Leak
% rear energy leakage
16
14
12
10
8
6
4
2
0
5
10
15
20
25
30
35
40
E 3

Longitudinal shower profile
measures
the rear energy leakage:
$E = E_1 + E_2 + E_3 + C\, E_3/(E_1 + E_2)$.
Resolution before and after correction:
0.5% -> 0.25% for 100 GeV e
0.6% -> 0.3% for 100 GeV γ's

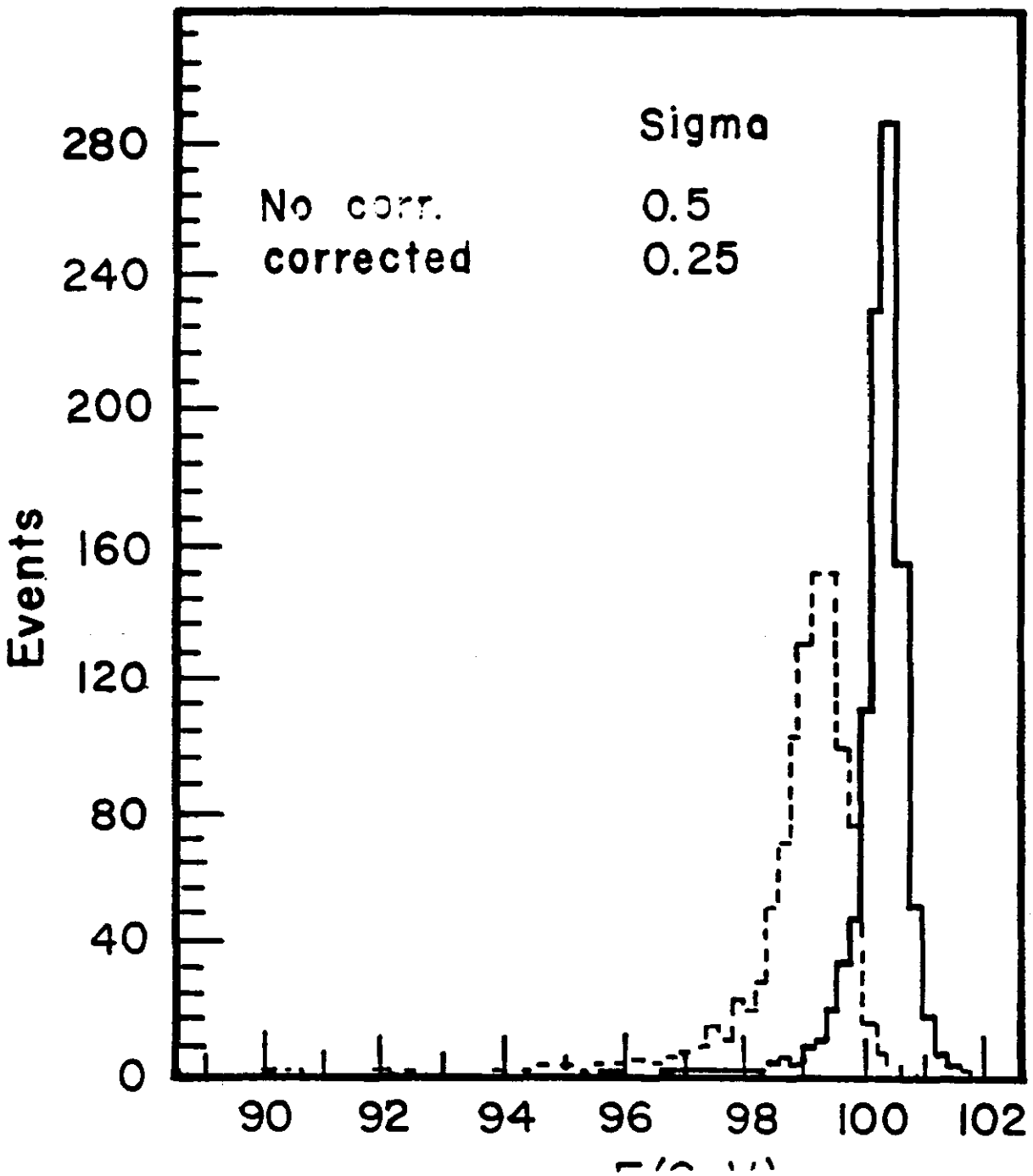

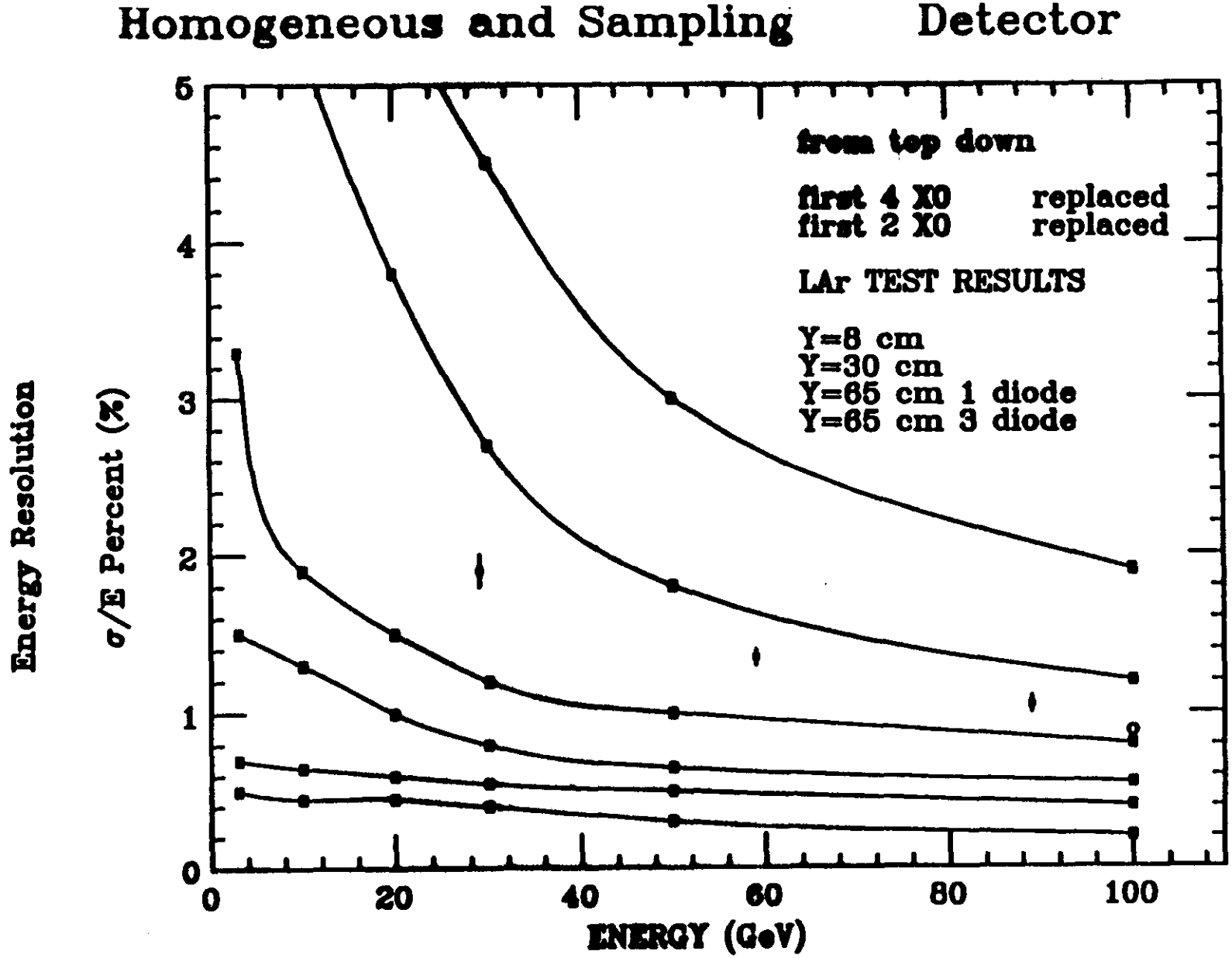

Fig. Resolution: Energy resolution of various EM calorimeters. The curves are for different calorimeters, ranging from bottom up (note all are GEANT except f and g.): a) homogenous LXe calorimeter with longitudinal sampling; b) homogenous LXe calorimeter with only 1 diode/cell; c) 30 cm homogeneous front section; d) Sandl (8 cm homogeneous front); e) recent data from Accordion at 100 GeV (open point); f) old data from Accordion (solid points); g) a sampling EM calorimeter with 1st 2 rad. dead; and h) a sampling

SandI SINGLE CELL AND SAMPLING AREA CROSS SECTION

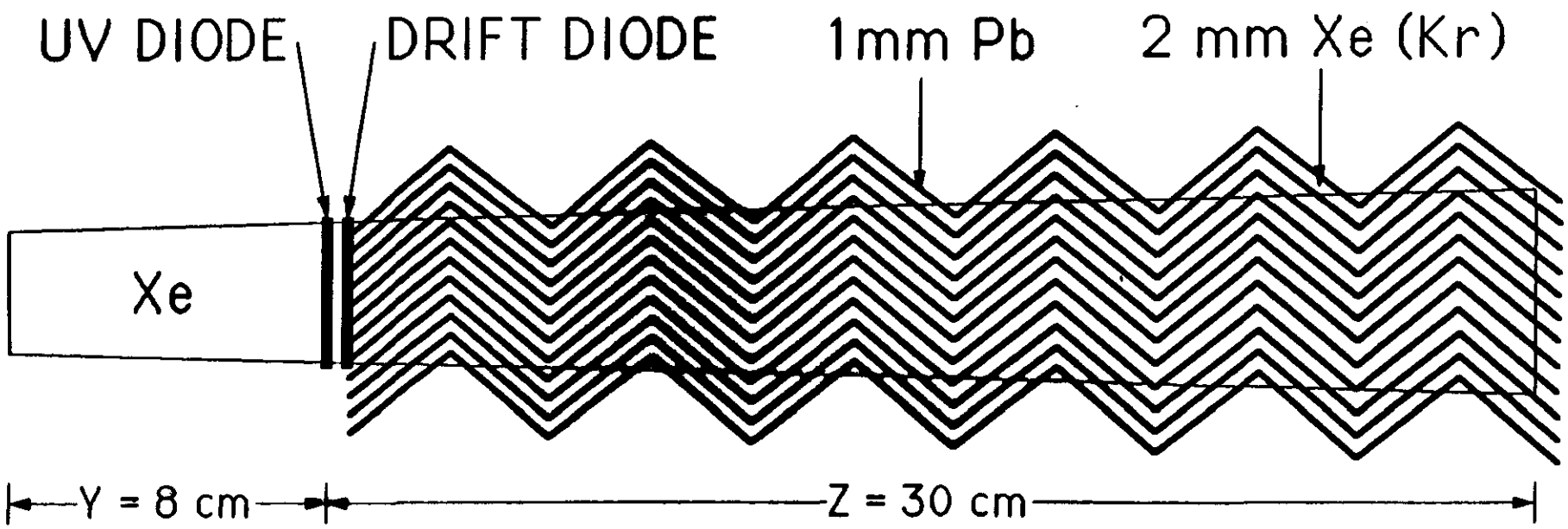

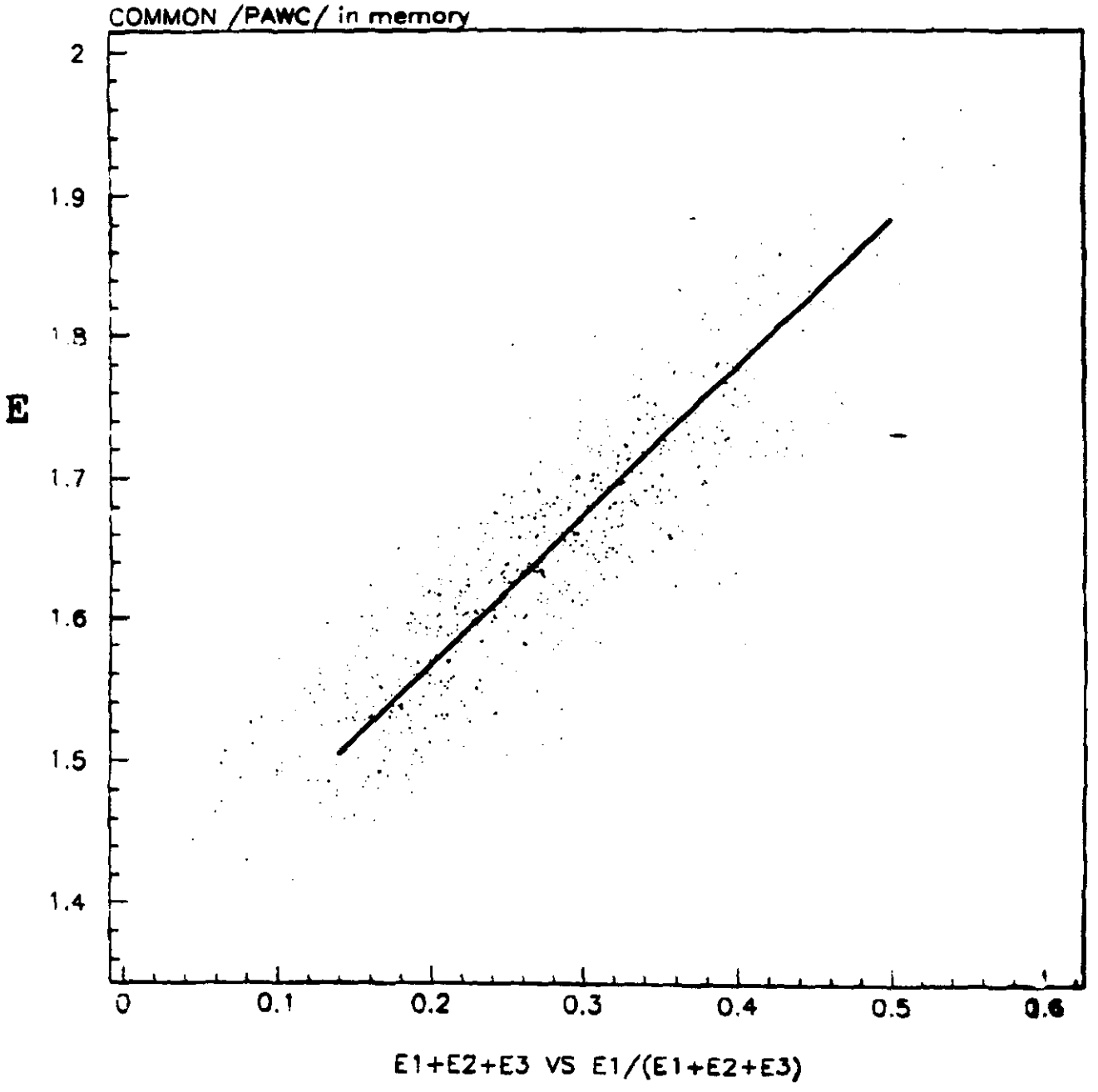
COMMON /PAWC/ in memory
E
2
1.9
1.8
1.7
1.6
1.5
1.4
0
0.1
0.2
0.3
0.4
0.5
0.6
E1+E2+E3 VS E1/(E1+E2+E3)

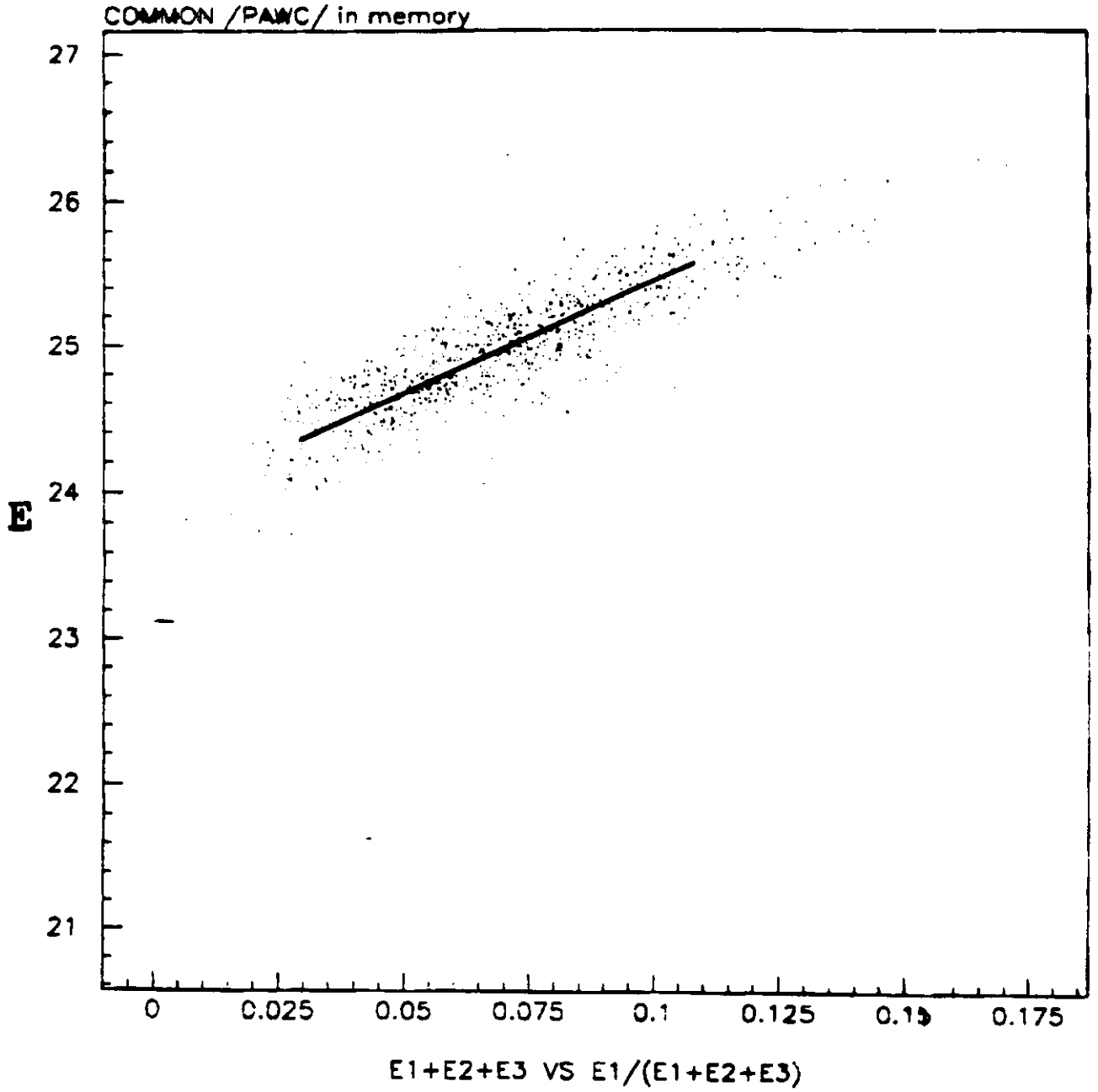
COMMON /PAWC/ in memory
27
26
25
24
23
22
21
E
0
0.025
0.05
0.075
0.1
0.125
0.175
E1+E2+E3 VS E1/(E1+E2+E3)

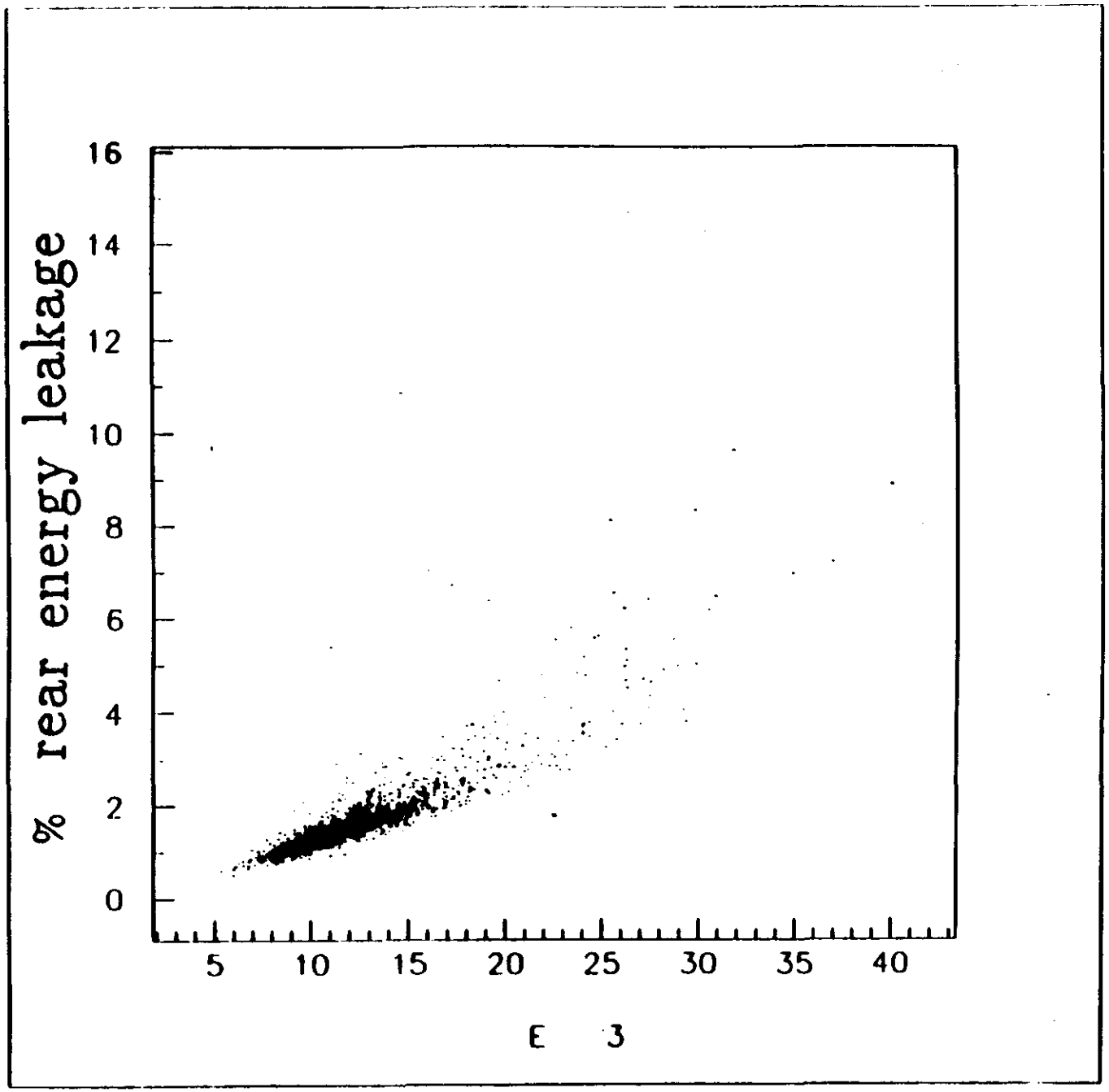
% rear energy leakage
16
14
12
10
8
6
4
2
0
5
10
15
20
25
30
35
40
E 3

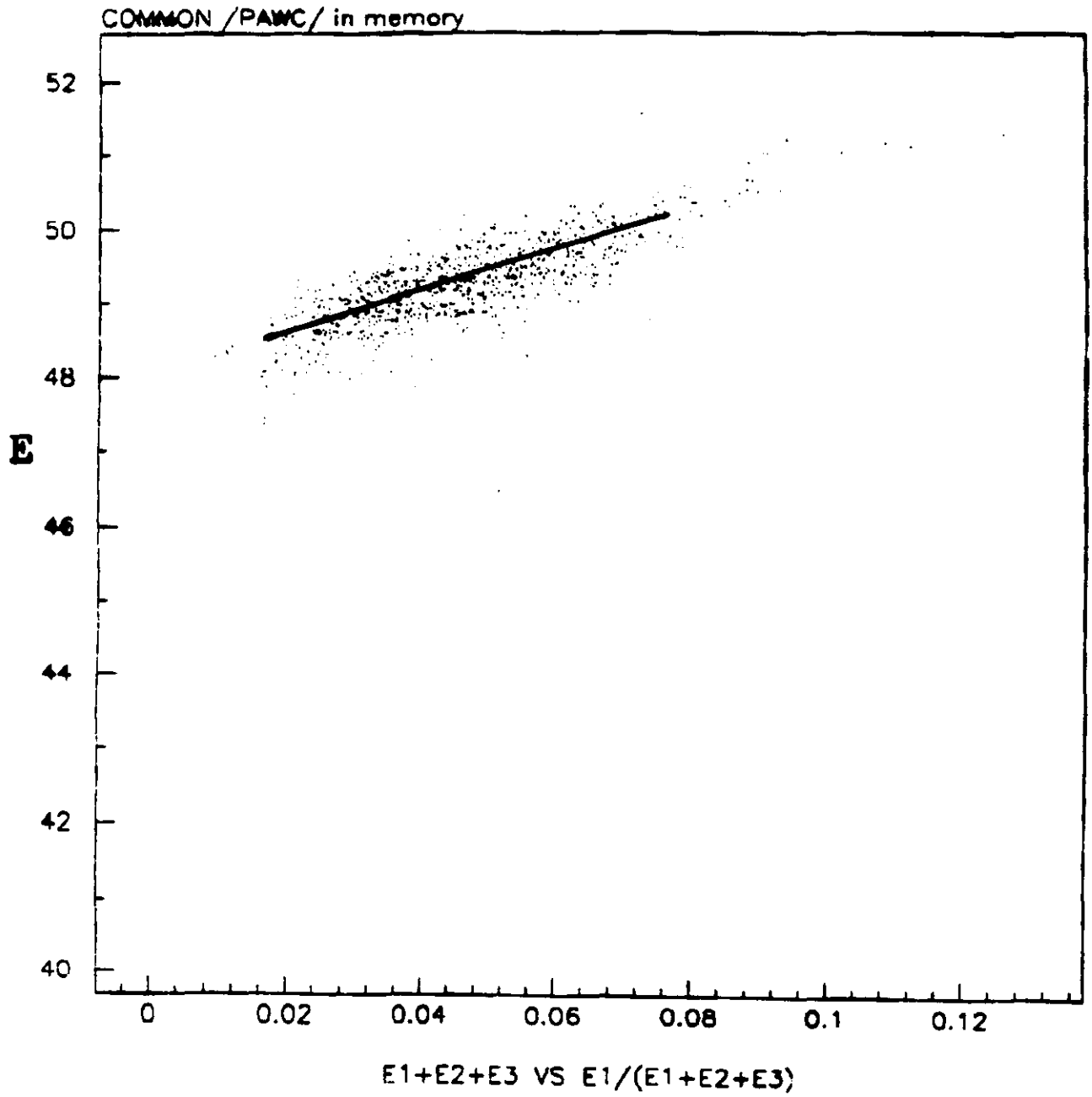
COMMON /PAWC/ in memory
52
50
48
E
46
44
42
40
0
0.02
0.04
0.06
0.08
0.1
0.12
E1+E2+E3 VS E1/(E1+E2+E3)

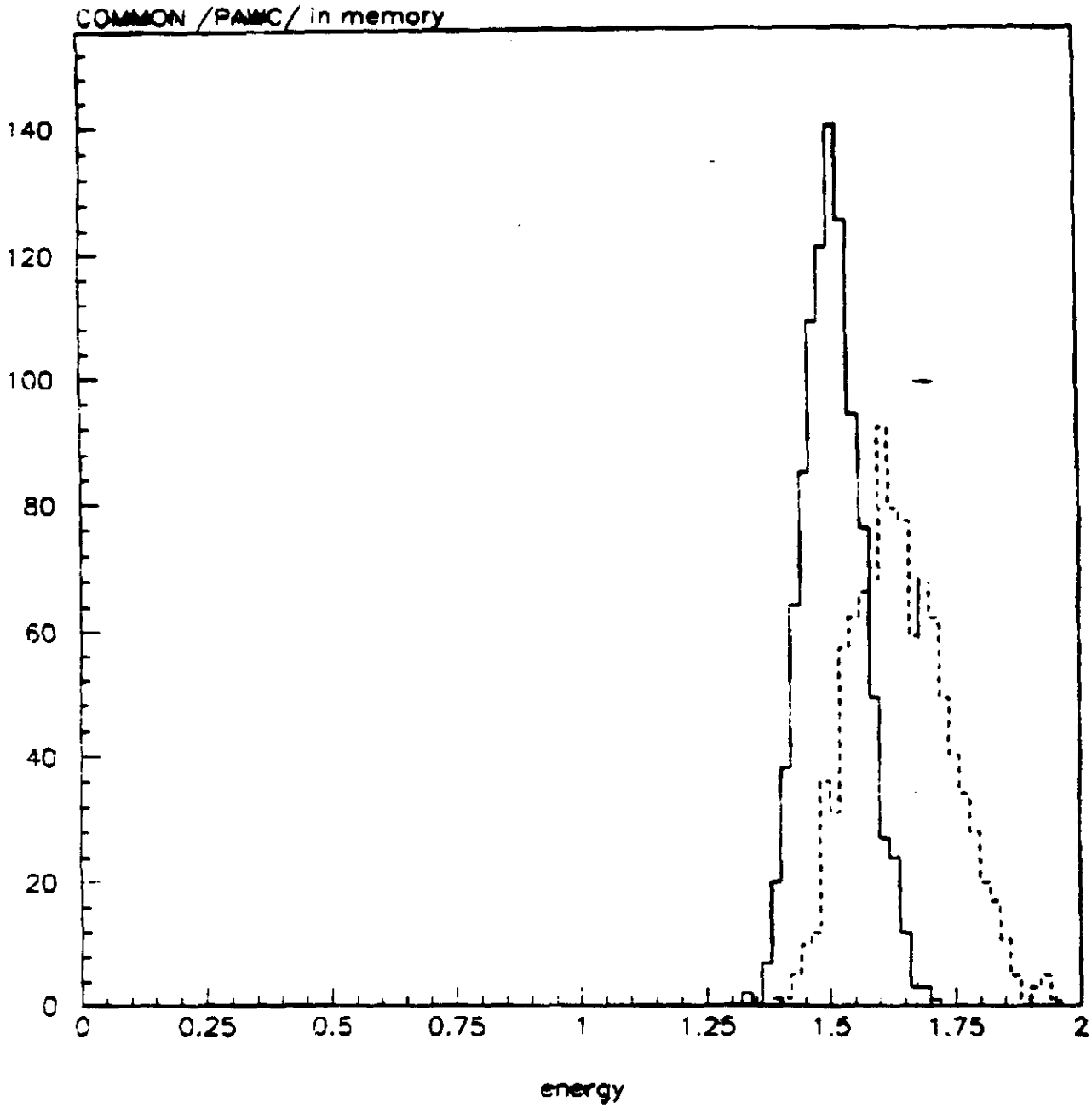
COMMON /PAWC/ in memory
140
120
100
80
60
40
20
0
0
0.25
0.5
0.75
1
1.25
1.5
1.75
2
energy

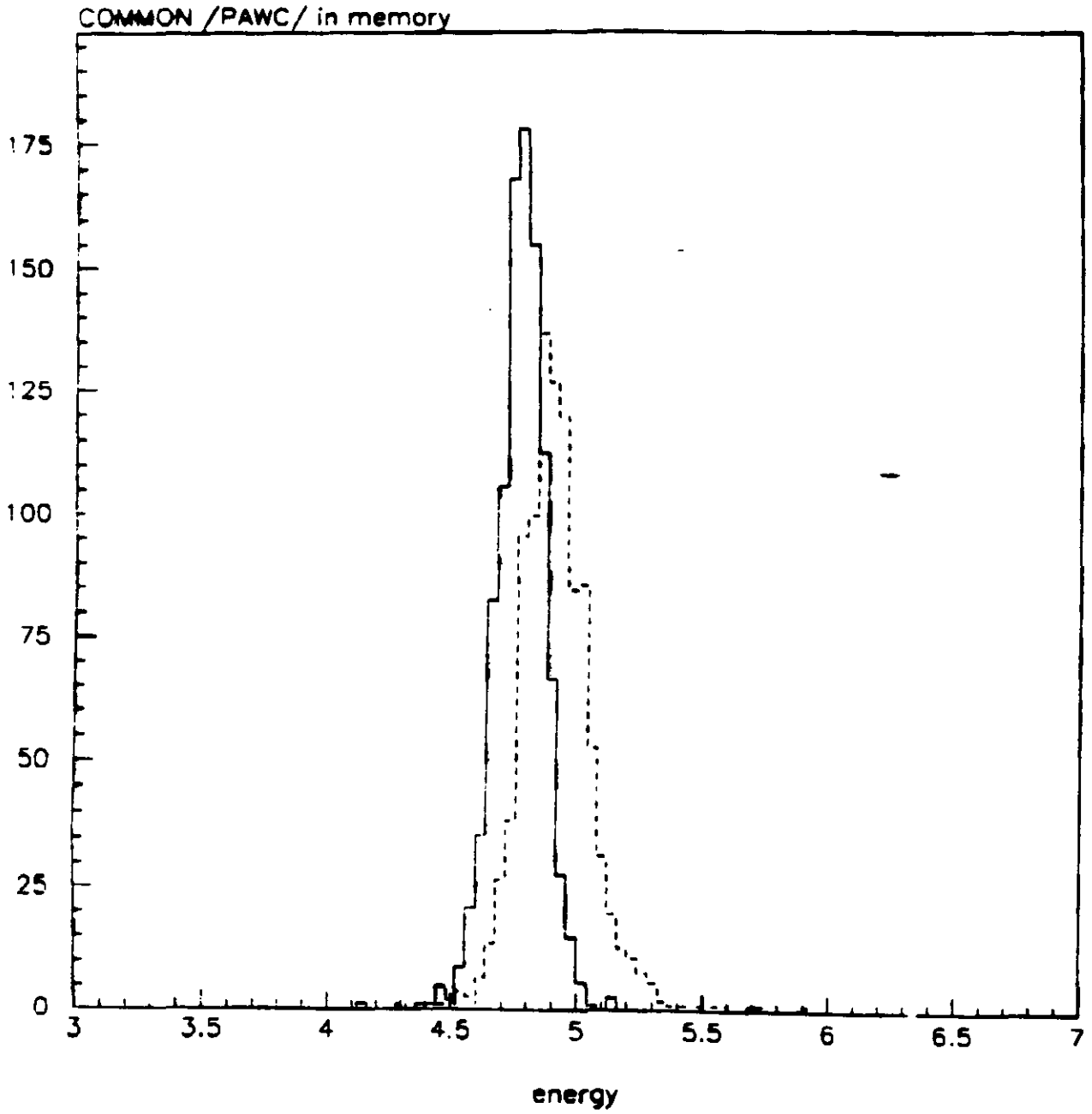
COMMON /PAWC/ in memory
175
150
125
100
75
50
25
0
3
3.5
4
4.5
5
5.5
6
6.5
7
energy

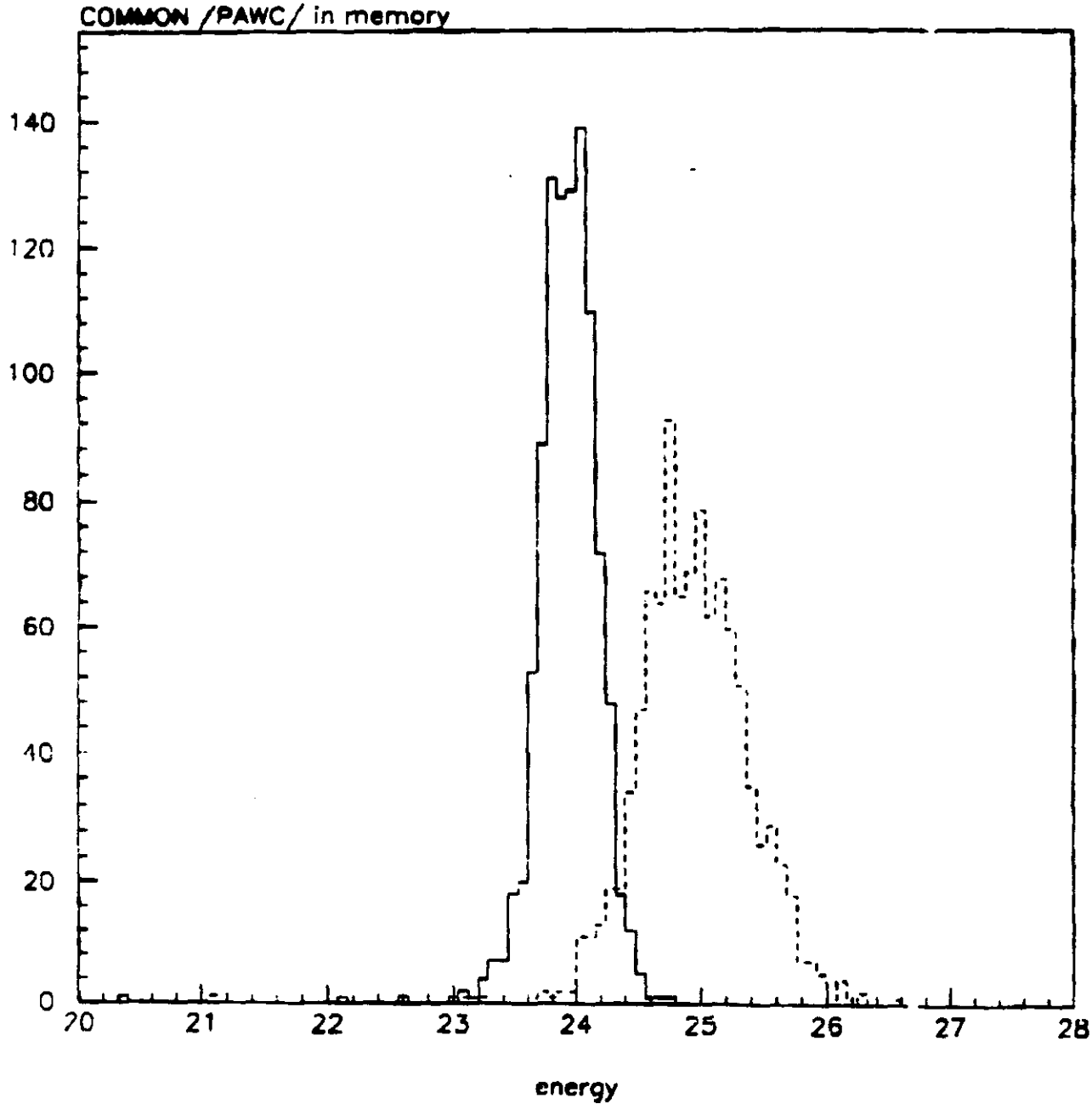
COMMON /PAWC/ in memory
140
120
100
80
60
40
20
0
20
21
22
23
24
25
26
27
28
energy

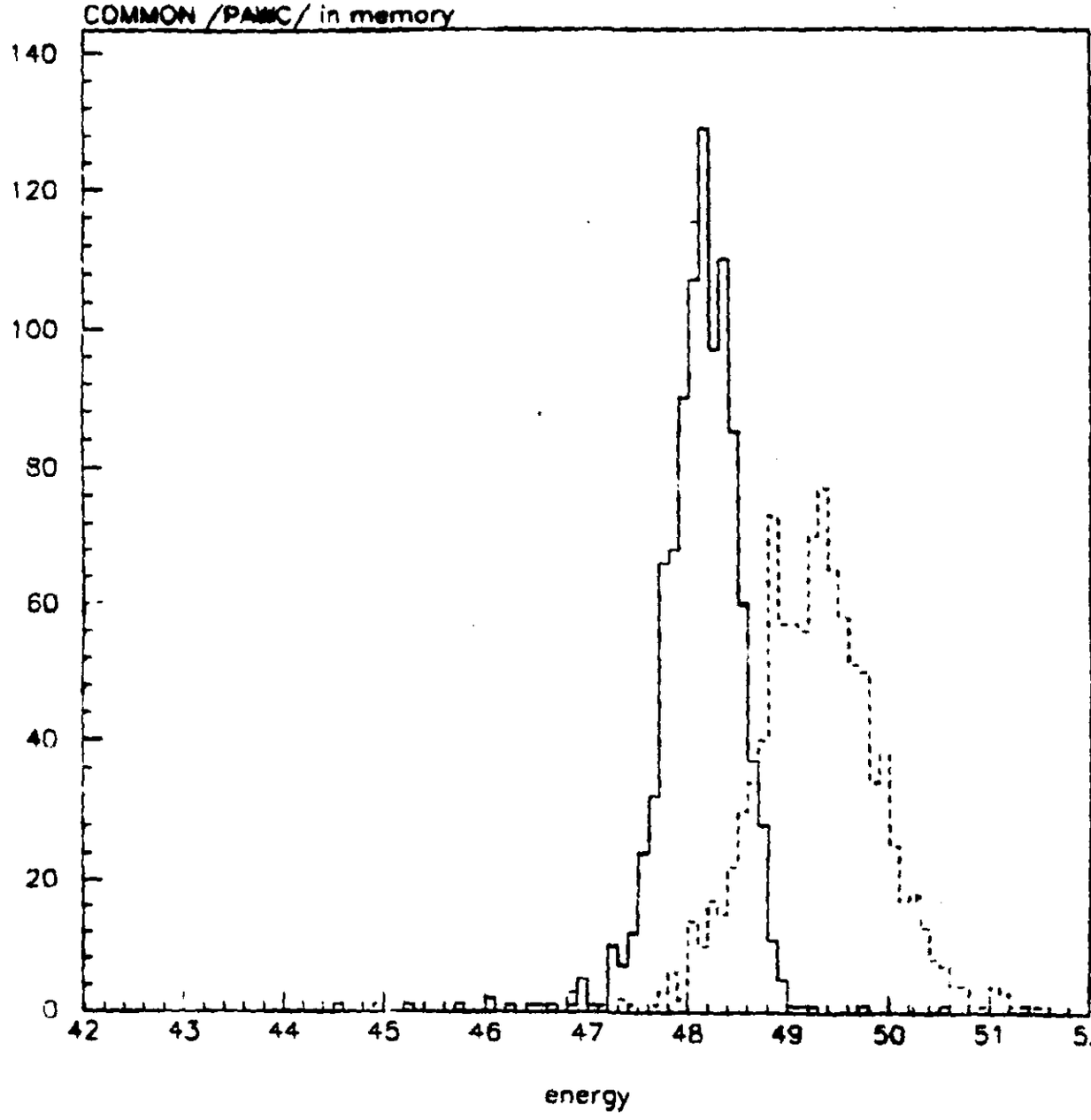
COMMON /PAWC/ in memory
140
120
100
80
60
40
20
0
42
43
44
45
46
47
48
49
50
51
52
energy

Homogeneous and Sampling LXe Detector

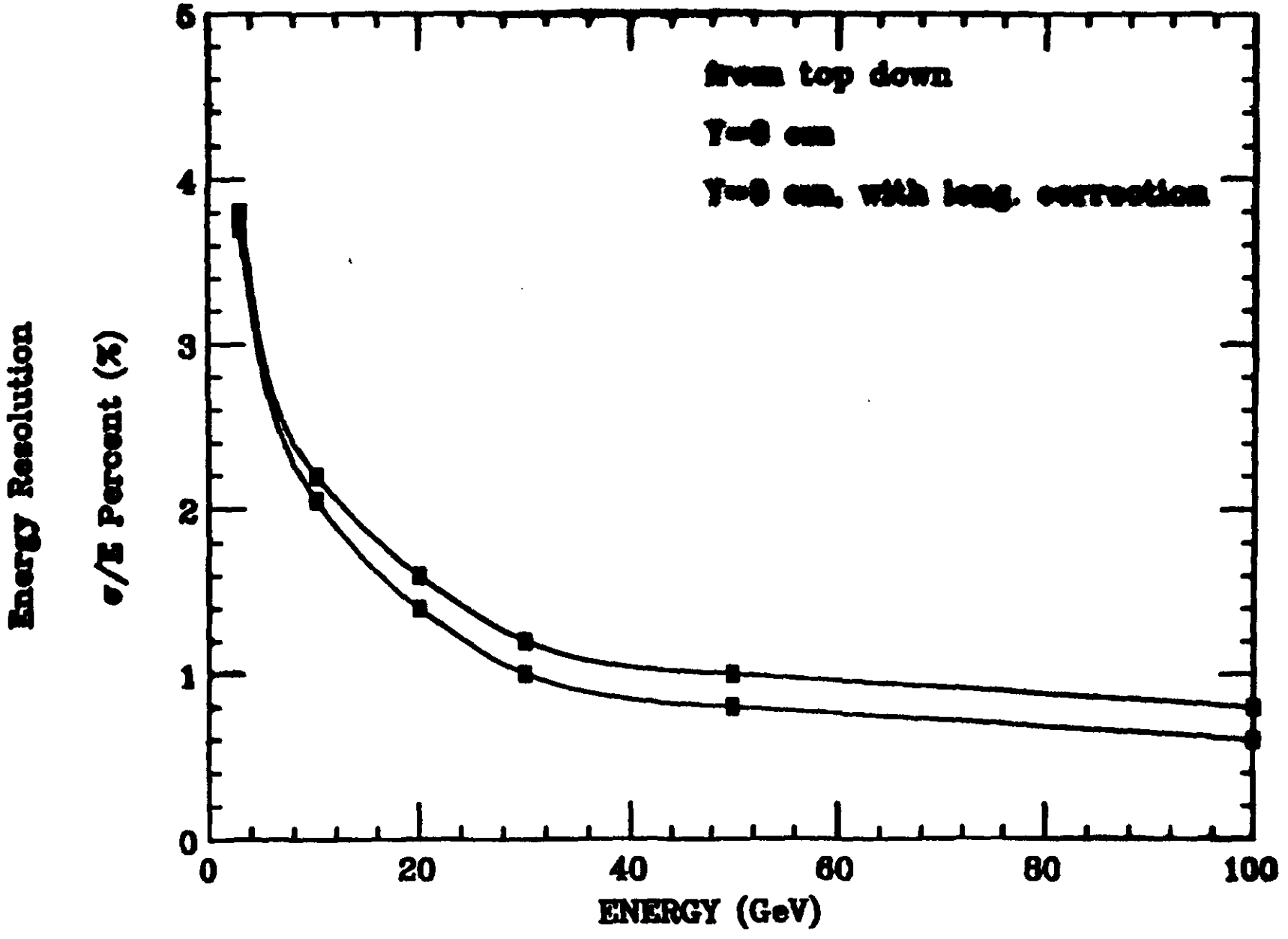

Side View of one quadrant of Sandl LXe EM detector

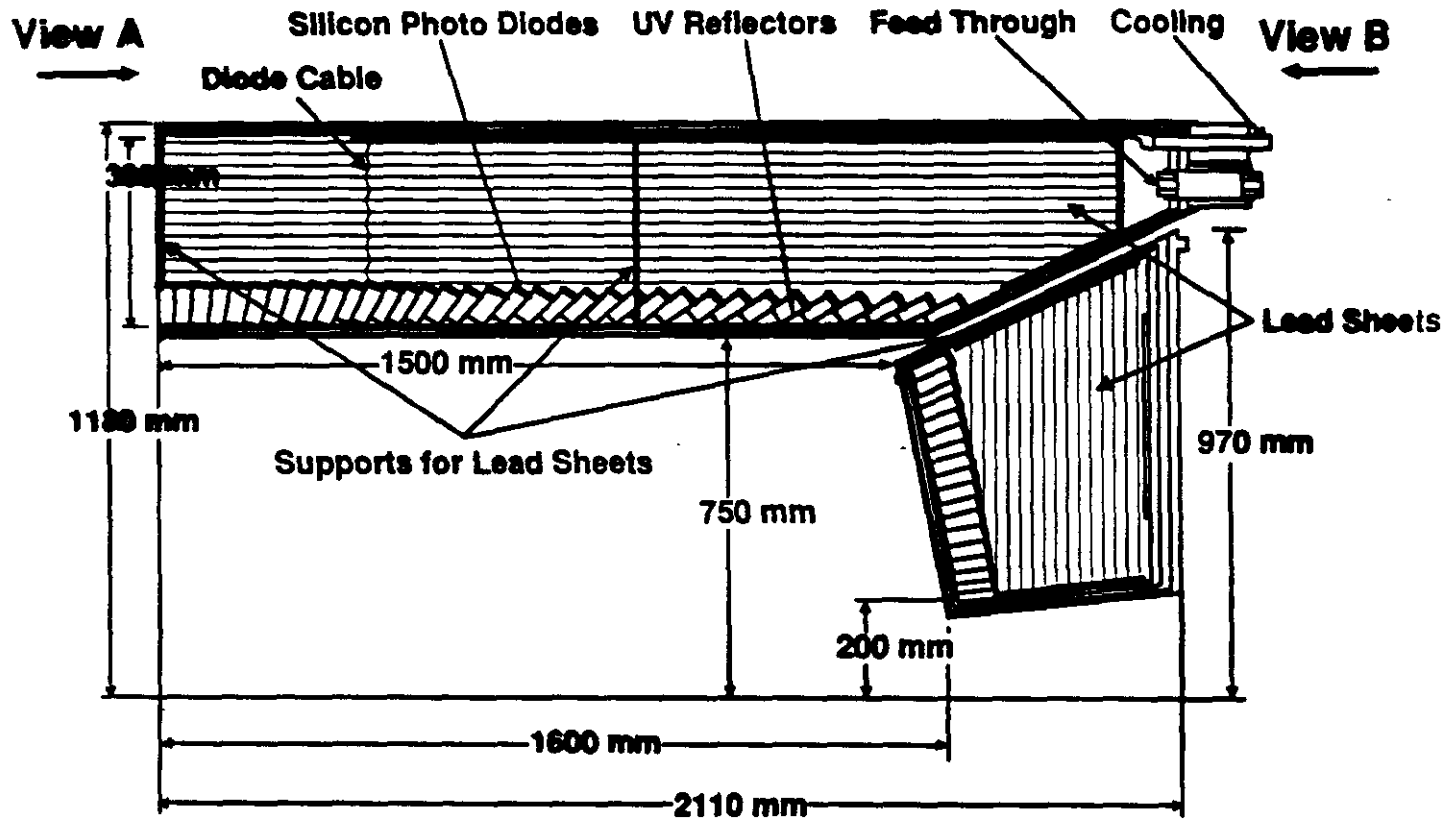

End Views

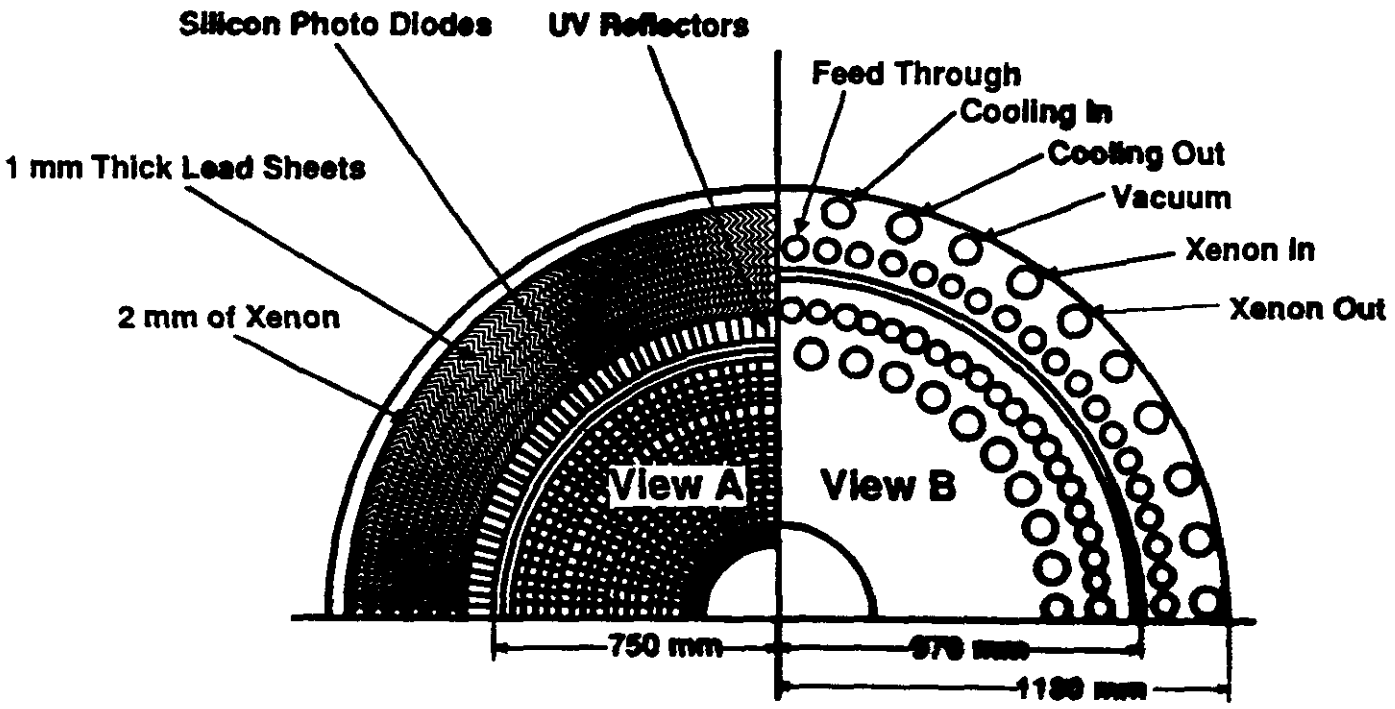

Question (3b) What uniformity has been measured when varying the incident position of particles across the front face of modules?

We are in the process of optimizing the UV reflectors to achieve uniformity. We note the following:

1. Liquids, unlike solids, are homogeneous due to diffusion.

2. Diodes are uniformly covered due to the very large numbers of photons emitted.

3. Transverse non-uniformity occurs primary due to the material in UV reflectors.

4. Uniformity for 65 cm LXe retains for 10, 13 and 15 mm see Fig. xxx, The nonuniformity is less than 1% at the very edge of the cell, which can be corrected to retain the energy resolution ($<< 0.5\%$).

Existing large uv-photodiodes are limited:

1. Low quantum efficiency if with a front window;
2. Large *RC* time if windowless.

Si Photodiode

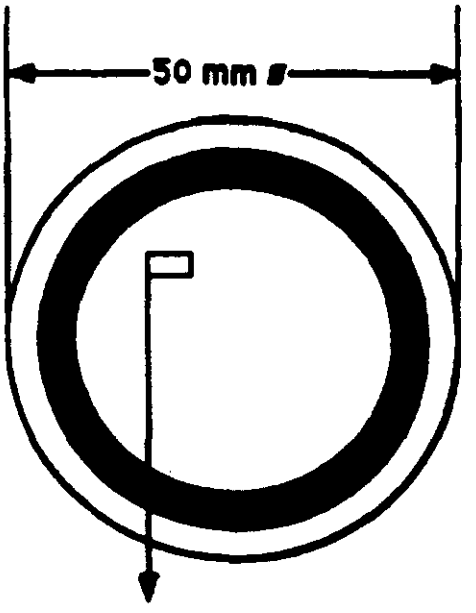

400 μ Si wafer

diameter as needed for L*

20 nm Au mesh

as transparent contact

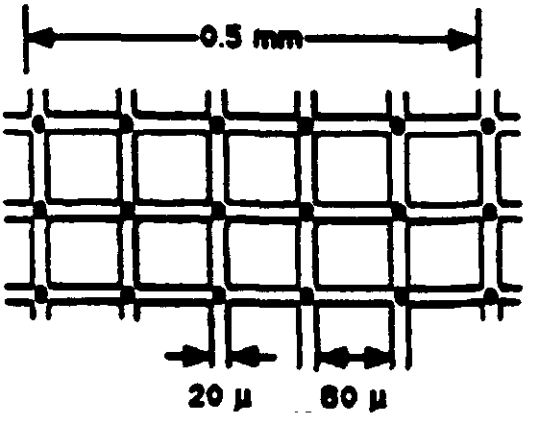

quantum efficiency

η (λ = 170 nm) > 50%

peaking time

$t_{10\text{-}90\%}$ 10 ns

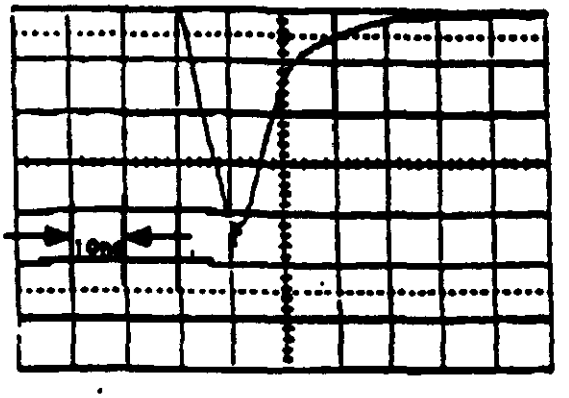

5. Reflection: MgF_2 mirrors are stable and radiation hard and can be i tored by α's after being checked with VUV spectrometer.

STRUCTURE OF PC LAYER MIRROR

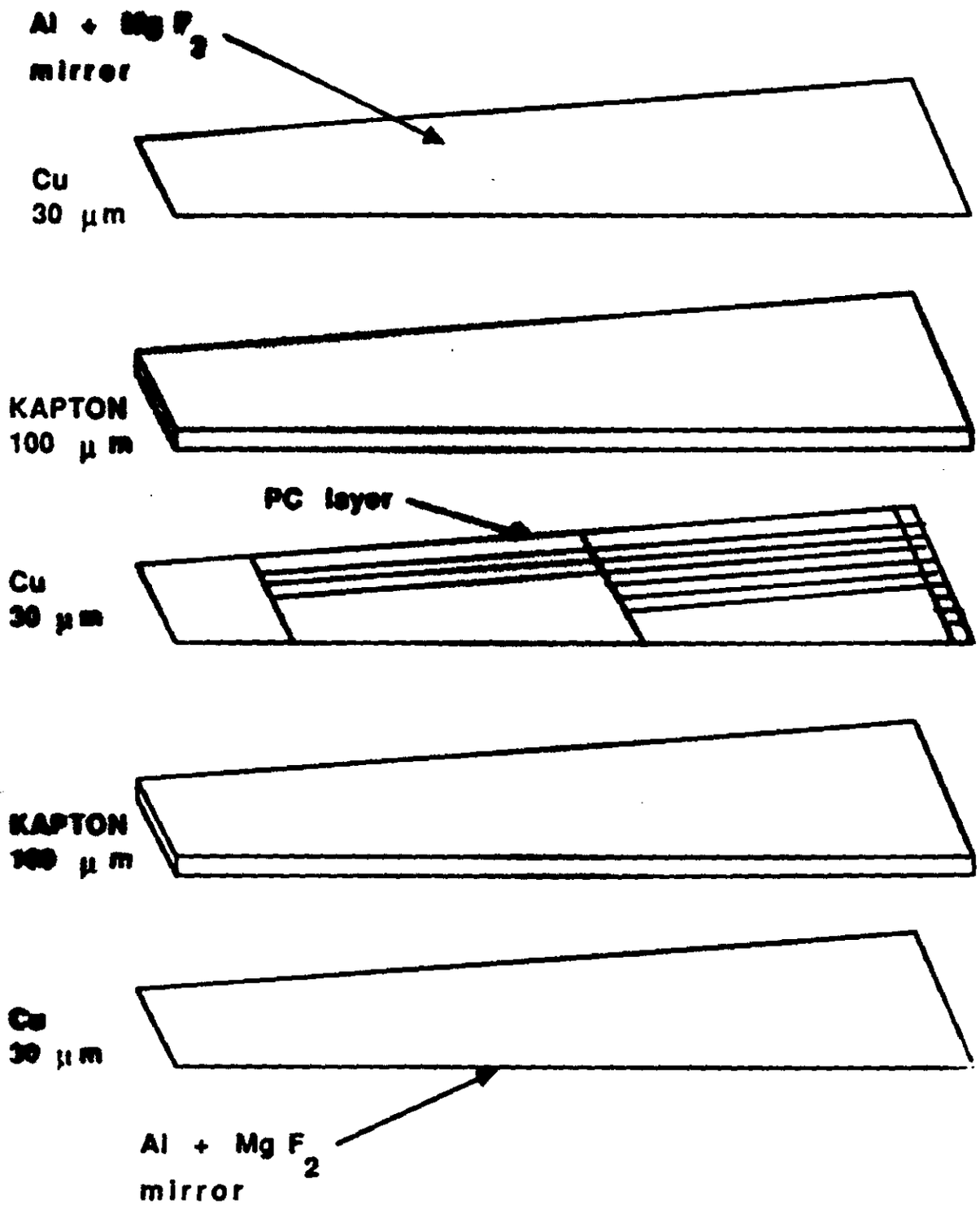

Arrangement of Diodes, Amplifiers, and UV Mirrors (printed boards) for the 5 × 5 LXe Prototype Detector

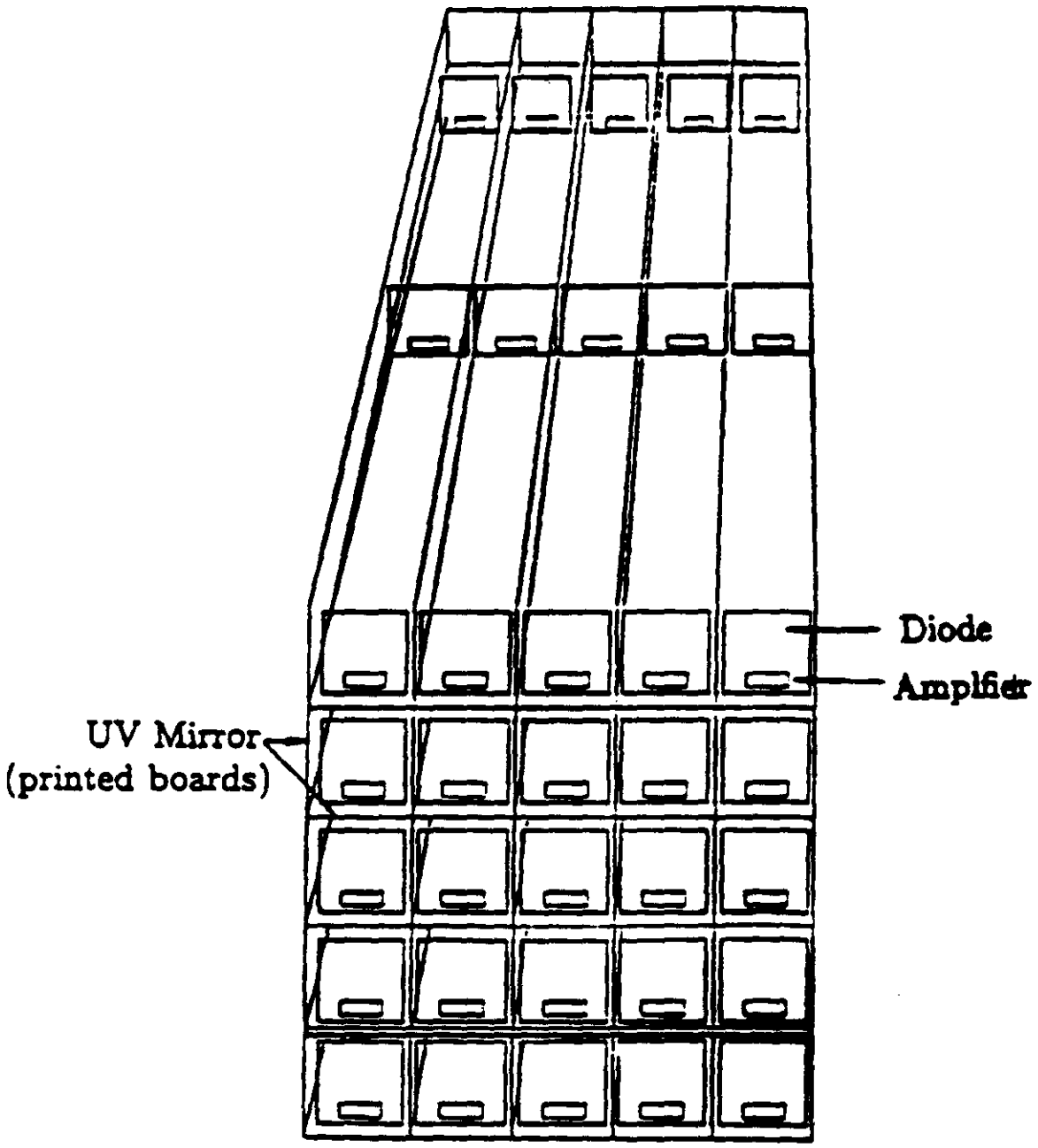

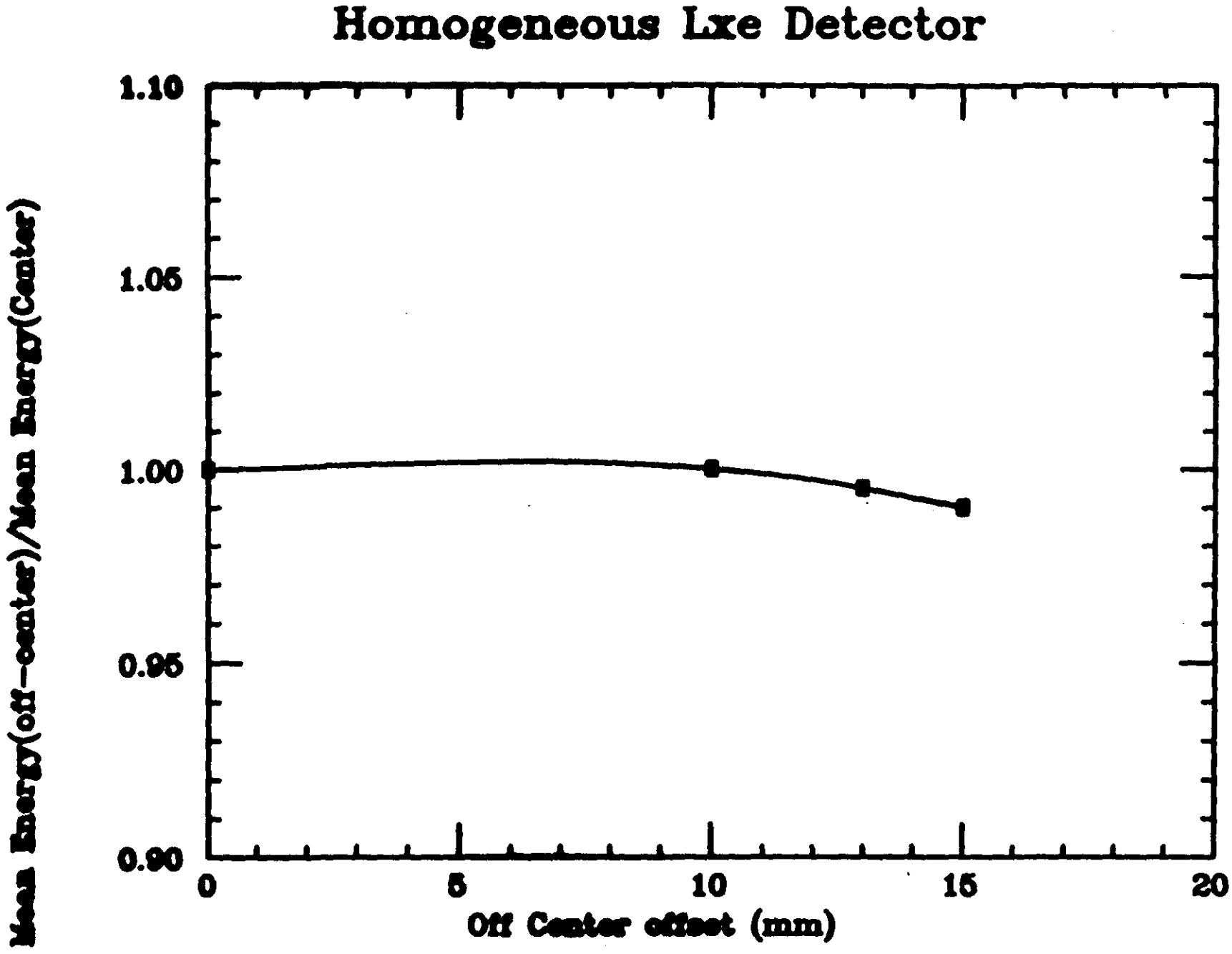
Homogeneous Lxe Detector
1.10
1.05
1.00
0.95
0.90
0
5
10
15
20
Off Center offset (mm)
Mean Energy(off-center)/Mean Energy(Center)

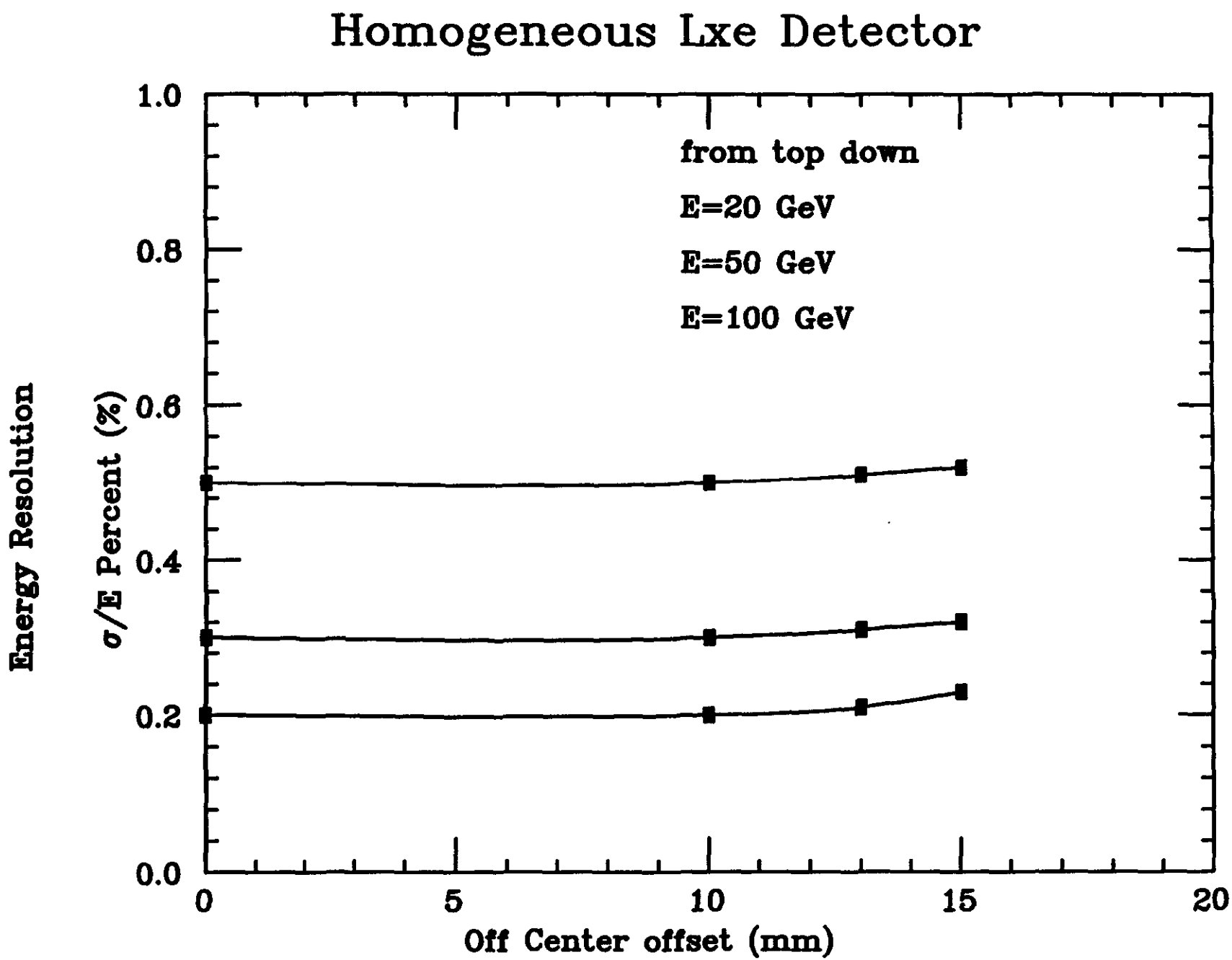
Homogeneous Lxe Detector
from top down
E=20 GeV
E=50 GeV
E=100 GeV
Energy Resolution
σ/E Percent (%)
1.0
0.8
0.6
0.4
0.2
0.0
0
5
10
15
20
Off Center offset (mm)

UV-Reflectors:
Mean reflectivity = 88% at 170 nm

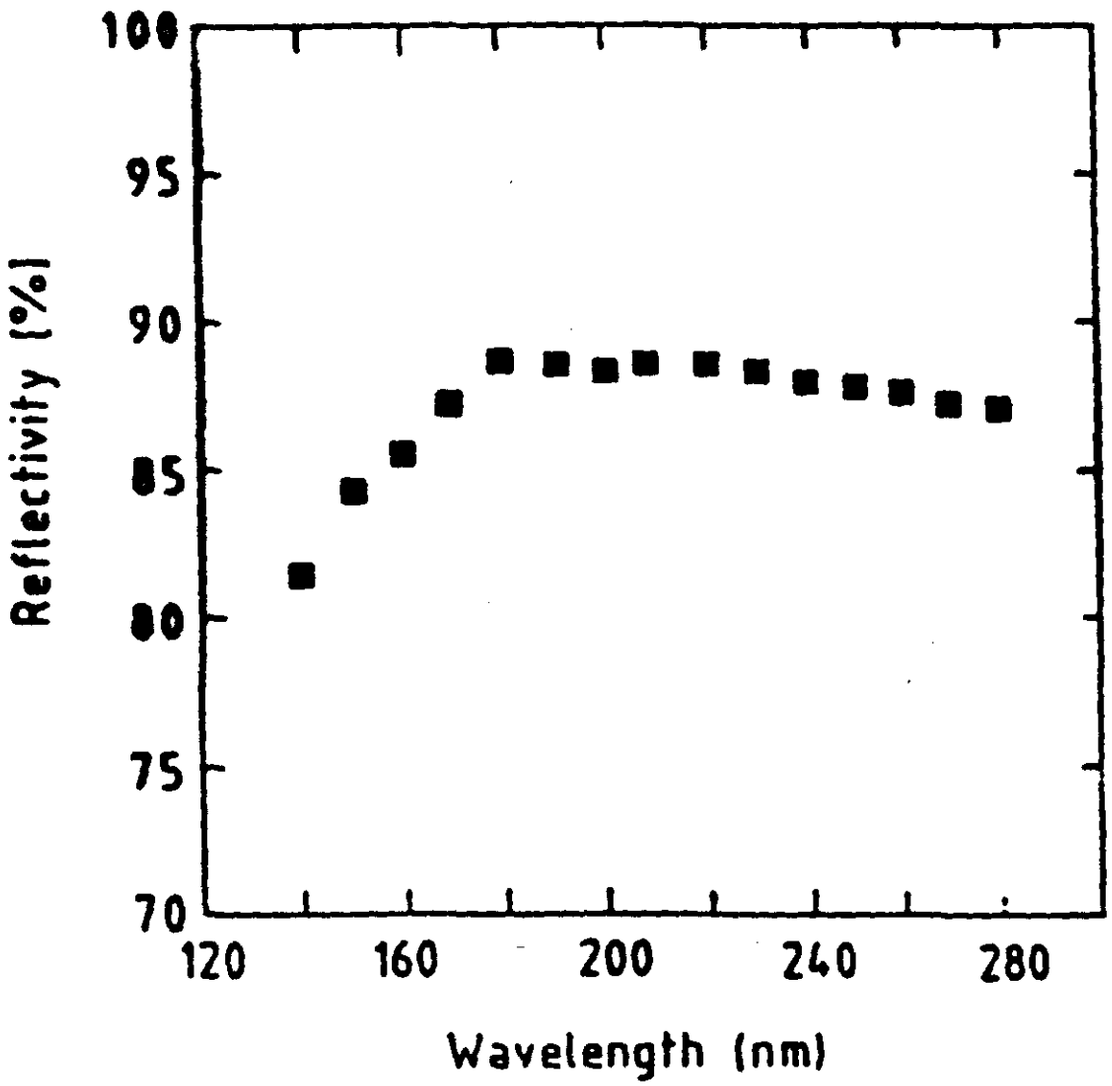

Average reflectivity as a function of wavelength for 300 mirrors as measured at CERN

RICH in DELPHI

3. **Examples: A single 66 cm long cell:**

- 1. **For diode without coating, i.e.** N_{Si} = 3.5, Rb=0.5, Rs=0.88, Dtop=1.0 cm, Db=0.3 cm, λ = 300 cm, D.R. = 12Fig. 2.6 shows that acceptance 25% ± 1.2% *or* < 5% deviation.
- 2. For diode with SiO2 coating, N_{SiO2}=1.55, Rb= 0.8 , Rs= 0.8, Dtop=0.0 cm, Db=0.5 cm, λ = 300 cm, D.R. = 20Fig 2B.9 shows that acceptance 26.2% ± 0.4% *or* < 1.5% deviation.

4. 26 cm case

- 1. For diode without coating, i.e. N_{Si} = 3.5, Rb=0.88, Rs=0.88, Dtop=0.3 cm, Db=0.0 cm, λ = 300 cm, D.R. = 12Fig. 4.1 shows that acceptance 42% ± 1.5% or < 4% deviation.
- 2. For diode with SiO2 coating, N_{SiO2}=1.55, Rb= 0.75 , Rs= 0.8, Dtop=0.0 cm, Db=0.7 cm, λ = 300 cm, D.R. = 20Fig 4B.1 shows that acceptance 29.5% ± 0.6% or < 2% deviation.

5. 8 cm case

- 1. For diode without coating, i.e. N_{Si} = 3.5, Rb=0.85, Rs=0.80, Dtop=0.2 cm, Db=0.0 cm, λ = 300 cm, D.R. = 20Fig. 3.16 shows that acceptance 48% ± 1% or < 2% deviation.
- 2. For diode with SiO2 coating, N_{SiO2}=1.55, Rb= 0.65 , Rs= 0.65, Dtop=0.0 cm, Db=0.5 cm, λ = 300 cm, D.R. = 35Fig 3B.11 shows that acceptance 31% ± 0.2% or < 0.6% deviation.

6. Uniformity for [illegible]

Light Acceptance VS Dist. from Photo Diode

Fig 2B.9

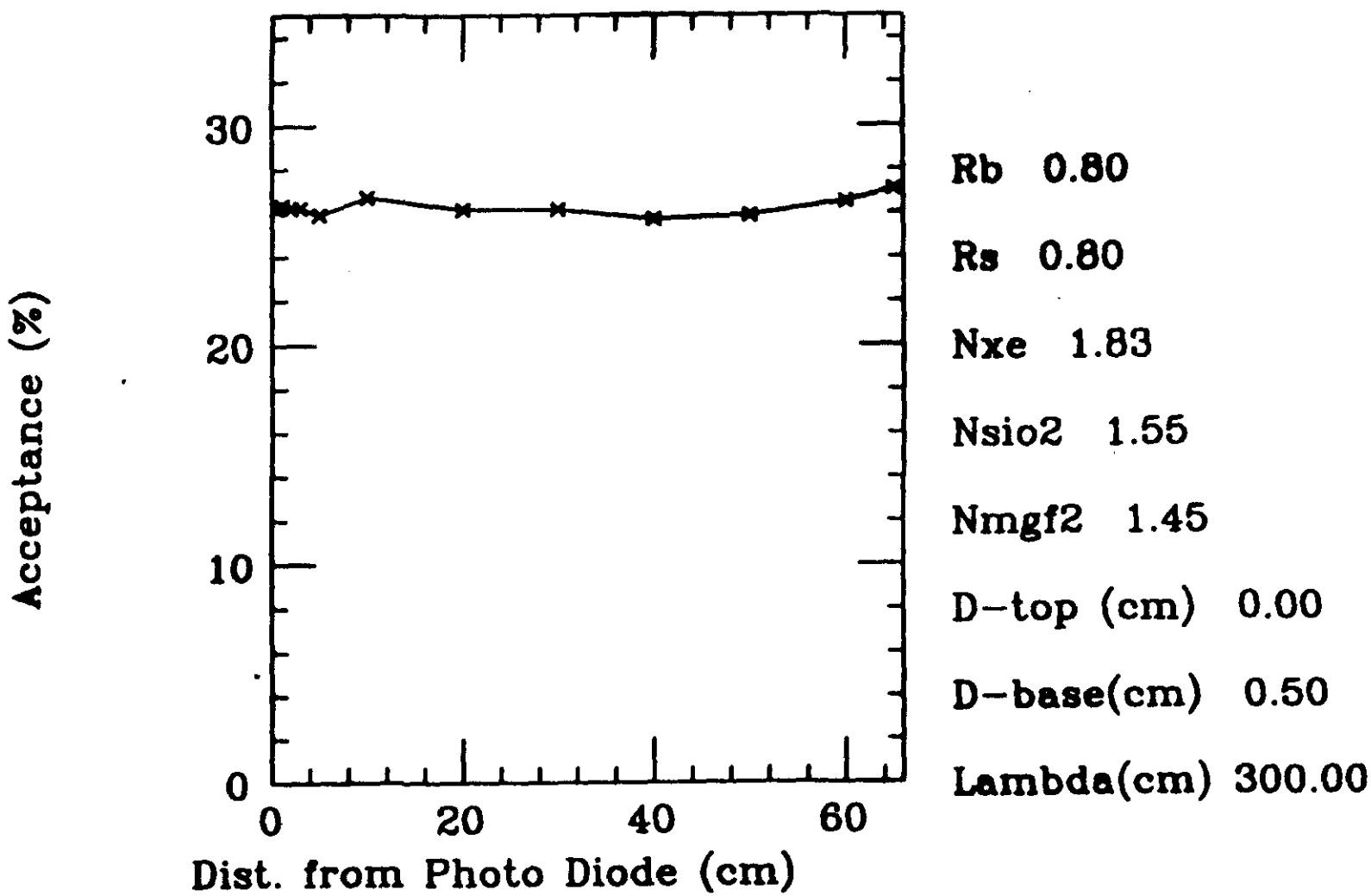

Light Acceptance VS Dist. from Photo Diode

Fig. 3.1

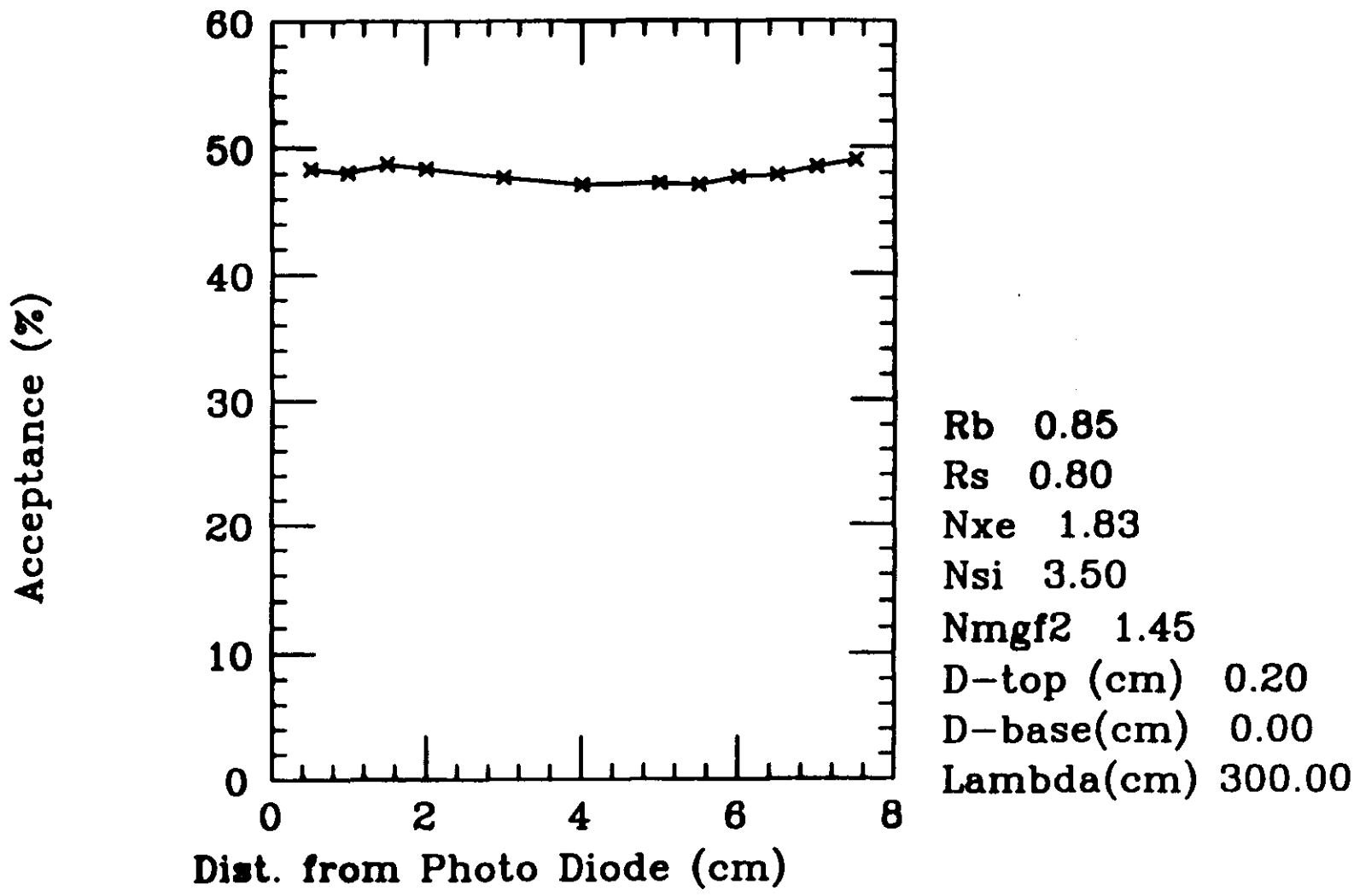

Light Acceptance VS Dist. from Photo Diode

Fig. 4.1

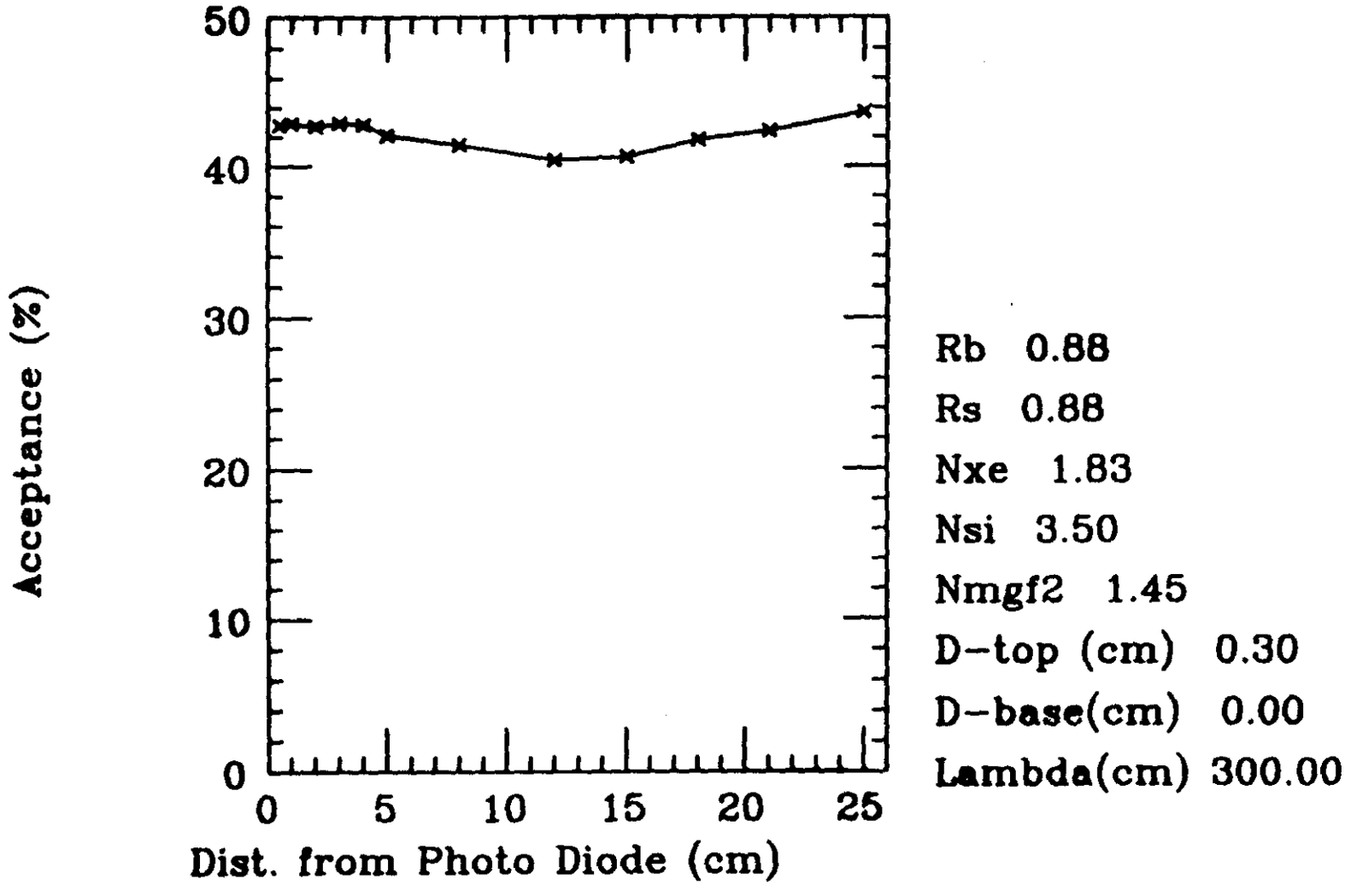

Light Acceptance VS Dist. from Photo Diode

Fig 3B.11

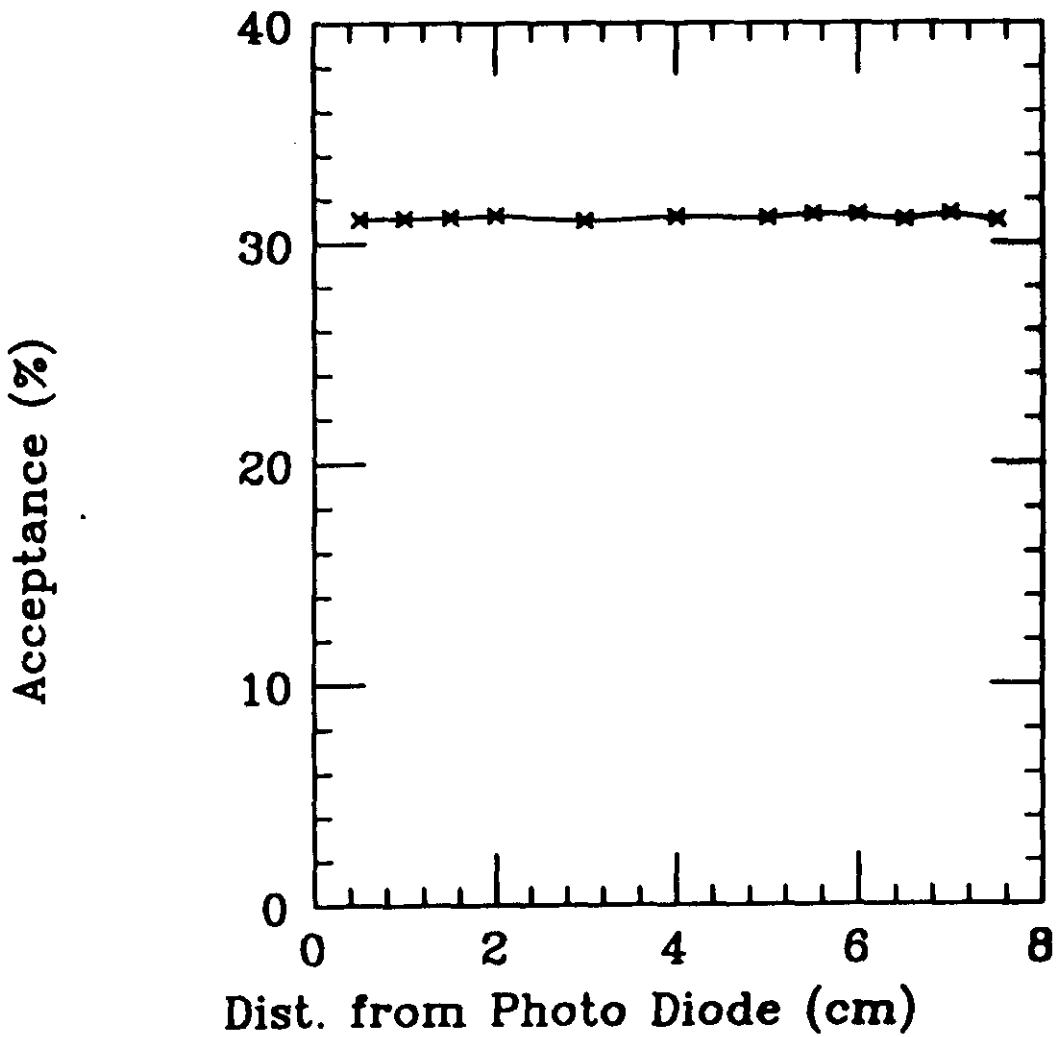

Rb 0.65

Rs 0.65

Nxe 1.83

Nsio2 1.55

Nmgf2 1.45

D-top (cm) 0.00

D-base(cm) 0.50

Lambda(cm) 300.00

Light Acceptance VS Dist. from Photo Diode

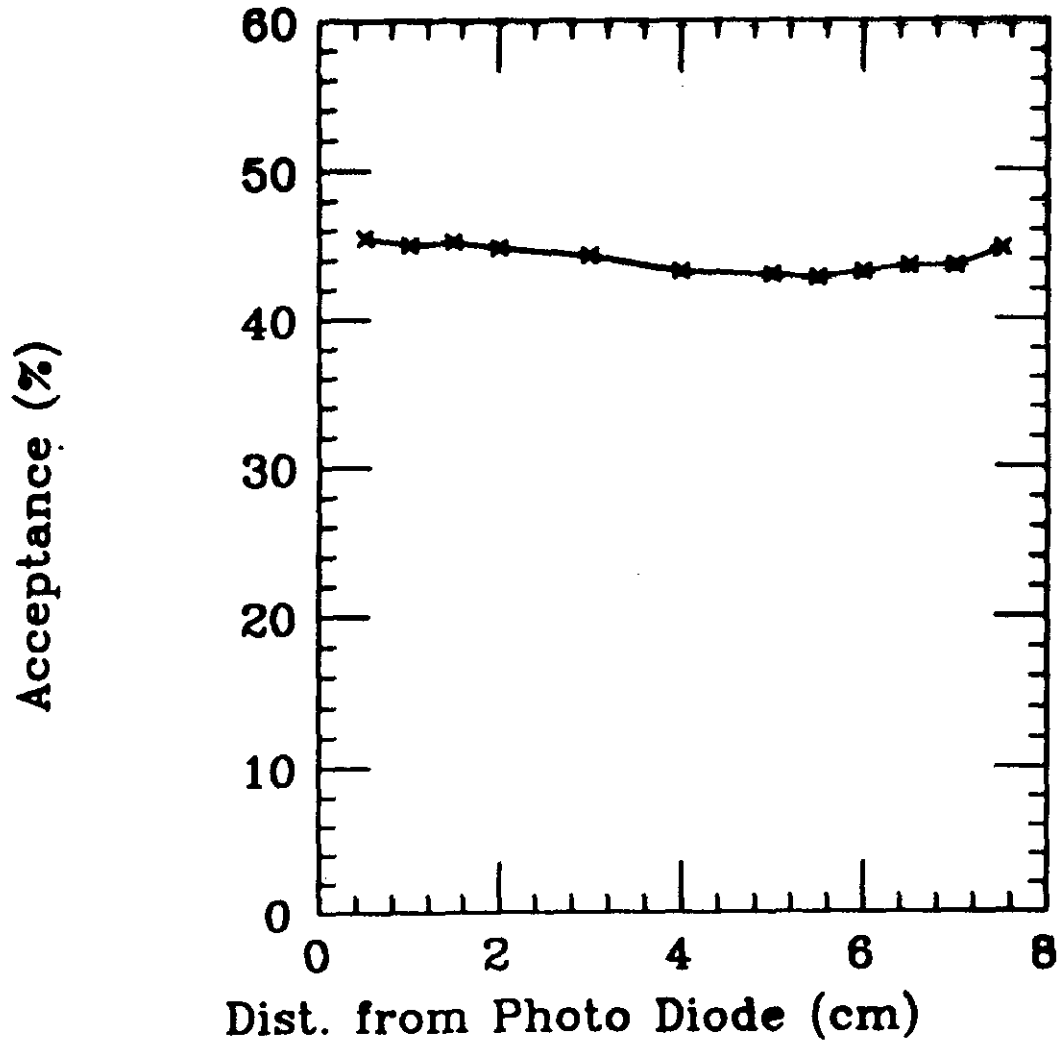

Fig. 3.8

Rb 0.85
Rs 0.80
Nxe 1.83
Nsi 3.50
Nmgf2 1.45
D-top (cm) 0.20
D-base(cm) 0.00
Lambda(cm) 100.00

Light Collection Acceptance
& Deviation in LXe cells **With diodes coated with SiO_2**

L	Liq	Rs	Rb	Db	λ	D.R.	Uniform
66cm	Xe	0.8	0.8	0.5 cm	300cm	20	26.2% ± 0.4%
66cm	Xe	0.88	0.88	0.0 cm	100cm	20	22.8% ± 1.2%
26cm	Xe	0.8	0.75	0.7 cm	300cm	20	29.5% ± 0.6%
26cm	Xe	0.8	0.75	0.5 cm	100cm	20	28.2% ± 0.4%
8cm	Xe	0.65	0.65	0.5 cm	300cm	35	31% ± 0.2%

Conclusions:

Uniform can be achieved for:

- Attenuation length $\lambda = 2 \pm 1$ m;
- Reflectivity of mirrors Rs = 75 to 88 %.
- Diffusion 20%, or
- Surface not very critical.

Light Collection Acceptance
& Deviation in LXe cells

With bare Si diodes.

L	Liq	Rs	Rb	Dt	Db	λ	D.R.	Uniform
66cm	Xe	0.88	0.5	1.0cm	0.3 cm	300cm	12	25% ± 1.2%
26cm	Xe	0.88	0.88	0.3cm	0.0 cm	300cm	12	42% ± 1.5%
26cm	Xe	0.88	0.88	1.0cm	0.0 cm	100cm	12	27% ± 1.5%
8cm	Xe	0.80	0.85	0.2cm	0.0 cm	300cm	12	48% ± 1%
8cm	Xe	0.80	0.85	0.2cm	0.0 cm	100cm	12	44% ± 1%

BGO

Light Collection Uniformity

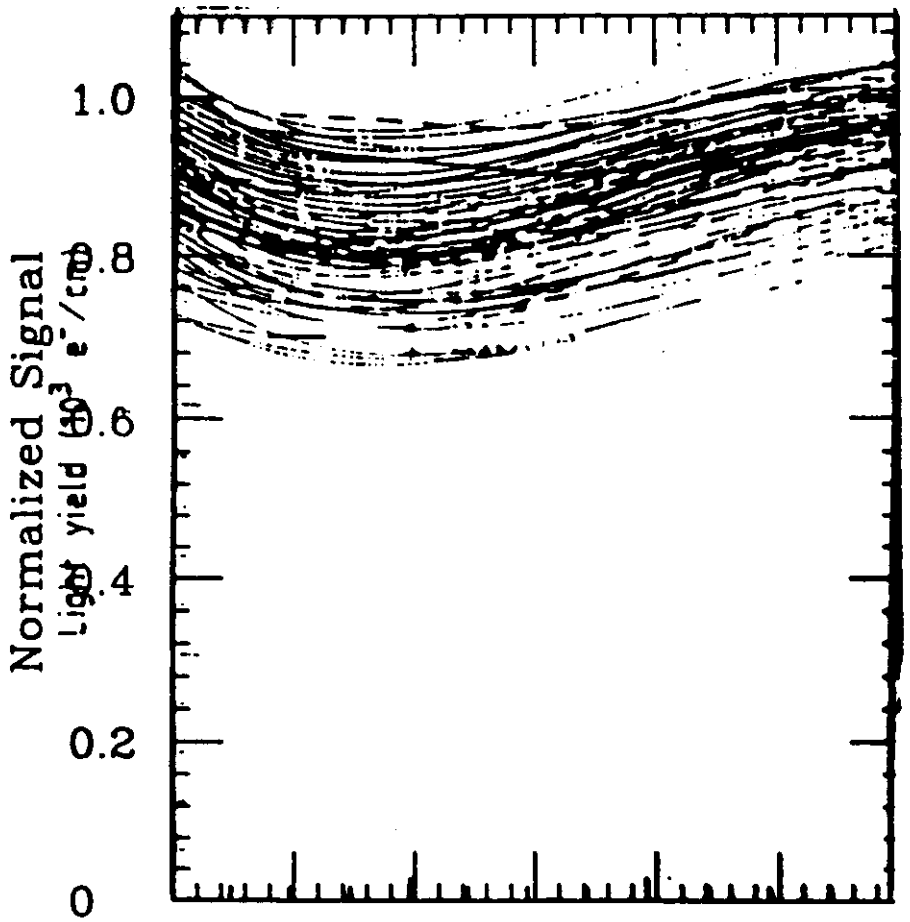

Question (3b) What nonuniformity of reflector surfaces and of photodetector across the output face have been assumed?

Definition:

Rb: reflectivity of normal incident light on BASE Al reflector.

Rs: reflectivity of normal incident light on SIDE Al reflector.

They will be $cos(\theta)^2$ interpolated between Rs(Rb) and 1, for θ, defined w.r. to the normal, > the critical angle, which is about 52°.

Refractive Index at 170 nm:

$N_{Xe} = 1.83$

$N_{Si} = 3.5$

$N_{SiO2} = 1.55$

$N_{MgF2} = 1.45$

Dtop : Darkening process on the side reflector, near top side (Ph. Diode)

Dbase: "" "" , near base side.

λ: Light attenuation length of LXe, vary between 100 and 300 cm.

D.R. : % of reflected light, which is Diffuse Reflection to simulate uneven surface.

The nonuniformity of reflector surfaces and of photodetector assumed are:

1. Uniformity is sufficient for 20% diffusion or 17 nm for surface smoothness. CERN mirror shop routinely produce mirror surface to 1 nm. Uniformity curve with 20% diffusion– see Fig. 3.5.

2. Uniformity with 20% diffusion and attenuation length 100 cm see Fig.3.8.

Question (3c)Are all reflective and support materials known to be sufficiently radiation hard?

Yes, they are known to be sufficiently radiation hard:

1. **Cu, Al, Au and ceramic are all hard;**
2. **MgF_2: 10^7 rad, the effect is not visible: <1% for 1500 μ thick window. Our mirror is < 1 μ, so the effect of radiation damage is > 1/1500 of 1%.**
3. **Kapton is hard up to $5 \times 10^{8-9}$ rad,;**
4. **Silicon diode can be calibrated and the leakage current is negligible at -100 ^{o} C. The frame of the diode is either ceramic or kapton, both are radiation hard.**

5.6 Radiation Damage to Selected Materials in Accelerator Components

Assuming a uniform distributed loss for 30 years of operation as described in Section 5.5, one may estimate the doses seen by the materials in the superconducting dipoles—see Fig. 5.6 for a cross section of a dipole showing the location of the various components. The results are given in Table 5.1.

Table 5.1

For the materials indicated, the 30 year doses, given the assumptions discussed in Section 5.1, are given and the approximate value of the damage threshold to the material of interest.

Subcomponent and material	30-year Dose (10^6 Gy)	Approx. Tol (10^6 Gy)
Beam tube	2.5	
Stainless steel (Cu plated)		—
Trim Coils	2.5	
Kapton film		50.0
Tefzel adhesive		0.5
PK102 thermosetting adhesive (mostly epoxy)		10.0
S.C. wire (.014" diam., Kapton wrapped)		50.0
S-2 glass ("PV" polyimide coated		50.0
Crest 7450 epoxy		10.0
Envex locating pins (Rogers polymide)		50.0
Kapton bumpers		50.0
Circulating helium	—	
Coils	1.4	—
S.C. wire		—
Cu		—
Nb		—
Ti		—
Cable insulation		
Kapton		50.0
Fiberglass (epoxy impregnated)		10.0
Wedges		—
Coil insulation and lubricant		
Kapton		50.0
Teflon		0.01
Collars (stainless steel)	—	—

The leakage current of silicon detectors at −20°C increases slightly after 10 Mrad of radiation.

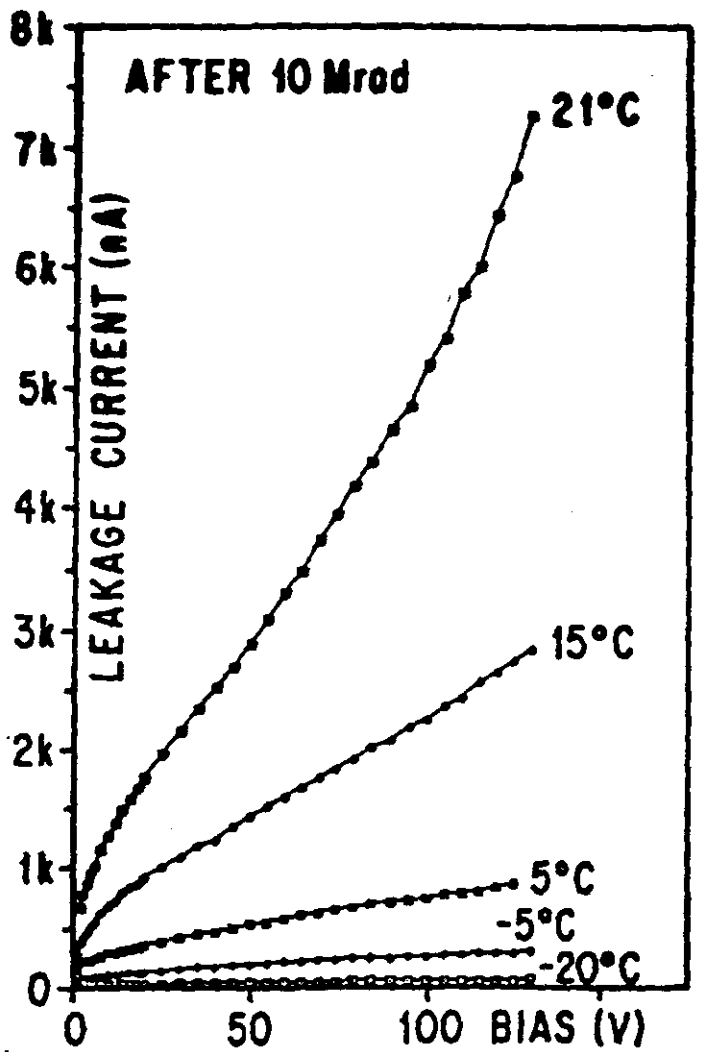

Fig. VII.6. Leakage current in silicon detectors after a 10 megarad exposure to 800 MeV/c protons, as a function of detector temperature.

Tests of similar **photodiodes** show that
the leakage **current of diodes**
decreases by 10^{-6} **from** $-20°C$ to $-108°C$
Conclusion: leakage current at $-108°C$ is negligible.

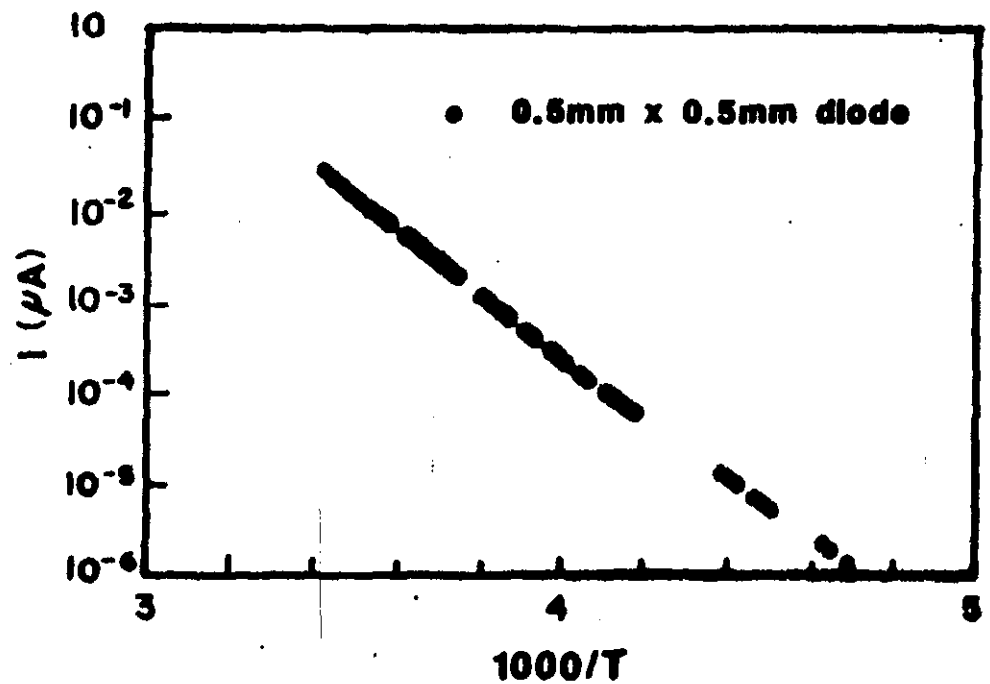

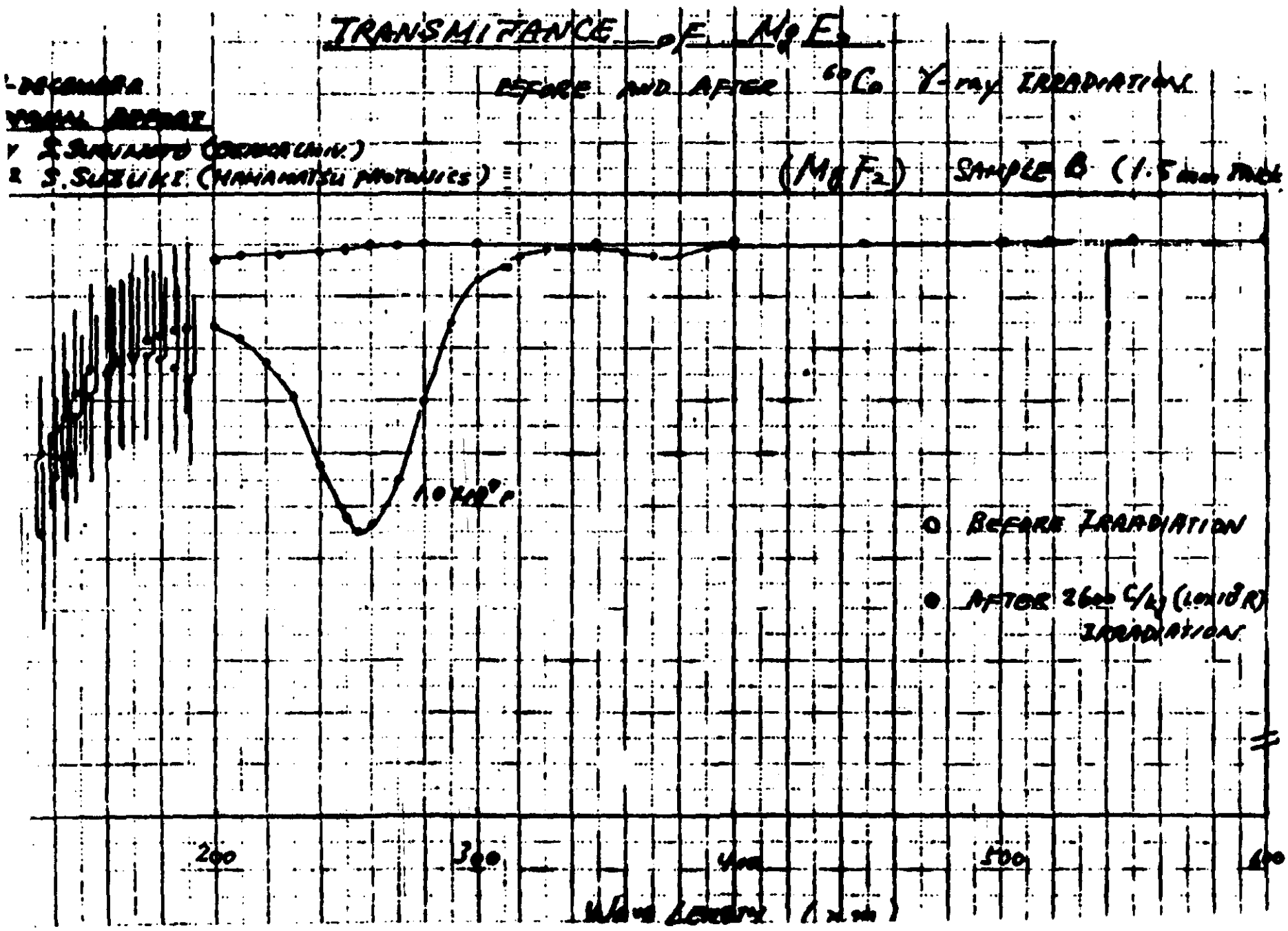
TRANSMITANCE OF MgF2
BEFORE AND AFTER 60Co γ-ray IRRADIATION
(MgF2) SAMPLE B (1.5 mm thick)
S. SUZUKI (HAMAMATSU PHOTONICS)
BEFORE IRRADIATION
AFTER 2600 C/kg (10×10^8 R) IRRADIATION
200
300
500

to be sufficiently radiation hard in response to neutrons and gammas?

Yes, VUV photodiodes and fast amplifiers are sufficiently radiation hard:

1. Silicon diode can be calibrated. Its leakage current is negligible at low T.
2. Due to the large capacitance and signal, fast amp. can be outside: with 5 m of cable, no additional noise.
3. Light production: Xe/Kr are radiation hard and homogeneous, which can be monitored externally.
4. Transmission: UV mirror is radiation hard.
5. Attenuation length: Xe/Kr are radiation hard and homogeneous, which can be monitored externally.
6. Mirror: MgF_2 is radiation hard. Substrates (Cu/Al/kapton) are radiation hard:
7. Collection: UV-diodes, calibrated by α's, see Fig.

Question (3e) Is the module response sufficiently uniform longitudinally through the entire chain of light production, transmission, and collection? If not, there may be an unacceptable constant term because of longitudinal shower fluctuations.

Using the Geant Monte Carlo shower program, we vary the acceptance by 2 ± 1% and found the resolution does not deteriote. This is supported by the 3 BGO data, that with an 6% deviation in light acceptance, a 0.5% resolution s achieved at the test beam above a few GeV.

Question (4) What are the measured effects of radiation damage on light yield, transmission, and collection of the 170nm VUV light?

By exposing the 1x1 chamber and Xe gas in high pressure cylinder separately instead of the chamber with LXe inside and using standard procedure of purification, we plan to measure,

1. uniformity before and after irradiation,

2. energy scale after calibration of quantum efficiency using α's.

α Calibration Spectrum

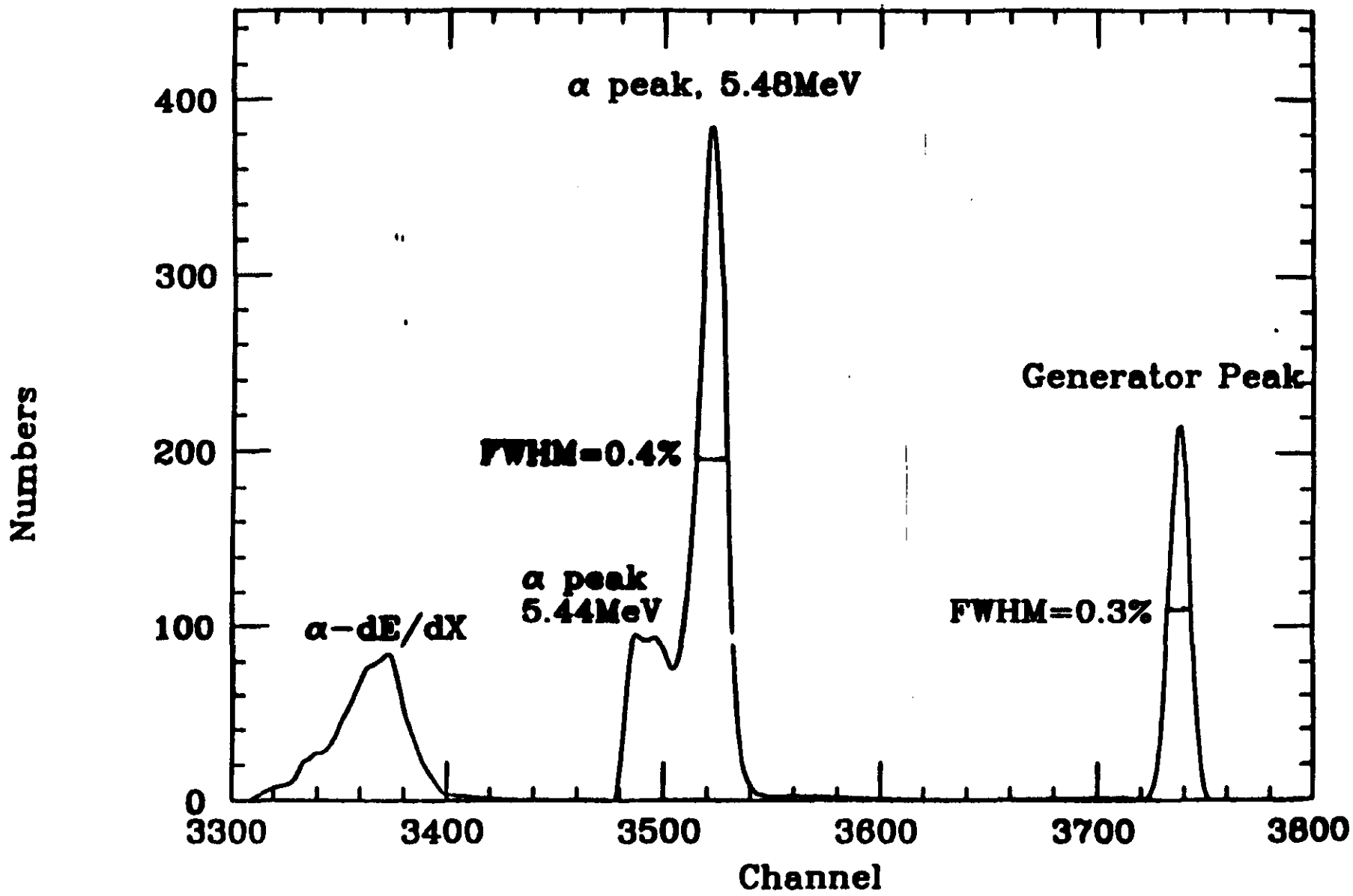

Question (5) Is the cost of the calibration system included in the baseline? How can one monitor system response along the length of a module?

The cost of the calibration system is basically included in the baseline, which over-estimated by 4M$ (40% contingency) or 9 M$ (25% contingency). The cost of the calibration system is:

1. **Generator (5k$) Fanout (4500 vac. relay at 5$ each, multiplex=25k) Capacitor(1$)**
2. **Total cost: 5 + 25 + 45k = 75k$ x 2 = 150 k$**
3. **Discriminator: 10$ + vac. relay 5 $ MUX = 15 $/channel, or x 45k = 700 k$ x 2 = 1.5 M$.**
4. **Auto VUV spectrometer: 300k$.**
5. **One monitor system calibrate along the length of a module, because**
   - **Liquid is homogeneous,**
   - **MgF_2 is radiation hard,**
   - **Diode has been crossed calibrated and is the only one to be calibrated.**

Question (6) What provision has been made for the rejection of pi-zero gammas from unfavorable jet fragmentations? (The rate of such fragmentation has large uncertainties, and these may dominate the Higgs –> gamma gamma background.) If very fine lateral segmentation is proposed, this must be included in the baseline cost.

The following devices are being considered for the rejection of π^o γ's:

1. **Drift diodes: Rehak/BNL,**
2. **Milli-Strip detector:**
   - **scale from UV-diodes: 14k strip detector at 100$ each,**
   - **scale from micro-strips: 13k$/5k ch = 3$/ch**
   - **30 ch each with 5 bit ADC = 3 $ * 30 * 2 = 18,**
   - **280 x 14k = 5 M$.**
3. **Scin. Fibre: J. Brau**
4. **TPC Wire chamber: E. Aprile, T. Doke, T. Ypsilantis**

The cost is basically included in the baseline, which over-estimates by 4M$ (40% contingency) or 9 M$ (25% contingency).

3-D Shower Measurement

Use 3 Layers of LXe Counters longitudinally

1st Layer: one transverse counter per shower

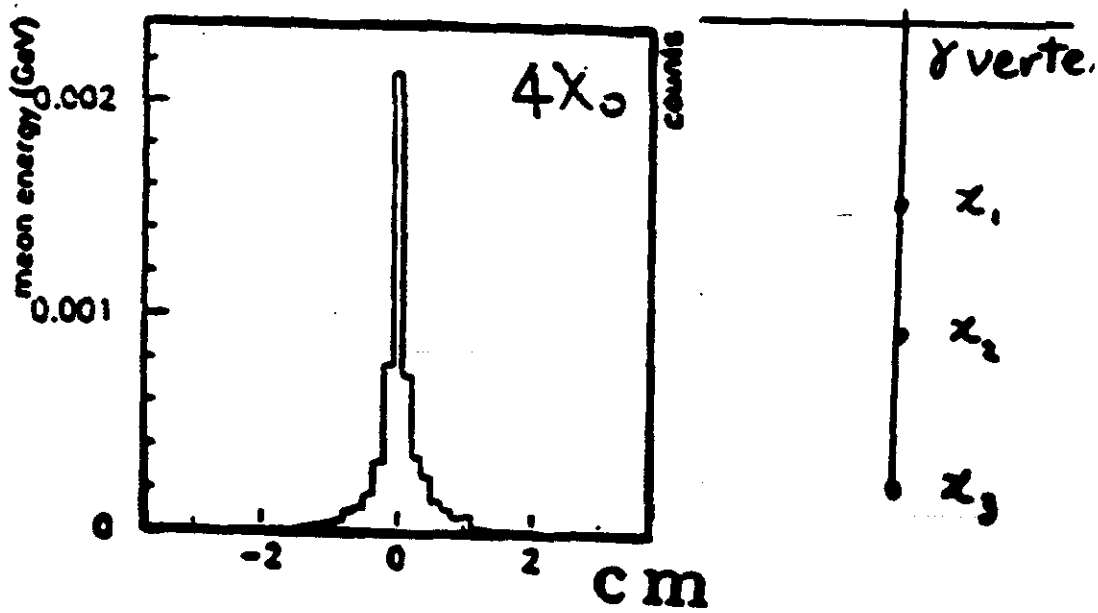

2nd & 3rd Layers: > 60% of energy in one counter

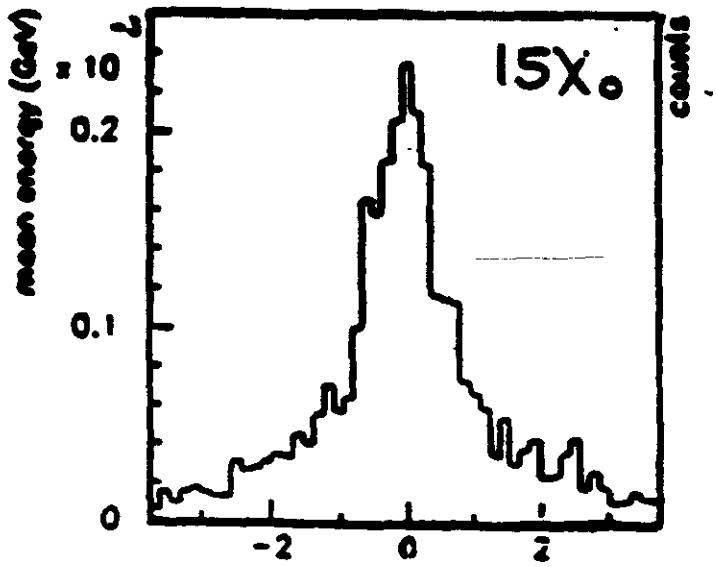

Whence transverse center of gravity determined to 1.5 mm in outer layers, Longitudinal separation of layers permit extrapolation to I.P. ;

or vertex — ≈ 2 mm / 300 mm × 1000 mm ≈ 7 mm

Veto $\pi^0 \to \gamma\gamma$

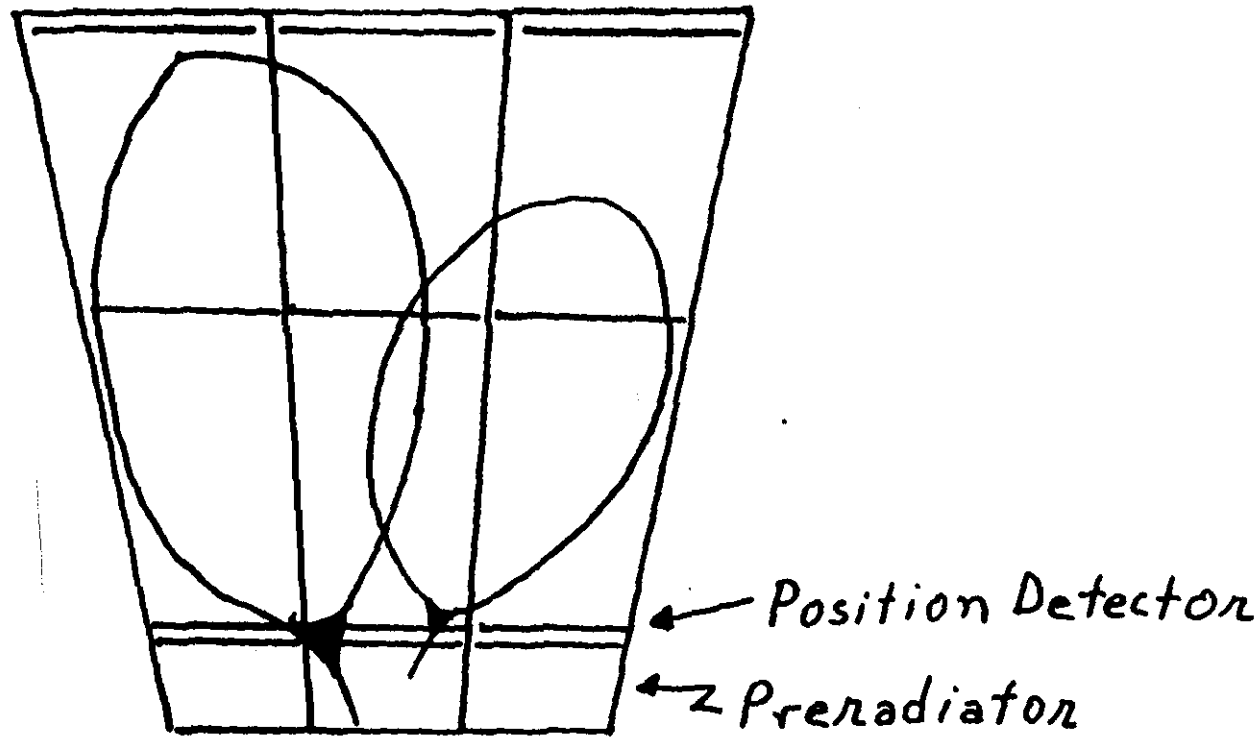

Active preradiator is more accurate than passive in E resolution and depth E distribution.

γ/π^0 Separation

- Isolation cuts.
- Drift diode veto of $\pi^0 \rightarrow \gamma\gamma$ if $\gamma\gamma > 1$ mm.

Energy distribution after 8 cm of LXe, for ten 50 GeV π^0 decaying into two 25 GeV γ's, 1 mm apart.

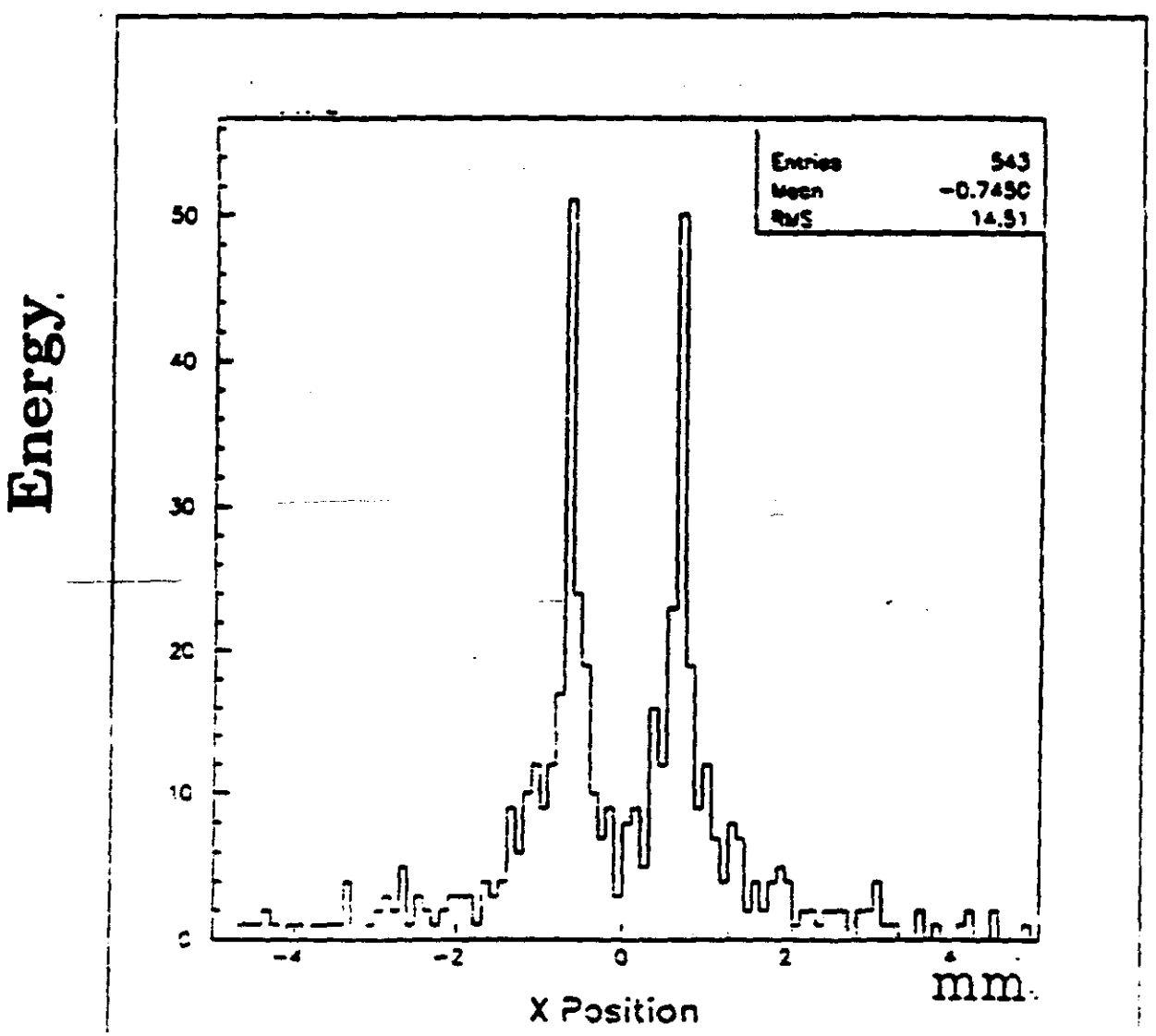

3-D Shower Measurement

Use 3 Layers of LXe Counters longitudinally

1st Layer: one transverse counter per shower

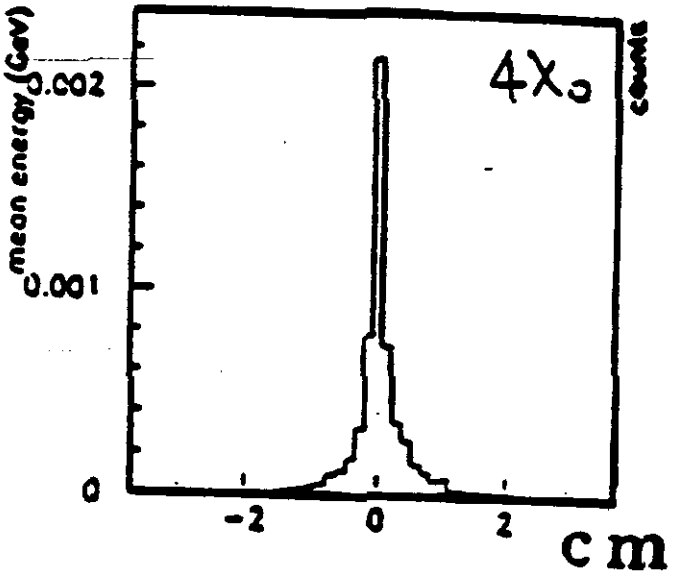

2nd & 3rd Layers: > 60% of energy in one counter

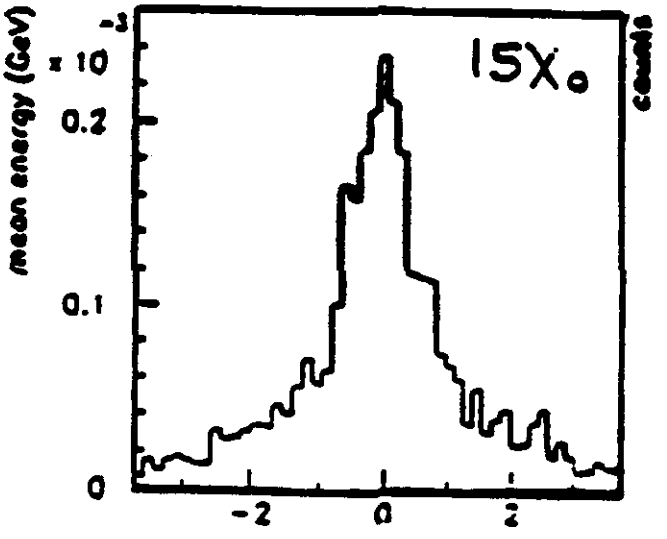

Whence transverse center of gravity determined to 1.5 mm in outer layers, Longitudinal separation of layers permit

Imperial College/S.I. Silicon drift diodes

The diodes are provided on small boards as shown below:

Detector boards, back and front:

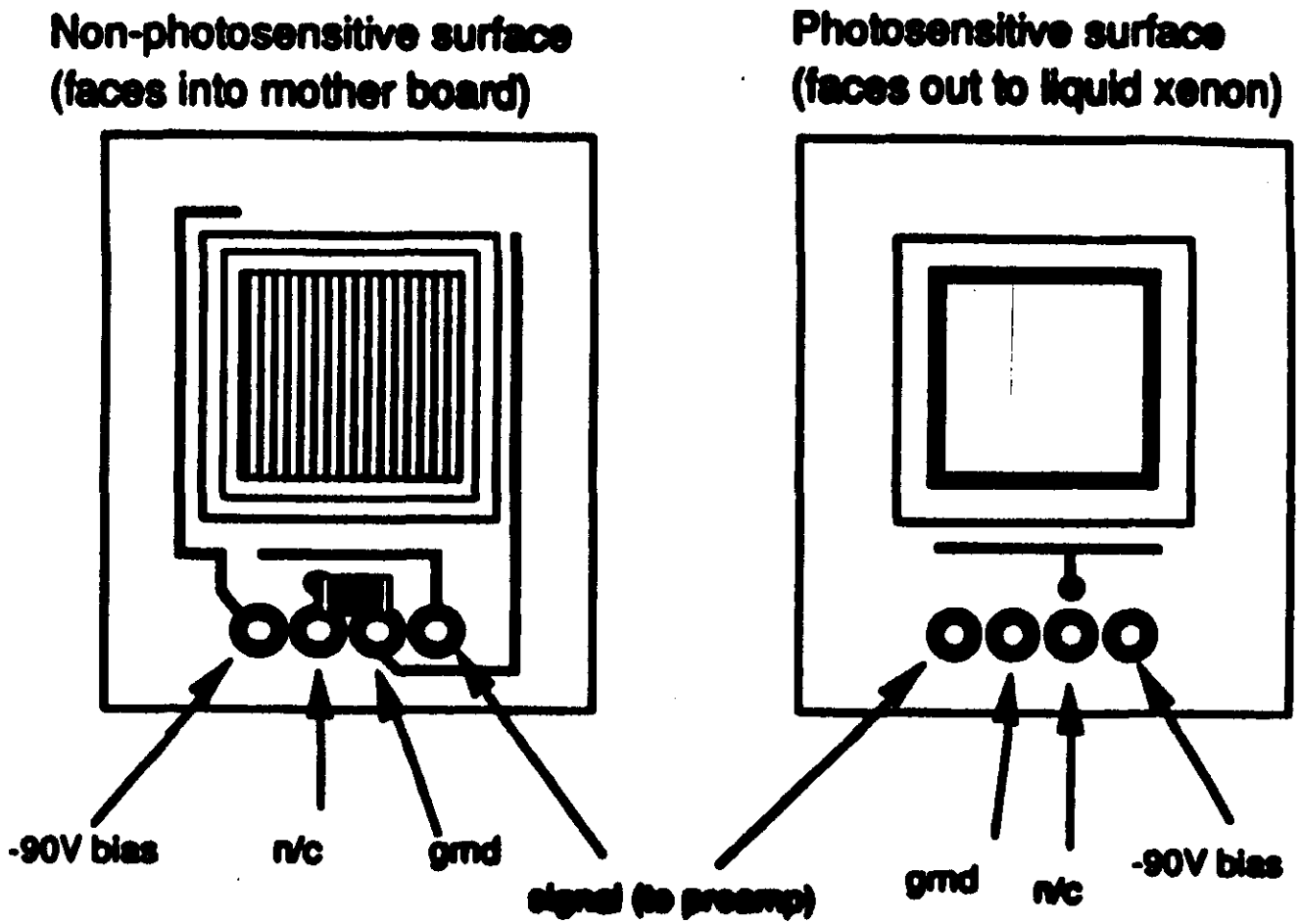

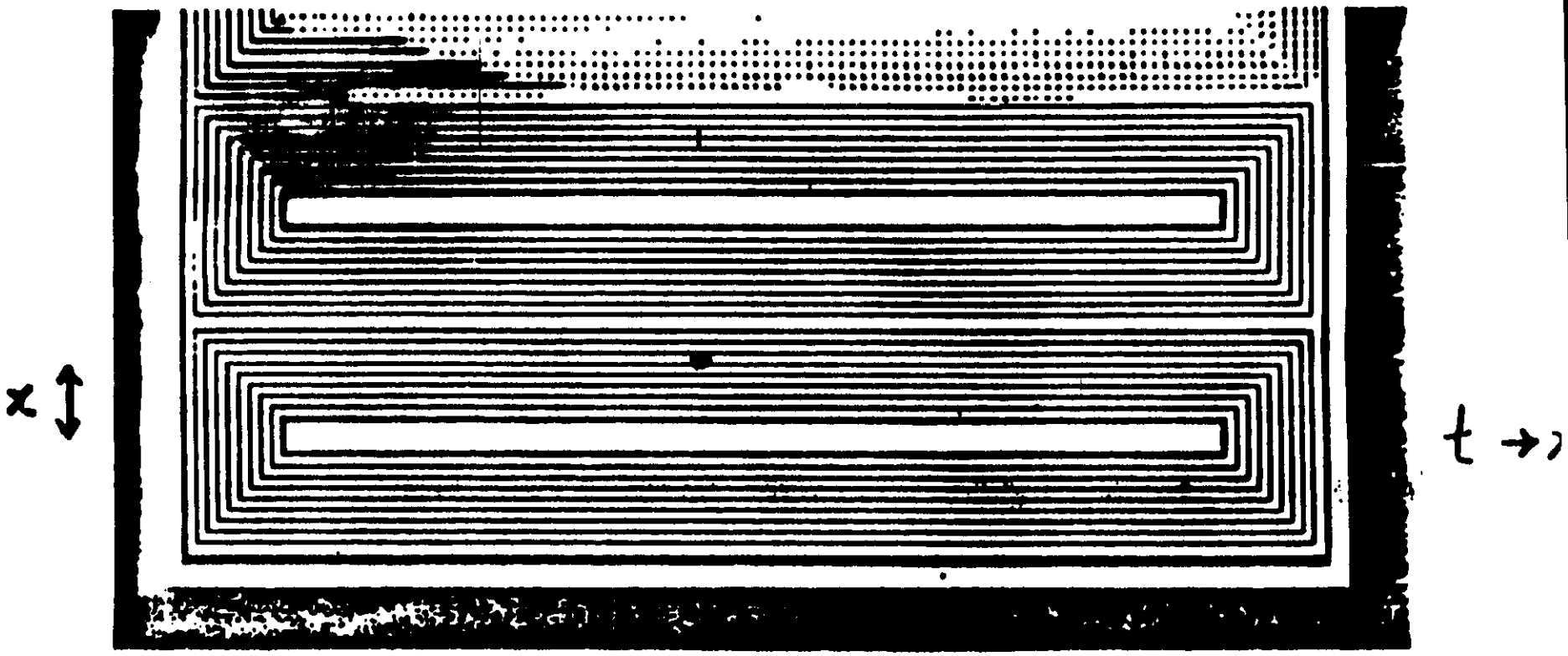

Fig.1 A section of one surface of a drift photodiode, showing two cells of the device. The photosensitive surface is opposite this one. Each of the five cells is 2mm by 10mm. In each a central anode is surrounded by field shaping cathodes to provide the drift field. The total active area is $1cm^2$.

Pulses from Wide Anode Drift Photodiode (200ns RC-CR shaping)

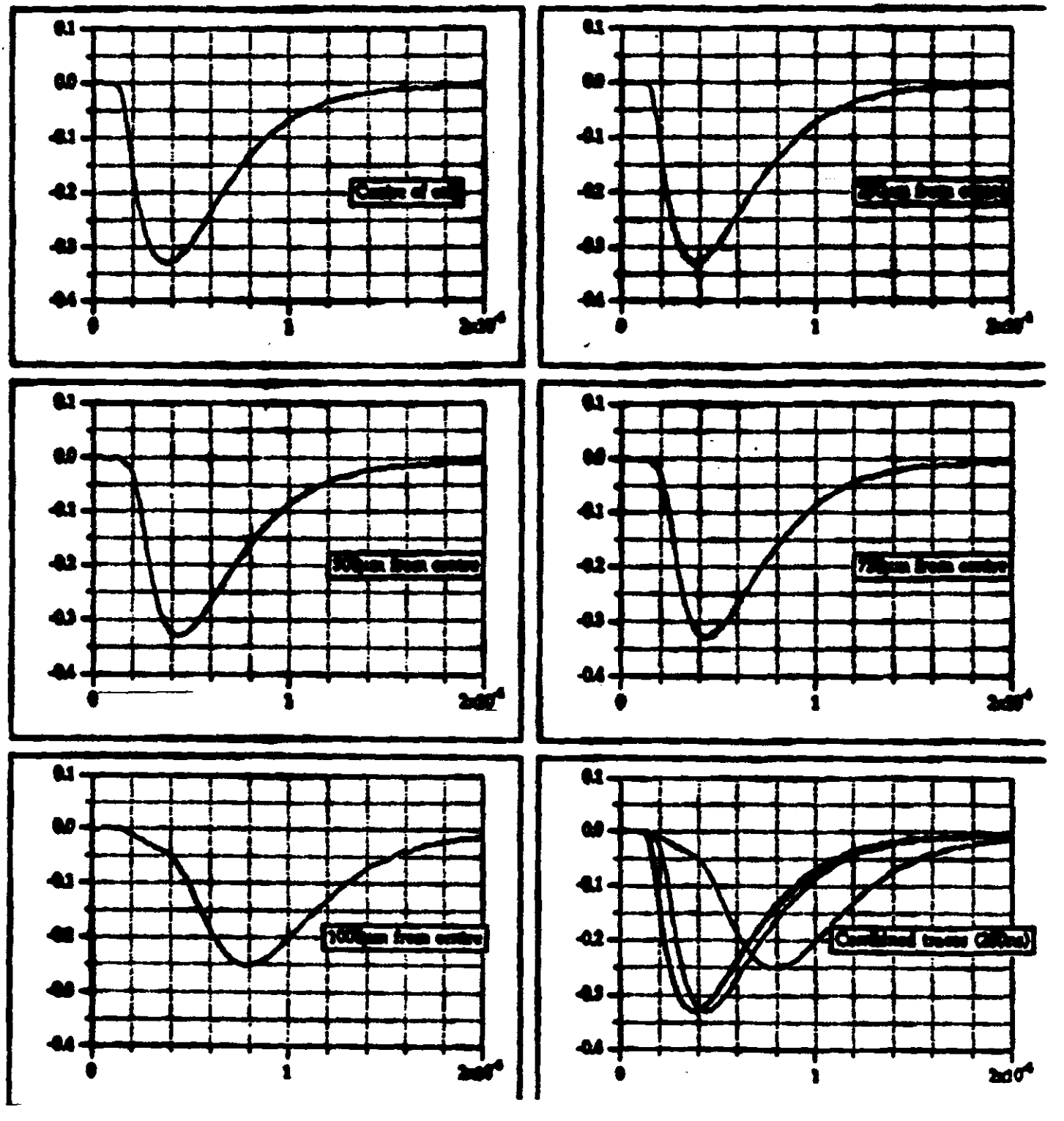

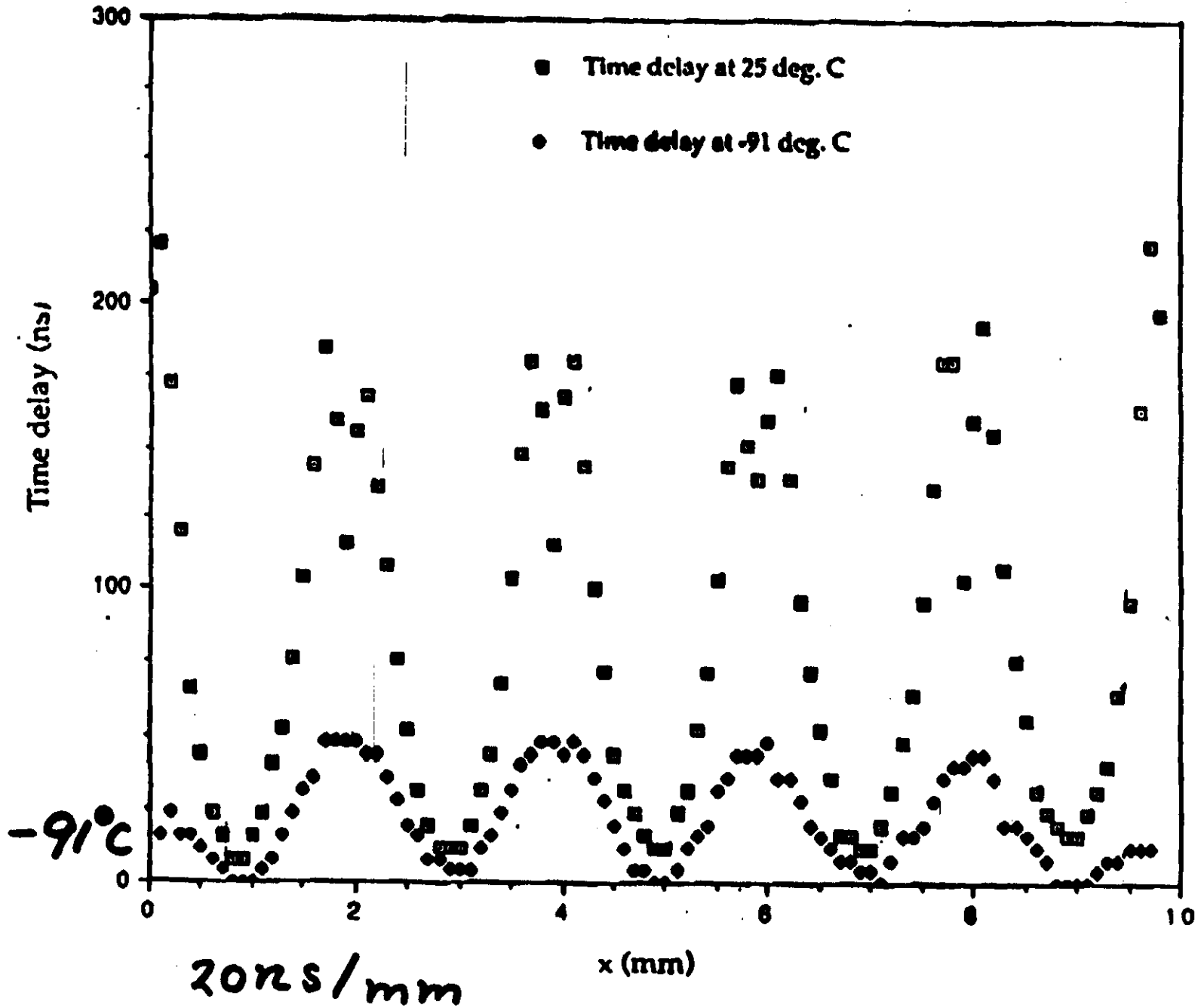
Time delay at 25 deg. C
Time delay at -91 deg. C
Time delay (ns)
300
200
100
0
0
2
4
6
8
10
x (mm)
-91°C
20ns/mm

$ttH \rightarrow \gamma + \gamma$ + lepton tag with isolated π^0 background

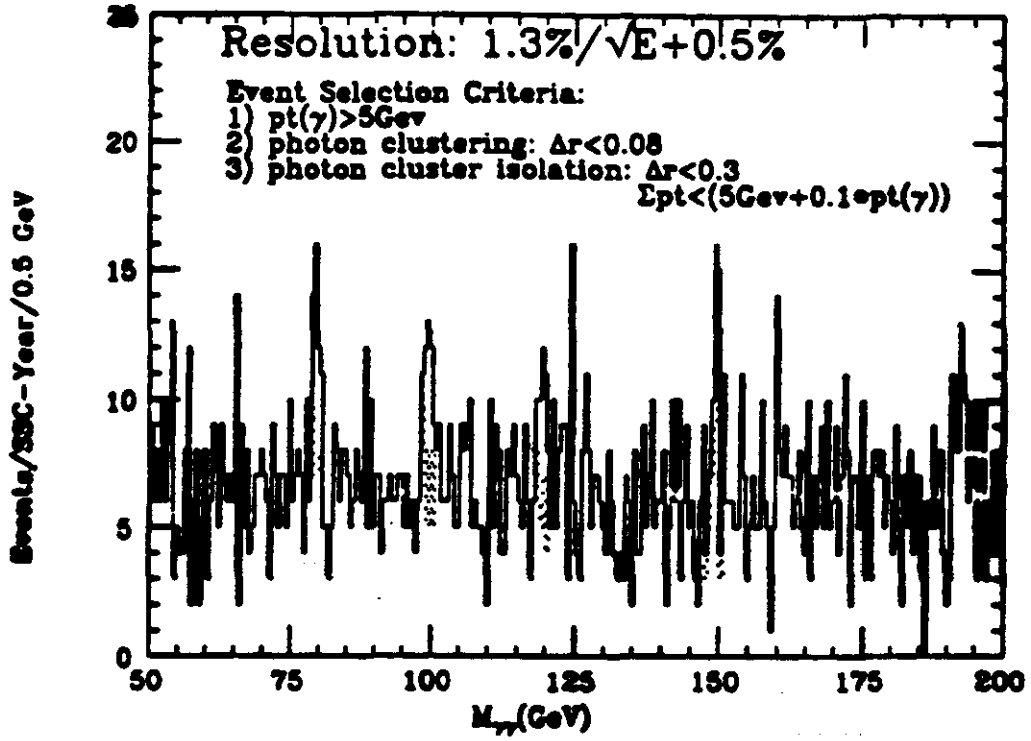

$t\bar{t}H \rightarrow \gamma + \gamma$ + lepton tag after vetoing isolated π^0

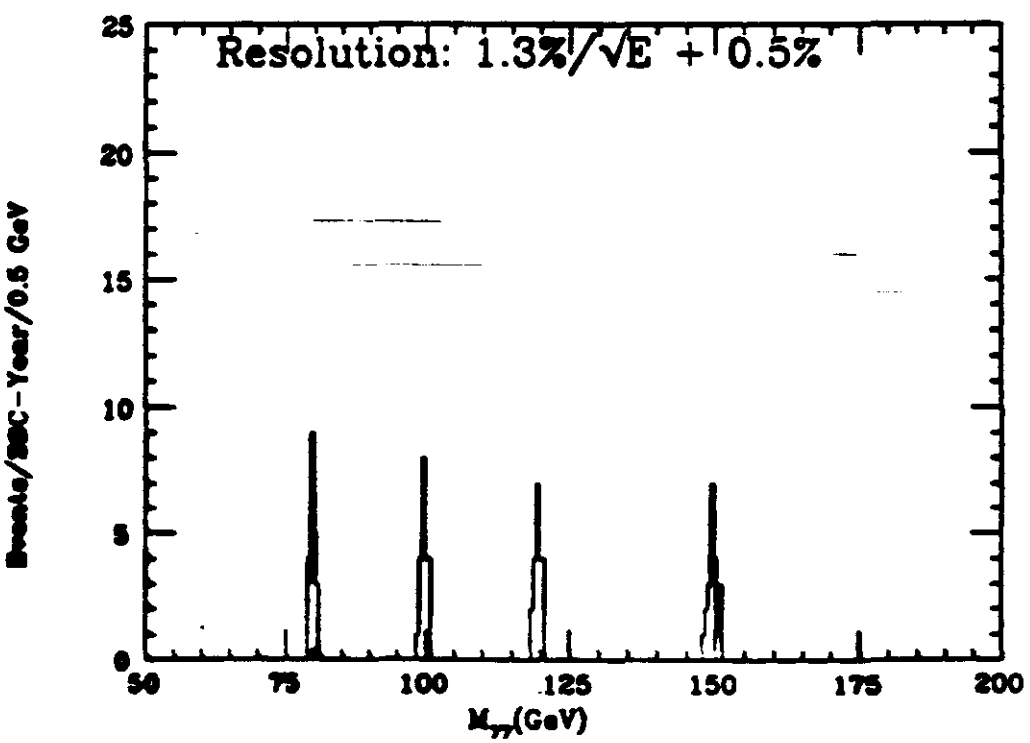

$t\bar{t}\gamma$ and $t \rightarrow \gamma$ + W + b background to be added.

Question (7) What is the constant term in the energy resolution for hadrons which one measures after more than an interaction length of non-compensating liquid xenon (with 3 depth segments)? Precisely how has this been simulated, and when will it be measured?

1. **Simulated with Geisha together with a compensating TMP calorimeter by Fesefeldt using a long gate time. e/π can be further tuned to be closer to 1 using faster gate time.**

2. **To be Measured in 92 at CERN.**

LXe scintillation:

1. intense:$4 - 6 \times 10^7$ photons/GeV;

2. Non-saturation;

3. $e/\pi = 1$.

New compensation mechanism:
The fast component enhanced for high dE/dx particles such as o or nuclear spallation fragments from hadron-nucleus interaction.

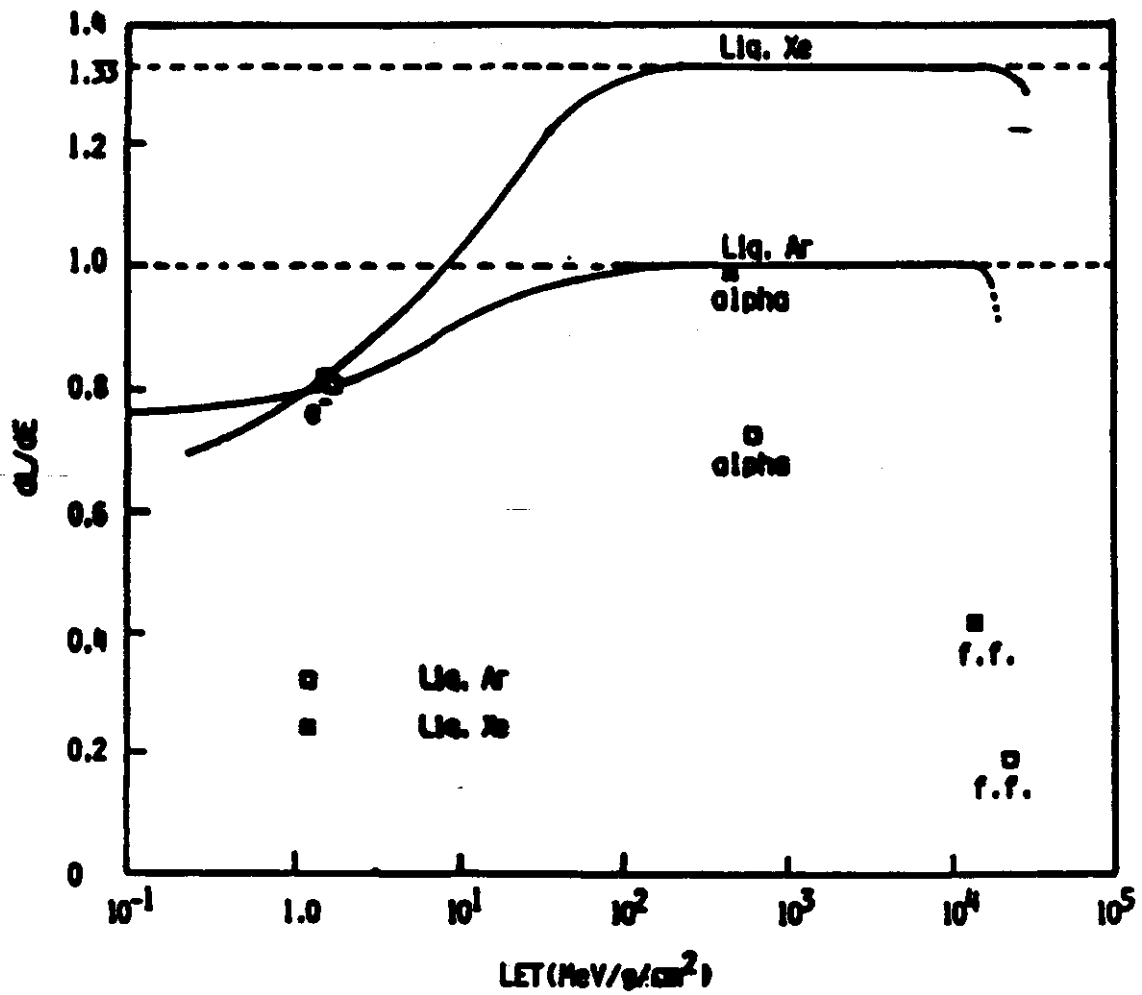

Fig. 7c Similar to Fig. 7b, dL/dE for relativistic ions and fission fragments for LXe (solid squares) and for LAr (open squares) versus dE/dx. For heavy ions, the electron/ion density and thus the scintillat-

Scintillation Mechanism in Noble Liquids

LXe scintillation:

1. intense: $4-6\times10^7$ photons/GeV;
2. Non-saturation;
3. $e/\pi = 1$.

Scintillating light includes
Molecular excitation and recombination luminescence

1. Molecular excitation luminescence (e, α):
   Energy loss -> Xe_2^* -> Xe_2 + UV,
   Any Xe atom can contribute:
   Thus high efficiency and
   No satuation.
2. Recombination luminescence (α):
   Molecular ions Xe_2^+ + e -> Xe^* + Xe.
   Xe^* -> Xe_2 + UV,
   dependent on the electron-ion density or dE/dx
   New compensation mechanism:
   The fast component is enhanced for high dE/dx particles such as α,
   or nuclear spallation fragments from hadron-nucleus interaction.

For relativistic particles($\beta > 0.9$),

I. Fast component:

$$I_f = \int_0^T i_f(t)\,dt = \int_0^T A_f e^{-t/\tau_f}\,dt = A_f\tau_f(1 - e^{-T/\tau_f})$$

II Slow component:

$$I_s = \int_0^T i_s(t)\,dt = \int_0^T A_s e^{-t/\tau_s}\,dt = A_s\tau_s(1 - e^{-T/\tau_s})$$

III Recombination component:

$$I_r = \int_0^T i_r(t)\,dt = \int_0^T S\cdot R_o(-dn/dt)\cdot dt = \int_0^T SR_o n_o^2\alpha/(1 + n_o\alpha t)^2\,dt$$
$$= SR_o n_o^2\alpha T/(1 + n_o\alpha T)$$

where S : the cross section of the column of ion pairs

R_o: the track length

n_o: the initial density of ion pairs

α : the recombination coefficient

($dn_\pm/dt = -\alpha n_\pm^2$)

T : the gate time

5 GeV jet

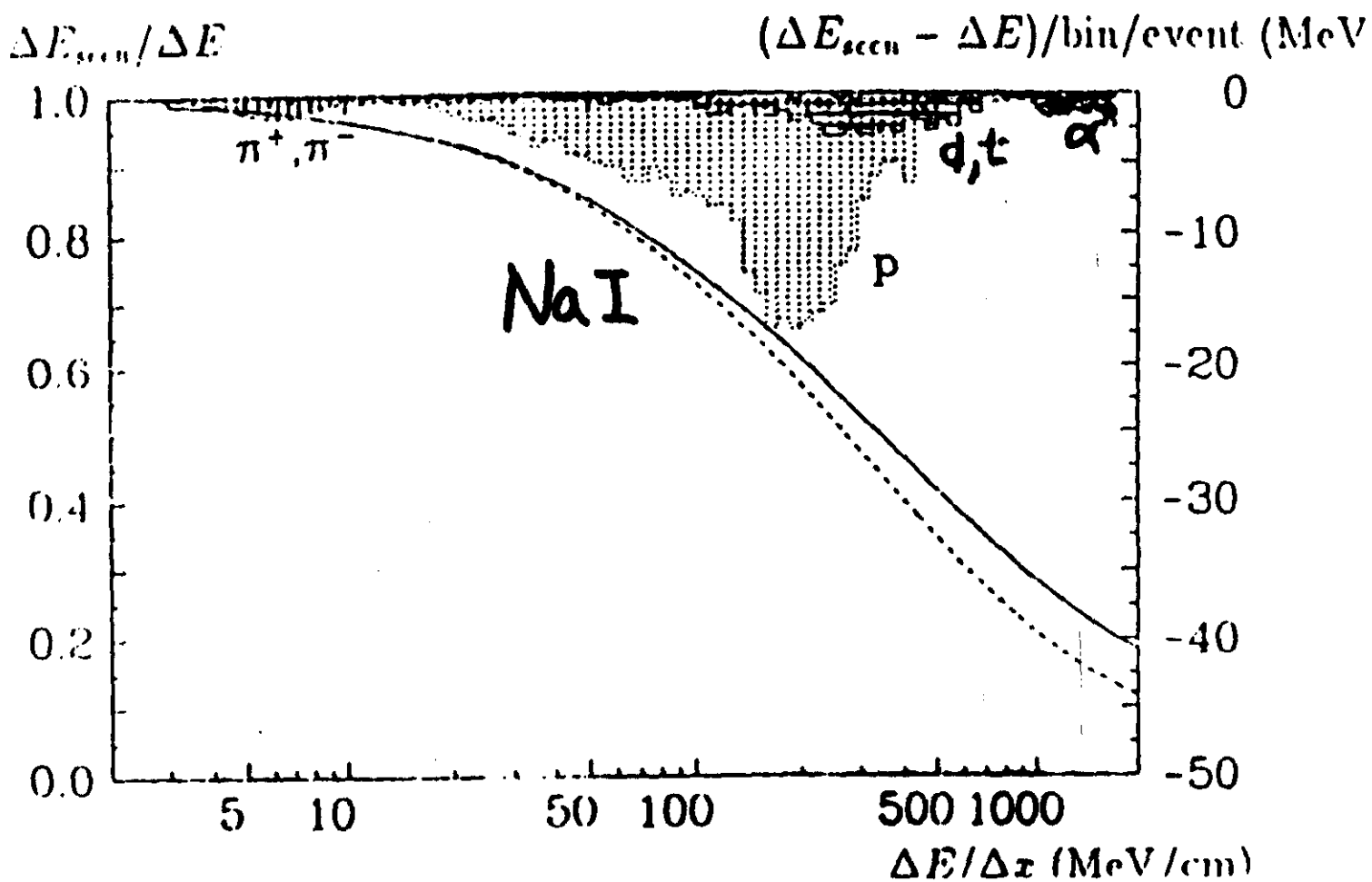
$\Delta E_{scen}/\Delta E$
$(\Delta E_{scen} - \Delta E)$/bin/event (MeV)
1.0
0.8
0.6
0.4
0.2
0.0
0
-10
-20
-30
-40
-50
π^+, π^-
d,t
α
p
NaI
5
10
50
100
500
1000
$\Delta E/\Delta x$ (MeV/cm)

Compensation in LXe

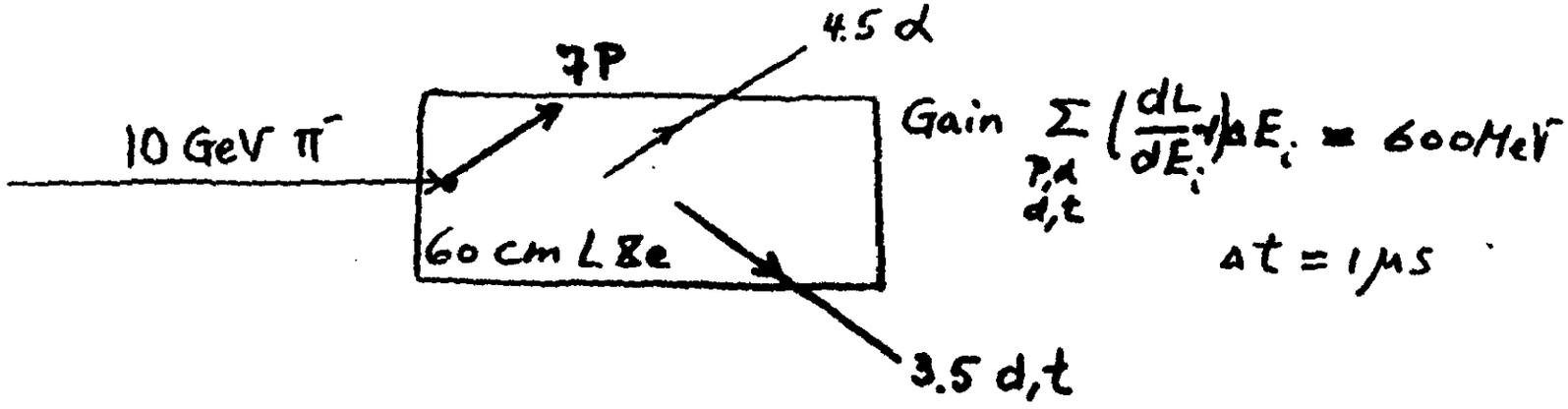

COMPENSATED

Nuclear binding energy loss
2.1 ± 1GeV

Enhanced light output
2 GeV at 15 ns

Compared with "neutron" compensation:

- faster
- smaller cone

Similarly, Monte Carlo shows compensation for 50 and 100 GeV π^-

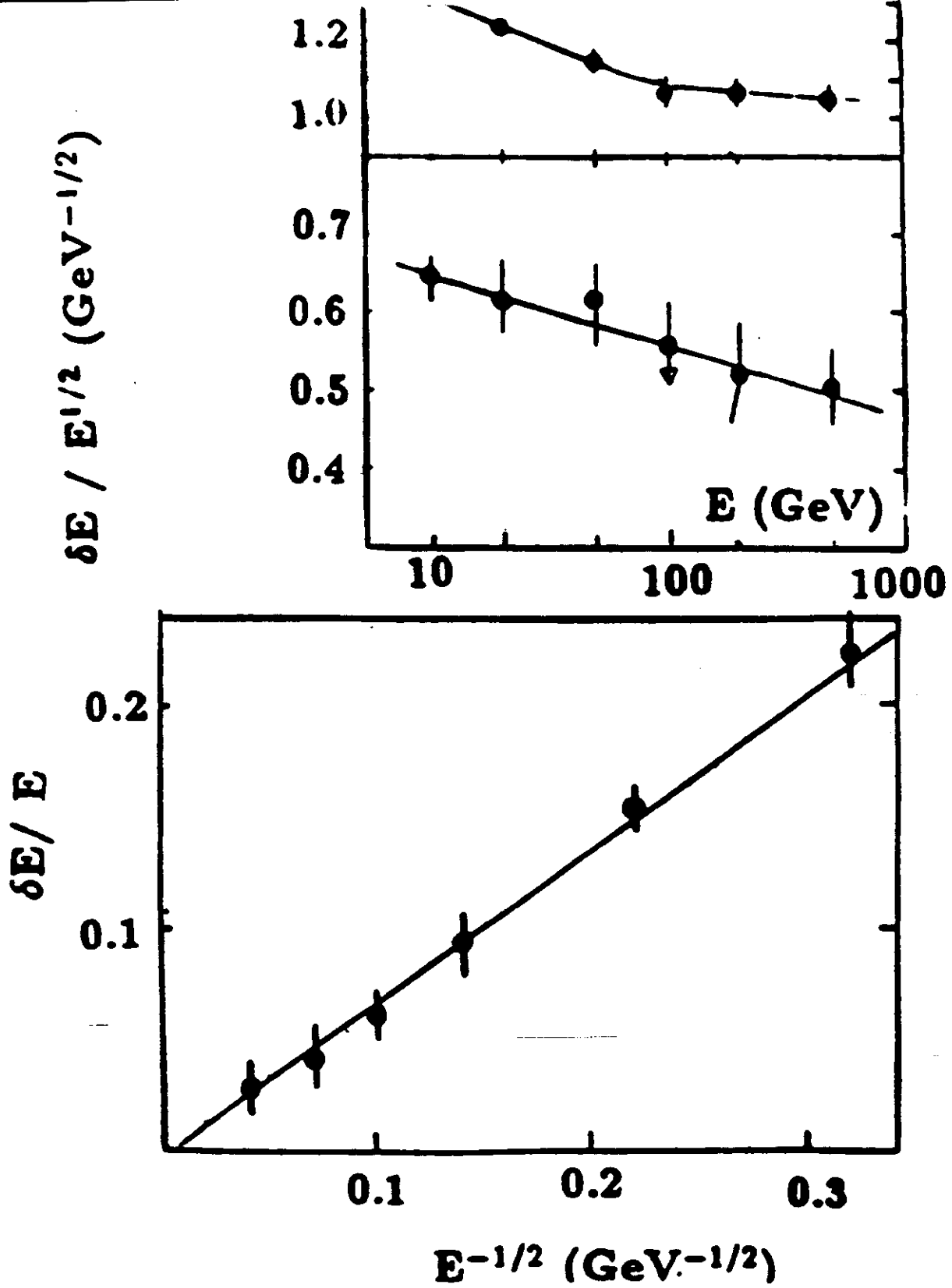

Figure 3: Monte Carlo results on a) the e/π ratio, b) jet energy resolution, and c) the $1/\sqrt{E}$ dependence of jet energy resolution, showing a very small constant term, for a combined system of scintillating liquid xenon EM calorimeters in front of some compensating hadron calorimeters (such as TMS + U plates).

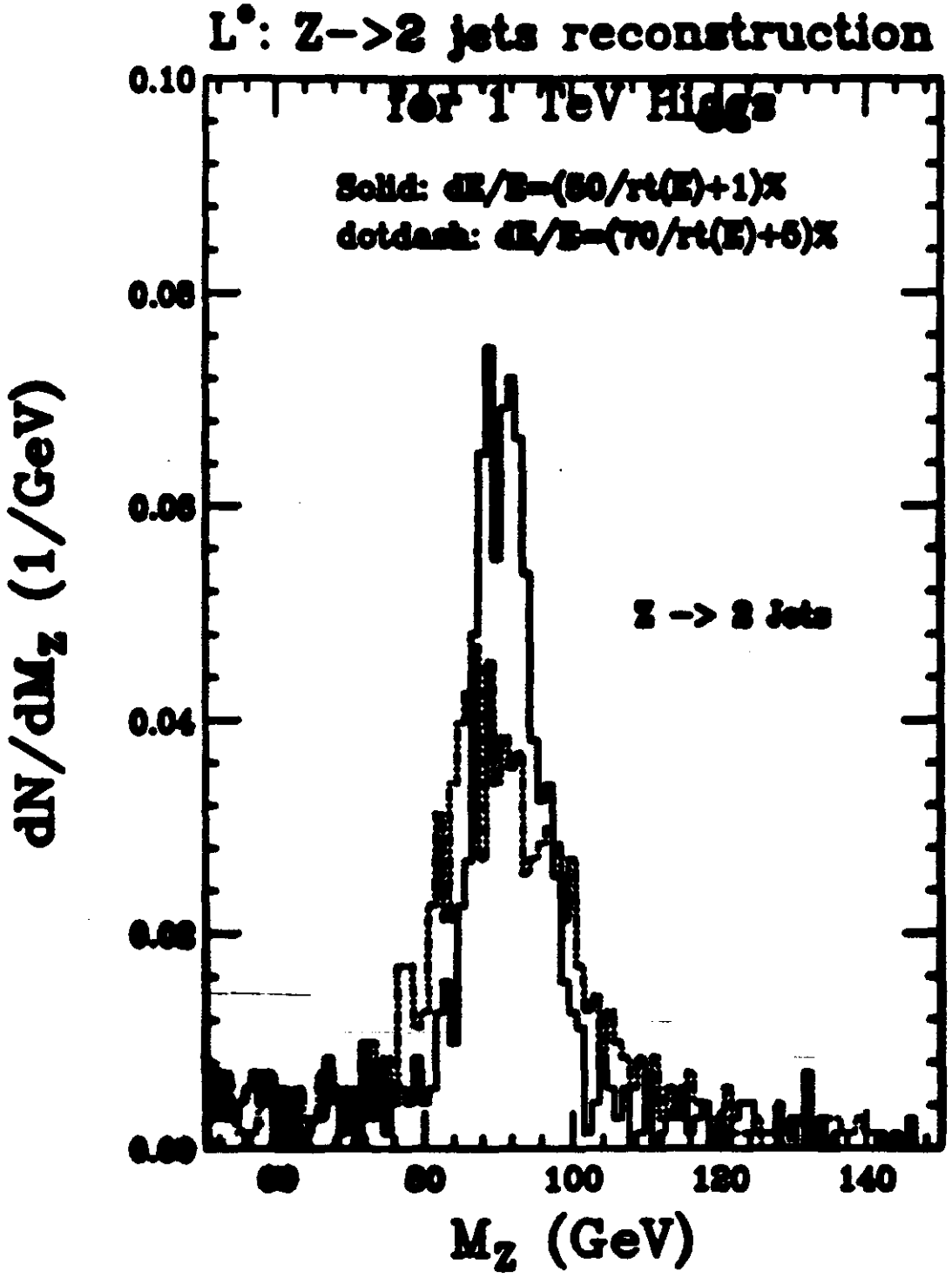
L*: Z->2 jets reconstruction
For 1 TeV Higgs
Solid: dE/E=(50/rt(E)+1)%
dotdash: dE/E=(70/rt(E)+5)%
Z -> 2 jets
dN/dM_Z (1/GeV)
M_Z (GeV)
0.10
0.08
0.06
0.04
0.02
0.00
60
80
100
120
140

Question (8) How confident can we be that liquid Xenon will in fact be available in the quantities required at the anticipated cost? Are there alternative sources in case of disruption of supply from the primary source, and what would be the cost from such an alternative source?

We note:

1. Xenon and krypton are both by-products of liquid air.

2. The price 2.5$/c.c. for liquid xenon assumes there is no market for krypton. More and more detectors are using krypton and this could cut the xenon price by a factor up to two.

3. Liq. Air Co. submitted formal letters stating that they can produce 30 cubic meters of liquid xenon using their existing facility in the next 8 years. The LXe calorimeter requires 16 cubic meters, while the proposed SandI for barrel and LXe endcap uses only 4 cubic meters of LXe. This is a small fraction of the potential production capacity.

4. We note that 0.8 cubic meters of LXe already exist inside a bubble chamber at ITEP, which may complete its mission this year.

5. ORT of USSR is the largest foreign supplier and is having discussion with